UC Riverside

UC Riverside Electronic Theses and Dissertations

Title

Proton NMR Studies of the Interaction of Heparin-Derived Oligosaccharide with Biological Molecules and the Cis/Trans Isomerization of Amide Bonds in Peptides and Peptide/Peptoid Hybrids

Permalink

https://escholarship.org/uc/item/1qp699nb

Author

Nguyen, Khanh Trong

Publication Date

2009

Peer reviewed|Thesis/dissertation

UNIVERSITY OF CALIFORNIA
RIVERSIDE

Proton NMR Studies of the Interaction of Heparin-Derived Oligosaccharide With
Biological Molecules and the Cis/Trans Isomerization of Amide Bonds in Peptides and
Peptide/Peptoid Hybrids

A Dissertation submitted in partial satisfaction
of the requirement for the degree of

Doctor of Philosophy

in

Chemistry

by

Khanh Trong Nguyen

March 2009

Dissertation Committee:
        Professor Dallas L. Rabenstein, Chairperson
        Professor Cynthia K. Larive
        Professor Yinsheng Wang

The Dissertation of Khanh Trong Nguyen is approved:

_____

_____

_____

Committee Chairperson

University of California, Riverside

Acknowledgements

This dissertation would have been impossible without the help of many people. First I would especially like to thank my research advisor, Professor Dallas L. Rabenstein, for giving me the opportunity to do research with him, for his patience and guidance through my PhD at UCR. Professor Rabenstein is a wonderful advisor, providing me with encouragement and endless source of ideas. His broad knowledge and enthusiasm for research impresses and inspires me. I am extremely grateful for the knowledge that I have gained from him, which is a special wealth to my life and will form the basis to my future career.

Special thanks to Professor Cynthia Larive and Professor Yinsheng Wang for their assistance, kindness and time served on my dissertation committee.

I would like to thank Dr. Dan Borchardt and Mr. Yi Meng for their help with NMR as well as Mr. Ron New for his assistance in MALDI-MS.

 I would like to thank Dr. Stephen Spain for teaching me how to use HPLC, CE, and NMR. He gave me a lot of help when I first joined the group.

I would like to thank Dr. Sui Qiang, a great friend, for teaching me kinetic experiments and sharing his knowledge of the peptide chemistry. I would also like to thank Dr. Tiesheng Shi for making the Platinum reagent for my peptide studies as well as his valuable suggestions and help.

I am grateful to the past and present members of the Rabenstein research group for their support, suggestions, and friendship, particularly Dr. Tiesheng Shi, Dr. Stephen Spain, and Dr. Sui Qiang, Mark Hamza, Emily Spencer, Bruce Ford and Robert Young.

I am thankful for the caring and help from all the staff members in the UCR chemistry department as well. Everyone made this department a friendly environment.

Finally, I would like to thank my parents and sister for their constant support and encouragement that they have given me, which kept me going through the difficult time over years. I also like to express my deep thankfulness to my wife Quyen Pham. She has been always there sharing with me the good and bad times.

ABSTRACT OF THE DISSERTATION

Proton NMR Studies of the Interaction of Heparin-Derived Oligosaccharide with
Biological Molecules and the Cis/Trans Isomerization of Amide Bonds in Peptides and
Peptide/Peptoid Hybrids

By

Khanh Trong Nguyen

Doctor of Philosophy, Graduate Program in Chemistry
University of California, Riverside, March 2009
Professor Dallas L. Rabenstein, Chairperson

Two diverse topics in biological chemistry are the subject of this dissertation. In
part I, the research focuses on heparin and the interaction of histidine-containing peptides
with heparin. Heparin is a linear polysaccharide, which is formed through the linkage of
variously sulfated uronic acid-($1 \rightarrow 4$)-D-glucosamine repeating disaccharide subunits by
glycosidic bonds. The structure of heparin is not yet completely understood due to its
extreme complexity. Consequently, details of the binding of peptides and proteins by
heparin is not well understood. One approach is to use well-defined heparin-derived
oligosaccharides with different structures as models to probe the question of specificity of
binding.

Three heparin-derived tetrasaccharides, one hexasaccharide and one
octasaccharide were isolated, purified and characterized. A structurally defined
tetrasaccharide was then used as a model to study heparin binding by histidine-containing
peptides and related molecules. The imidazolium group of all the molecules studied was
found to bind site specifically to a binding pocket formed by an iduronic acid-
glucosamine-iduronic acid trisaccharide sequence. Binding constants were determined for
the complexes by NMR. Binding constants and relative binding affinities were also

determined for the binding of the same molecules by intact heparin by isothermal titration calorimetry and heparin affinity chromatography, respectively.

In part II, the kinetics and thermodynamics of cis/trans isomerization of Xaa-sarcosine tertiary amide bonds in peptide/peptoid hybrids were studied. Xaa represents an amino acid and sarcosine is N-methyl glycine. Specifically, the effect of amino acid sequence on the kinetics and equilibria of cis/trans isomerization across Xaa-sarcosine peptide bonds in three series of peptide/peptoid hybrids having the sequences Ac-Cys-Sar-His-Xaa-(Ala)$_3$-Cys-NH$_2$, where Xaa is His, Gly, Lys, Phe, Asp and Glu, Ac-Cys-Sar-(Ala)$_x$-His-(Ala)$_y$-Cys-NH$_2$, x = 0-4 and y = 4-0, and Ac-Cys-Sar-His-(Ala)$_3$-Cys-NH$_2$, Ac-Cys-His-Sar-(Ala)$_3$-Cys-NH$_2$, etc., were studied. The populations of the cis and trans isomers and the kinetics of cis/trans interconversion were found to depend on the amino acid preceding sarcosine.

The kinetics and equilibria of cis/trans isomerization across the Xaa-Xaa secondary amide bonds in a series of peptides of the sequence Ac-Cys-Xaa-Xaa-Cys-His-NH$_2$, where Xaa is Ala, Tyr and Phe, were also studied. These peptides were studied as model peptides for oxido-reductase enzymes with the Cys-Xaa-Xaa-Cys motif. The effects of the type and position of the central Xaa residues on the kinetics and equilibria of cis/trans isomerization were examined. Rate and equilibrium constants for cis/trans isomerization together with thermodynamic parameters were determined for all the peptides and peptide/peptoid hybrids studied in both their dithiol and disulfide forms. Rate constants for interconversion between the cis and trans configurational isomers were determined by inversion-magnetization transfer NMR methods and equilibrium constants for the cis/trans isomerization were determined from resonance intensities.

Table of Contents

Table of Contents

Table of Contents

Table of Contents

Table of Contents

Table of Contents

Part II

Cis/tran Isomerization of Amide Bonds in Peptides and Peptide/Peptoid Hybrids

Table of Contents

Table of Contents

Table of Contents

List of Figures

List of Figures

List of Figures

List of Figures

List of Figures

Chapter 4

List of Figures

List of Figures

List of Figures

List of Figures

Chapter 5

Part II

Chapter 1

Chapter 2

List of Figures

List of Figures

Chapter 4

List of Figures

List of Tables

Chapter 5

List of Tables

Part II

Chapter 3

List of Tables

Chapter 4

Part I

Isolation and Characterization of Heparin and its Binding with Biological Molecules

Chapter 1

Introduction

1.1 Structure, Biosynthesis, and Therapeutic Applications of Heparin

1.1.1 Heparin Sources

Heparin, together with heparan sulfate, chondroitin sulfate, dermatan sulfate, keratan sulfate and hyaluronic acid, is a glycoaminoglycan (GAG), a class of polysaccharides. Heparin is primarily present in the dense, membrane-enclosed granules of mast cells.[1] The granules are composed mainly of heparin and basic protein, which accounts for about 50% of the total mast cell volume.[2] In the granules of mouse mast cells, for example, heparin forms an insoluble complex with the basic protein mast cell protease-7, a tryptase. Heparin is present in many tissues, including the intestine and the lung. Heparin was originally isolated from canine liver cells. Today, the most common source of heparin is porcine intestines. Heparin is used in medicine to prevent blood coagulation; most of the heparin used as an anticoagulant is prepared from porcine intestinal mucosa.[3]

1.1.2 Heparin Structure

Heparin is a complex, sulfated polysaccharide. Heparin binds to a number of biologically important proteins, including growth factors, which leads to its potentially exploitable use in therapy, for example for inhibition of tumor growth[4] and viral invasion[5]. Despite its binding interactions with a wide range of proteins, the specificity requirements for binding of heparin by proteins are not well understood due to the extremely complex structure of heparin. The complexity of heparin's structure results

2

from its heterogeneity, polydispersity, monosaccharide composition, and iduronic acid ring conformation.

1.1.2.1 The Composition of Heparin

Heparin is a linear polysaccharide, which is formed through the linkage of uronic acid-(1→4)-α-D-glucosamine repeating disaccharide subunits by glycosidic bonds (Figure 1.1). The uronic acid residue can be either α-L-iduronic acid (IdoA) or β-D-glucuronic acid (GlcA). L-iduronic acid and D-glucuronic acid may contain a 2-O-sulfo group (IdoA(2S) and GlcA(2S) (Figure 1.2). α-D-glucosamine residues can either be N-sulfo-α-D-glucosamine (GlcNS) or N-acetyl-α-D-glucosamine (GlcNAc). The 3- and 6-positions of the N-sulfo-α-D-glucosamine can either or both be substituted with an O-sulfo group (GlcNS(3S), GlcNS(6S) and GlcNS(3S, 6S)) or unsubstituted. The 6-position of N-acetyl-α-D-glucosamine may be substituted with an O-sulfo group (GlcNAc(6S)) or unsubstituted. As seen from Figure 1.3, twenty-four uronic acid-(1→4)-α-D-glucosamine disaccharide units are possible, which gives rise to a large number of complex heparin polysaccharide sequences. Among the twenty-four disaccharides, IdoA(2S)-(1→4)-GlcNS(6S) is the most abundant in heparin (Figure 1.1). In fact, heparin from bovine lung consists of up to 90% of this disaccharide while up to 70% of heparin from porcine intestinal mucosa is this repeating disaccharide unit.[6]

1.1.2.2 Ring Conformation of Heparin Monosaccharides

The pyranose rings of the monosaccharide residues within heparin adopt the $^4C_1$, and $^1C_4$ chair conformations, as well as the ^2S_o skew boat conformation (Figure 1.4).
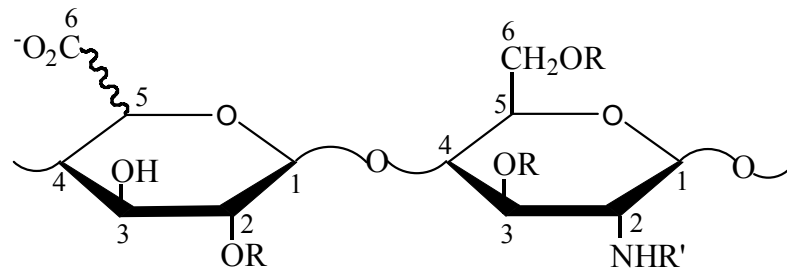
R = H or SO$_3^-$
R' = SO$_3^-$ or COCH$_3$
Minor disaccharide sequences
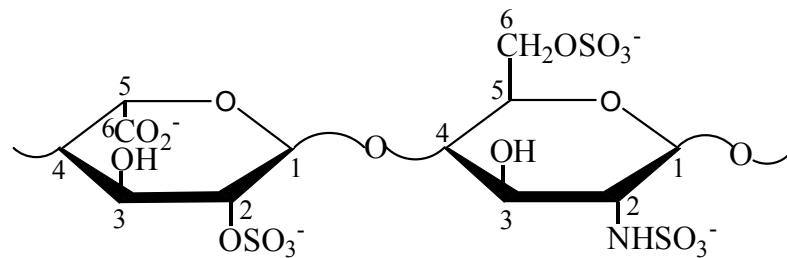
Major repeating disaccharide sequence

Figure 1.1. The major and minor disaccharide sequences of heparin.

Uronic Acid → α-L-Iduronic Acid → IdoA / IdoA(2S)

Uronic Acid → β-D-Glucuronic Acid → GlcA / GlcA(2S)

α-D-Glucosamine → N-Sulfo-α-D-Glucosamine → GlcNS / GlcNS(3S) / GlcNS(6S) / GlcNS(3S, 6S)

α-D-Glucosamine → N-Acetyl-α-D-Glucosamine → GlcNAc / GlcNAc(6S)

IdoA
IdoA(2S)
GlcA
GlcA(2S)
GlcNS

GlcNS(3S)
GlcNS(6S)
GlcNS(3S, 6S)
GlcNAc
GlcNAc(6S)

CO_2^-, OH, OSO_3^-, CH_2OH, $CH_2OSO_3^-$, $NHSO_3^-$, $NHCOCH_3$
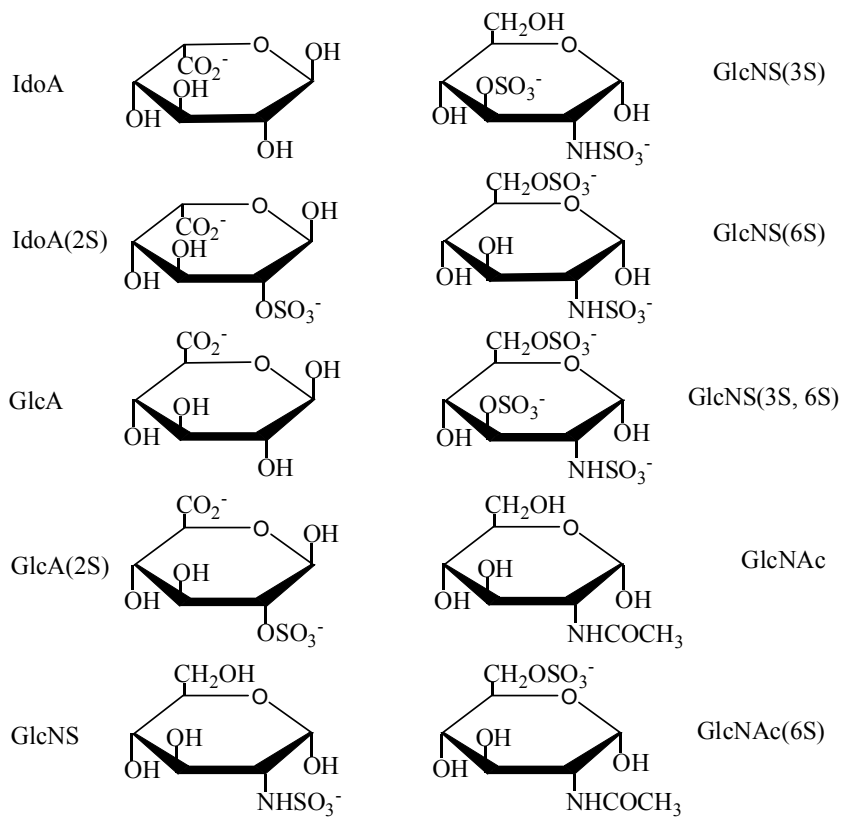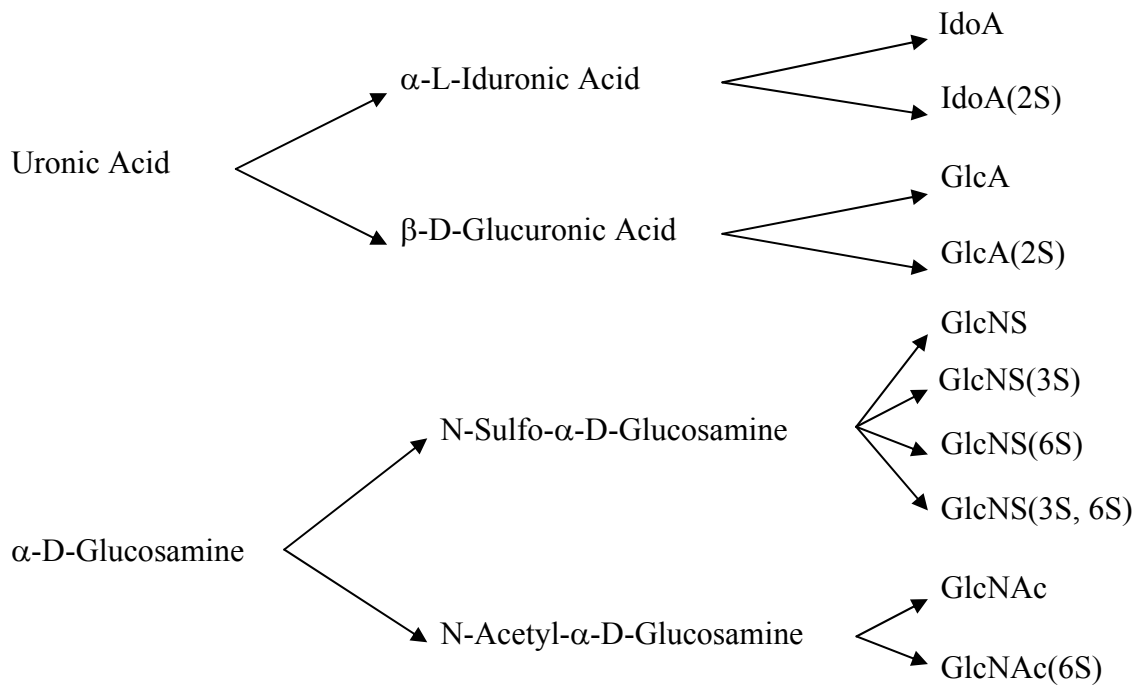
Figure 1.2. Monosaccharide building blocks of heparin and heparan sulfate.
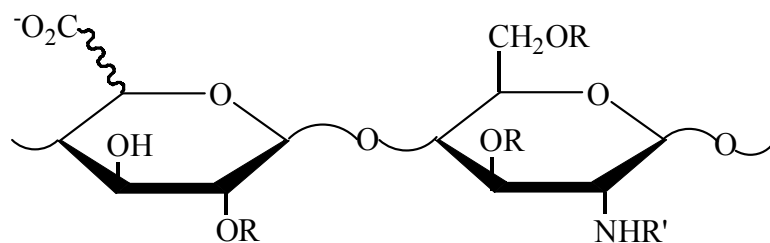
R= SO$_3^-$ or H

R' = SO$_3^-$ or COCH$_3$

IdoA-GlcNS	GlcA-GlcNS
IdoA-GlcNS(3S)	GlcA-GlcNS(3S)
IdoA-GlcNS(6S)	GlcA-GlcNS(6S)
IdoA-GlcNS(3S, 6S)	GlcA-GlcNS(3S, 6S)
IdoA-GlcNAc	GlcA-GlcNAc
IdoA-GlcNAc(6S)	GlcA-GlcNAc(6S)
IdoA(2S)-GlcNS	GlcA(2S)-GlcNS
IdoA(2S)-GlcNS(3S)	GlcA(2S)-GlcNS(3S)
IdoA(2S)-GlcNS(6S)	GlcA(2S)-GlcNS(6S)
IdoA(2S)-GlcNS(3S, 6S)	GlcA(2S)-GlcNS(3S, 6S)
IdoA(2S)-GlcNAc	GlcA(2S)-GlcNAc
IdoA(2S)-GlcNAc(6S)	GlcA(2S)-GlcNAc(6S)

Figure 1.3. The twenty-four uronic acid-(1→4)-D-glucosamine disaccharides that can be formed from the monosaccharides in Figure 1.2.

$^4C_1$ (GlcNS(6S)) $^4C_1$ (GlcA)

$^4C_1$ $^1C_4$ ^2S_O
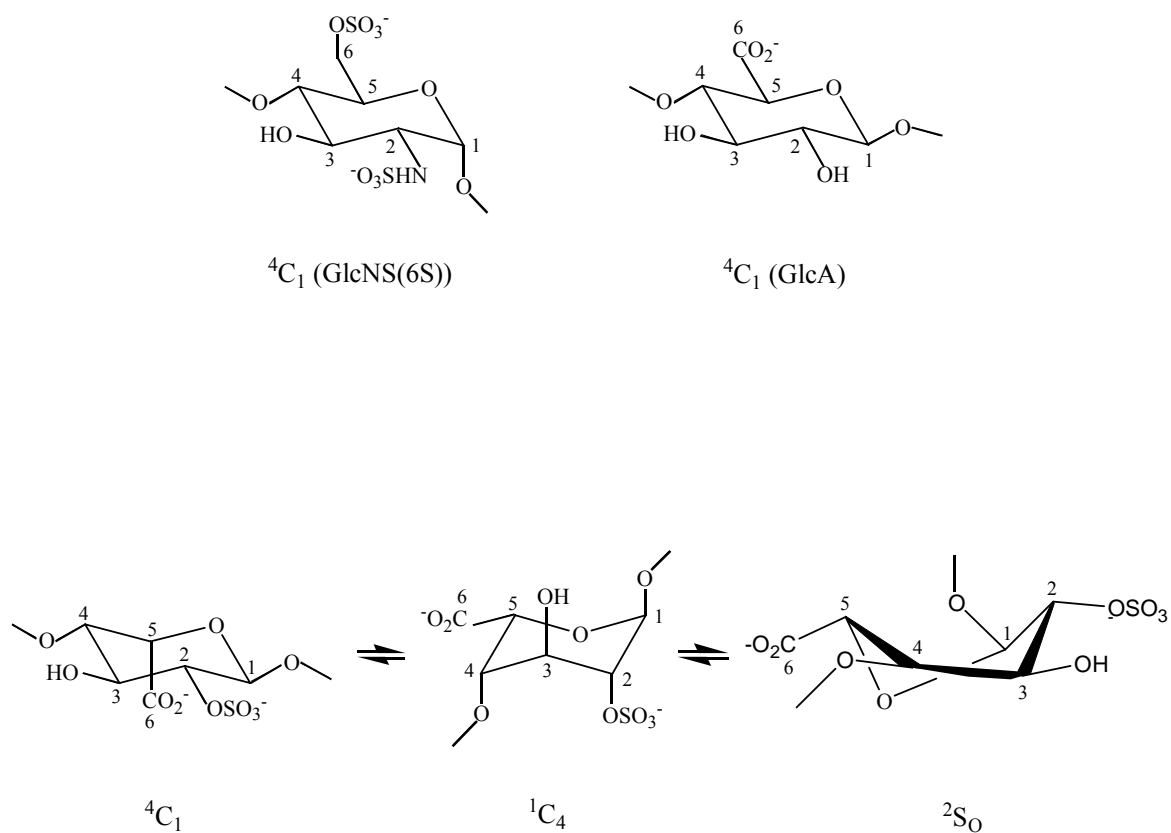
Figure 1.4. The top shows the conformations of the pyranose rings of the GlcNS and GlcA residues of heparin and heparan sulfate. The bottom shows the three possible conformers of the iduronic acid residue (IdoA(2S)).

NMR studies and X-ray structures show that glucosamine and glucuronic acid residues prefer the $^4C_1$ chair conformation.[1] The pyranose ring of iduronic acid is more flexible. In solution, evidence suggests that when it is at the reducing end of an oligosaccharide, it can be present as all three possible conformers (Figure 1.4).[7] When the iduronic residue is internal, only the $^1C_4$ chair and the ^2S_o skew boat are accessible.[8] The position of the $^1C_4$ $\leftrightarrow$ ^2S_o equilibrium of iduronic acid residues is sensitive to the binding of proteins and other biological molecules. In short, the flexibility of the L-iduronic acid residue most probably explains in part the remarkable ability of heparin and heparan sulfate (HS) to bind to a wide range of proteins by facilitating the interaction of their anionic sulfo and carboxyl groups with cationic sites on proteins, such as the guanidinium group of arginine and the ammonium group of lysine.

The unsaturated uronic acid residue of the non-reducing end in oligosaccharides formed upon cleavage of heparin by heparinase enzymes can exist in either the $^2H_1$ or $^1H_2$ conformations, and the equilibrium between these two conformers is controlled by their substitution pattern (Figure 1.5).[9, 10] Crystallography data show that the $^2H_1$ and $^1H_2$ forms can coexist within the same unit cell, suggesting that they are equal in energy.[11] However, the solution structures of heparin-derived oligosaccharides determined by NMR spectroscopy indicate that the non-reducing terminus unsaturated uronic acid unit exists predominantly in the $^1H_2$ form with minor contribution from the $^2H_1$ form.[12, 13]

1.1.3 Biosynthesis of Heparin

Heparin is biosynthesized inside mast cells as a proteoglycan, which has a MW ranging from 750,000 to 1,000,000 Daltons. The proteoglycan consists of a core protein

$^2H_1$ $^1H_2$
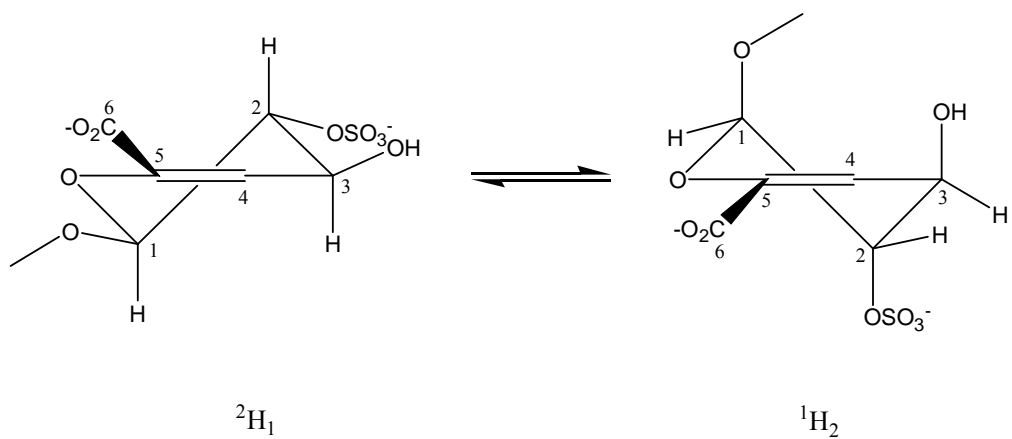
Figure 1.5. The two possible conformers of the unsaturated uronic acid residue (ΔUA(2S)).

(serglycin) and heparin oligosaccharide chains. Biosynthesis of the heparin begins with chain initiation followed by polymerization and then polymer modification.[14]

Chain initiation begins with attachment of the tetrasaccharide primer β-GlcA-(1→3)-β-Gal (1→3)-β-Gal (1→4)-β-Xyl to specific serine residues of the serglycin by glycosyltransferases.[15] Serglycin contains a large number of serine and glycine repeats. Due to the high content of serine residues, multiple heparin polysaccharide chains are covalently attached to the core protein.

After chain initiation, chain polymerization takes place via the alternating addition of N-Acetyl-D-glucosamine (GlcNAc) and D-glucuronic acid (GlcA) monosaccharide units to the linker tetrasaccharide by transferase enzymes. As the polysaccharide chain elongates, it also undergoes a series of modification reactions (Figure 1.6).

Modification of the polymer is initiated by removal of acetyl groups by N-deacetylase and addition of N-sulfate groups by N-sulfotransferase (Figure 1.6). C5 epimerase then catalyzes transformation of some of the GlcA residues to L-iduronic acid (IdoA) residues.[16-19] Due to the substrate specificity of C5 epimerase, only GlcA residues attached to the reducing end of a GlcNS unit are converted to IdoA saccharides.[17, 20] Finally, the polysaccharide is O-sulfated at varying locations by O-sulfotransferase.[20, 21] 2-O-sulfation of iduronic acid and glucuronic acid residues take place by an iduronosyl 2-O-sulfotransferase and a glucuronosyl 2-O-sulfotransferase, respectively. 2-O-sulfation of the uronic acid is followed by 6-O-sulfation of the glucosamine ring by glucosamine 6-O-sulfotransferase. Eventually, the 3-O-sulfation reaction, a modification required for
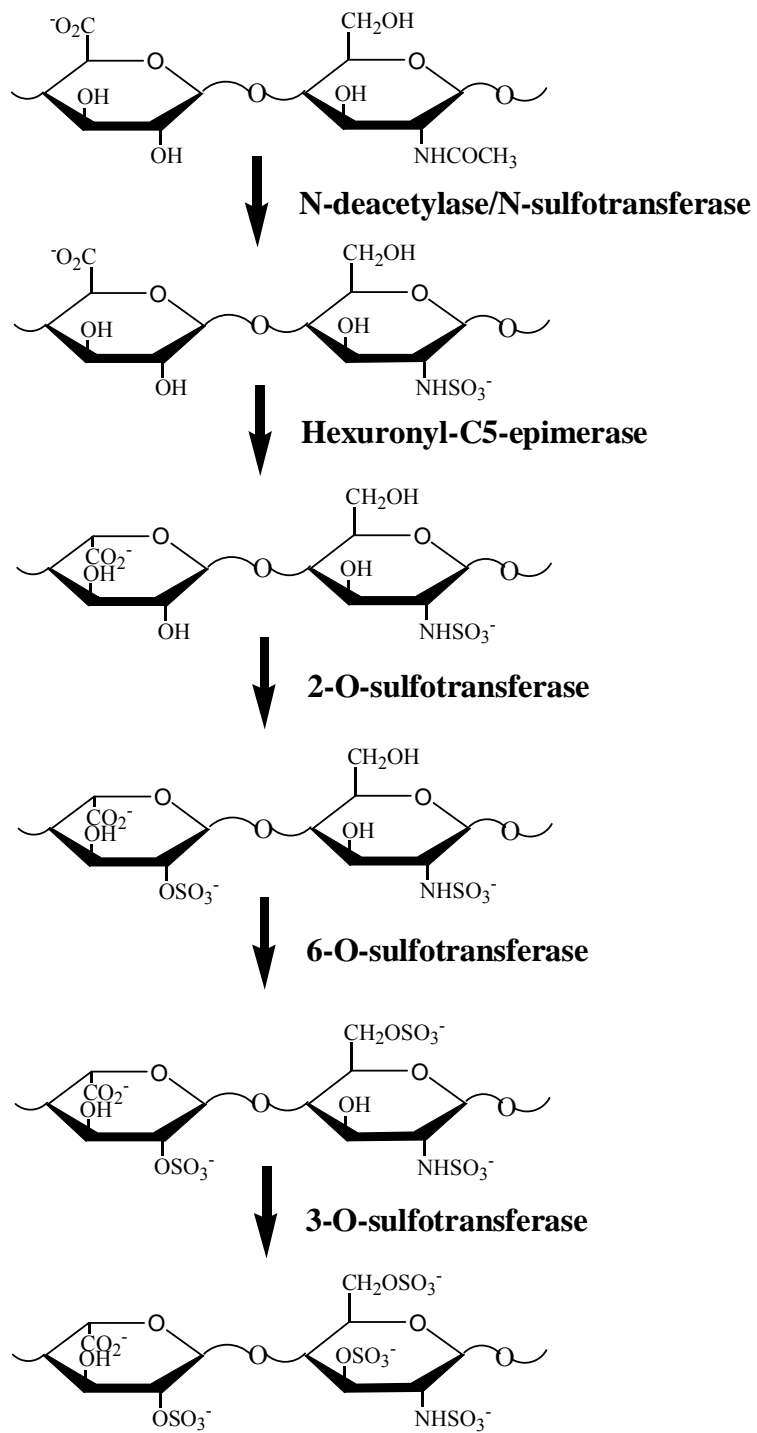
Figure 1.6. Scheme of step-by-step modifications that occur during the biosynthesis of heparin and heparan sulfate.

anticoagulation activity of heparin, occurs last.[22] Not all substrate residues are modified by the sequence of reactions in Figure 1.6, resulting in microheterogeneity along the heparin polymer.

After approximately 300 sugar residues are added to each linker tetrasaccharide, the core protein is broken down by tissue proteases to heparin peptidoglycans. Each heparin peptidoglycan is a small peptide containing only a single long polysaccharide chain with a MW of about 100 kDa, which is equivalent to the total mass of ~ 300 sugar residues. The peptidoglycan has a short life as it's immediately degraded by β-endoglucuronidase producing a number of smaller polysaccharide chains called glycosaminoglycan (GAG) heparin, having an average MW of about 15 kDa.[23] Due to an incomplete modification of the heparin polymer by the biosynthetic enzymes, the structural complexity and heterogeneity of a heparin chain increases throughout the modification process.

1.1.4 Therapeutic Applications of Heparin

Heparin is a natural blood anticoagulant. It is used to treat and prevent blood clot formation in patients prior to surgery if the risk of a blood clot is high. About 500 million doses of heparin are produced annually for clinical use, worlwide.[24]

The anticoagulant activity of natural and synthetic heparins is mediated primarily via the activation of antithrombin III (AT III), a plasma serpin that circulates at 2.3 μM and has the ability to inhibit all of the serine proteases that promote blood coagulation. AT III, the most important serpin in hemostasis,[25] together with heparin cofactor II, plasminogen activator inhibitor-1, protease nexin 1, and protein C inhibitor, are the five

serpins known to bind heparin among thirty-five serpins that have been identified in the human genome.[26]

The anticoagulation effect of heparin resides in a unique pentasaccharide sequence (Figure 1.7). The mechanism by which heparin inhibits blood coagulation has been well studied.[27] Briefly, the binding of the pentasaccharide sequence to AT III results in an increase in the activity of AT III of about 1000 fold due to a change in its conformation upon binding, which activates it to bind to either of the enzymes factor Xa or thrombin. Upon formation of the AT III-heparin-thrombin ternary complex, formation of fibrin, the protein that polymerizes into the mesh that underlies a blood clot, is shut off. Inhibition of thrombin requires heparin having a length of 14-20 monosaccharide units, about three times the length of the minimal AT-specific pentasaccharide.[28] The AT III-pentasaccharide complex binds factor Xa via a serine residue on factor Xa and inhibits it from converting prothrombin to thrombin, a key step in the coagulation mechanism.

The binding constant for the interaction of heparin with AT III was determined to be 10-20 nM at physiologic ionic strength and pH.[29] Heparin-AT III binding is mediated by both electrostatic and site specific interactions. The 3-O-sulfo group on the central glucosamine residue, a rare modification required for the anticoagulant activity of heparin, makes the pentasaccharide sequence in Figure 1.7 a unique one. Only approximately one-third of heparin polysaccharide chains in mast cells and about 1% of heparan sulfate on the cell surfaces contain this unique pentasaccharide sequence.[6] Binding studies of AT III with synthetic pentasaccharides without the 3-O-sulfate group
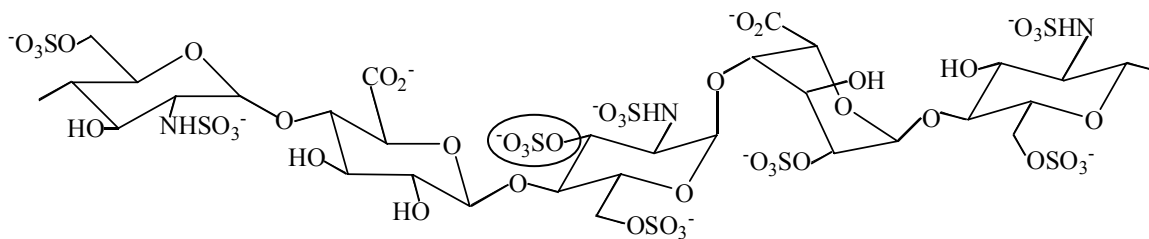
Figure 1.7. Structure of the antithrombin III binding pentasaccharide sequence of heparin. The 3-O-sulfate group on the internal glucosamine ring (in circle) is essential for high affinity binding of heparin to AT III.

gave dissociation constants of ~ 2 mM, which suggests that the 3-O-sulfate group is essential for high affinity binding of heparin to AT III.[30]

In addition to its anticoagulant activity, heparin has been shown to inhibit the growth and replication of human immunodeficiency virus (HIV) by binding to an extended loop of glycoprotein gp 120 on the surface of the virus. HIV infects $CD4^+$ T lymphocytes by binding to heparan sulfate proteoglycans on the surface of T lymphocytes through the same loop of gp 120.[31, 32]

It has also been reported that heparin may modulate cell growth processes. For instance, heparin is believed to inhibit cell proliferation in a process involving internalization of the glycosaminoglycan moiety and its migration to the cell nucleus. Heparin was found to bind tightly to many fibroblast growth factors (e.g. FGF-1[33], FGF-2[34], and FGF-7[35]), which are members of a large family of proteins that are involved in developmental and physiological processes including cell proliferation, differentiation, morphogenesis, and angiogenesis. Formation of the FGF-heparin complex protects the growth factor from being degradated by enzymes and thus enhances its activity. There is evidence that binding of FGFs by proteoglycans and glycosaminoglycans in the extracellular matrix creates a reservoir of growth factors for cells to use.

1.1.5 Heparin versus Heparan Sulfate

Unlike heparin which only occurs in mast cells, heparan sulfate (HS) is found on cell surfaces and in the extracellular matrix. HS is bound to different core proteins and thus exists as HS proteoglycans. Free unbound HS chains are rare.

HS is structurally related to heparin. It is constructed from the same monosaccharide building blocks (Figure 1.2). Nevertheless, the primary structure of HS is significantly different than that of heparin. HS consists of repeating disaccharide units composed of predominantly GlcA and GlcNAc. It is less substituted with sulfo groups than heparin. The primary structure of HS was found to depend on the type of tissue, and it can be different for different cells from the same tissue.[36, 37] HS chains normally contain on average approximately one sulfo group per disaccharide. They are also polydisperse but are longer than heparin chains, ranging in molecular weight from 5 to 50 kDa, with an average molecular weight of about 30 kDa.[38]

HS is also biosynthesized as a proteoglycan through the same pathway as heparin. HS chains on HS proteoglycans have been shown to bind to different proteins, which mediate various important biological processes including cell adhesion[39], inhibition of blood coagulation[40] and regulation of cellular growth and proliferation.[41, 42] Although HS is involved in many physiologically important functions, only a few studies of HS-protein binding have been reported due to the very small amount of HS available. Much of what has been learned about HS-protein binding is from heparin-protein binding studies; heparin is used as a model for the interaction of highly sulfated regions of HS chains with proteins since heparin and heparin-derived oligosaccharide are more abundant.[43]

1.2 Binding of Peptides and Proteins by Heparin

1.2.1 Amino Acids Involved in Binding

Peptides and proteins with consensus sequences XBBXBX, XBBBXXBX, and XBBBXXBBBXXBBX, where X represents a hydropathic (either a neutral or a

16

hydrophobic amino acid residue) and B represents a basic residue (either arginine or lysine), were found to bind to heparin.[44, 45] The binding of peptides and proteins by heparin is mediated primarily by non-specific electrostatic interaction between the basic side chains of arginine and lysine residues and the sulfo and carboxyl groups of heparin. Peptides enriched in arginine and lysine were found to bind to heparin with greatest affinity. Fromm and coworkers have reported that arginine-containing peptides bind to heparin 2.5 times stronger than lysine-containing peptides.[46]

1.2.2 Site Specific Binding of the Histidine Side Chain by Heparin

1.2.2.1 Binding of Histamine and Imidazole by Heparin

In a previous study, this research laboratory determined that histamine binds to heparin and that the binding is site-specific.[47] The binding interaction of histamine with heparin in aqueous solution was characterized by ^{1}H and ^{13}C NMR spectroscopy. In the NMR studies, binding at specific sites in heparin was monitored by measuring the chemical shift of each proton of heparin as a function of pD over the pD range 2-12, both free in solution and in solution with histamine.

Site-specific binding of histamine was indicated by an upfield shift of the resonance for the proton on C3 of GlcNS(6S) residues of heparin (Figure 1.1), the A-H3 proton of heparin, when heparin is in solution with histamine. In the absence of histamine, the chemical shift of the A-H3 resonance is independent of pD. In the presence of histamine, the proton shifts upfield over the pD region of 2-6 where the carboxylic acid groups of heparin are titrated. The upfield shift reaches its maximum at pD ~ 6. As the pD is further increased, the chemical shift of the A-H3 proton moves back toward its

17

value in the absence of histamine, indicating dissociation of the heparin-histamine complex. It was proposed that when the carboxylic acid groups of the IdoA(2S) residues of heparin are titrated, a binding site with a high affinity for the positively charged imidazolium group of histamine is created. The upfield shift indicates the H3 proton of the A ring is located right above the imidazolium ring, an aromatic ring, which causes its resonance to shift upfield due to an increase in shielding from ring current effects.[48] The truth of this hypothesis will be discussed in the next section based on further studies also performed in this laboratory.

To elucidate the nature of the binding of histamine by heparin, the binding interaction of imidazole with heparin was also studied. The upfield shift of the A-H3 resonance is analogous to the behavior observed for the A-H3 proton of heparin in solution with histamine, which suggests that the imidazolium ion is complexed by heparin.

1.2.2.2 Binding of Histamine by Chemically Modified Heparin and Heparin Derived Oligosaccharides

To characterize the details of the binding of histamine by heparin, the binding of histamine by six heparin-derived oligosaccharides and four chemically modified heparins (Figure 1.8) was studied.[49] Binding at specific sites in the heparin-derived oligosaccharides was monitored by measuring the chemical shift of each proton of the oligosaccharide as a function of pD over the pD range 2-12, both free in solution and in solution with histamine. In the presence of histamine, H5 of the I residue and H3 of the A residue are the two heparin resonances that shift the most.

| Ia | Ab | Ic | Ad | Ie | Af |
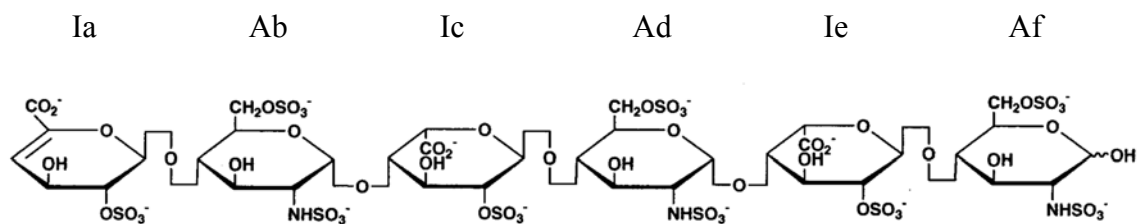
Upon binding of histamine, the Ab-H3 and Ad-H3 resonances of fully sulfated hexasaccharide III in Figure 1.8 both shift upfield, while the Af-H3 resonance is not affected by the presence of histamine, indicating site-specific binding at the Ab and Ad residues, but not the Af residue. It was determined from a molecular modeling study in which an IAI trisaccharide was constructed and histamine was then docked into the binding cleft formed by the IAI triad with the help of a systematic search algorithm to obtain the lowest energy complex, the proximity (2.8 Å) of the A-H3 proton to the imidazolium ring of histamine roughly centers the histamine between two I residues (Figure 1.9). This together with the absence of site-specific binding of histamine at residue Af of hexasaccharide III indicates that the IAI triad is the minimum heparin sequence for site-specific binding of histamine.

Results for the binding of histamine by fully sulfated di- and tetrasaccharides (I and II in Figure1.8) confirmed that site-specific binding of histamine requires two I rings, one linked to the nonreducing end and the other linked to the reducing end of residue A of the IAI triad.

From studies of the binding of histamine by the other heparin-derived oligosaccharides in Figure 1.8, it was found that binding depends on the configuration of uronic acid at the reducing end of the IAI minimum binding sequence, the 2-O-sulfate
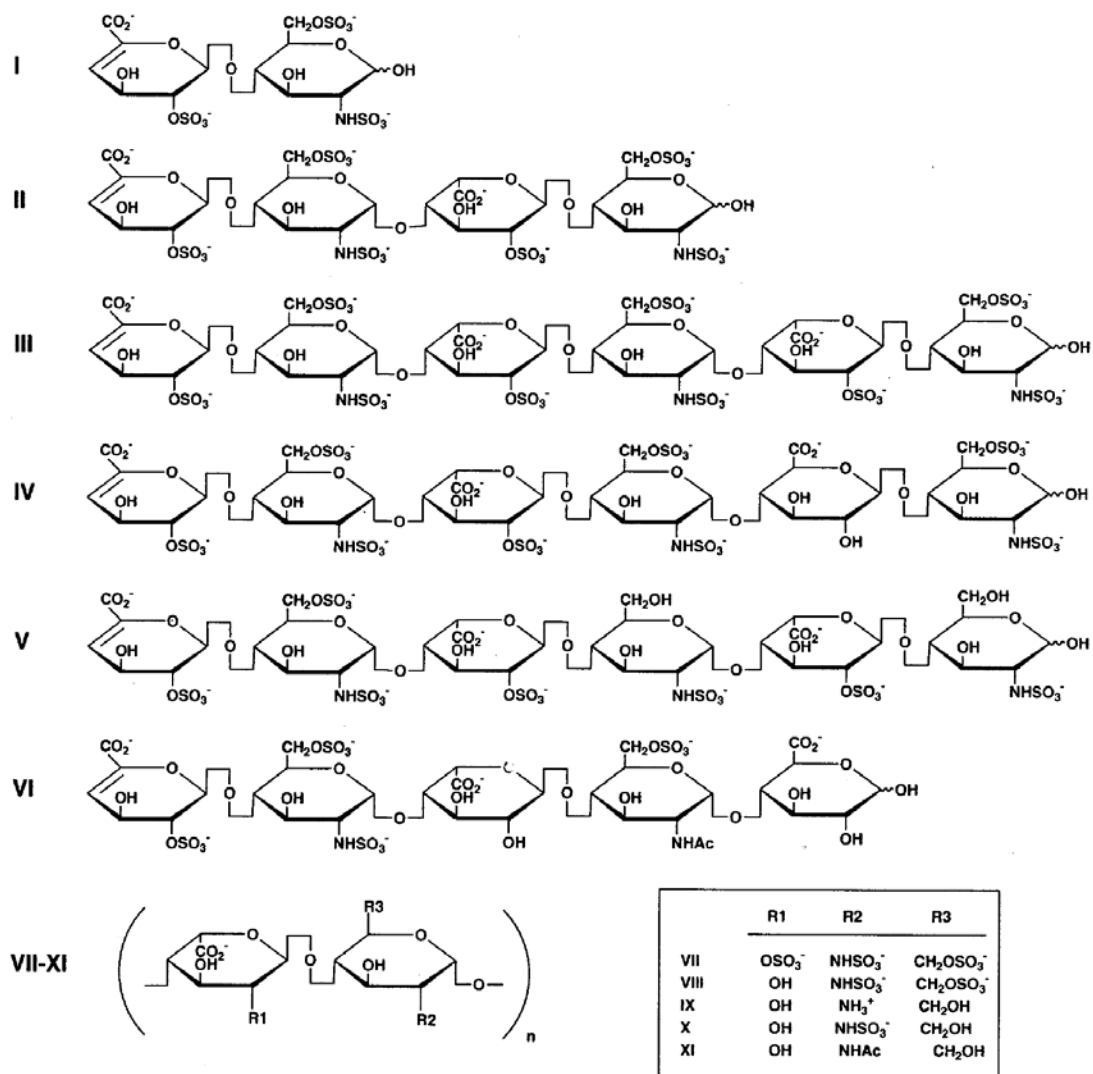
Figure 1.8. Heparin-derived oligosaccharides and chemically modified polysaccharides.
[Ref. 49]

groups of the I rings of the IAI triad are not essential for site-specific binding of histamine, the I residue at the reducing end of the A ring of the IAI minimum binding sequence has to be an iduronic acid residue, but not glucuronic acid, and that the 6-O-sulfate substituent on the A ring of the trisaccharide sequence is not essential for site-specific binding of histamine, whereas the N-sulfate substituent is necessary for site-specific binding of histamine. The molecular modeling study found that the imidazolium ring of histamine fits in a binding pocket formed by the IAI triad of heparin, to form a complex in which the two imidazolium NH protons of histamine are hydrogen bonded to the carboxylate groups of the two I rings, while the ammonium group of histamine interacts with the N-sulfate group of the A ring of heparin (Figure 1.9).

1.2.2.3 Binding of Imidazole by a Heparin-Derived Hexasaccharide

The binding of imidazole by fully sulfated hexasaccharide III in Figure 1.8 was studied to determine if the ammonium group of histamine is essential for site-specific binding.[49] In the presence of imidazole, the resonances for Ab-H3 and Ad-H3 of III are shifted upfield, indicating that the imidazolium ion by itself binds site-specifically to sites Ab and Ad of the hexasaccharide. However, the magnitudes of the shifts for both Ab-H3 and Ad-H3 are smaller than observed for histamine binding, indicating that the imidazolium group of histamine is critical in directing site-specific binding of histamine while the ammonium group increases the amount of binding of histamine by heparin.

1.2.2.4 Binding of the Growth Factor GHK by Heparin

As discussed above, the imidazolium ring binds site specifically to heparin. The imidazolium ring is present in peptides and proteins as the side chain of histidine residue.
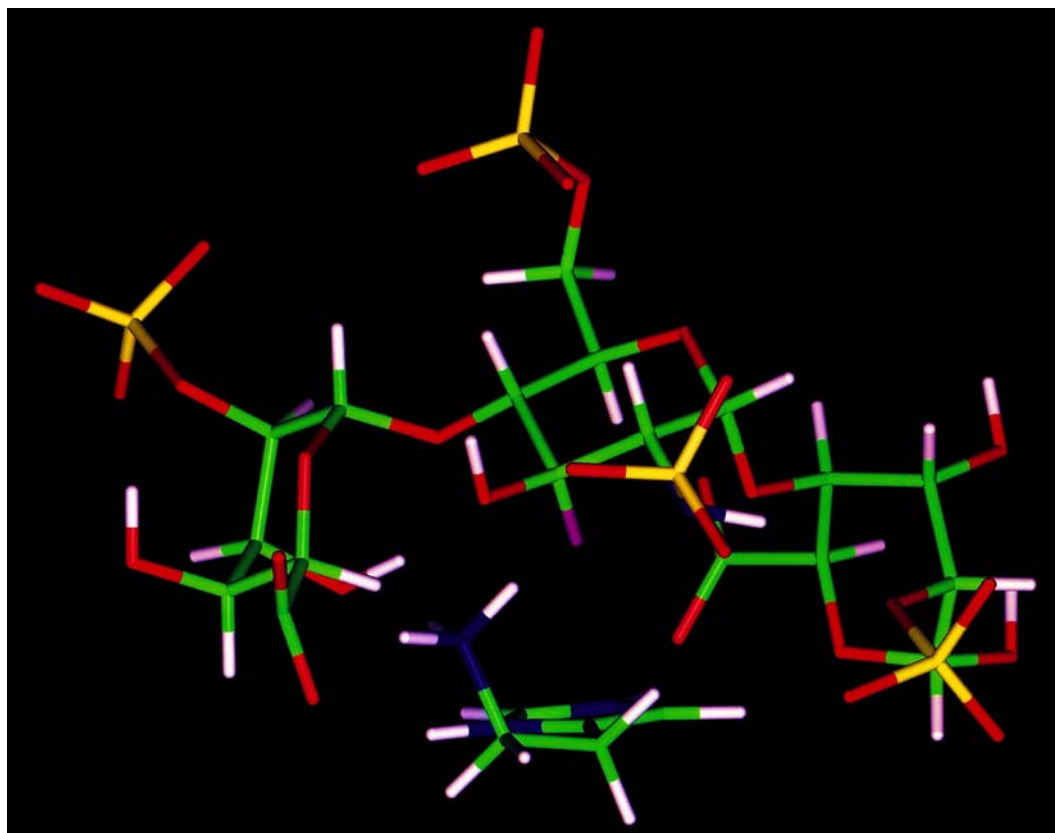
Figure 1.9. A stick model of the heparin-histamine complex. The complex is oriented with the reducing end of the IAI trisaccharide on the right (I'AI'') and the ammonium tail of histamine facing out of the plane of the paper. [Ref. 49]

Nevertheless, there is only one reported study of the interaction of a histidine-containing peptide with heparin. The growth factor glycyl-histidyl-lysine (GHK) has been reported to bind to heparin site-specifically.[50] The binding interaction was characterized by ^{1}H NMR spectroscopy. Evidence for formation of GHK-heparin complex and site-specific binding of the histidyl imidazolium group to the imidazolium binding site on heparin were provided by the behavior of the chemical shift-pD titration curves for specific resonances of the tripeptide and heparin.

GHK has three potential sites for its interaction with heparin: the N-terminal glycyl ammonium group, the lysine ammonium group, and the histidyl imidazolium group. An upfield displacement of the A3 resonance of heparin provided evidence for site-specific binding of the imidazolium group of GHK by heparin. Chemical shift data suggest that the ammonium groups of the glycyl and lysine residues are hydrogen bonded to the carboxylate groups of heparin, while the histidyl imidazolium group lies in the binding pocket formed by the IAI trisaccharide. It was suggested that histidine side chains of β-amyloid peptides, platelet factor 4, and mouse mast cell protease-7 bind site specifically to imidazolium binding sites on heparin in the same way as the imidazolium side chain of GHK.

1.3 Heparin-Derived Oligosaccharides

Direct determination of the structure of heparin is not possible due to its polydispersity and its microheterogeneity as a result of incomplete modification of some residues by the reactions in Figure 1.6. Glycosaminoglycan heparin has a molecular weight ranging from 5 to 40 kDa with an average molecular weight of 15 kDa.[38] To

23

overcome the polydispersity and microheterogeneity issues, researchers have depolymerized heparin into smaller oligosaccharides using either chemical or enzymatic methods and then purified the fragments to obtain homogeneous heparin-derived oligosaccharides in terms of size and charge in order to establish its structure.[51]

1.3.1 Low Molecular Weight Heparin (LMWH)

As a result of its molecular heterogeneity in terms of size and microheterogeneity in terms of sulfation patterns, heparin possesses multiple functional domains, which can elicit many biological activities. As a result, the use of intact heparin often causes a great risk of thrombosis after major surgery.[52] Thus, attempts have been made to produce better defined heparin preparations. Better defined heparin in terms of more or less uniform mass has been achieved in part by the generation of so called low molecular weight heparin (LMWH; MW 5000-8000 Da) by either gel filtration[53] or by partial enzymatic[54] or chemical[55] depolymerization of heparin. A LMWH standard prepared by partial nitrous acid depolymerization has been introduced by the National Institute of Biological Standards and Control (NIBSC, London, England).[56]

Studies have shown that LMWH induces less hypocoagulation, prolongs inhibition of factor Xa activity, and is less haemorrhagic than unfractionated heparin.[57, 58] With subcutaneous injection, LMWH offers a four to nine fold higher bioavailability compared to heparin.[59] Moreover, it has been reported that the use of LMWH reduces adverse side-effects such as lipolysis and thrombocytopenia associated with the administration of heparin.[58]

1.3.2 Separation Methods for Heparin-Derived Oligosaccharides

Although LMWH was recently introduced as a heparin substitute due to its efficacy as an antithrombotic agent and its decreased toxic side effects compared to the parent drug unfractionated heparin[59], it still shows a considerable structural heterogeneity, thereby impeding predictions about its bioactivity and pharmacokinetics. Furthermore, chemical depolymerization of heparin to form LMWH often results in a loss of the unique pentasaccharide sequence and hence proportional loss of anticoagulant activity. Thus, the preparation of structurally defined pure heparin-derived oligosaccharides is crucial in understanding heparin's interaction with proteins and in determining the precise structural requirements within heparin essential for the binding.

Structurally defined heparin-derived oligosaccharides can be obtained from the mixtures of heparin-derived oligosaccharides produced by depolymerization of heparin. The mixtures are first fractionated by low pressure gel permeation chromatography into size-uniform mixtures of disaccharides, tetrasaccharides, hexasaccharides and higher oligosaccharides. Each size-fractionated mixture is then separated either by strong anion exchange or reversed-phase ion-pairing high performance liquid chromatography. The purity of oligosaccharides can be confirmed by capillary electrophoresis and one-dimensional ^{1}H nuclear magnetic resonance spectroscopy. The structure of the oligosaccharide is established using two-dimensional nuclear magnetic resonance spectroscopy.

1.3.2.1 Low Pressure Gel Permeation Chromatography

Heparin-derived oligosaccharide mixtures produced by depolymerization of

heparin can be fractionated according to their size by low pressure gel permeation chromatography (GPC).

Yang *et al*. have resolved heparin fragments from di- through dodecasaccharide on a 4.8 x 100 cm column packed with Bio-Gel P6 (superfine) from Bio-Rad.[60] Oligosaccharides of different degrees of polymerization (DP 2-DP 12) were eluted with 0.1 M NaCl at a flow rate of 1.5 mL/min. Pervin and coworkers demonstrated size fractionation of heparin fragments ranging from disaccharides to tetradecasaccharides using sephadex G-50 (superfine) on 4.8 x 100 cm column.[61] Size-uniform oligosaccharides were eluted with 0.2 M sodium chloride at a flow rate of 2 mL/min.

1.3.2.2 Strong Anion Exchange High Performance Liquid Chromatography (SAX HPLC)

SAX-HPLC has been the preferred technique for the separation of size-fractionated heparin-derived oligosaccharide mixtures.[60, 62-65] The separation by SAX-HPLC is based on the charge of the heparin-derived oligosaccharides. The most highly charged components elute last due to their strong interactions with the column stationary phase. While SAX-HPLC provides high resolution and availability for quantitation, it requires microgram amounts of sample, long separation time (>90 min), extensive desalting of purified oligosaccharide compounds, and it can not be coupled to mass spectrometry due to the high sodium chloride concentration.

1.3.2.3 Reversed-Phase Ion-Pairing High Performance Liquid Chromatography (RPIP-HPLC)

RPIP-HPLC offers an alternative to SAX-HPLC in the separation of size-

fractionated heparin-derived oligosaccharide mixtures. The basis for RPIP separation of heparin-derived oligosaccharides is still controversial. Two different retention processes are possible.[66] In the first process, ion-pairs form between the positively charged ion-pairing reagent and negatively charged sulfo and carboxyl groups on the oligosaccharide; the ion-pairs are retained by interaction of the hydrophobic alkyl groups of the ion-pairing reagent with the hydrophobic stationary phase of the octadecyl (C_{18}) silica column. In the second process, ion-pairing cations are adsorbed onto the C_{18} column, which renders it into an anion exchange column.

A number of researchers have investigated the use of RPIP-HPLC for analysis of mixtures of heparin-derived oligosaccharides.[67-72] For instance, Thanawiroon *et al*. have designed the first method that can separate a complex mixture of more than 30 oligosaccharide components ranging from disaccharide (DP 2) to tetradecasaccharide (DP 14).[66] Several tetraalkyl ammonium salts were investigated as ion-pairing reagents including tetraethyl-, tetrabutyl-, and tetrahexylammonium salts. Ion-pairing reagents with large alkyl groups were found to retain small oligosaccharides for very long times, while reagents with small alkyl groups did not give satisfactory retention of large oligosaccharides. Tetrabutylammonium (TBA) salt was found to be capable of retaining oligosaccharides ranging from disaccharide to tetradecasaccharide. Optimum resolution was obtained at pH 7, where both sulfo and carboxyl groups in all oligosaccharides present in the mixture are expected to be completely ionized, allowing their maximum interaction with TBA cations. A mobile phase of 25% CH_3CN was determined to give excellent resolution for oligosaccharides from DP 2 to DP 14. In comparison to the

conventional SAX-HPLC separation, RPIP-HPLC shows better resolution in the separation of both small and large heparin oligosaccharides as well as shorter analysis time. However, removal of TBA is problematic. To facilitate the removal of ion-pairing reagent, TBA was replaced by a volatile ion-paring reagent, tributylamine (TrBA).

1.3.2.4 Capillary Electrophoresis (CE)

Due to the limited amount of heparin-derived oligosaccharides and their inherently high potential for mircoheterogeneity in terms of sulfation pattern, a number of efforts have been made to develop new methods for the analysis of heparin-derived oligosaccharides. CE has proven to be an attractive separation technique for heparin-derived oligosaccharides. Compared with other analytical methods, CE offers several advantages including extremely high separation efficiency, short analysis time, on-line CE-MS, and extremely small amounts (picograms) of sample are consumed.

For the separation of oligosaccharides, CE can be operated in both modes: normal polarity (positive mode) and reversed polarity (negative mode). In the normal polarity mode, the sample is applied at the anode and detected at the cathode $(+ \rightarrow -)$, and basic or neutral buffer (e.g. tris, borate) is required. In reversed polarity, the sample is injected at the cathode and migrates under electrophoresis toward the anode $(- \rightarrow +)$, and acidic buffer (e.g. phosphate) is required. In reversed polarity, the silanol (SiOH) groups on the inner surface of the capillary are uncharged because of the low pH. Under acidic condition, the electroosmotic flow (EOF) is relatively weak compared to the electrophoretic mobility of negatively charged species and therefore the mobility of the ions is the major force in the separation under electrophoresis.

Analysis and separation of acidic disaccharide components of glycoaminoglycans was first reported by Al-Halkim *et al*. using capillary zone electrophoresis (CZE).[73] Separation in CZE is based on differences in mass-to-charge ratios of sample components. It is a fast and simple method, which employs a single buffer system in free solution. For example, an eight-component disaccharide mixture was resolved within 40 minutes on a 70 cm fused silica capillary using a single buffer system under a constant voltage. The elution profile was monitored by absorbance at 232 nm. Ampofo and coworkers have also investigated the use of CZE using positive mode for the analysis of eight disaccharide standards in a pH 8.80 borate buffer.[74] All eight disaccharides were resolved after adjusting the length of the capillary together with the use of sodium dodecyl sulfate. In CZE, the most highly charged components elute first as a result of their smaller mass-to-charge ratios.

Recently, CZE has also been used increasingly to detect impurities in peptide samples as well as to check the purity of heparin-derived oligosaccharides. Sample purity is confirmed by the presence of a single symmetrical peak.

1.4 Research Described in Part I of this Thesis

Characterizing the interaction of heparin with peptides and proteins at the molecular level is essential for understanding the biological activity of heparin. The use of structurally well-defined heparin-derived oligosaccharides to study the binding of heparin by peptides and proteins has resulted in breakthroughs in understanding the binding events and in determining the exact structural requirements within heparin that are critical for each binding. The studies reported in part I of this thesis describe the

isolation, purification, and structural characterization of a number of homogenous well-defined heparin-derived oligosaccharides using various methods. A structurally defined heparin-derived tetrasaccharide was then used to explore site specific binding of heparin with histidine-containing peptides. The information gained from studies reported in part I of this dissertation may help in the design of new highly specific therapeutic agents.

Chapter 2 details the experimental methods used for the isolation, purification, and structural characterization of heparin-derived oligosaccharides and the methods used to study binding of the tetrasaccharide by histidine-containing peptides.

Chapter 3 reports the results obtained from the isolation, purification, and characterization of heparin-derived oligosaccharides. Three tetrasaccharides, one hexasaccharide, and one octasaccharide were purified and characterized.

Chapter 4 presents results from a study of the binding of the fully sulfated heparin-derived tetrasaccharide to imidazole, L-histidine, histamine, β-amyloid peptide, and several other histidine-containing peptides by ^{1}H NMR.

Chapter 5 reports results of a study of the binding of imidazole, histamine, and histidine-containing peptides by heparin by isothermal titration calorimetry and affinity chromatography.

1.5 References

1. Lagunoff, D.; Phillips, M. T.; Iseri, O. A.; Benditt, E. P. *Lab. Invest*. **1964**, *13*, 1331.

2. Martin, T. W.; Lagunoff, D. (1984) in *Mast Cell Secretion* (Cantin, M., Ed.) S. Karger, Basel.

3. Lane, D.; Lindahl, U. (eds) (1989) Heparin, Chemical and Biological Properties, Clinical Applications. CRC Press, Boca Raton, FL.

4. Crum, R; Szabo, S.; Folkman, J. *Science* **1985**, *230*, 1375.

5. Holondniy, M; Kim, S.; Katzenstein, D.; Konrad, M.; Groves, E. T.; Merigan, T. C. *J. Clin. Microbiol.* **1991**, *29*, 676.

6. Casu, B.; in *Heparin: Chemical and Biological Properties, Clinical Applications*, ed. Lane, D. A.; Lindahl, U. CRC Press, Inc., Boca Raton, Fl, **1989**, p. 25.

7. Ferro, D. R.; Provas, A. *J. Am. Chem. Soc*. **1986**, *108*, 6773-6778.

8. Mulloy, B.; Forster, M. J.; Jones, C.; Davies, D. B. *Biochem. J*. **1993**, *293*, 849-858.

9. Bazin, H. G.; Capila, I.; Linhardt, R. J. *Carbohydr. Res*. **1998**, *309*, 135-144.

10. Ragazzi, M.; Ferro, D. R.; Provasoli, A.; Pumilia, P.; Cassinara, A.; Torri, G. ; Guerrini, M. ; Casu, B. ; Nader, H. B. ; Dietrich, C. P. *J. Carbohydr. Chem*. **1993**, *12*, 523-535.

11. Gould, S. E. B. ; Gould, R. O.; Rees, D. A.; Wight, A. W. *J. Chem. Soc. Perkin Trans*. **1975**, *2*, 392-399.

12. Mikhailow, D.; Linhardt, R. J.; Mayo, K. H. *Biochem. J*. **1997**, *328*, 51-61.

13. Mikhailow, D.; Mayo, K. H.; Vlahov, I. R.; Toida, T.; Pervin, A.; Linhardt, R. J. *Biochem. J*. **1996**, *318*, 93-102.

14. Rabenstein, D. L. *Nat. Prod. Rep.* **2002**, *19*, 312-331.

15. Lindahl, U. in *Heparin: Chemical and Biological Properties, Clinical Applications*, ed. Lane, D. A.; Lindahl, U. CRC Press, Inc., Boca Raton, FL, **1989**, p. 159.

16. Li, J. P.; Hagner-McWhirter, A.; Kjellen, L.; Palgi, J.; Jalkanen, M.; Lindahl, U. *J. Biol. Chem.* **1997**, *272*, 28158.

17. Hagner-McWhirter, A.; Lindahl, U.; Li, J. P. *Biochem. J.* **2000**, *347*, 69.

18. Crawford, B. E.; Olson, S. K.; Esko, J. D.; Pinhal, M. A. S. *J. Biol. Chem.* **2001**, *276*, 21538.

19. Hagner-McWhirter, A.; Hannesson, H. H.; Campbell, P.; Westley, J.; Roden, L.; Lindahl, U.; Li, J. P. *Glycobiology*, **2000**, *10*, 159.

20. Conrad, H. E.; *Heparin-Binding Proteins*, Academic Press, New York, **1998**.

21. Rong, J.; Habuchi, H.; Kimata, K.; Lindahl, U.; Kusche-Gullberg, M. *Biochemistry* **2001**, *40*, 5548.

22. Rosenberg, R. D.; Shworak, N. W.; Liu, J.; Schwartz, J. J.; Zhang, L.; *J. Clin. Invest.* **1997**, *100*, S67-S75.

23. Linhardt, R. J.; Toida, T. in *Carbohydrates in Drug Design* (Eds.: Witczak, Z. J.; Nieforth, K. A.), Marcel Dekker, New York, **1997**, pp. 277-341.

24. Linhardt, R. J.; *Chemistry & Industry* **1991**, *2*, 45-50.

25. Bjork, I; Olson, ST. *Adv Exp Med Biol*. **1997**, *425*, 17-33.

26. Gettins, PGW; Patston, PA; Olson, ST. Serpins: Structure, Function and Biology. Austin, TX:R. G. Landes Co., **1996**.

27. Boeckel, C.A.A. V.; Petitous, M. *Angew. Chem. Int. Ed. Engl*. **1993**, *32*, 1671-1690.

28. Hirsh, J; Warkentin, T. E.; Shaughnessy, S. G.; Anand, S. S.; Halpernin, J. L.; Raschke, R.; Granger, C. *Chest* **2001**, *119*, 64S-94S.

29. Capila, I.; Linhardt, R. J. *Angew. Chem. Int. Ed*. **2002**, *41*, 390-412.

30. Petitou, M.; Casu, B.; Lindahl, U. *Biochimie* **2003**, *85*, 83-89.

31. Baba, M. ; Pauwels, R. ; Balzarini, J. ; Arnout, J.; Desmyter, J.; DeClercq, E. *Proc. Natl. Acad. Sci., U.S.A*., **1988**, *85*, 6132-6136.

32. Ito, M.; Baba, M.; Pauwels, R.; DeClercq, E.; Shigeta, S. *Antiviral Res*. **1987**, *7*, 361-367.

33. DiGabriele, A. D.; Lax, I.; Chen, D. I.; Svahn, C. M.; Jaye, M.; Schlessinger, J.; Hendrickson, W. A. *Nature* **1998**, *393*, 812-817.

34. Faham, S.; Hileman, R. E.; Fromm, J. R.; Linhardt, R. J.; Rees, D. C. *Science* **1996**, *271*, 1116-1120.

35. Ye, S.; Luo, Y.; Lu, W. ; Jones, R. B. ; Mohamedali, K. A. ; Linhardt, R. J.; Capila, I.; Toida, T. ; Kan, M. ; Pelletier, H. ; McKeehan, W. L. *Biochemistry* **2001**, *40*, 14429-14439.

36. Born, J.; Gunnarson, K.; Bakker, M. A. H.; Kjellen, L.; Kusche-Gullberg, M.; Maccarana, M.; Berden, J. H. M.; Lindahl, U. *J. Biol. Chem*. **1995**, *270*, 31303.

37. Born, J.; Jann, K.; Assmann, K. J. M.; Lindahl, U.; Berden, J. H. M. *J. Biol. Chem*. **1996**, *271*, 22802.

38. Capila, I.; Linhardt, R. J. *Angew. Chem. Int. Ed*. **2002**, *41*, 390-412.

39. Lindahl, U.; Lidholt, K.; Spillmann, D.; Kjellen, L. *Thromb. Res*. **1994**, *75*, 1.

40. Marcum, J. A.; McKenney, J. B.; Galli, S. J.; Jackman, R. W.; Rosenberg, R. D. *Am. J. Physiol.*, **1986**, *250*, H879.

41. Castellot, J. J.; Hoover, R. L.; Harper, P. A.; Karnovsky, M. *J. Am. J. Pathol.*, **1985**, *120*, 427.

42. Perrimon, N.; Bernfield, M. *Nature* **2000**, *404*, 725.

43. Sasisekharan, S.; Venkataraman, G. *Curr. Opin. Chem. Biol*. **2000**, *4*, 626.

44. Cardin, A. D.; Weintraub, H. J. R. *Arteriosclerosis* **1989**, *9*, 21-32.

45. Sobel, M.; Soler, D. F.; Kermode, J. C.; Harris, R. B. *J. Biol. Chem*. **1992**, *267*, 8857-8862.

46. Fromm, J. R.; Hileman, R. E.; Caldwell, E. E. O.; Weiler, J. M.; Linhardt, R. J. *Arch. Biochem. Biophys*. **1995**, *323*, 279-287.

47. Rabenstein, D. L.; Bratt, P.; Schierling, T. D.; Robert, J. M.; Guo, W. *J. Am. Chem. Soc.* **1992**, *114*, 3278-3285.

48. Wuthrich, K. *NMR of proteins and Nucleic Acids*; John Wiley: New York, **1986**.

49. Chuang, W.-L.; Christ, M. D.; Peng, J.; Rabenstein, D. L. *Biochemistry* **2000**, *39*, 3542-3555.

50. Rabenstein, D. L.; Robert, J. M. ; Hari, S. *FEBS Lett*. **1995**, *376*, 216-220.

51. Loganathan, D.; Wang, H. M.; Mallis, L. M.; Linhardt, R. J. *Biochemistry* **1990**, *29*, 4362-4368.

52. Hyers, T. M.; Hull, R. D.; Weg, J. G. *Arch. Intern. Med*. **1986,** *146*, 467.

53. Pangrazzi, P.; Abbadini, M.; Zametta, M.; Naggi, A.; Torri, B.; Donati, M. B. *Biochem. Pharmacol* **1985**, *34*, 3305.

54. Linhardt, R. J. ; Rice, K. G.; Zohar, Z. M.; Yeong, K. S.; Lohse, D. L. *J. Biol. Chem.* **1986**, *261*, 14448.

55. Guo, Y. C.; Conrad, H. E. *Anal. Biochem.* **1988**, *168*, 54.

56. Barrowcliffe, T. W.; Curtis, A. D.; Tomilson, T. D.; Hubbard, A. R.; Johnson, E. A.; Thomas, D. P. *Thromb. Haemostasis* **1985**, *54*, 675.

57. Albada, J.; Nieuwenhuis, H. K; Sixma, J. J. in D. A. Lane and U. Lindahl (Editors) *Heparin: Chemical and Biological Properties, Clinical Applications*, Edward Arnold, London, **1989**, p. 417 and references cited therein.

58. Holmer, E. in D. A. Lane and U. Lindahl (Editors), *Heparin: Chemical and Biological Properties, Clinical Applications*, Edward Arnold, London, **1989**, p. 575, and references cited therein.

59. Breddin, H. K.; Fareed, J.; Bender, N. *Haemostasis* **1988**, *18*, 1.

60. Yang, H. O.; Gunay, N. S.; Toida, T.; Kuberan, B.; Yu, G.; Kim, Y. S.; Linhardt, R. J. *Glycobiology* **2000**, *10*, 1033-1039.

61. Pervin, A.; Gallo, C.; Jandik, K. A.; Han, X. J.; Linhardt, R. J. *Glycobiology* **1995**, *5*, 83-95.

62. Bienkowski, M. J.; Conrad, H. E. *J. Bio. Chem.* **1985**, *260*, 356-365.

63. Guo, Y.; Conrad, H. E. *Anal. Biochem.* **1989**, *176*, 96-104.

64. Linhardt, R. J.; Turnbull, J. E.; Wang, H. M.; Loganathan, D.; Gallagher, J. T. *Biochem. J.*, **1990**, *29*, 2611-2617.

65. Rice, K. G.; Kim, Y. S.; Grant, A. G.; Merchant, Z. M. ; Linhardt, R. J. *Anal Biochem.* **1985**, *150*, 325-331.

66. Thanawiroon, Charuwan; Linhardt, R. J. *J. of Chromatogr. A* **2003**, *1014*, 215-223.

67. Guo, Y. C.; Conrad, H. E. *Anal Biochem.* **1988**, *168*, 54-62.

68. Toyoda, H.; Yamamoto, H.; Ogino, N.; Toida, T.; Imanari, T. *J. Chromatogr. A* **1999**, *830*, 197.

69. Karamanos, N. K.; Vanky, P.; Tzanakakis, G. N. ; Tsegenidis, T. ; Hjerpe, A. *J. Chromatogr. A*, **1997**, *765*, 169-179.

70. Korir, A. K.; Limtiaco, J. F. K. ; Gutierrez, S. M. ; Larive, C. K. *Anal. Chem.* **2008**, *80*, 1297-1306.

71. Chen, J. ; Duncan, M. B. ; Carrick, K.; Pope, R. M.; Liu, J. *Glycobiology* **2003**, *13*, 785-794.

72. Linhardt, R. J.; Toida, T.; in : Z. J. Witczak, Nieforth, K. A. (Eds.), Carbohydrates in Drug Design, Marcel Dekker, *New York*, **1997**, p. 277.

73. Al-Halkim, A.; Linhardt, R. J. *Anal. Biochem.* **1991**, *195*, 68-73.

74. Ampofo, S. A.; Wang, H. M.; Linhardt, R. J. *Anal Biochem.* **1991**, *199*, 249-255.

Chapter 2

Experimental Methods and Materials

2.1 Materials

Porcine intestinal mucosal heparin, sodium 3-(trimethylsilyl)-propionate-2, 2, 3, 3-d4 (TMSP), imidazole, histamine, L-histidine, histidyl-glycine, glycyl-histidine, glycyl-histidyl-glycine and glycyl-histidyl-lysine were purchased from Sigma Chemical Co. β-amyloid peptide (FRHDSGY) was purchased from AnaSpec. NaOD (40%), DCl (35%) and D_2O were purchased from Cambridge Isotope Laboratories Inc. NaCl, NaH_2PO_4 and sodium acetate were obtained from Fisher Scientific. Millipore water was obtained from the Chemistry Department. Sephadex G-10 was purchased from Amersham Biosciences. Capillary electrophoresis reagents (e.g. 0.1 M phosphate buffer, pH 2.5, capillary wash solution and the peptide calibrator) were purchased from Biorad. A semi-preparative scale (9 x 250 mm) CarboPac PA column was purchased from Dionex Co. A semi-preparative scale (10 x 250 mm) Spherisorb SAX column was purchased from Waters (Milford, MA). A pH microelectrode for measuring pH in NMR tubes was obtained from Microelectrodes Inc.

2.2 pH Measurements

pH measurements were performed with an Orion Research EA 920 pH meter equipped with a pH microelectrode designed for pH measurements within a 5 mm NMR tube. The pH meter was calibrated with Fisher Scientific certified pH 4.00, 7.00 and 10.00 pH standard solutions. Since the pH meter was standardized with aqueous buffers, pD values reported for D_2O solutions were obtained by using the equation pD = pH meter

reading + 0.40 to correct for the deuterium isotope effect.[1]

2.3 Separation of Size-Homogeneous Oligosaccharide Mixture by Strong Anion Exchange High Performance Liquid Chromatography (SAX-HPLC)

SAX-HPLC was used to purify mixtures of size-homogeneous oligosaccharides by charge. The size-homogeneous mixtures were obtained using gel permeation chromatography (GPC). Separations were performed on a Dionex 500 ion chromatography system equipped with a GP40 gradient pump and an AD20 UV/visible detector. The polyether ether ketone (PEEK) tubing and ceramic pump heads in the Dionex HPLC system makes it the HPLC of choice for the separation of heparin-derived oligosaccharides, which requires a high salt buffer and NaCl gradient that is corrosive to the stainless steel used in most HPLC pumps.

Charge separation of size-uniform oligosaccharide fractions was carried out on a semi-preparative scale CarboPac PA1 SAX column. The sample was eluted from the SAX column using a linear gradient of NaCl from 0 to 2 M at pH 3.0. The separation times for the tetrasaccharide, hexasaccharide and octasaccharide fractions were 140, 160 and 170 min, respectively. Separations began with 100% of mobile phase A (a 70 mM phosphate buffer in Millipore water) for the first 10 minutes and then mobile phase B (2.0 M sodium chloride solution in 70 mM phosphate buffer) was increased over time to elute the oligosaccharides. Both mobile phases were adjusted to pH 3.0 with hydrochoric acid. The elution profile was monitored by absorbance at 232 nm. The heparin-derived oligosaccharides were eluted from the column at a flow rate of 3.3 mL/min. Major peaks with the same retention time from multiple injections of the same sized oligosaccharide

38

were pooled together, lyophilized and desalted. The purity of each oligsaccharide was next confirmed by the presence of a single symmetrical peak on analysis using capillary zone electrophoresis as will be discussed in a later section of this chapter.

After each run, the column was washed with 100% mobile phase B for 1 column volume (16 mL) at 1 mL/min and was then equilibrated with mobile phase A before the next injection. Samples were prepared by dissolving a certain sample mass in an appropriate volume of mobile phase A to fully dissolve the sample. Prior to injection, samples were filtered through a 0.22 μm membrane filter. Mobile phases A and B were filtered as well after pH adjustment. The injection volume was optimized without scarificing peak resolution as well as avoiding column fronting.

2.4 Concentrating Oligosaccharide Solution for Desalting

Desalting of the heparin-derived oligosaccharides separated by SAX-HPLC was necessary for the binding studies of oligosaccharide with heparin binding ligands reported in chapter 4. The pooled solutions of oligosaccharide eluting from the SAX column contain a high concentration of Na^+, which affects the binding affinity of ligand. For instance, the binding constant for the interaction of histamine with heparin has been reported to be reduced as the Na^+ concentration increases.[2] Na^+ counterions compete with the ligand for negative binding sites on heparin.

SAX-HPLC was used in the first step of a two-step desalting process. Oligosaccharide solution collected from peaks eluting at the same retention time from repetitive injections of the same sized oligosaccharide were combined and were diluted with Millipore water to lower the NaCl concentration down to below 0.4 M. The diluted

39

oligosaccharide solution was then reloaded onto the Spherisorb SAX column as the mobile phase.

With the sodium concentration below 0.4 M, the oligosaccharide was retained in the column while the sodium chloride was eluted from the column. Thus, the trapped oligosaccharide inside the column was concentrated and was eventually eluted from the column using the same salt gradient that was used to separate the oligosaccharide mixture. The volume of oligosaccharide solution collected from this last step was a lot smaller than that of all collections combined together; it contained all the oligosaccharide from the pooled fractions at the same NaCl concentration as an individual fraction, i.e. the oligosaccharide/salt ratio was increased. By concentrating the oligosaccharide, the desalting step by gel permeation chromatography was much less work intensive. This concentrating procedure also allows repurifying the oligosaccharide if unwanted peaks were collected during the SAX-HPLC separation. An example of the sample concentrating procedure is illustrated in Figure 2.1.

2.5 Desalting the Size Fractionated Oligosaccharides

The concentrated oligosaccharide fractions were desalted on a custom-made size exclusion chromatography column (9 x 250 mm) packed with sephadex G-10, which was connected to the Dionex HPLC. The elution profiles were monitored by absorbance at 232 nm. Heparin oligosaccharides were eluted with Millipore water as the mobile phase at a flow rate of 3.3 mL/min. Eluent peaks were collected and freeze-dried.

2.6 Lyophilization

After desalting, heparin-derived oligosaccharide solution was frozen in dry ice (-
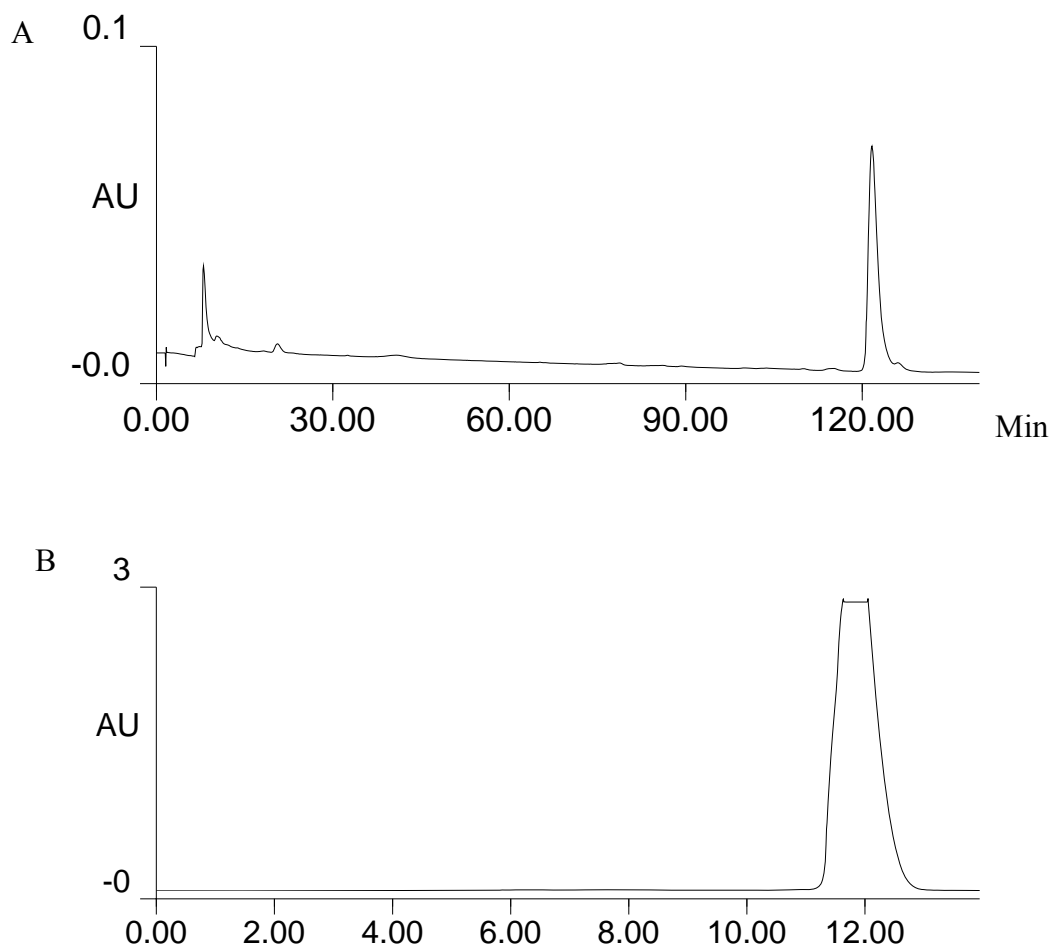
Figure 2.1. SAX-HPLC chromatograms of pure heparin-derived tetrasaccharide. (A)

Obtained from one single collected fraction using the CarboPac PA1 column; (B)

Obtained after reloading a combined volume of more than 30 collected fractions back

onto the SAX column (a Spherisorb column this time) as the mobile phase once the NaCl

concentration was reduced to below 0.4 M. The concentrated oligosaccharide was eluted

from the Spherisorb SAX column using the same salt gradient condition as used to obtain

the top chromatogram.

78.5 °C) followed by lyophilizing on a Virtis lyophilizer under a vacuum of about 400 millitorr and at low temperature (-40 ^{o}C) to remove solvent (water).

2.7 Capillary Zone Electrophoresis (CZE)

In this research, CZE was used to check the purity of heparin-derived oligosaccharides after they were first separated by size by gel permeation chromatography and then by charge using SAX-HPLC, followed by desalting.

All separations were performed on a Biorad Biofocus 3000 CE system operated by Microsoft Windows 3.1. Analytes were monitored by using UV detection at 232 nm and were separated on custom-made fused silica capillary cartridges (i.d. 25 μm, o.d. 363 μm, l$_{det.}$ of 24 cm or 40 cm where l$_{det.}$ is the distance from the inlet to the detector). The internal surface of the capillary was coated to prevent electroosmotic flow (EOF). The electrolyte used was a solution of 0.1 M phosphate buffer, pH 2.5. Separations were carried out at a constant voltage of 8 kV for heparin-derived tetrasaccharides and of 10 kV for heparin-derived octasaccharide. The sample ions were loaded into the capillary using electrophoretic injection mode for a few seconds with the anode at the detector side (reversed polarity, - → +). Since the quantity of sample ions that migrate into the capillary during electrophoretic injection is strongly dependent on the ionic strength of the sample solution, heparin-derived oligosaccharides were desalted first to reduce the sample salt concentration in order to achieve optimum sensitivity. The carousel setpoint temperature was set to 20 °C for every separation reported in this thesis. A blank injection was always done prior to injecting a sample to ensure that the capillary was clean.

A peptide calibrator solution was used to check the functionality of the CE instrument and the capillary cartridge. The electropherogram of the peptide calibrator is shown in Figure 2.2. The components of the peptide calibrator were separated on the custom-made cartridge (i.d. 25 μm, o.d. 363 μm, $l_{det.}$ 24 cm). All 9 peptides (bradykinin, angiotensin II, α-MSH, TRH, LHRH, leucine enkephalin, bombesin, methionine enkephalin, and oxytocin) in the peptide calibrator were detected at 200 nm at a constant voltage of 8 kV using the same buffer mentioned above. The peptide calibrator was loaded into the capillary using eletrophoretic injection mode at 8 kV for 2 seconds with the cathode at the detector side (normal polarity, $+ \rightarrow -$). All samples were prepared by dissolving a known sample mass into a certain volume of the running phosphate buffer. The sample solution was transferred to a 0.45 μm spinning filter vial and was then centrifuged to remove air bubbles and particulates.

2.8 ^{1}H NMR Measurements

2.8.1 NMR Instrumentation

NMR spectra were obtained using a Varian Unity Inova 500 MHz pulsed Fourier transform NMR spectrometer, which is controlled by a Sun Ultra 140E Unix workstation running Varian VNMR 6.1C software. An Oxford 11.94 Tesla superconducting magnet was used. Data were processed on a Silicon Graphics Indigo Octane computer. NMR experiments were carried out either on a 5mm Varian Triax (^{1}H/^{13}C/^{15}N) pulse field gradient (PFG) probe or on a 5 mm Varian (^{1}H, ^{19}F) probe. All of NMR experiments in part I of this thesis were done at 25 ^{o}C.

43
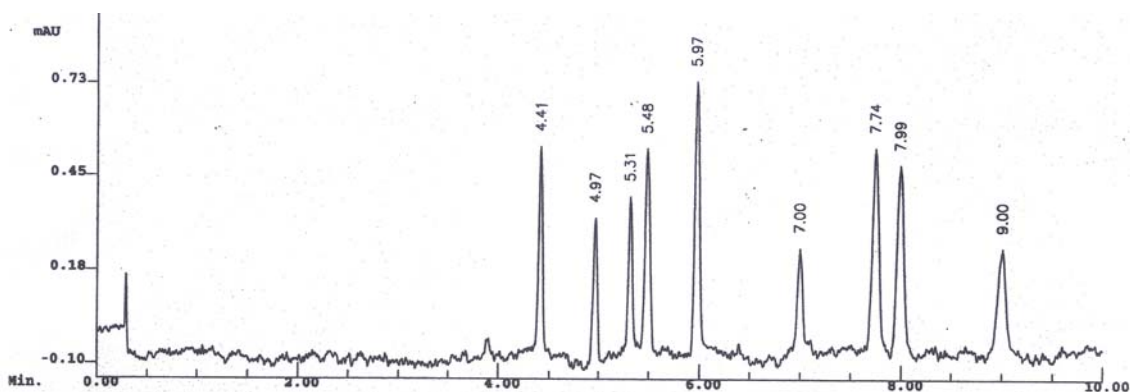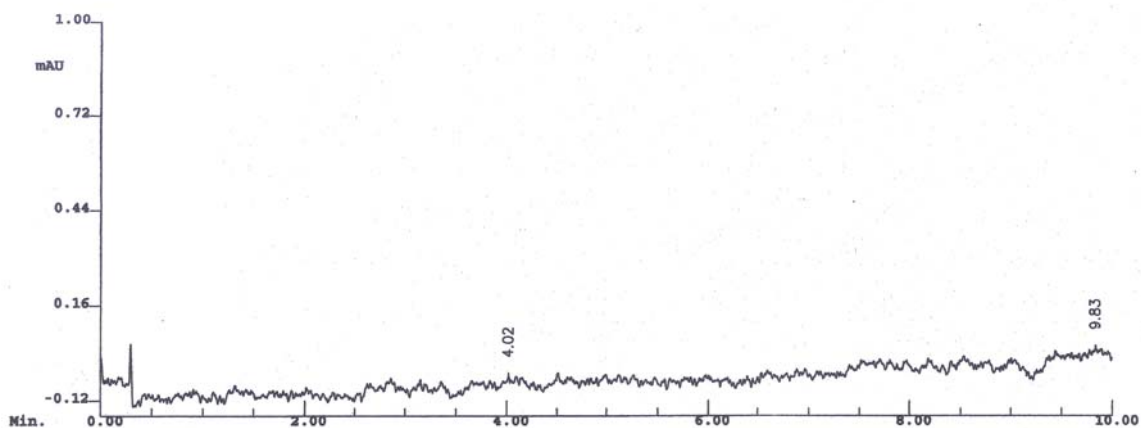
Bradykinin	4.41 min	Angiotensin II	4.97 min
α-MSH	5.31 min	TRH	5.48 min
LHRH	5.97 min	Leucine enkephalin	7.00 min
Bombesin	7.74 min	Methionine enkephalin	7.99 min
Oxytocin	9.00 min		

Figure 2.2. The top shows the blank electropherogram without sample injection. The bottom shows the typical capillary electropherogram of the nine peptides in the peptide calibrator. The CE conditions were 0.1 M phosphate buffer (pH 2.5) and positive to negative polarity at 8 kV. The absorbance was measured at 200 nm.

2.8.2 Sample Preparation

NMR spectra were measured for the heparin-derived oligosaccharides in D_2O solution. To reduce the intensity of the residual HOD resonance, heparin-derived oligosaccharides were dissolved in D_2O and then lyophilized to exchange labile oligosaccharide OH protons with deuterium. This D_2O exchange procedure was repeated three times.

Samples were weighed out on a Mettler Microbalance in plastic Eppendorf vials and were dissolved in 100% D_2O solution. For structural identification of heparin-derived oligosaccharides, a solution volume of 320 μL was prepared. For NMR titration experiments, a volume of 500 μL was required. Sodium 3-(trimethylsilyl) propionate-2,2,3,3-d_4 (TMSP) was added as a chemical shift reference, where the methyl singlet of TMSP was assigned to be 0.000 ppm. A trace amount of EDTA-d16 was added to the oligosaccharide samples to reduce line broadening caused by trace amounts of paramagenetic cations (e.g. Cu^{2+}, Mn^{2+} and Fe^{3+}) via the interaction between electron and nuclear spins. Dissolved molecular oxygen can also shorten relaxation time by the electron-nuclear dipolar mechanism as well. Molecular oxygen was removed by sonicating the sample solution under a vacuum for about ½ hour.

The sample pH was adjusted with 0.1 M DCl or NaOD solutions. Samples were filtered through a 0.45 μm Microspin filter to remove particulates. Filtered sample solutions were transferred to a Shigemi NMR tube (Figure 2.3) obtained from Shigemi Co. The use of Shigemi tubes helps reduce solution volume and improves suppression of the water resonance. A Shigemi tube consists of a cylindrical tube with a solid glass base
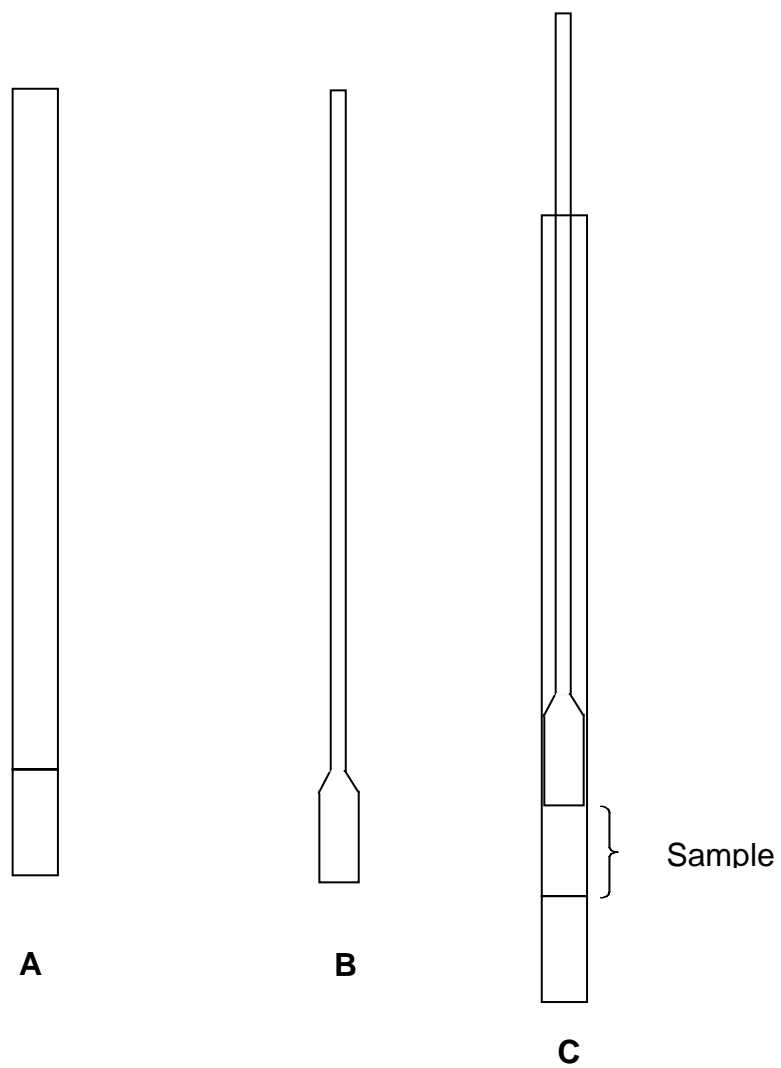
Figure 2.3. Shigemi NMR tube. (A) tube; (B) insert; (C) insert in a tube with sample.

at the bottom and a glass insert, both of which are made from a special type of glass with a magnetic susceptibility matched to that of D_2O to remove magnetic field inhomogeneity resulting from an interface of two zones (the sample solution region and the region either above or below it) having dissimilar magnetic susceptibility. With this design, a 5 mm Shigemi tube requires a sample volume of only about 320 μL. The low sample volume requirement of Shigemi tubes is particularly beneficial for working with the limited amount of heparin-derived oligosaccharides.

2.8.3 One Dimensional ^{1}H NMR Experiments

All 1-D spectra in this thesis were obtained using the single pulse experiment with suppression of the H_2O or HOD resonance by the selective saturation method. Although samples were dissolved in 100% D_2O to eliminate the resonance from solvent protons, heparin-derived oligosaccharides and peptides both contain OH and NH protons, which exchange with deuterons from the solvent resulting in the presence of the residual HOD resonance. As described in the sample preparation section, the intensity of the residual HOD resonance was minimized by a D_2O exchange procedure.

No matter how well the D_2O exchange procedure was done, the concentration of residual HOD was always larger than the analytes, which were typically 0.5-2 mM. Since the spectrum contains both strong and weak signals, suppression of the residual HOD resonance was necessary to avoid a dynamic range problem in digitization of the FID.[3, 4] By saturating the residual HOD resonance, the Signal-to-Noise (S/N) ratio of the solute resonances can be improved.

One-dimensional ^{1}H NMR spectra were measured by the single pulse sequence

shown in Figure 2.4. As seen from Figure 2.4, a selective presaturation pulse (typically 4 seconds) was applied just before the 90° observation pulse, at the frequency of the water resonance to suppress the HOD resonance. The saturation pulse serves to equalize the populations of the two energy levels of the HOD protons, and thus the HOD resonance is eliminated. However, solute resonances at frequencies close to the water frequency are also suppressed due to saturation. To minimize the loss of analyte resonances, a low water saturation power (typically 13 dB) was used.[5] The pulse sequence is repeated with coherent addition of successive FID's in the computer to enhance S/N. The relaxation delay between pulses allows the nuclear magnetization to recover to equilibrium by spin-spin (T_2) and spin-lattice (T_1) relaxation.

The presaturation single pulse experiments were performed using the following parameters: spectral width (sw) was 5500 Hz, the number of points (np) collected was either 8196 or 16392, the number of transients (nt) collected was 64-256, the transmitter offset (tof) and the saturation frequency (satfrq) were optimized and set to the frequency of the water resonance using the wfrq macro, the transmitter power (tpwr) was 63 dB, the water saturation power (satpwr) was 13 dB and the transmitter pulse width (pw) was about 8.4 μs. All 1-D experiments were conducted without spinning the sample.

2.8.4 Two-Dimensional ^{1}H NMR Experiments

Heparin-derived tetrasaccharides and larger oligosaccharides reported in this thesis are composed of repeating disaccharide units. For instance, the hexasaccharide ΔUA(2S)-GlcNS(6S)-IdoA(2S)-GlcNS(6S)-IdoA(2S)-GlcNS(6S) has 2 IdoA(2S) residues and 3 GlcNS(6S) residues. Due to significant overlap of resonances of the same
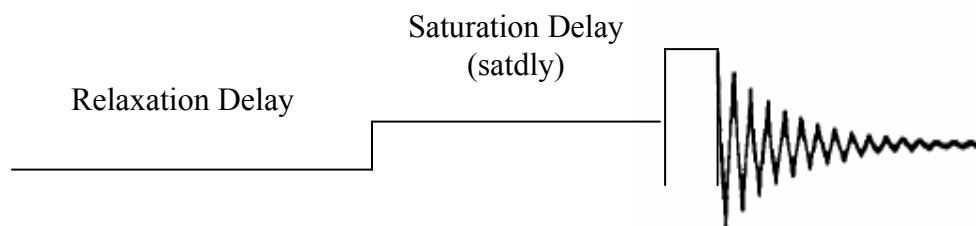
Figure 2.4. Pulse sequence for the measurement of ^{1}H NMR spectra with water resonance suppression by presaturation.

residues, it is not possible to resolve all resonances of this hexasaccharide in a 1-D

spectrum, as shown by the 500 MHz spectrum of the hexasaccharide obtained at pD 6.68

in Figure 2.5. Therefore, 2-D NMR experiments were used to obtain the complete

structural characterization of heparin-derived oligosaccharides. The 2-D NMR

experiments used in this research include the TOtal Correlation SpectroscopY (TOCSY),

Nuclear Overhauser Effect SpectroscopY (NOESY), and Rotating Frame Overhauser

Effect SpectroscopY (ROESY) experiments. Each type of 2-D experiment yields specific

information about the oligosaccharide, which will be described in detail in the following

sections.

2.8.4.1 The TOtal Correlation SpectroscopY (TOCSY) Experiments

The TOCSY experiment, also known as the HOHAHA (HOmonuclear

HArtmann-HAhn) experiment, permits the assignment of all the resonances of an isolated

spin system based on scalar (through-bond) ^{1}H-^{1}H spin-spin couplings (Figure 2.6).[6] As

seen from the structure of the heparin-derived hexasaccharide at the top of Figure 2.6, the

^{1}H nuclei of each sugar ring are an isolated spin system since there is no scalar coupling

of ^{1}H nuclei across the glycosidic bond. The middle of Figure 2.6 is the TOCSY

spectrum of the hexasaccharide obtained at pD 3.02.

The TOCSY spectrum consists of the normal 1D spectrum along the diagonal,

with off-diagonal peaks linking resonances for the same spin system. A trace through a

resolved resonance yields a 1-D subspectrum corresponding to a specific sugar ring of the

hexasaccharide. For instance, a trace through the most downfield resonance (in circle),

gives the subspectrum shown at the bottom of Figure 2.6, which allows one to identify
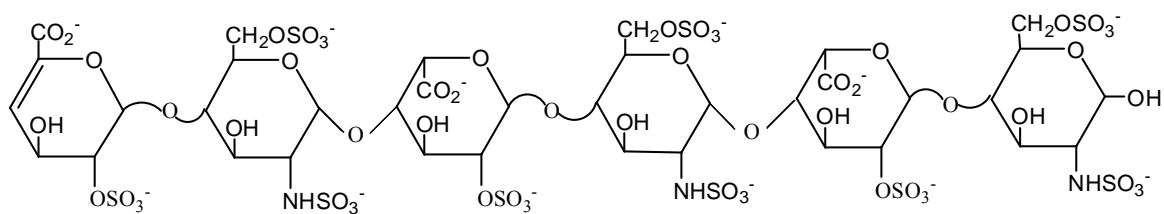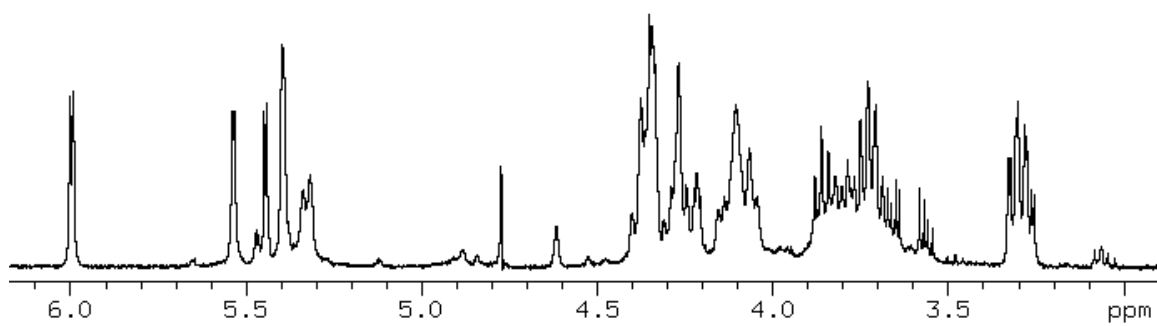
Figure 2.5. 1-D ^{1}H NMR spectrum (500 MHz, 298 K, pD 6.68) of a heparin-derived hexasaccharide. The spectrum was measured with water suppression in 100% D_2O.
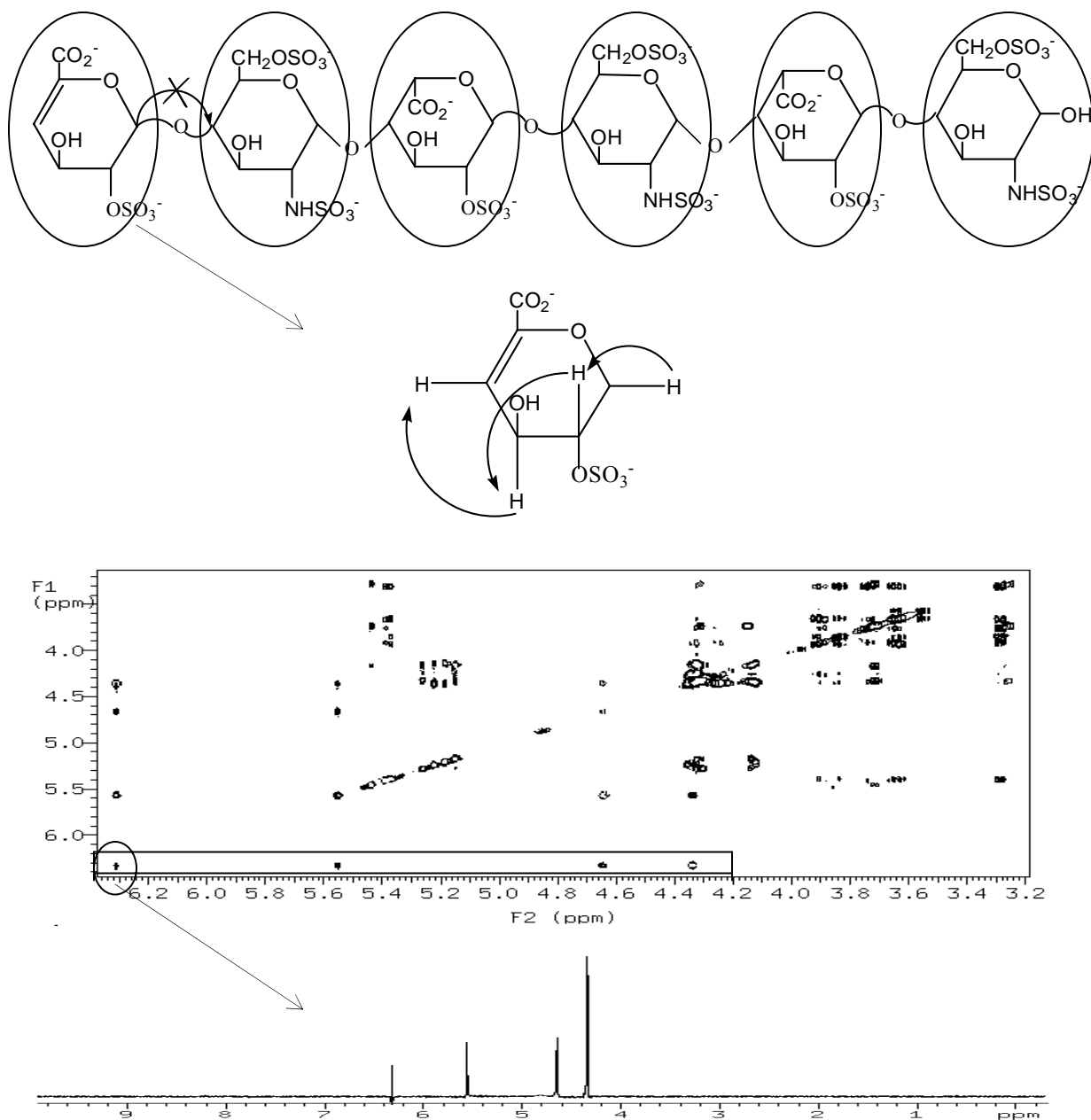
Figure 2.6. Structure of heparin-derived hexasaccharide is shown at the top with a circle around each sugar unit to indicate an isolated spin system. The arrows within the non-reducing end sugar ring below the hexasaccharide illustrate relay of magnetization within a spin system in the TOCSY experiment. The arrow with the cross sign on hexasaccharide structure indicates that magnetization is not transferred across glycosidic bonds. The middle of the figure shows the TOCSY spectrum of the hexasaccharide measured with water suppression at pD 3.02 in 100% D_2O. A trace taken from the TOCSY spectrum through the well-resolved resonance in the circle yields a subspectrum, which allows identification of the sugar residues to be the unsaturated uronic acid residue $\Delta UA(2S)$.

52

the sugar unit giving this subspectrum to be the unsaturated uronic acid residue ΔUA(2S) by comparing the chemical shift of each resonance with literature values. Resonances in the subspectrum are observed for all the protons within ΔUA(2S) because magnetization that is transferred between two scalar coupled spins is further relayed through the entire spin system. The pulse sequence of the TOCSY experiment with suppression of the residual HOD or H_2O resonance by the selective saturation method used in this research is shown in Figure 2.7.

As seen from Figure 2.7, a selective presaturation pulse of 1 second is first applied via the transmitter channel just before the 90° pulse to suppress the HOD resonance. The 90° pulse is applied to put the sample magnetization onto the transverse plane. Trim pulses of a couple of msec are applied at the beginning and the end of the mixing period to defocus any antiphase magnetization. The spin lock is applied during the mixing period to align magnetization along the Y-axis in order to induce the transfer of magnetization between scalar coupled spins.[7] A composite pulse (MLEV-17) was used for the spin lock.[8]

Parameters used in the TOCSY experiment were as follows: spectral widths (sw and sw1) in F_1 and F_2 dimenstions were 5500 Hz each, the number of points (np) collected in the F_2 dimension was either 8196 or 16392, the number of transients (nt) collected was 32-96, the number of t_1 increments (ni) was 64-192, the transmitter power (tpwr) was 63dB, the water saturation power (satpwr) was 13dB, the transmitter pulse width (pw) for a 90° pulse was 8.4 µs, the transmitter offset (tof) and the saturation frequency (satfrq) were optimized and set to the frequency of the water resonance using
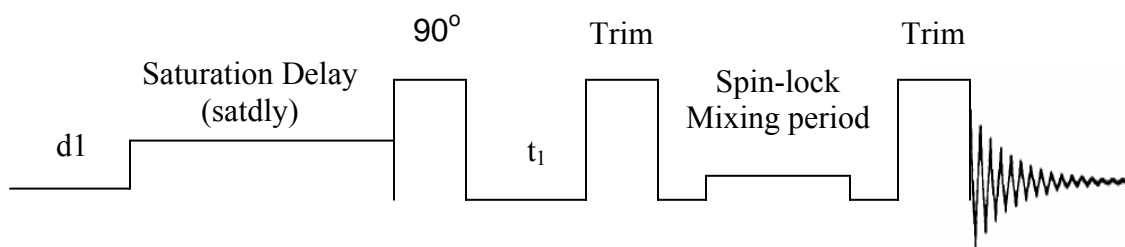
Figure 2.7. 2-D ^{1}H TOCSY pulse sequence with presaturation of the solvent resonance.

the wfrq macro, trim pulses were in the range between 0 and 3 msec, mixing times (mix) of 120 msec and a presaturation delay (d1) of 0 second were used, the saturation delay was 1 second, the spin lock power (slpwr) and pulse width (slpw) were determined using the attval(pw,tpwr) macro where the values for slpwr and slpw were selected with a field strength as close as possible to 9 KHz. Because the high duty cycle of the spin lock pulse may cause heating, 16 to 64 dummy scans (ss) were performed prior to acquisition to bring the sample to thermal equilibrium. All TOCSY experiments were run in the nonspinning mode.

2.8.4.2 The Rotating Frame Overhauser Effect SpectroscopY (ROESY) Experiments [9-13]

The ROESY experiment provides information based on dipolar (through-space) connectivities between protons within 5 Angstroms of each other in space (Figure 2.8). The top of Figure 2.8 shows the connection between two protons close in space, H_1 of $\Delta UA(2S)$ and H_4 of GlcNS (6S) (in circle) of a heparin-derived hexasaccharide. The cross peaks identified in the spectrum in Figure 2.8 between the H_1 and H_4 protons allows one to distinguish the GlcNS(6S) residue connected to $\Delta UA(2S)$ from the other two GlcNS(6S) residues. The cross peaks for $1 \rightarrow 4$ linkages between the other sugar units enable assignment of the sequence of the hexasaccharide as shown.

In this dissertation, the ROESY experiment is used to assign the sequence of monosaccharides in oligosaccharides and the sequence of amino acids in peptides with molar masses of 1000 – 3000 Daltons. Nuclear Overhauser Effect (NOE) cross peaks are weak for molecules with masses in the 1000-3000 Dalton range and thus the Nuclear
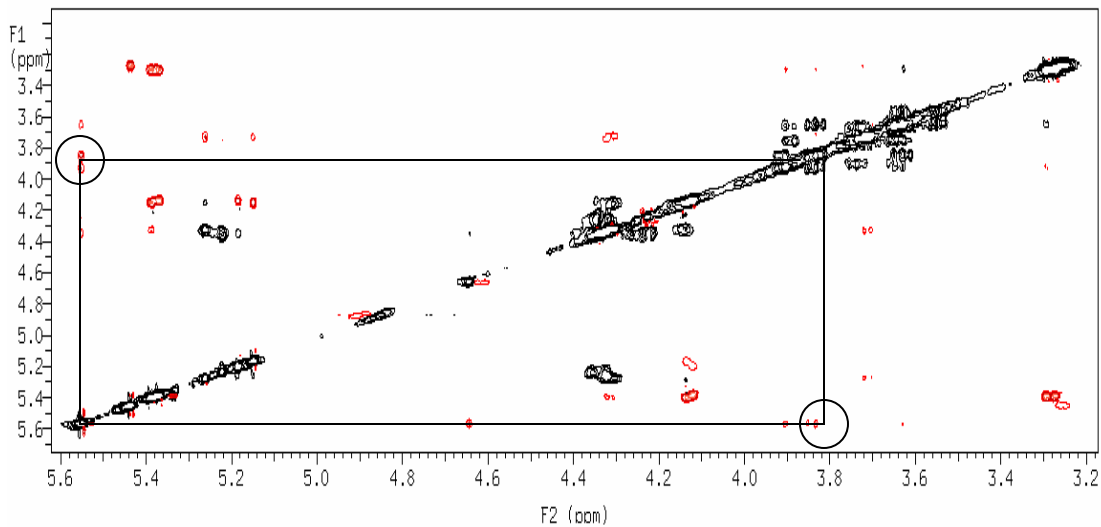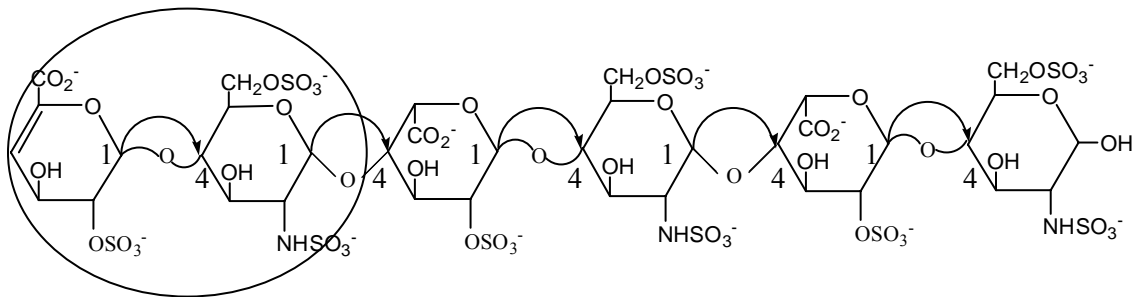
Figure 2.8. The top of this figure shows the connection between the two protons close in space, H_1 of $\Delta UA(2S)$ and H_4 of GlcNS (6S) (in circle) of a heparin-derived hexasaccharide. Arrows outside of the circle represent other connectivities established by magnetization transfer via through-space (dipolar) coupling from H_1 of I ring to H_4 of A ring as well as from H_1 of A ring to H_4 of I ring. The bottom of the figure shows the ROESY spectrum of the heparin-derived hexasaccharide measured with water suppression at pD 3.02 in 100% D_2O. ROESY cross peaks between the H_1 proton of $\Delta UA(2S)$ and the H_4 proton of the GlcNS(6S) residue, linked to $\Delta UA(2S)$ are shown in little circles.

Overhauser Effect SpectroscopY (NOESY) experiment is inappropriate for molecules in this mass range as is discussed in the next section. In the ROESY experiment, the rotating frame NOE (or ROE) is always positive due to $\varpi\tau_c$ always being $\ll 1$[12], where ϖ is the spectrometer operating frequency, and τ_c is the motional correlation time, the time taken for the molecule to rotate by roughly 1 radian about any axis.

ROESY cross peaks arising from transfer of magnetization through chemical exchange are positive in phase (the same sign as the diagonal resonances), while those arising from dipolar transfer of magnetization are negative (opposite in sign to the diagonal resonances). Thus, the ROESY experiment allows one to differentiate between NOE type interactions and exchange phenomena, which are less readily distinguished by NOESY experiment since NOESY chemical exchange and dipolar cross peaks are both positive. TOCSY cross peaks can also appear in the ROESY spectrum due to the similarity between the ROESY and the TOCSY pulse sequences.

The pulse sequence for the ROESY experiment with water suppression by presaturation is shown in Figure 2.9. In the pulse sequence, the spin-lock is applied for a designated time called the mixing time, which varies between 100 and 300 msec and is experimentally determined for each molecule studied by setting up an array for the mixing time (mix) from 0 – 300 msec. To minimize TOCSY cross peaks, the spin lock was generated with 30° pulses.

Parameters used in the collection of data in the ROESY experiment were as follows: spectral widths (sw and sw1) in F_1 and F_2 dimensions were 5500 Hz each, the number of points (np) collected in the F_2 dimension was either 8196 or 16392, the
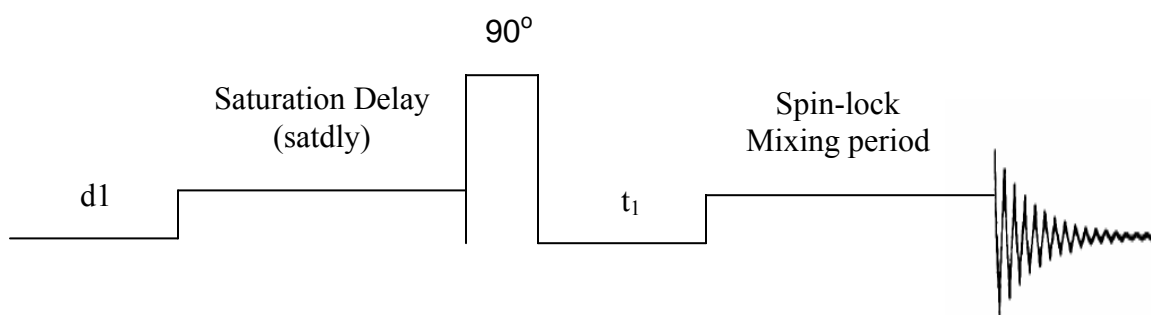
Figure 2.9. 2-D ^{1}H ROESY pulse sequence.

number of transients (nt) collected was 32-96, the number of t_1 increments (ni) was 64-192, the transmitter power (tpwr) was 63dB, the water saturation power (satpwr) was 13dB, the transmitter pulse width (pw) for a 90° pulse was 8.4 μs, the transmitter offset (tof) and the saturation frequency (satfrq) were optimized and set to the frequency of the water resonance using the wfrq macro, mixing times (mix) of 200 msec and the relaxation delay (d1) of 0 sec were used, the saturation delay was 1 sec, the spin lock power (slpwr) and pulse width (slpw) were determined using the attval (pw,tpwr) macro where the values for slpwr and slpw were selected with a field strength as close as possible to 4 KHz. Because the high duty cycle of the spin lock pulse may cause heating, 16 to 64 dummy scans (ss) were performed at the beginning of the experiment to allow the system to reach an equilibrium temperature prior to data acquisition. All ROESY experiments were run in the nonspinning mode.

2.8.4.3 The Nuclear Overhauser Effect SpectroscopY (NOESY) Experiments [14-17]

The NOESY experiment is widely used for identifying resonances from protons that are close together in space; usually within 5 Å. Cross peaks in the NOESY spectrum result from transfer of magnetization through space by dipolar cross relaxation between these spins or by transfer of protons between two sites by chemical exchange during the mixing time. In the NOESY spectrum, cross peaks from chemical exchange and those from through space dipolar cross relaxation are both positive. Like ROESY spectra, NOESY spectra are used in this work to establish the sequence of monosaccharides in heparin-derived oligosaccharides.

The intensity of NOESY cross peaks goes through a null point when $\varpi\tau_c$ equals

1.12, where again ϖ is the spectrometer operating frequency, and τ_c is the motional

correlation time. The motional correlation time (τ_c) is field dependent, which can be

roughly estimated by multiplying the molecular weight (M_r) by 10^{-12}. For the 500 MHz

NMR spectrometer used in this research, the zero cross-over point (null point) occurs for

molecules with a mass of 2240 Daltons. Molecules with molecular weights of 1000-3000

Daltons have $\varpi\tau_c$ in the range of 0.500-1.500, which fall near the null point and thus the

NOE enhancement is very little. Thus, in this thesis, the NOESY experiment was only

used for molecules with masses less than 1000 Daltons or more than 3000 Daltons. The

maximum NOE enhancement (η_{max}) depends upon both the molecular rotational

correlation time τ_c and the spectrometer frequency ω as described by the following

equation:

$$\eta_{max} = \frac{5 + \varpi^2\tau^2 - 4\omega^4\tau^4}{10 + 23\varpi^2\tau^2 - 4\omega^4\tau^4} \qquad (2.1)$$

The NOESY pulse sequence with solvent suppression by the selective saturation

method is given in Figure 2.10. A selective presaturation pulse is first applied to saturate

the solvent resonance. The first 90^o_x pulse is applied to create transverse magnetization

by putting the net magnetization in the transverse plane. The transverse magnetization

evolves during the variable evolution time t, encoding the phase in the second dimension.

The second 90^o_x pulse places magnetization of all spins onto the –Z-axis to generate a

population inversion, which allows the transfer of magnetization between spins within 5

Å of each other to take place by dipolar cross relaxation during the mixing time τ_m.

60
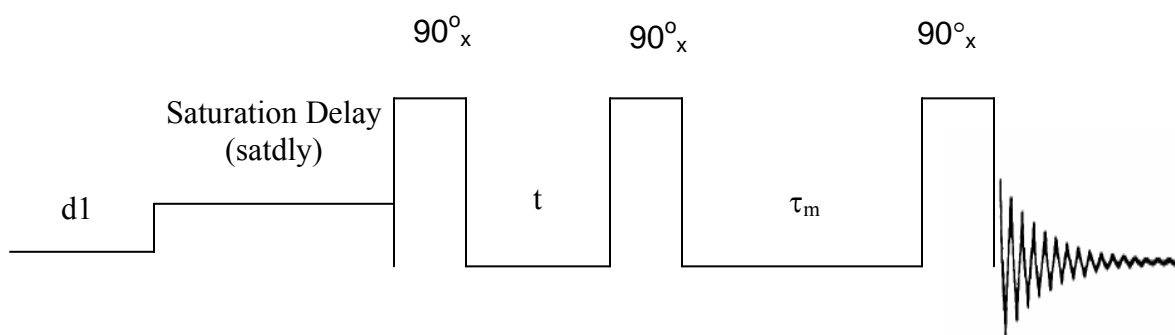
Figure 2.10. 2-D ^{1}H NOESY pulse sequence.

During the mixing time, the Nuclear Overhauser Effect (NOE) builds up. The final 90^o_x pulse puts the –Z-axis magnetization back into the XY plane for sampling.

Parameters used in the collection of data in the NOESY experiment were as follows: spectral widths (sw and sw1) in F_1 and F_2 dimensions were 5500 Hz each, the number of points (np) collected in the F_2 dimension was either 8196 or 16392, the number of transients (nt) collected was 32-96, the number of t_1 increments (ni) was 64-192, the transmitter power (tpwr) was 63dB, the water saturation power (satpwr) was 13dB, the transmitter pulse width (pw) for a 90° pulse was 8.4 μs, the transmitter offset (tof) and the saturation frequency (satfrq) were optimized and set to the frequency of the water resonance using the wfrq macro, mixing times (mix) of 200 msec and the relaxation delay (d1) of 0 sec were used, the saturation delay was 1 sec, the spin lock power (slpwr) and pulse width (slpw) were determined using the attval(pw,tpwr) macro where the values for slpwr and slpw were selected with a field strength as close as possible to 4 KHz. Because the high duty cycle of the spin lock pulse may cause heating, 16 to 64 dummy scans (ss) were performed prior to acquisition to allow the system to reach thermal equilibrium. All NOESY experiments were run in the nonspinning mode.

2.8.4.4 Band-Selective Homonuclear-Decoupled (BASHD) 2D NMR Experiments [18-21]

BASHD experiments are powerful 2-D NMR tools since they offer an increase in resolution in the F_1 dimension. Enhancement of resolution in the F_1 dimension is achieved by homonuclear decoupling and by reducing the spectral width. Band selective homonuclear decoupling improves resolution and sensitivity by converting multiplets

into singlets in the indirectly detected (F_1) dimension. In this research, BASHD experiments enable structural characterization of large heparin-derived oligosaccharides and peptides, which exhibit extensive resonance overlap. For heparin-derived oligosaccharides, the anomeric proton region was selectively excited and decoupled in the F_1 dimension; while the NH region of peptides was selectively excited and decoupled.

The spectral bandwidth of the region to be selectively excited varied between 300 and 500 Hz. Excitation of such a narrow bandwidth significantly improves the digital resolution. Band selection in the F_1 dimension is achieved using a double pulse field gradient spin echo (DPFGSE) pulse sequence to refocus only the interested resonances. The band selective pulse used in a BASHD experiment is a phase-modulated q3 Gausian cascade pulse, which has superior selectivity, phase and amplitude characteristics.[21] Because the BASHD spectrum does not have a resonance corresponding to the chemical shift reference TMSP, the resonance for one of the anomeric protons was used as the reference.

The parameters for the BASHD experiments are almost the same as for the non-BASHD experiments with several exceptions. The band-selective power (selpwr) and the pulse width (selpw) must be determined. To obtain selpwr and selpw, a 1-D ^{1}H NMR spectrum was first acquired and the cursors were then placed at the two ends of the proton region to be excited. The selex macro was executed, which displayed the shape macro. Q3 was typed into the shape macro to bring up the phase-modulated q3 Gaussian cascade pulse to be used, which yielded the bandwidth (bw) and offset (off) values. The bw and off values were entered into the pxshape macro, which has the format

pxshape('q3 bw off','filename'). The pxshape macro output the slpwr in dB and selpw in msec for the selective shape. Selpw was converted to μsec before inputting in the computer. The number of points collected in the F_2 dimension was either 4096 or 8192. The number of transients was 64, and the number of t_1 increments (ni) was either 64 or 128. Lastly, the spectral width in the indirectly detected dimension (sw1) was calculated by adding 100 Hz to the bandwidth (bw) that covered the region of protons to be excited. The pulse sequences for the BASHD-TOCSY, BASHD-ROESY and BASHD-NOESY experiments are shown in Figures 2.11, 2.12 and 2.13, respectively.
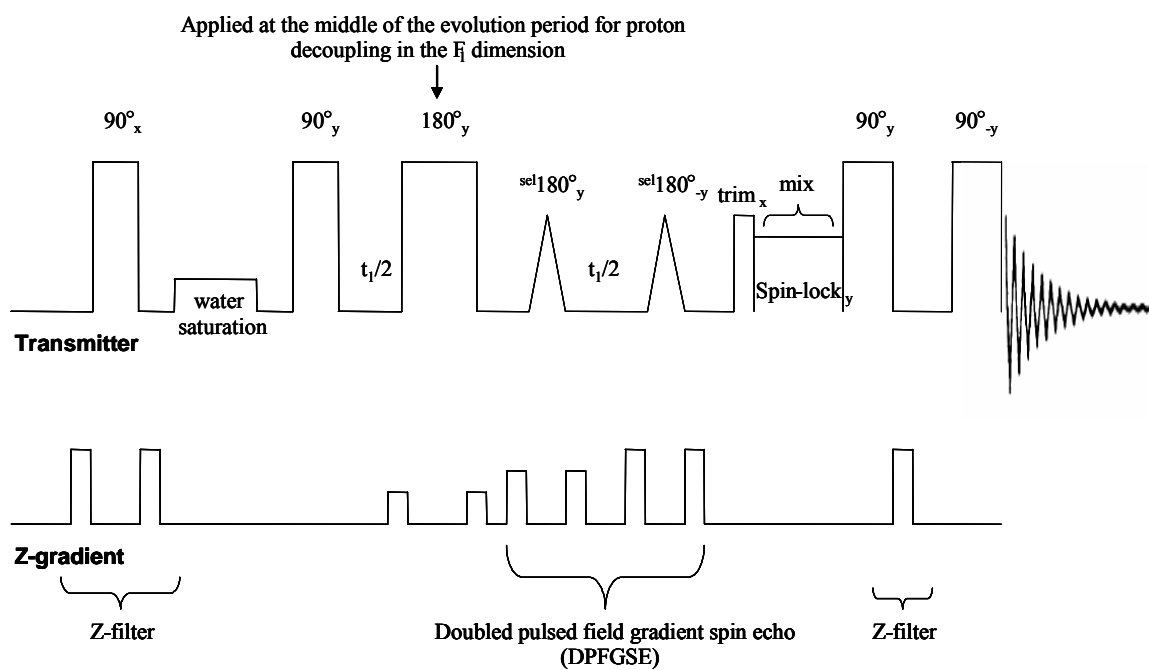
Figure 2.11. 2-D BASHD-TOCSY pulse sequence.

Applied at the middle of the evolution period for proton
decoupling in the F_1 dimension

$90°_x$ $90°_y$ $180°_{-y}$ $^{sel}180°_y$ $^{sel}180°_{-y}$ mix $90°_y$ $90°_{-y}$

$t_1/2$ $t_1/2$ Spin-lock $_x$

water
saturation

Transmitter

Z-gradient

Z-filter   Doubled pulsed field gradient spin echo
(DPFGSE)   Z-filter
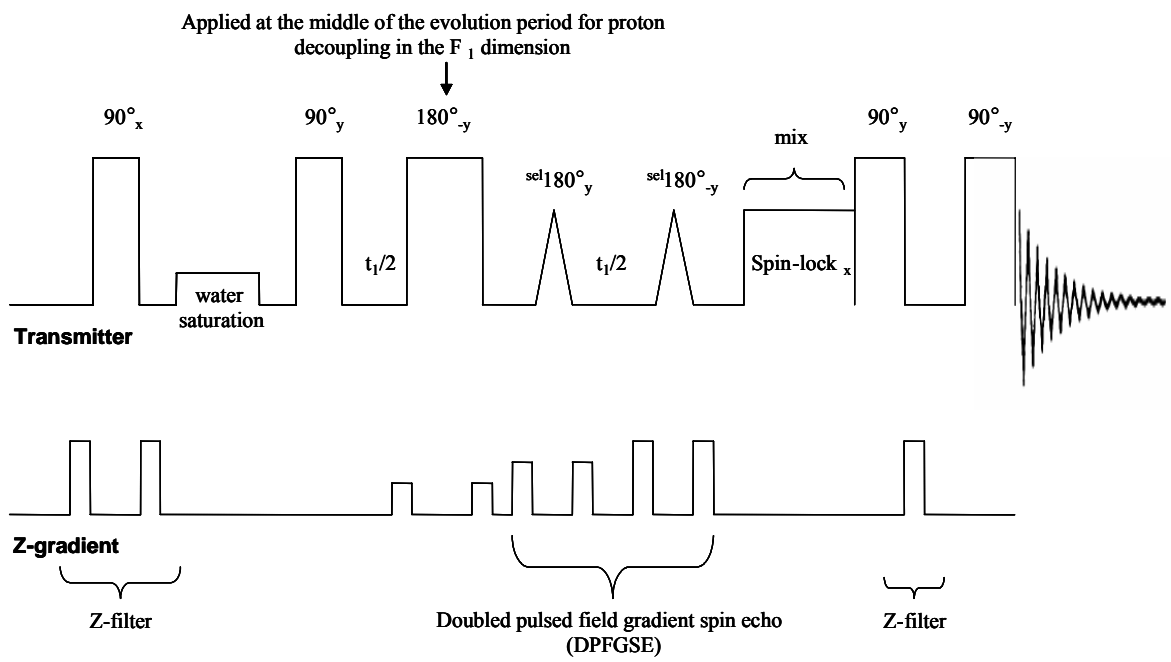
Figure 2.12. 2-D BASHD-ROESY pulse sequence.
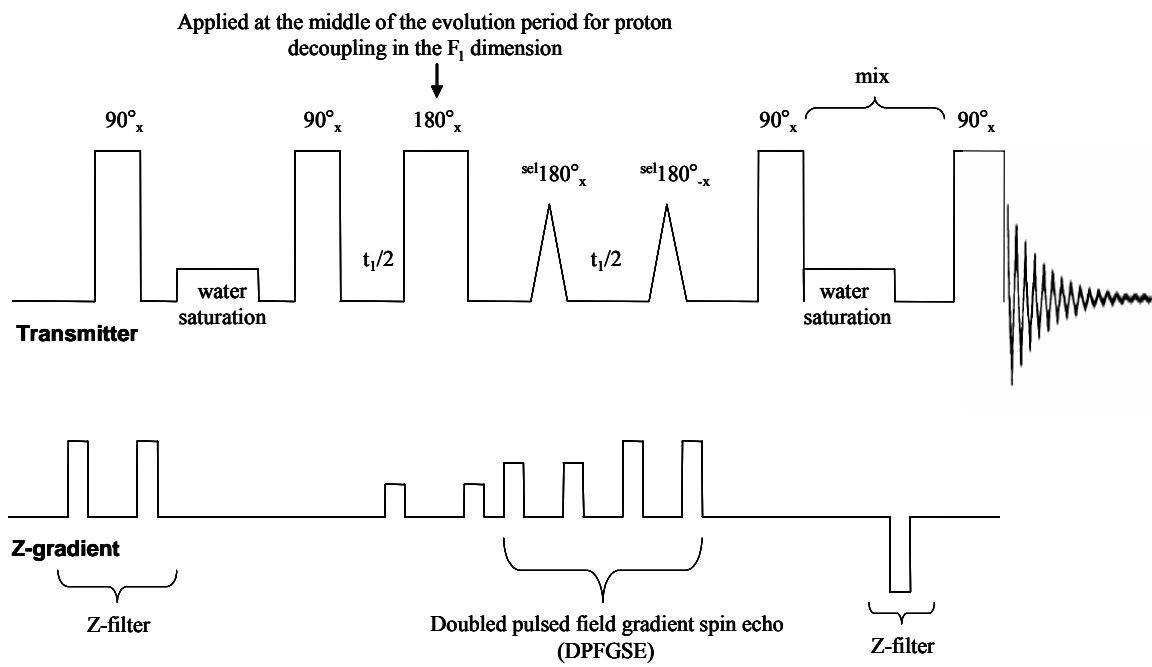
Figure 2.13. 2-D BASHD-NOESY pulse sequence.

2.8.5 NMR Data Processing

1-D NMR spectra were processed without apodization. Linear prediction and zero filling in the F_1 dimension were done on all 2-D spectra using the custom made macros 'lpset' and 'tsu'. The 'tsu' macro contains the following set of commands: center, f full, pmode='full', rp1=0, lp1=0, lsfrq=0, lsfrq1=0, refpos=0, refpos1=0, parfidss, ssfilter=100, sb='n', sbs='n', fn=np, lpset, sb1=-(lpext1+1)/sw1, sbs1=sb1, and dg. The 'lpset' macro is given in the box below:

LPSET-setup parameters for linear prediction in the F_1 dimension

parlp(1) lpopt1='f' lpfilt1=8 $1=ni lpnupts1=$1
strtlp1=$1 strtext1=$1+1 lpext1=(4*$1-$1) $2=2*(lpext1+strtlp1)
if   64>$2≥1 then fn1=64 else
if   128≥$2>64 then fn1=128 else
if   256≥$2>128 then fn1=256 else
if   512≥$2>256 then fn1=512 else
if 1024≥$2>512 then fn1=1024 else
if 2048≥$2>1024 then fn1=2048 else
if 4096≥$2>2048 then fn1=4096 else
if 8192≥$2>4096 then fn1=8192 else
Endif endif endif endif endif endif endif endif
proc1='lp'

After Fourier transformation of the ni spectra (the t_2 dimension of the t_1-t_2 data set), the 'lpset' macro predicts the "FID" in the t_1 dimension that is three times the number of points collected (ni), adds these points to the FID and then zero fills it to the fn1 value. For instance, if the number of increments (ni) was set to be 64 then 192 data points were added to each t_1 "FID" to produce a 256 point "FID". This FID was then

zero-filled by adding zero-intensity data points to the end of the FID to give a Fourier

number in the indirectly detected F_1 dimension (fn1) of 512 data points.

2-D spectra were automatically apodized in the F_1 dimension by executing the

"tsu" macro, which was also set up to apply a combination of the sine bell (sb1) and

shifted sine bell (ssb1) apodization functions; sb1 = -(lpext1 + 1) / sw1, sbs1 = sb1. A

gaussian weighting function was manually applied in the F_2 dimension to force the FID to

zero at the point that the FID disappeared into the noise.

For BASHD experiments, the frequency shift in the F_1 dimension (lsfrq1)

parameter was adjusted manually via trial and error until the bandwidth being selectively

excited was centered on the F_1 dimension of the contour plot.

2.8.6 Determination of pK$_a$ Values by NMR

Heparin-derived oligosaccharides contain multiple carboxylic acid groups (Figure

2.14). A specific pK$_a$ value can be determined for each carboxylic acid group by [1]H

NMR. As a proton is titrated off a functional group, the chemical environment and thus

the chemical shift of nuclei near by the functional group are affected. The affected proton

is called the 'reporter' proton (see Figure 2.14), where the change in its chemical shift is

monitored as the pD of the sample solution is varied. This generates a chemical shift-pD

titration curve from which the pK$_a$ value of the carboxylic acid group can be calculated. It

should be noted that the acidic proton of the carboxylic acid group being titrated cannot

be monitored directly since it is constantly exchanging with the solvent.

Before the chemical shift of the resonance was plotted versus pD to determine

pK$_a$ value, it was corrected since the chemical shift of the trimethyl protons of the

Reporter protons

Carboxylic acid groups (pK_a = 3 - 4)

Sulfonic acid groups
pK_a of OSO_3^- < 1
pK_a of NSO_3^- = 1.0 - 1.5
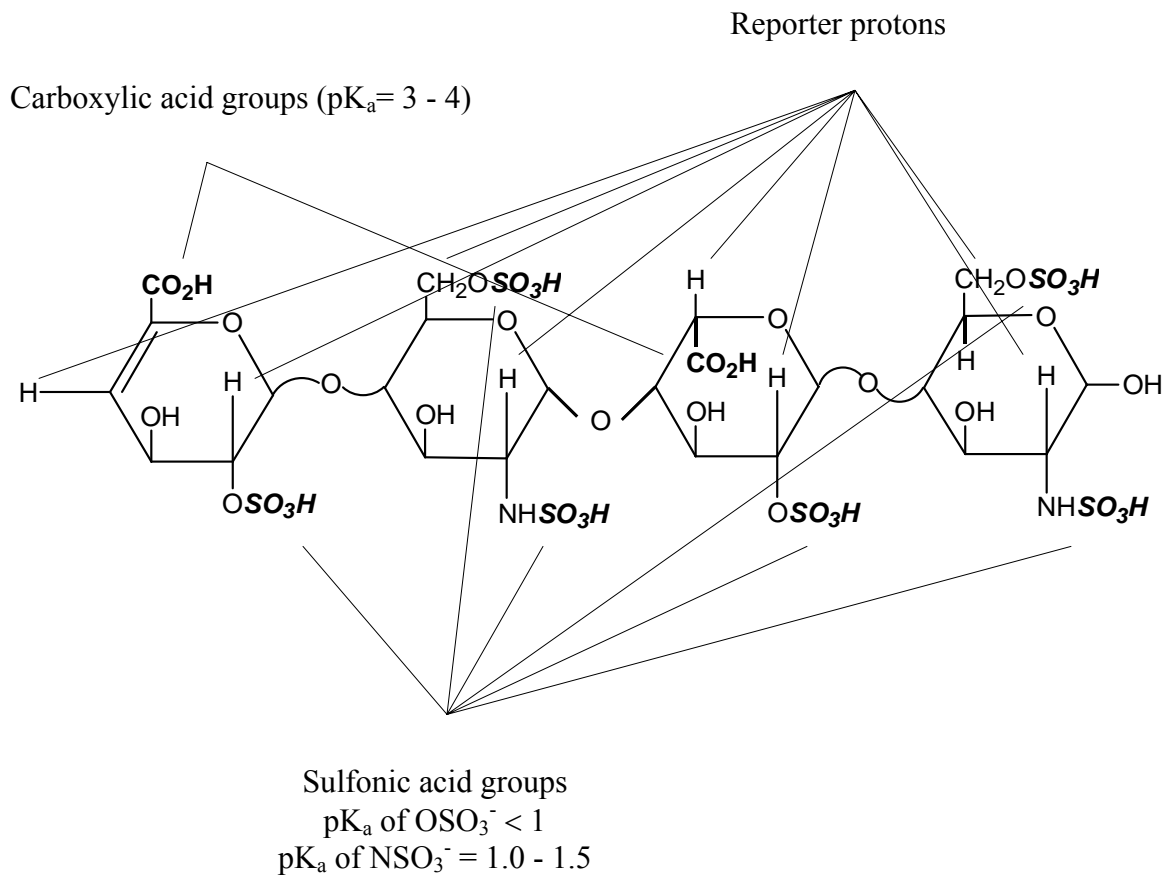
Figure 2.14. Acidic groups and reporter protons of a fully sulfated heparin-derived tetrasaccharide.

chemical shift reference is pD dependent.[22] The pD dependence of TMSP is accounted

for with the following equation:

$$\delta = \delta_{observed} - \frac{0.019}{1 + 10^{(5.0 - pD)}} \qquad (2.2)$$

where δ is the corrected chemical shift of the resonance and $\delta_{observed}$ is the chemical shift

of the resonance relative to the TMSP reference.

2.8.6.1 Monoprotic Acid Model

In determining the pK_a of a carboxylic acid group, titration data points were

collected at 25 °C as the pD of the sample solution was increased from 2 to 11. The pD of

the sample was adjusted to the desired pD by adding a few µL of 0.1 M NaOD directly

into the NMR tube. The top of the tube was sealed with parafilm and was shaken. 1-D ^1H

and 2D-TOCSY and/or BASHDTOCSY spectra were measured to obtain the chemical

shift of the 'reporter' proton at each pD value. The observed chemical shift of the

'reporter' proton (δ_{Obs}) is a function of the fractional concentrations of carboxylate and

carboxylic acid forms (f_{A^-} and f_{HA}, respectively):

$$\delta_{Obs} = \delta_{A^-} f_{A^-} + \delta_{HA} f_{HA} \qquad (2.3)$$

where δ_{A^-} is the chemical shift of the 'reporter' proton when the carboxylic acid group

has been fully titrated (upper pD limit), δ_{HA} is the chemical shift of the 'reporter' proton

prior to titration (lower pD limit). The acid dissociation constant (K_a) is defined as

follows:

$$HA \leftrightarrow H^+ + A^-$$

$$K_a = \frac{[H^+][A^-]}{[HA]} \qquad (2.4)$$

The fractional concentrations f_{A^-} and f_{HA} can be expressed as follows:

$$f_{A^-} = \frac{[A^-]}{[HA] + [A^-]} \qquad (2.5)$$

$$f_{HA} = \frac{[HA]}{[HA] + [A^-]} \qquad (2.6)$$

$$f_{A^-} + f_{HA} = 1 \qquad (2.7)$$

Combining equations 2.3, 2.4, 2.5, 2.6 and 2.7 gives an equation for δ_{Obs} in terms of only pH, K_a and chemical shift.

$$\delta_{Obs} = \left(\frac{[H^+]}{[H^+] + K_a} \right) \delta_{HA} + \left(\frac{K_a}{[H^+] + K_a} \right) \delta_{A^-} \qquad (2.8)$$

The K_a value of a carboxylic acid was obtained by fitting titration data to equation 2.8 using the nonlinear least squares program Scientist.[23] In the nonlinear least squares fit, pD is the independent variable while δ_{Obs} is the dependent variable. A rough estimate is first given for the parameters, δ_{A^-}, δ_{HA} and K_a, which are then refined by the Scientist program. Figure 2.15 shows an example of a chemical shift-pD titration curve for C4H of the unsaturated uronic acid residue of a fully sulfated heparin-derived tetrasaccharide.

2.8.6.2 Diprotic Acid Model

The chemical shift of the C3H proton (see the bottom of Figure 2.16) of the glucosamine residue located between the nonreducing end residue and the IdoA(2S) residue of a fully sulfated heparin-derived tetrasaccharide was monitored during the course of the titration of the tetrasaccharide free in solution. It was observed that the
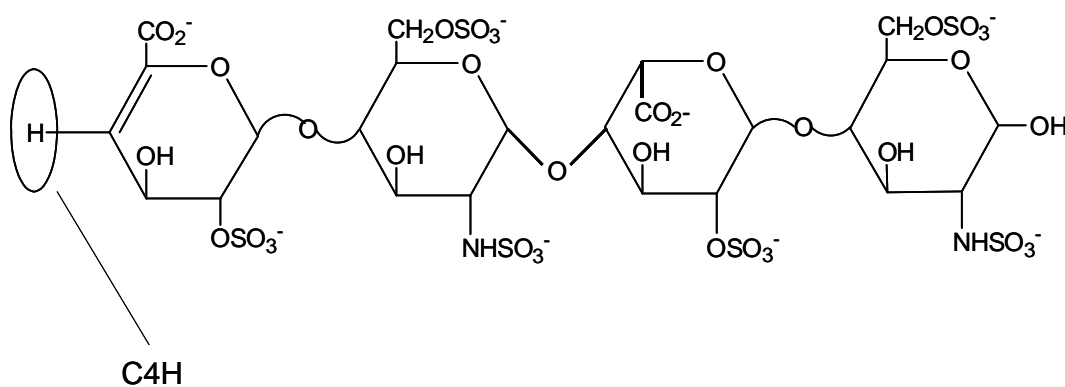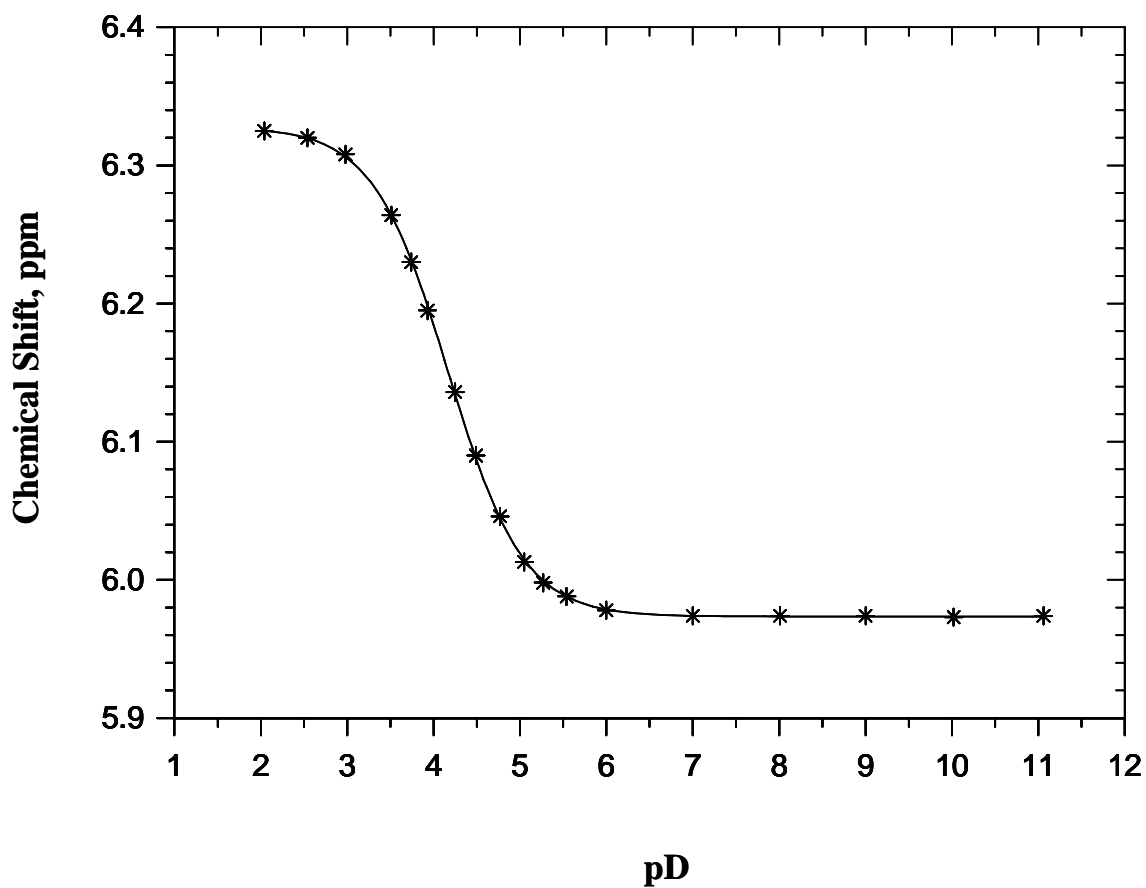
Figure 2.15. The chemical shift-pD titration curve for C4H (in circle) of the unsaturated

uronic acid residue of a fully sulfated heparin-derived tetrasaccharide free in solution

with the total Na^+ concentration of 0.020M.
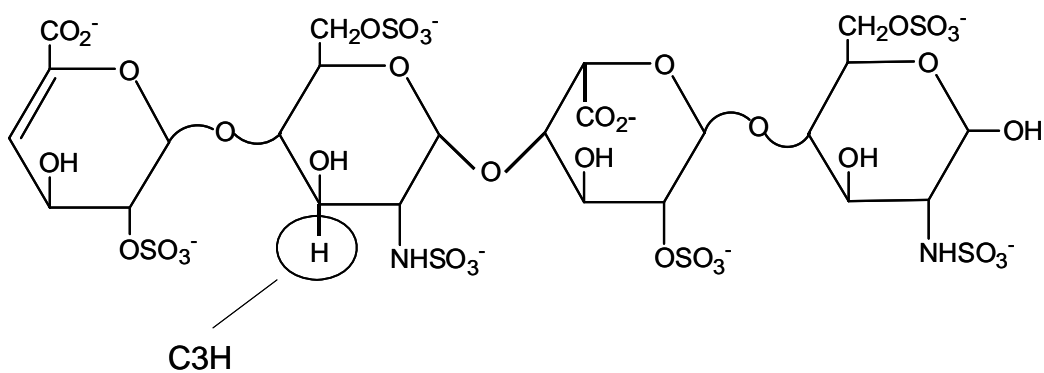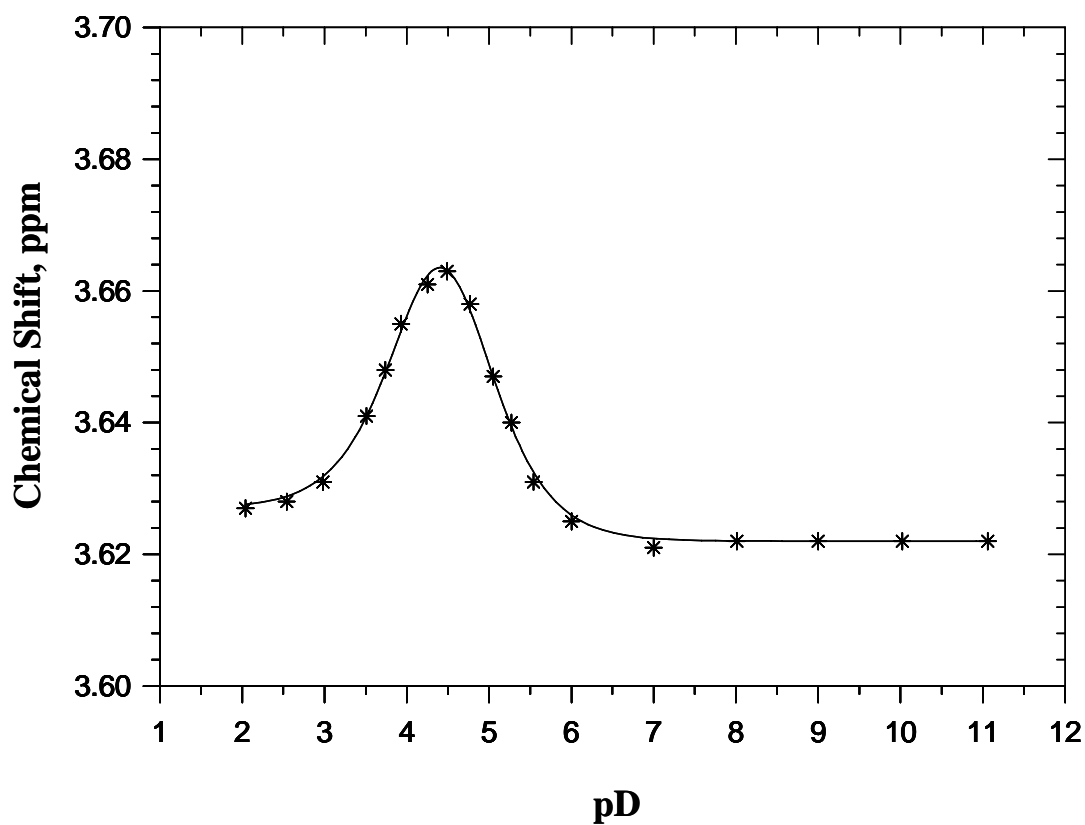
Figure 2.16. The chemical shift-pD titration curve for C3H proton (in circle) of the glucosamine residue of a fully sulfated heparin-derived tetrasaccharide free in solution.

chemical shift of the C3H proton changed as the two carboxylic acid groups of the two I residues were titrated. The carboxylic acid group of the nonreducing end residue was titrated first due to its lower pK_a value compared to that of the IdoA(2S) unit as determined by the monoprotic acid model.

The diprotic acid model used to fit the chemical shift-pD titration data of the C3H proton of the glucosamine residue is derived as follows:

$$H_2A + H_2O \leftrightarrow HA^- + H_3O^+$$

$$K_{a1} = \frac{[HA^-][H_3O^+]}{[H_2A]} = \frac{[HA^-]}{[H_3O^+]} \tag{2.9}$$

$$HA^- + H_2O \leftrightarrow A^{2-} + H_3O^+$$

$$K_{a2} = \frac{[A^{2-}][H_3O^+]}{[HA^-]} \tag{2.10}$$

where K_{a1} and K_{a2} are acid dissociation constants for the carboxylic acid groups of the nonreducing end and IdoA(2S) rings, respectively.

The fractional concentrations f_{H2A}, f_{HA-} and f_{A2-} can be expressed as follows:

$$f_{H2A} = \frac{[H_2A]}{D} = \frac{[H_3O^+]^2}{D} \tag{2.11}$$

$$f_{HA-} = \frac{[HA^-]}{D} = \frac{K_{a1}[H_3O^+]}{D} \tag{2.12}$$

$$f_{A2-} = \frac{[A^{2-}]}{D} = \frac{K_{a1}K_{a2}}{D} \tag{2.13}$$

where $D = [H_2A] + [HA^-] + [A^{2-}] = [H_3O^+]^2 + K_{a1}[H_3O^+] + K_{a1}K_{a2}$ (2.14)

The observed chemical shift of the C3H proton (δ_{Obs}) as a function of pD is given by

equation 2.15:

$$\delta_{Obs} = f_{H2A}\delta_{H2A} + f_{HA^-}\delta_{HA^-} + f_{A2^-}\delta_{A2^-}$$ (2.15)

where δ_{H2A} is the chemical shift of the C3H proton prior to titration of the first acidic

proton, δ_{HA^-} is the chemical shift of the C3H proton after the first acidic proton has been

titrated, and δ_{A2^-} is the chemical shift when the acidic protons of the two carboxylic acid

groups have been fully titrated.

Combining equations 2.11, 2.12, 2.13, 2.14 and 2.15 gives an equation for δ_{Obs} in

terms of only pD, K_{a1}, K_{a2} and the chemical shifts of indicated forms. δ_{H2A} and δ_{A2^-} are

known from the chemical shifts at the low and high pD ends of the titration curve.

$$\delta_{Obs} = \frac{1}{[H_3O^+]^2 + K_{a1}[H_3O^+] + K_{a1}K_{a2}}\left([H_3O^+]^2\delta_{H2A} + K_{a1}[H_3O^+]\delta_{HA^-} + K_{a1}K_{a2}\delta_{A2^-}\right)$$

(2.16)

The chemical shift-pD titration data for the C3H proton were fit to equation

2.16.[24] In the Scientist program, pD is the independent variable while δ_{Obs} is the

dependent variable. A rough estimate was given for δ_{HA^-}, K_{a1} and K_{a2}, which were then

refined by Scientist program. The smooth curve through the points in Figure 2.16 is the

fit of the chemical shift-pD titration data for the C3H proton to the diprotic acid model.

The nonlinear least squares fit of the data yielded values of 4.17 and 4.69 for pK_{a1} and

pK_{a2}.

2.8.7 Measurement of Binding Constants by NMR

In this research, imidazole, histamine, L-histidine and histidine-containing

peptides were found to bind site specifically to a fully sulfated heparin-derived

tetrasaccharide. The chemical shift of the C3H proton (see Figure 2.17) of the glucosamine residue located between the nonreducing end sugar ΔUA(2S) and the IdoA(2S) residue of the tetrasaccharide changed upon binding of the imidazolium side chain to the tetrasaccharide.

The first step in determining a binding constant for the interaction of a ligand with the tetrasaccharide was to obtain the chemical shift-pD titration curve for the C3H proton of the tetrasaccharide in solution with the binding ligand. Figure 2.17 shows the chemical shift titration curve for the C3H proton, for example, for the binding interaction of imidazole with a fully sulfated tetrasaccharide. The pH at which the ligand binds strongest to the tetrasaccharide was then determined by looking for the biggest change in the chemical shift value of the C3H proton from the titration curve. The binding constant was determined at this pD by measuring the chemical shift of the C3H proton as a function of the ligand : tetrasaccharide molar ratio. The concentration of the tetrasacchride was held constant while the concentration of the ligand was varied. It should be noted that for every binding study the chemical shift of the C3H resonance of tetrasaccharide was corrected using equation 2.2 before it was plotted versus the concentration of the ligand in order to determine the binding constant.

The binding constant K_{Bd} can be expressed according to the binding reaction below where T and HA^+ represent the free forms of the tetrasaccharide and the ligand, respectively:

$$T + HA^+ \leftrightarrow T\text{-}HA$$
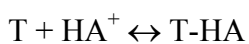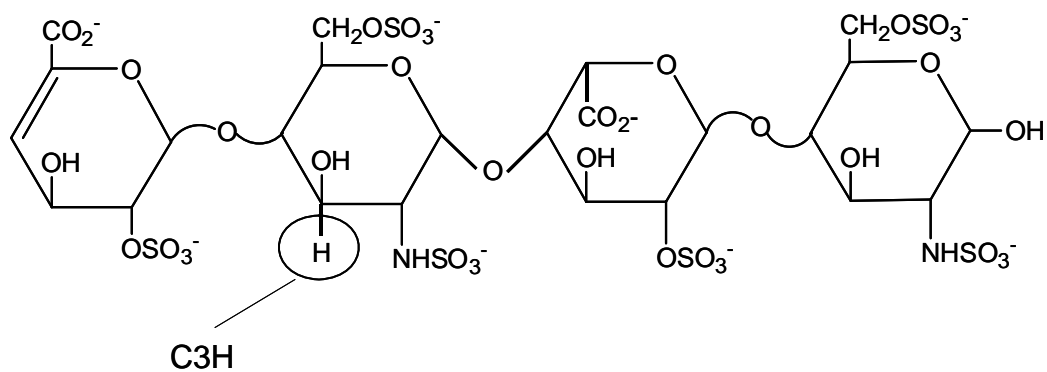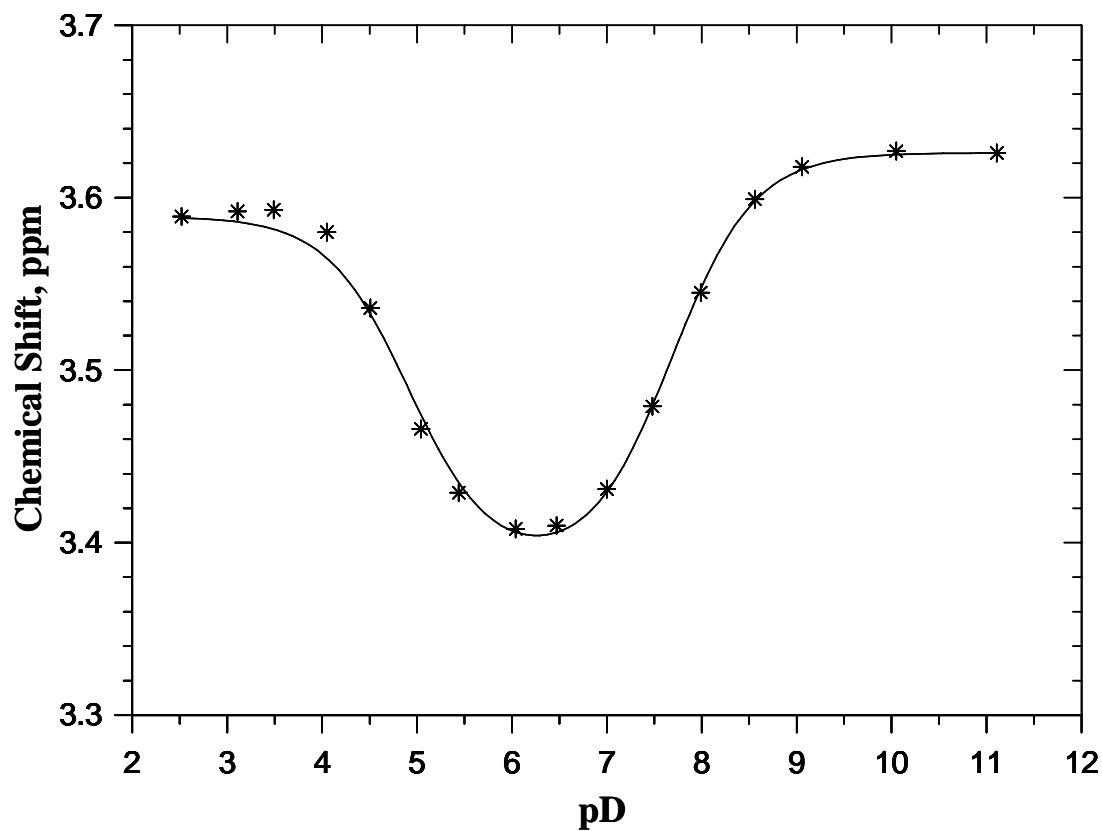
Figure 2.17. The chemical shift-pD titration curve for C3H proton (in circle) of the glucosamine residue of a fully sulfated heparin-derived tetrasaccharide in solution with imidazole. The tetrasaccharide concentration was 0.834 mM and the imidazole concentration was 33.4 mM. The tetrasaccharide : imidazole molar ratio of 1:40 was studied in D_2O solution with $[Na^+]_{total}$ of ~ 0.020 M.

$$K_{Bd} = \frac{[T - HA]}{[T][HA^+]} \qquad (2.17)$$

The concentration of the ligand in the free form [HA$^+$] is given by equation 2.18:

[HA$^+$] = [HA]$_t$ – [T-HA] = [HA]$_t$ – K$_{Bd}$[T][HA$^+$] $\qquad$ (2.18)

Rearranging equation 2.18 gives:

$$[HA^+] = \frac{[HA]_t}{1 + K_{Bd}[T]} \qquad (2.19)$$

where [HA]$_t$ is the total concentration of the ligand, which is known, and [T-HA] is the concentration of the ligand in the complex form. The total concentration of the tetrasaccharide [T]$_t$, which is also known, is expressed by equation 2.20:

[T]$_t$ = [T] + [T-HA] $\qquad$ (2.20)

where [T] is the concentration of the tetrasaccharide in the free form and [T-HA] is the concentration of the tetrasaccharide in the complex form. By substituting [T-HA] in terms of K$_{Bd}$, [T] and [HA$^+$], obtained from equation 2.17 into equation 2.20; [T]$_t$ can now be expressed as follows:

[T]$_t$ = [T] + K$_{Bd}$[T][HA$^+$] $\qquad$ (2.21)

Further substitution of [HA$^+$] in terms of [HA]$_t$, K$_{Bd}$ and [T] as expressed by equation 2.19 into equation 2.21, [T]$_t$ is now expressed as follows:

$$[T]_t = [T] + K_{Bd}[T]\frac{[HA]_t}{1 + K_{Bd}[T]} \qquad (2.22)$$

Rearrangement of Equation 2.22 gives equation 2.23, which has the form of a quadratic equation (AX^2 + BX + C = 0):

$$K_{Bd}[T]^2 + \left(1 + K_{Bd}[HA]_t - K_{Bd}[T]_t\right)[T] - [T]_t = 0 \qquad (2.23)$$

Let:

$$B = 1 + K_{Bd}[HA]_t - K_{Bd}[T]_t \qquad (2.24)$$

Then:

$$[T] = \frac{-B + \sqrt{B^2 - [4K_{Bd}(-[T]_t)]}}{2K_{Bd}} \qquad (2.25)$$

The fractional concentrations of the tetrasaccharide in the free form (f_f) and the complex

form (f_c) are given by equations 2.26 and 2.27:

$$f_f = \frac{[T]}{[T]_t} \qquad (2.26)$$

$$f_c = \frac{[T - HA]}{[T]_t} \qquad (2.27)$$

Since $f_f + f_c = 1$ therefore:

$$fc = 1 - \frac{[T]}{[T]_t} \qquad (2.28)$$

Binding constants were calculated by a nonlinear least squares fit of the observed

chemical shift of the C3H proton (δ_{Obs}) as a function of the total concentration of the

ligand to the model equation 2.29 below:

$$\delta_{Obs} = f_f \delta_f + f_c \delta_c \qquad (2.29)$$

where δ_f is the chemical shift of the C3H proton of the tetrasaccharide free in solution at

the pD where the binding is strongest (this value of δ_f is known); and δc is the chemical

shift of C3H proton of the tetrasaccharide-ligand complex, which is unknown. The data

were fit with Scientist program, where $[HA]_t$ was the independent variable; while δ_{Obs}

was the dependent variable. δ_c, and K_{Bd}, the parameters determined by fitting, were

estimated first and then the software refined the values according to the least squares of

the residuals criterion. Figure 2.18 shows the binding curve for the interaction of a fully

sulfated heparin-derived tetrasaccharide with imidazole at pD 3.00 ± 0.08. The nonlinear

least squares fit of the data yielded a binding constant of 11 ± 5 M^{-1}.

2.9 Isothermal Titration Calorimetry (ITC) [25-28]

2.9.1 ITC Theory

Microcalorimetry can be used to study all types of binding reactions including

protein-protein, protein-DNA, protein-ligand, receptor-target and DNA-drug binding,

since heat is either released or absorbed in essentially all binding events. It is the method

of choice for measuring the thermodynamic parameters that characterize interacting

molecules. A single ITC experiment affords the independent variables binding enthalpy

(ΔH), binding constant (K_B) and the number of binding sites (n), as well as the dependent

variables entropy (ΔS) and free energy (ΔG).

In a typical ITC experiment, a solution of a ligand is titrated against a solution of

a binding partner or vice versa at a constant temperature. A computer controlled power

compensation mechanism is used to maintain the temperature constant. The ITC unit has

two cells: a reference cell and a sample cell. The heat released or absorbed upon

interaction of the ligand with its binding partner is reflected by a temperature difference

between the reference cell and the sample cell, which is monitored over time by a

thermopile thermal detector. The major heat change experienced in the sample cell arises

from the binding interaction. A minor contribution to the change in heat comes from the

background heat of dilution of titrant experienced in the titration cell.
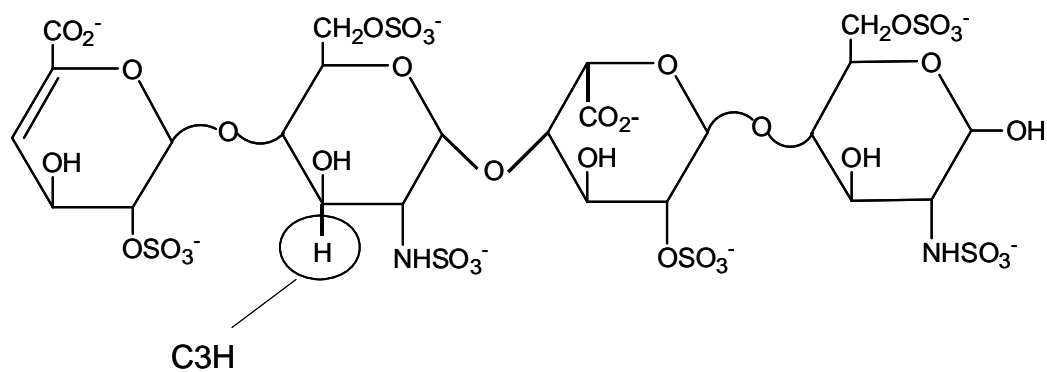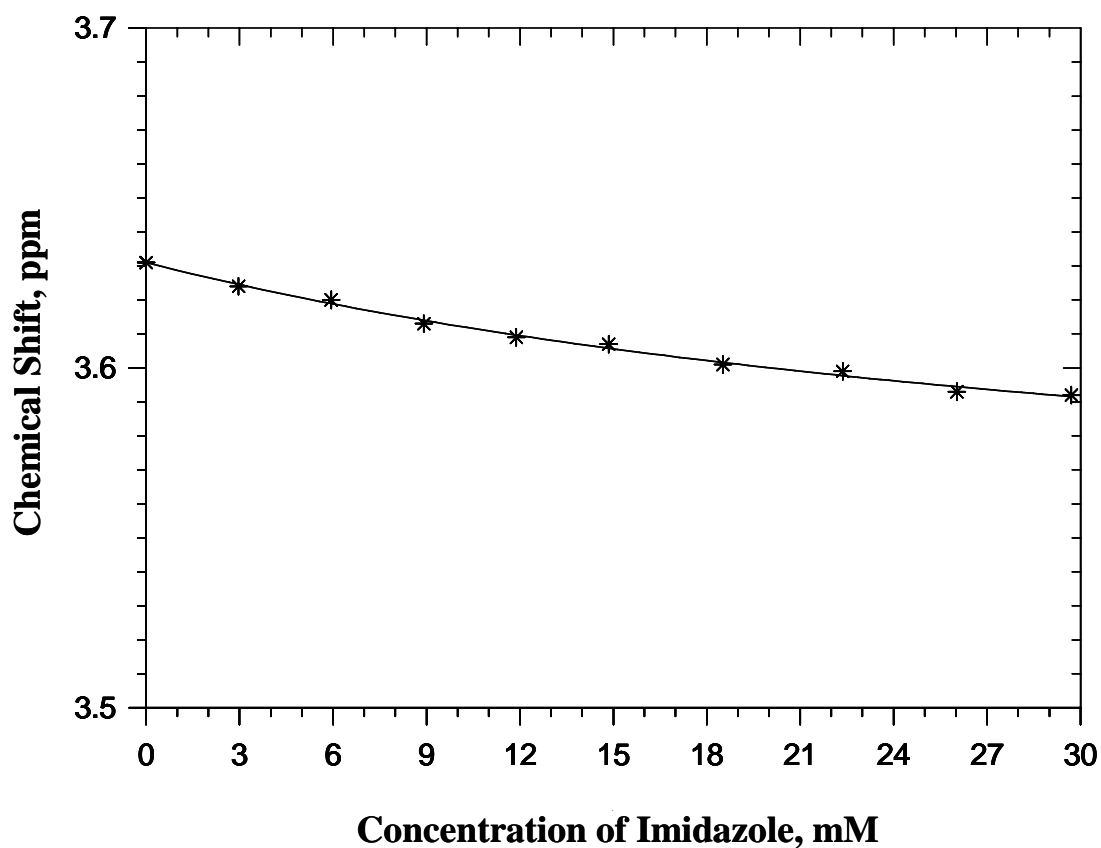
Figure 2.18. The chemical shift-concentration titration curve for C3H proton (in circle) of the glucosamine residue of a fully sulfated heparin-derived tetrasaccharide binding to imidazole at pD 3.00 ± 0.08. The concentration of tetrasaccharide was fixed (0.834 mM) while the concentration of imidazole was varied.

The heat involved in the interaction is a function of the molar ratio of the ligand and its binding partner as well as the binding affinity of the interaction. The titration data is composed of a series of peaks as shown in Figure 2.19. The area under each peak represents the amount of heat absorbed or generated following each addition of titrant. As the system reaches saturation, the signal diminishes until only the background heat of dilution is observed. A binding curve (Figure 2.20) is then obtained from a plot of the heats from each injection against the ratio of the ligand and its binding partner. Fitting the binding curve to an appropriate model allows determination of ΔH, K_B and n as well as ΔS and ΔG. The fitting model used in this research is described in the next section.

2.9.2 Single Set of Identical Binding Sites Model

The reaction stoichiometry n, binding constant K_B and molar heat of ligand binding ΔH reported in this dissertation were obtained by fitting experimental data to equation (2.34) below, the model for a single set of identical sites. In this model, the binding constant K_B is defined as follows:

$$K_B = \frac{\Theta}{(1-\Theta)[X]} \tag{2.30}$$

where Θ is fraction of sites occupied by ligand X and [X] is the free concentration of the ligand.

The bulk concentration (X_t) of the ligand was determined as follows:

$$X_t = [X] + n\Theta M_t \tag{2.31}$$

where M_t is the bulk concentration of the macromolecule. Substituting [X] in terms of K_B and Θ obtained from equation (2.30) into equation (2.31) gives
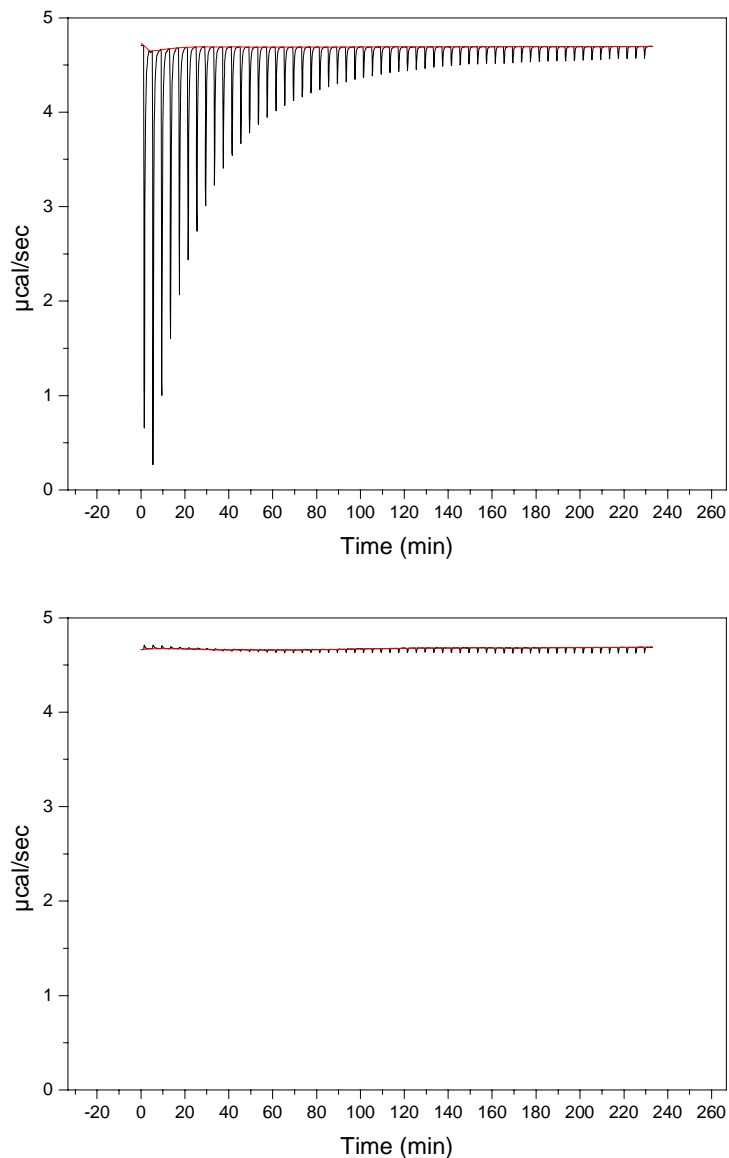
Figure 2.19. ITC raw data (top panel) for the titration of 0.378 mM β-amyloid peptide (FRHDSGY) with 2.48 mM heparin. Temperature 25 °C, buffer 20.0 mM sodium acetate, pH 5.63. The bottom panel shows the raw titration data for the background heat of dilution of titrant (heparin), which is subtracted from titration data in the top panel prior to fitting the data to obtain the binding constant and other parameters.
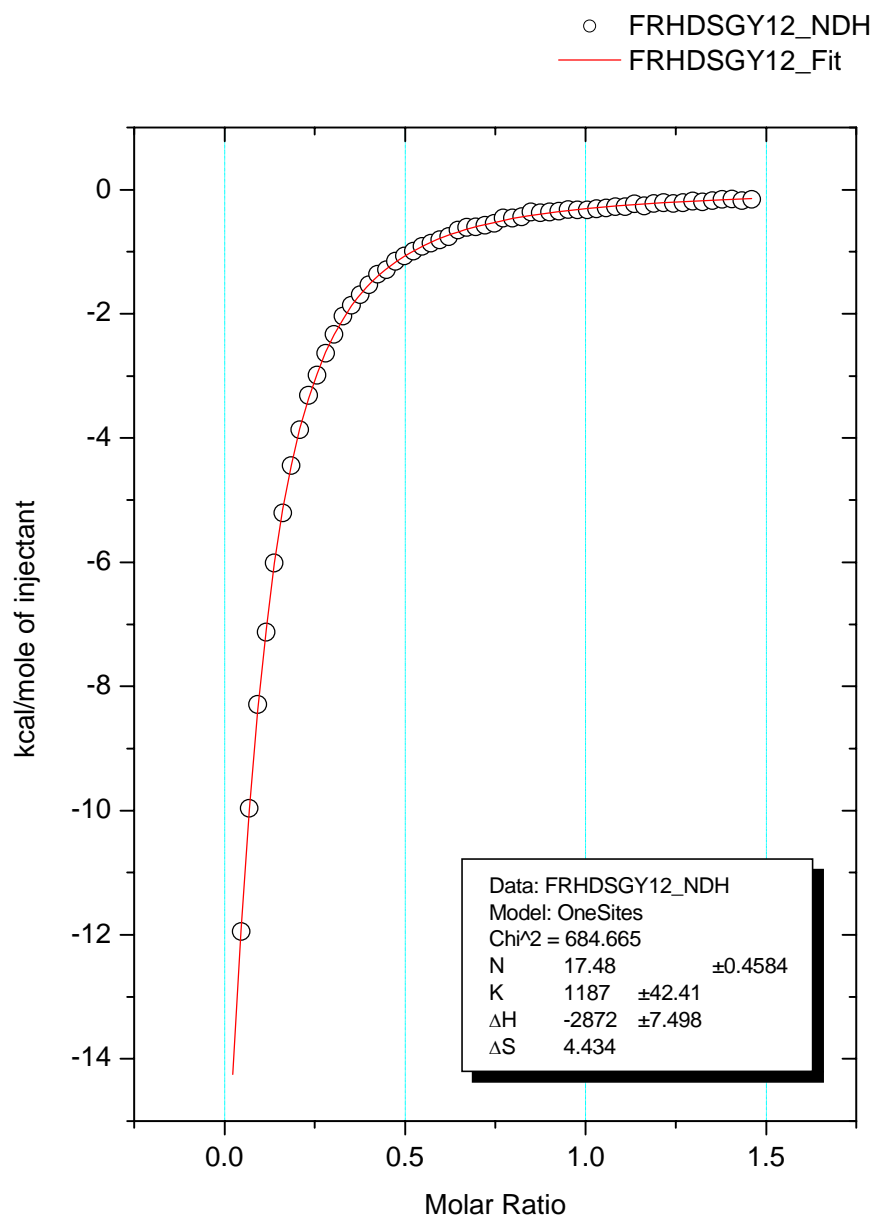
Figure 2.20. ITC fitted data for the titration of 0.378 mM β-amyloid peptide (FRHDSGY)

with 2.48 mM heparin. Temperature 25 °C, buffer 20.0 mM sodium acetate, pH 5.63.

$$\Theta^2 - \Theta\left(1 + \frac{X_t}{nM_t} + \frac{1}{nKM_t}\right) + \frac{X_t}{nM_t} = 0 \qquad (2.32)$$

The total heat content Q of the solution contained in the active cell volume V_0 at

fractional saturation Θ is:

$$Q = n\Theta M_t \Delta H V_0 \qquad (2.33)$$

The value of Θ obtained from solving the quadratic equation (2.32) is substituted into

equation (2.33), which then gives:

$$Q = \frac{nM_t \Delta H V_0}{2}\left[1 + \frac{X_t}{nM_t} + \frac{1}{nKM_t} - \sqrt{(1 + \frac{X_t}{nM_t} + \frac{1}{nKM_t})^2 - \frac{4X_t}{nM_t}}\right] \qquad (2.34)$$

The Q value is measured by the instrument. The heat content after any injection i is

designated as Q(i). The heat released, $\Delta Q(i)$, from the ith injection after a correction for

displaced volume, dV_i, is:

$$\Delta Q(i) = Q(i) + \frac{dV_i}{V_0}\left[\frac{Q(i) + Q(i-1)}{2}\right] - Q(i-1) \qquad (2.35)$$

The first step in the process of fitting experimental data is to guess the initial

values for n, K_B and ΔH, which is done by the Origin software (version 5.0). Next, the

software then calculates $\Delta Q(i)$ for each injection and compares it with the measured heat

for the corresponding experimental injection. The Origin software then improved the

initial values of n, K_B and ΔH. Iteration of this step-by-step procedure was performed

until no further improvement in fit occurs, as judged by the sum of the squares of the

residuals, in order to obtain best values for the three fitting parameters.

2.9.3 Sample Preparation

All ITC experiments were conducted at 25 °C on a VP-ITC MicroCalorimeter (Figure 2.21) manufactured by Microcal Inc. A bulk stock buffer solution (20 mM sodium acetate at various pH values) was prepared. Weighed amounts of heparin and the binding ligands (histamine and histidine-containing peptides) were dissolved in appropriate volumes of buffer to make sample solutions with desired concentrations. The sodium concentration was calculated from the mass of the sodium from the sodium acetate buffer solution. Sample solutions were degassed for 30 minutes prior to use with the ThermoVac Accessories unit to remove dissolved gases.

A minimum of 1.8 ml of ligand solution was drawn into a loading syringe, even though the working volume of the cell is only 1.4359 mL. After removing air bubbles from the syringe, the ligand solution was slowly loaded into the sample cell. The syringe plunger was pulled back and forth for at least 20 times to get rid of air bubbles clinging onto the edge of the sample cell. The excess solution above the rim of the sample cell was removed. Heparin titrant solution was loaded into the auto-pipette syringe injector (see Figure 2.22). The plunger was fully lowered and raised several times to purge air bubbles from the syringe injector.

2.9.4 ITC Titration Procedure

Prior to first use and between runs, the syringe injector was washed with 50 mL of 5% Contrad-70 solution followed by 200 mL of Millipore water and 50 mL of methanol by a vacuum setup. The injector was dried under vacuum to remove residual methanol. The reference and sample cells were cleaned with 5% Contrad-70 solution followed by
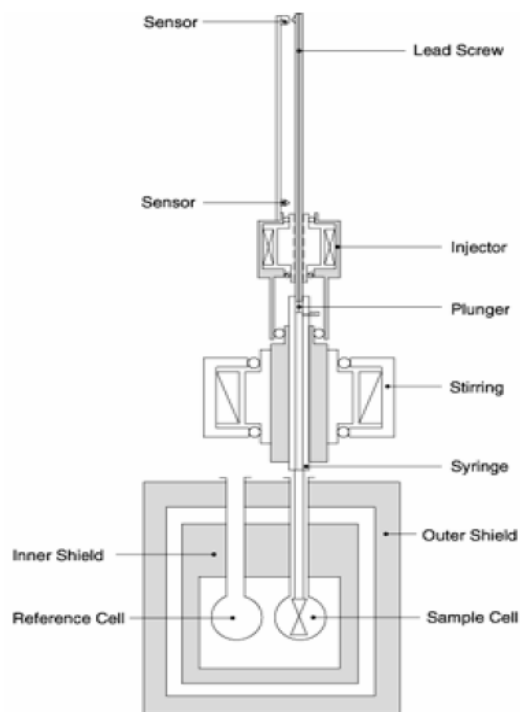
Figure 2.21. A schematic diagram of the isothermal titration calorimetry apparatus. In this research, the sample cell contains peptide (ligand) solution while the heparin (macromolecule) solution is loaded into the auto-pipette syringe injector as shown in Figure 2.22.
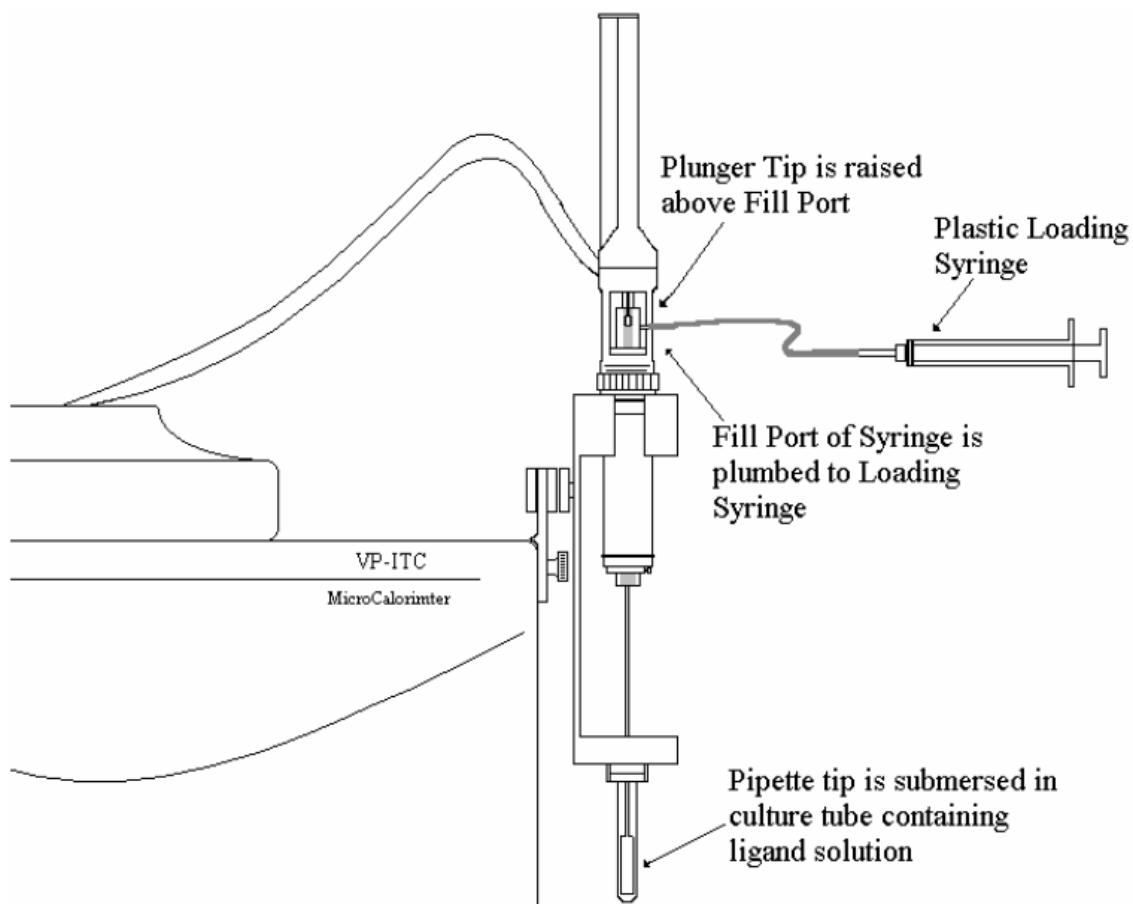
Figure 2.22. Schematic diagram of the auto-pipette syringe injector. The titrant is loaded

into the syringe injector by pulling the plastic syringe.

Millipore water and buffer solution, about 100 mL each.

Before injection the system was allowed to reach thermal equilibrium. The heparin solution in the syringe injector was injected into the sample cell according to the setup parameters involving injection volume, spin rate, injection rate and duration time. For each titration, 58 injections (5 μL per injection), an injection duration time of 10 seconds, a spacing time of 240 seconds between injections, and a stirring speed of 310 revolutions per minute were used.

Heat evolved or absorbed upon injecting the heparin solution into the ligand solution was measured. The reported binding constants are the average of at least three replicate measurements. For each experiment, the heat of dilution measured upon addition of heparin solution into the titration cell containing only the buffer solution was subtracted from the heat absorbed or released from the interaction of heparin with its binding ligand.

2.10 Heparin Affinity Chromatography [29-31]

Heparin affinity chromatography experiments were carried out on a Dionex 500 ion chromatography system equipped with a GP40 gradient pump and an AD20 UV/visible detector. The polyether ether ketone (PEEK) tubing and ceramic pump heads in the Dionex HPLC system makes it the HPLC of choice for binding affinity studies since a high salt buffer is required to elute imidazole, histamine and histidine-containing peptides from the heparin affinity column. The relative binding strengths of these ligands to heparin were determined by comparing their retention times. Elution of ligand from the heparin affinity column was monitored by measuring the absorbance at 215 nm. Elution

buffers of several pH values were used.

A HiTrap Heparin HP column (2.5 x 0.7 cm-i.d., column volume 1 mL) was used for affinity chromatography experiments. The column is packed with heparin covalently coupled to highly cross-linked spherical agarose beads via a N-hydroxysuccinamide coupling method. Before use the column was washed with 10 column volumes of mobile phase A (10 mM phosphate without NaCl) to remove the preservative as well as to equilibrate the column. Between runs the column was washed with 5 column volumes of mobile phase B (10 mM phosphate plus 1 M NaCl) followed by 10 column volumes of mobile phase A to equilibrate the column prior to the next injection. A linear gradient started out with 100% mobile phase A and an increase in the mobile phase B of 0.5 %/min was used with a flow rate of 0.6 mL/min.

2.11 References

1. Glasoe, P. K.; Long, F. A. J. *Phys. Chem.* **1960**, *64*, 188-190.

2. Rabenstein, D. L.; Bratt, P.; Peng, J. *Biochemistry* **1998**, *37*, 14121-14127.

3. Claridge, T. in *High-Resolution NMR Techniques in Organic Chemistry*, Elsevier Science Ltd., Kidlington, United Kingdom, **1999**, pp. 13-31, 277-337.

4. Braun, S.; Kalinoski, H.; Berger, S. *150 and More Basic NMR Experiments*, Wiley-VCH, Weinheim, Germany, **1998**, pp. 45-49, 401-412, 445-448.

5. Bax, A.; Davis, D. *J. Mag. Reson.* **1985**, *65*, 355-360.

6. Martin, G.; Zektzer, A. *Two-Dimensional NMR Methods for Establishing Molecular Connectivities*, VCH, Weinheim, Germany **1988**, pp. 303-316.

7. Braunschweiler, L.; Ernst, R. *J. Mag. Reson.* **1983**, *53*, 521-528.

8. Bax, A.; Davis, D. *J. Mag. Reson.* **1985**, *65*, 355-360.

9. Bothner-By, A.; Stephens, R.; Lee, J.; Warren, C.; Jeanloz, R. *J. Am. Chem. Soc.* **1984**, *106*, 811-813.

10. Bax, A.; Davis, D. *J. Magn. Reson.* **1985**, *63*, 207-213.

11. Hwang, T.; Shaka, A. *J. Am Chem Soc.* **1992**, *114*, 3157-3159.

12. Braunschweiler, R.; Roux, B.; Blackledge, M.; Griesinger, C.; Karplus, M.; Ernst, R. R. *J. Am. Chem. Soc.* **1992**, *114*, 2289-2302.

13. Neuhaus, D.; Williamson, M. *The Nuclear Overhauser Effect in Structural and Conformational Analysis*, VCH, Weinheim, Germany, **1989**, 312-327.

14. Neuhaus, D.; William, M. *The Nuclear Overhauser Effect in Structural and Conformation Analysis*, VCH, Weinheim, Germany, **1989**, 312-327.

15. Jeener, J.; Meirer, B.; Bachmann, P.; Ernst, R. *J. Chem. Phys*. **1979**, *71*, 4546-4563.

16. States, D.; Haberkorn, R.; Rubben, D. *J. Magn. Reson*. **1982**, *48*, 286-292.

17. Bodenhausen, G.; Kogler, H.; Ernst, R. *J Magn. Reson*. **1984**, *58*, 370-388.

18. Krishnamurthy, V. *Mag. Res. Chem*. **1997**, *35*, 9-12.

19. Krishnamurthy, V. *J. Mag. Res. B* **1996**, *113*, 46-52.

20. Kaerner, A; Rabenstein, D. *Mag. Res. Chem*. **1998**, *36*, 601-607.

21. Emsley, L; Bodenhausen, G. *J. Magn. Reson*. **1992**, *97*, 135-148.

22. Wishart, D. S.; Bigam, C. G.; Yao, J.; Abildgaard, F.; Dyson, H. J.; Oldfield, E.; Markley, J. L.; Sykes, B. D. *J. Biomolecular NMR*, **1995**, *6*, 135-140.

23. Rabenstein, D. L.; Hari, S. P.; Kaerner, A. *Anal. Chem*. **1997**, *69*, 4310-4316.

24. Rabenstein, D. L.; Bratt, P.; Peng, J. *Biochemistry* **1998**, *37*, 14121-14127.

25. Ladbury, J.; Chowdhry, B. *Biocalorimetry*, John Wiley & Sons Ltd. Chinchester, England, **1998**.

26. Wiseman, T.; Williston, S.; Brandts, J.; Lin, L. *Analytical Biochemistry*, **1989**, *179*, 131-137.

27. Freire, E.; Mayorga, O.; Straume, M. *Anal. Chem*. **1990**, *62*, 950A-959A.

28. Brandts, J.; Lin, L.; Wiseman, T.; Williston, S.; Yang, C. *American Laboratory* **1990**, *22*, 30.

29. Thanawiroon, C; Linhardt, R. *Journal of Chromatography A* **2003**, *1014*, 215-223.

30. Brunden, K. R.; Richter-Cook, N. J.; Chaturvedi, N.; Frederickson, R. C. A. *J. Neurochem*. **1993**, *61*, 2147-2154.

31. Matsumoto, R.; Sali, A.; Ghildyal, N.; Karplus, M.; Stevens, R. L. *J. Biol. Chem.* **1995**, *270*, 19524-19531.

Chapter 3

Preparation, Isolation, and Characterization of Heparin-Derived Oligosaccharides

3.1 Introduction

Incomplete biosynthetic modification of proteoglycan (PG) heparin by enzymes (Figure 1.6) gives rise to structural complexity and heterogeneity of heparin chains. Random and incomplete modification by N-deacetylase at an early stage of heparin biosynthesis is an example of the incomplete modification process.[1] Thus, identification of heparin-binding domains that interact with biological molecules (i.e. peptides/proteins) essentially requires the use of structurally well-defined heparin-derived oligosaccharides, which are prepared, isolated, and characterized as outlined in Scheme 3.1. Briefly, intact heparin is first depolymerized into heparin-derived oligosaccharides. Mixtures of heparin-derived oligosaccharides are then size fractionated by size exclusion chromatography. Size-uniform fractions of oligosaccharides are then separated by strong anion exchange chromatography. Homogenous fractions in terms of size and charge are desalted, and capillary zone electrophoresis is next used to check the purity of oligosaccharides. Structures of heparin-derived oligosaccharides are finally characterized by one- and two-dimensional ^{1}H NMR.

3.2 Separation of Heparin-Derived Oligosaccharides by Strong Anion Exchange High Performance Liquid Chromatography (SAX-HPLC)

Heparin-derived oligosaccharides reported in this dissertation were obtained by depolymerizing intact heparin using heparinase I, which cleaves a glucosamine-(1→4)-uronic acid glycosidic bond (Figure 3.1). Heparinase I, an enzyme isolated from

Heparin

Depolymerization

Heparin-Derived Oligosaccharide Mixture

Size-Exclusion Chromatography
"Separate oligosaccharides by size"

| Di- | Tetra- | Hexasaccharide | Etc |

Strong Anion Exchange HPLC
"Separate size-fractionated
oligosaccharides by charge"

| Pure Tetra-I | Pure Tetra-II | Pure Tetrasaccharide-III |

Desalting

CZE

1-D & 2-D ^{1}H NMR

"Lower [NaCl]"   "Purity Analysis"   "Structure Analysis"

Scheme 3.1. Outline of the procedures used for the preparation, separation, and

characterization of heparin-derived oligosaccharides.
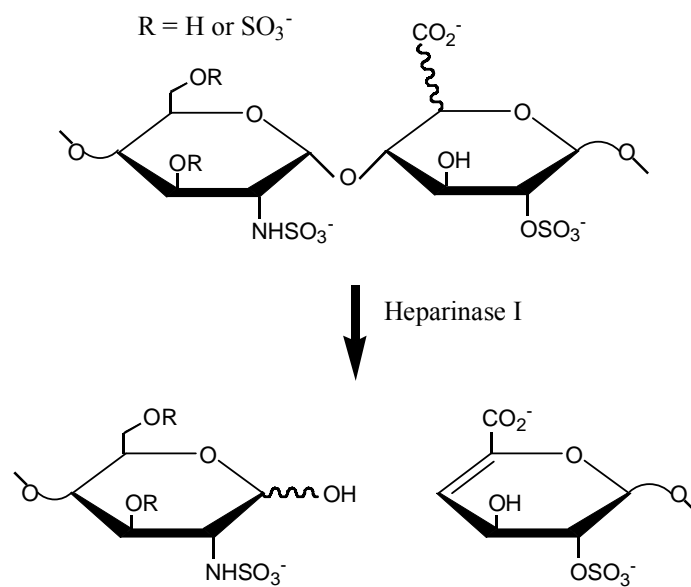
Figure 3.1. Scheme illustrating heparin being cleaved by heparinase I. Glucosamine residue can be GlcNS, GlcNS(6S), or GlcNS(3S, 6S) and uronic acid can be either IdoA(2S) or GlcA(2S).

flavobacterium heparinium, has high specificity for IdoA(2S) glycosidic bonds, where the glucosamine can be GlcNS, GlcNS(6S), or GlcNS(3S, 6S).[2, 3] It also cleaves GlcA(2S) glycosidic bonds in highly sulfated regions of heparin.[2] As seen from Figure 3.1, after the cleavage, the glucosamine residue remains intact; however, a terminal uronic acid with an unsaturated 4, 5 carbon bond is produced. The double bond on the unsaturated uronic acid (ΔUA) is a UV chromophore (absorbance maximum at 232 nm), which allows monitoring the progress of depolymerization and detecting oligosaccharides separated by GPC, SAX-HPLC, and CE. Heparin-derived oligsaccharides were fractionated by GPC on a 3 cm x 2 m column packed with Bio-Rad Bio-Gel P6 resin using 0.5 M NH_4HCO_3 as a mobile phase at a flow rate of 8-12 mL/hr.

In this work, size-uniform fractions of heparin-derived oligosaccharides obtained from GPC with degree of polymerization, i.e. the number of monosaccharide residues, ranging from 4 to 8 were separated on a semi-preparative (9 x 250 cm) CarboPac PA 1 column according to their charges. Separations of tetrasaccharides, hexasaccharides, and octasaccharides were performed at pH 3 to achieve the best resolution as well as to avoid oligosaccharides being modified under alkaline elution conditions.

Size-uniform heparin-derived tetrasaccharides, hexasaccharides, and octasaccharides were separated at a flow rate of 3.3 mL/min using a sodium chloride gradient where mobile phase A was a 70 mM pH 3 phosphate buffer in Millipore water and mobile phase B was a 2.0 M NaCl solution in 70 mM pH 3 phosphate buffer. Mobile phase B was increased at 2%/min for the first 10 min and then 0.5%/min thereafter. For tetrasaccharide, eluent peaks I, II, and III as seen from Figure 3.2 were collected and their
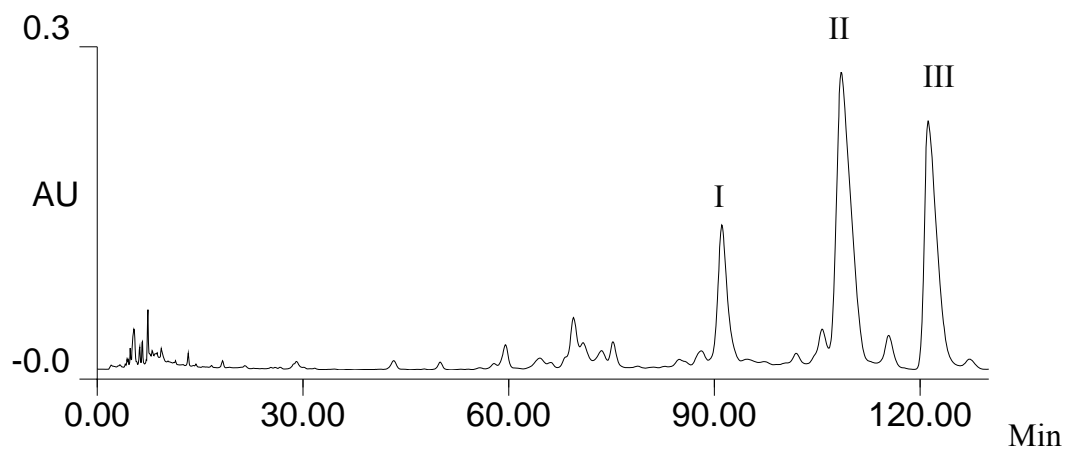
Figure 3.2. SAX-HPLC chromatogram of heparin-derived tetrasaccharide mixture on a semi-preparative CarboPac PA1 column.

structures were characterized using ^{1}H NMR. Eluent peaks identified by arrows in the chromatograms of hexasaccharide and octasaccharide in Figures 3.3 and 3.4, respectively, were collected, and their structures were also characterized by ^{1}H NMR.

The CarboPac PA 1 column provided highly reproducible elution profiles even after hundreds of injections, which allowed combining peaks eluted at similar retention times with confidence. Repetitive injections of the same sized heparin-derived oligosaccharide were performed to obtain enough sample for structural characterization and binding studies.

3.3 Desalting Oligosaccharides by Size Exclusion Chromatography (SEC)

Due to a large volume of oligosaccharide solution being collected from repetitive injections using SAX-HPLC, desalting was a daunting task. To ease the desalting step, sample solution from repetitive injections was combined and was diluted with Millipore water to lower the salt concentration to below 0.4 M. The diluted oligosaccharide solution was then pumped back onto the SAX column as the mobile phase. Because of the low salt concentration, the sample was trapped at the inlet of the column while salt was eluted off the column. The concentrated oligosaccharide was then eluted from the column using the same NaCl gradient that was used to separate the oligosaccharide mixture, as described in the previous section.

The collected concentrated oligosaccharide fractions were desalted online by connecting a custom-made SEC column (9 x 250 mm) packed with sephadex G-10 to the Dionex HPLC. The oligosaccharide was eluted with Millipore water at a flow rate of 3.3 mL/min. The desalting chromatogram of heparin-derived tetrasaccharide (peak III), for
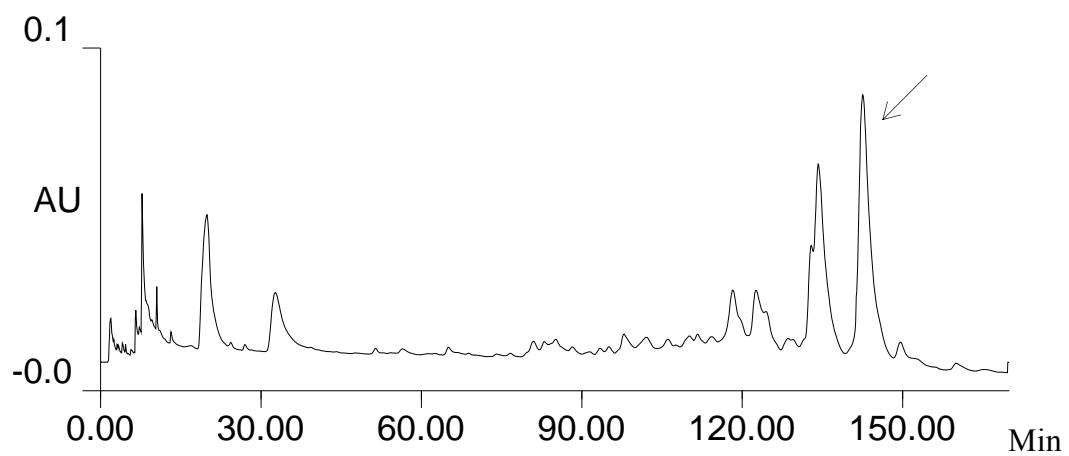
Figure 3.3. SAX-HPLC chromatogram of heparin-derived hexasaccharide mixture on a semi-preparative CarboPac PA1 column.
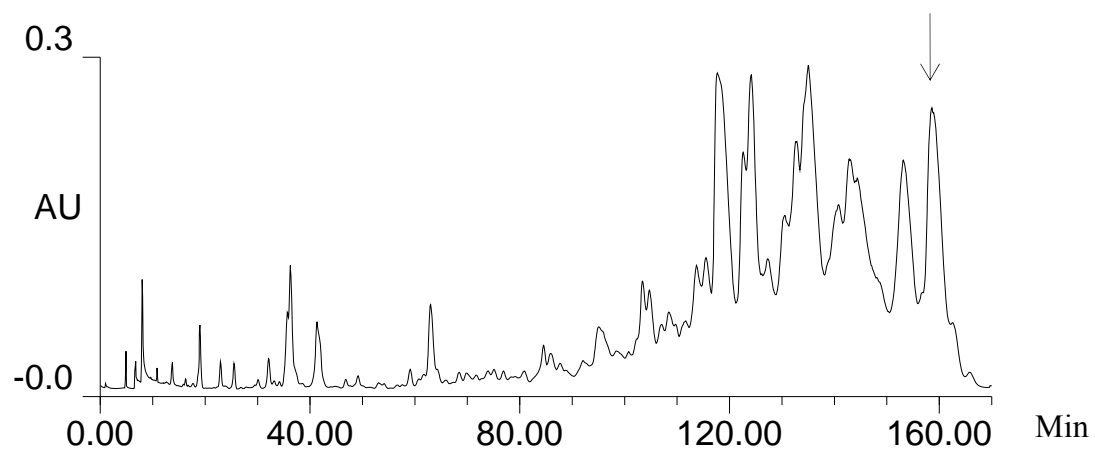
Figure 3.4. SAX-HPLC chromatogram of heparin-derived octasaccharide mixture on a semi-preparative CarboPac PA1 column.

example, is shown in Figure 3.5. Other heparin-derived oligosaccharides were desalted using the same desalting procedure.

3.4 Purity Assessment of Oligosaccharides by Capillary Zone Electrophoresis (CZE)

The purity of the heparin-derived tetrasaccharides obtained by collecting peaks I, II, and III from the SAX-HPLC separation was checked by CZE. Peaks I, II and III were analyzed on a custom-made silica capillary cartridge (i.d. 25 μm, o.d. 363 μm, $l_{det.}$ of 40 cm) at a constant voltage of 8 kV using 0.1 M phosphate buffer at pH 2.5. Figure 3.6 shows electropherograms of collected peaks I, II, and III and of the three peaks combined. The elution order of different tetrasaccharides agrees with the mass-to-charge ratio of each tetrasaccharide, which was calculated after its structure was determined by ^{1}H NMR (Table 3.1). The presence of a single peak in each electropherogram indicates that each collected SAX-HPLC peak is a pure tetrasaccharide, which makes it ready for NMR analysis.

Figure 3.7 shows an electropherogram of the octasaccharide peak obtained by SAX-HPLC with desalting. Separation of octasaccharide was performed on a custom-made silica capillary cartridge (i.d. 25 μm, o.d. 363 μm, $l_{det.}$ of 24 cm) at a constant voltage of 10 kV using 0.1 M phosphate buffer at pH 2.5. A single peak in the electropherogram suggests the octasaccharide is pure and ready for structural analysis.

3.5 Step-by-Step Procedure for Structural Characterization of Heparin-Derived Oligosaccharides by ^{1}H NMR

The first step in determining the structure of a heparin-derived oligosaccharide is
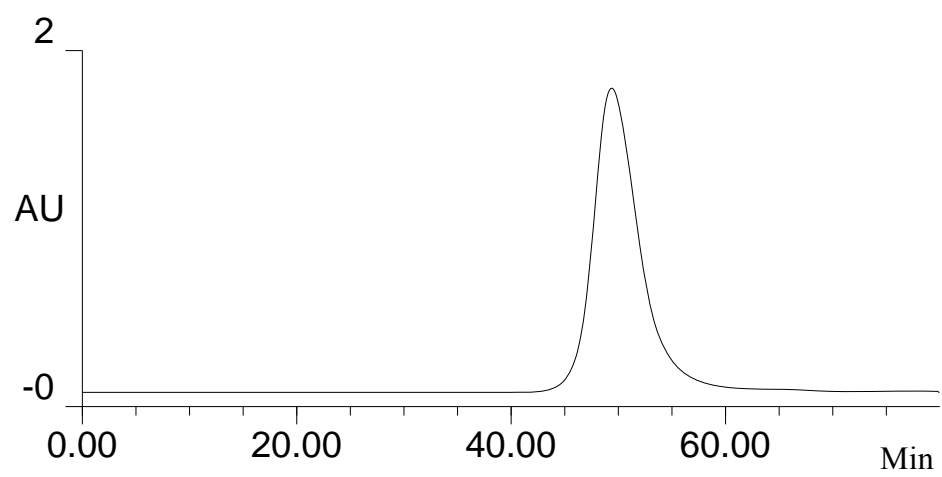
Figure 3.5. Desalting chromatogram of heparin-derived tetrasaccharide (peak III) obtained by size exclusion chromatography.
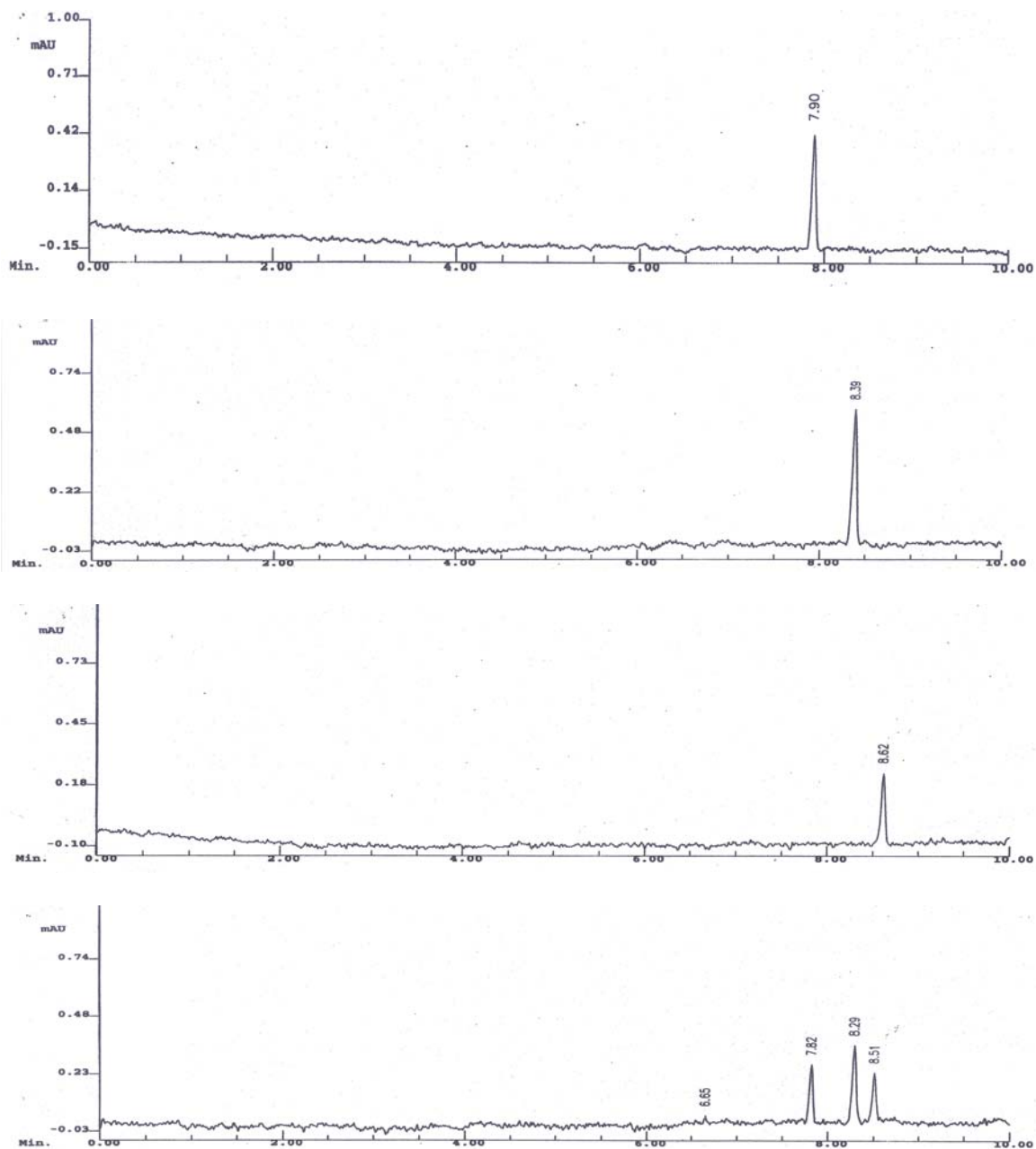
Figure 3.6. Electropherograms of the three heparin-derived tetrasaccharides obtained from SAX-HPLC. Top (Peak III, Figure 3.2); second from top (Peak II); third from top (Peak I); bottom (mixture of peaks I, II, and III). Separations were performed at a constant voltage of 8 kV using 0.1 M phosphate buffer at pH 2.5 in the reversed polarity mode (232 nm).

Peak No.	Time (min)	m/z
III	7.90	214.134
II	8.39	231.943
I	8.62	236.552

Table 3.1. Illustrating the CZE elution order of eluent peaks I, II, and III (Figure 3.2) of heparin-derived tetrasaccharide based on mass-to-charge ratio.
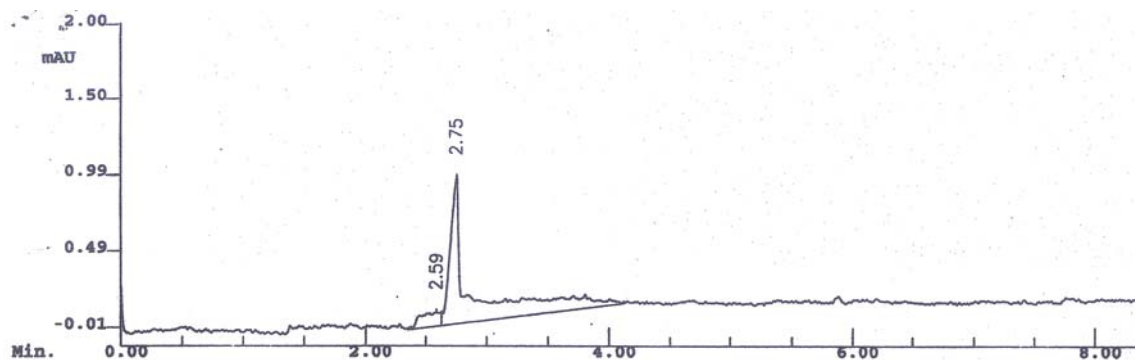
Figure 3.7. Electropherogram of heparin-derived octasaccharide obtained from SAX-

HPLC. Separation was performed at a constant voltage of 10 kV using 0.1 M phosphate

buffer at pH 2.5 in the reversed polarity mode (232 nm).

to determine the length of the oligosaccharide. A 1-D ^{1}H NMR experiment was always performed first. The length of an oligosaccharide could be determined by counting the number of anomeric resonances in the 1D spectrum, which occur in the anomeric region (5.2-5.5 ppm). Each anomeric resonance represents a monosaccharide residue. The number of monosaccharide units determines the degree of polymerization of an oligosaccharide. Due to the well-resolved H4 resonance (the most downfield resonance) of the unsaturated uronic acid residue (ΔUA), the peak area of the H4 resonance is used to determine if each anomeric resonance is a single proton.

In the case where anomeric resonances are overlapped, a BASHD-TOCSY spectrum was obtained with band selection of the anomeric region. Once the number of anomeric resonances was determined based on integration relative to H4 resonance of ΔUA, each monosaccharide that gave rise to each anomeric resonance was identified using subspectra obtained by taking a trace through the TOCSY spectrum at the chemical shift of the anomeric resonance. Characterization of each monosaccharide unit will be discussed in the next section.

When the identities of all the monosaccharide residues were determined, the oligosaccharide sequence was next established using dipolar connectivity between the H1 and H4 protons on adjacent monosaccharide residues of the oligosaccharide; the dipolar connectivities were obtained from a ROESY/NOESY spectrum, depending on the size of the heparin-derived oligosaccharide (Sections 2.8.5.2 and 2.8.5.3). The sequence assignment began by determining the chemical shift of the H1 proton of the ΔUA residue by taking a trace through the TOCSY spectrum at the chemical shift of the H4 proton of

ΔUA. The next step in the sequential assignment was to look for the NOE cross peak between the H1 proton of ΔUA and the H4 proton of the next residue by taking a trace through the ROESY/NOESY spectrum at the chemical shift of the H1 proton of ΔUA; the NOE cross peak in the trace yields the chemical shift of the H4 proton of the glucosamine residue connected to the reducing end of ΔUA. This sequential assignment procedure was repeated until the reducing end glucosamine ring was identified, which gave a complete assignment of the ^{1}H NMR spectrum of the heparin-derived oligosaccharide.

3.6 Monosaccharide Characterization by ^{1}H NMR

As shown in Figure 1.2, there are two types of α-D-glucosamine: GlcNS and GlcNAc. They can be differentiated either by the presence of the methyl resonance of the N-acetyl group at 2.03 ppm or by the chemical shift of the H2 proton[4]: 3.27 ppm for GlcNS and 3.91 ppm for GlcNAc. Chemical shifts of neighboring protons, H1 and H3, are affected differently, depending on whether the substituent on the C2 position is an acetyl or a sulfo group (Figure 3.8).

The uronic acid residues can be either iduronic acid (IdoA) or glucuronic acid (GlcA) (Figure 1.2). IdoA can be distinguished from GlcA by comparing the chemical shift of the H1 proton: 4.99 ppm for IdoA and 4.58 ppm for GlcA. The vicinal coupling constant, $^3J_{H, H}$, also can be used to differentiate IdoA from GlcA: 3 Hz for IdoA and 9 Hz for GlcA (Figure 3.9).

Sulfation can take place at C3 and C6 on GlcNS (Figure 1.2). When there is a sulfate group attached to C3 of GlcNS, the H3 resonance is displaced downfield by about 0.8 ppm (3.73 → 4.46 ppm). The chemical shifts of neighboring protons (H2 and H4) are

GlcNS　　　　　　　vs　　　　　GlcNAc

R= H or SO_3^-
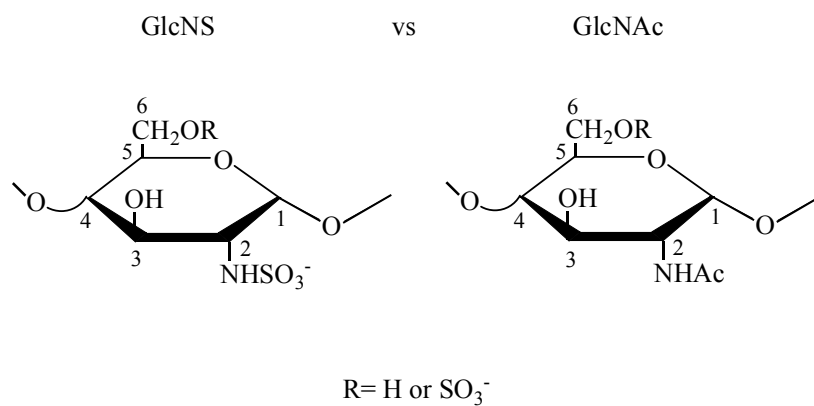
	GlcNS	GlcNAc
H_1	5.43	5.36
H_2	3.27	3.91
H_3	3.67	3.77
Ac	Not Applicable	2.03

Figure 3.8. ^{1}H NMR chemical shift values for GlcNS and GlcNAc residues. [Ref. 4 & 5]

IdoA   vs   GlcA

R= H or SO_3^-
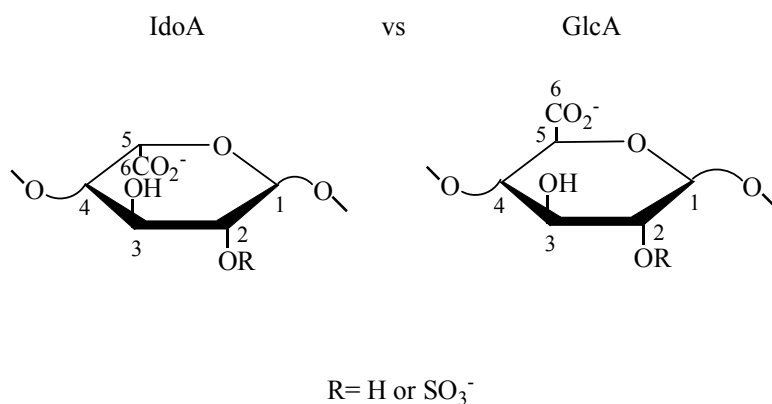
	IdoA		GlcA	
	H	SO_3^-	H	SO_3^-
H_1	4.99	5.21	4.58	4.58
H_2	3.76	4.32	3.37	4.10
H_3	4.12	4.22	3.73	4.00

Figure 3.9. ^{1}H NMR chemical shift values for IdoA and GlcA residues. [Ref. 4]

affected by the downfield shift of the H3 proton. In the case where a sulfate group is attached to C6 of GlcNS, H6 is shifted downfield by about 0.5 ppm (3.84 → 4.31 ppm). The downfield shift of the H6 resonance influences the chemical shift of the neighboring proton H5 (Figure 3.10).

For GlcNAc residue, a sulfate group can only be attached to C6 but not C3 due to substrate specificity of 3-O-sulfotransferase. In the presence of the sulfate group at C6, H6 is shifted downfield by about 0.4 ppm (3.83 → 4.24 ppm). The presence of the sulfate group at C6 affects the chemical shift of the neighboring proton H5 (Figure 3.11).

IdoA can only be sulfated at the C2 position by 2-O-sulfotransferase. The presence of a sulfate group at C2 of IdoA causes a downfield shift for H2 by about 0.6 ppm (3.76 → 4.32 ppm). H1 and H3 protons are affected by the presence of the sulfate group at C2 (Figure 3.9).

Like IdoA, GlcA can also be sulfated only at the C2 position due to substrate specificity. Upon being sulfated at the C2 position, H2 is shifted downfield by about 0.4 ppm (3.37 → 4.10 ppm). The effect on the chemical shift of the H3 proton by the presence of the sulfate group is shown in Figure 3.9.

3.7 Identification of Heparin-Derived Oligosaccharides by ^{1}H NMR

Structures of three tetrasaccharides, one hexasaccharide, and one octasaccharide were characterized by ^{1}H NMR. The characterization strategy described in Sections 3.5 and 3.6 was applied in determining the structures of these heparin-derived oligosaccharides.

GlcNS
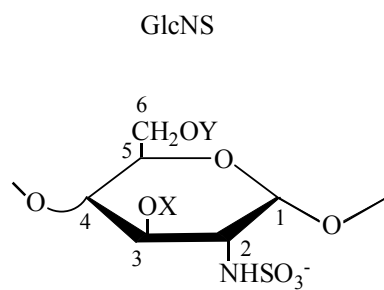
	X		Y	
	H	SO_3^-	H	SO_3^-
H_2	3.25	3.41		
H_3	3.73	4.46		
H_4	3.69	3.94		
H_5			3.86	4.04
$H_{6\,a,\,b}$			3.84, 3.86	4.27, 4.35

Figure 3.10. ^{1}H NMR chemical shift values for the various sulfated form of GlcNS residue. [Ref. 4]

GlcNAc

R = H or SO_3^-
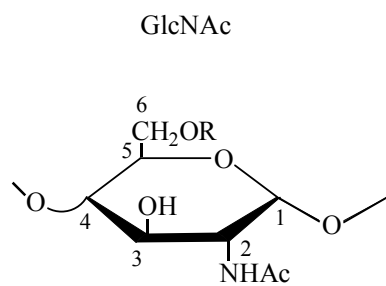
	R	
	H	SO_3^-
H_5	3.87	4.05
$H_{6\,a,\,b}$	3.83, 3.79	4.24, 4.34

Figure 3.11. ^{1}H NMR chemical shift values for H_5 and $H_{6\,a,\,b}$ of GlcNAc and GlcNAc(6S). [Ref. 4]

3.7.1 Characterization of Heparin-Derived Tetrasaccharides

Peak I was determined by ^{1}H NMR to have the following structure: ΔUA(2S)-GlcNS(6S)-IdoA(2S)-GlcNS. Figure 3.12 shows the 1-D and TOCSY ^{1}H spectra of peak I at pD 6.75, 25 °C. The chemical shifts of all the protons of the tetrasaccharide were obtained from traces through the TOCSY spectrum (Figure 3.13). The assigned chemical shifts within each monsaccharide (Table 3.2) are in good agreement with literature values[4], which confirms that each residue is correctly assigned. The sequential assignment was unambiguously established by clear ROESY cross peaks (bottom of Figure 3.14) between H1 and H4 resonances and vice versa. The top of Figure 3.14 shows the full ROESY spectrum of peak I at pD 6.75, 25 °C.

The structure of peak II was assigned to: ΔUA(2S)-GlcNS-GlcA-GlcNS(6S). Figure 3.15 shows the 1-D and TOCSY ^{1}H spectra of a solution of 2.5 mM of peak II in 100% D_2O at pD 6.99, 25 °C. All four subspectra obtained by taking traces through the TOCSY spectrum in Figure 3.15 at the chemical shifts of the anomeric resonances are shown in Figure 3.16. Figure 3.17 shows the full ROESY spectrum and ROESY cross peaks of peak II at pD 6.99, 25 °C. The assigned chemical shifts within each monosaccharide are shown in Table 3.3. The presence of GlcA was suggested by the characteristic chemical shift of the H1 proton at 4.601 pppm and a large coupling constant of 8 Hz due to being in the $^4C_1$ conformation. Tetrasaccharide II is different from tetrasaccharide I in that its internal glucosamine does not have a sulfo group at the C6 position and the internal uronic acid is a glucuronic acid. It also has a 6S on the reducing end.
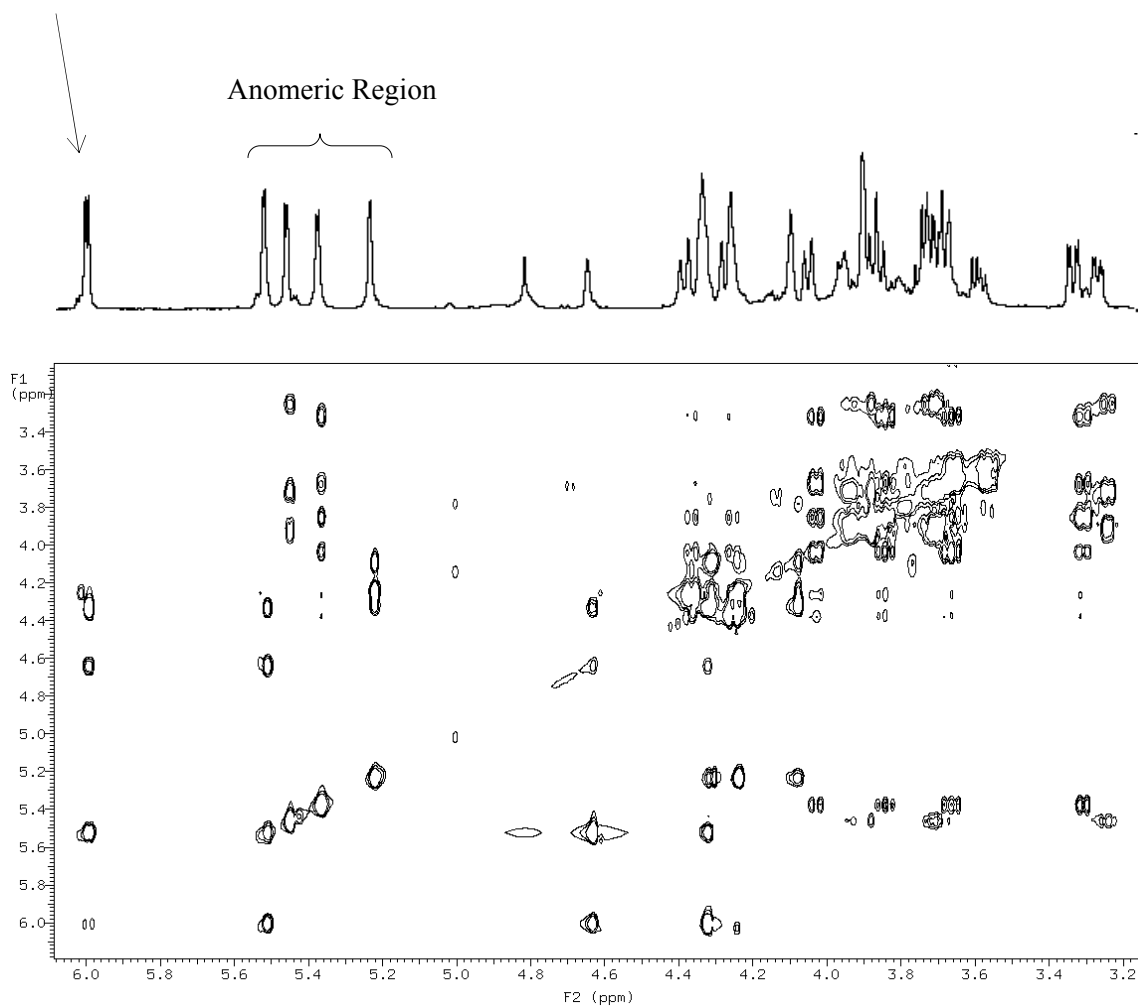
Figure 3.12. 1-D (top) and TOCSY (bottom) spectra of heparin-derived tetrasaccharide

peak I at pD 6.75, 25 °C.

Trace at 5.51 ppm

Trace at 5.45 ppm

Trace at 5.37 ppm

Trace at 5.22 ppm
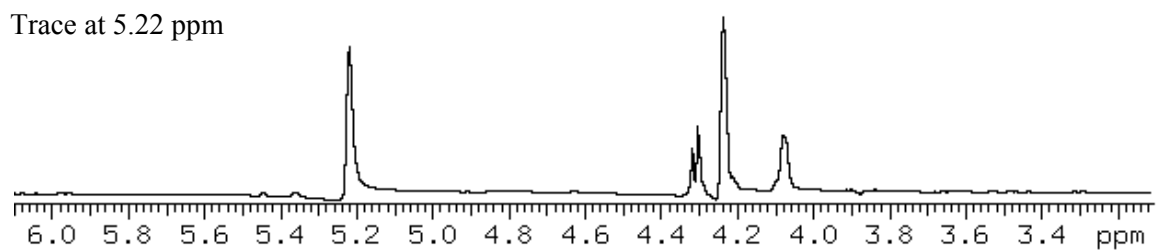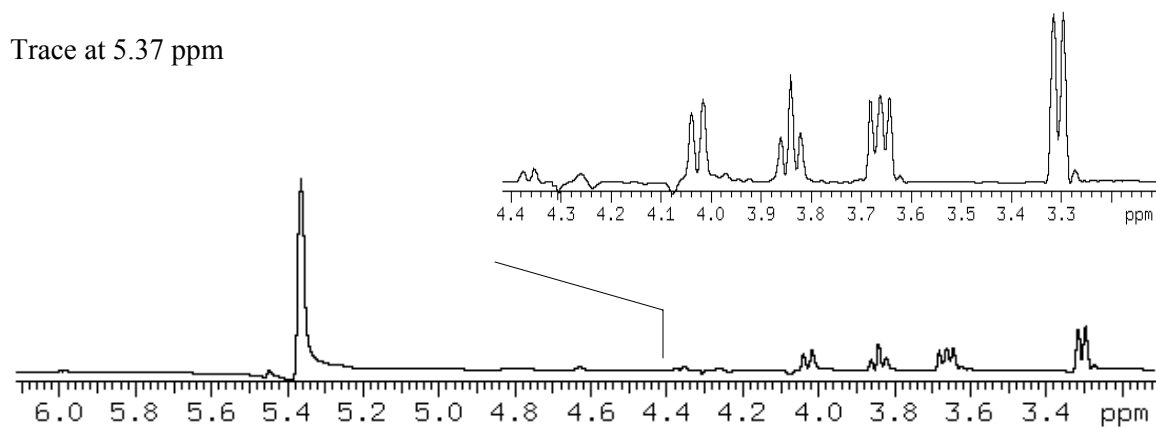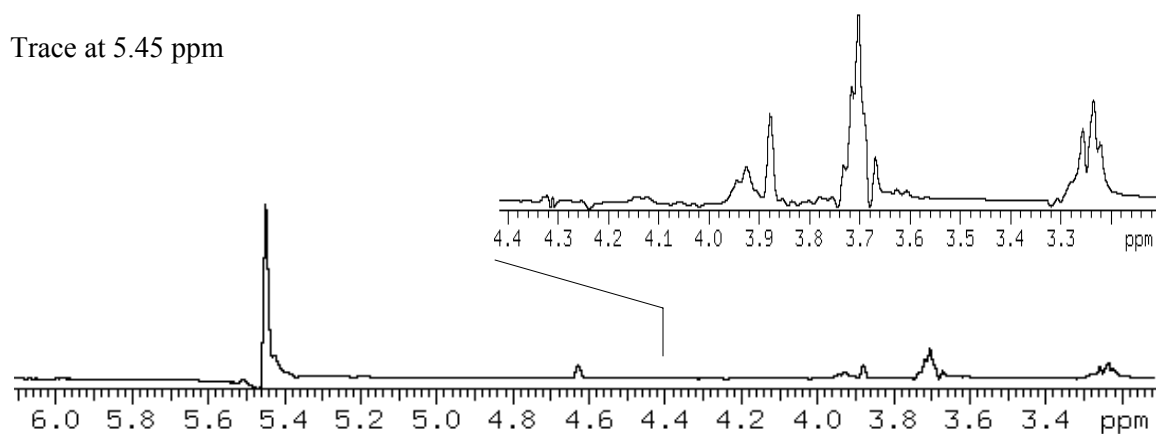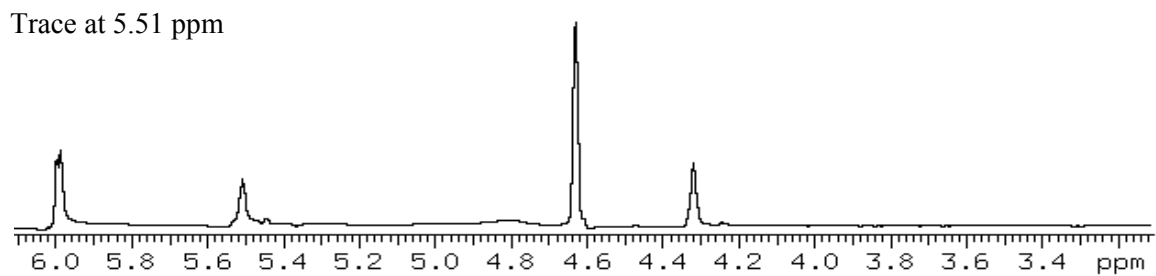
Figure 3.13. Traces through 2-D TOCSY (Figure 3.12) of heparin-derived tetrasaccharide peak I at the chemical shifts of the anomeric resonances.

	Monosaccharides			
Proton	ΔUA(2S)	GlcNS(6S)	IdoA(2S)	GlcNS
H_1	5.505	5.362	5.218	5.445
H_2	4.628	3.296	4.316	3.253
H_3	4.319	3.659	4.234	3.688
H_4	5.997	3.840	4.081	3.702
H_5		4.015	4.800	3.878
H_{6a}		4.259		3.926
H_{6b}		4.353		3.945
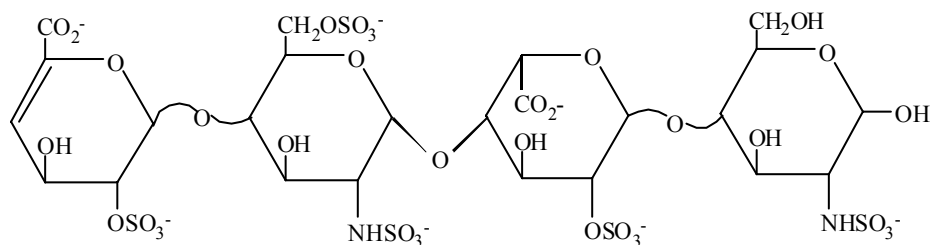
Table 3.2. ^{1}H NMR chemical shift data for peak I of the heparin-derived tetrasaccharide.
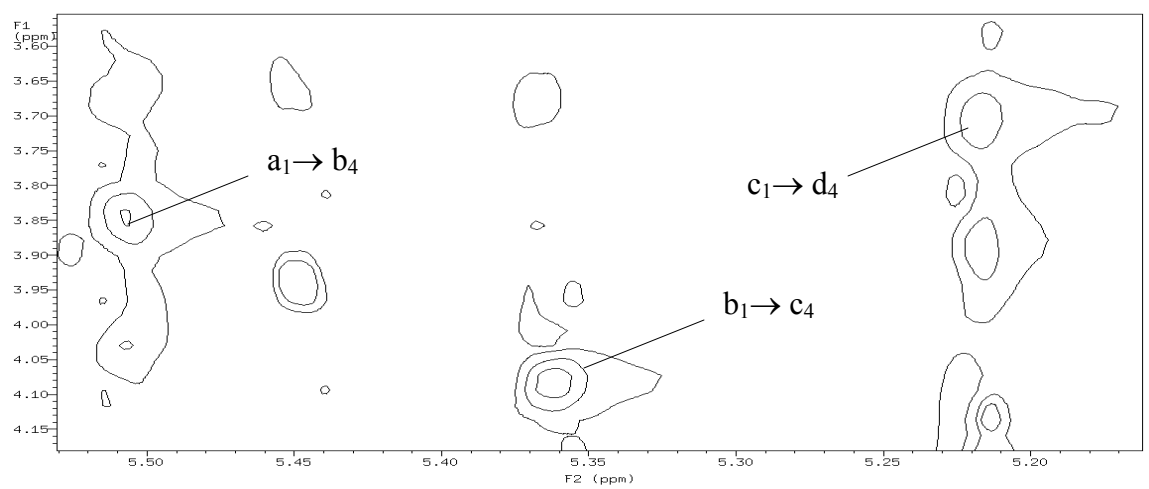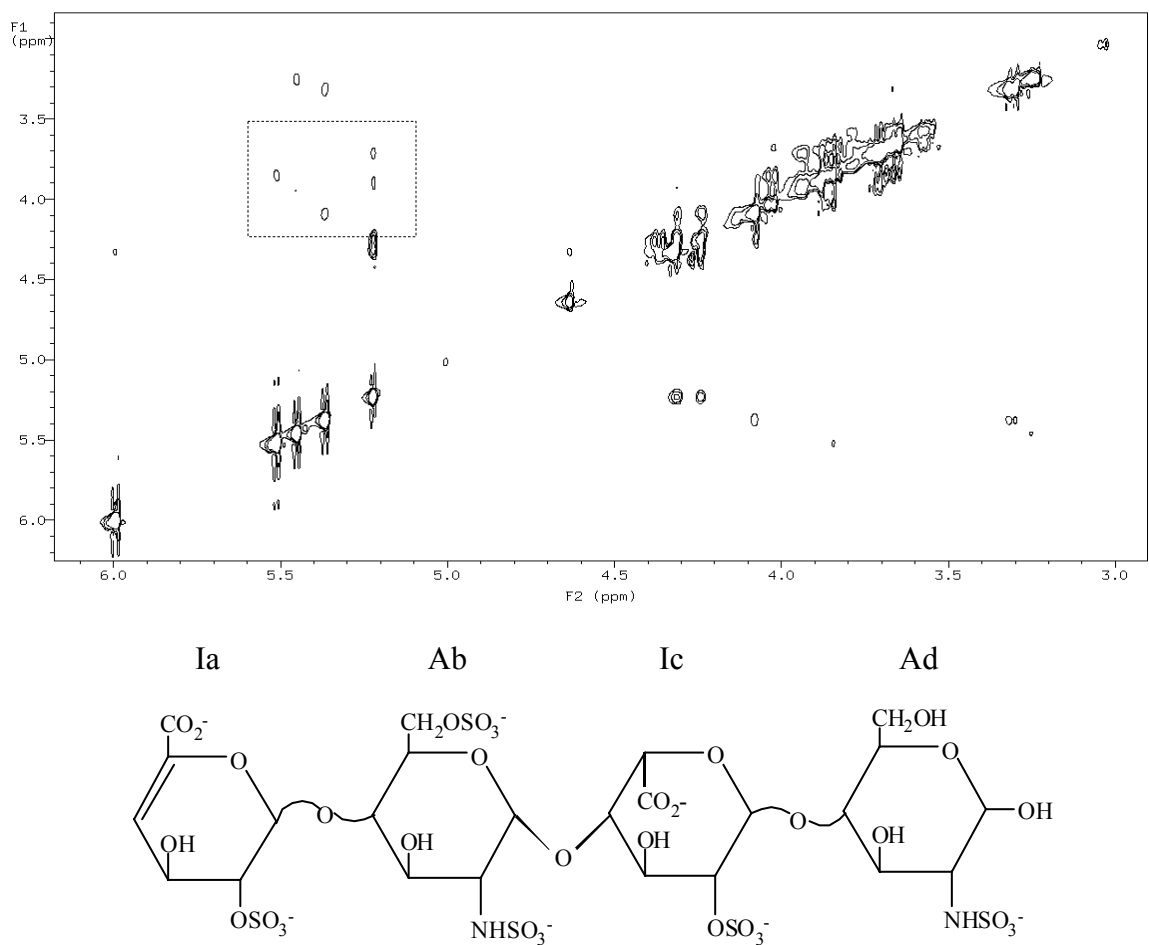
Figure 3.14. The full ROESY spectrum (top) and the ROESY cross peaks (bottom) of heparin-derived tetrasaccharide peak I at pD 6.75, 25 °C.

119
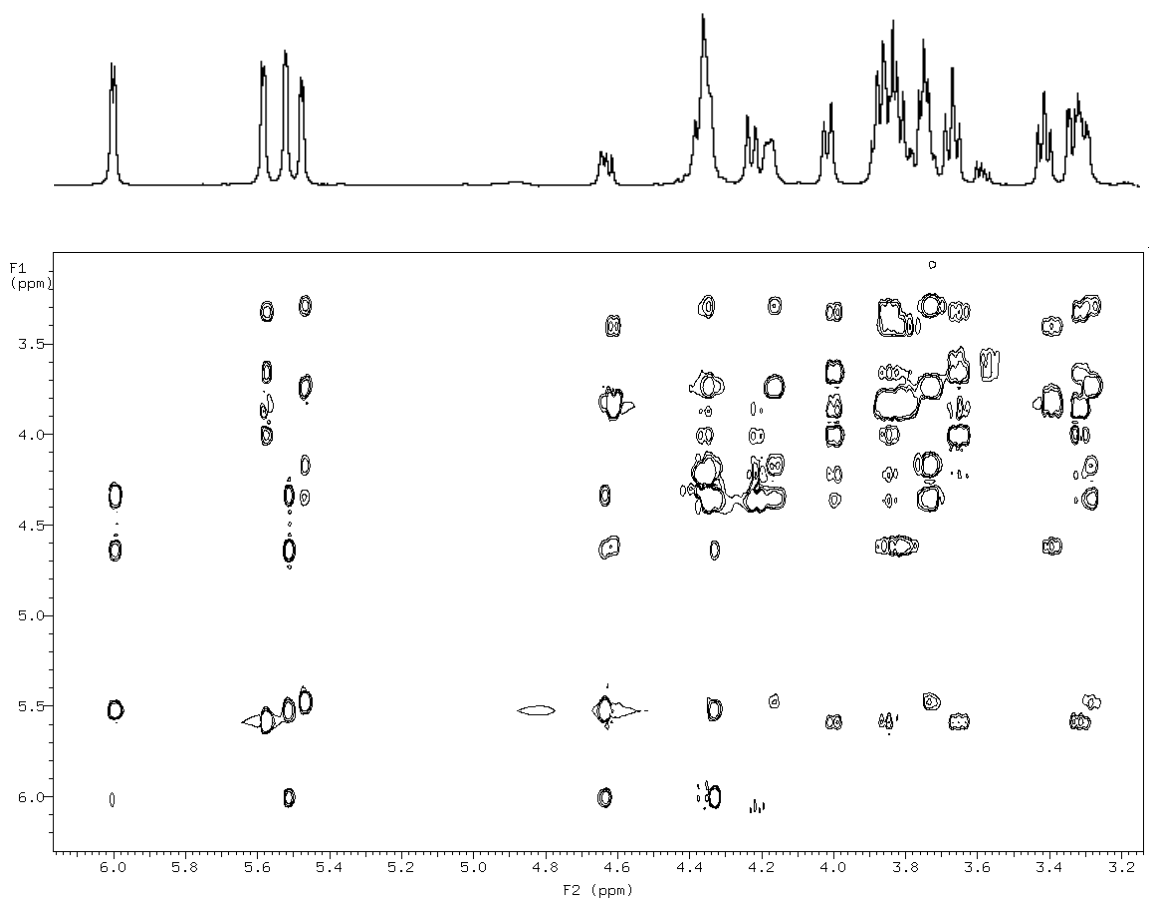
Figure 3.15. 1-D (top) and TOCSY (bottom) spectra of heparin-derived tetrasaccharide

peak II at pD 6.99, 25 °C.

120
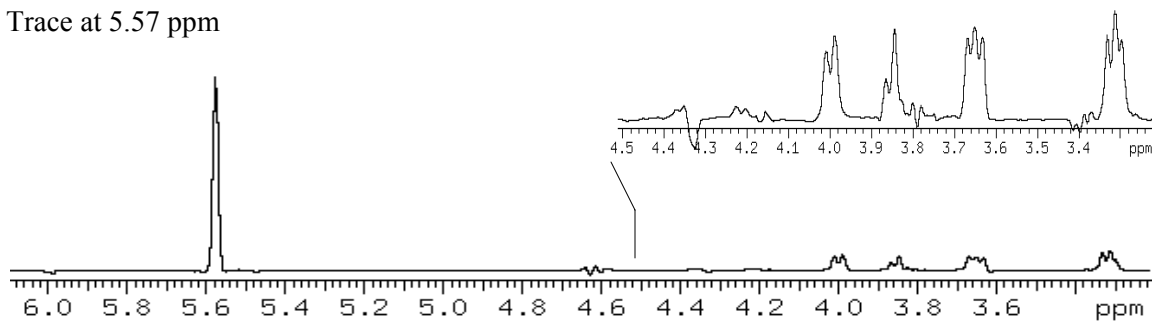
Trace at 5.57 ppm

Trace at 5.51 ppm
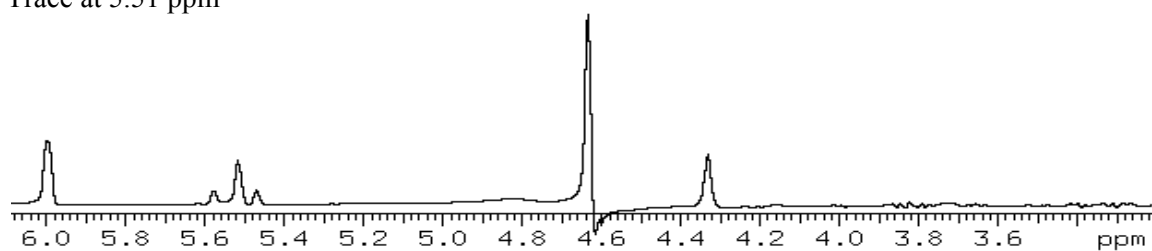
Trace at 5.46 ppm
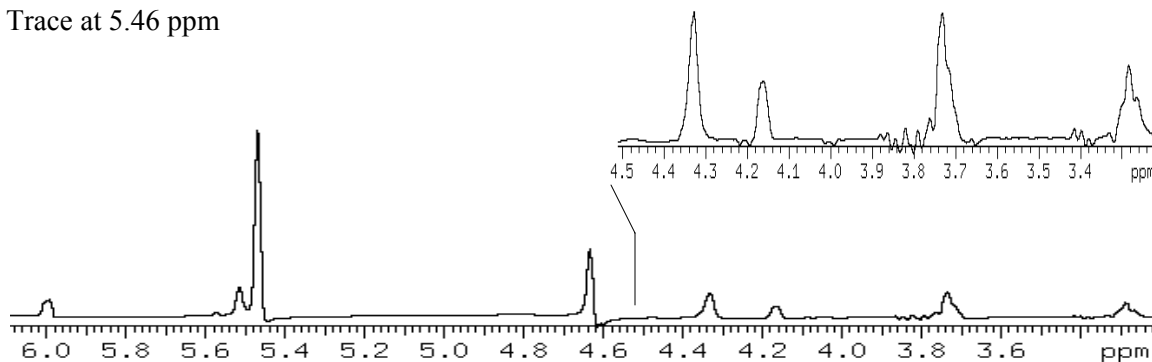
Trace at 4.60 ppm
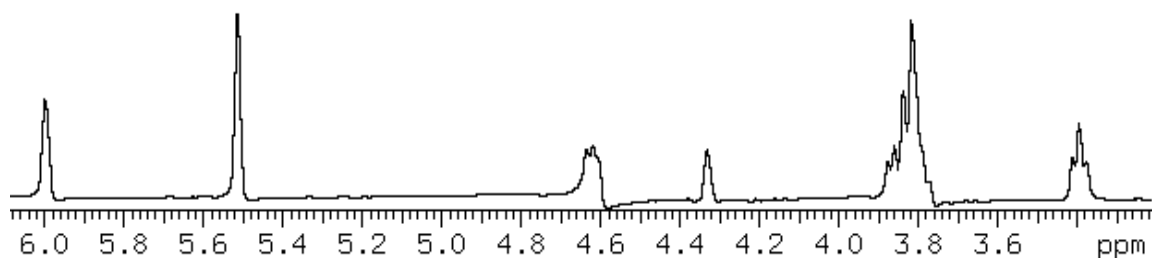
Figure 3.16. Traces through 2-D TOCSY in Figure 3.15 of heparin-derived tetrasaccharide peak II at the chemical shifts of the anomeric resonances.

121
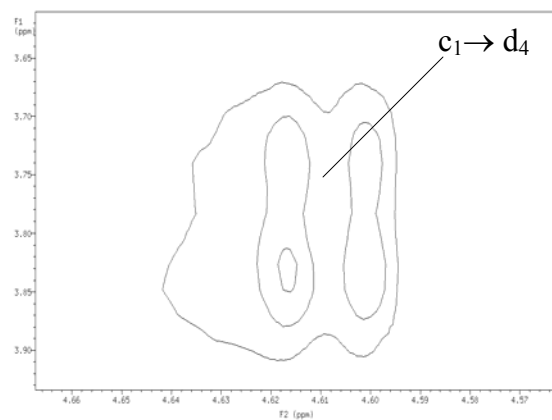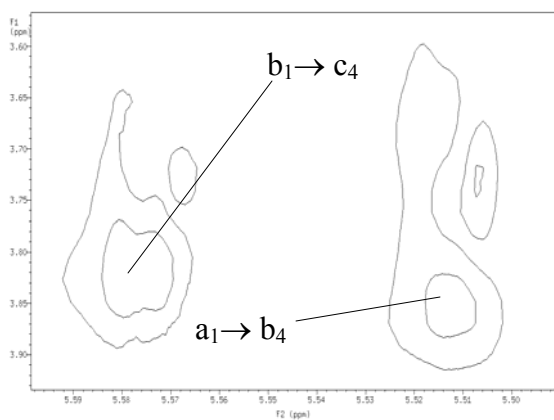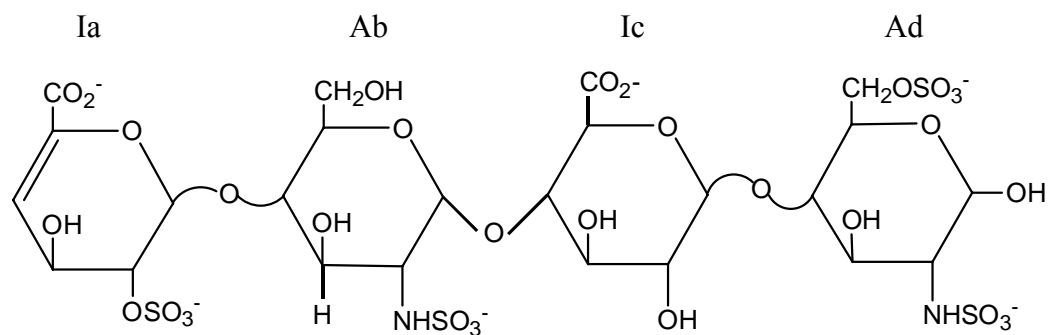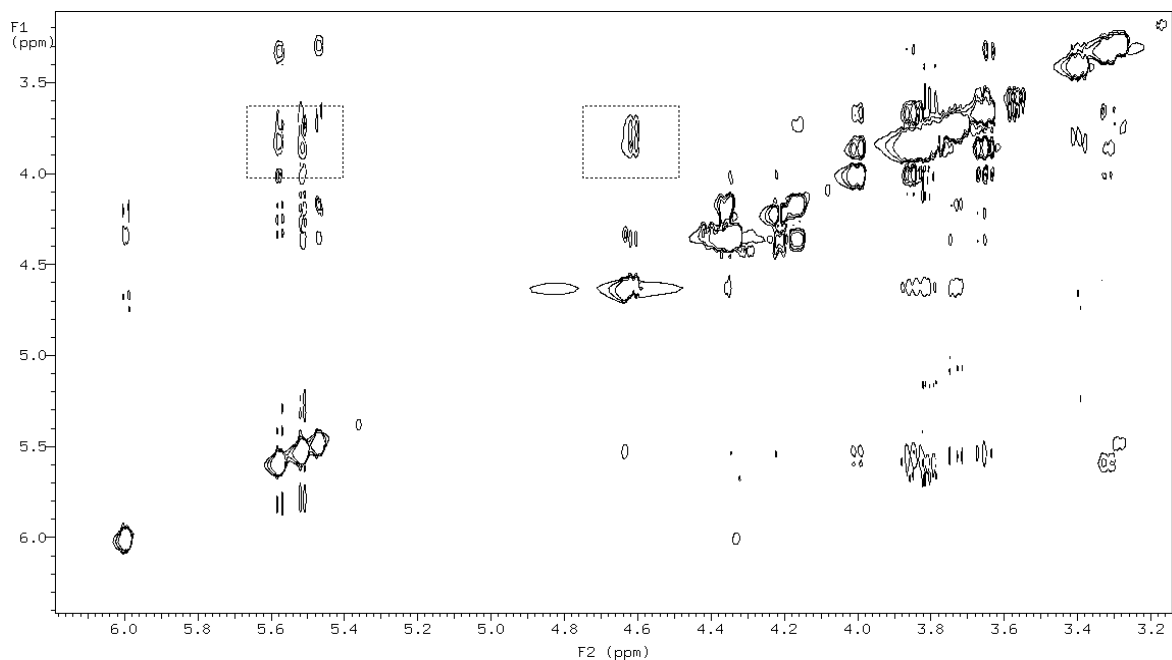
Figure 3.17. The full ROESY spectrum (top) and the ROESY cross peaks (bottom) of heparin-derived tetrasaccharide peak II at pD 6.99, 25 °C.

	Monosaccharides			
Proton	ΔUA(2S)	GlcNS	GlcA	GlcNS(6S)
H_1	5.508	5.571	4.601	5.461
H_2	4.630	3.314	3.391	3.285
H_3	4.327	3.651	3.803	3.644
H_4	5.989	3.843	3.815	3.729
H_5		3.863	3.874	4.168
H_{6a}		3.987		4.315
H_{6b}		4.007		4.336
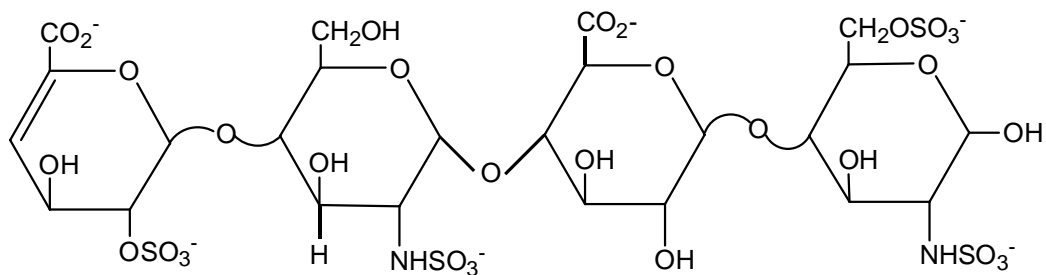
Table 3.3. ^{1}H NMR chemical shift data for peak II of the heparin-derived tetrasaccharide.

The structure of peak III was determined to be: ΔUA(2S)-GlcNS(6S)-IdoA(2S)-GlcNS(6S). 1D and TOCSY spectra of a 2.5 mM solution of peak III in 100% D_2O at pD 6.57 and 25 °C are shown in Figure 3.18. Compared to traces (Figure 3.19) taken through the bottom left TOCSY spectrum in Figure 3.18, traces (Figure 3.20) through the bottom right TOCSY spectrum in Figure 3.18 give better resonance shape due to better digital resolution in the F2 dimension. Figure 3.21 shows the full ROESY spectrum and ROESY cross peaks of peak III at pD 6.57, 25 °C. The assigned chemical shifts within each monosaccharide are shown in Table 3.4.[4] According to the TOCSY assignment, tetrasaccharide III differs from tetrasaccharide I in that the reducing end glucosamine residue has a sulfo group at the C6 position. This fully sulfated tetrasaccharide will be used to study the binding of histidine-containing peptides in Chapter 4.

3.7.2 Characterization of the Heparin-Derived Hexasaccharide

The hexasaccharide obtained from the SAX-HPLC separation was identified to be: ΔUA(2S)-GlcNS(6S)-IdoA(2S)-GlcNS(6S)-IdoA(2S)-GlcNS(6S). The presence of two additional resonances in the anomeric region at pD 3.02 (Figure 3.22) were assigned to the H5 protons of the two iduronic acid residues, which confirms the oligosaccharide is a hexasaccharide. Figure 3.22 also shows the 1-D ^{1}H NMR spectrum of the same hexasaccharide at pD 6.68. At pD 6.68, anomeric resonances of the two internal glucosamine residues as well as those of the two uronic acid residues are overlapped, which makes assignment of the identity at this pH ambiguous. Figure 3.23 shows the 1-D and TOCSY of the hexasaccharide at pD 3.02, 25 °C. Subspectra from traces through the TOCSY spectrum in Figure 3.23 are shown in Figure 3.24. The ROESY spectrum and
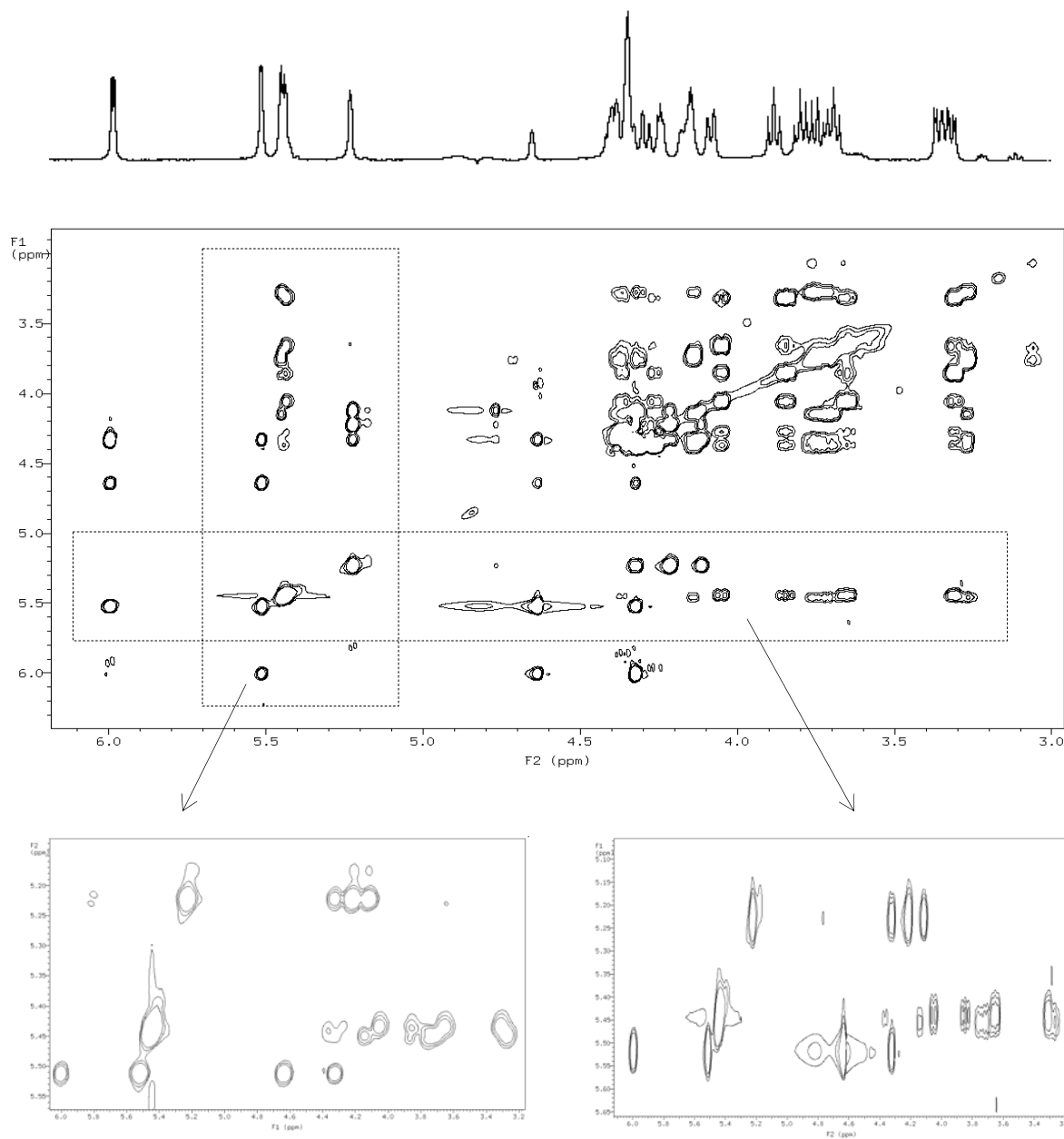
Figure 3.18. 1-D (top) and TOCSY (middle) spectra of heparin-derived tetrasaccharide

peak III at pD 6.57, 25 °C. The bottom right spectrum is a portion of the middle TOCSY

spectrum and the bottom left one is the same portion of the middle TOCSY spectrum

except the axes are switched (F1-horizontal and F2-vertical).

Trace at 5.51 ppm
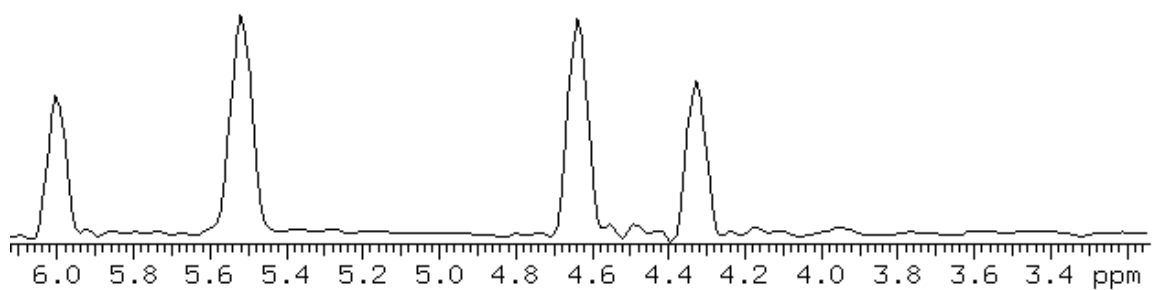
Trace at 5.45 ppm
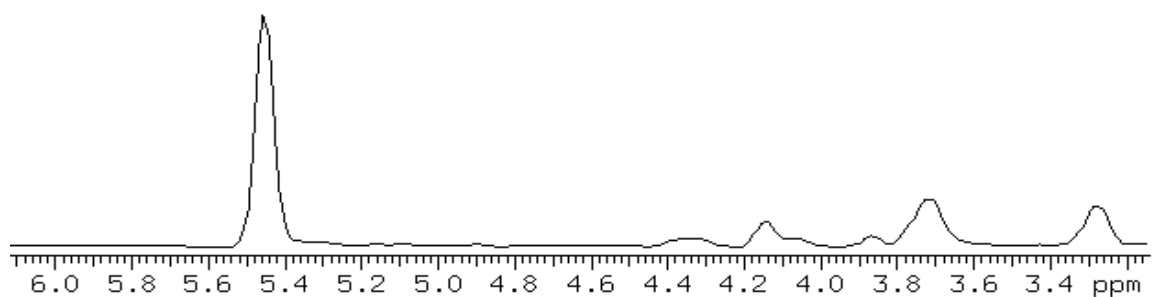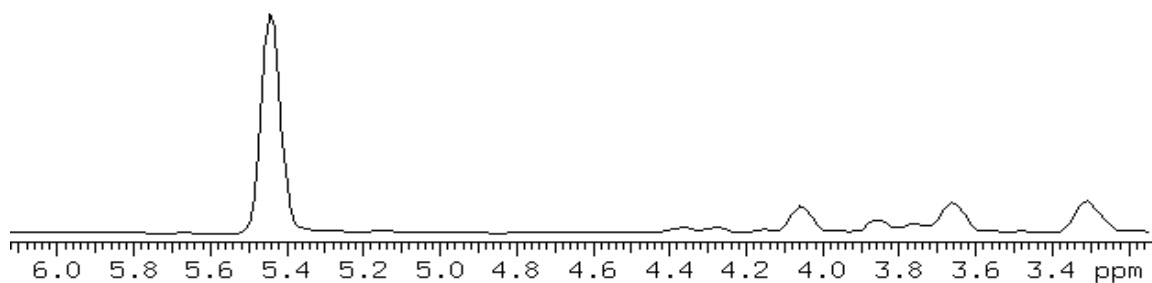
Trace at 5.43 ppm
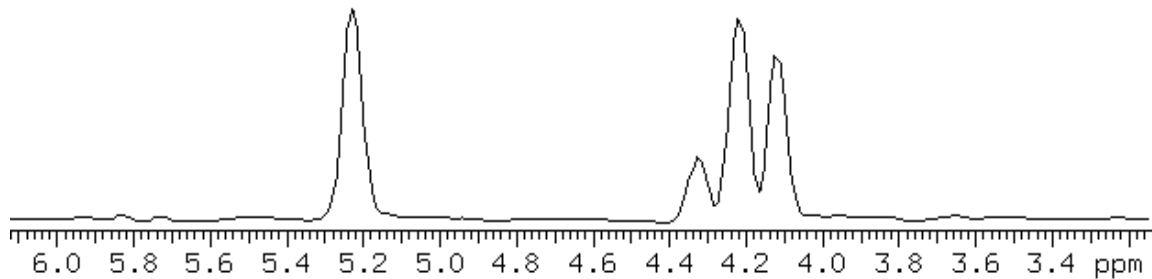
Trace at 5.22 ppm

Figure 3.19. Traces through the bottom left TOCSY spectrum in Figure 3.18 of heparin-derived tetrasaccharide peak III at the chemical shifts of the anomeric resonances.

Trace at 5.51 ppm
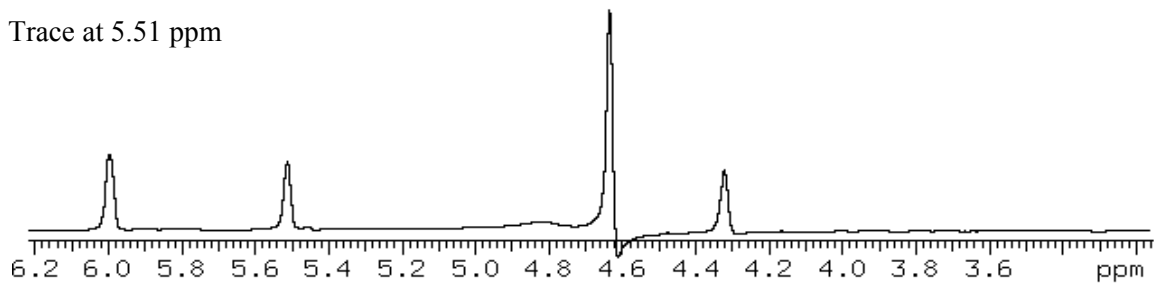
Trace at 5.45 ppm
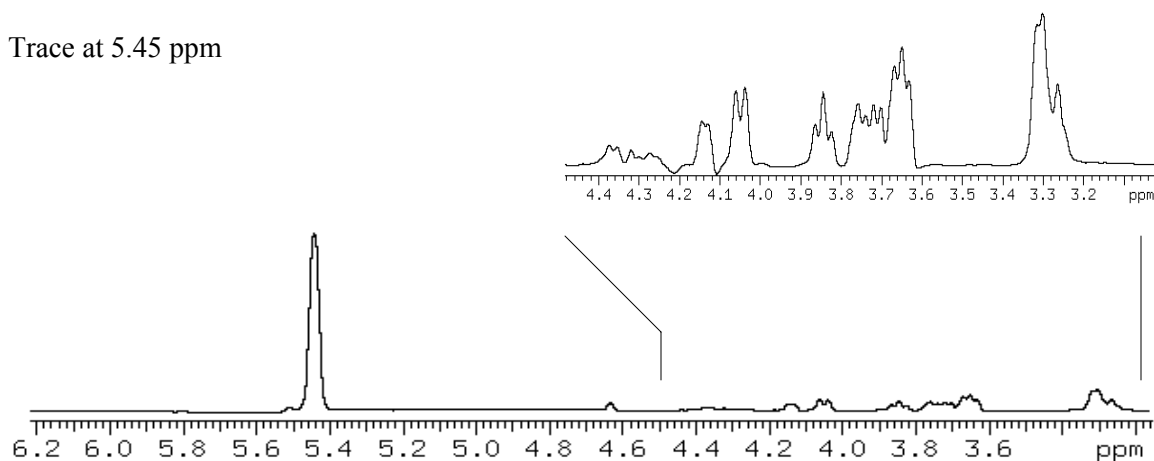
Trace at 5.43 ppm
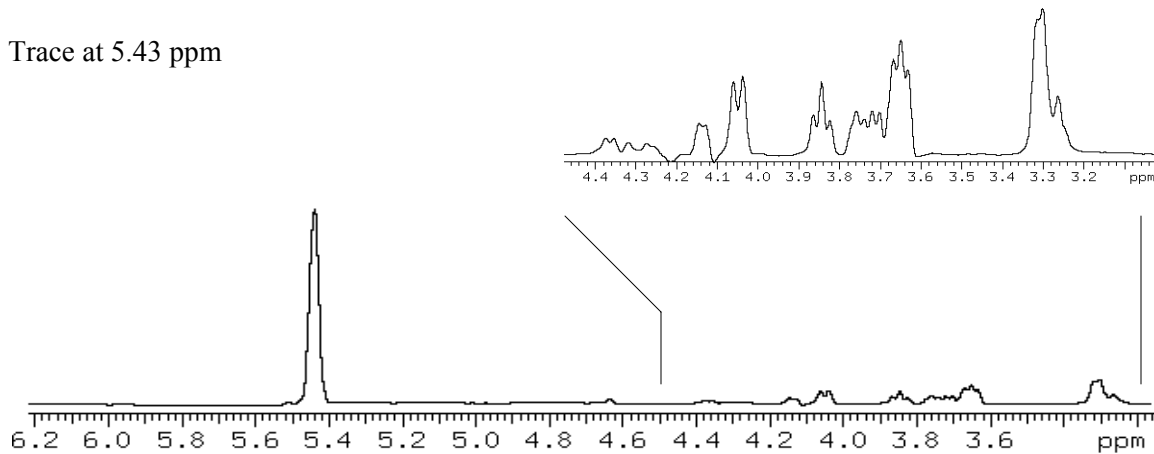
Trace at 5.22 ppm
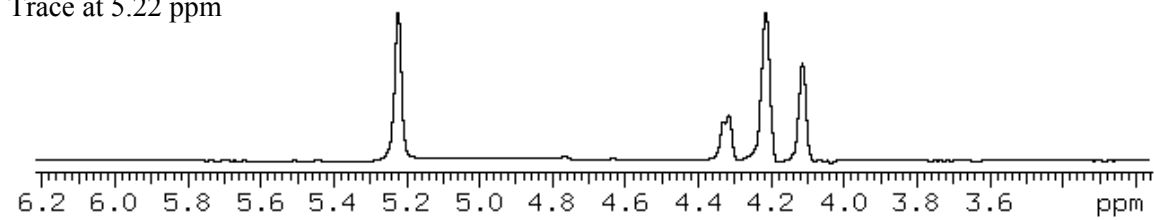
Figure 3.20. Traces through the bottom right TOCSY spectrum in Figure 3.18 of heparin-derived tetrasaccharide peak III at the chemical shifts of the anomeric resonances.
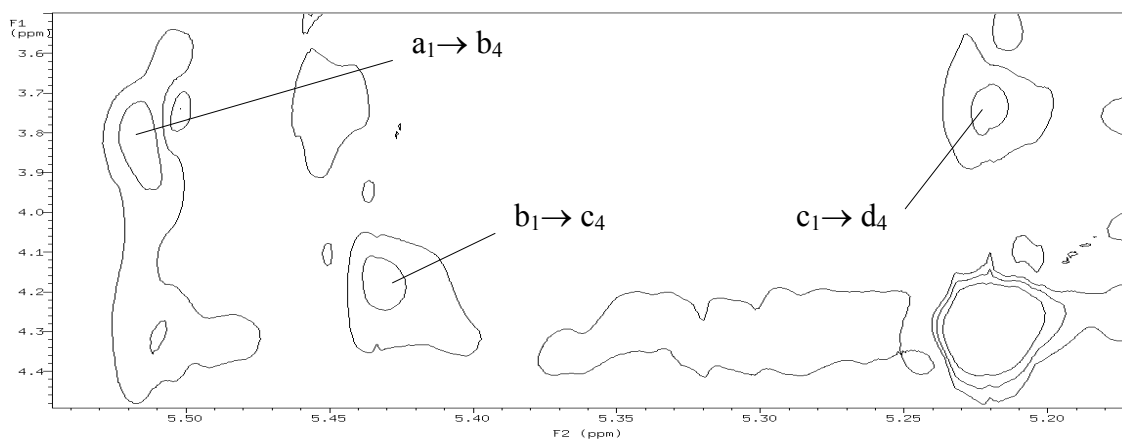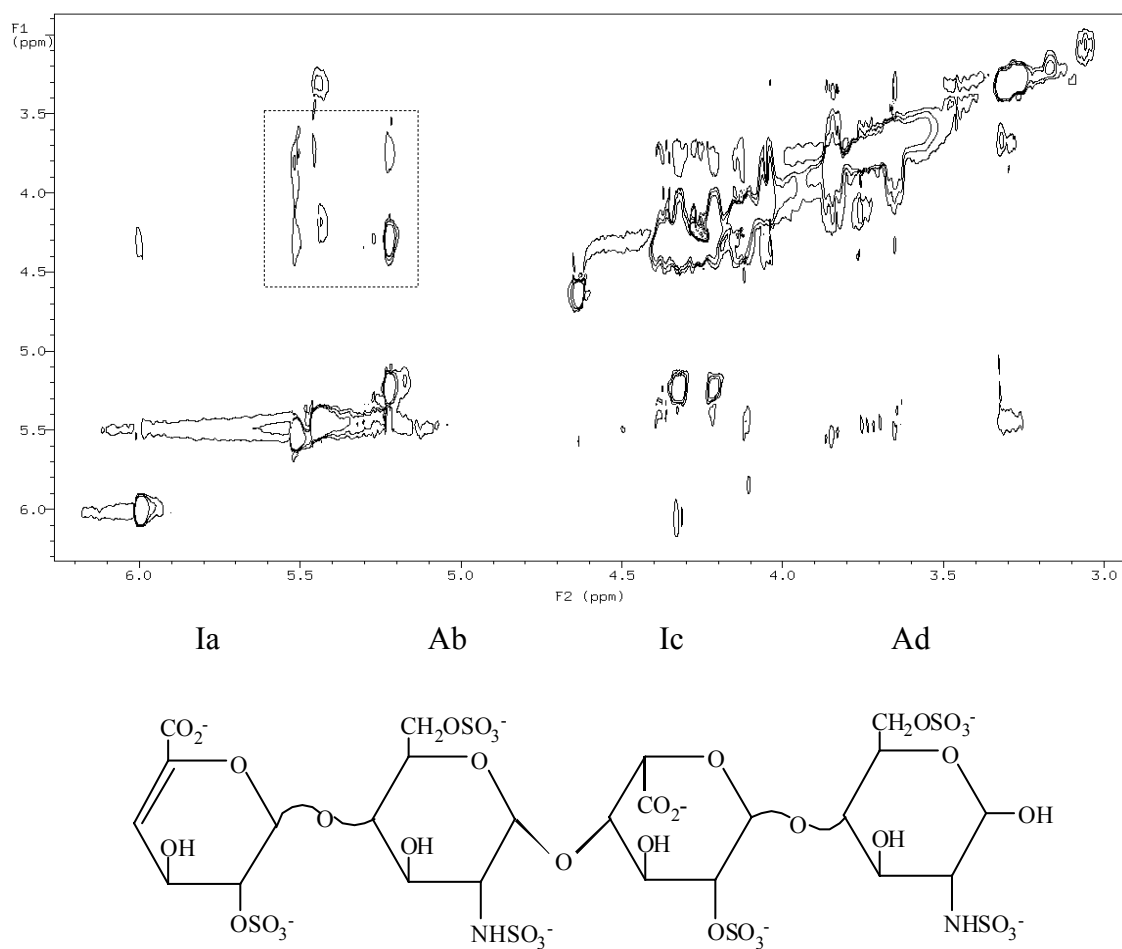
Figure 3.21. The full ROESY spectrum (top) and the ROESY cross peaks (bottom) of heparin-derived tetrasaccharide peak III at pD 6.57, 25 °C.

	Monosaccharides			
Proton	ΔUA(2S)	GlcNS(6S)	IdoA(2S)	GlcNS(6S)
H_1	5.509	5.436	5.219	5.447
H_2	4.631	3.298	4.313	3.259
H_3	4.319	3.629	4.220	3.719
H_4	5.998	3.842	4.111	3.756
H_5		4.036	4.760	4.040
H_{6a}		4.319		4.126
H_{6b}		4.354		4.145
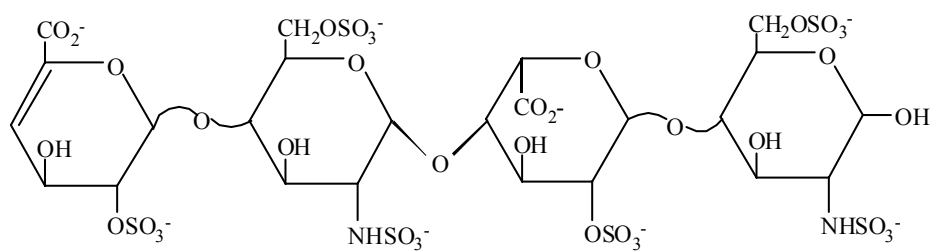
Table 3.4. ^{1}H NMR chemical shift data for peak III of the heparin-derived tetrasaccharide.
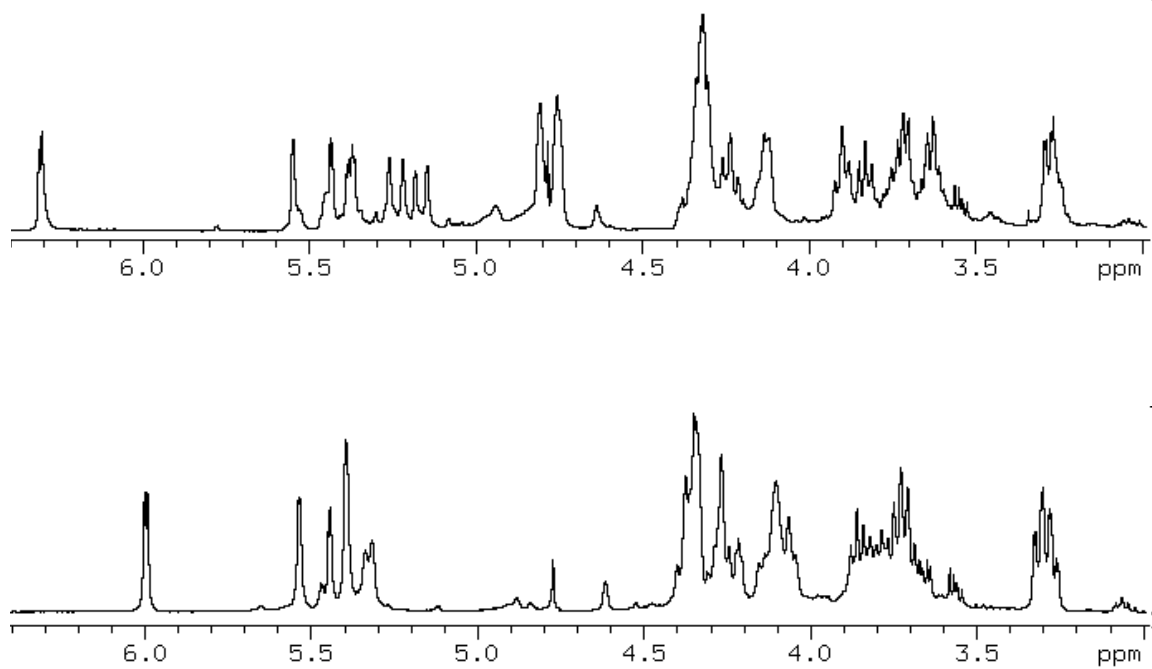
Figure 3.22. 1-D ^{1}H NMR spectra of the heparin-derived hexasaccharide. The top spectrum was obtained at pD 3.02, and the bottom spectrum was obtained at pD 6.68.
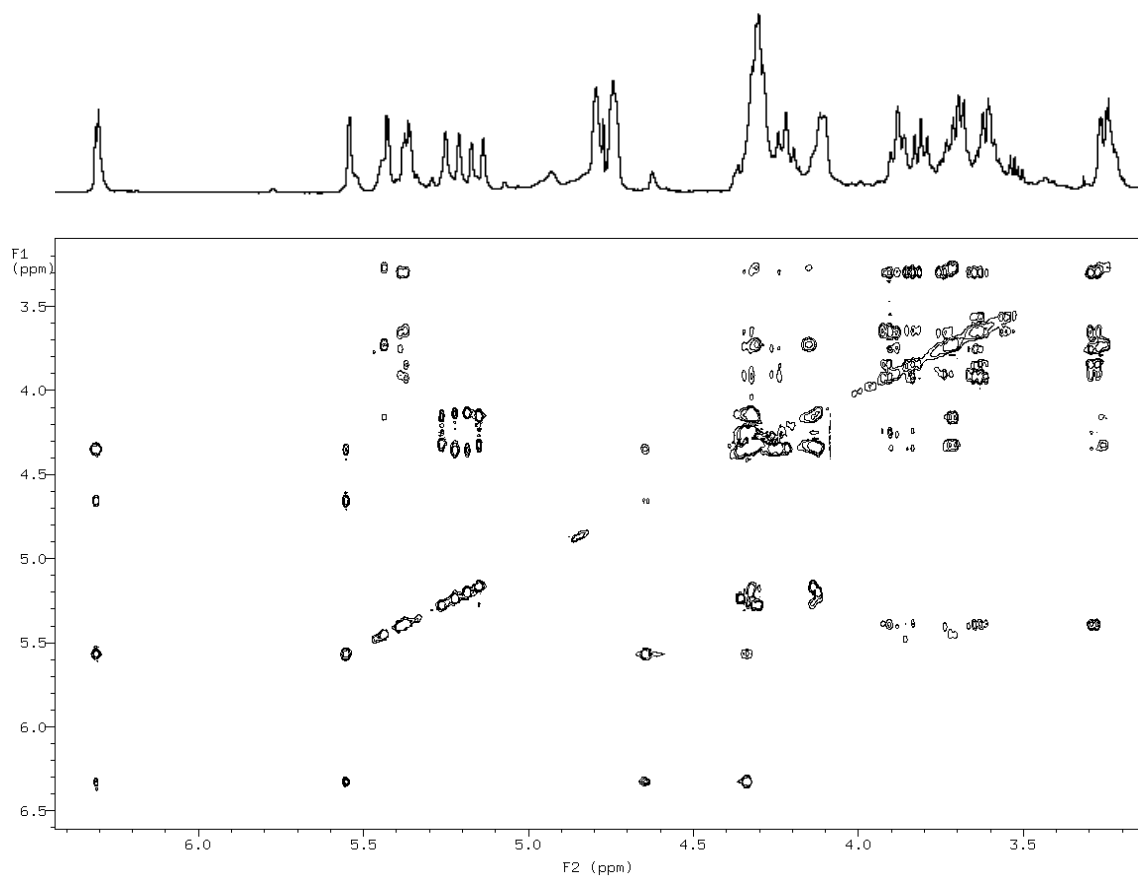
Figure 3.23. 1-D (top) and TOCSY (bottom) spectra of heparin-derived hexasaccharide at pD 3.02, 25 °C.

131

Trace at 5.56 ppm

Trace at 5.37 ppm

Trace at 5.44 ppm

Trace at 5.27 ppm

Trace at 5.39 ppm

Trace at 5.23 ppm
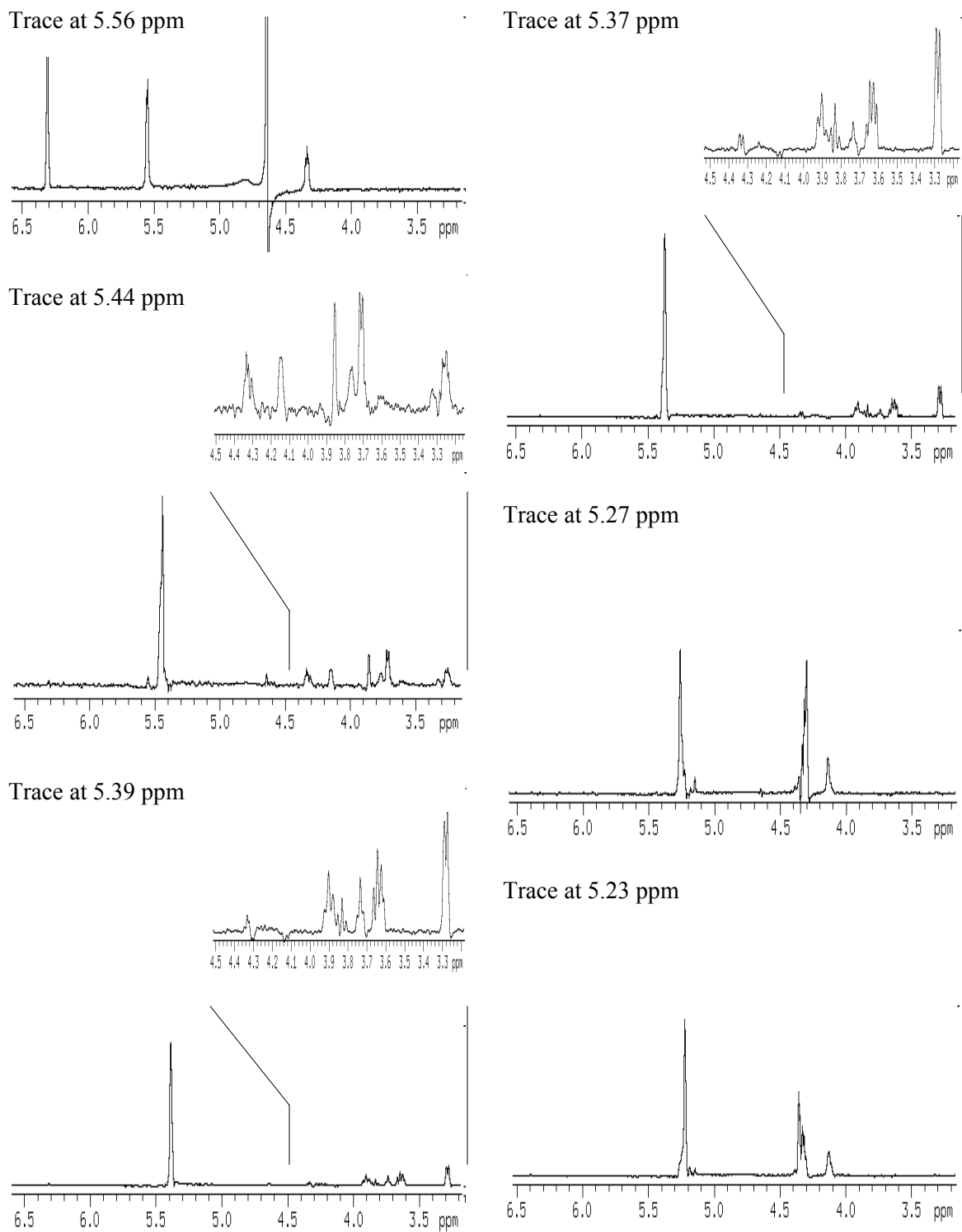
Figure 3.24. Traces through the TOCSY spectrum in Figure 3.23 of heparin-derived

hexasacccharide at the chemical shifts of anomeric resonances.

ROESY cross peaks of the hexasaccharide at pD 3.02 are shown in Figure 3.25. The

identity and chemical shifts of each residue of the hexasaccharide (Table 3.5) were

assigned at pD 3.02, where the anomeric protons are resolved.

3.7.3 Characterization of the Heparin-Derived Octasaccharide

The structure of one octasaccharide was assigned as follows: ΔUA(2S)-GlcNS-

IdoA(2S)-GlcNS(6S)-IdoA(2S)-GlcNS-IdoA(2S)-GlcNS(6S). Like the hexasaccharide,

this octasaccharide was identified by taking advantage of better resolution at a low pD

value of 2.55. Figure 3.26 shows the 1-D ^{1}H NMR spectrum of the octasaccharide

obtained at pD 5.32, with severe resonance overlap in the anomeric region (all three

uronic acid residues are overlapped into one single peak). At pD 2.55, there is less

overlap of the three uronic acid anomeric resonances (Figure 3.26). Although the

anomeric resonances are better resolved at low pD, BASHD experiments were still

needed to further enhance the resolution of the anomeric resonances for complete

assignment of the spectrum. All anomeric resonances and the three uronic acid residues

are well resolved in 2-D spectra obtained from the BASHD-TOCSY and BASHD-

NOESY experiments. Figure 3.27 shows the 1-D, and BASHD-TOCSY of the

octasaccharide at pD 2.55, 25 °C. Figure 3.28 shows traces through the BASHD-TOCSY

spectrum at the chemical shifts of the anomeric resonances. The BASHD-NOESY

spectrum and BASHD-NOESY cross peaks of the octasaccharide are shown in Figure

3.29. The identity and chemical shifts of each residue of the octasaccharide were assigned

at pD 2.55 (Table 3.6).
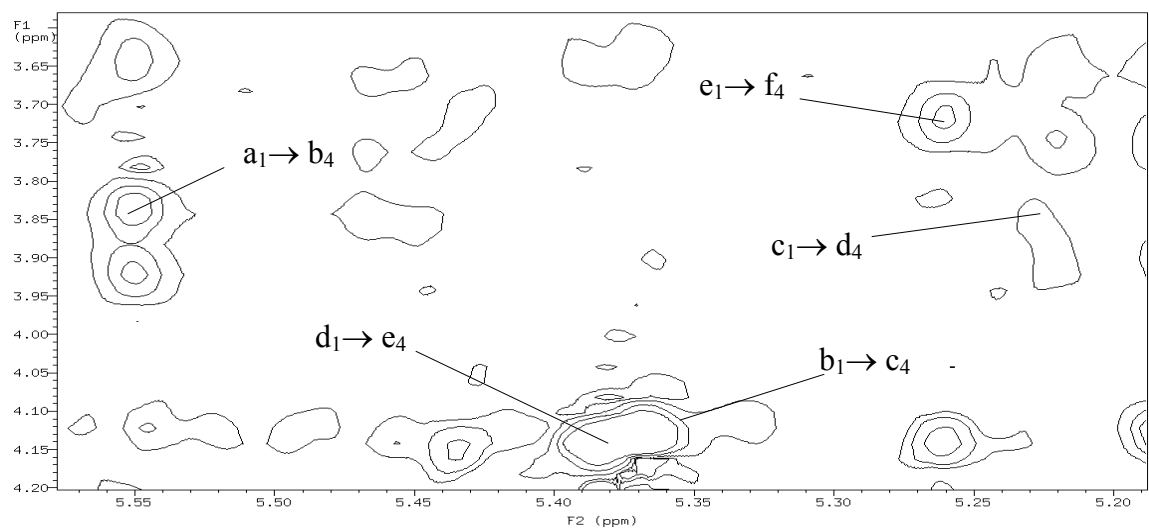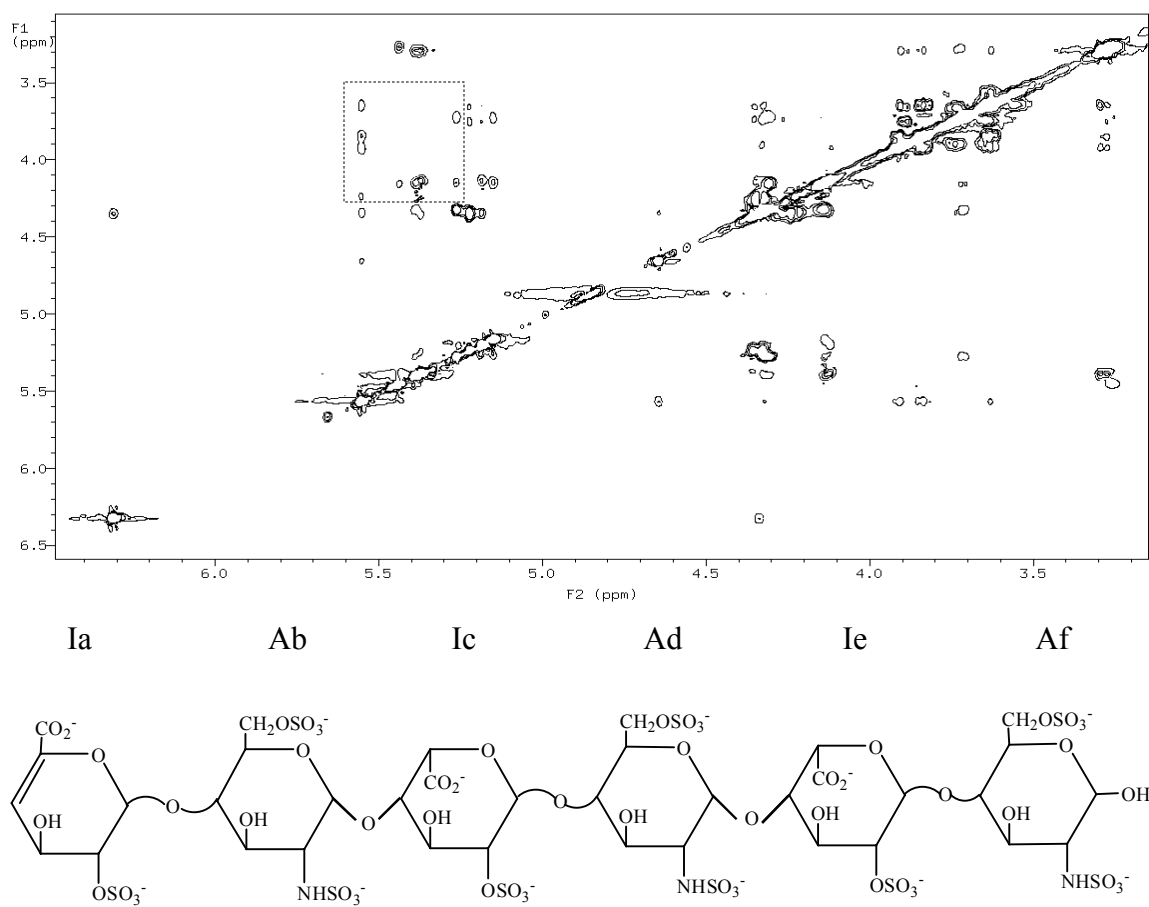
Figure 3. 25. The full ROESY spectrum (top) and the ROESY cross peaks (bottom) of heparin-derived hexasaccharide at pD 3.02, 25 °C.

	Monosaccharides					
Proton	ΔUA(2S)	GlcNS(6S)	IdoA(2S)	GlcNS(6S)	IdoA(2S)	GlcNS(6S)
H_1	5.551	5.369	5.222	5.388	5.262	5.435
H_2	4.641	3.282	4.355	3.282	4.323	3.253
H_3	4.334	3.627	4.322	3.735	4.292	3.701
H_4	6.310	3.830	4.119	3.830	4.135	3.720
H_5		3.902	5.185	3.902	5.148	4.148
H_{6a}		4.224		4.249		4.316
H_{6b}		4.334		4.332		4.341
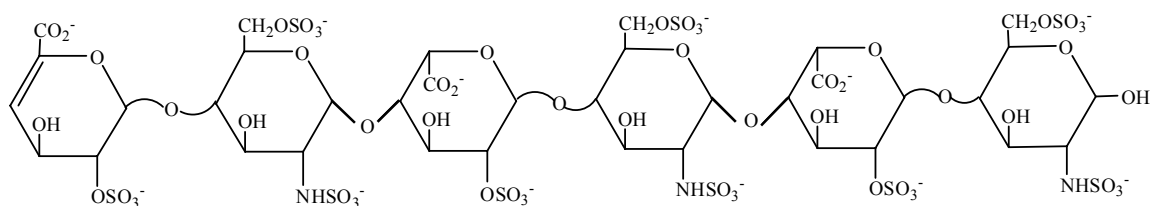
Table 3.5. ^{1}H NMR chemical shift data for the heparin-derived hexasaccharide at pD 3.02.
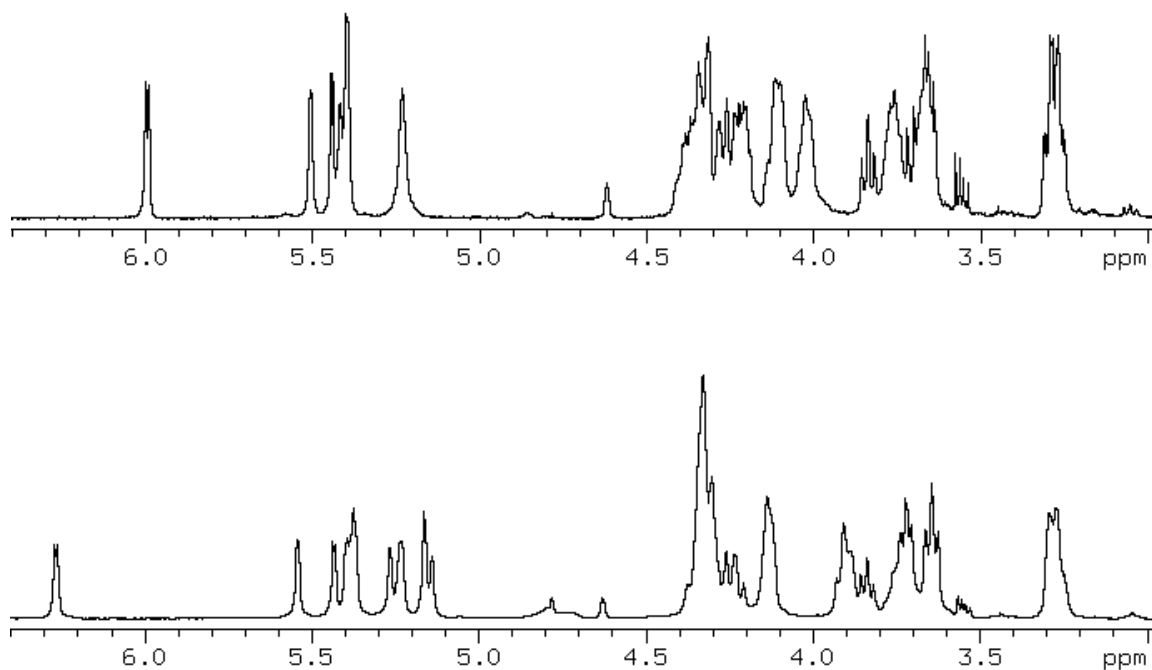
Figure 3.26. 1-D ^{1}H NMR spectra of the heparin-derived octasaccharide. The top spectrum was obtained at pD 5.32, and the bottom spectrum was obtained at pD 2.55.
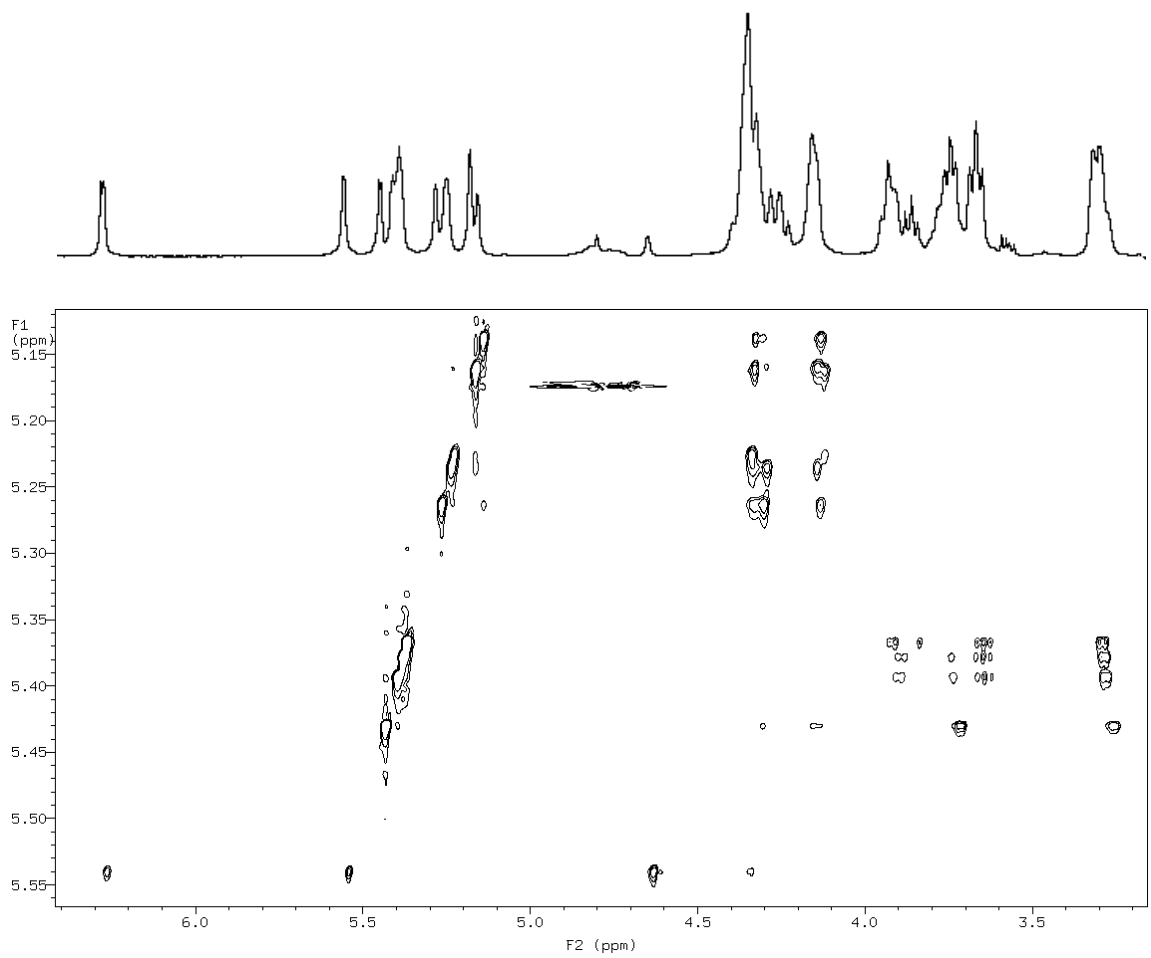
Figure 3.27. 1-D (top) and BASHD-TOCSY (bottom) spectra of heparin-derived

octasaccharide at pD 2.55, 25 °C.

Trace at 5.54 ppm

Trace at 5.37 ppm

Trace at 5.43 ppm

Trace at 5.26 ppm

Trace at 5.39 ppm

Trace at 5.24 ppm

Trace at 5.38 ppm

Trace at 5.23 ppm
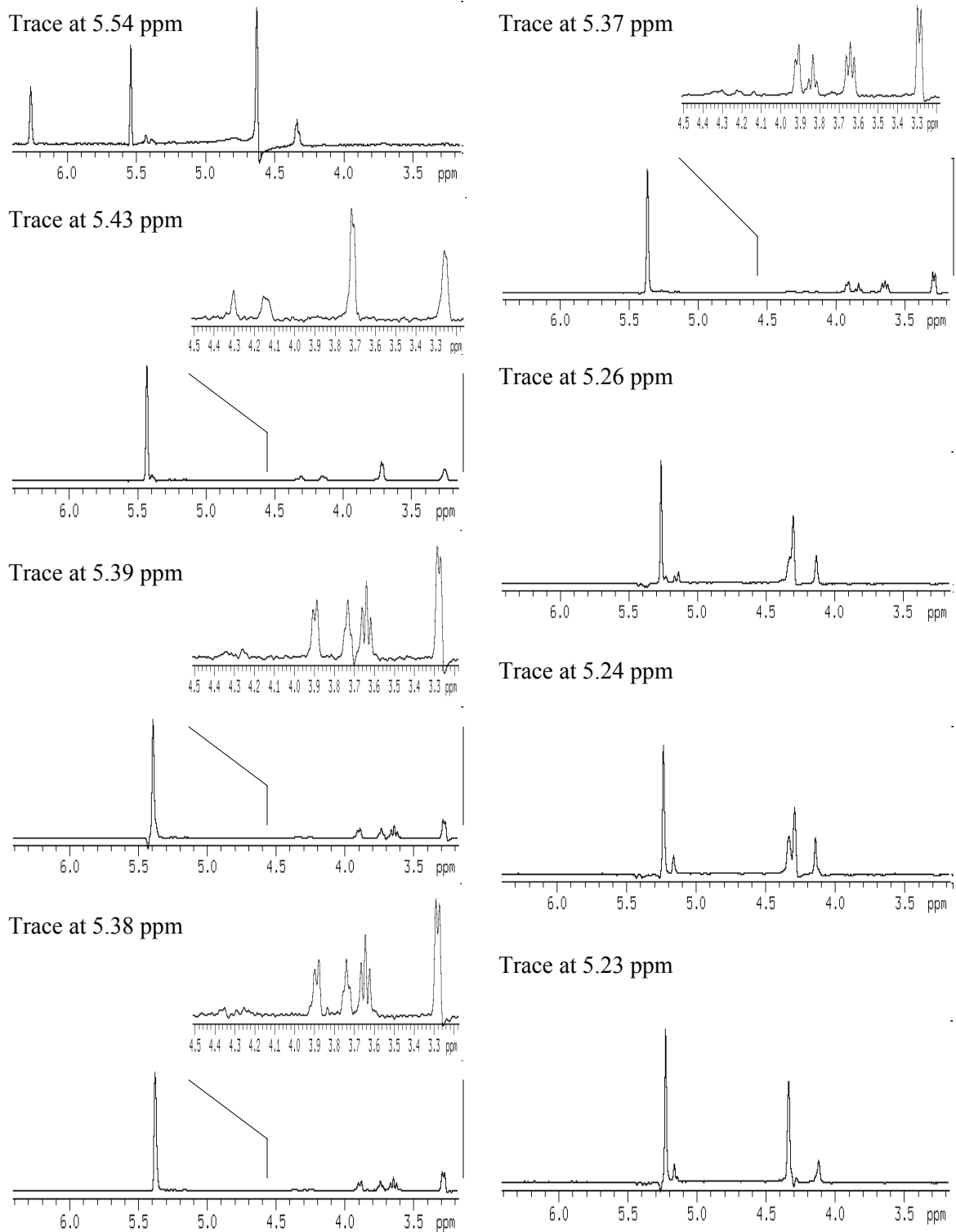
Figure 3.28. Traces through the BASHD-TOCSY spectrum in Figure 3.27 of heparin-derived octasaccharide at the chemical shifts of anomeric resonances.
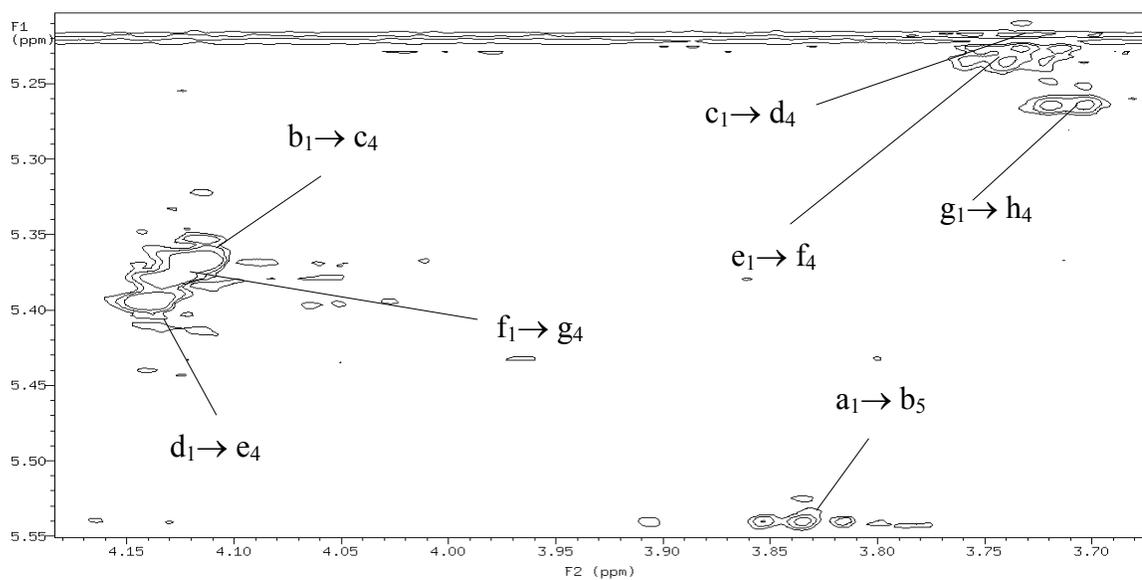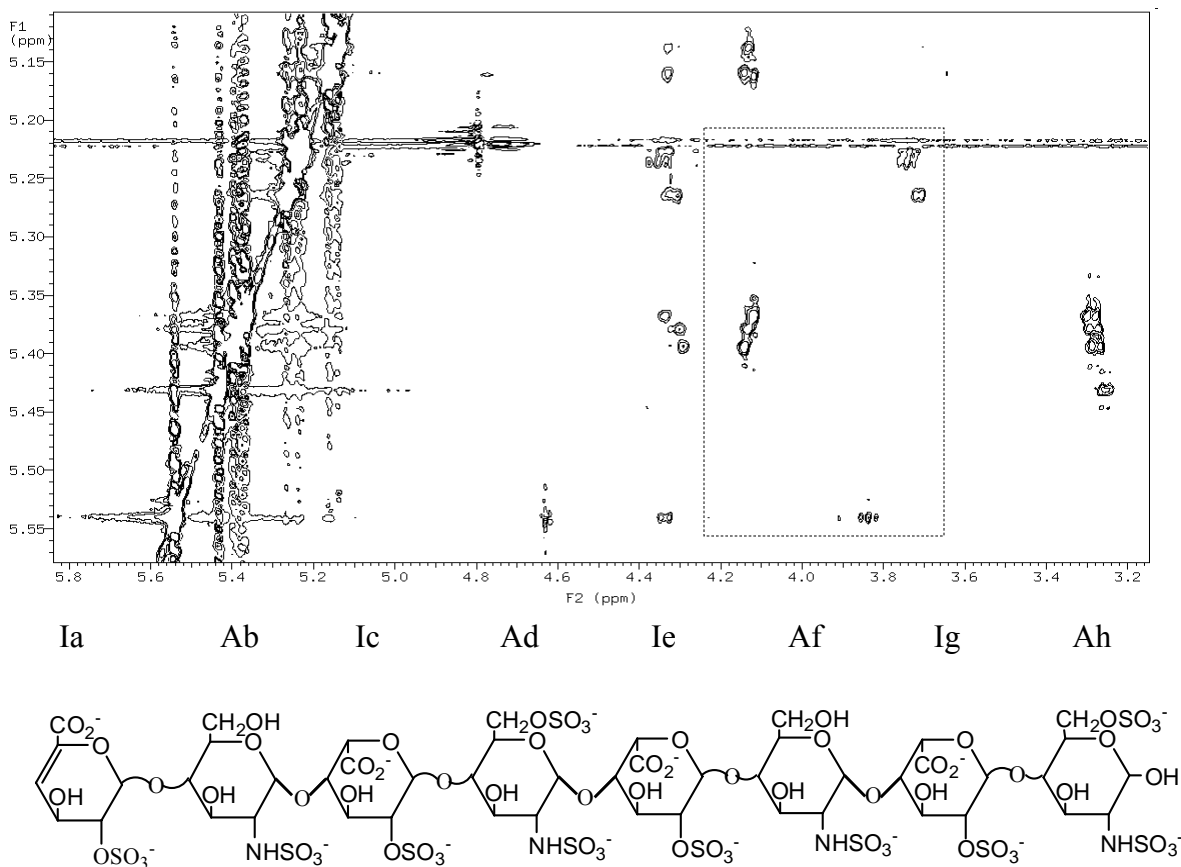
Figure 3. 29. The BASHD-NOESY spectrum (top) and the BASHD-NOESY cross peaks (bottom) of heparin-derived octasaccharide at pD 2.55, 25 °C.

139

Proton	Monosaccharides							
	ΔUA(2S)	GlcNS	IdoA(2S)	GlcNS(6S)	IdoA(2S)	GlcNS	IdoA(2S)	GlcNS(6S)
H_1	5.540	5.366	5.225	5.392	5.233	5.377	5.263	5.429
H_2	4.626	3.286	4.336	3.276	4.327	3.279	4.323	3.250
H_3	4.334	3.641	4.287	3.637	4.289	3.643	4.297	3.704
H_4	6.263	3.738	4.115	3.731	4.138	3.738	4.127	3.715
H_5		3.834	5.159	3.896	5.159	3.833	5.135	4.156
H_{6a}		3.915		4.254		3.887		4.301
H_{6b}		3.915		4.351		3.887		4.372
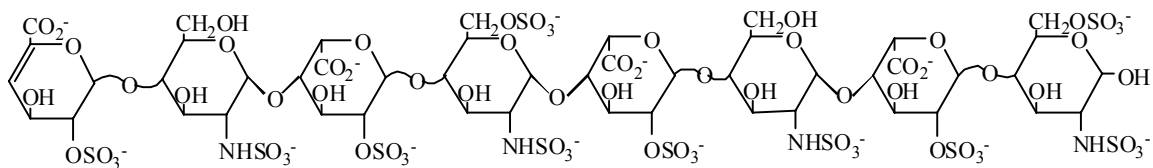
Table 3.6. ^{1}H NMR chemical shift data for the heparin-derived octasaccharide.

3.8 References

1. Capila, I.; Linhardt, R. *J. Angew. Chem. Int. Ed*. **2002**, *41*, 390-412.

2. Venkataraman, G; Shriver, Z; Raman, R.; Sasisekharan, R. *Science*, **1999**, *289*, 537.

3. Desai, U. R.; Wang, H. M.; Linhardt, R. J. *Biochemistry*, **1993**, *32*, 8140.

4. Chuang, W.L; Christ M. D.; Rabenstein, D. L. *Anal. Chem*. **2001**, *73*, 2310-2316.

5. Hileman, R. E.; Smith, A. E.; Toida, T.; Linhardt, R. J. *Glycobiology* **1997**, *7*, 231-239.

6. Tsuda, H.; Yamada, S.; Yamane, Y.; Yoshida, K.; Hopwood, J. J.; Sugahara, K. *J. Biol. Chem.* **1996**, *27*, 10495-10502.

<center>**Chapter 4**</center>

<center>**The Binding of Imidazole, Histamine, L-Histidine and Histidine-Containing Peptides to a Fully Sulfated Heparin-Derived Tetrasaccharide by NMR**</center>

4.1 Introduction

It has been reported that the histidyl imidazolium ring of several peptides and proteins, including synthetic β-amyloid peptide[1], histidine-rich glycoprotein[2], platelet factor 4[3], mouse mast cell protease 7 (mMCP-7)[4], binds to heparin. For instance, in the case of β-amyloid peptide, a major component of neuritic plaques located in the cortex and hippocampus of the Alzheimer's disease brain[5,6], was found to be aggregated in the presence of heparin. Histidine residues at positions 13 and 17 were demonstrated to be responsible for the association of β-amyloid peptide with heparin, as indicated by pH dependence of the binding affinity (tightly at pH 4.0 and essentially no association at pH 8.0) and the loss of the binding (both at pH 4.0 and 8.0) when the two histidines were replaced with serines.

mMCP-7, a tryptase bound to heparin-containing serglycin proteoglycans stored in secretory granules of mast cells, was reported to bind to a heparin affinity column at the acidic pH 5.5 of the granule.[7] The ability of mMCP-7 to bind heparin via ionic interaction depends on the ionization state of histidines at positions 8, 68, and 70, as supported by no binding observed at pH > 6.5 since the positively charged side-chains ($pK_a = 6.5$) of these histidines are eliminated at this pH due to being deprotonated. Additionally, site-directed mutagenesis confirmed that a mutation of His[8], His[68], or His[70] into Glu greatly diminished the binding of mMCP-7 to the heparin affinity column at pH

<center>142</center>

5.0-5.5. In another study reported by this research group, histidine side chain of the growth factor GHK was demonstrated to bind to heparin, as indicated by the displacement of the histidyl imidazolium ring proton (C2H) to higher pD in the presence of heparin.[8]

In this chapter, results from research on the site specific binding of the imidazolium ring of imidazole, histamine, L-histidine, and histidine-containing peptides by a fully sulfated heparin-derived tetrasaccharide (ΔUA(2S)-GlcNS(6S)-IdoA(2S)-GlcNS(6S), tetrasaccharide III), are presented. In Chapter 5, results from a study of the binding of the same molecules by intact heparin are presented. The histidine-containing peptides studied include GH, HG, GHK, GHG, and FRHDSGY, a β-amyloid peptide (4-10). The binding interactions of imidazole, histamine, L-histidine, and histidine-containing peptides with tetrasaccharide III in aqueous solution were characterized by ^{1}H NMR spectroscopy. Due to the strong dependence of the binding constant on Na$^+$ concentration[9], it should be noted that binding constants and pK_a values reported in this chapter were determined with a total NaCl concentration of ~ 0.020 M.

4.2 pK_a Determination of Tetrasaccharide

Prior to determination of the binding constants for the interaction of ligands with tetrasaccharide III, pK_a values were determined for the two carboxylic acid groups of the tetrasaccharide. The pK_a values of the carboxylic acid groups of tetrasaccharide were determined directly from the pD dependence of the chemical shifts of the H4 and H5 protons of the ΔUA(2S) and IdoA(2S) residues, respectively, as well as from chemical shift data for the Ab-H3 resonance.

The chemical shifts of the H4 and H5 protons of ΔUA(2S) and IdoA(2S) residues were used as an indicator to study the acid/base chemistry of the two residues because the H4 and H5 protons are closest to their carboxylic acid groups, and thus their chemical shifts are affected the most by titration of the carboxylic acids. The changes in the chemical shifts of the ΔUA-H4 and Ic-H5 protons as a function of pD measured using one-dimensional ^{1}H NMR are shown in Figures 4.1 and 4.2, respectively. Figure 2.15 in Chapter 2 shows the chemical shift-pD titration curve for H4 of the ΔUA(2S) unit. The chemical shift titration curve for Ic-H5 of tetrasaccharide III is shown in Figure 4.3.

Acid dissociation constants of the two carboxylic acid groups were obtained by fitting chemical shift-pD titration data to equation 2.7 in Chapter Two using the nonlinear least squares program Scientist. The pK_a values of the carboxylic acid groups of ΔUA(2S) and IdoA(2S) residues are shown in Table 4.1.

4.3 Purity Determination of Tetrasaccharide

In order to determine the binding constant for the interaction of heparin-derived tetrasaccharide III with ligands, the purity of tetrasaccharide III was determined using 4-hydroxybenzoic acid (99.0%) as an internal intensity reference. The 1-D ^{1}H NMR spectrum of free 4-hydroxybenzoic acid solution is shown in Figure 4.4. The two aromatic resonances of 4-hydroxybenzoic acid are well resolved from each other and are far away from resonances of tetrasaccharide III, which makes it a good compound for determining the purity of tetrasaccharide III. Figure 4.5 shows a 1-D ^{1}H NMR spectrum of a solution containing a known concentration of 4-hydroxybenzoic acid and tetrasaccharide III. By comparing the peak area of the ΔUA-H4 resonance to the peak

144
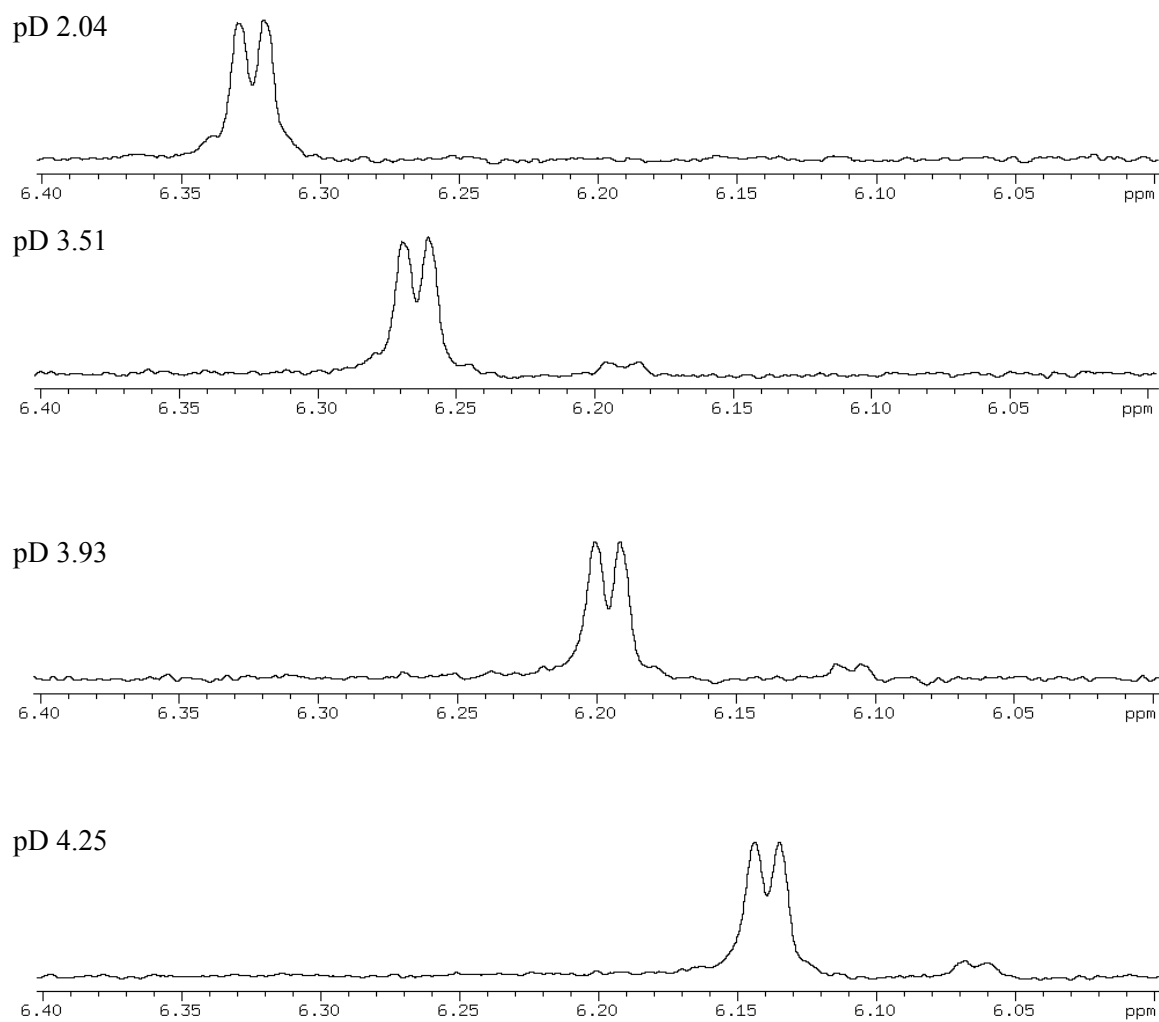
Figure 4.1. 1-D ^{1}H NMR spectra showing the pD dependence of the chemical shift of the H4 resonance of the ΔUA(2S) residue of free fully sulfated heparin-derived tetrasaccharide (tetrasaccharide III) in D$_2$O solution with [Na$^+$]$_{total}$ of ~ 0.020 M.
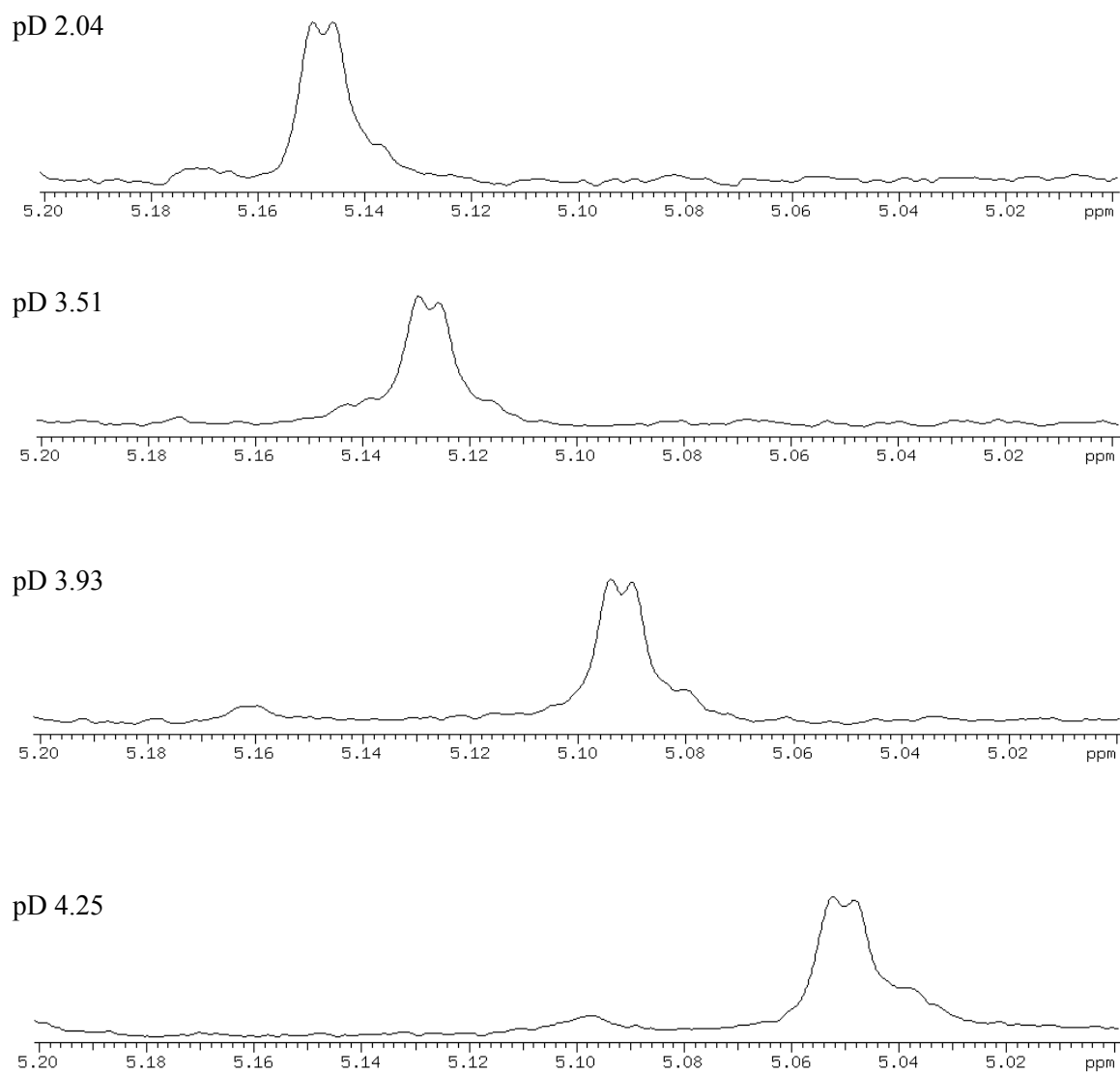
Figure 4.2. 1-D ^{1}H NMR spectra showing the pD dependence of the chemical shift of the H5 resonance of the IdoA(2S) residue of free tetrasaccharide III in D$_2$O solution with [Na$^+$]$_{total}$ of ~ 0.020 M.
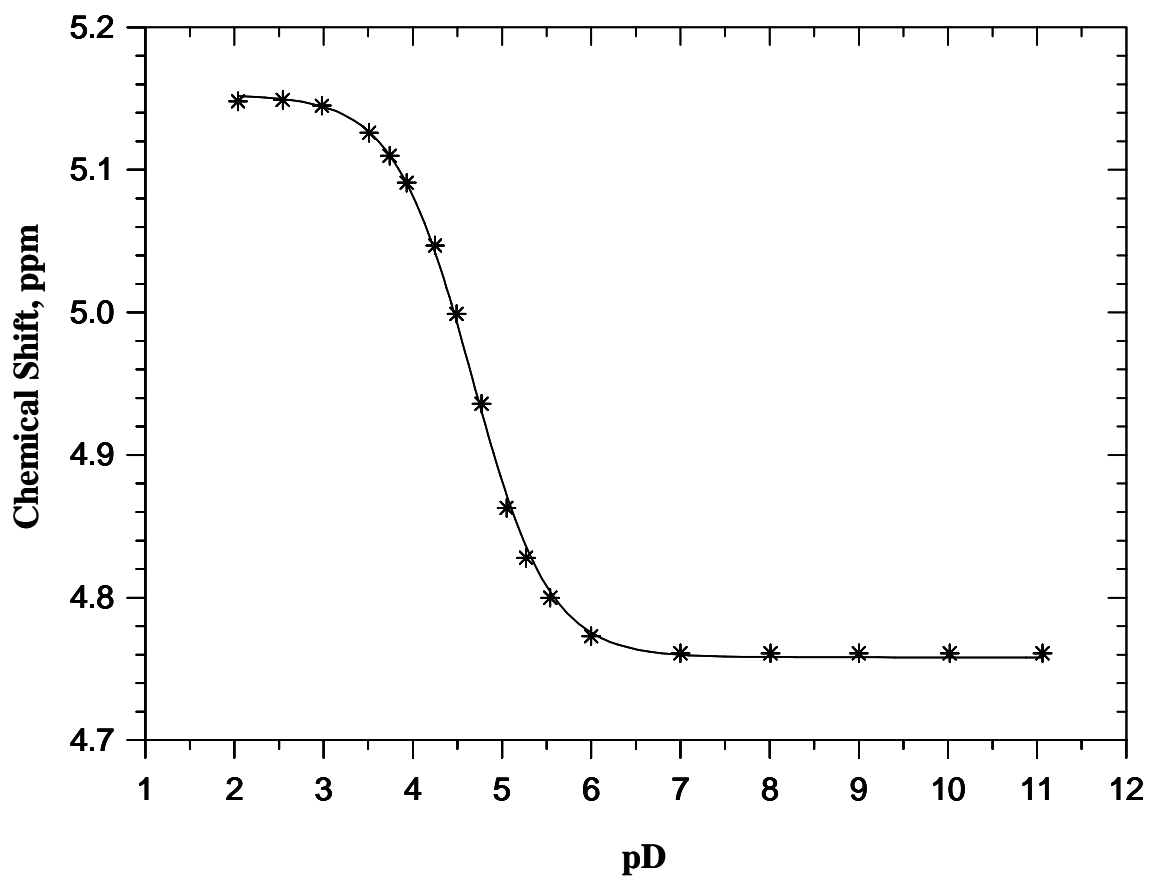
Figure 4.3. The chemical shift-pD titration curve for the H5 proton of the IdoA(2S) residue of 0.193 mM free tetrasaccharide III in D$_2$O solution with [Na$^+$]$_{total}$ of ~ 0.020 M.

	pK$_a$	δ$_{HA}$	δ$_A$
ΔUA-H4	4.17 ± 0.01	6.328 ± 0.001	5.973 ± 0.001
Ic-H5	4.66 ± 0.01	5.153 ± 0.002	4.758 ± 0.002

Table 4.1. Acid dissociation constants of the carboxylic acid groups of tetrasaccharide III.
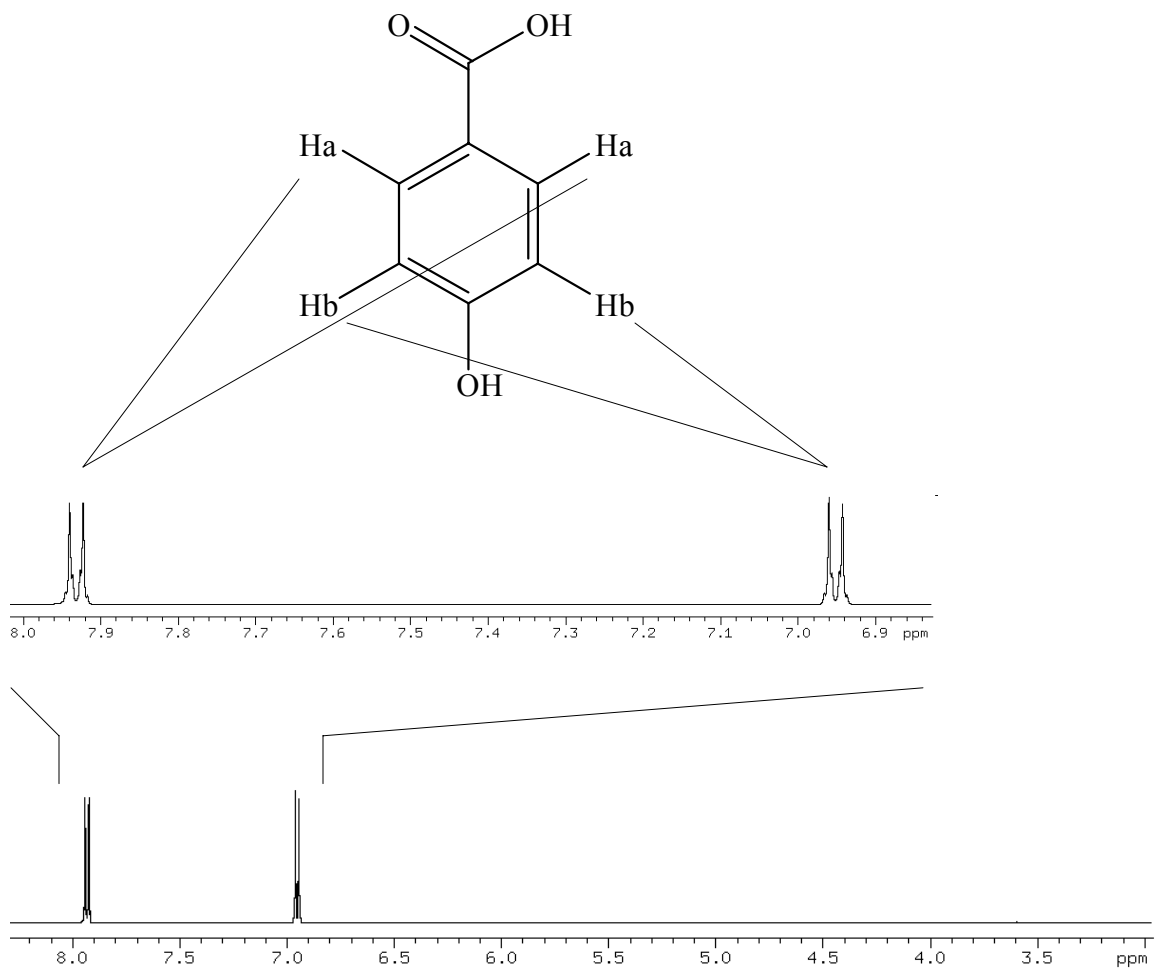
Figure 4.4. Portion of the 1D ^{1}H NMR spectrum of free 4-hydroxybenzoic acid at pD 2.97 and 25 °C.

149
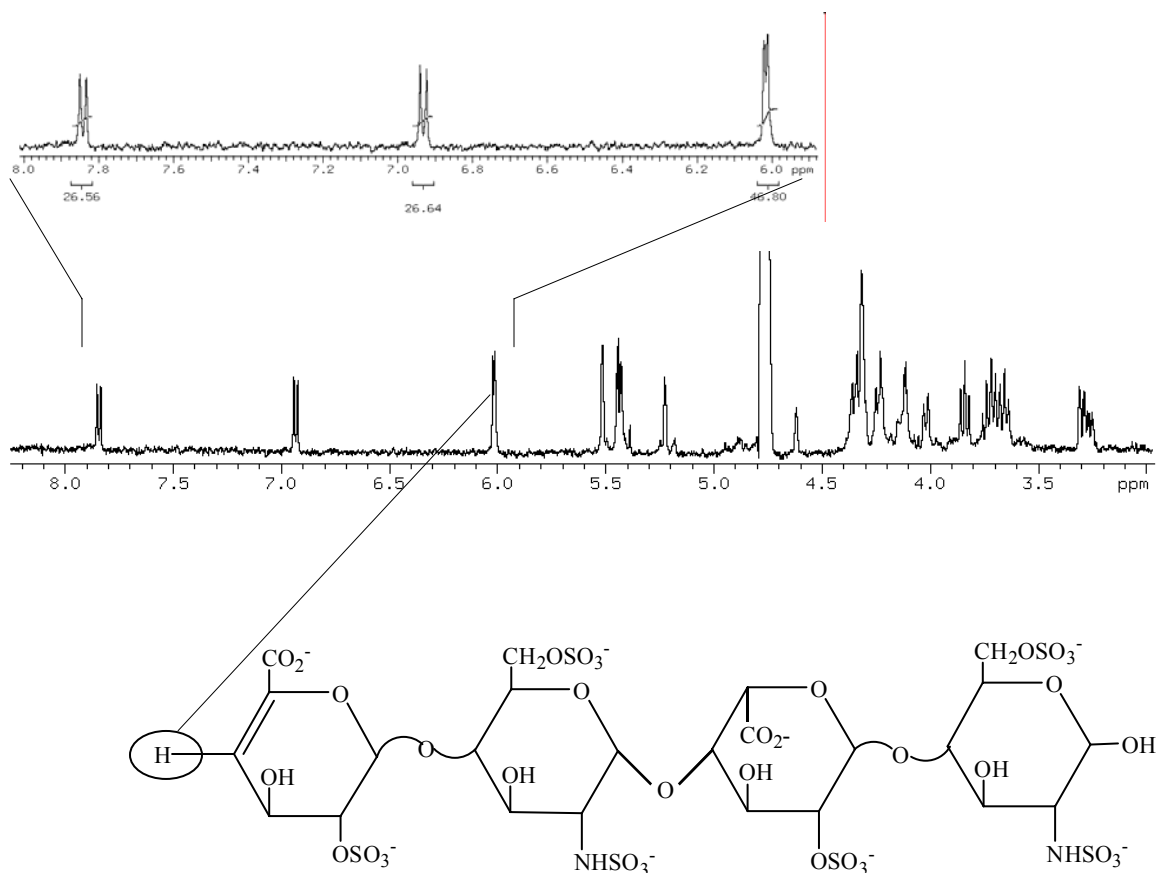
Figure 4.5. Portion of the 1-D ^{1}H NMR spectrum of a solution of 4-hydroxybenzoic acid and tetrasaccharide III at pD 5.43 and 25 °C. The resonance for the ΔUA-H4 proton (in circle) was used to determine the purity of tetrasaccharide III. The peak area of the ΔUA-H4 resonance was measured relative to the peak areas of the two resonances of 4-hydroxybenzoic acid.

areas of the two resonances of 4-hydroxybenzoic acid, an average purity of 98.3% was obtained for tetrasaccharide III. Because no impurity peaks were detected in the CE of tetrasaccharide III, it seems likely the small impurity is residual water.

4.4 Binding of Histamine by Tetrasaccharide

4.4.1 Acid Dissociation Constants of Histamine

The acid/base chemistry of the imidazolium ring and the ammonium group of histamine in the absence and presence of tetrasaccharide can provide evidence for the binding interaction of histamine by tetrasaccharide III.

In the presence of tetrasaccharide III, the pK_a values of the imidazolium ring and the ammonium group of histamine both increase, indicating the involvement of the imidazolium ring and the ammonium group in the binding of histamine by tetrasaccharide. The pK_a values of the imidazolium ring and the ammonium group in the absence and presence of tetrasaccharide III are reported in Table 4.2. They were determined by fitting chemical shift-pD titration data of different reporter protons using the diprotic acid model described in Chapter Two. The chemical shift vs pD titration curves for C2H, C4H, CH$_2$a, and CH$_2$b protons of the imidazolium ring of histamine are shown in Figure 4.6.

Figure 4.7 shows the upfield shift of C2H and C4H resonances of free histamine over the pD range 4-8, which reflects titration of the imidazolium ring of histamine. The upfield shift of CH$_2$a and CH$_2$b resonances of free histamine over the pD range of 8-12 shown in Figure 4.8 corresponds to titration of the ammonium group of histamine. 1-D ^{1}H NMR spectra of free histamine and histamine in solution with tetrasaccharide III are

151

	pK$_a$							
	Free histamine				Histamine-Tetrasaccharide III Complex			
	C2H	C4H	CH$_2$a	CH$_2$b	C2H	C4H	CH$_2$a	CH$_2$b
Imidazolium ring	6.16 ± 0.01	6.17 ± 0.01	6.15 ± 0.02	6.12 ± 0.05	6.28 ± 0.01	6.28 ± 0.02	n.d.	n.d.
Ammonium group	10.19 ± 0.13	10.12 ± 0.02	10.05 ± 0.01	10.07 ± 0.01	n.d.	n.d.	n.d.	n.d.

n.d., Not determined.
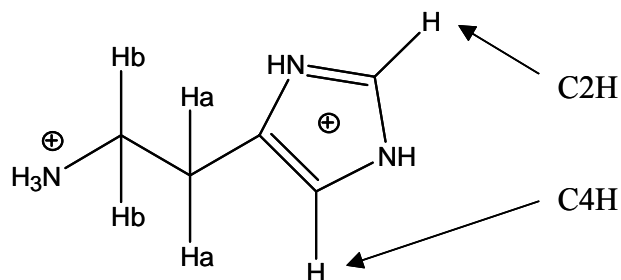
Table 4.2. Acid dissociation constants of the imidazolium ring and the ammonium group of histamine using the C2H, C4H, CH$_2$a, and CH$_2$b reporter protons. The C2H and C4H protons give more reliable pK$_a$ value for the imidazolium ring, and the CH$_2$a and CH$_2$b protons gives more reliable pK$_a$ value for the ammonium group.
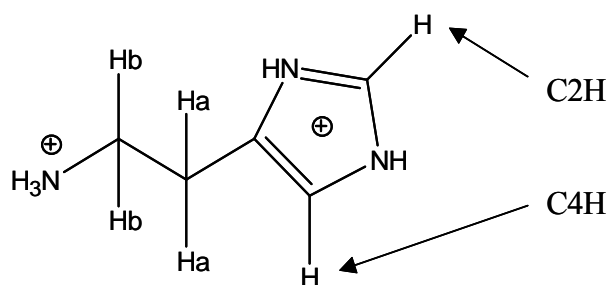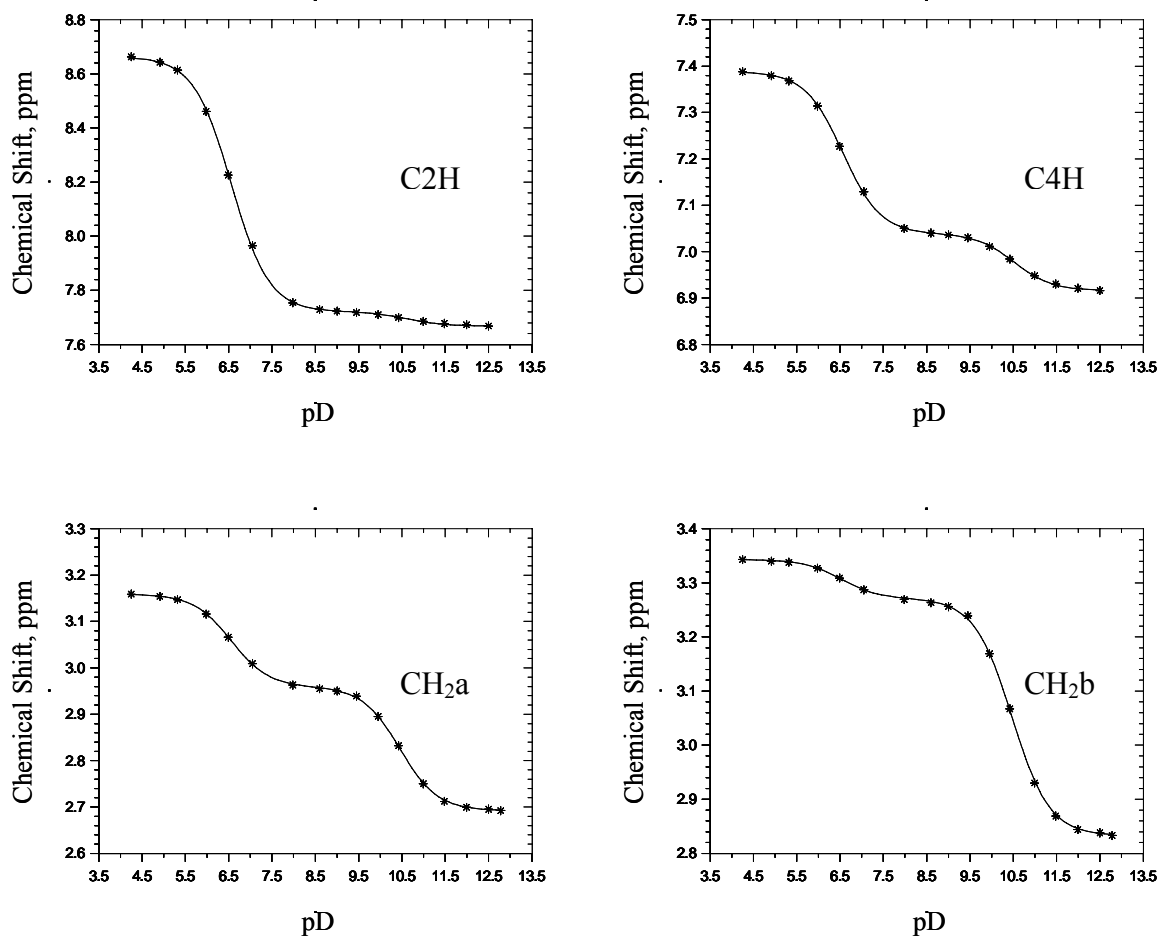
Figure 4.6. Chemical shift-pD titration curves for the C2H, C4H, CH$_2$a, and CH$_2$b

reporter protons of 0.020 M free histamine in D$_2$O solution with [Na$^+$]$_{total}$ of ~ 0.020 M.
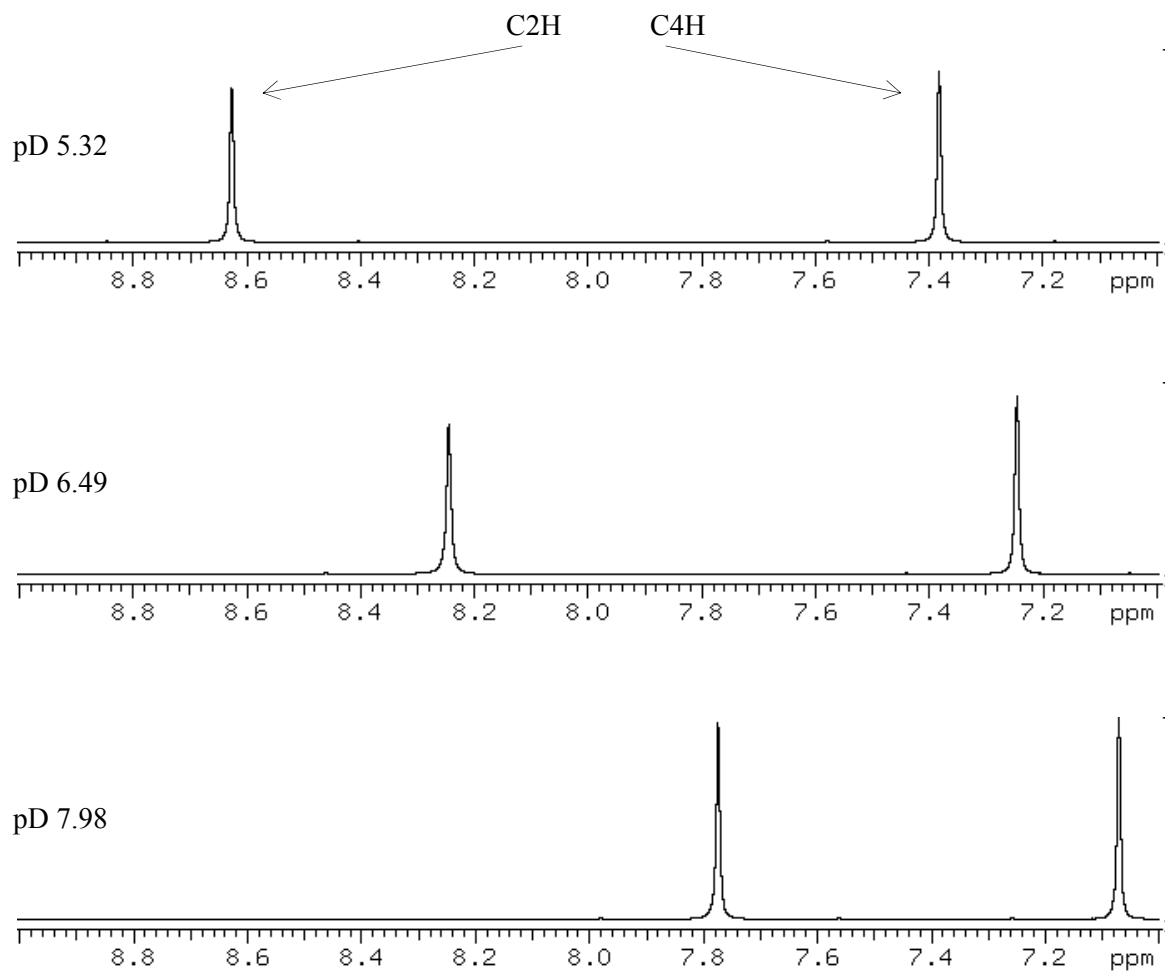
Figure 4.7. Portions of 1-D ^{1}H NMR spectra of a D_2O solution which contained 20.0 mM histamine with $[Na^+]_{total}$ of ~ 0.020 M at various pD values.
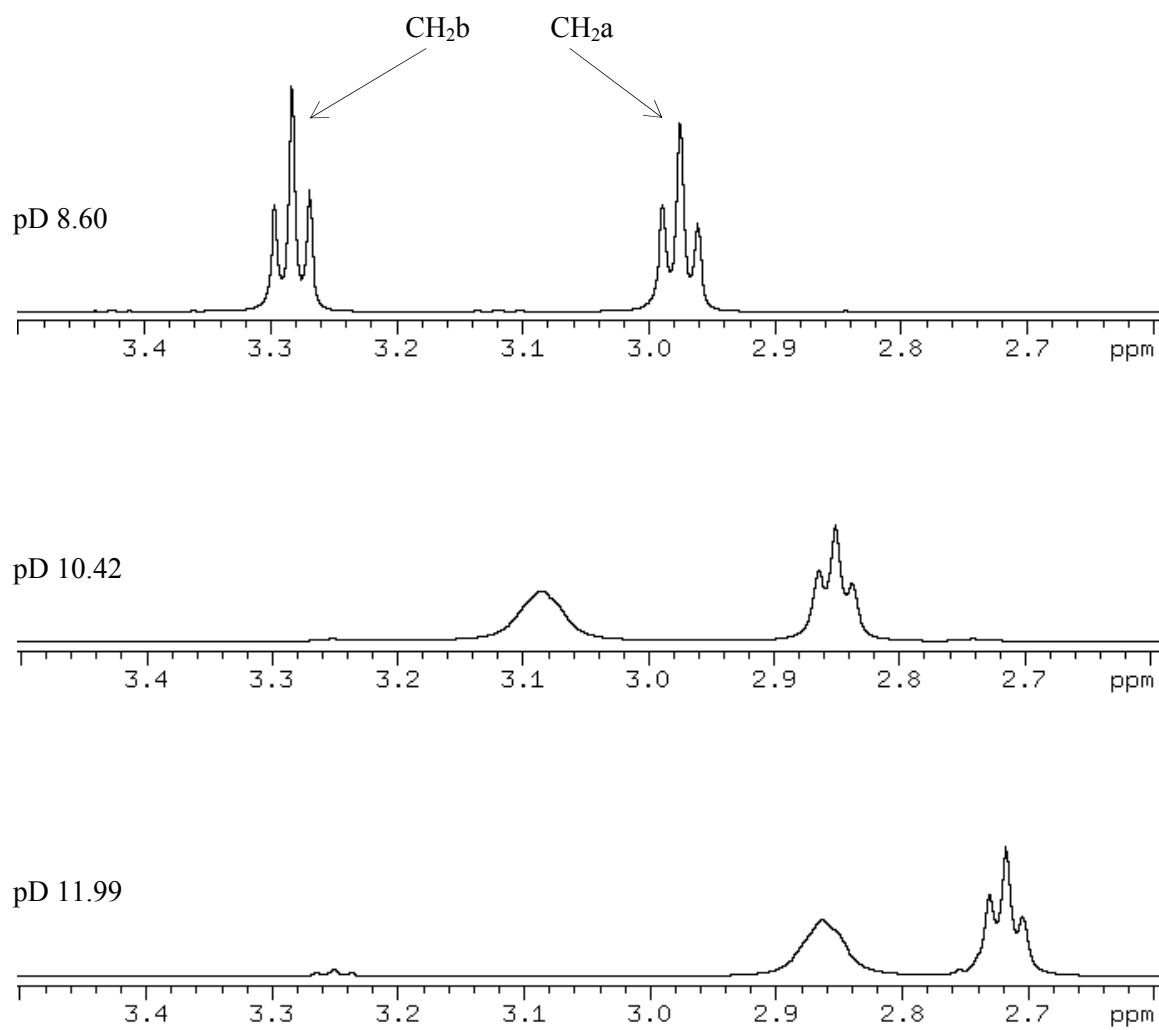
Figure 4.8. Portions of 1-D ^{1}H NMR spectra of a D_2O solution containing 20.0 mM histamine with $[Na^+]_{total}$ of ~ 0.020 M at various pD values.

shown in Figure 4.9. Figure 4.10 shows the downfield shift of C2H, C4H, CH$_2$a, and CH$_2$b resonances of histamine in the presence of tetrasaccharide III, indicating the involvement of the imidazolium ring and the ammonium group of histamine in the interaction of histamine with tetrasaccharide.

4.4.2 Evidence for Binding Interaction

The binding interaction was further confirmed by comparing the chemical shift-pD titration curves for Ic-H5 and ΔUA-H4 protons of tetrasaccharide III in the free and complex forms. Figures 4.11 and 4.12 show chemical shift titration curves for Ic-H5 and ΔUA-H4 protons, which shift to lower pD when tetrasaccharide III is in solution with histamine, suggesting the interaction of histamine with tetrasaccharide III. As seen from Figures 4.11 and 4.12, Ic-H5 and ΔUA-H4 protons of tretrasaccharide III free in solution are pD dependent. They shift upfield over the pD range 2-6, which reflects titration of the carboxylic acid groups of IdoA(2S) and ΔUa(2S) residues. The lower pD displacement of the chemical shift titration curves for Ic-H5 and ΔUA-H4 protons are consistent with formation of the histamine-tetrasaccharide III complex as described by the following equilibria:

TetrasaccCO$_2$H $\leftrightarrow$ TetrasaccCO$_2^-$ + H$^+$

TetrasaccCO$_2^-$ + H$_2$A^{2+} $\leftrightarrow$ TetrasaccCO$_2^-$-H$_2$A^{2+}

H$_2$A^{2+} $\leftrightarrow$ HA$^+$ + H$^+$
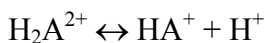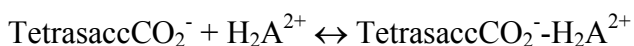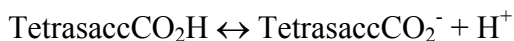
Where TetrasaccCO$_2$H and TetrasaccCO$_2^-$ represent the carboxylic acid and carboxylate groups of the IdoA(2S) and ΔUA(2S) residues of tetrasaccharide III, H$_2$A^{2+} represents the
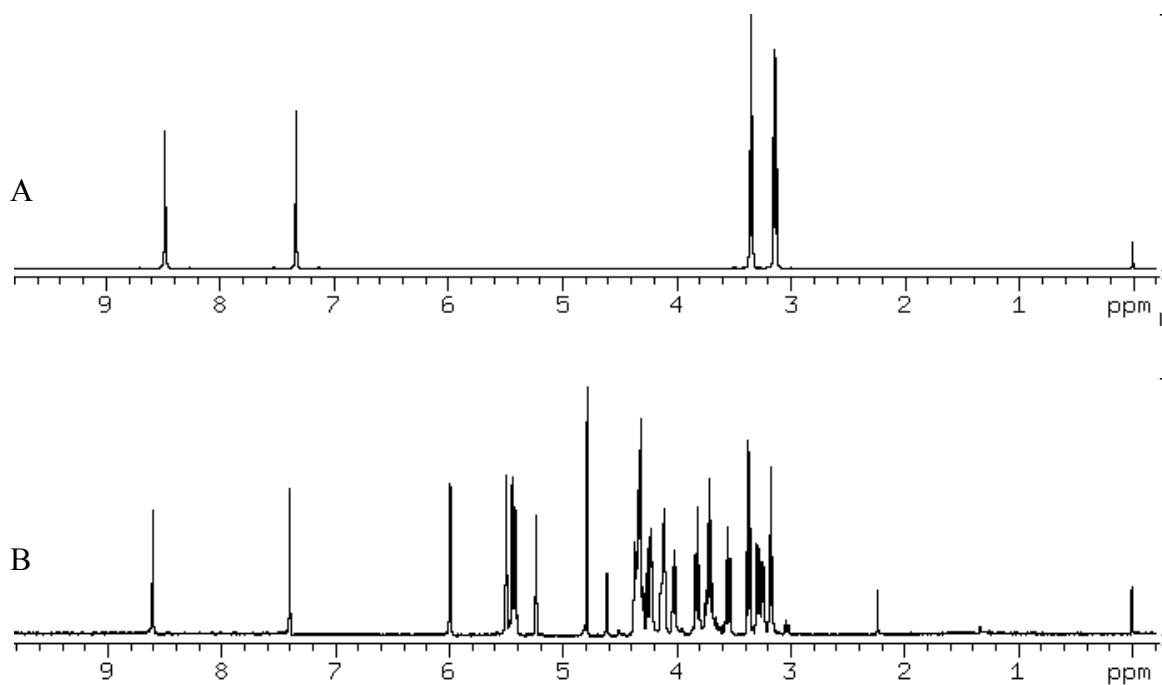
Figure 4.9. 1-D ^{1}H NMR spectra of D$_2$O solutions containing (A) 0.020 M histamine at pD 5.98 and (B) 0.474 mM histamine with 1.01 mM tetrasaccharide III at pD 6.04. The total sodium concentration for free and bound histamine was ~ 0.020 M.
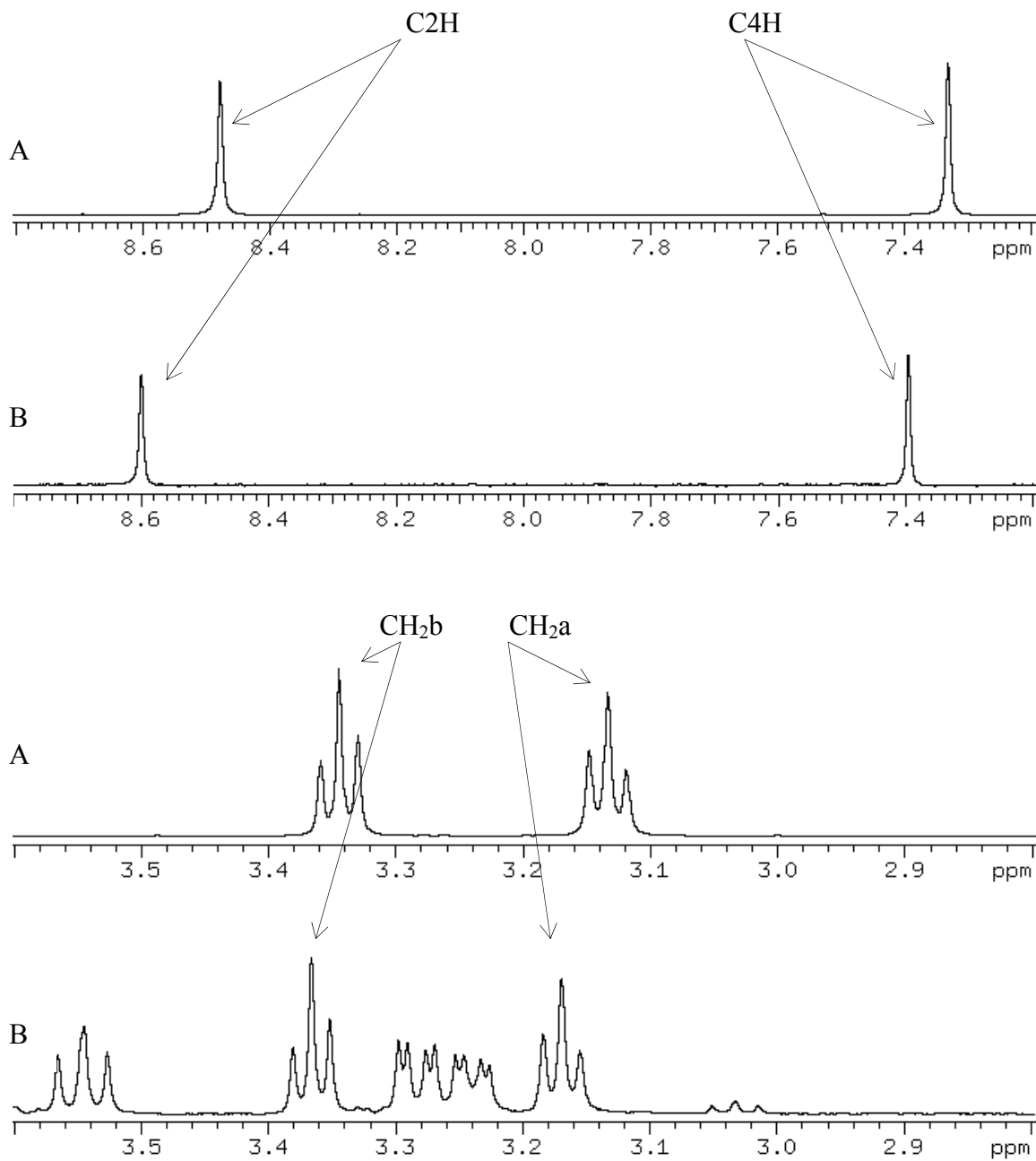
Figure 4.10. Portions of 1-D ^1H NMR spectra of D_2O solutions containing (A) 20.0 mM

histamine at pD 5.98 and (B) 0.474 mM histamine plus 1.01 mM tetrasaccharide III at pD

6.04. The total sodium concentration for free and bound histamine was ~ 0.020 M.
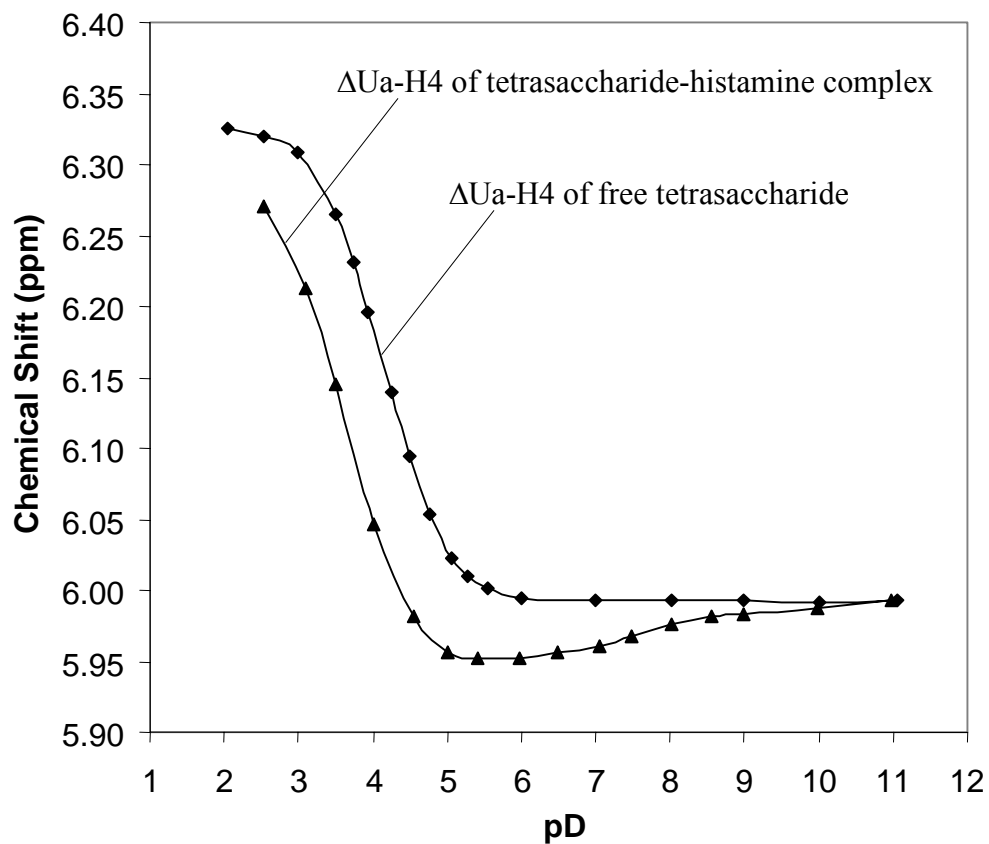
Figure 4.11. Chemical shift-pD titration data for the H4 proton of the ΔUA residue of tetrasaccharide III in the absence and presence of histamine. The histamine-tetrasaccharide III complex solution contains 0.020 M histamine and 0.001 M tetrasaccharide III with $[Na^+]_{total}$ of ~ 0.020 M.
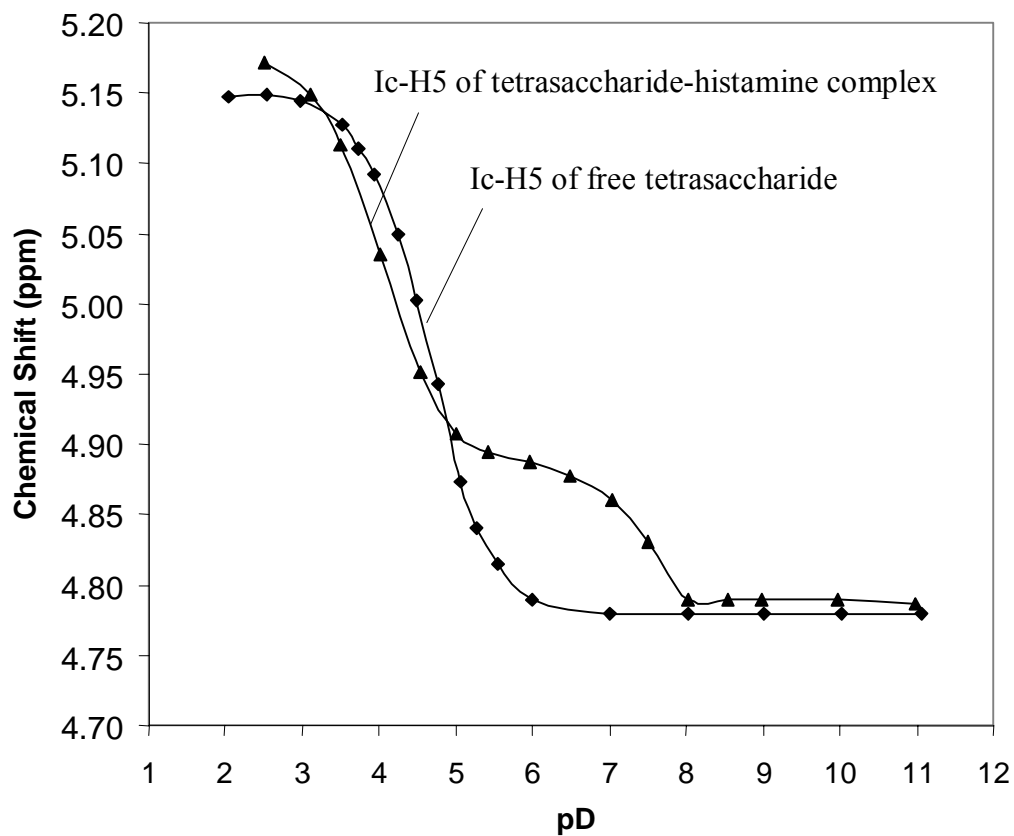
Figure 4.12. Chemical shift-pD titration data for the H5 proton of the Ic residue of tetrasaccharide III in the absence and presence of histamine. The tetrasccharide III-histamine complex solution contains 0.020 M histamine and 0.001 M tetrasaccharide III with $[Na^+]_{total}$ of ~ 0.020 M.

160

diprotonated form of histamine, and TetrasaccCO$_2^-$-H$_2$A^{2+} is for the histamine-tetrasaccharide III complex.

Formation of the TetrasaccCO$_2^-$-H$_2$A^{2+} complex shifts the TetrasaccCO$_2$H deprotonation equilibrium to the right, which displaces the chemical shift titration curve for the Ic-H5 proton to lower pD, corresponding to an increase in the apparent acidity of the carboxylic acid group of the IdoA(2S) residue. On the other hand, for histamine, formation of TetrasaccCO$_2^-$-H$_2$A^{2+} shifts the H$_2$A^{2+} deprotonation equilibrium to the left and thus shifts the chemical shift titration curve for the C2H proton (Figure 4.13) of the imidazolium ring of histamine to higher pD, corresponding to an increase in the apparent basicity of the diprotonated form of histamine.

Figure 4.14 shows the chemical shift vs pD titration curves for the Ab-H3 proton of tetrasaccharide III free and in the presence of histamine. The chemical shift titration curve in the presence of tetrasaccharide III indicates complex formation upon titration of the carboxylic acid groups of tetrasaccharide III and dissociation of the complex upon titration of the imidazolium group of histamine. The chemical shift data over the pD range 9-11 also suggest the ammonium group of the HA$^+$ form of histamine binds to tetrasaccharide III. It should be noted that titration of the ammonium group of histamine occurs over the pD range 8-12 (Figure 4.6), which is where the proposed binding of the ammonium group of histamine by tetrasaccharide III takes place. The downfield shift of the CH$_2$ protons of histamine in the presence of tetrasaccharide as seen in Figure 4.10 also suggests the involvement of the ammonium group of histamine in the binding of histamine by tetrasaccharide III.
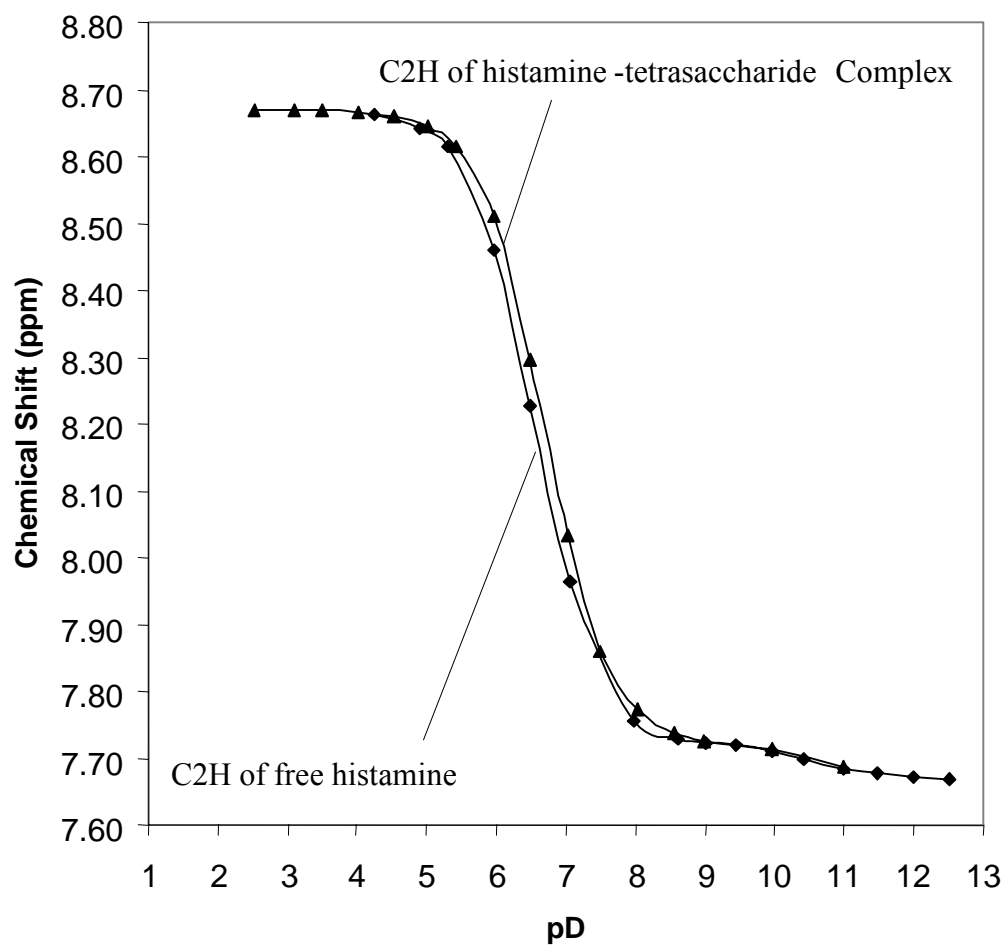
Figure 4.13. pD dependence of the chemical shift of the C2H proton of histamine in D_2O

solutions containing 0.020 M histamine, and 0.020 M histamine + 0.001 M

tetrasaccharide III. Both free and complex solutions contain $[Na^+]_{total}$ of ~ 0.020 M.
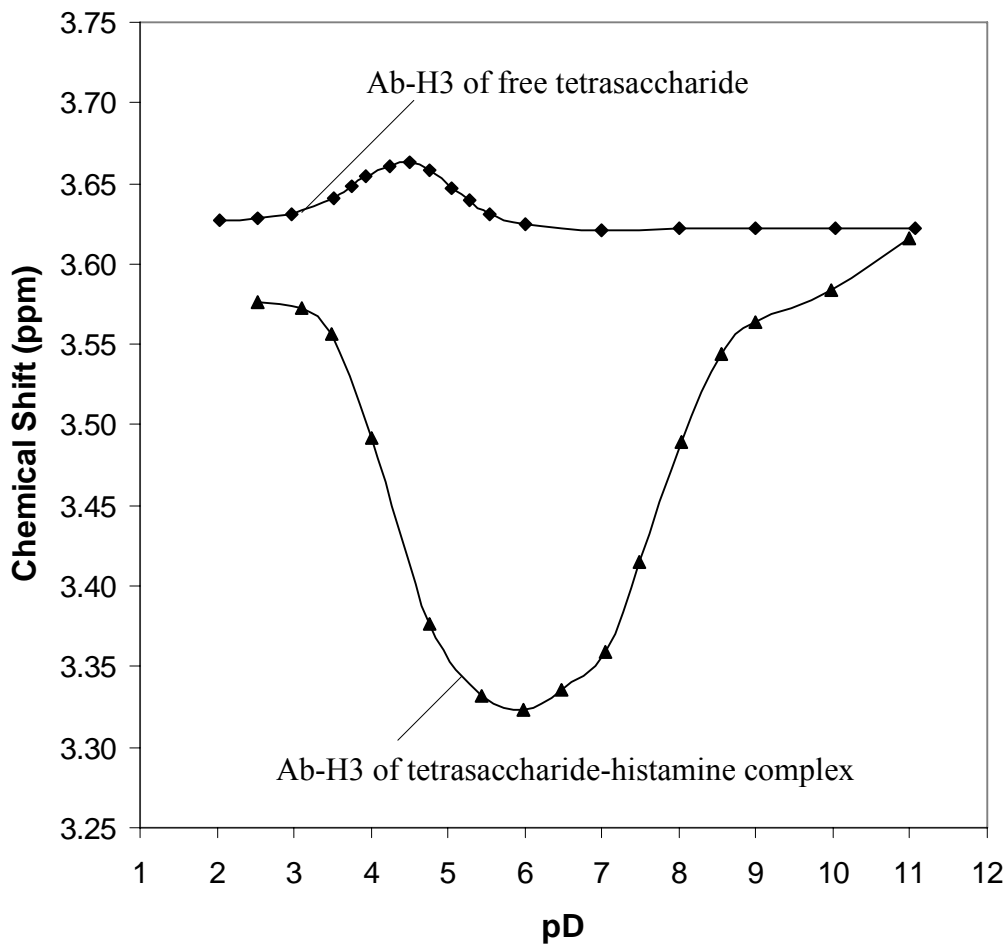
Figure 4.14. Chemical shift-pD titration data for the Ab-H3 proton of tetrasaccharide for a solution containing only tetrasaccharide and a solution containing 0.020 M histamine plus 0.001 M tetrasaccharide. Both free and complex solutions contain ~ 0.020 M Na^+.

4.4.3 Site Specific Binding

Site specific binding of histamine by tetrasaccharide III was suggested by an upfield displacement of the Ab-H3 resonance when the tetrasaccharide is in solution with histamine (Figure 4.14). When tetrasaccharide III is free in solution, the chemical shift of the Ab-H3 resonance shows a small change in chemical shift due to titration of the carboxylic acid groups. In the presence of histamine, the Ab-H3 resonance is displaced upfield over the pD region where the carboxylic acid groups of ΔUA(2S) and IdoA(2S) residues of tetrasaccharide III are titrated. Since the upfield shift of the Ab-H3 resonance and titration of the carboxylic acid groups occur at the same pD range of 2-6, titration of the carboxylic acid groups is believed to be necessary for the site specific binding of histamine by tetrasaccharide.[10] The upfield shift of the Ab-H3 resonance reaches its maximum at pD ~6 (see Figure 4.14). Beyond pD 6 where titration of the imidazolium group occurs, the chemical shift of the Ab-H3 resonance returns to its value in the absence of histamine, suggesting dissociation of the tetrasaccharide-histamine complex. 1-D ^{1}H NMR spectra showing the upfield shift of the Ab-H3 resonance at various pD values are presented in Figure 4.15.

The chemical shift data in Figure 4.14 shows that there is some binding of histamine to tetrasaccharide III at low pD where the carboxyl groups of ΔUA(2S) and IdoA(2S) residues of III are in the carboxylic acid form.

4.4.4 Association Constant Determination

The association constant for the interaction of histamine with tetrasaccharide III was determined by measuring the chemical shift of the resonance for the Ab-H3 proton as
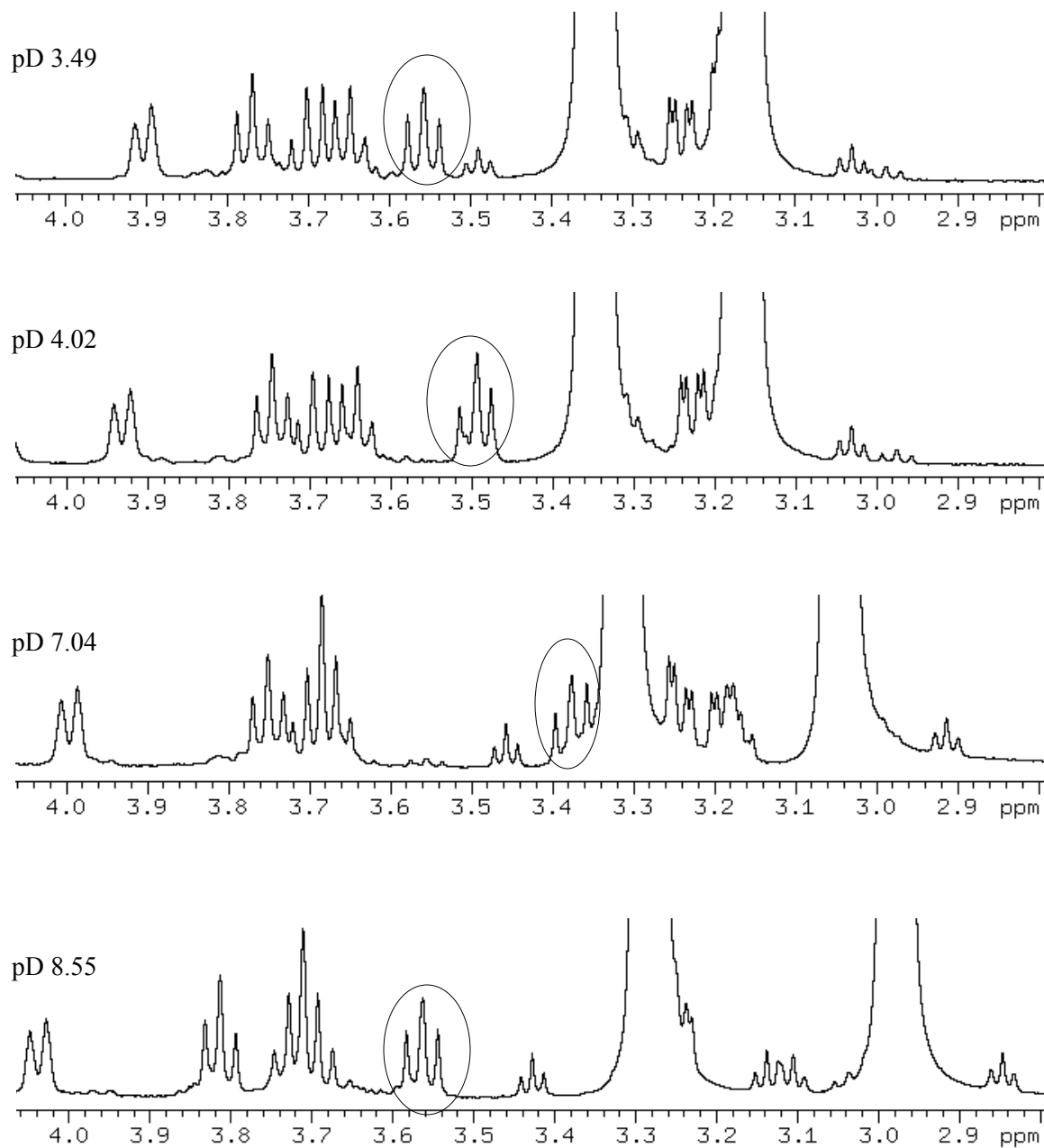
Figure 4.15. Portions of 1-D ^{1}H NMR spectra of a D_2O solution containing 0.020 M histamine plus 0.001 M tetrasaccharide III with $[Na^+]_{total}$ of ~ 0.020 M at various pD values. The circled resonance corresponds to the Ab-H3 proton of tetrasaccharide III.

165

a function of the concentration of histamine at pD 6.02, where histamine binds strongest

to tetrasaccharide (see Figure 4.14). The concentration of tetrasaccharide III was held

constant at 1.01 mM. The chemical shift-concentration data (Figure 4.16) were fit with

Scientist program by the nonlinear least-squares fitting procedure described in Chapter 2

to obtain the binding constant. A binding constant of 2,368 $\pm$ 128 M^{-1} was obtained at pD

6.02 $\pm$ 0.07. The dependence of the chemical shift of the Ab-H3 resonance of

tetrasaccharide III on histamine : tetrasaccharide ratio is shown in Figure 4.17.

4.5 Binding of Imidazole by Tetrasaccharide

1-D ^{1}H NMR spectra for free imidazole and the tetrasaccharide III complex with

imidazole are shown in Figure 4.18. Figure 4.19 shows the chemical shift vs pD titration

curves for the C2H and C4, 5H protons of imidazole free in solution. Acid dissociation

constants of the imidazolium ring in the absence and presence of tetrasaccharide III are

reported in Table 4.3. The increase in the pK_a of the imidazole in the presence of

tetrasaccharide III suggests the binding of imidazole by tetrasacccharide.

Chemical shift-pD titration curves for ΔUA-H4 and Ic-H5 protons of

tetrasaccharide III in the absence and presence of imidazole are shown in Figure 4.20. In

the presence of imidazole, chemical shift titration curves are displaced to lower pD,

indicating the formation of the tetrasaccharide III-imidazolium ion complex. The pK_a

values of the carboxylic acid groups of ΔUA(2S) and IdoA(2S) residues in the absence

and presence of imidazole are reported in Table 4.4.

Site specific binding of imidazole by tetrasaccharide III was indicated by an

upfield displacement of the Ab-H3 resonance (Figure 4.21). It should be noted that the
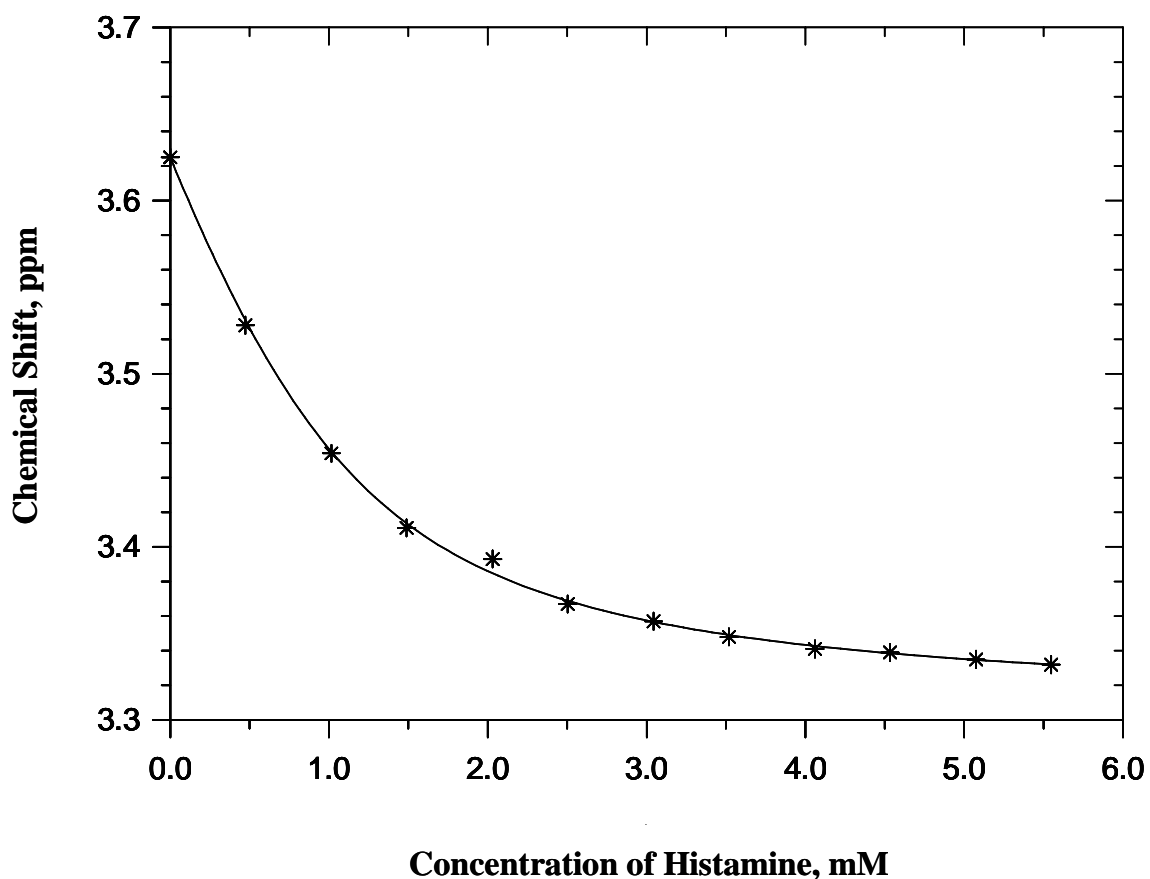
Figure 4.16. Determining the binding constant (K_{Bd}) between histamine and tetrasaccharide III. The concentration of tetrasaccharide III was held constant at 1.01 mM while histamine concentration was varied. The dependence of the chemical shift of the Ab-H3 proton on the concentration of histamine was obtained at pD 6.02 ± 0.07. Non-linear least squares fit of the chemical shift-concentration data yields a binding constant of 2396 ± 135 M^{-1}. [Na$^+$]$_{total}$ = 0.020 M.

Free Tetrasaccharide; pD 6.00
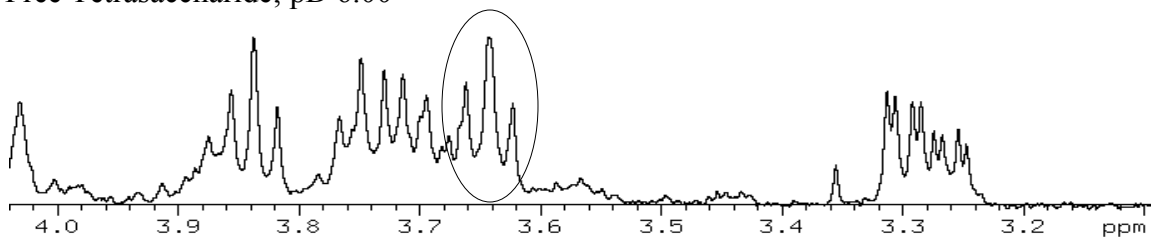
$$\frac{[Histamine]}{[Tetrasaccharide]} = 0.5 \text{; pD } 6.04$$
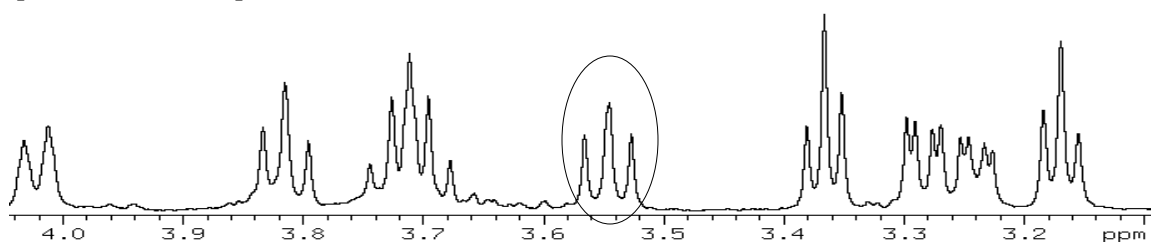
$$\frac{[Histamine]}{[Tetrasaccharide]} = 1 \text{; pD } 6.01$$
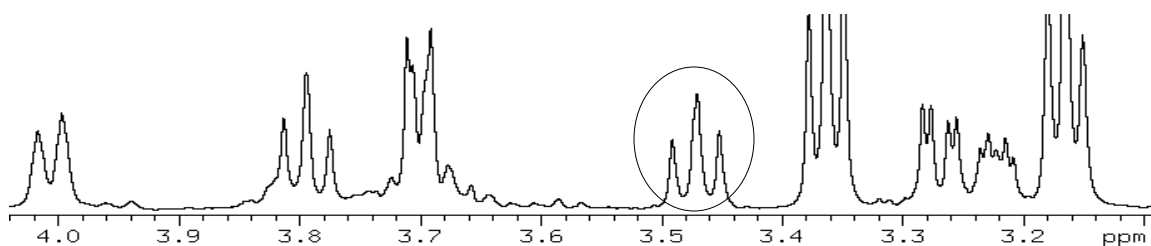
$$\frac{[Histamine]}{[Tetrasaccharide]} = 2 \text{; pD } 6.01$$
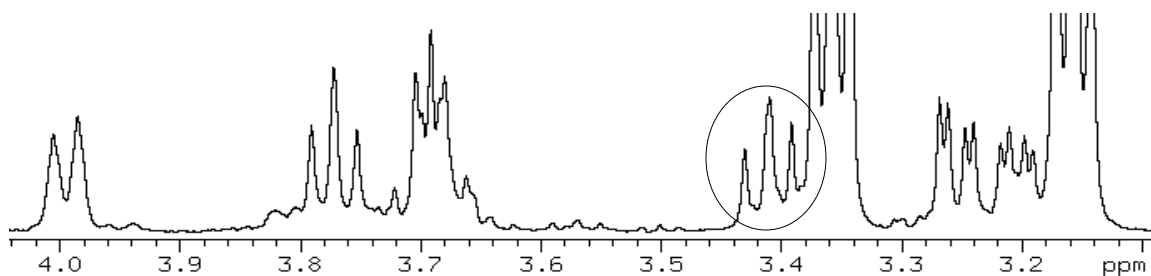
Figure 4.17. The dependence of the chemical shift of the Ab-H3 resonance of tetrasaccharide III on the histamine : tetrasaccharide III molar ratio. The circled resonance corresponds to the Ab-H3 proton of tetrasaccharide III. $[Na^+]_{total} = 0.020$ M.
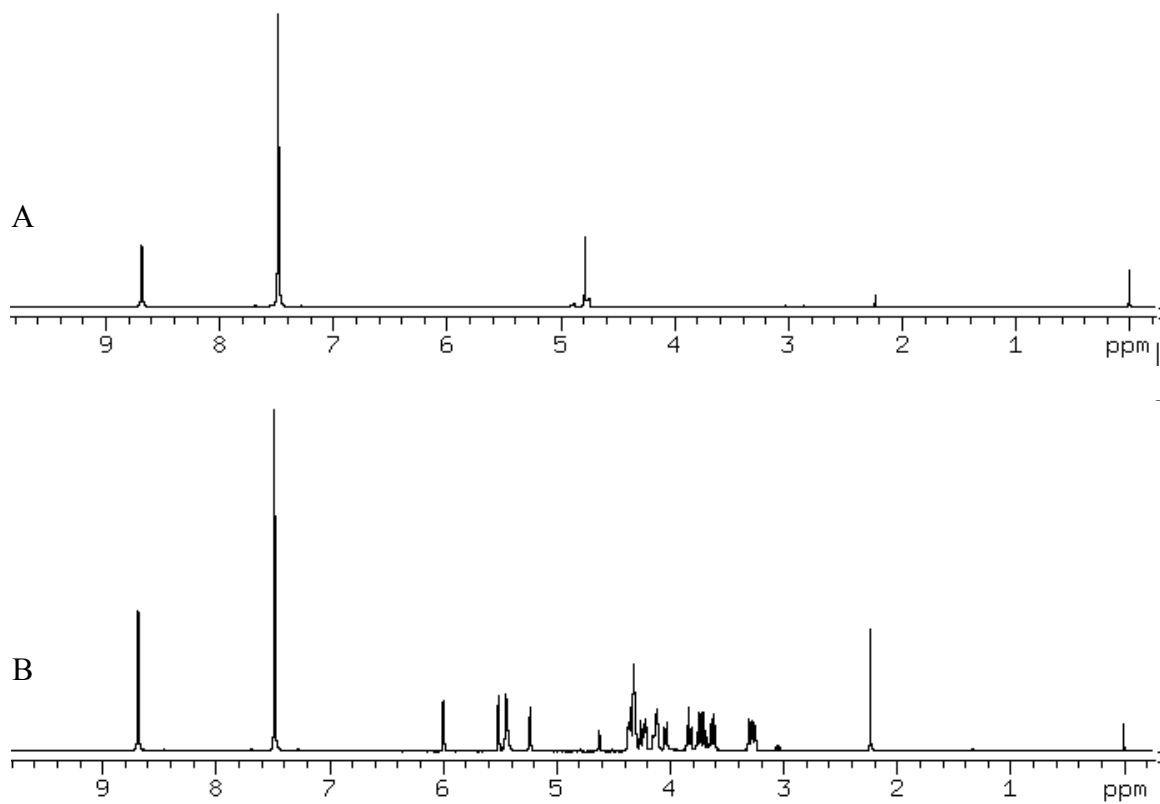
Figure 4.18. 1-D ^{1}H NMR spectra of D_2O solutions containing (A) 0.010 M imidazole at

pD 6.01 and (B) 0.002 M imidazole with 0.001 M tetrasaccharide III at pD 6.01. The

total sodium concentration for free and bound imidazole was ~ 0.020 M.

169
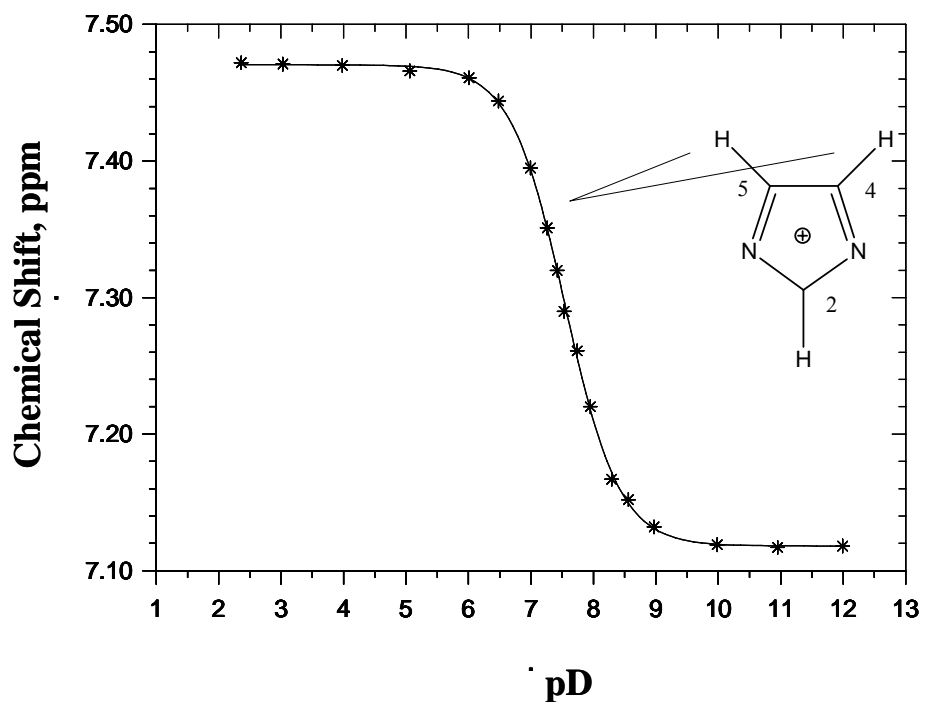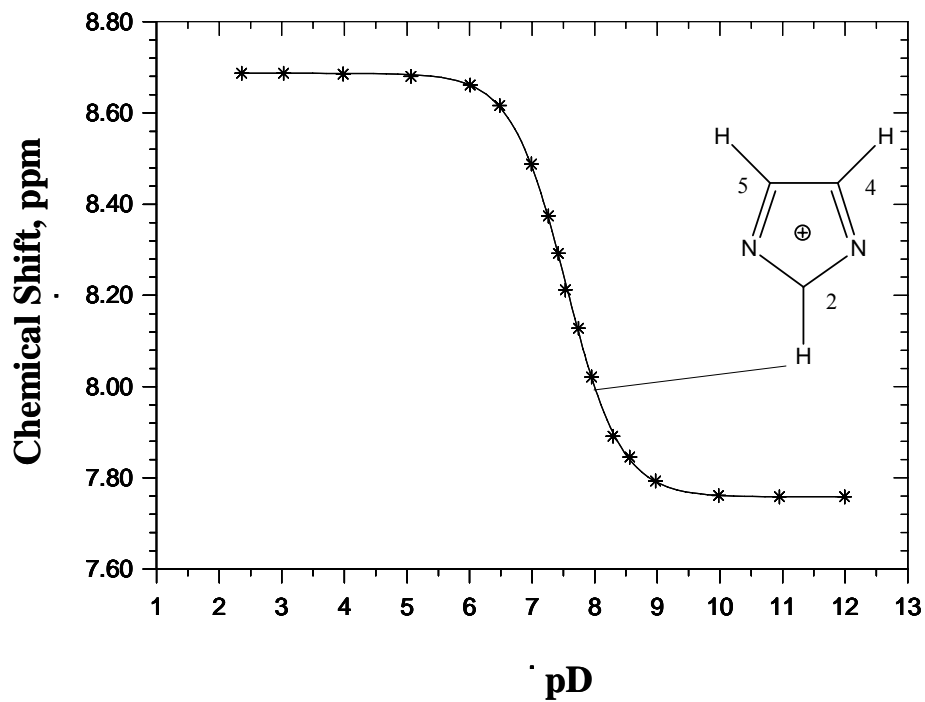
Figure 4.19. The chemical shift-pD titration curves for the C2H and C4, 5H protons of

0.010 M imidazole free in solution with the total sodium concentration of ~ 0.020 M.

	pK$_a$	
	C2H	C4, 5H
Free imidazole	7.14 ± 0.01	7.15 ± 0.01
I/T = 20/1	7.22 ± 0.01	7.22 ± 0.01
I/T = 1/2	7.25 ± 0.01	7.26 ± 0.01
I/T = 1/20	7.32 ± 0.01	7.34 ± 0.01
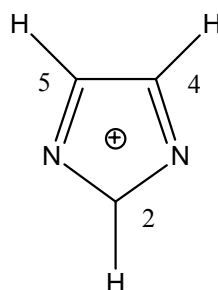
Table 4.3. Acid dissociation constants of the imidazolium ring in the absence and presence of tetrasaccharide III. The acid dissociation constants were measured using the C2H and C4, 5H reporter protons. The free 0.010 M imidazole solution was prepared with [Na$^+$]$_{total}$ of ~ 0.020 M. The complex solutions were prepared by mixing: a) 0.020 M imidazole with 0.001 M tetrasaccharide III; b) 0.001 M imidazole with 0.002 M tetrasaccharide III; c) 0.251 mM imidazole with 5.34 mM tetrasaccharide III, with [Na$^+$]$_{total}$ of ~ 0.020 M for each complex solution.
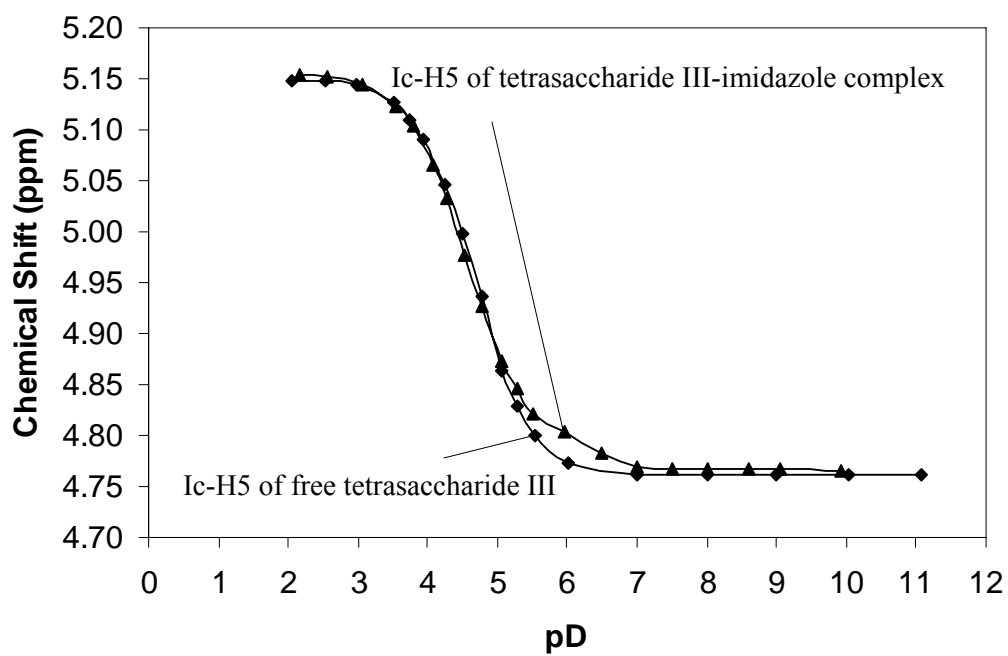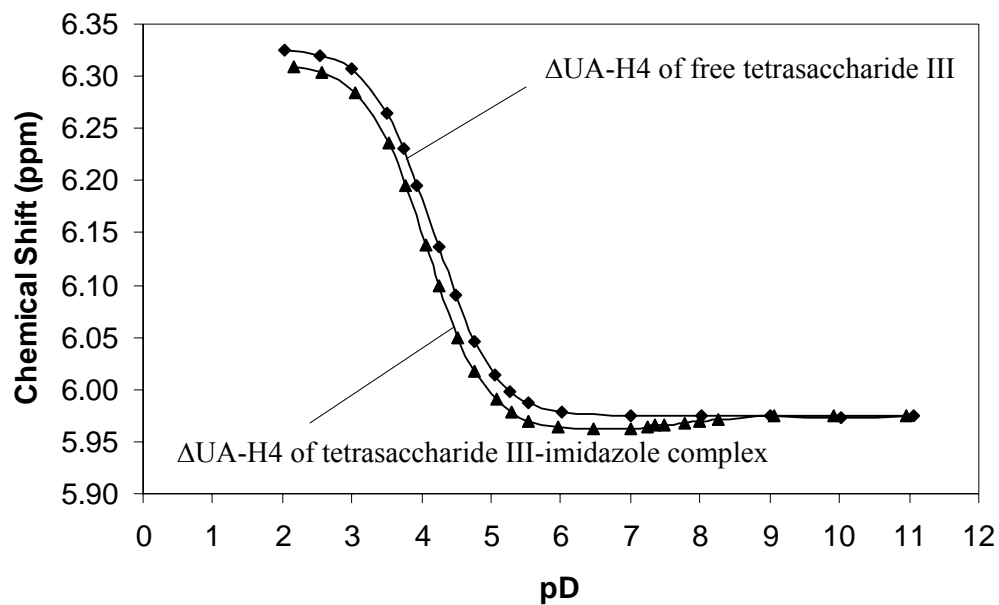
Figure 4.20. Chemical shift-pD titration curves for the ΔUA-H4 and Ic-H5 protons of tetrasaccharide III in the absence and presence of imidazole. The complex solution contains 0.001 M tetrasaccharide III and 0.020 M imidazole with $[Na^+]_{total}$ of ~ 0.020 M.

	pK$_a$	
	ΔUA	Ic
Free tetrasaccharide III	4.17 ± 0.01	4.66 ± 0.01
I/T = 20/1	4.09 ± 0.01	4.56 ± 0.01

Table 4.4. Acid dissociation constants of the carboxylic acid groups of ΔUA and Ic residues of tetrasaccharide III in the absence and presence of imidazole. The complex solution contained 0.001 M tetrasaccharide III plus 0.020 M imidazole with [Na$^+$]$_{total}$ of ~ 0.020 M.
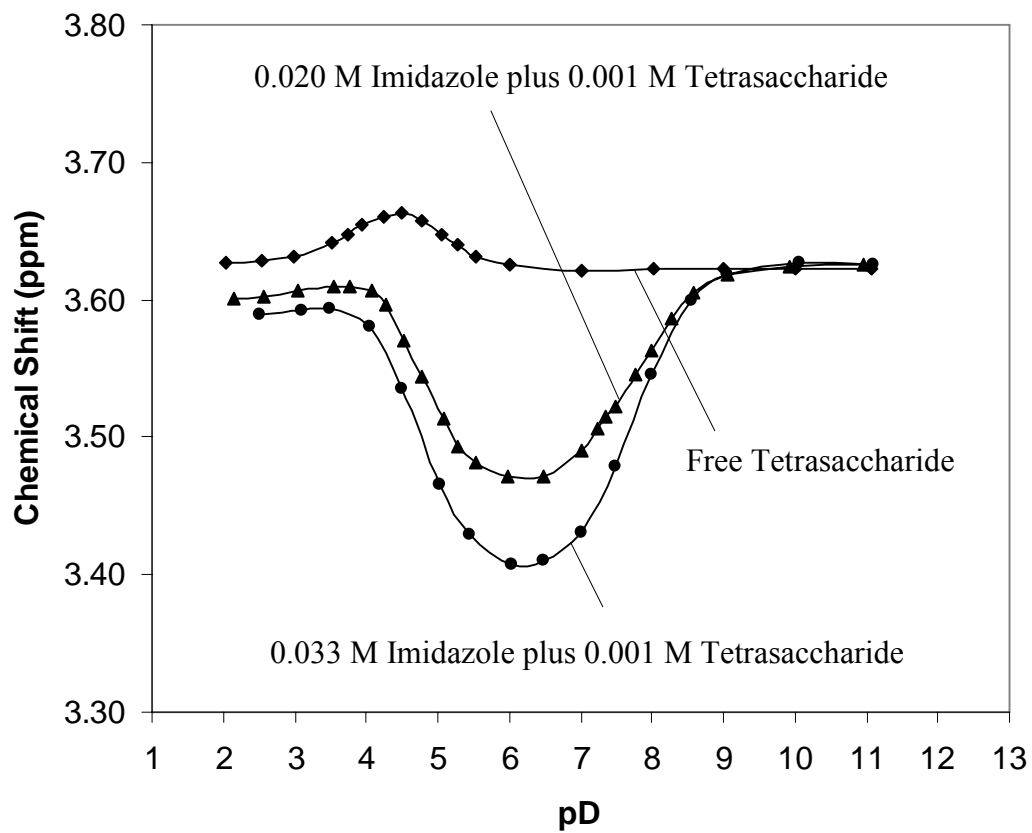
Figure 4.21. Chemical shift-pD titration data for the Ab-H3 proton of tetrasaccharide III free in solution and in solution with imidazole. Both free and complex solutions contain ~ 0.020 M Na$^+$.

upfield shift of Ab-H3 observed for the tetrasaccharide III-imidazolium ion complex is less than that observed for the tetrasaccharide III-histamine complex, suggesting that binding of tetrasaccharide III to imidazole is weaker than histamine. As the imidazole : tetrasaccharide III molar ratio is increased, the displacement of the chemical shift titration curves increases, indicating increased binding of imidazole by tetrasaccharide. Figure 4.22 shows the dependence of the chemical shift of the Ab-H3 resonance as a function of pD when tetrasaccharide III is in solution with imidazole. The upfield shift of the Ab-H3 resonance reaches its maximum at pD ~ 6. Figure 4.23 shows the binding curve for the interaction of imidazole with tetrasaccharide III. The dependence of the chemical shift of the Ab-H3 resonance on the imidazole : tetrasaccharide III ratio is shown in Figure 4.24. A binding constant of 36 ± 3 M^{-1} was determined at pD 6.00 ± 0.05.

The interaction of imidazole with tetrasaccharide III also occurs at pD ~ 3. However, the binding is weak as suggested by a little upfield shift of the Ab-H3 resonance (Figure 4.21). A binding constant of 11 ± 5 M^{-1} was obtained at pD 3.03 ± 0.05.

4.6 Binding of Histidine-Containing Peptides by Tetrasaccharide

4.6.1 β-Amyloid Peptide (FRHDSGY)

1-D ^{1}H NMR spectra for free tetrasaccharide III and the tetrasaccharide III-β-amyloid peptide complex are shown in Figure 4.25. Figure 4.26 shows the chemical shift vs pD titration curves for the Ab-H3 proton both in the absence and presence of the peptide. In the presence of the peptide, the upfield shift of the Ab-H3 resonance reaches
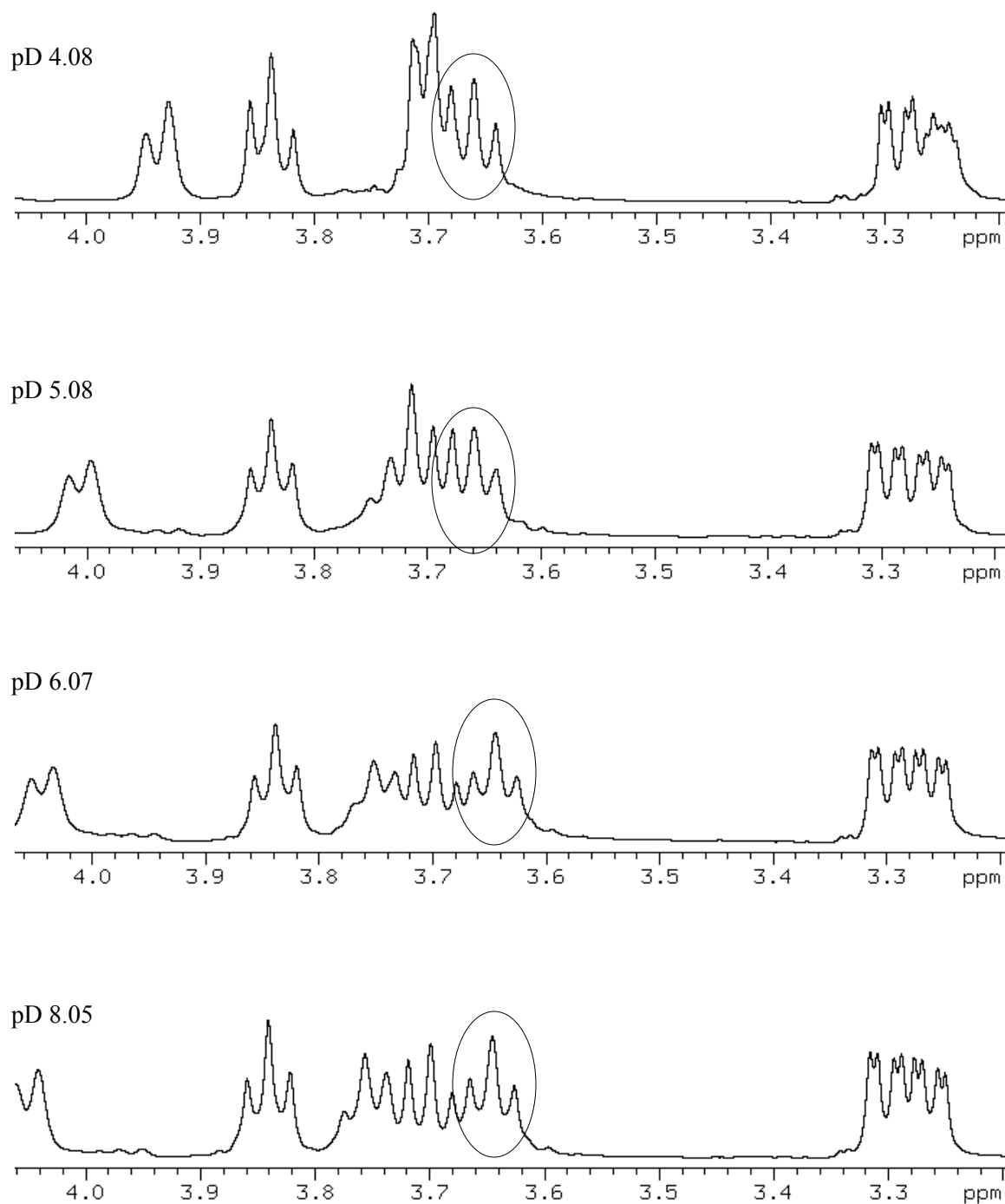
Figure 4.22. Portions of 1-D ^{1}H NMR spectra of a D_2O solution containing 0.020 M imidazole plus 0.001 M tetrasaccharide III with $[Na^+]_{total}$ of ~ 0.020 M at various pD values. The circled resonance corresponds to the Ab-H3 proton of tetrasaccharide III.
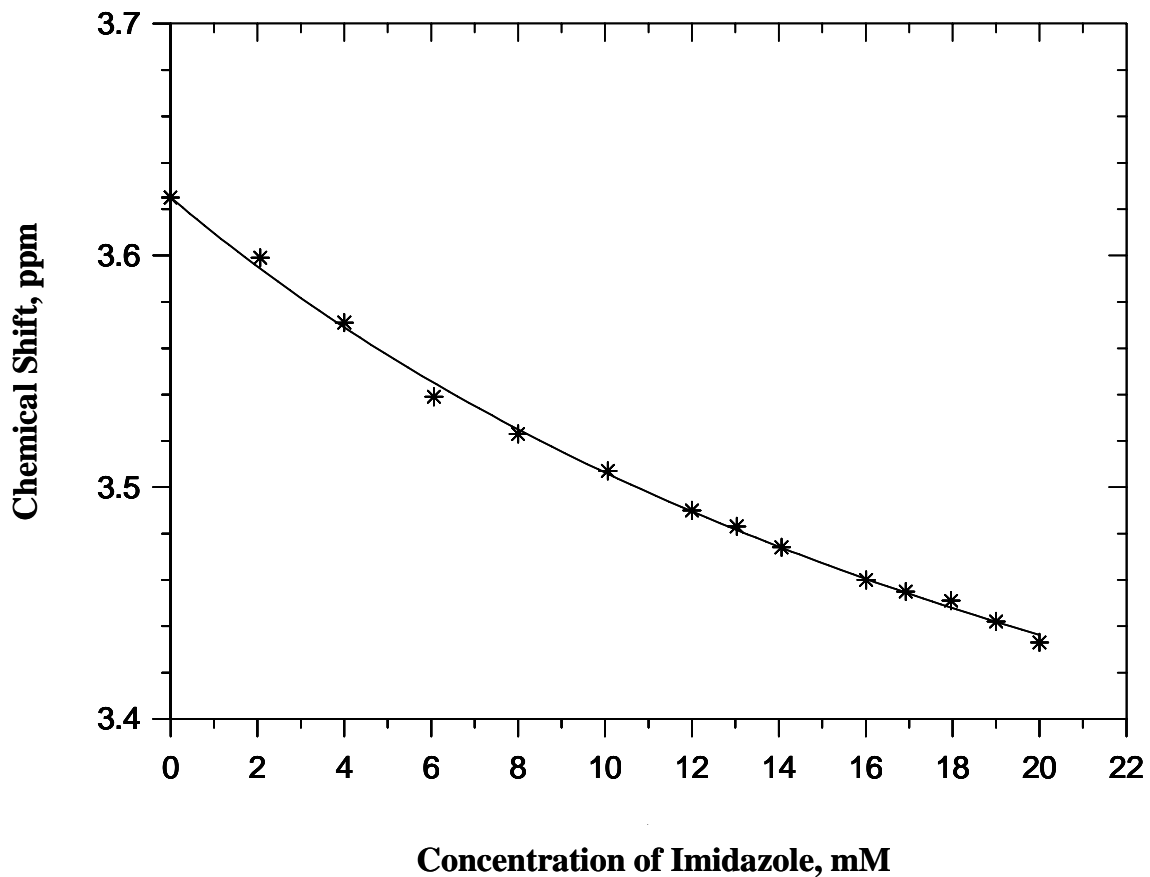
Figure 4.23. Determining the binding constant (K_{Bd}) between imidazole and tetrasaccharide III. The concentration of tetrasaccharide III was held constant at 1.02 mM while imidazole concentration was varied. The dependence of the chemical shift of the Ab-H3 proton on imidazole concentration was obtained at pD 6.00 ± 0.05. Non-linear least squares fit of the chemical shift-concentration data yields a binding constant of 36 ± 3 M^{-1}. [Na^{+}]$_{total}$ = 0.020 M.

Free Tetrasaccharide; pD 6.00
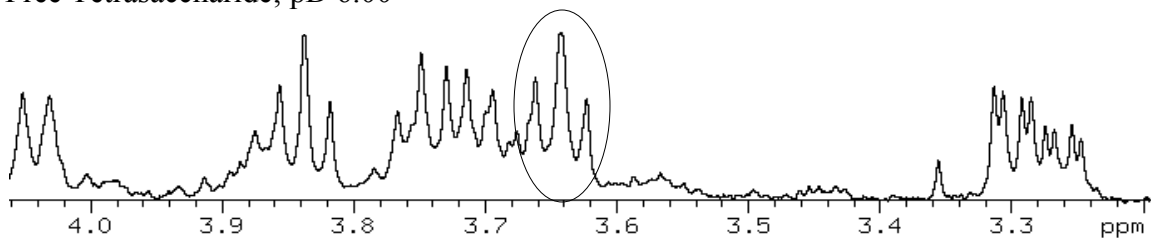
$$\frac{[\text{Im}idazole]}{[\textit{Tetrasaccharide}]} = 6\,;\,\text{pD } 6.03$$
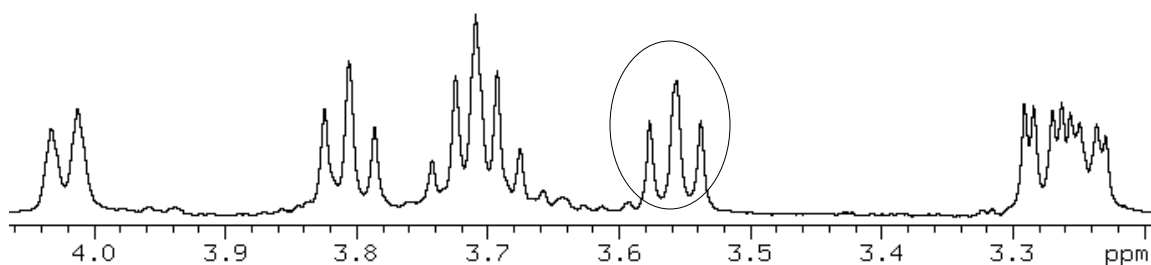
$$\frac{[\text{Im}idazole]}{[\textit{Tetrasaccharide}]} = 12\,;\,\text{pD } 6.04$$
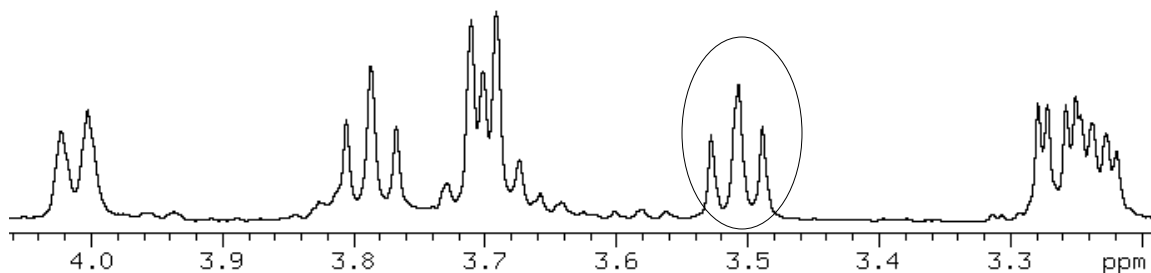
$$\frac{[\text{Im}idazole]}{[\textit{Tetrasaccharide}]} = 18\,;\,\text{pD } 5.99$$
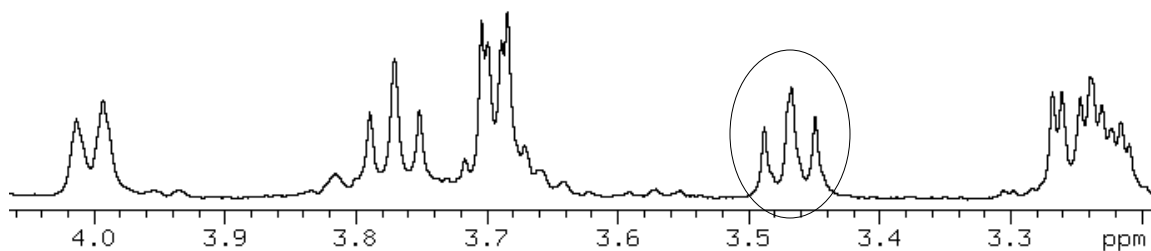
Figure 4.24. The dependence of the chemical shift of the Ab-H3 resonance of tetrasaccharide III on the imidazole : tetrasaccharide III ratio. The circled resonance corresponds to the Ab-H3 proton of tetrasaccharide III. $[Na^+]_{total} = 0.020$ M.
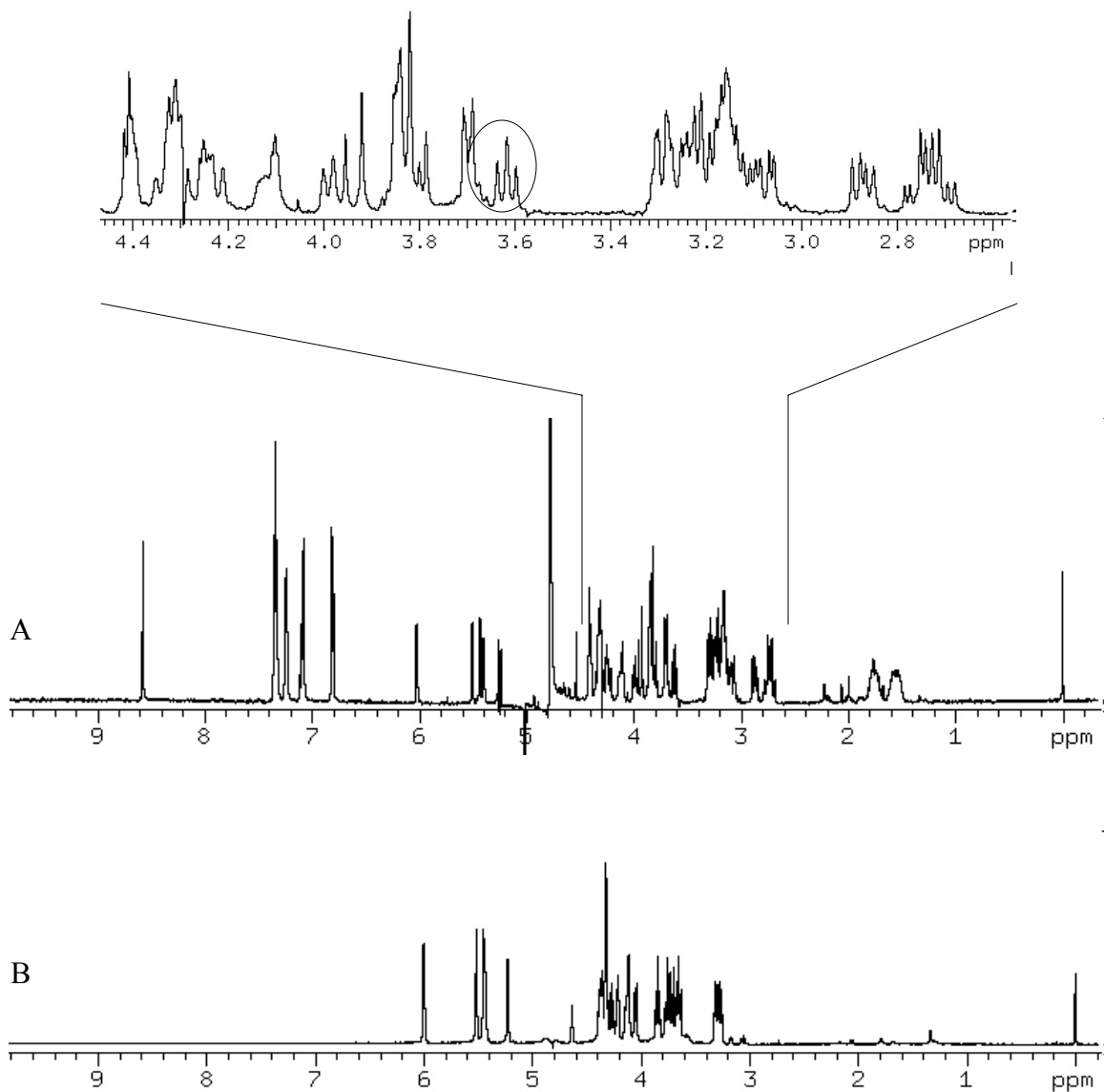
Figure 4.25. 1D ^{1}H NMR spectra of D$_2$O solutions containing (A) 0.775 mM β-amyloid peptide (FRHDSGY) with 0.516 mM tetrasaccharide III at pD 5.01 and (B) 2.607 mM tetrasaccharide III at pD 6.57. The circled resonance corresponds to the Ab-H3 proton of tetrasaccharide III. The total sodium concentration for free and bound FRHDSGY was ~ 0.020 M.

179
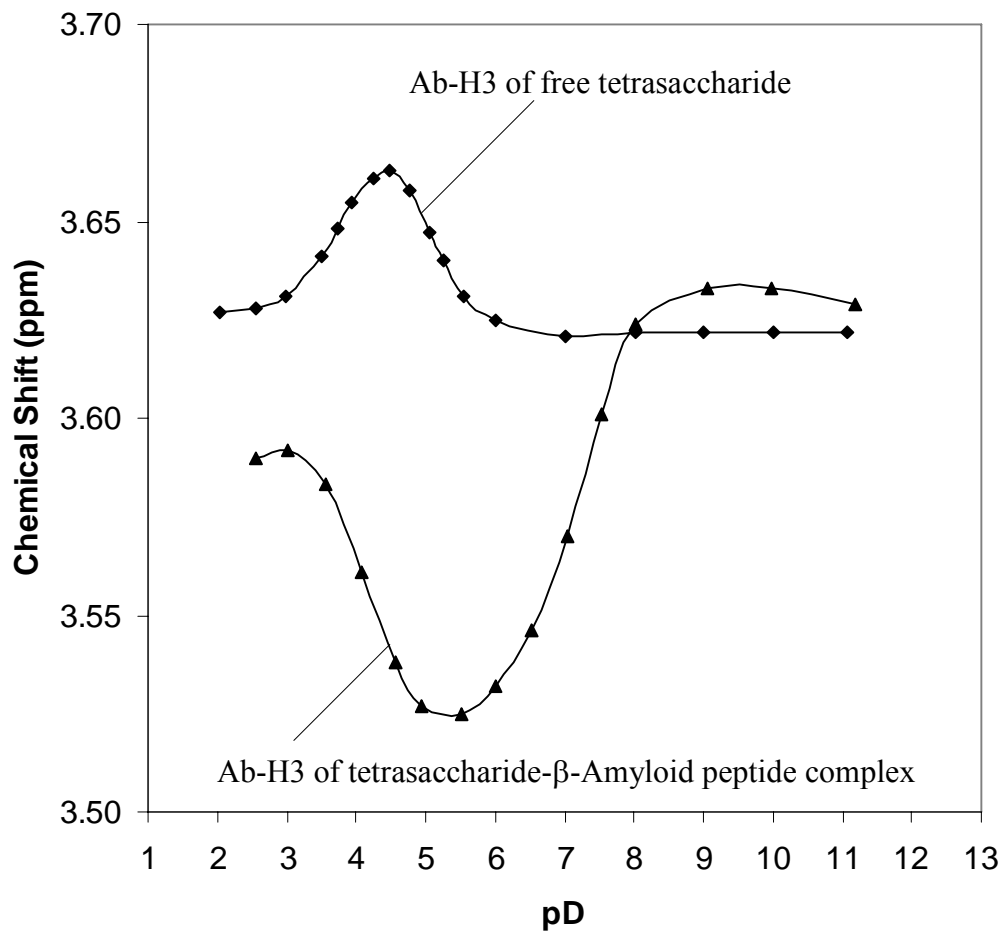
Figure 4.26. pD dependence of the chemical shift of the resonance for the Ab-H3 proton

of tetrasaccharide III for a solution containing only tetrasaccharide III and a solution

containing 5.45 mM β-amyloid peptide plus 0.502 mM tetrasaccharide III. Both free and

complex solutions contain ~ 0.020 M Na$^+$.

its maximum at pD ~ 5.5. As seen from the chemical shift titration curve, the upfield

displacement characteristic of site specific binding at site Ab of tetrasaccharide III results

from the ring current effect induced by the presence of the histidyl imidazolium ring of β-

amyloid peptide located below the Ab-H3 proton. Figure 4.27 shows the dependence of

the chemical shift of the Ab-H3 resonance as a function of pD when tetrasaccharide III is

in solution with the peptide. The resonance for the Ab-H3 proton shifts upfield over the

pD range 2-5. Beyond pD 5.5, the Ab-H3 resonance moves back to its chemical shift in

the absence of β-amyloid peptide. The binding curve for the interaction of the peptide

with tetrasaccharide III is shown in Figure 4.28. Figure 4.29 shows the dependence of the

chemical shift of the Ab-H3 resonance on the β-amyloid peptide : tetrasaccharide III

molar ratio. A binding constant of 329 ± 30 M^{-1} was determined at pD 5.00 ± 0.06.

4.6.2 The Growth Factor glycyl-L-histidyl-L-lysine (GHK)

1-D ^{1}H NMR spectra for free tripeptide growth factor GHK and the

tetrasaccharide III-GHK complex are shown in Figure 4.30. Assignment of resonance

chemical shifts for the growth factor GHK free in solution is shown in Table 4.5. Figure

4.31 shows the chemical shift-pD titration curves for the Ab-H3 proton in the absence

and presence of GHK. For the complex solution, the upfield shift of the resonance for the

Ab-H3 proton reaches its maximum at pD ~ 6. The upfield shift of the Ab-H3 resonance

indicates that the histidyl imidazolium group of GHK binds site specifically to the

imidazolium-binding site on tetrasaccharide III. The upfield displacement of the Ab-H3

resonance also indicates formation of tetrasaccharide III-GHK complex. The binding of

GHK by tetrasaccharide III suggests one molecule of III would accommodate one
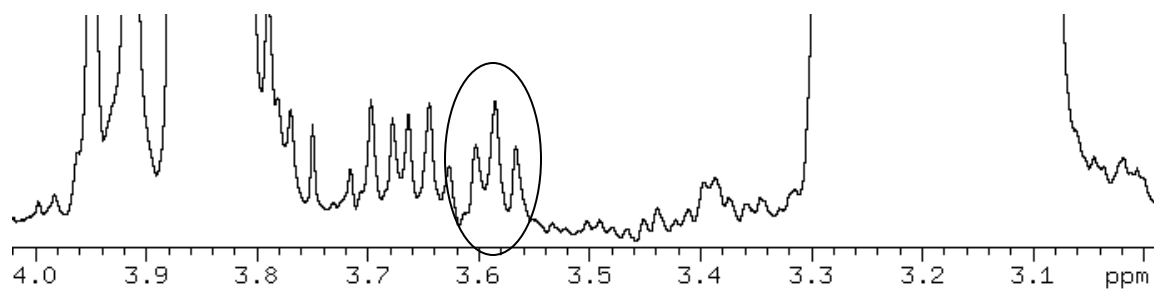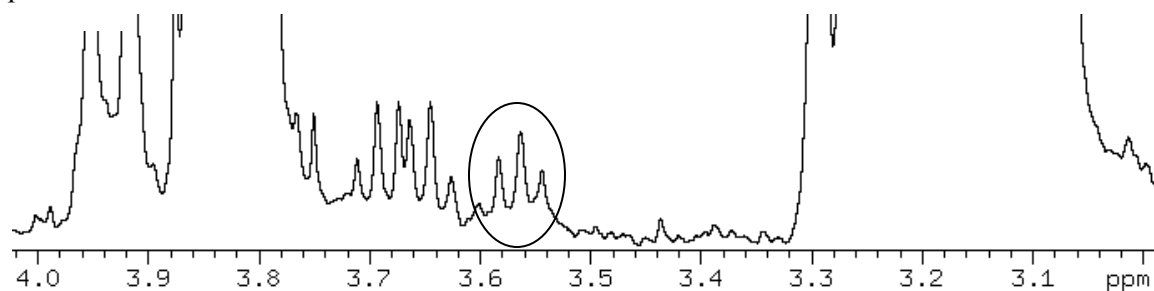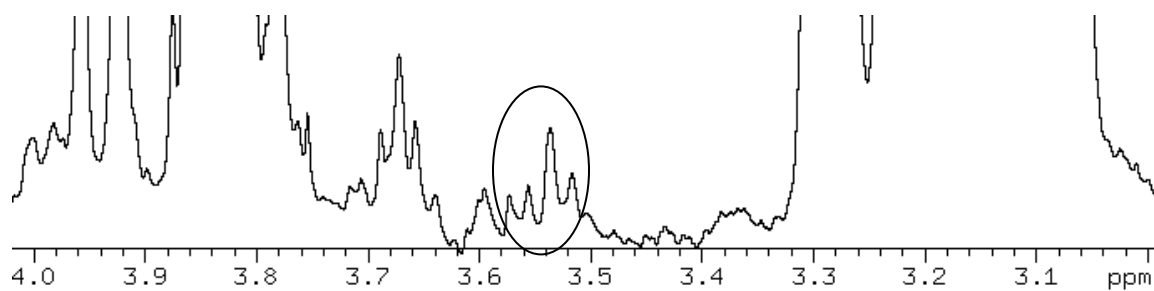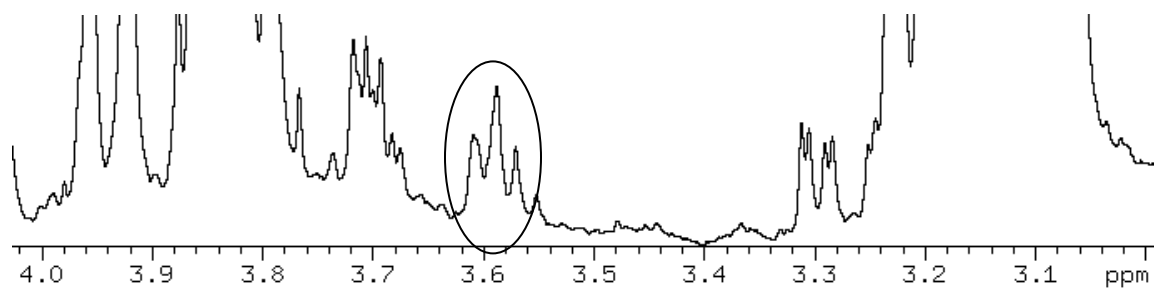
Figure 4.27. Portions of 1-D ^{1}H NMR spectra of a D$_2$O solution containing 5.45 mM β-amyloid peptide plus 0.502 mM tetrasaccharide III with [Na$^+$]$_{total}$ of ~ 0.020 M at various pD values. The circled resonance corresponds to the Ab-H3 proton of tetrasaccharide III.
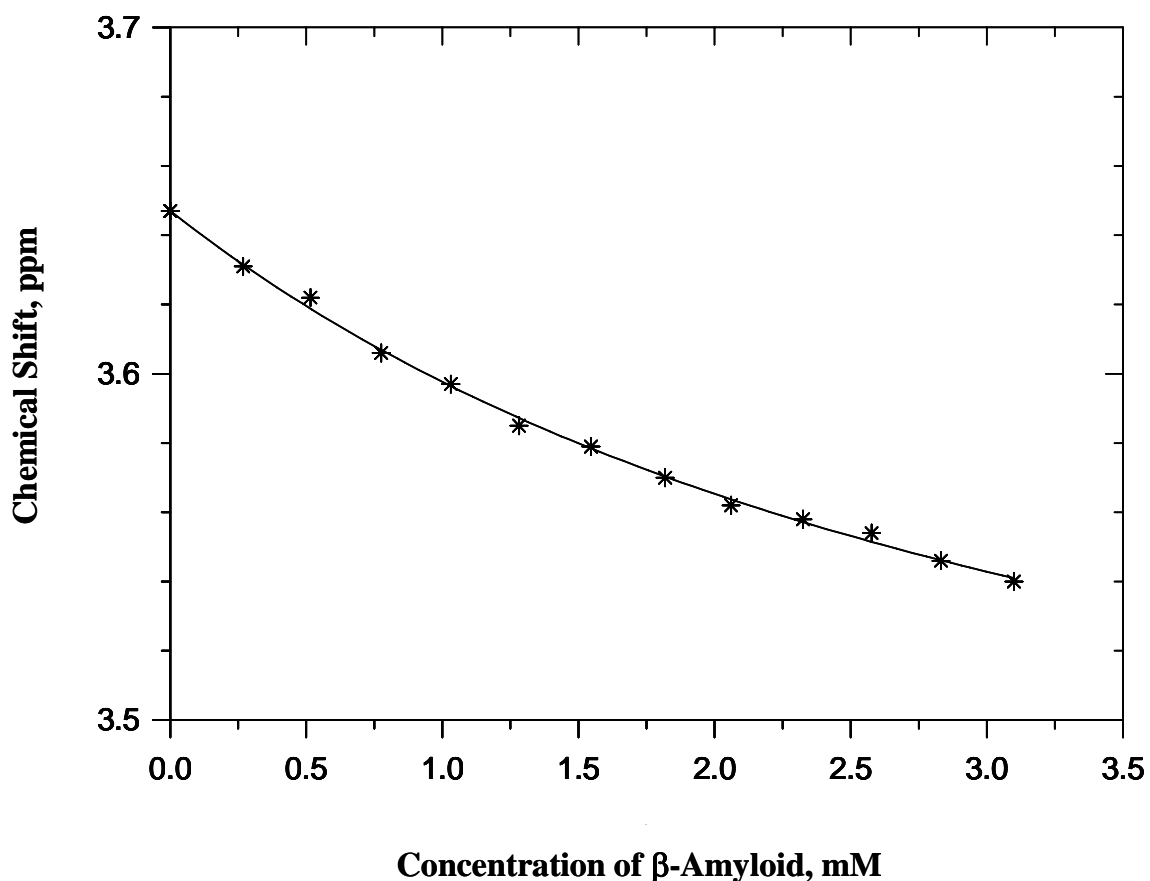
Figure 4.28. Determining the binding constant (K_{Bd}) between β-amyloid peptide (FRHDSGY) and tetrasaccharide III. The concentration of tetrasaccharide III was held constant at 0.516 mM while the β-amyloid peptide concentration was varied. The chemical shift dependence of the Ab-H3 proton on the peptide concentration was obtained at pD 5.00 ± 0.06. Non-linear least squares fit of the chemical shift-concentration data yields a binding constant of 329 ± 30 M^{-1}. [Na$^+$]$_{total}$ = 0.020 M.

Free Tetrasaccharide; pD 5.05
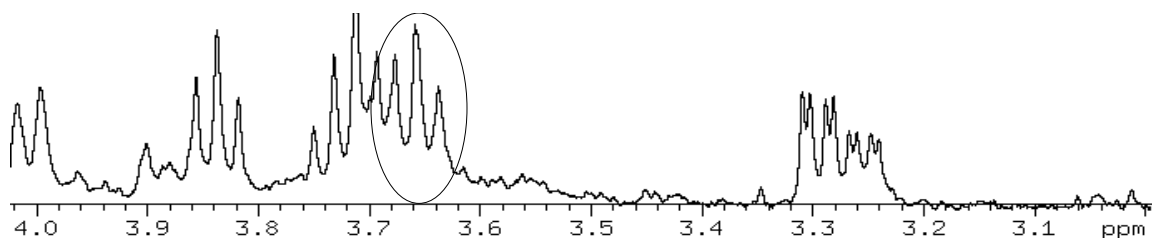
$$\frac{[FRHDSGY]}{[Tetrasaccharide]} = 0.5 \, ; \text{pD } 5.03$$
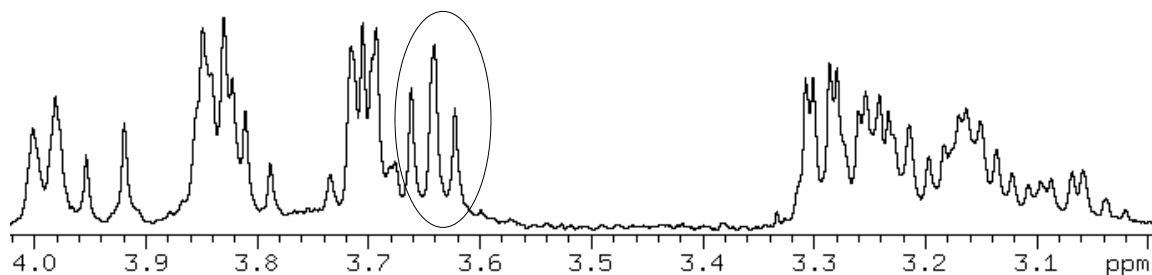
$$\frac{[FRHDSGY]}{[Tetrasaccharide]} = 1.5 \, ; \text{pD } 5.01$$
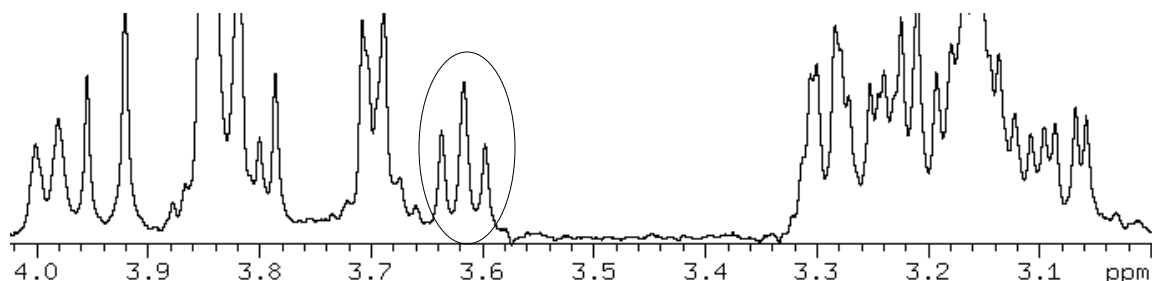
$$\frac{[FRHDSGY]}{[Tetrasaccharide]} = 6 \, ; \text{pD } 5.03$$
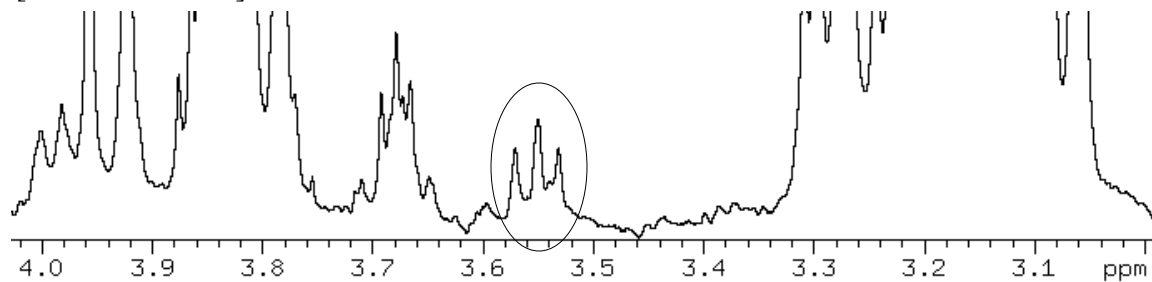
Figure 4.29. The dependence of the chemical shift of the Ab-H3 resonance of tetrasaccharide III on the β-amyloid peptide : tetrasaccharide III molar ratio. The circled resonance corresponds to the Ab-H3 proton of tetrasaccharide III. $[Na^+]_{total} = 0.020$ M.
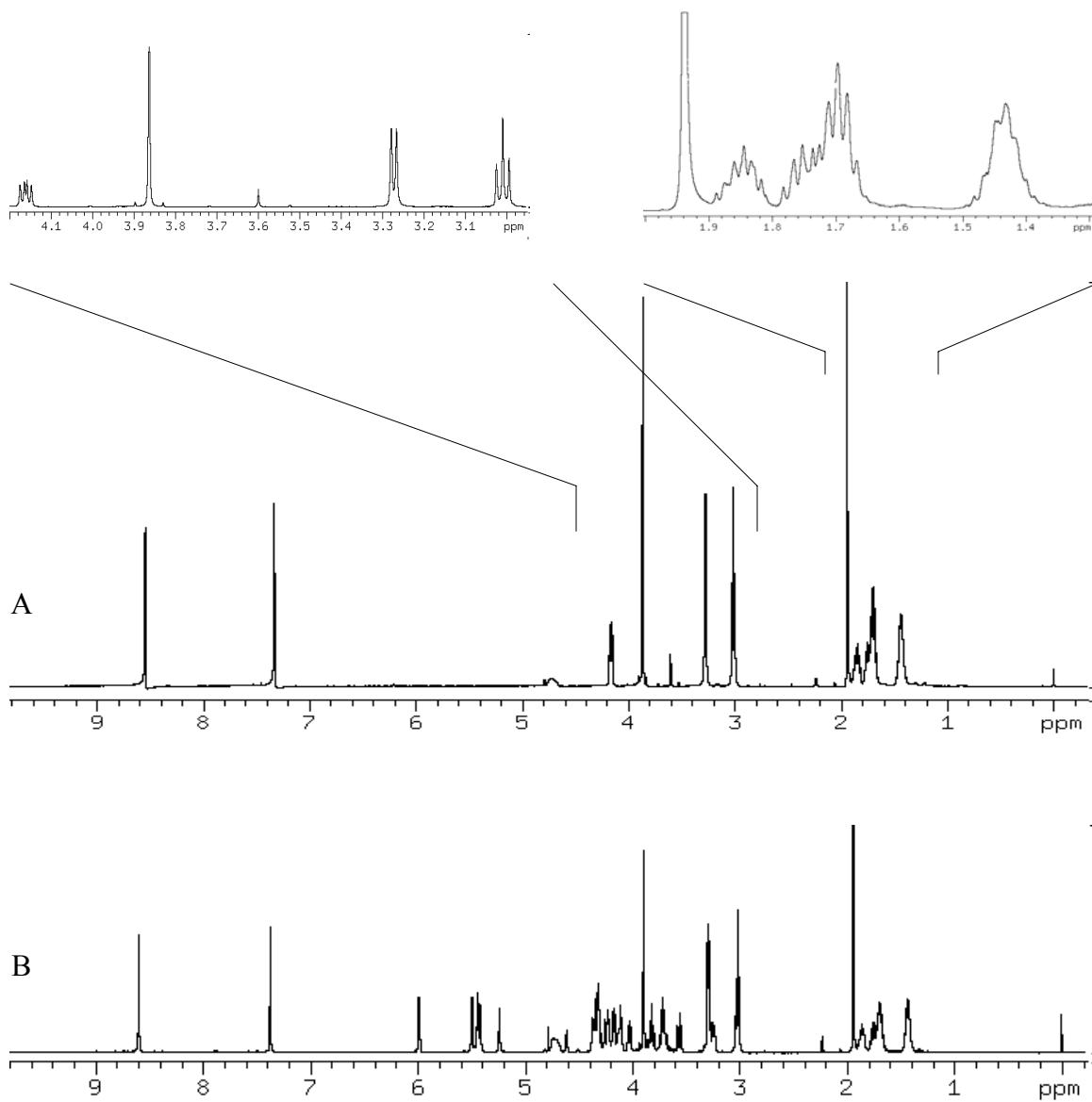
Figure 4.30. (A) 1-D ^{1}H NMR spectrum of free tripeptide GHK at pD 6.03 and (B) 1-D ^{1}H NMR spectrum of the GHK-tetrasaccharide III complex containing 1.01 mM GHK + 1.01 mM tetrasaccharide III at pD 5.99. The total sodium concentration for free and bound GHK was ~ 0.020 M.

Residue	NH	αH	βH	Others
Gly[1]	n.d.	3.863		
His[2]	n.d.	4.698	3.273	H_2 7.327
				H_4 8.541
Lys[3]	n.d.	4.161	1.846, 1.759	γCH_2 1.432, 1.432
				δCH_2 1.697, 1.697
				εCH_2 3.010, 3.010

n.d., not determined because of deuterium exchange with the D_2O solvent.

Table 4.5. Assignment of chemical shifts of resonances for the growth factor GHK free in solution at pD 6.03 and 25 °C.
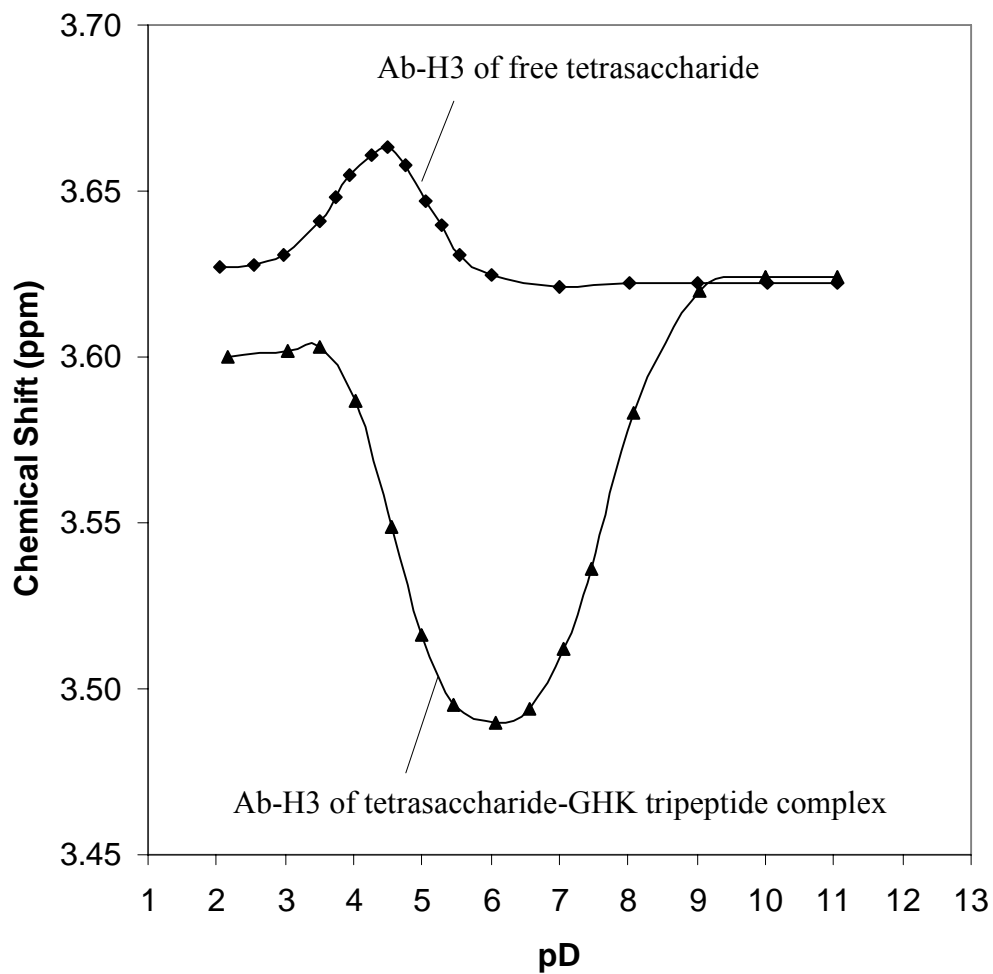
Figure 4.31. pD dependence of the chemical shift of the resonance for the Ab-H3 proton of tetrasaccharide III for a solution containing only tetrasaccharide III and a solution containing 0.005 M GHK plus 0.001 M tetrasaccharide III. Both free and complex solutions contain ~ 0.020 M Na$^+$.

molecule of GHK. Figure 4.32 shows the pD dependence of the chemical shift of the Ab-H3 resonance when tetrasaccharide III is in solution with GHK. The resonance for the Ab-H3 proton shifts upfield over the pD range of 2-6. As the pD is further increased, the Ab-H3 resonance returns to its chemical shift in the absence of GHK. The binding curve for GHK-tetrasaccharide III interaction is shown in Figure 4.33. Figure 4.34 shows the dependence of the chemical shift of the Ab-H3 resonance on the GHK : tetrasaccharide III ratio. A binding constant of 1855 ± 43 M^{-1} was determined at pD 6.00 ± 0.06.

4.6.3 TriPeptide glycyl-L-histidyl-L-glycine (GHG)

1-D ^{1}H NMR spectra for free tetrasaccharide III and the tetrasaccharide III-GHG complex are shown in Figure 4.35. Figure 4.36 shows the chemical shift titration curves for the Ab-H3 proton in the absence and presence of the tripeptide GHG. In the presence of GHG, the Ab-H3 resonance is displaced upfield and reaches its maximum at pD ~ 6. The upfield displacement of the Ab-H3 resonance indicates that the histidyl imidazolium group of GHG binds site specifically to the imidazolium-binding site on tetrasaccharide III. The binding of GHG by tetrasaccharide III suggests one molecule of III would accommodate one molecule of GHG. The pD dependence of the Ab-H3 resonance of tetrasaccharide III in the presence of GHG is presented in Figure 4.37. The binding curve for the interaction of tetrasaccharide III with GHG is shown in Figure 4.38. Figure 4.39 shows the dependence of the chemical shift of the Ab-H3 resonance on the GHG : tetrasaccharide III ratio. A binding constant of 257 ± 11 M^{-1} was determined at pD 6.04 ± 0.05.
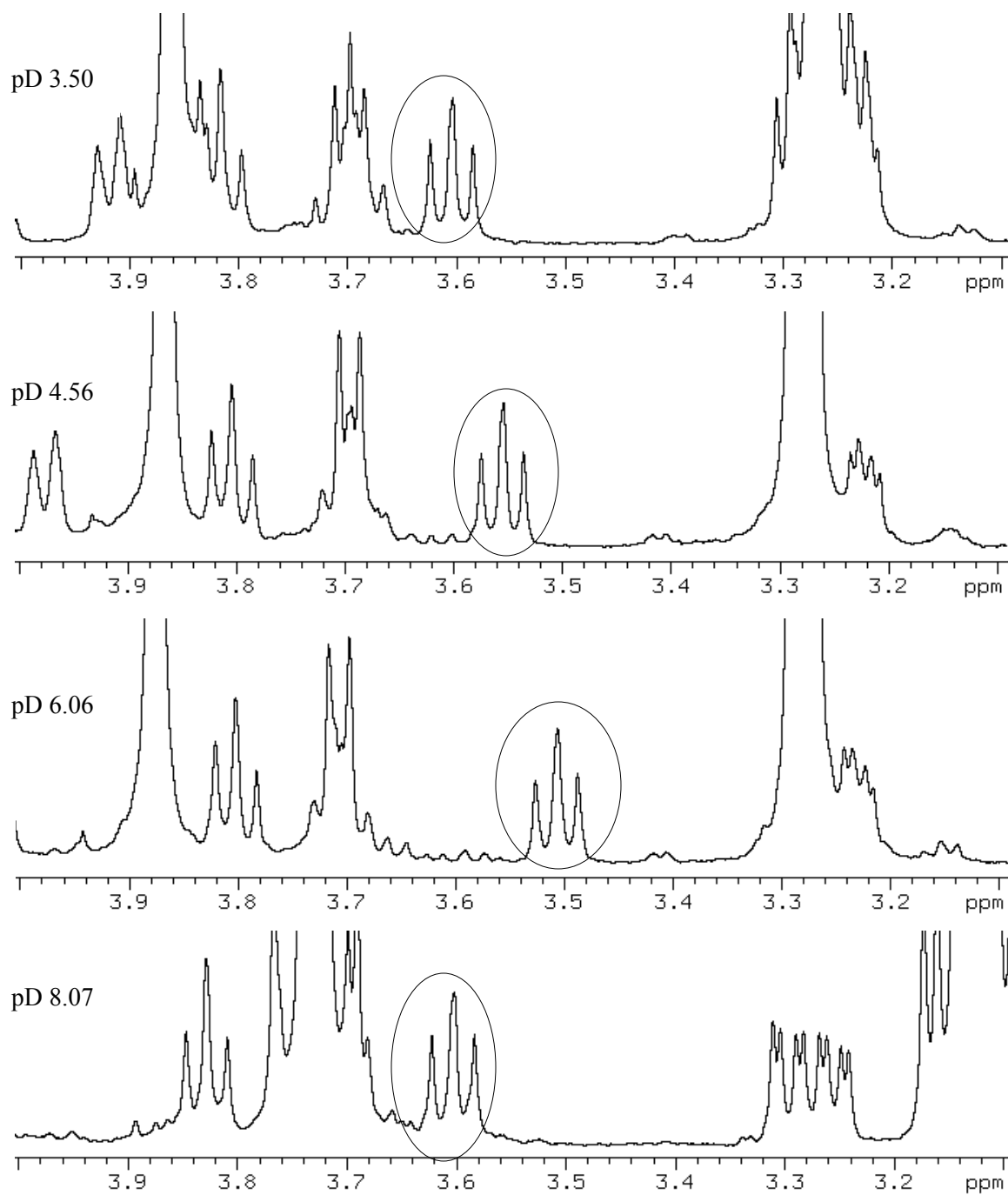
Figure 4.32. Portions of 1-D ^{1}H NMR spectra of a D_2O solution containing 0.005 M tripeptide GHK plus 0.001 M tetrasaccharide III with $[Na^+]_{total}$ of ~ 0.020 M at various pD values. The circled resonance corresponds to the Ab-H3 proton of the tetrasaccharide III.
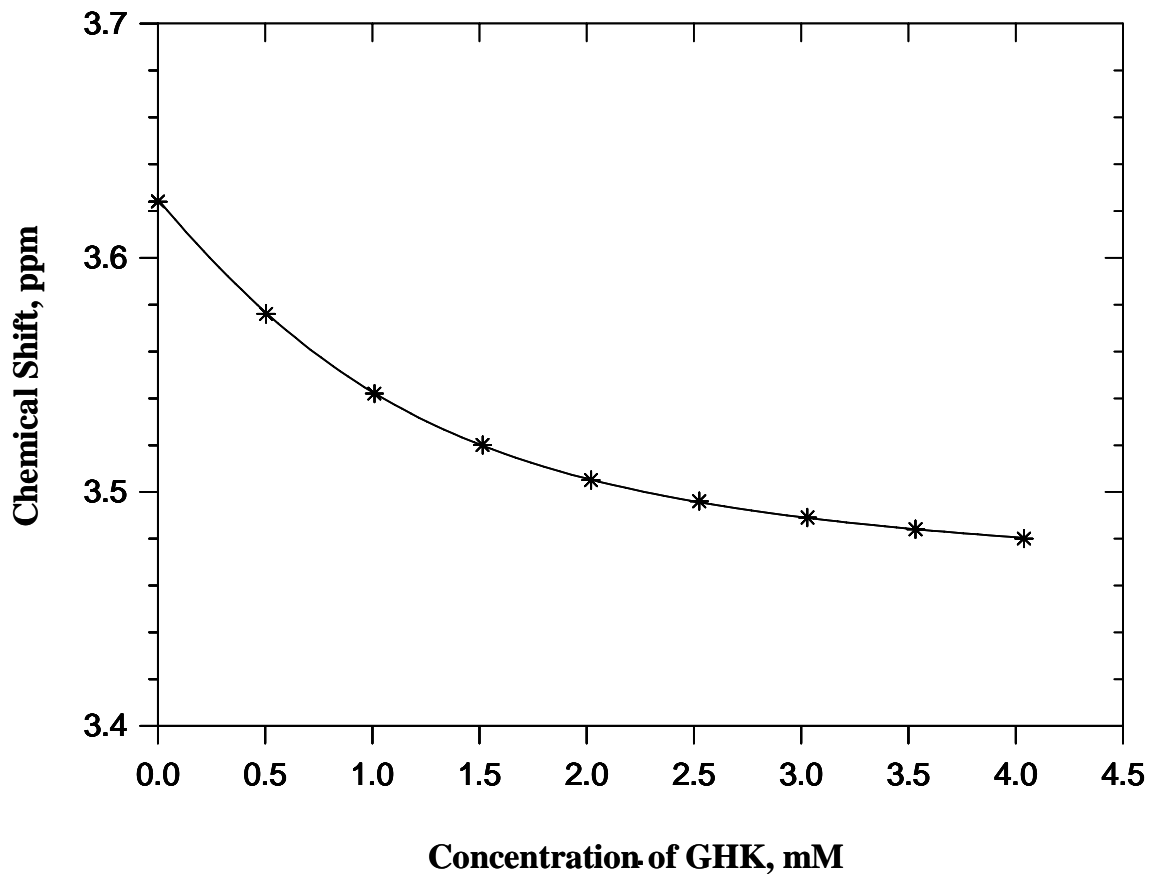
Figure 4.33. Determining the binding constant (K_{Bd}) between the growth factor GHK and tetrasaccharide III. The concentration of tetrasaccharide III was held constant at 1.01 mM while GHK concentration was varied. The dependence of the chemical shift of the Ab-H3 proton on GHK concentration was obtained at pD 6.00 ± 0.06. Non-linear least squares fit of the chemical shift-concentration data yields a binding constant of 1855 ± 43 M^{-1}. [Na$^+$]$_{total}$ = 0.020 M.

Free Tetrasaccharide; pD 6.00
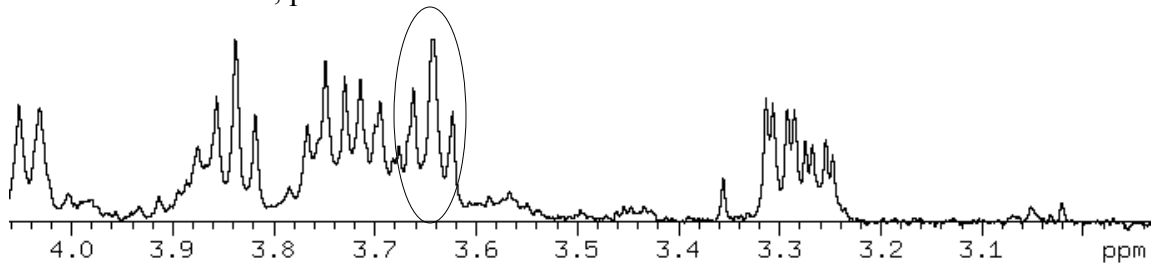
$$\frac{[GHK]}{[Tetrasaccharide]} = 0.5 \text{ ; pD 5.99}$$
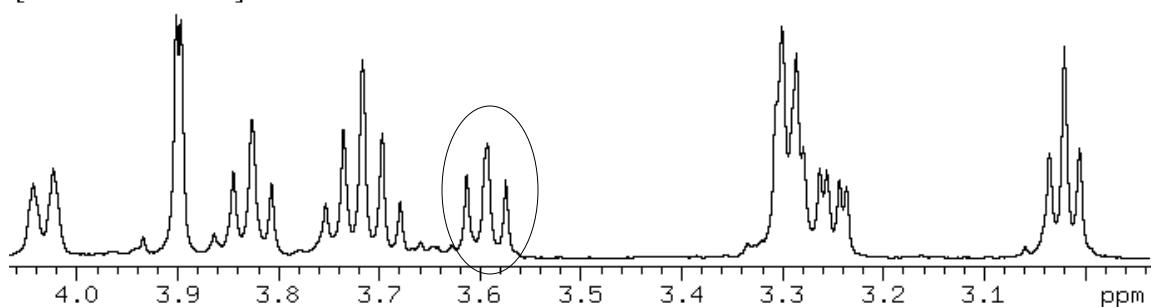
$$\frac{[GHK]}{[Tetrasaccharide]} = 1 \text{ ; pD 5.99}$$
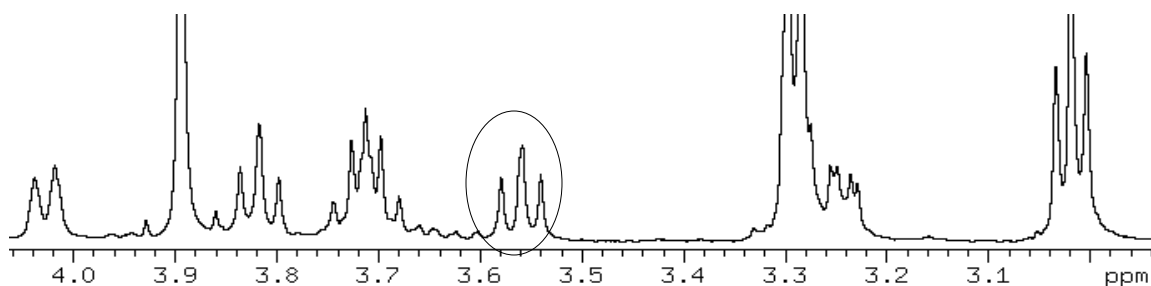
$$\frac{[GHK]}{[Tetrasaccharide]} = 2 \text{ ; pD 6.01}$$
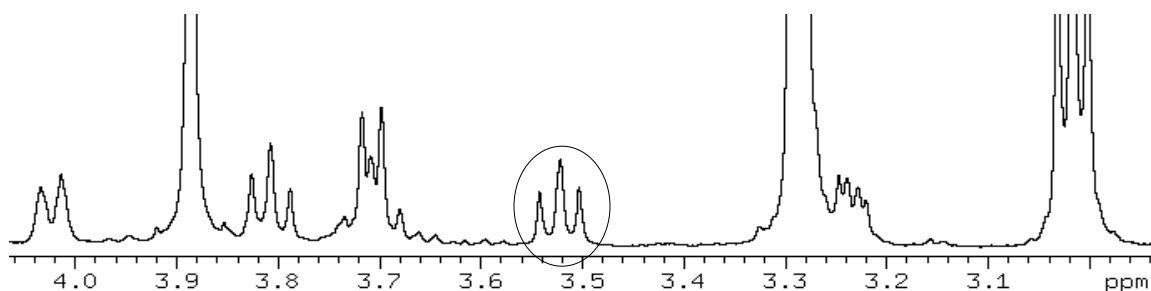
Figure 4.34. The dependence of the chemical shift of the Ab-H3 resonance of tetrasaccharide III on the GHK : tetrasaccharide III molar ratio. The circled resonance corresponds to the Ab-H3 proton of tetrasaccharide III. $[Na^+]_{total} = 0.020$ M.
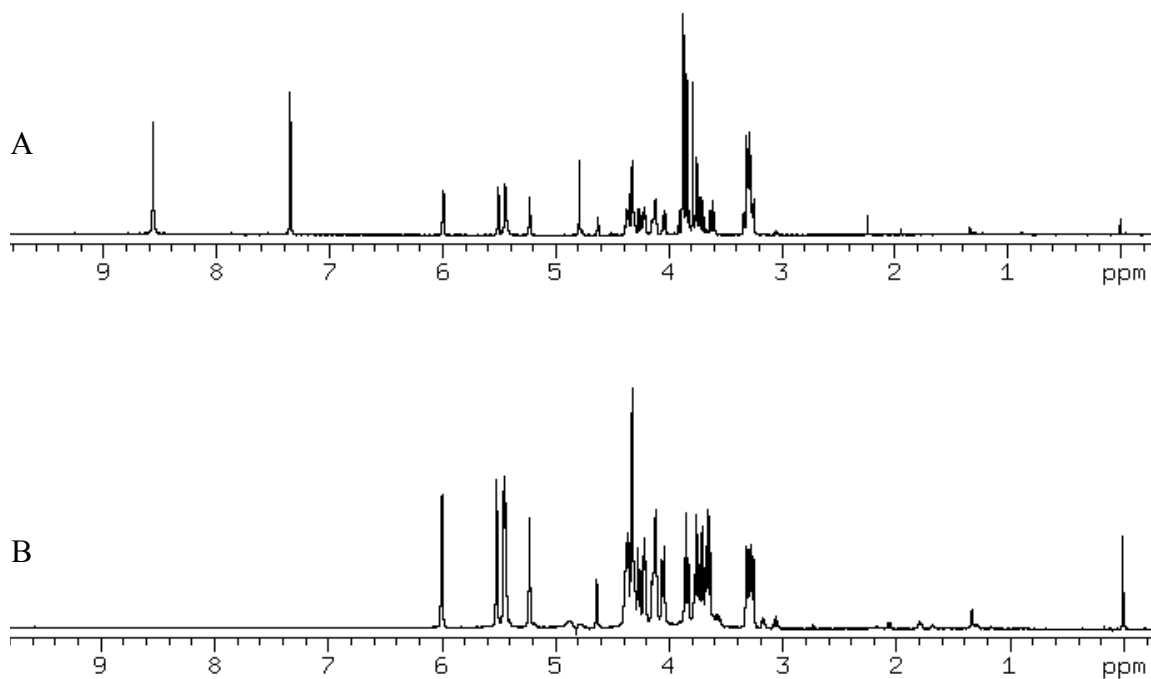
Figure 4.35. 1-D ^{1}H NMR spectra of D_2O solutions containing (A) 1.00 mM tripeptide GHG with 0.506 mM tetrasaccharide III at pD 6.06 and (B) 2.607 mM tetrasaccharide III at pD 6.57. The total sodium concentration for free and bound GHG was ~ 0.020 M.
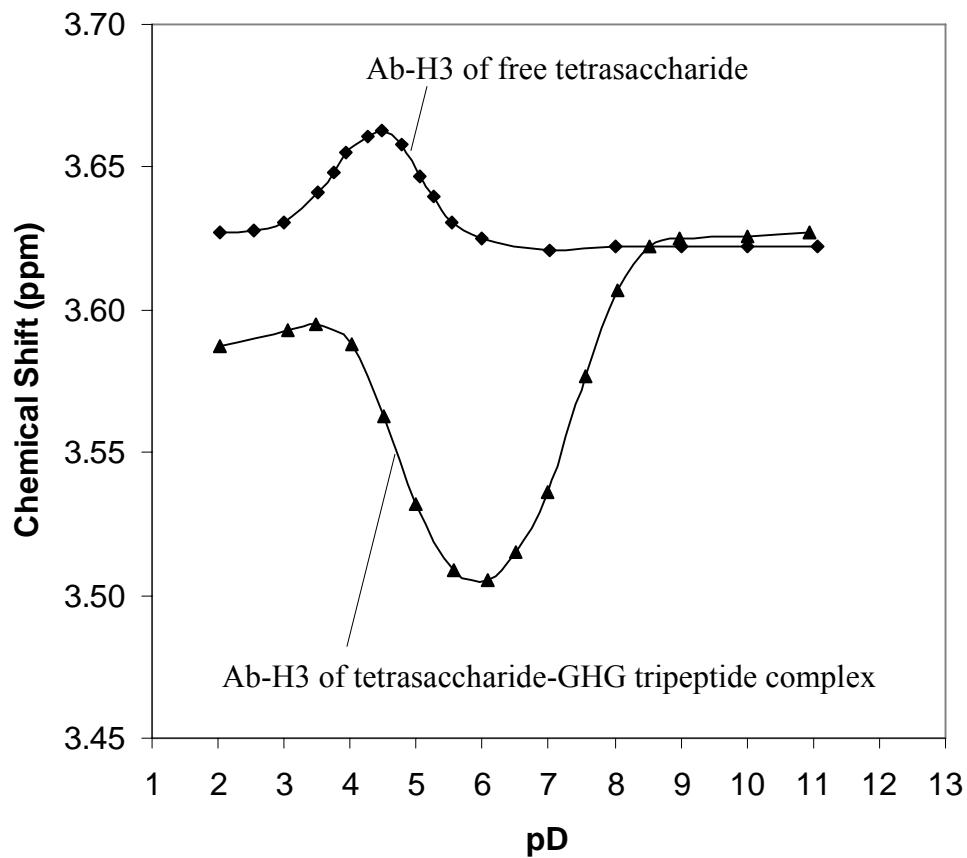
Figure 4.36. pD dependence of the chemical shift of the resonance for the Ab-H3 proton of tetrasaccharide III for a solution containing only tetrasaccharide III and a solution containing 10.2 mM GHG with 0.511 mM tetrasaccharide III. Both free and complex solutions contain ~ 0.020 M Na^+.
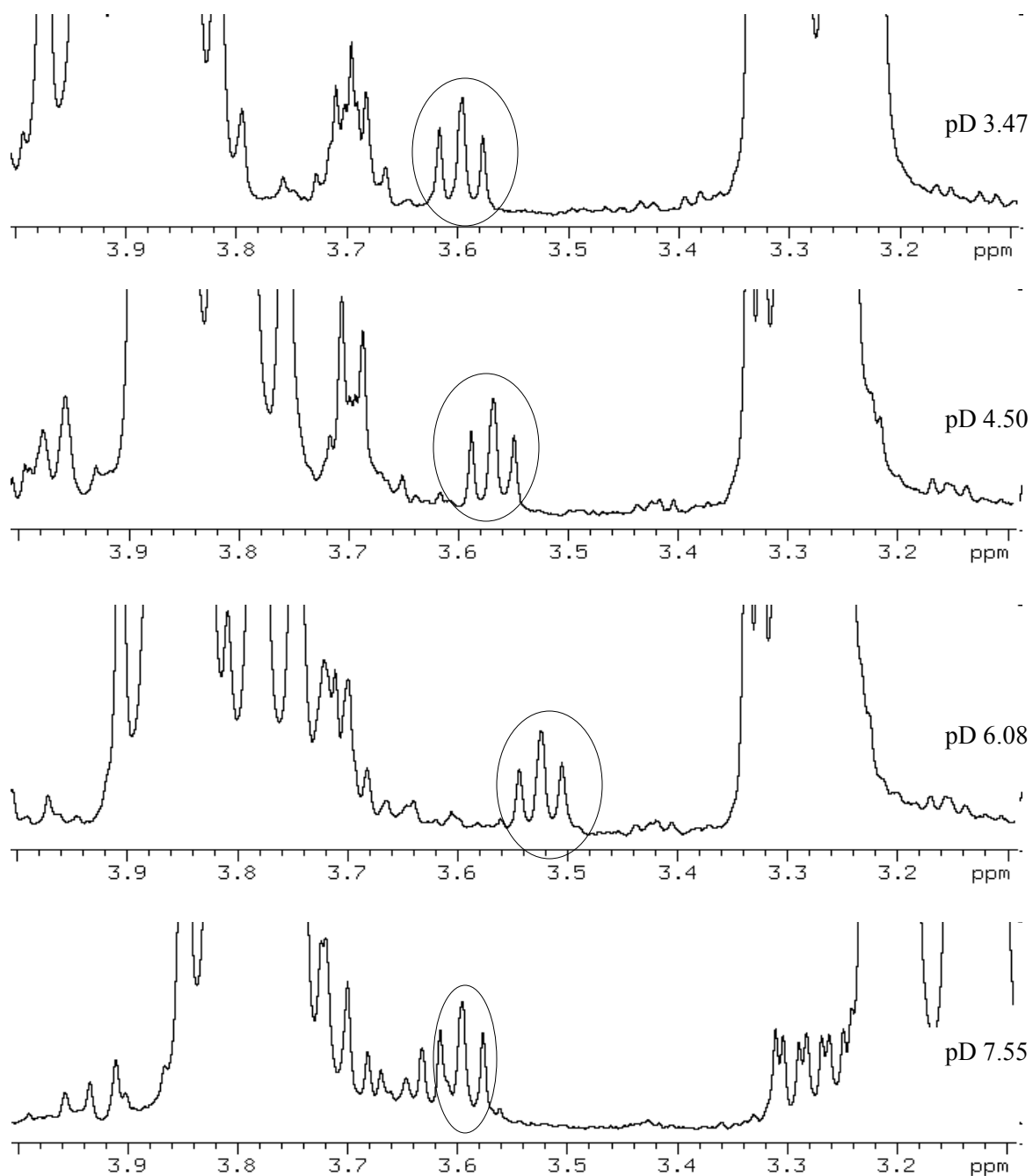
Figure 4.37. Portions of 1-D ^{1}H NMR spectra of a D$_2$O solution containing 10.2 mM GHG plus 0.511 mM heparin-derived tetrasaccharide III with [Na$^+$]$_{total}$ of ~ 0.020 M at various pD values. The circled resonance corresponds to the Ab-H3 proton of the tetrasaccharide III.
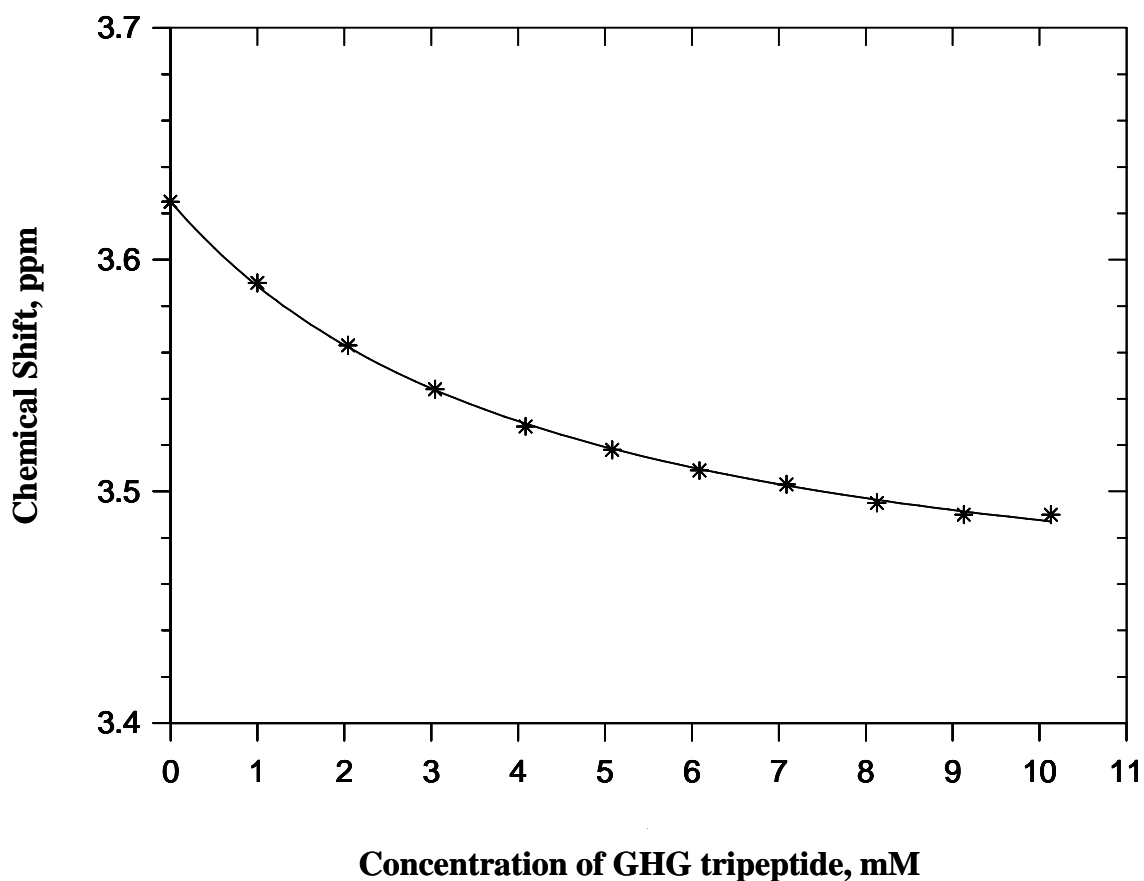
Figure 4.38. Determining the binding constant (K_{Bd}) between tripeptide GHG and tetrasaccharide III. The concentration of tetrasaccharide III was held constant at 0.506 mM while the GHG concentration was varied. The dependence of the chemical shift of the Ab-H3 proton on GHG concentration was obtained at pD 6.04 ± 0.05. Non-linear least squares fit of the chemical shift-concentration data yields a binding constant of 257 ± 11 M^{-1}. $[Na^+]_{total}$ = 0.020 M.

Free Tetrasaccharide; pD 6.00
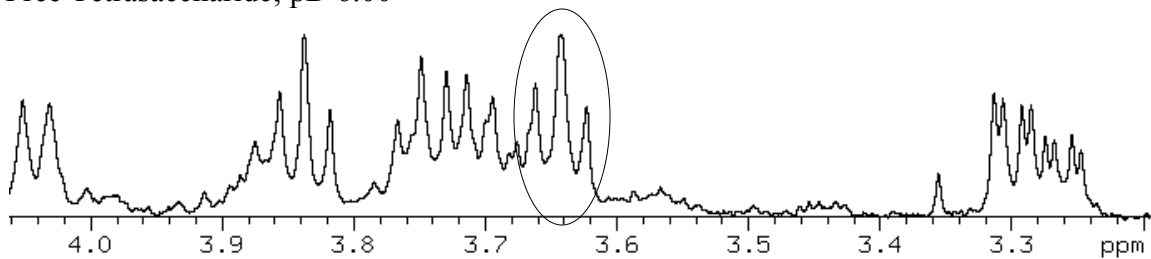
$$\frac{[GHG]}{[Tetrasaccharide]} = 2 \text{ ; pD 6.06}$$
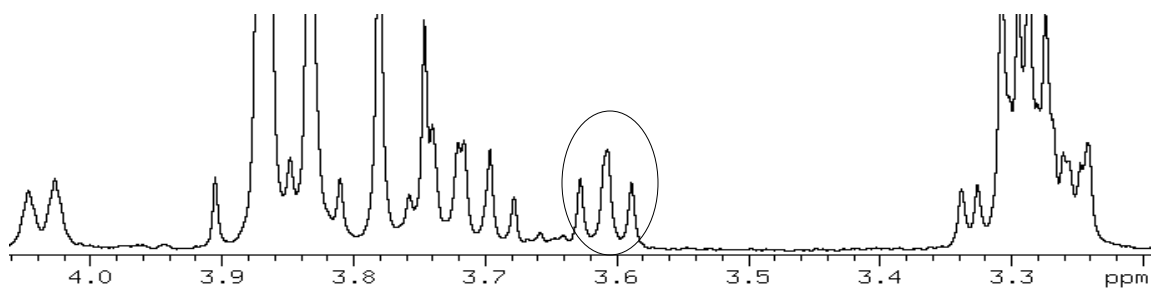
$$\frac{[GHG]}{[Tetrasaccharide]} = 6 \text{ ; pD 6.00}$$
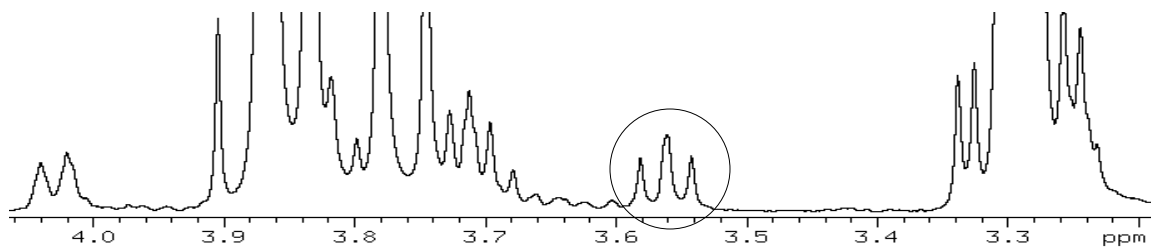
$$\frac{[GHG]}{[Tetrasaccharide]} = 12 \text{ ; pD 5.99}$$
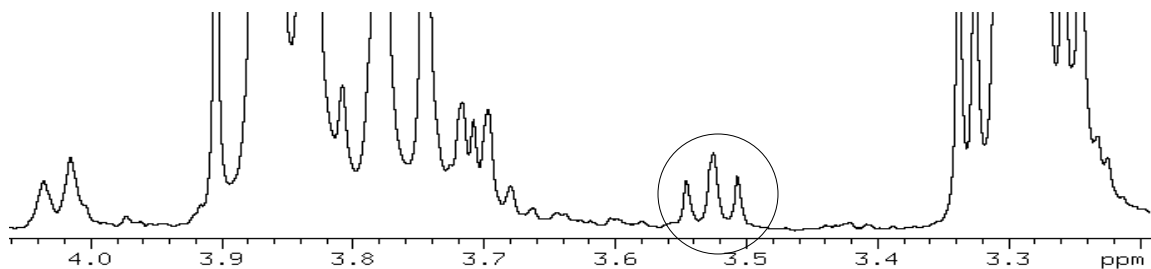
Figure 4.39. The dependence of the chemical shift of the Ab-H3 resonance of tetrasaccharide III on the GHG : tetrasaccharide III ratio. The circled resonance corresponds to the Ab-H3 proton of tetrasaccharide III. $[Na^+]_{total} = 0.020$ M.

4.6.4 DiPeptide L-histidyl-L-glycine (HG)

1-D ^{1}H NMR spectra for the free dipeptide HG and the tetrasaccharide III-HG

complex are shown in Figure 4.40. Assignment of chemical shifts of resonances for free

HG is shown in Table 4.6. Chemical shift vs pD data for CαH, C2H, and C4H protons of

the histidyl residue of HG free in solution are presented in Figure 4.41. The lines through

the points are predicted by the nonlinear least-squares fit of the data to the diprotic acid

model described in Chapter 2. The pK$_a$ values of the imidazolium ring and histidyl

ammonium group of free HG are reported in Table 4.7. Figure 4.42 shows the chemical

shift data for the Ab-H3 proton of tetrasaccharide III in the absence and presence of HG.

In the presence of HG, the Ab-H3 resonance is shifted upfield with a maximum

displacement at pD ~ 5.7. The upfield shift characteristic of site specific binding at

residue Ab of tetrasaccharide III indicates that the histidyl imidazolium group of HG

binds site specifically to the imidazolium-binding site on tetrasaccharide III. Upfield

displacement of the Ab-H3 resonance also provides evidence for formation of the

tetrasaccharide III-HG complex. The shift of the Ab-H3 resonance back to its chemical

shift of free tetrasaccharide III indicates dissociation of the complex upon titration of the

imidazolium ring. Figure 4.43 shows the dependence of the chemical shift of the Ab-H3

resonance as a function of pD when tetrasaccharide III is in solution with HG. The

binding curve for the HG-tetrasaccharide III binding is presented in Figure 4.44. Figure

4.45 shows the dependence of the chemical shift of the Ab-H3 resonance on the HG :

tetrasaccharide III ratio. A binding constant of 171 ± 4 M^{-1} was obtained at pD $5.67 \pm$

0.12.
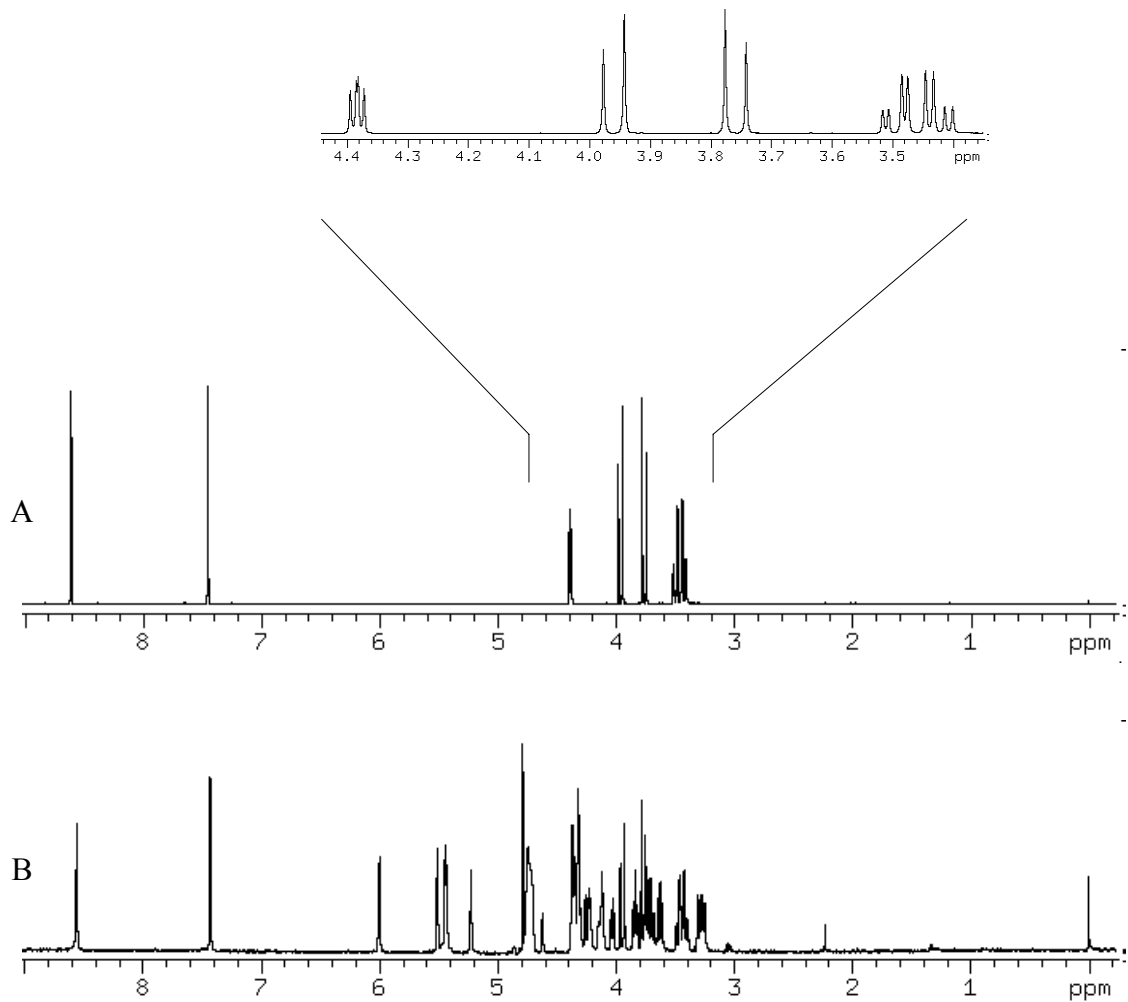
Figure 4.40. 1-D ^{1}H NMR spectra of D$_2$O solutions containing (A) 34.1 mM dipeptide HG at pD 5.49 and (B) 0.531 mM HG + 0.506 mM tetrasaccharide III at pD 5.75. The total sodium concentration for free and bound HG was ~ 0.020 M.

Residue	NH	αH	βH	Others
His[1]	n.d.	4.383	3.423, 3.495	H_2 7.447
				H_4 8.605
Gly[2]	n.d.	3.859		

n.d., not determined because of deuterium exchange with the D_2O solvent.

Table 4.6. Assignment of chemical shifts of resonances for dipeptide HG free in solution at pD 5.49 and 25 °C.
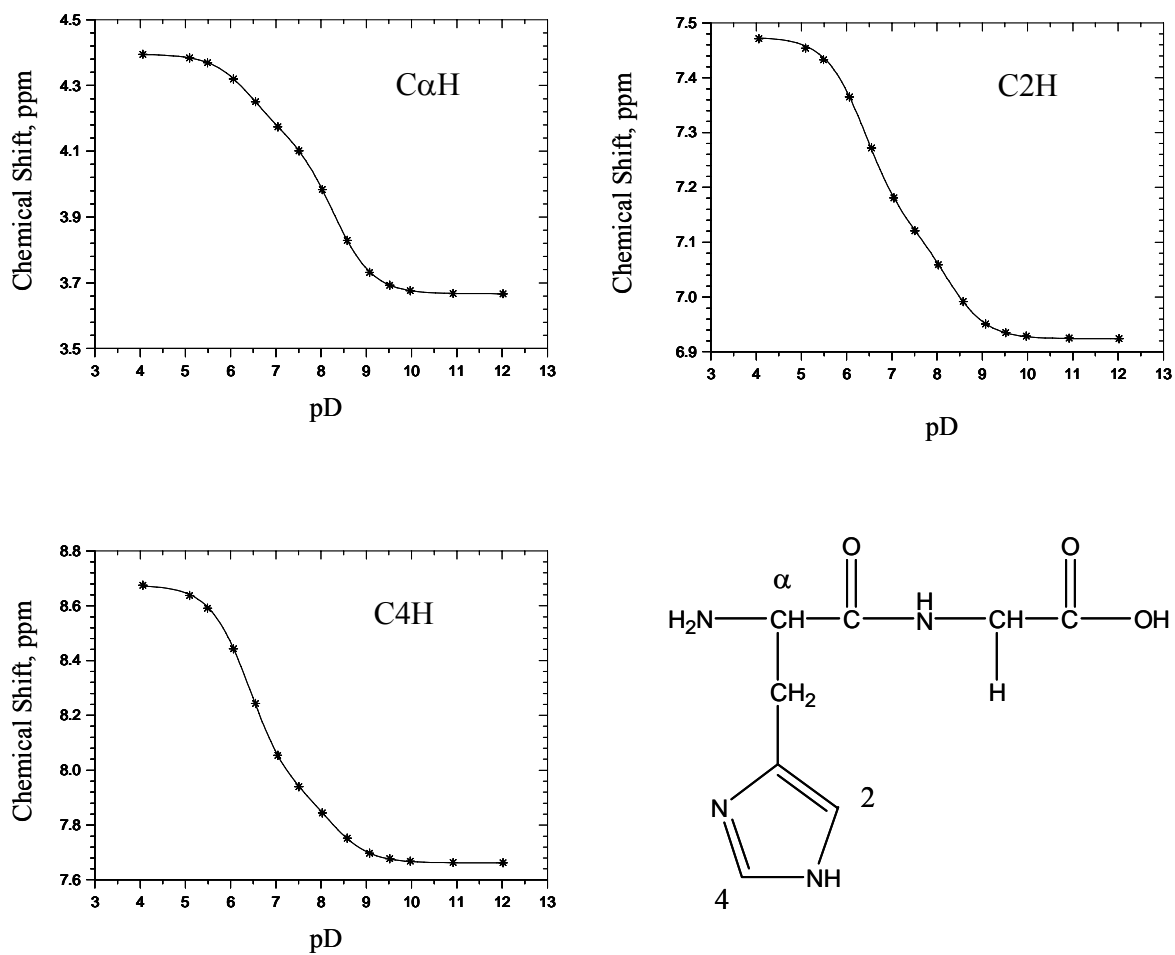
Figure 4.41. The chemical shift-pD titration curves for the CαH, C2H, and C4H protons

of the histidine residue of dipeptide HG free in solution with $[Na^+]_{total}$ of ~ 0.020 M.

	pK$_a$		
	CαH	C2H	C4H
Imidazolium ring	6.03 ± 0.01	6.00 ± 0.01	6.01 ± 0.01
N-terminal ammonium group	7.87 ± 0.01	7.85 ± 0.03	7.85 ± 0.02

Table 4.7. Acid dissociation constants of the imidazolium ring and N-terminal ammonium group of histidyl of dipeptide HG free in solution with [Na$^+$]$_{total}$ of ~ 0.020 M based on chemical shift data of the CαH, C2H, and C4H protons.
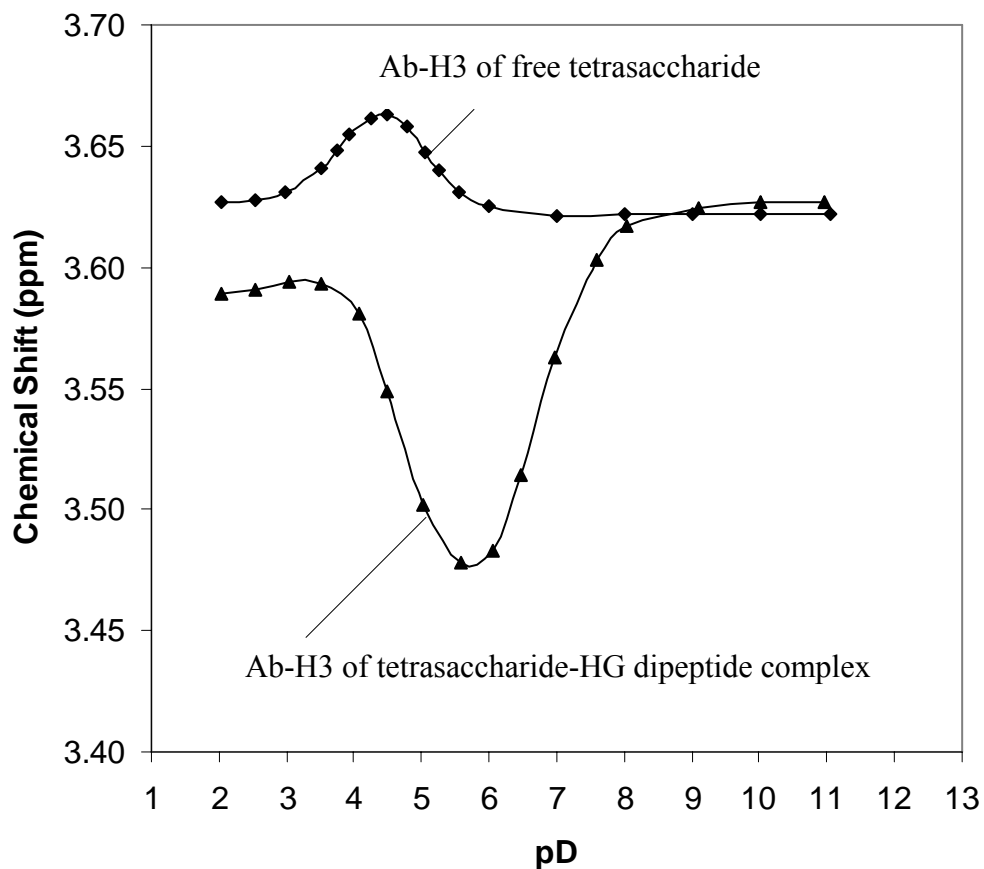
Figure 4.42. Chemical shift of the resonance for the Ab-H3 proton of tetrasaccharide III as a function of pD for a solution containing only tetrasaccharide III and a solution containing 0.511 mM tetrasaccharide III plus 10.2 mM HG. Both free and complex solutions contain ~ 0.020 M Na^+.
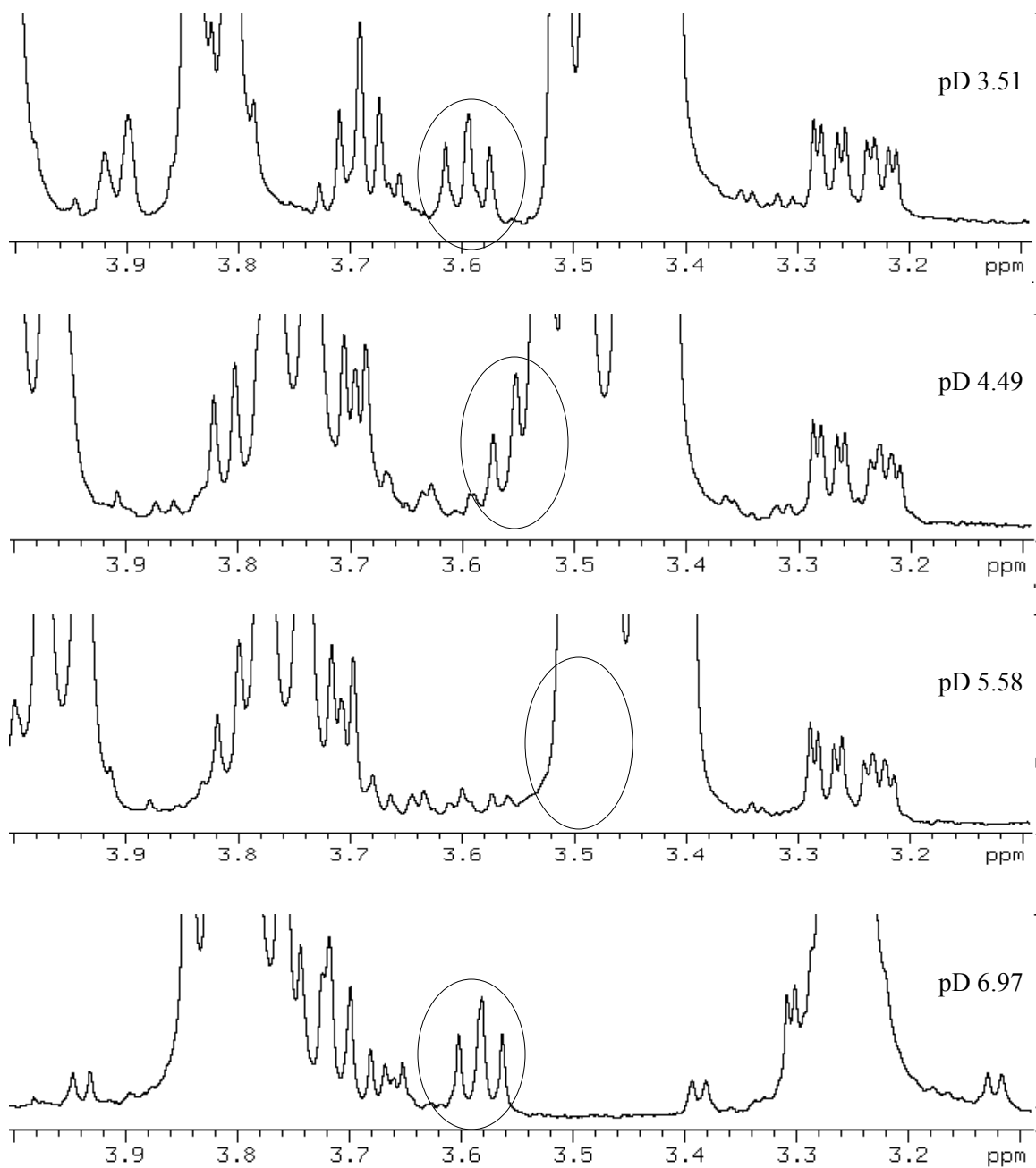
Figure 4.43. Portions of 1-D ^{1}H NMR spectra of a D_2O solution containing 10.2 mM HG plus 0.511 mM tetrasaccharide III with $[Na^+]_{total}$ of ~ 0.020 M at various pD values. The circled resonance corresponds to the Ab-H3 proton of the tetrasaccharide III. At pD 5.58, Ab-H3 resonance lies underneath the intense resonance and its chemical shift was determined to be 3.493 ppm from the TOCSY spectrum.
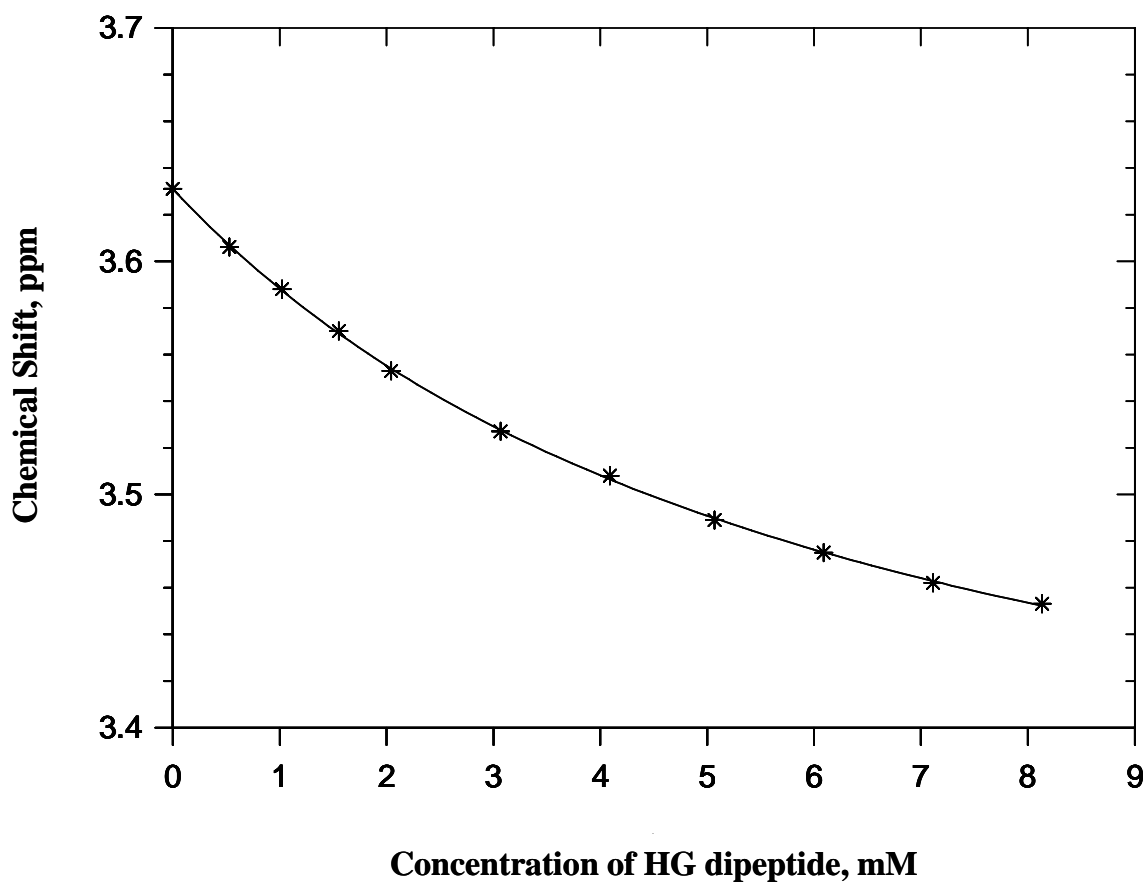
Figure 4.44. Determining the binding constant (K_{Bd}) between dipeptide HG and
tetrasaccharide. The concentration of tetrasaccharide was held constant at 0.506 mM
while HG concentration was varied. The dependence of the chemical shift of the Ab-H3
proton on HG concentration was obtained at pD 5.67 ± 0.12. The fitting yields a binding
constant of 171 ± 4 M^{-1}. $[Na^+]_{total}$ = 0.020 M.

Free Tetrasaccharide; pD 5.54
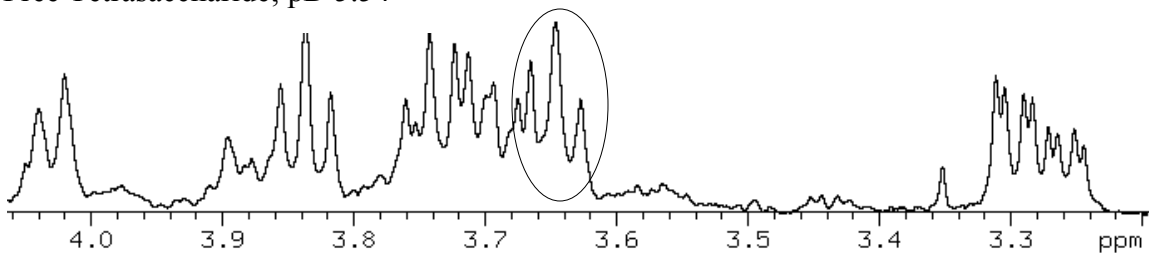
$$\frac{[HG]}{[Tetrasaccharide]} = 2 \,; \text{pD } 5.68$$
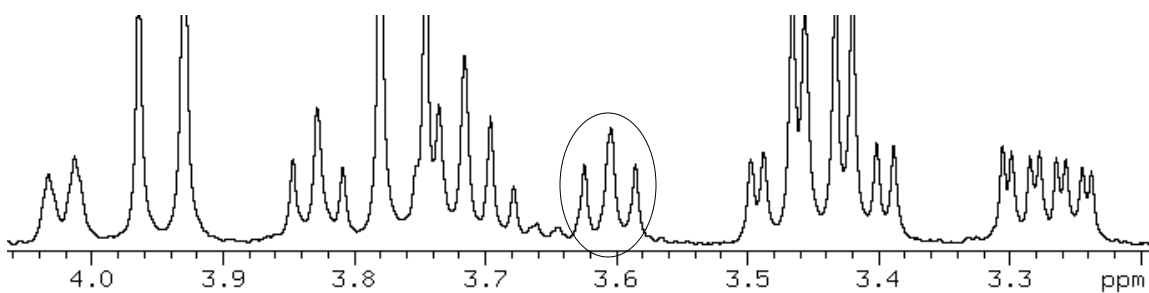
$$\frac{[HG]}{[Tetrasaccharide]} = 4 \,; \text{pD } 5.79$$
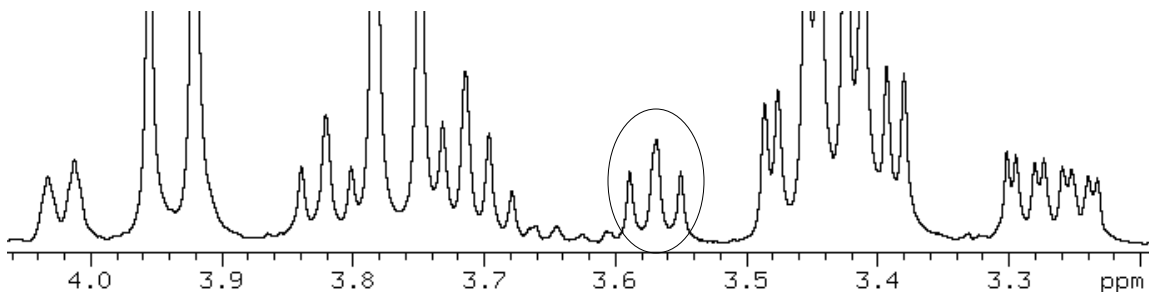
$$\frac{[HG]}{[Tetrasaccharide]} = 6 \,; \text{pD } 5.77$$
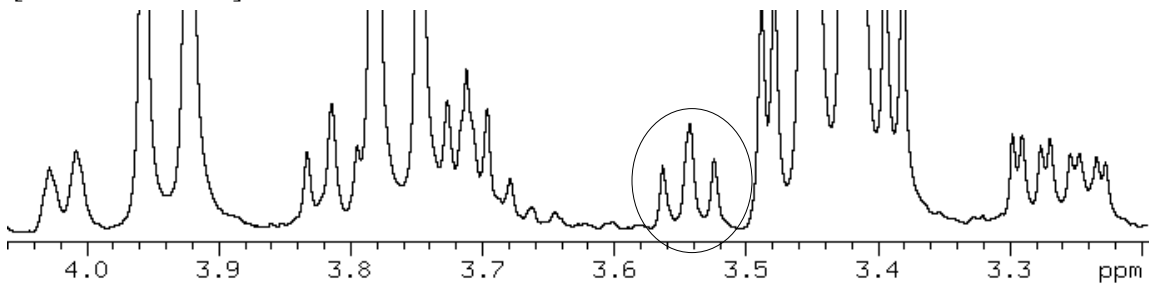
Figure 4.45. The dependence of the chemical shift of the Ab-H3 resonance of tetrasaccharide III on HG : tetrasaccharide III ratio. The circled resonance corresponds to the Ab-H3 proton of tetrasaccharide III. $[Na^+]_{total} = 0.020$ M.

4.6.5 DiPeptide L-glycyl-L-histidine (GH)

1-D ^{1}H NMR spectra for the free dipeptide GH and the tetrasaccharide III-GH complex are shown in Figure 4.46. Assignment of chemical shifts of resonances for free GH is shown in Table 4.8. Chemical shift data are presented in Figure 4.47 for the CαH proton of the glycyl, and the CαH, C2H and C4H protons of the histidine of GH free in solution. The pK$_a$ values of the histidine imidazolium group and the glycyl ammonium group of free GH are reported in Table 4.9. It should be noted that the pK$_a$ of the imidazolium group for GH is higher than that for HG. Figure 4.48 shows the chemical shift titration curves for the Ab-H3 proton of tetrasaccharide III in the absence and presence of GH. The upfield shift of the Ab-H3 resonance of tetrasaccharide III in the presence of GH reaches its maximum at pD ~ 6, which is consistent with a higher pK$_a$ value for the imidazolium group. The upfield displacement of the Ab-H3 resonance indicates that the histidine imidazolium group of GH binds site specifically to the imidazolium-binding site on tetrasaccharide III. Figure 4.49 shows the pD dependence of the Ab-H3 resonance of tetrasaccharide III in the presence of GH. The binding curve for the GH-tetrasaccharide III interaction is presented in Figure 4.50. Figure 4.51 shows the dependence of the chemical shift of the Ab-H3 resonance on the GH : tetrasaccharide III ratio. A binding constant of 87 ± 5 M^{-1} was determined at pD 6.05 ± 0.05.

4.6.6 L-Histidine

1-D ^{1}H NMR spectra for the free L-histidine and the tetrasaccharide III-L-histidine complex are shown in Figure 4.52. Chemical shift vs pD titration curves for the CαH, C2H, and C4H protons of L-histidine free in solution are presented in Figure 4.53. The
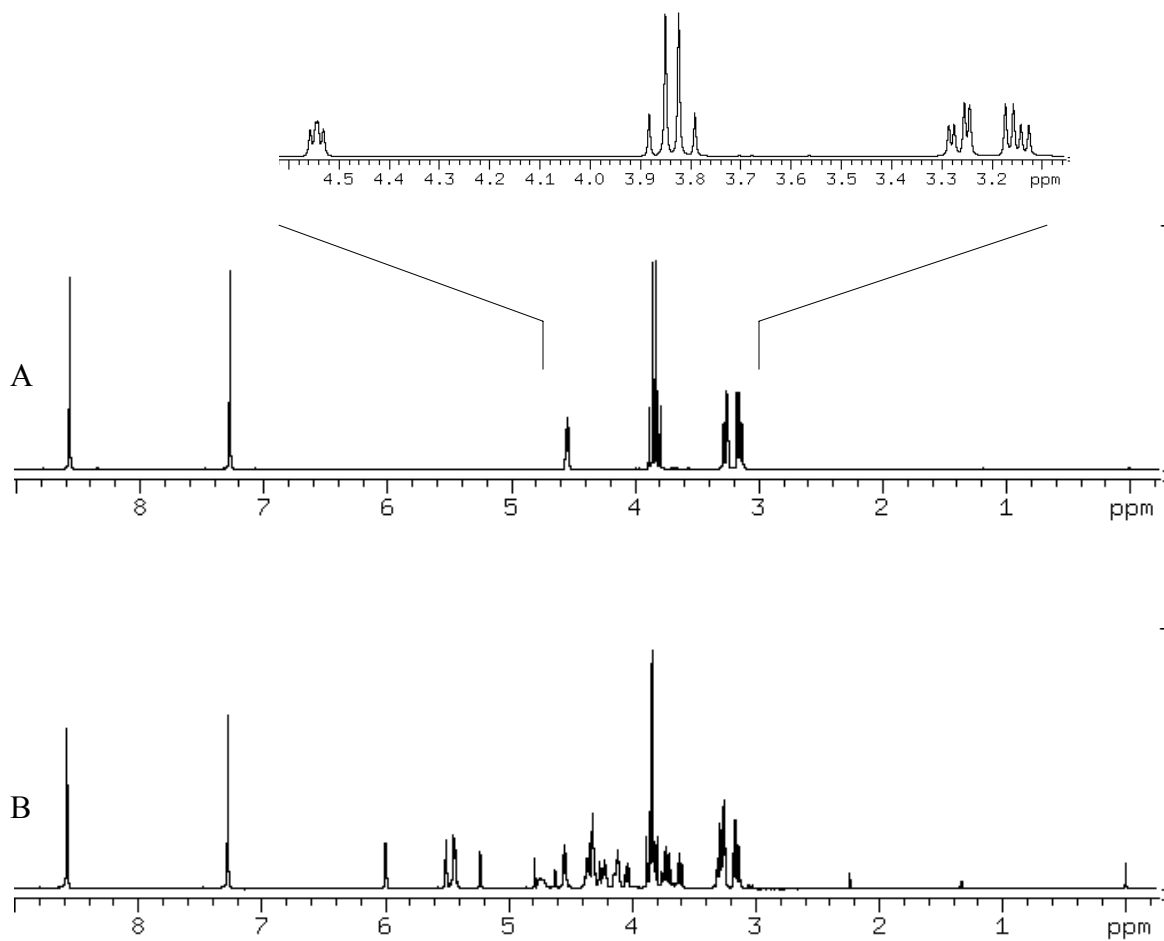
Figure 4.46. 1-D ^{1}H NMR spectra of D_2O solutions containing (A) 0.036 M dipeptide GH at pD 6.09 and (B) 0.002 M GH plus 0.001 M tetrasaccharide III at pD 6.00. The total sodium concentration for free and bound HG was ~ 0.020 M.

Residue	NH	αH	βH	Others
Gly[1]	n.d.	3.836		
His[2]	n.d.	4.543	3.149, 3.264	H_2 7.268
				H_4 8.563

n.d., not determined because of deuterium exchange with the D_2O solvent.

Table 4.8. Assignment of chemical shifts of resonances for dipeptide GH free in solution at pD 6.09 and 25 °C.

Figure 4.47. The chemical shift-pD titration curves for CαH of glycyl (A), and CαH (B), C2H (C), and C4H (D) protons of histidine of dipeptide GH free in solution with $[Na^+]_{total}$ of ~ 0.020 M.

	pK$_a$			
	Glycyl	Histidine		
	CαH	CαH	C2H	C4H
Imidazolium ring		7.29 ± 0.07	7.00 ± 0.02	6.98 ± 0.01
N-terminal ammonium group	8.31 ± 0.02			

Table 4.9. Acid dissociation constants of the imidazolium ring of histidine and the glycyl ammonium group of free GH with [Na$^+$]$_{total}$ of ~ 0.020 M based on chemical shift data of the CαH, C2H, and C4H protons.
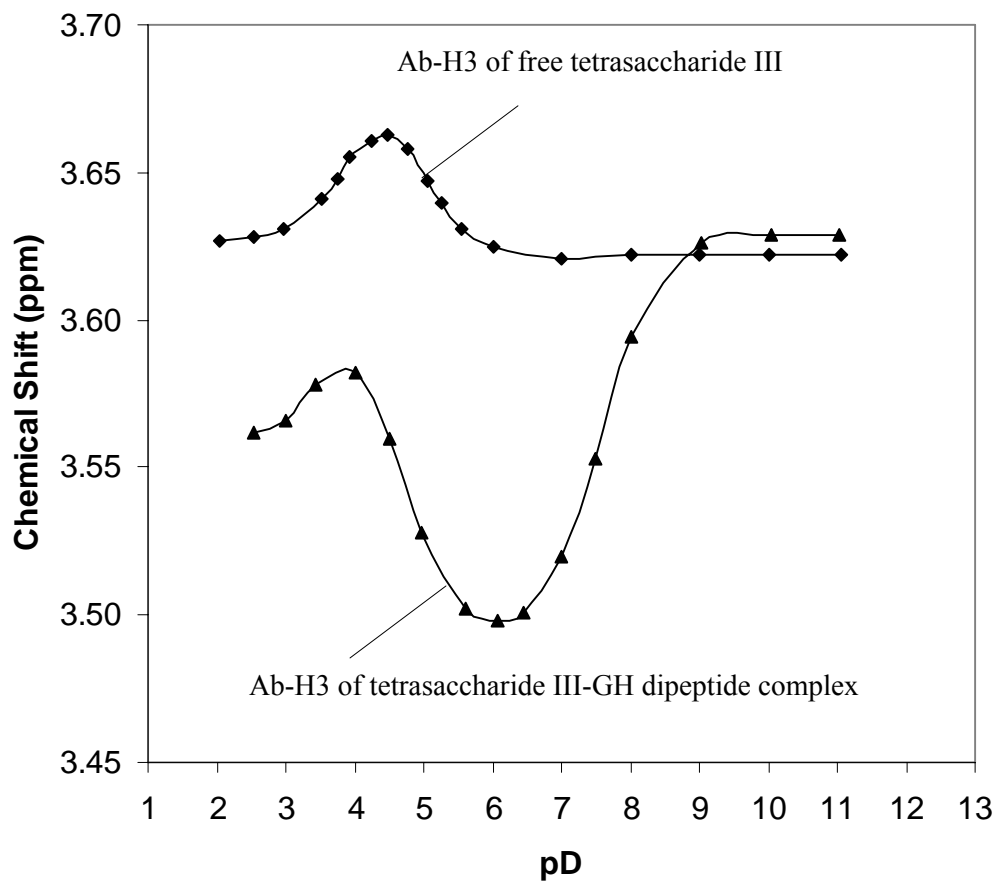
Figure 4.48. Chemical shift of the resonance for the Ab-H3 proton of tetrasaccharide III as a function of pD for a solution containing only tetrasaccharide III and a solution containing 0.001 M tetrasaccharide III plus 0.020 M GH. Both free and complex solutions contain ~ 0.020 M Na$^+$.
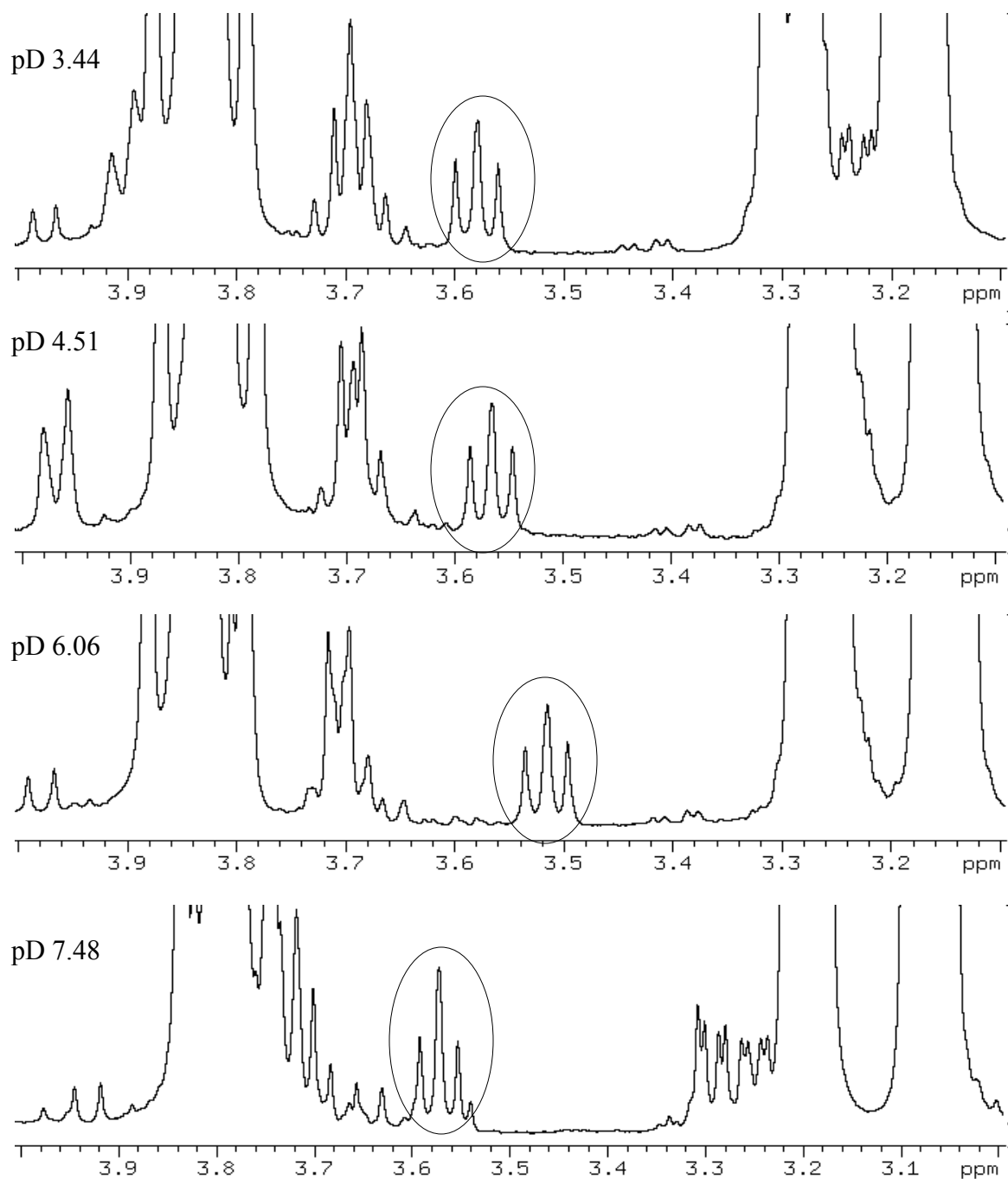
Figure 4.49. Portions of 1-D ^{1}H NMR spectra of a D_2O solution containing 0.020 M dipeptide GH plus 0.001 M tetrasaccharide III with $[Na^+]_{total}$ of ~ 0.020 M at various pD values. The circled resonance corresponds to the Ab-H3 proton of the tetrasaccharide III.

212
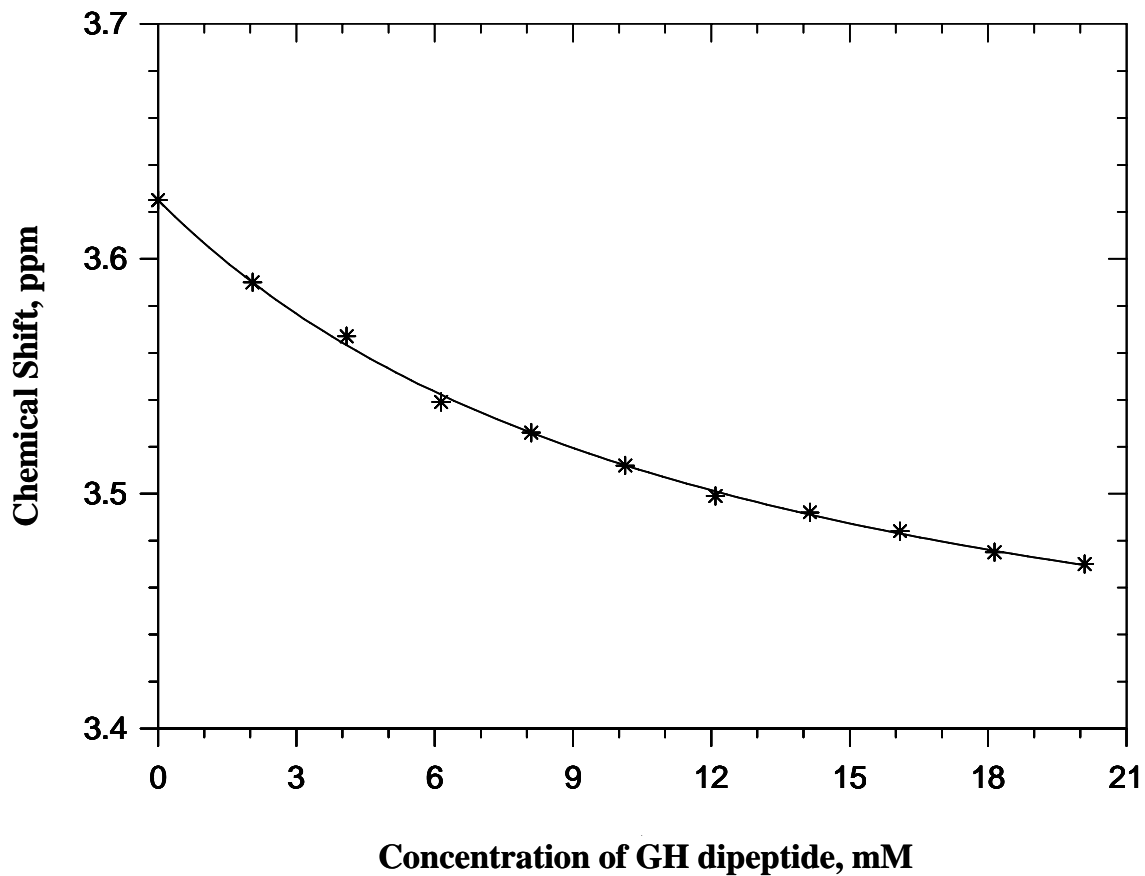
Figure 4.50. Determining the binding constant (K_{Bd}) between dipeptide GH and tetrasaccharide III. The concentration of tetrasaccharide III was held constant at 1.01 mM while GH concentration was varied. The dependence of the chemical shift of the Ab-H3 proton on the concentration of GH was obtained at pD 6.05 ± 0.05. The fitting yields a binding constant of 87 ± 5 M^{-1}. [Na$^+$]$_{total}$ = 0.020 M.

Free Tetrasaccharide; pD 6.00
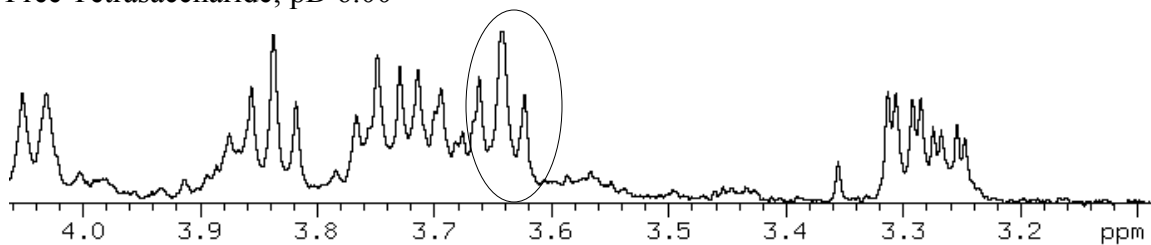
$$\frac{[GH]}{[Tetrasaccharide]} = 2\,; \text{pD } 6.00$$
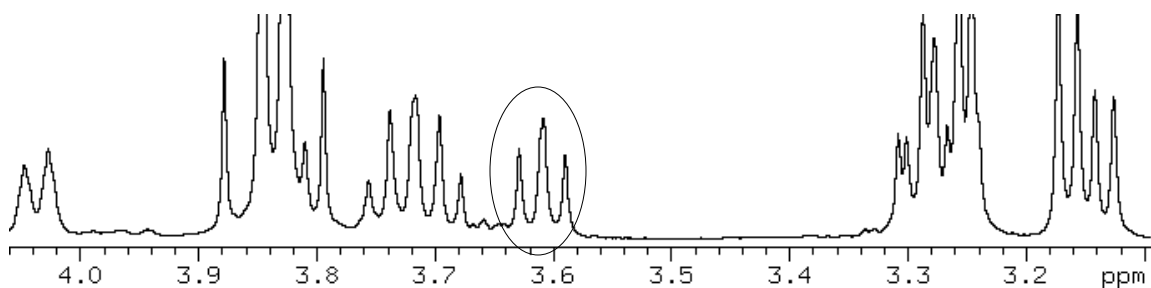
$$\frac{[GH]}{[Tetrasaccharide]} = 8\,; \text{pD } 6.01$$
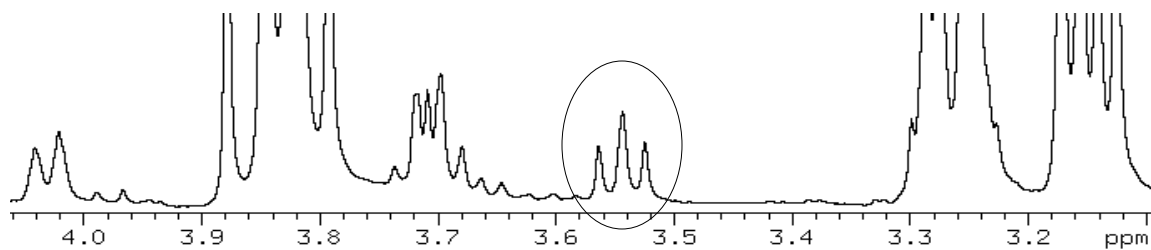
$$\frac{[GH]}{[Tetrasaccharide]} = 14\,; \text{pD } 6.03$$
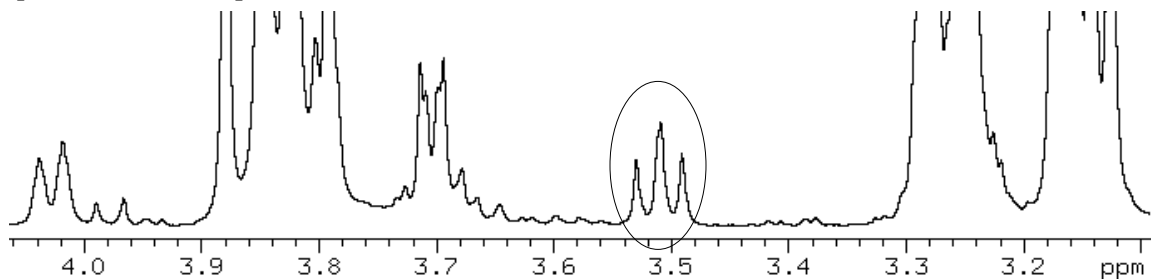
Figure 4.51. The dependence of the chemical shift of the Ab-H3 resonance of tetrasaccharide III on the GH : tetrasaccharide III molar ratio. The circled resonance corresponds to the Ab-H3 proton of tetrasaccharide III $[Na^+]_{total} = 0.020$ M.
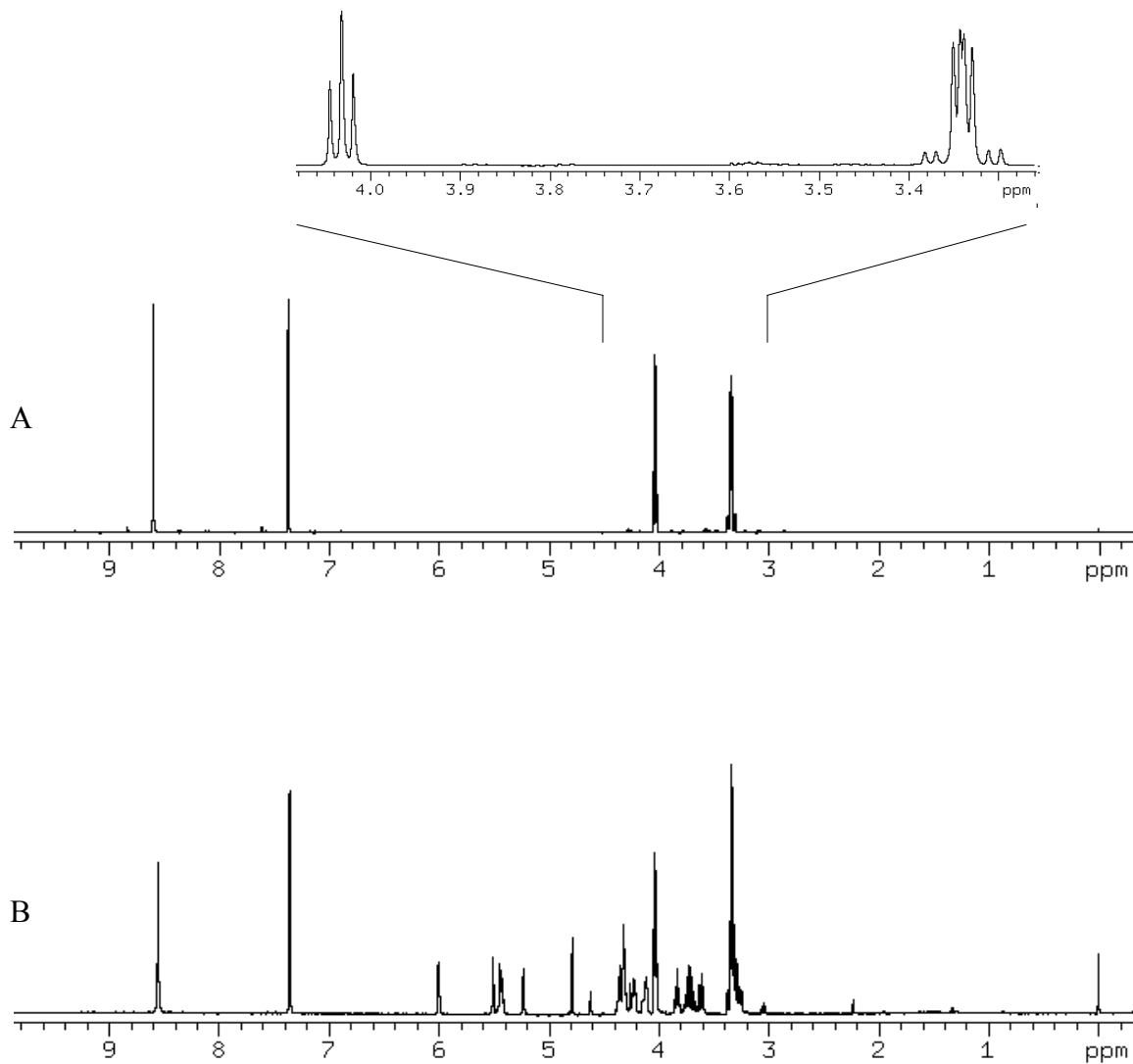
Figure 4.52. 1-D ^{1}H NMR spectra of D_2O solutions containing (A) 0.034 M L-histidine at pD 5.58 and (B) 1.04 mM L-histidine with 0.516 mM tetrasaccharide III at pD 5.79. The total sodium concentration for free and bound L-histidine was ~ 0.020 M.
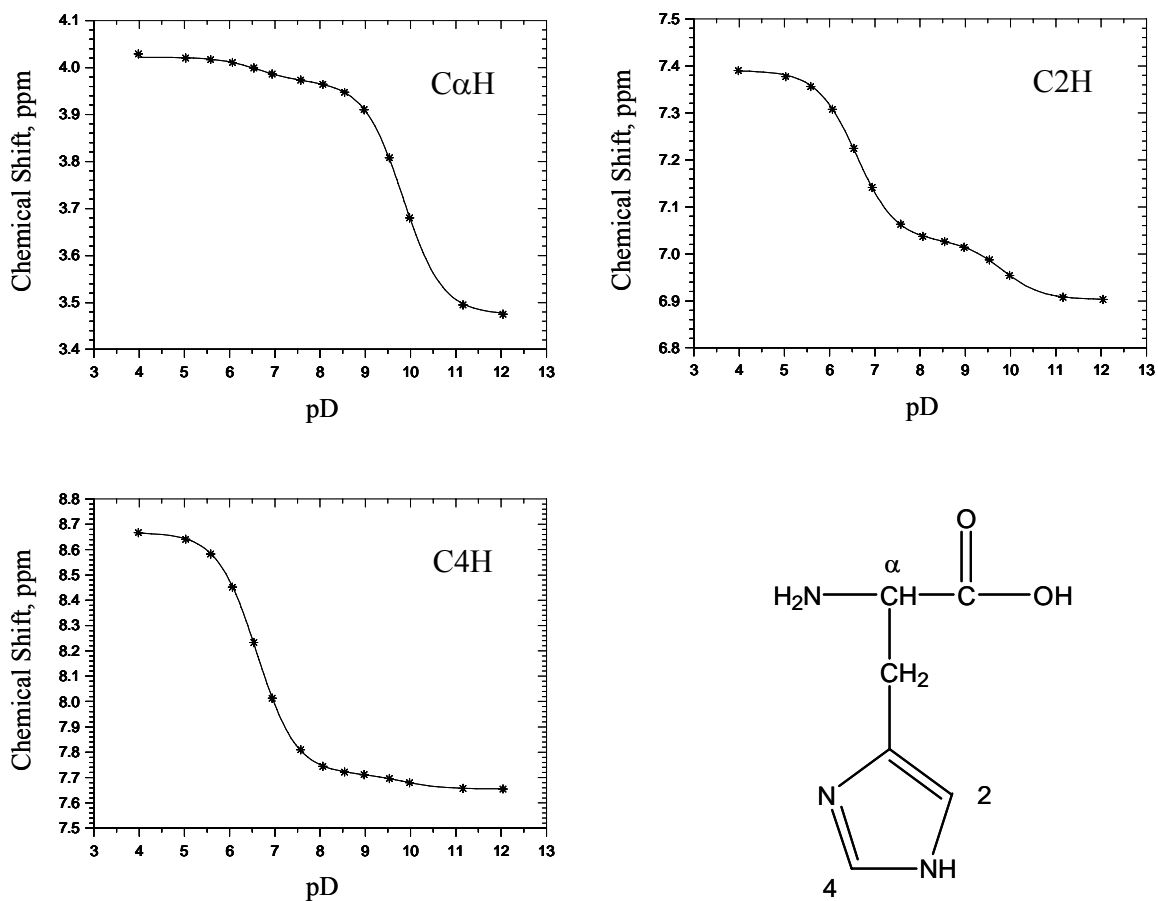
Figure 4.53. The chemical shift-pD titration curves for the CαH, C2H, and C4H protons of L-histidine free in solution with $[Na^+]_{total}$ of ~ 0.020 M.

pK_a values of the imidazolium and the N-terminal ammonium groups of free L-histidine are reported in Table 4.10. Figure 4.54 shows the chemical shift data for the Ab-H3 proton of tetrasaccharide III in the absence and presence of L-histidine. The upfield shift of the Ab-H3 resonance of tetrasaccharide III in the presence of L-histidine reaches its maximum at pD ~ 5.7, a similar behavior as for the dipeptide HG since the pK_a values of the imidazolium groups for L-histidine and HG are almost identical. The upfield displacement at site Ab of tetrasaccharide III indicates that the imidazolium group of L-histidine binds site specifically to the imidazolium-binding site on tetrasaccharide III created by the trisaccharide ΔUA(2S)-GlcNS(6S)-IdoA(2S). Figure 4.55 shows the pD dependence of the chemical shift of the Ab-H3 resonance of tetrasaccharide III in the presence of L-histidine. The binding curve for the L-histidine-tetrasaccharide III binding is presented in Figure 4.56. Figure 4.57 shows the dependence of the chemical shift of the Ab-H3 resonance on the L-histidine : tetrasaccharide III ratio. A binding constant of 118 $\pm$ 4 M^{-1} was determined at pD 5.66 $\pm$ 0.12.

4.7 Discussion

As seen from the chemical shift-pD titration curves, the Ab-H3 proton of free tetrasaccharide III displays a small change in chemical shift over the pD range 2-6 where its carboxylic acid groups are titrated presumably due to a small rotation around the IdoA(2S)-GlcNS(6S) glycosidic bond.[11] For all the binding studies reported, the upfield shift of the Ab-H3 proton was induced by a ring current effect caused by the imidazolium group, an aromatic ring, which is located close to the Ab-H3 proton in the tetrasaccharide III-ligand complexes.[10] The binding is mediated primarily by electrostatic interaction.[9, 11]

	pK$_a$		
	CαH	C2H	C4H
Imidazolium ring	6.22 ± 0.07	6.19 ± 0.01	6.20 ± 0.01
N-terminal ammonium group	9.43 ± 0.01	9.42 ± 0.02	9.42 ± 0.05

Table 4.10. Acid dissociation constants of the imidazolium ring and N-terminal ammonium group of L-histidine free in solution with [Na$^+$]$_{total}$ of ~ 0.020 M based on chemical shift data of the CαH, C2H, and C4H protons.
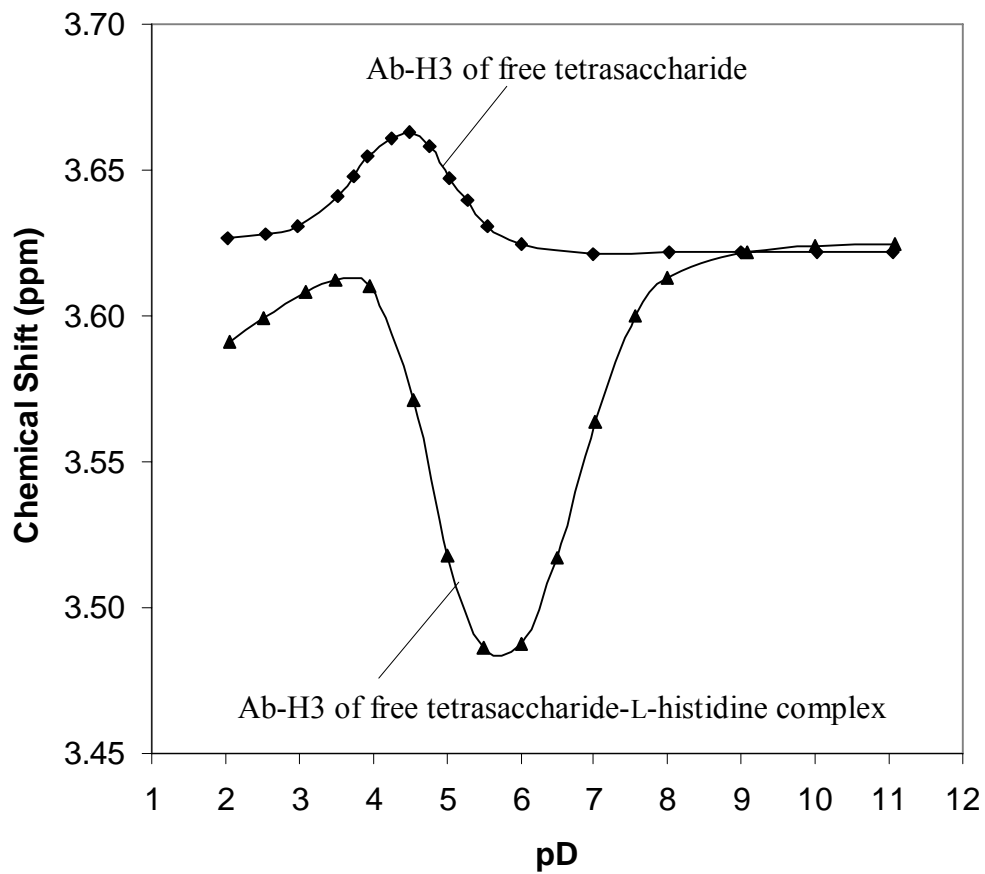
Figure 4.54. Chemical shift of the resonance for the Ab-H3 proton of tetrasaccharide III as a function of pD for a solution containing only tetrasaccharide III and a solution containing 0.511 mM tetrasaccharide III plus 10.2 mM L-histidine. Both free and complex solutions contain ~ 0.020 M Na^+.
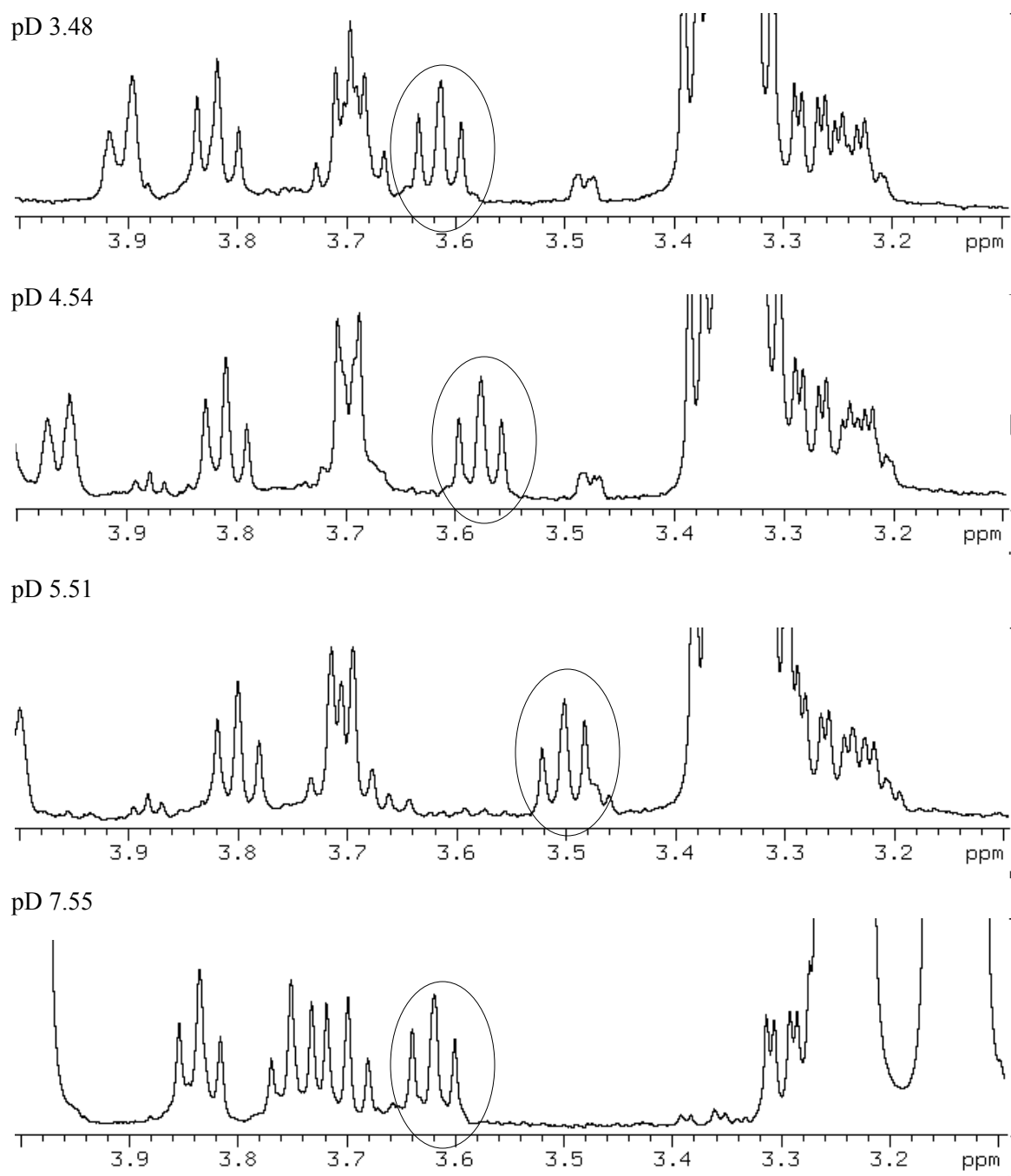
Figure 4.55. Portions of 1-D ^{1}H NMR spectra of a D$_2$O solution containing 10.2 mM L-histidine plus 0.511 mM tetrasaccharide III with [Na$^+$]$_{total}$ of ~ 0.020 M at various pD values. The circled resonance corresponds to the Ab-H3 proton of tetrasaccharide III.
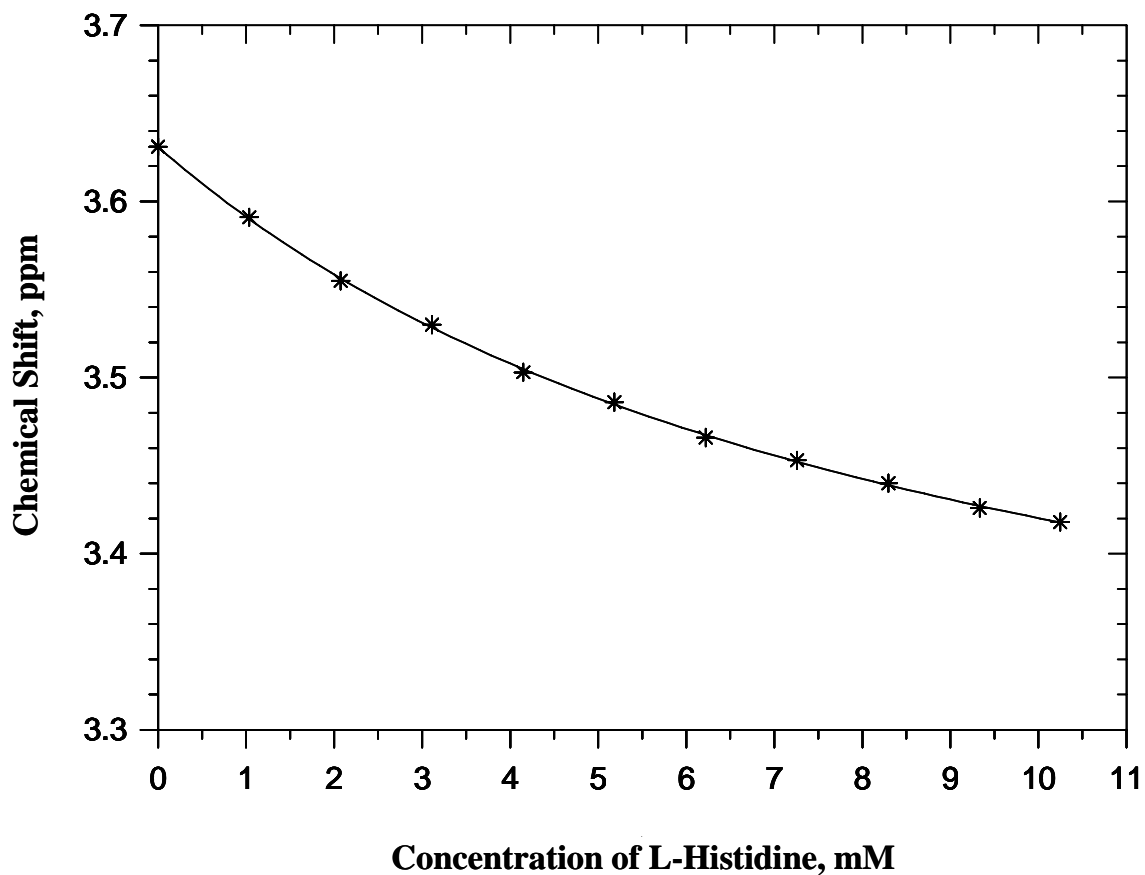
Figure 4.56. Determining the binding constant (K_{Bd}) between L-histidine and tetrasaccharide III. The concentration of tetrasaccharide III was held constant at 0.516 mM while L-histidine concentration was varied. The dependence of the chemical shift of the Ab-H3 proton on the concentration of L-histidine was obtained at pD 5.66 ± 0.12. The fitting yields a binding constant of 118 ± 4 M^{-1}. [Na$^+$]$_{total}$ = 0.020 M.

Free Tetrasaccharide; pD 5.54
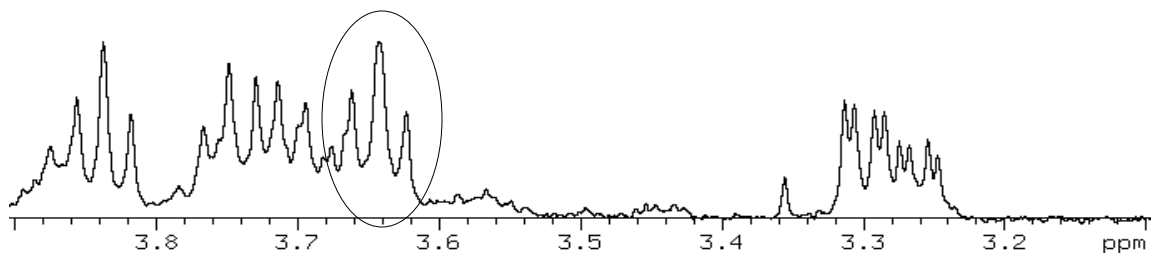
$$\frac{[Histidine]}{[Tetrasaccharide]} = 2 \, ; \text{pD } 5.79$$
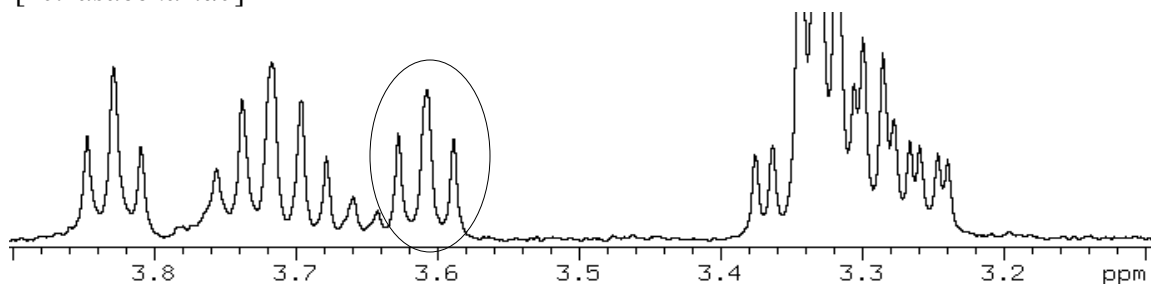
$$\frac{[Histidine]}{[Tetrasaccharide]} = 4 \, ; \text{pD } 5.77$$
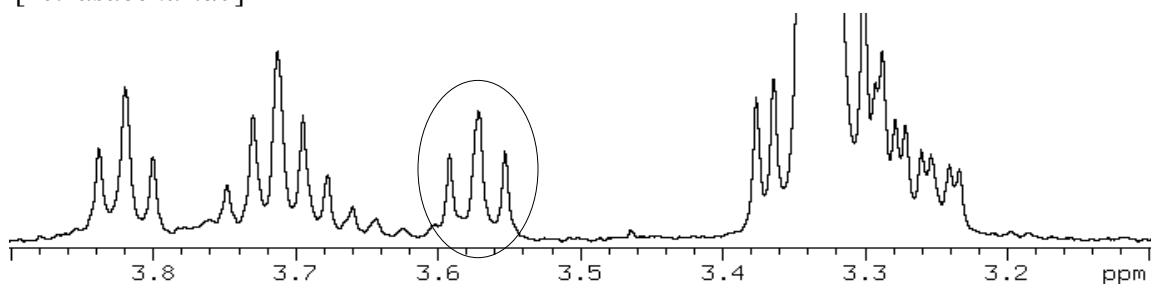
$$\frac{[Histidine]}{[Tetrasaccharide]} = 8 \, ; \text{pD } 5.77$$
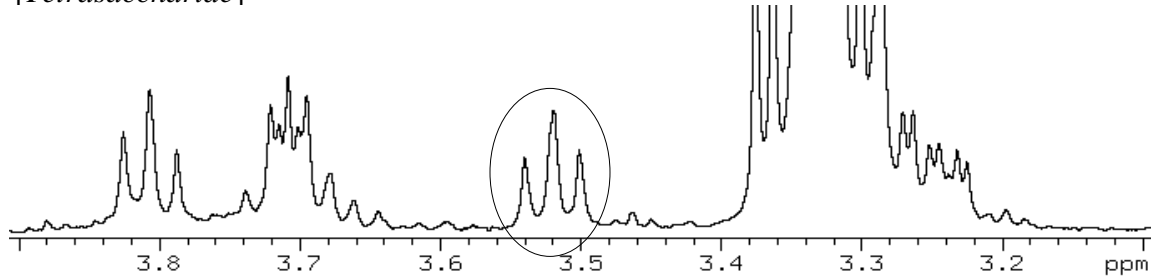
Figure 4.57. The dependence of the chemical shift of the Ab-H3 resonance of tetrasaccharide III on the L-histidine : tetrasaccharide III ratio. The circled resonance corresponds to the Ab-H3 proton of tetrasaccharide III. $[Na^+]_{total} = 0.020$ M.

The results in Table 4.11 indicate that the binding of histamine by tetrasaccharide III is strongest among the ligands. Figure 4.58 show structures of imidazole, histamine, L-histidine, dipeptides GH and HG, tripeptide GHG, the growth factor GHK, and β-amyloid peptide. From the steric and electrostatic repulsions point of view, histamine can be more easily in close contact with binding sites on heparin compared to others, with the only exception being imidazole.

A molecular modeling study has shown that the two imidazolium NH protons hydrogen bonded to the carboxylate groups of the two I residues, while the ammonium group of histamine interacts with the N-sulfate group of GlcNS(6S) of the IdoA(2S)-GlcNS(6S)-IdoA(2S) trisaccharide binding sequence, resulting in an enhancement for the histamine-heparin binding affinity.[10] It should be noted that the binding constant for histamine-tetrasaccharide III interaction reported in this dissertation is 3 times smaller than histamine-heparin binding reported in literature, at the same $[Na^+]$.[9] Weaker binding for the interaction of histamine with tetrasaccharide III might be due to there being a ΔUA residue rather than an IdoA residue at the nonreducing end of residue Ab of tetrasaccharide III. In addition, a smaller entropic contribution for the tetrasaccharide III-histamine interaction is expected compared to that of the heparin-histamine binding as a result of the smaller degree of polymerization of tetrasaccharide III compared to that of a heparin polymer presumably contributes to the weaker binding of III for histamine.

The results in Table 4.11 also indicate that dipeptide GH binds to tetrasaccharide III tighter than imidazole. The tighter GH-tetrasaccharide III binding is presumably due to a contribution from the electrostatic interaction between the glycyl ammonium group

Ligands	pD	K_{Bd} (M^{-1})	$\delta_{Complex}$ (ppm)
Imidazole	3.0	11 ± 5	3.482 ± 0.049
Imidazole	6.0	36 ± 3	3.171 ± 0.025
GH	6.0	87 ± 5	3.377 ± 0.006
L-Histidine	5.7	118 ± 4	3.237 ± 0.007
HG	5.7	171 ± 4	3.319 ± 0.004
GHG	6.0	257 ± 11	3.432 ± 0.003
FRHDSGY	5.0	329 ± 30	3.428 ± 0.011
GHK	6.0	1855 ± 43	3.456 ± 0.001
Histamine	6.0	2396 ± 135	3.306 ± 0.003

Table 4.11. Summary of binding constants for the interaction of imidazole, histamine, L-histidine, and histidine-containing peptides with tetrasaccharide III. The last column shows the upfield shift of the Ab-H3 resonance in the tetrasaccharide-ligand complex. $[Na^+]_{total} = 0.020$ M.
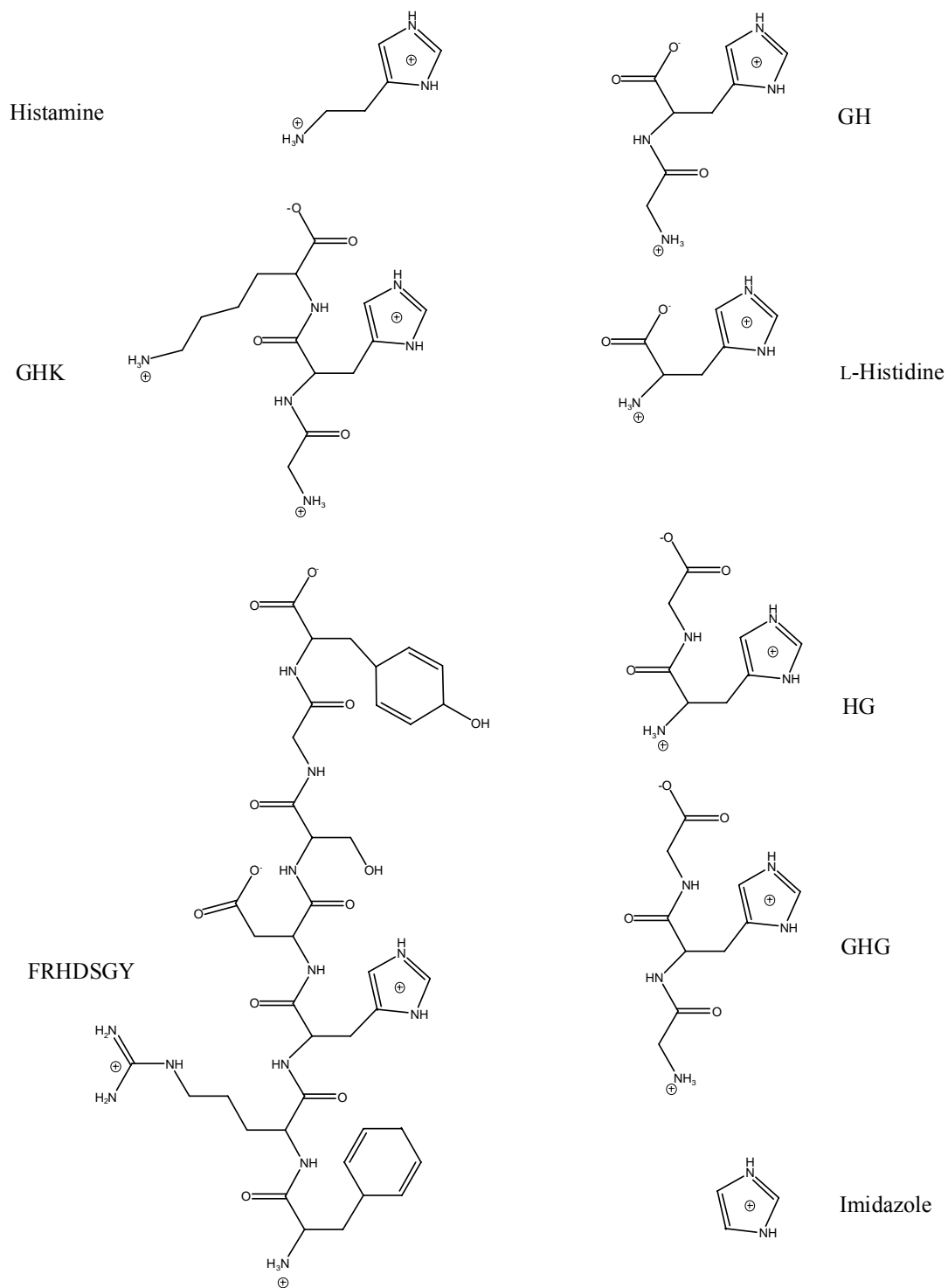
Figure 4.58. structures of imidazole, histamine, L-histidine, dipeptides GH and HG, tripeptides GHG and GHK, and β-amyloid peptide.

and sulfate groups on tetrasaccharide III.

L-histidine binds to tetrasaccharide III more tightly than dipeptide GH. A larger upfield displacement of the Ab-H3 resonance for L-histidine suggests that the imidazolium group fits more tightly into the binding pocket formed by ΔUA(2S)-GlcNS(6S)-IdoA(2S), which brings the N-terminal ammonium group of L-histidine closer to sulfate groups on tetrasaccharide III and thus enhances the binding.

Dipeptide HG binds to tetrasaccharide III stronger than L-histidine. Tighter binding of the dipeptide HG to tetrasaccharide III might be due to the presence of the glycine residue, which moves the carboxy terminus away from the position in L-histidine reducing charge repulsion (see Figure 4.58).

Tripeptide GHG binds to tetrasaccharide III stronger than dipeptide HG. The ionic bonding between the glycyl ammonium group and sulfate groups on tetrasaccharide III likely contributes to enhancement of the binding of GHG by tetrasaccharide III.

β-amyloid peptide binds to tetrasaccharide III more tightly than tripeptide GHG. Electrostatic interactions between the guanidinium group of the arginine side-chain and sulfate groups on tetrasaccharide III might contribute to stronger binding of β-amyloid peptide by tetrasaccharide III than GHG. Additionally, the hydrogen bonding between the carboxyl group from the side-chain of aspartic acid and the hydroxyl groups on tetrasaccharide III might contribute to the increase of binding affinity of β-amyloid peptide.

The growth factor GHK has a stronger affinity for tetrasaccharide III than β-amyloid peptide. Stronger binding of tripeptide GHK might result from electrostatic

interaction of the ammonium group of lysine with sulfate groups on tetrasaccharide III than the guanidinium group of the arginine side-chain.

4.8 References

1. Brunden, K. R.; Richter-Cook, N. J.; Chaturvedi, N.; Frederickson, R. C. A. *J. Neurochem.* **1993**, *61*, 2147-2154.

2. Burch, M. K.; Blackburn, M. N.; Morgan, W. T. *Biochemistry* **1987**, *26*, 7477-7482.

3. Talpas, C. J.; Lee, L. J. *Protein Chem.* **1993**, *12*, 303-309.

4. Matsumoto, R.; Sali, A.; Ghildyal, N.; Karplus, M.; Stevens, R. L. *J. Biol. Chem.* **1995**, *270*, 19524-19531.

5. Terry, R. D.; Peck, A.; DeTeresa, R.; Schecter, R.; Horoupian, D. S. *Ann. Neurol.* **1981**, *10*, 184-192.

6. Terry, R.; Katzman, R. in *Neurology of Aging*, **1983**, p.51.

7. De Young, M. B.; Nemeth, E. F.; Scarpa, A. *Arch Biochem. Biophys.* **1987**, *254*, 222-233.

8. Rabenstein, D. L.; Robert, J. M.; Hari, S. *FEBS Lett.* **1995**, *376*, 216-220.

9. Rabenstein, D. L.; Bratt, P.; Peng, J. *Biochemistry* **1998**, *37*, 14121-14127.

10. Chuang, W.-L.; Christ, M. D.; Peng, J.; Rabenstein, D. L. *Biochemistry* **2000**, *39*, 3542-3555.

11. Rabenstein, D. L.; Bratt, P.; Schierling, T. D.; Robert, J. M.; Guo, W. *J. Am Chem Soc*. **1992**, *114*, 3278-3285.

Chapter 5

Determination of Binding Constants for Heparin Complexes with Imidazole, Histamine, L-Histidine, and Histidine-Containing Peptides by Isothermal Titration Calorimetry and Relative Heparin-Binding Affinities by Heparin Affinity Chromatography

5.1 Introduction

In Chapter 4, the results of a study of the binding of imidazole, histamine, L-histidine, and histidine-containing peptides by the heparin-derived tetrasaccharide were presented. In this chapter, results of a study of the binding of the same molecules by intact heparin are reported. Thermodynamic parameters, including the binding constant K_{bd}, were determined by isothermal titration calorimetry. Additionally, the relative binding strengths for the binding interactions of intact heparin with imidazole, histamine, L-histidine, and histidine-containing peptides were also determined by affinity chromatography.

5.2 Binding Studies by Isothermal Titration Calorimetry (ITC)

ITC, a high-sensitivity calorimetric technique capable of providing the full thermodynamic characterization of a binding event[1], was used to measure the thermodynamic parameters for the interaction of heparin with histamine, the growth factor GHK, β-amyloid peptide, and tripeptide GHG. Each experiment was repeated three times to verify reproducibility. The binding stoichiometry (N), association constant (K), binding enthalpy (ΔH), and entropy (ΔS) are reported as the average of triplicate measurements. Setup parameters are the same for every binding interaction studied: the total number of injections (58), cell temperature (25 °C), reference power (5 μcal/sec),

initial delay (60 sec), stirring speed (310), injection volume (5μ), injection duration time (10 sec), delay between injections (240 sec), and filter period (5 sec).

For each experiment, the effect of dilution of the heparin solution in the titration cell containing only the buffer solution was subtracted from the heat absorbed or released from the interaction of heparin with the binding ligand. It should be noted that the first injection shows a smaller heat effect than it should (see Figure 5.1 A, for example), which results from leakage due to having the syringe in the cell for ~ ½ hour before the first injection was made. This time period was needed to equilibrate the ITC in preparation for a titration run. As a result, the first data point was removed before curve-fitting.

5.2.1 Interaction of Histamine with Heparin

20 mM sodium acetate buffer (pH 5.66) was used to prepare solutions of 1.00 mM heparin (pH 5.67) and 0.400 mM histamine (pH 5.63). An average molecular weight of 12 kDa was used to calculate the concentration of the heparin solution. Figure 5.1 A shows the calorimetric trace obtained by injecting 5 μL aliquots of heparin into the sample cell containing histamine solution. The calorimetric trace for heat of heparin dilution (Figure 5.1 B) was obtained by titration of buffer with heparin. The integrated heats in Figure 5.1 D represent the net heat of each injection after subtracting the heat of dilution of heparin into pure acetate buffer (Figure 5.1 C). The downward deflection of the titration peaks (Figure 5.1 A) indicates that binding of histamine to heparin is an exothermic reaction. The small heats measured in the last few injections (Figure 5.1 A) are due to the dilution of heparin into acetate buffer alone. Values for thermodynamic
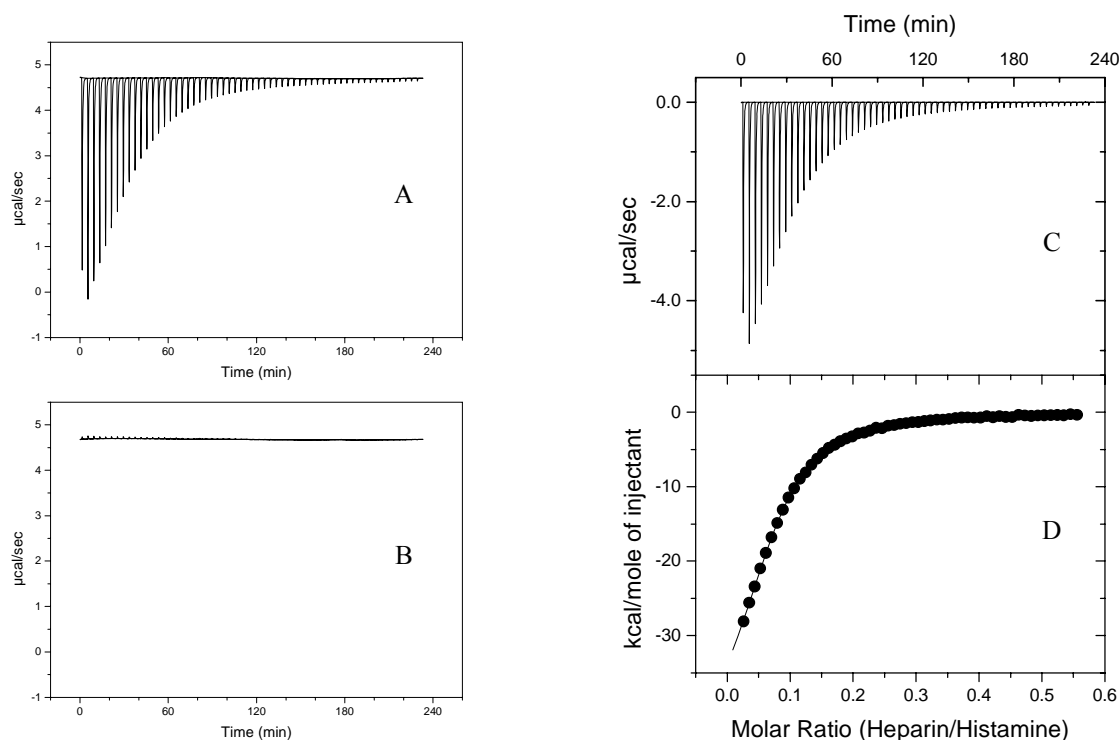
Figure 5.1. ITC determination of thermodynamic parameters for the binding of histamine with heparin. Histamine solution (0.400 mM, pH 5.63) in the sample cell was titrated with heparin (1.00 mM, pH 5.67) in the syringe. (A) Calorimetric data obtained by titration of heparin into histamine solution. Each peak represents the heat released after each injection of 5 μL of heparin. (B) Background heat of heparin dilution obtained by titration of heparin into the sample cell containing only acetate buffer (20 mM, pH 5.66). (C) Corrected calorimetric data for the titration of histamine with heparin. The corrected data was obtained by subtracting peak areas in panel B from those in panel A. (D) Integrated data. Peak areas in panel C were fitted and the total heat (kcal) per mole of heparin added was plotted as a function of molar ratio of heparin to histamine. The line through the points represents the nonlinear least squares fit of the ITC data. Solutions of histamine and heparin were prepared in 20 mM acetate buffer (pH 5.66) without addition of NaCl. The binding parameters obtained are listed in Table 5.1.

parameters obtained are reported in Table 5.1.

By using the Origin 5.0 nonlinear least squares program to fit calorimetric titration data to the binding model described in Chapter 2, a binding constant of 5880 $\pm$ 102 M^{-1} was found, corresponding to a dissociation constant in the micromolar range (170 μM).

5.2.2 Binding of the Growth Factor (GHK) to Heparin

Solutions of 0.411 mM growth factor glycyl-histidyl-lysine (GHK, pH 5.63) and 1.00 mM heparin (pH 5.67) were prepared in 20 mM sodium acetate buffer (pH 5.66). Figures 5.2 A and B show calorimetric traces obtained following the addition of 5 μL aliquots of heparin into the calorimeter cell containing GHK and into the cell containing pure acetate buffer, respectively. Figure 5.2 C and D present the corrected calorimetric trace after the removal of heat of dilution and the corresponding titration curve, respectively. The heparin-GHK interaction is an exothermic reaction, as indicated by the downward direction of the titration peaks (Figure 5.2 A). The small heats measured in the last few injections (Figure 5.2 A) correspond to the heat of dilution of heparin into the buffer. Thermodynamic parameters are summarized in Table 5.1.

The binding isotherm of GHK was obtained by fitting corrected calorimetric data to a single set of identical binding sites model presented in Chapter 2, yielding an average association constant of 4620 $\pm$ 145 M^{-1}.

5.2.3 Binding of β-Amyloid Peptide (FRHDSGY) to Heparin

The β-amyloid peptide is a 40-43 residue peptide derived from the amyloid precursor protein (APP).[2] In this study, only a portion of β-amyloid peptide (4-10) (Phe-

232

Binding Ligands	pH	K_{bd} (M^{-1})	N	ΔH (cal/mol)	ΔS (cal mol^{-1} °C^{-1})
Histamine	5.63	5880 ± 102	13.7 ± 0.1	-3429 ± 9	5.7 ± 0.1
GHK	5.63	4620 ± 145	18.7 ± 0.2	-1909 ± 8	10.4 ± 0.6
β-amyloid Peptide	5.63	1212 ± 60	16.8 ± 0.6	-2832 ± 10	4.6 ± 0.1
β-amyloid Peptide	4.65	2706 ± 133	15.0 ± 0.4	-1958 ± 13	9.2 ± 0.8
Tripeptide GHG	5.63	368 ± 19	15.2 ± 0.6	-1291 ± 5	7.4 ± 0.3

Table 5.1. Thermodynamic values for the interaction of heparin with histamine, the growth factor GHK, β-amyloid peptide, and tripeptide GHG at 25 °C. All data were collected in 20 mM sodium acetate buffer (at the indicated pH) without addition of NaCl (thus, [Na$^+$]$_{total}$ = 20 mM), at 25 °C, and are reported as the average of triplicate determinations.
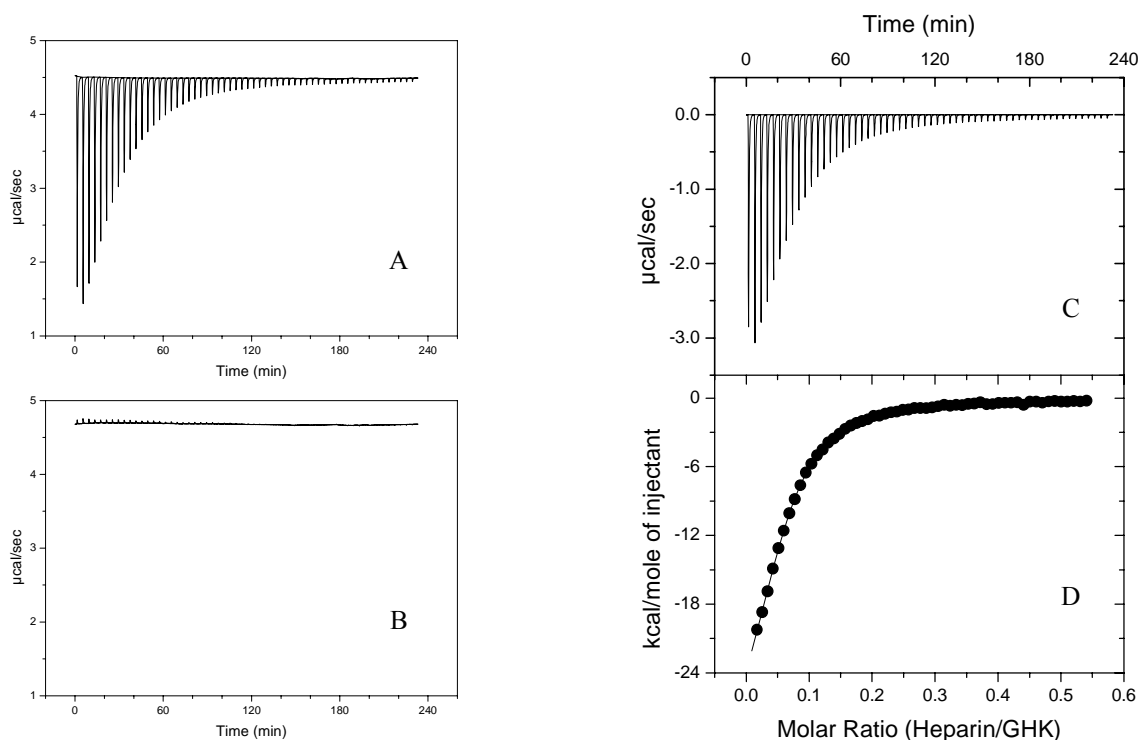
Figure 5.2. ITC determination of thermodynamic parameters for the interaction of the growth factor GHK with heparin. GHK solution (0.411 mM, pH 5.63) in the sample cell was titrated with heparin (1.00 mM, pH 5.67) in the syringe. (A) Calorimetric data obtained by titration of heparin into GHK solution. Each peak represents the heat released after each injection of 5 µL of heparin. (B) Heat of dilution of heparin obtained by titration of heparin into the sample cell containing only acetate buffer (20 mM, pH 5.66). (C) Corrected calorimetric data for the titration of GHK with heparin. The corrected data was obtained by subtracting peak areas in panel B from those in panel A. (D) Integrated data. Peak areas in panel C were fitted and the total heat (kcal) per mole of heparin added was plotted as a function of molar ratio of heparin to GHK. The line through the points represents the nonlinear least squares fit of the ITC data. Solutions of GHK and heparin were prepared in 20 mM acetate buffer (pH 5.66) without addition of NaCl. The thermodynamic parameters are reported in Table 5.1.

Arg-His-Asp-Ser-Gly-Tyr) was examined. From the NMR study of the binding of β-amyloid peptide (FRHDSGY) with a fully sulfated heparin-derived tetrasaccharide reported in Chapter 4, we learned that tetrasaccharide III interacts with the peptide in a pH dependent manner, with the tightest affinity at pH 4.6 where the histidine residue would be protonated Thus, the ITC experiment was performed at pH 4.6. The β-amyloid peptide-heparin binding was also studied at pH 5.6 where most other binding ligands bound tightly to heparin.

5.2.3.1 pH 5.6

A 2.48 mM heparin solution (pH 5.64) and a 0.378 mM peptide solution (pH 5.61) were prepared in 20 mM sodium acetate buffer (pH 5.63). Calorimetric data obtained upon titration of heparin into β-amyloid peptide solution and pure buffer are shown in Figure 5.3 A and B, respectively. Figures 5.3 C and D show the calorimetric data after subtracting heat of heparin dilution and the binding isotherm, respectively. The interaction of β-amyloid peptide with heparin is an exothermic reaction, as indicated by the downward direction of the titration peaks (Figure 5.3 A). The small heats detected at the end of the titration process (Figure 5.3 A) correspond to the heats of heparin dilution. The parameters K, ΔH, and N are listed in Table 5.1.

A binding constant of 1212 ± 102 M^{-1} was determined by fitting the net calorimetric titration data to the binding model described in Chapter 2. The peptide-to-heparin stoichiometry was found to be ~ 17, indicating that one molecule of β-amyloid peptide binds to a disaccharide segment of heparin.
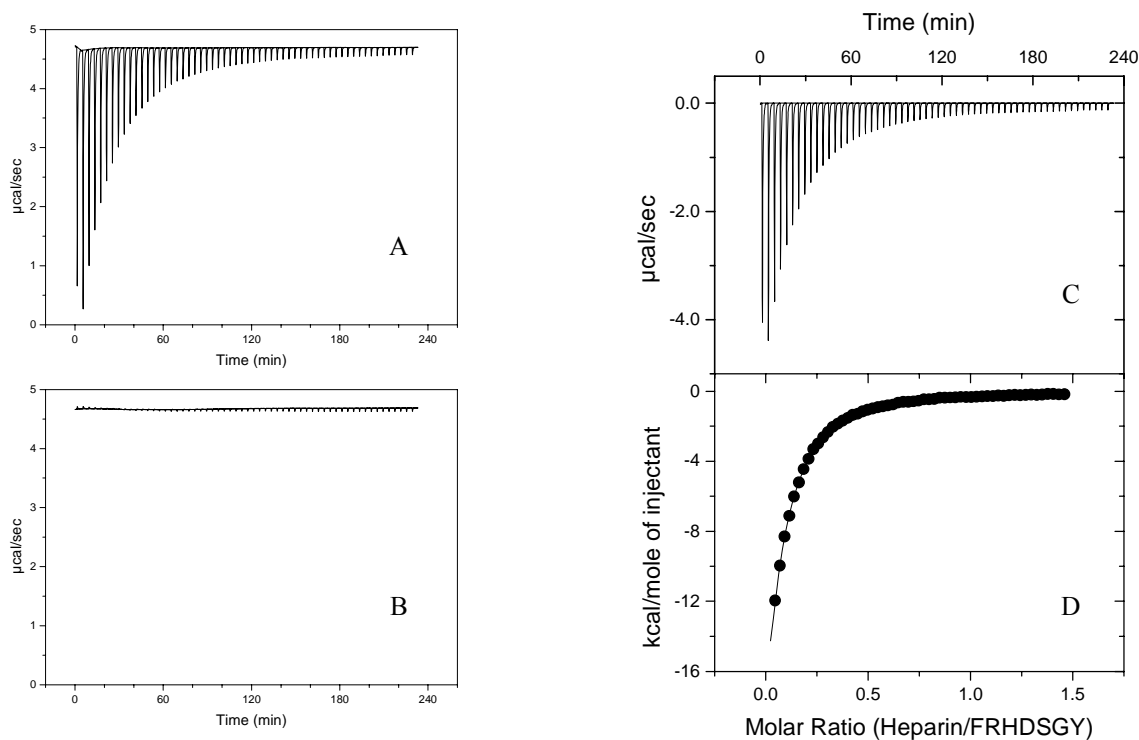
Figure 5.3. ITC determination of thermodynamic parameters for the binding of β-amyloid peptide FRHDSGY with heparin at pH 5.61. The peptide solution (0.378 mM, pH 5.61) in the sample cell was titrated with heparin (2.48 mM, pH 5.64) in the syringe. (A) Calorimetric data obtained by titration of heparin into peptide solution. Each peak represents the heat released after each injection of 5 μL of heparin. (B) Background heat of heparin dilution obtained by titration of heparin into the sample cell containing only acetate buffer (20 mM, pH 5.63). (C) Corrected calorimetric data for the titration of peptide with heparin. The corrected data was obtained by subtracting peak areas in panel B from those in panel A. (D) Integrated data. Peak areas in panel C were fitted and the total heat (kcal) per mole of heparin added was plotted as a function of molar ratio of heparin to peptide. The line through the points represents the nonlinear least squares fit of the ITC data. Solutions of peptide and heparin were prepared in 20 mM acetate buffer (pH 5.63) without addition of NaCl. The binding parameters obtained are presented in Table 5.1.

5.2.3.2 pH 4.6

Solutions of 0.756 mM heparin (pH 4.63) and 0.378 mM β-amyloid peptide (pH 4.60) were prepared in 20 mM sodium acetate buffer (pH 4.65). Figures 5.4 A and B present calorimetric titration of β-amyloid peptide and buffer with heparin, respectively. Figure 5.4 C and D show calorimetric data being corrected for heat of dilution and the binding curve, respectively. A binding constant of 2706 ± 133 M^{-1} was obtained. Other binding parameters are reported in Table 5.1.

5.2.4 Binding of TriPeptide GHG to Heparin

Solutions of 1.00 mM tripeptide GHG (pH 5.62) and 6.00 mM heparin (pH 5.67) were prepared in 20 mM sodium acetate (pH 5.66). The titration curves in Figures 5.5 A and B were obtain by adding 5 μL aliquots of 6.00 mM heparin to 1.00 mM GHG solution and to the titration cell containing only acetate buffer, respectively. Figure 5.5 C shows the calorimetric data for GHG binding to heparin after the background heat of dilution shown in Figure 5.5 B was subtracted from heat released from the interaction of GHG with heparin. Figure 5.5 D shows integrated data. Heparin-GHG binding interaction is an exothermic reaction, as indicated by the downward direction of the titration peaks (Figure 5.5 A). As the tripeptide GHG in the cell became saturated with added heparin, only small heats were detected for the last few injections, corresponding to the background heats of dilution of heparin (Figure 5.5 A). The binding parameters obtained are presented in Table 5.1.

A binding constant of 368 ± 19 M^{-1} was obtained by fitting the titration data to the binding model described in Chapter 2. 15 tripeptide GHG molecules are bound per
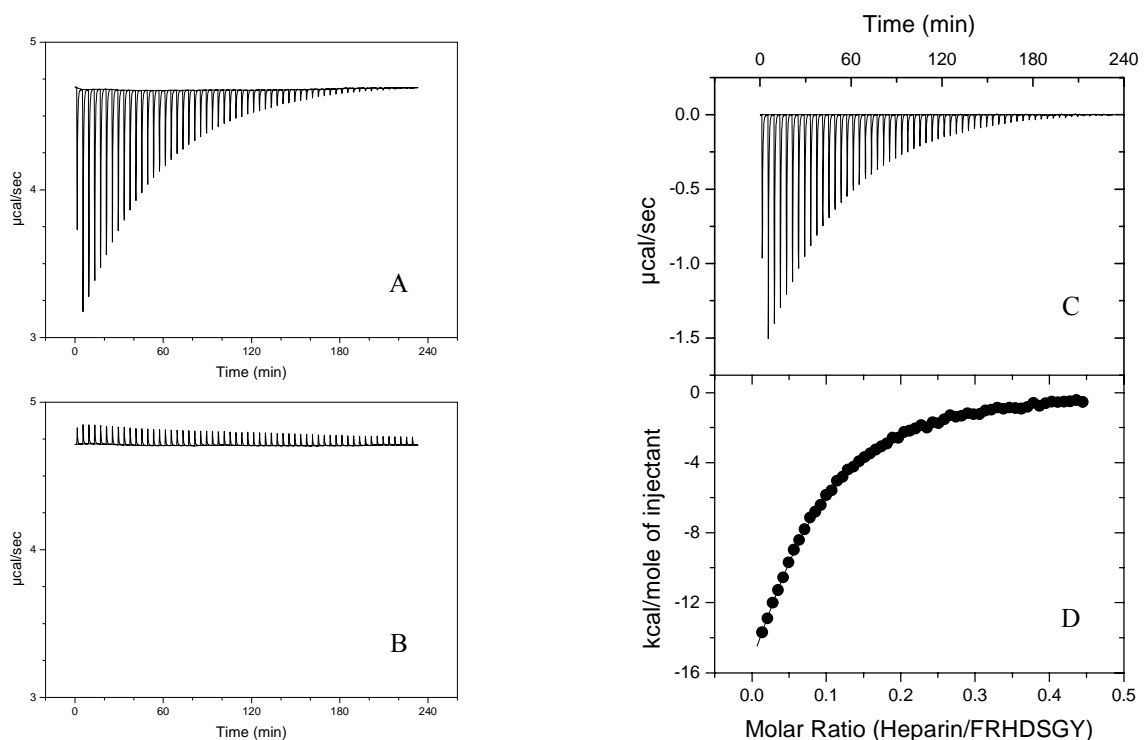
Figure 5.4. ITC determination of thermodynamic parameters for the binding of β-amyloid peptide FRHDSGY with heparin at pH 4.60. The peptide solution (0.378 mM, pH 4.60) in the sample cell was titrated with heparin (0.756 mM, pH 4.63) in the syringe. (A) Calorimetric data obtained by titration of heparin into peptide solution. Each peak represents the heat released after each injection of 5 μL of heparin. (B) Background heat of heparin dilution obtained by titration of heparin into the sample cell containing only acetate buffer (20 mM, pH 4.65). (C) Corrected calorimetric data for the titration of peptide with heparin. The corrected data was obtained by subtracting peak areas in panel B from those in panel A. (D) Integrated data. Peak areas in panel C were fitted and the total heat (kcal) per mole of heparin added was plotted as a function of molar ratio of heparin to peptide. The line through the points represents the nonlinear least squares fit of the ITC data. Solutions of peptide and heparin were prepared in 20 mM acetate buffer (pH 4.65) without addition of NaCl. The thermodynamic parameters are shown in Table 5.1.
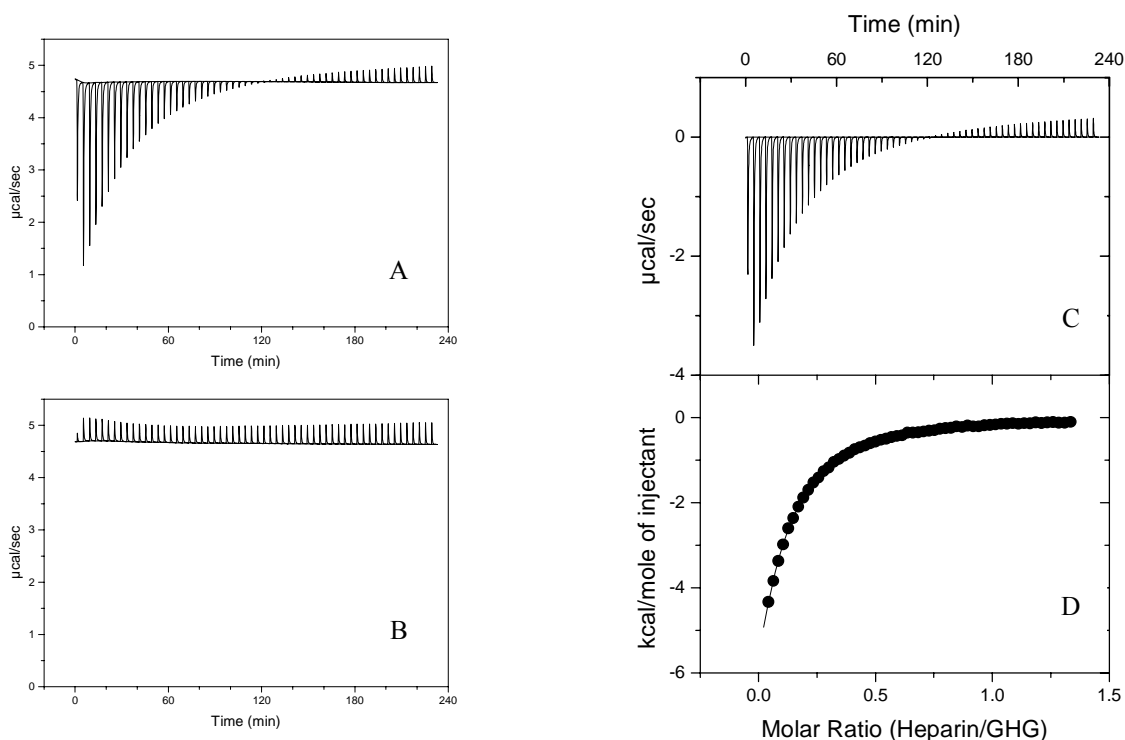
Figure 5.5. ITC determination of thermodynamic parameters for the interaction of tripeptide GHG with heparin. The peptide solution (1.00 mM, pH 5.62) in the sample cell was titrated with heparin (6.00 mM, pH 5.67) in the syringe. (A) Calorimetric data obtained by titration of heparin into peptide solution. Each peak represents the heat released after each injection of 5 μL of heparin. (B) Background heat of heparin dilution obtained by titration of heparin into the sample cell containing only acetate buffer (20 mM, pH 5.66). (C) Corrected calorimetric data for the titration of peptide with heparin. The corrected data was obtained by subtracting peak areas in panel B from those in panel A. (D) Integrated data. Peak areas in panel C were fitted and the total heat (kcal) per mole of heparin added was plotted as a function of molar ratio of heparin to peptide. The line through the points represents the nonlinear least squares fit of the ITC data. Solutions of peptide and heparin were prepared in 20 mM acetate buffer (pH 5.66) without addition of NaCl. The thermodynamic values obtained are reported in Table 5.1.

heparin chain, as indicated by the stoichiometry of N = 15.

5.3 A Study of the Relative Binding Strengths by Heparin Affinity Chromatography

The interactions of heparin with imidazole, histamine, L-histidine, and histidine-containing peptides were further characterized by heparin affinity chromatography.

5.3.1 The Relative Binding Strengths of Imidazole, Histamine, L-Histidine, and Histidine-Containing Peptides in 10 mM pH 5.6 Phosphate Buffer

The relative binding strengths of imidazole, histamine, L-histidine, and histidine-containing peptide, including dipeptides glycyl-histidine (GH) and histidyl-glycine (HG), tripeptides glycyl-histidine-glycine (GHG) and glycyl-histidine-lysine (GHK), and β-amyloid peptide, were studied using heparin affinity chromatography. Separate solutions of imidazole, histamine, L-histidine and histidine-containing peptides were prepared in 10 mM phosphate buffer (pH 5.6) and were injected onto a HiTrap heparin HP column (2.5 x 0.7 cm-i.d., 1 mL column volume). They were eluted using a linear gradient of low-salt and high-salt buffers [10 mM phosphate (pH 5.6), and 10 mM phosphate (pH 5.6) plus 1.0 M NaCl, respectively] at a flow rate of 0.6 mL/min. The separation began with 100% of low-salt buffer and then high-salt buffer was increased at 0.5%/min. Elution was monitored by determining the absorbance at 215 nm.

5.3.1.1 Single Column

A single heparin affinity column was first used to study the binding of each ligand with heparin. Retention time data for each ligand is reported in Table 5.2. The results in Table 5.2 indicate the binding affinity order at pH 5.6: imidazole < L-histidine < HG <

Ligands	Retention time (Min)					
	Single column			Two columns in series		
	pH 4.6	pH 5.3	pH 5.6	pH 4.6	pH 5.3	pH 5.6
Imidazole	n.d.	n.d.	4.89	n.d.	n.d.	9.15
GH	n.d.	n.d.	7.17	n.d.	n.d.	12.77
L-Histidine	n.d.	6.25	5.91	n.d.	12.19	11.55
HG	n.d.	7.85	7.07	n.d.	13.95	13.52
GHG	n.d.	n.d.	8.71	n.d.	n.d.	14.95
β-Amyloid	24.08	n.d.	19.08	32.04	n.d.	27.26
GHK	n.d.	n.d.	24.42	n.d.	n.d.	33.49
Histamine	n.d.	n.d.	27.47	n.d.	n.d.	36.77

n.d., not determined

Table 5.2. Affinity chromatography retention times for imidazole, histamine, L-histidine, and histidine-containing peptides using HiTrap heparin column in 10 mM phosphate buffer (at indicated pH).

GH < GHG < β-amyloid peptide < GHK < histamine. Imidazole, GH, GHG, GHK, and histamine were all found in Chapter 4 to bind to a fully sulfated heparin-derived tetrasaccharide with a maximum binding affinty at pH 5.6. The binding affinity order determined by affinity chromatography agrees with the binding affinity order determined by NMR in Chapter 4. It should be noted that at pH 5.6 the binding of β-amyloid peptide to heparin is still tighter than the GHG-heparin binding interaction, as indicated by its longer retention time. The binding of β-amyloid peptide to heparin at pH 4.6 will be presented in the following section.

It should also be noted that L-histidine and HG were eluted before GH, indicating that they are bound to heparin weaker than GH at pH 5.6. This result was expected since it was learned from the binding studies of L-histidine and HG with tetrasaccharide III that they both interacted most strongly with tetrasaccharide III at pH 5.3. As a result, the binding of L-histidine and HG by heparin were also studied by affinity chromatography at pH 5.3, as will be described in the next section.

5.3.1.2 Two Columns in Series

Two columns in series were used to resolve the close elution between dipeptides GH and HG at pH 5.6. Solutions of imidazole, histamine, L-histidine, and other histidine-containing peptides were also injected onto the two columns connected in series in order to rank the binding affinity order among them with confidence. Retention times for each heparin ligand are presented in Table 5.2. The results in Table 5.2 indicate the following binding affinity order: imidazole < L-histidine < GH < HG < GHG < β-amyloid peptide < GHK < histamine. By doubling the length of the heparin column, dipeptide HG was

found to bind heparin tighter than dipeptide GH at pH 5.6, as evidenced by its longer retention time (see Table 5.2). This is consistent with the result found in Chapter 4.

5.3.2 The Binding Strength of L-Histidine and DiPeptide HG in 10 mM pH 5.3 Phosphate Buffer

5.3.2.1 Single Column

A single column was used to study the binding of L-histidine and dipeptide HG with heparin at pH 5.3 under the same separation conditions at pH 5.6 reported in the previous section since they were both found in Chapter 4 to interact most strongly with tetrasaccharide III at pH 5.3.

Retention times of L-histidine at pH 5.3 and 5.6 are reported in table 5.2. L-histidine was retained longer at pH 5.3 than at pH 5.6, indicating that it binds to heparin tighter at pH 5.3 and that the nature of the binding interaction is pH dependent. This result obtained by affinity chromatography is consistent with the result obtained by NMR reported in Chapter 4 that L-histidine binds strongest to tetrasaccharide III at pH 5.3. However, the binding of L-histidine to heparin is still weaker than dipeptide GH as indicated by its shorter retention time, which contradicts the results determined by NMR for the binding of L-histidine and GH with tetrasaccharide III.

As anticipated, dipeptide HG also had a longer retention time at pH 5.3 than at pH 5.6 (see Table 5.2), indicating that HG-heparin binding is stronger at pH 5.3. The affinity chromatography results also suggest that the binding of HG by heparin is pH dependent. These results agree with the NMR results reported in Chapter 4 that the nature of HG-tetrasaccharide III interaction is pH dependent and that the binding is strongest at pH 5.3.

243

It is important to note that the longer retention time for HG at pH 5.3 compared to that of GH at pH 5.6 indicates that, at pH 5.3, HG binds to heparin more tightly than does GH. This binding affinity order based on affinity chromatography is in agreement with the binding affinity order determined by NMR: GH < HG, for the binding interactions of GH and HG with tetrasaccharide III. The explanation for the tighter binding at pH 5.3 is likely that the Na^+ concentration is less at pH 5.3, as discussed in Section 5.4.

5.3.2.2 Two Columns in Series

The binding affinities of dipeptide HG and L-histidine for heparin at pH 5.3 were measured again with the use of two columns connected in series under the same elution conditions used for a single column to determine if both L-histidine and HG will be retained longer than dipeptide GH. Retention times for HG and L-histidine are presented in Table 5.2. The bigger difference in retention time between GH at pH 5.6 and HG at pH 5.3 with the use of two columns in series further confirms the finding with a single column that HG binds to heparin with tighter affinity than GH.

It should be noted also that with two columns in series and a pH of 5.3, L-histidine still shows weaker binding by heparin than dipeptide GH, which again disagrees with the results found for the relative binding strengths of L-histidine and GH for tetrasaccharide III reported in Chapter 4. One reason for this might be due to over adding NaOH upon pH adjustment to 5.3. Na^+ counterion is known to compete with heparin binding ligands, which likely weakens the binding affinity of L-histidine for heparin, resulting in shorter retention time than expected.

244

5.3.3 The Binding Strength of β-Amyloid Peptide (FRHDSGY) in 10 mM pH 4.6 Phosphate Buffer

The results in Chapter 4 indicate that the tetrasaccharide has the highest affinity for the β-amyloid peptide at pH 4.6. To determine if this is the case for the binding of β-amyloid peptide by heparin, the affinity chromatography experiments were repeated at pH 4.6. The β-amyloid peptide was injected onto the same heparin affinity column under the same chromatography conditions as for the binding studies at pH 5.6. The results in Table 5.2 indicate that β-amyloid peptide binds to heparin tighter at pH 4.6 than at pH 5.6, as indicated by the longer retention time at pH 4.6.

5.4 Discussion

The ITC results indicate that the binding affinity of histamine for heparin is 2.5-fold stronger than the binding affinity of histamine for tetrasaccharide III reported in Chapter 4 (see Table 5.3). The difference in the binding strength might result from the structural difference between heparin and tetrasaccharide III where the residue at the nonreducing end of the A ring of heparin is an iduronic acid, while that of III is an unsaturated uronic acid. Also charge density is higher for heparin than for III, resulting in stronger binding of histamine by heparin. Higher charge density of heparin most likely contributes more Na^+ in the counterion condensation volume (0.59 Na^+/anionic charge on heparin[3]). Upon binding to heparin, more Na^+ counterions are displaced, yielding a larger entropic contribution. In other words, it is expected that the entropic value from the binding of histamine to tetrasaccharide III should be smaller than 5.7 cal mol^{-1} °C^{-1} (see Table 5.1). Although there is no experimental ΔS value for histamine-tetrasaccharide III

Ligands	Binding Constant, M^{-1}	
	Heparin-Derived Tetrasaccharide (by NMR)	Intact Heparin (by ITC)
Tripeptide GHG	257 ± 11	368 ± 19
β-Amyloid peptide	329 ± 30	2706 ± 133
Growth Factor GHK	1855 ± 43	4620 ± 145
Histamine	2396 ± 135	5880 ± 102

Table 5.3. Comparison of the binding constants for heparin and heparin-derived
tetrasaccharide binding by histidine-containing peptides and histamine, determined by
ITC and ^{1}H NMR, respectively.

binding interaction to directly support the argument, the interaction of L-HIPAP and D-HIPAP with heparin in reference 4 demonstrates that heparin has high charge density and thus more Na^+ counterions are displaced, as indicated by a large entropic contribution to binding ($\sim$ 24 cal mol^{-1} $°C^{-1}$). Histamine was reported to interact with heparin via electrostatics.[5] Two ionic bonds were formed for the histamine-heparin binding interaction, as determined from the dependence of the binding constant on Na^+ concentration using counterion condensation theory of polyelectrolytes and confirmed in molecular modeling study.[5]

A study by Kobayaski for the interaction of histamine with heparin using equilibrium dialysis reported a 1:1 (histamine : heparin disaccharide) stoichiometry.[6] In a recent study reported by this group, histamine was found to bind to heparin site specifically with the imidazolium group located in the binding cleft formed by the IAI trisaccharide, the minimum heparin binding sequence required for site specific binding.[7] Structurally, the requirements for a N-sulfate group and an iduronic acid residue at the reducing end of the A ring of the IAI triad are essential for site specific binding. Heparin with a molecular weight of 12 kDa is composed of $\sim$ 18 (12000/665) repeating disaccharide units. In porcine mucosal heparin, the content of glucosamine residue with N-sulfate group is 88%.[8] Thus, there are $\sim$ 16 (18 x 0.88) GlcNS residues present in the heparin polymer, which means 17 possible binding pockets can be formed along the heparin backbone. With $\sim$ 14 histamine molecules bound to one heparin molecule, as indicated by the binding stoichiometry of 13.7, it suggests that the heparin is essentially saturated.

The GHK-heparin binding interaction is 2.5-fold stronger than the GHK-tetrasaccharide III binding interaction presented in Chapter 4 presumably due to the same reasons as for the case of histamine, as discussed (see Table 5.3). The obtained binding stoichiometry (N = 18.7) suggests that each GHK molecule interacts with a disaccharide segment of heparin. The binding constant obtained (4620 M^{-1}) indicates that GHK-heparin binding is strong, but weaker than the binding of histamine by heparin. The glycyl ammonium, histidyl imidazolium, and lysine ammonium groups of GHK provide three potential sites for interactions with the sulfo and carboxylate groups of heparin chain. A study reported by this group using ^{1}H NMR spectroscopy indicated that ammonium groups of GHK hydrogen bonded to heparin carboxylate groups, while the histidyl imidazolium ring binds site specifically to the imidazolium binding site on heparin formed by the IAI trisaccharide.[7]

The ITC result indicates that the binding affinity of β-amyloid peptide to heparin is pH dependent, as indicated by different binding constant values obtained at pH 4.6 and 5.6. Tighter binding at pH 4.6 was expected since the binding of β-amyloid peptide to a fully sulfated heparin-derived tetrasaccharide reported in Chapter 4 was found to be strongest at pH 4.6. Weaker binding for β-amyloid peptide-heparin interaction at pH 5.6 might be due to two reasons. First, more NaOH was added to the buffer to adjust the pH to 5.6 compared to that at pH 4.6, and the added Na^+ competed with β-amyloid peptide in binding to heparin, which therefore weakened β-amyloid peptide-heparin binding. Secondly, the aspartic acid side chain group (pK_a 3.65) is less negative charge at pH 4.6 (89.9% in the deprotonated form) than at pH 5.6 (98.9% in the deprotonated form) and

hence there is less electrostatic repulsion between carboxylate group of aspartic acid and negatively charged groups of heparin. This likely contributes to stronger binding of β-amyloid peptide by heparin at pH 4.6 as well. The tight binding of β-amyloid peptide to heparin occurred at lower pH compared to other binding ligands studied might be a result of the presence of the aspartic acid residue adjacent to the histidine residue, which lowered the pK_A of the imidazolium ring.

The stoichiometry of N = 15 for the β-amyloid-heparin binding interaction indicates that one molecule of β-amyloid peptide binds to a heparin disaccharide or tetrasaccharide repeat unit. It should be noted that pH does not influence the stoichiometry of this reaction, as indicated by the small variation in N. The β-amyloid peptide (4-10) was found to bind heparin 7-fold stronger than GHG. This is likely due to the presence of the arginine residue in the peptide sequence. The positively charged guanidinium group of arginine forms an ion pair with negatively charged sulfo and carboxylate groups of the heparin chain.[8] In addition to ionic bonding, hydrogen bonds (N-H…O) can be formed between the NH protons of the arginyl guanidinium group of the peptide and the oxygens of heparin sulfate and/or carboxylate if the distance is close enough (normally ≤ 2 Å). In addition to ionic and hydrogen bonding contributed from the arginine residue, polar residues (Ser and Tyr) of β-amyloid peptide might involve in heparin binding through forming hydrogen bonds with the hydroxyl or carboxyl groups on heparin.

5.5 Summary

The complexation of histamine, the growth factor GHK, β-amyloid peptide, and

tripeptide GHG by heparin was studied by both microcalorimetry and affinity chromatography. The ITC measurements presented here indicate that the positively charged side-chain of the histidine residue of the histidine-containing peptides studied here is involved in the association of each peptide with heparin. The ITC results fully support the results obtained by heparin affinity chromatography and vice versa. The experimental results obtained from ITC and heparin affinity chromatography described in this chapter in turn support the binding constants obtained by NMR for the site specific interactions of the fully sulfated heparin-derived tetrasaccharide with imidazole, histamine, L-histidine, and histidine-containing peptides presented in Chapter 4. The ionization state of the imidazolium ring in general was found to modulate the binding affinity of ligand to heparin, as indicated by the pH-dependence of the ligand-heparin binding interactions. The information reported here contributes to a greater understanding for the interactions of histidine-containing peptides with heparin.

5.6 References

1. Wiseman, T.; Williston, S; Brandts, J. F.; Lin, L. N. *Anal. Biochem.* **1989**, *179*, 131-137.

2. Glenner, G. G.; Wong, C. W. *Biochem. Biophys. Res. Commun.* **1984**, *120*, 885-890.

3. Rabenstein, D. L.; Robert, J. M. ; Peng, J. *Carbohydr. Res*. **1995**, *278*, 239-256.

4. Wang, J.; Rabenstein, D. L. *Biochemistry* **2006**, *45*, 15740-15747.

5. Rabenstein, D. L.; Bratt, P.; Peng, J. *Biochemistry* **1998**, *37*, 14121-14127.

6. Kobayaski, Y. *Arch Biochem. Biophys*. **1962**, *96*, 20-27.

7. Chuang, W.-L.; Christ, M. D.; Peng, J.; Rabenstein, D. L. *Biochemistry*, **2000**, *39*, 3542-3555.

8. Rabenstein, D. L. *Nat. Prod. Rep*. **2002**, *19*, 312-331.

Part II

Cis/Tran Isomerization of Amide Bonds in Peptides and Peptide/Peptoid Hybrids

Chapter 1

The kinetics and Equilibria of Cis/Trans Isomerization of Amide Bonds in Peptides and Peptide/Peptoid Hybrids

1.1 Introduction

Amino acids in peptides and proteins are linked together by amide (peptide) bonds (Figure 1.1). The C-N bond has a partial double bond character because the nitrogen lone pair of electrons is conjugated with the carbonyl group. The six atoms of the peptide bond are planar, as required for the nitrogen lone pair to interact with the carbonyl π-bond in order for the conjugation to take place. The planar framework of the amide group can exist in two conformations: the cis conformation, where the two α-C atoms are on the same side of the C-N bond, and the trans conformation, where they are on the opposite side of the C-N bond (see Figure 1.2).

For nineteen of the twenty naturally occurring amino acids, the exception being proline, the trans conformation across the peptide bond is highly populated, as indicated by conformational energy calculations.[1-3] Formation of the unfavorable cis conformation requires higher energy than the trans conformation, as a result of steric strain between the substituents attached to the α-C atoms. Figure 1.2.A shows cis/trans isomerization of a secondary amide peptide bond. To minimize steric interactions, the trans conformation is favored. For example, the cis conformation appears to be approximately 0.5% per peptide bond in dipeptides and 0.15% in longer oligopeptides and unfolded proline-free proteins.[4] Although peptide bonds in most native proteins exist almost exclusively in the trans conformation, Weiss and coworker reported that nonprolyl cis peptide bonds were found
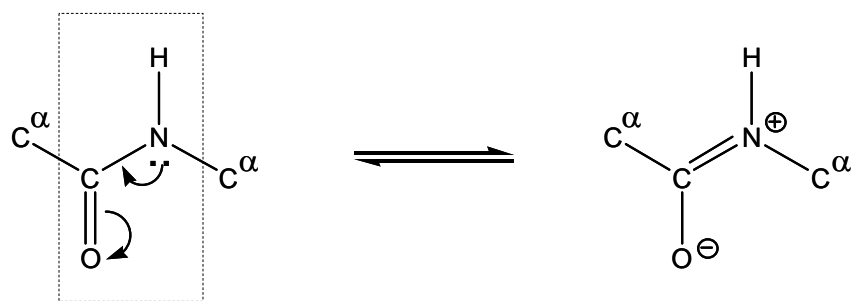
Figure 1.1. Resonance stablilization of the amide group. The amide (peptide) bond is shown in the box.
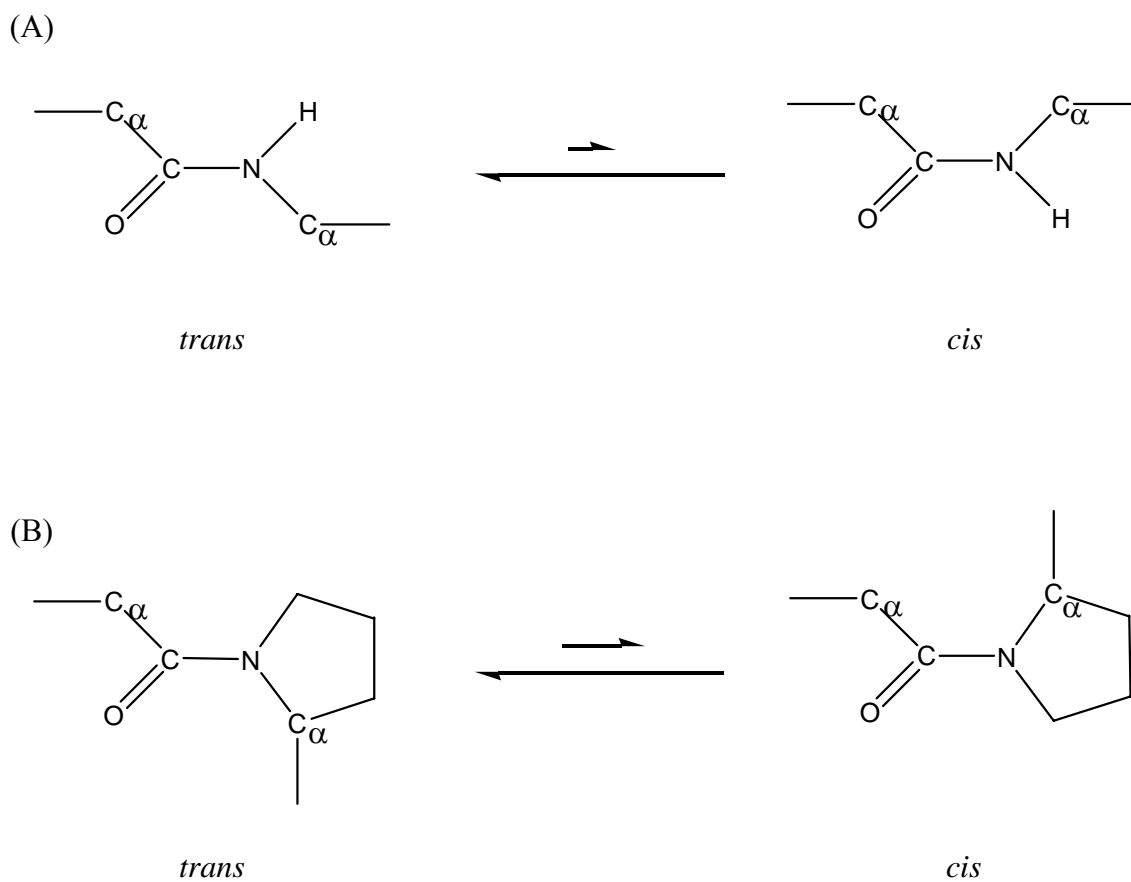
Figure 1.2. (A) Cis/trans isomerization of a secondary amide peptide bond. (B) Cis/trans isomerization of a peptidyl-prolyl peptide bond.

in the native structure of several proteins (e.g. ribonuclease T_1).[5] According to Odefey *et al.*, nonprolyl cis peptide bonds can give rise to very slow refolding reactions.[6] The function of cis peptide bonds in native proteins is not clear.[7]

In native proline-containing proteins, approximately 6% of Xaa-Pro peptide bonds, where Xaa represents one of the non-proline amino acids, are in the cis conformation[8], which is 40 times larger than that of nonprolyl peptide bonds as a result of more steric hindrance in the trans conformation, as compared to the secondary amide (peptide) bond. Figure 1.2.B shows cis/trans isomerization about a peptidyl-prolyl bond. The cis population of Xaa-Pro peptide bond was found to depend on the amino acid residue preceding the proline residue; the highest content of cis isomer follows aromatic residues.[9]

Protein folding has been an area of interest for many researchers. A major focus of protein folding studies is to characterize the rate limiting events for formation of the protein native structure. In the native state of folded proteins, the peptide bonds that link adjacent amino acid residues are almost exclusively in the trans conformation. However, in unfolded proteins and peptides, the proteins and peptides exist as a mixture of cis and trans isomers across the peptide bond. The rate limiting step in protein folding can be the rate at which the cis conformers of peptide bonds interconvert to the trans conformers.

Heterogeneities in unfolded proteins caused by a slow cis→trans equilibration reaction have been shown to complicate analysis of the folding mechanism. Cis/trans isomerization of peptidyl-prolyl peptide bonds is the common heterogeneity.[10, 11] Another source of heterogeneities in denatured proteins is cis/trans isomerization of secondary

amide (or "normal") peptide bonds.[10] Thus, study of the rates of cis-to-trans and trans-to-cis isomerization of peptide bonds is essential to understand the kinetics behind protein folding.

Cis→trans isomerization of peptidyl-prolyl peptide bonds is the rate limiting step for the refolding of denatured proline-containing proteins.[12] For an unfolded nonproline-containing protein, cis→trans isomerization of secondary amide peptide bonds was proposed to be the rate limiting step in the refolding of proline-free proteins.[13] Although the cis population per normal peptide bond for an unfolded protein is only ~ 0.15%[4], the overall cis content from a large number of normal peptide bonds in the protein is big enough to significantly slow down the folding process.

1.1.1 Cis/Trans Isomerization of Secondary Amide Peptide Bonds in Peptides

An ^{1}H NMR study of the cis/trans isomerization of secondary amide peptide bonds by Scherer and coworkers found that the cis isomer population of peptide bonds adjacent to the aromatic amino acids (i.e. Tyr and Phe) was in the range 0.15-0.50%.[4] The cis content was reported to decrease upon extending the peptide chain in both directions of the dipeptide Ala-Tyr. The rate constant $k_{trans \to cis}$ of dipeptide Ala-Tyr, for example, was determined to be 2.4 x 10^{-3} s^{-1} at 298 K, which is similar to that of the trans → cis isomerization in Ala-Pro (1 x 10^{-3} s^{-1}).[14] Nevertheless, the rate constant determined for $k_{cis \to trans}$ of 0.6 s^{-1} for Ala-Tyr is much faster than $k_{cis \to trans}$ of 0.085 s^{-1} for prolyl peptide bonds in tendamistat[15].

Another study of cis/trans isomerization rates of secondary amide peptide bonds using a direct UV/vis spectrophotometric method was reported by Schiene *et al*. In this

study, the cis/trans isomerization rates of several dipeptides including Gly-Gly were examined. A rate constant $k_{cis \rightarrow trans}$ of 0.3 s^{-1} obtained for Gly-Gly, for instance, proves the idea that the rate of cis→trans isomerization of secondary amide peptide bonds can result in slow rate limiting steps in the refolding of many denatured proteins.

Cis/trans equilibrium of the Tyr^{38}-Ala^{39} peptide bond in ribonuclease T$_1$ variant (RNase T$_1$), where prolyl at position 39 of RNase T$_1$ was replaced with an alanine residue to possibly generate a nonprolyl cis peptide bond, was studied by Mayr *et al.* using ^{1}H NMR.[15] The Tyr^{38}-Ala^{39} peptide bond of RNase T$_1$ variant was determined to have a cis content of 0.17%, consistent with the average cis content reported by Scherer. A rate constant $k_{trans \rightarrow cis}$ of 1.4 s^{-1} was obtained. It should be noted that for RNase T$_1$variant in the native state, the Tyr^{38}-Ala^{39} bond exists in the cis form. Thus, it was proposed that the trans → cis isomerization of the Tyr^{38}-Ala^{39} peptide bond was the slow step in the refolding of RNase T$_1$ variant.

Nonprolyl peptide bond isomerization in proline-free tendamistat reported by Pappenberger *et al* was also examined by ^{1}H NMR.[13] Tendamistat, an inhibitor of α-amylase, is a small protein of 74 amino acids containing three prolyl residues, which are in the trans conformation in the native state.[16] To simplify the folding mechanism of tendamistat, prolyl residues at positions 7, 9, and 50 of tendamistat were replaced with alanines and hence prolyl isomerization with a slow rate constant $k_{cis \rightarrow trans}$ of 0.085 s^{-1} was eliminated. Alanine was chosen to replace proline since Ala and Gly have been found to form cis secondary amide peptide bonds in some native proteins (i.e. RNase T$_1$).[15, 17] Although all prolyl residues were mutated with alanines, the refolding of 5.0%

(as indicated by the amplitude of the tryptophan fluorescence change) of the unfolded

molecules occurs slowly with a rate constant $k_{cis \rightarrow trans}$ of 2.5 s^{-1}. It should be noted that a

fast reaction occurs with a rate of constant of ~ 10 s^{-1}.[13] Pappenberger proposed that the

observed 5% is presumably as a result of either an average cis content of ~ 0.07%

(instead of 0.15% as reported by Scherer) per peptide bond for all 73 peptide bonds of

tendamistat or that only approximately half of the cis peptide bonds prevent the refolding.

In short, Pappenberger argues for cis $\rightarrow$ trans isomerization of nonprolyl peptide bonds as

the rate limiting step in the refolding of 5.0% of the unfolded molecule.

In research reported in Part II of this dissertation, the distribution and kinetics of

interchange between the cis and trans conformations of secondary amide peptide bonds of

several peptides in their reduced linear dithiol and oxidized cyclic disulfide forms were

investigated by ^{1}H NMR.

1.1.2 Cis/Trans Isomerization of Tertiary Amide Peptide Bonds in Peptide/Peptoid Hybrids

Despite many important bioactivities of peptides, they are normally poor drugs,

are quickly broken down by proteases in vivo, and have low oral bioavailability.[18] Thus,

peptidomimetics are of interest as potential drug candidates. Peptoids (N-substituted

glycine oligomers, Figure 1.3) are resistant to degradation by proteases and were

demonstrated to have interesting biological activities.[19] In addition, peptoids were among

the first sequence specific oligomers called foldamers[20] that can mimic protein structure

and function. Recently, helical peptoids were successfully designed to mimic the

functionalities of antimicrobial peptide and lung surfactant proteins in vitro.[18] The fate of

no chirality

No H-bond donor

Protease stability
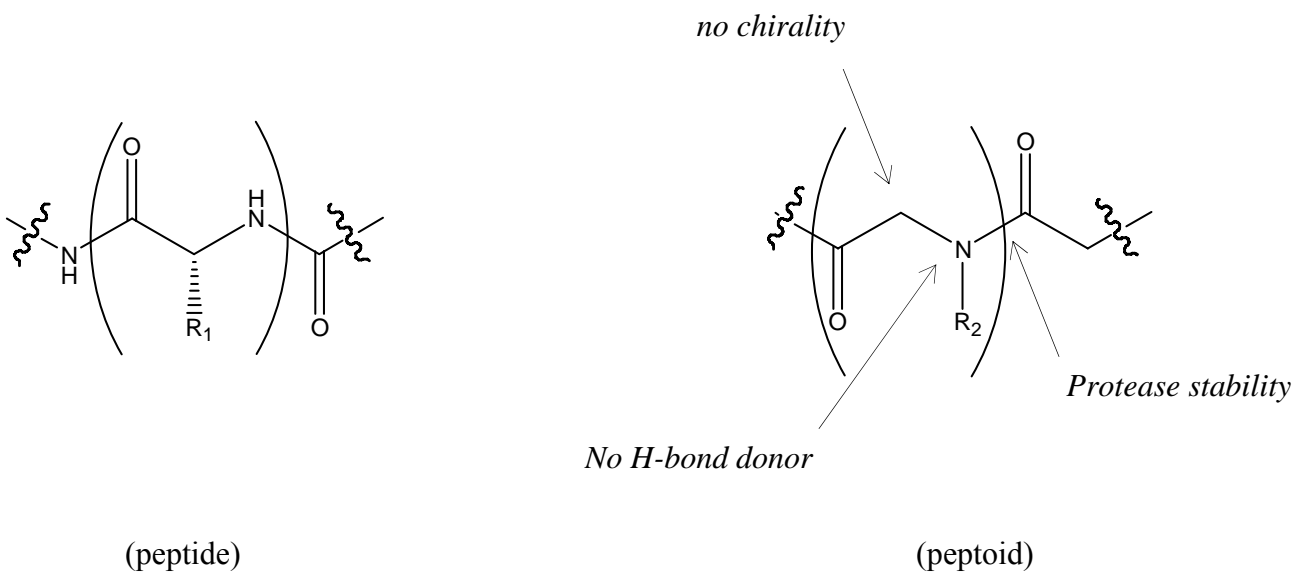
(peptide)

(peptoid)

Figure 1.3. Building blocks (in parenthesis) of peptides and peptoids. Major differences

for peptoids are illustrated.

these peptoids in biological systems has been under active investigation. Currently, no peptoid-based therapeutics are available.

Peptoids are structurally similar to peptides. Major differences between structures of peptoids and peptides are shown in Figure 1.3. As seen, unlike the basic amino acid building block of peptides, where the side chain group is attached to the α-C atom of the amino acid, the side chain of the basic peptoid building block (N-substituted glycine) is shifted to the backbone nitrogen atom. Another difference between peptoids and peptides is that monomers of peptoids are linked via tertiary amide bonds, whereas the amino acids in peptides are linked through secondary amide bonds with the exception of proline. Furthermore, the peptoid monomer unit does not have a hydrogen attached to its amide nitrogen, and thus can not establish hydrogen bonding networks to stabilize secondary structures (i.e. α-helix, β-pleated sheet) as in peptides. Compared with the large data bank of information about protein structures, detailed structural information for peptoids is limited but growing.

In a family of related oligomers, peptide/peptoid hybrids, the replacement of individual peptide residues of a bioactive peptide sequence by peptoid monomers in order to maintain its activity but also to enhance specificity has been reported with success. However, attempts to fully transform bioactive peptides into peptoid-based oligomers have so far been only successful for peptoids with short chain lengths.[21]

In research reported here, we replaced one amino acid residue of several peptide sequences with N-methyl glycine (sarcosine, Sar) as model peptide/peptoid hybrids to study the equilibrium distribution and the kinetics of interconversion between the cis and

trans isomers of a peptoid-like tertiary amide bond.

1.2 Research Described in this Thesis

Part II of this thesis presents the results obtained from studies of cis/trans isomerization of secondary amide bonds in peptides and the tertiary bonds in peptide/peptoid hybrids.

Chapter 2 describes the experimental methods used, including synthesis, purification, and characterization of the peptides and peptide/peptoid hybrids that were studied.

Chapter 3 reports the results of a study of the rate and equilibrium constants for cis/trans isomerization across cysteine-sarcosine peptide bonds in two series of peptides: Ac-Cys-Sar-His-Xaa-(Ala)$_3$-Cys-NH$_2$, where Xaa is histidine (His), glycine (Gly), lysine (Lys), phenylalanine (Phe), aspartic acid (Asp), and glutamic acid (Glu), and Ac-Cys-Sar-(Ala)$_x$-His-(Ala)$_y$-Cys-NH$_2$, x = 0-4 and y = 4-0. The results of a study of the kinetics and equilibria of cis/trans isomerization across the Xaa-Sar peptide bonds in a series of peptides in which the Sar residue is moved along the peptide sequence Ac-Cys-Sar-His-(Ala)$_3$-Cys-NH$_2$, Ac-Cys-His-Sar-(Ala)$_3$-Cys-NH$_2$, etc, are also presented in this chapter. Peptides in the three series were studied in their reduced linear dithiol and oxidized cyclic disulfide forms.

Chapter 4 reports the results of a study of the kinetics and equilibria of cis/trans isomerization across the Ala-Tyr, Tyr-Ala, Ala-Phe, and Phe-Ala peptide bonds in two series of peptides: Ac-Cys-Xaa-Ala-Cys-His-NH$_2$ and Ac-Cys-Ala-Xaa-Cys-His-NH$_2$,

where Xaa represents either Tyr or Phe. Peptides in both the linear dithio and cyclic disulfide forms were studied.

1.3 References

1. Radzicka, A.; Pedersen, L.; Wolfenden, R. *Biochemistry*, **1998**, *27*, 4538.

2. Fisher, G. *Chem. Soc. Rev*. **2000**, 119-127.

3. Zimmerman, S. S.; Scheraga, H. A. *Macromolecules*, **1976**, *9*, 408-416.

4. Scherer, G.; Kramer, M. L.; Schutkowski, M.; Reimer, U.; Fischer, G. *J. Am. Chem. Soc.* **1998**, *120*, 5568-5574.

5. Weiss, M. S.; Jabs, A.; Hilgenfeld, R. *Nature Struct. Biol*. **1998**, *5*, 676.

6. Odefey, C.; Mayr, L.; Schmid, F. X. *J. Mol. Biol*. **1995**, *245*, 69-78.

7. Herzberg, O.; Moult. J. *Proteins: Struct. Funct. Genet*. **1991**, *11*, 223-229.

8. MacArthur, M. W.; Thornton, J. M. *J. Mol. Biol*. **1991**, *218*, 397-412.

9. Reimer, U. *J. Mol. Bio.* **1998**, *279*, 449-460.

10. Brandts, J. F.; Halvorson, H. R.; Brennan, M. *Biochemistry* **1975**, *14*, 4953-4963.

11. Schmid, F. X.; Baldwin, R. L.; *Proc. Natl. Acad. Sci. USA* **1978**, *75*, 4764-4768.

12. Fischer, G.; Schmid, F. X.; *Biochemistry* **1990**, *29*, 2205-2212.

13. Pappenberger, Gunter; Aygun, H.; Engels, J. W.; Reimer, U.; Fischer, G.; Kiefhaber, T. *Nature Struct. Biol*. **2001**, *8*, 452-458.

14. Perrin, C. L.; Thoburn, J. D.; Kresge, A. J. *J. Am. Chem. Soc*. **1992**, *114*, 8800-8807.

15. Mayr, L. M.; Willbold, D.; Rosch, P.; Schmid, F. X. *J. Mol. Biol*. **1994**, *240*, 288-293.

16. Pfugrath, J.; Wiegand, I.; Huber, R.; Vertesy, L. *J. Mol. Biol*. **1986**, *189*, 383-386.

17. Jabs, A; Weiss, M. S.; Hilgenfeld, R. *J. Mol. Biol*. **1998**, *286*, 291-304.

18. Patch, J. A.; Kirshenbaum, K.; Seurynck, S. L.; Zuckermann, R. N.; In Pseudo-peptides in Drug Discovery; Nielson, P. Ed.; Wiley-VCH Verlag GmbH & Co.: Weinheim, 2004; pp 1-27.

19. Patch, J. A.; Barron, A. E.; *Curr. Opin. Chem. Biol*. **2002**, *6*, 871-877.

20. Gellman, S. H. *Acc. Chem. Res*. **1998**, *31*, 173-180.

21. Thompson, D. A.; Chai, B. X. ; Rood, H. L. E.; Siani, M. A.; Douglas, N. R.; Grantz, I.; Millhauser, G. L. *Bioorg. Med. Chem. Lett*. **2003**, *13*, 1409-1413.

Chapter 2

Experimental Methods and Materials

2.1 Chemicals

Trifluoroacetic acid (TFA) and 9-Fluorenylmethoxycarbonyl (Fmoc)-protected amino acids were purchased from Chem-Impex International Inc. N, N'-dicyclohexylcarbodiimide (DCC), 2-(1H-benzotriazol-1-yl)-1,1,3,3-tetramethyluronium hexafluorophosphate (HBTU), and N-methyl-2-pyrrolidone (NMP) were purchased from Applied Biosystems. Triisopropylsilane (TIPS), α-Cyano-4-hydroxy-cinnamic acid (CHCA), piperidine (PIP), sodium 3-(trimethylsilyl)-propionate-2,2,3,3-d4 (TMSP), and N, N'-diisopropylcarbodiimide (DIPCDI) were purchased from Sigma-Aldrich. N, N'-dimethylformide (DMF), phenol, methanol, acetonitrile, acetic anhydride, and methyl t-butyl ether (MTBE) were obtained from Fisher Scientific. DTT (1,4-dithiol-DL-threitol) was obtained from Fluka. NaOD (40%), DCl (35%), D_2O, and deuterated (98%) dithiothreitol were purchased from Cambridge Isotope Laboratories. Rink amide 4-methylbenzhydrylamine (MBHA) resin was purchased from NovaBiochem.

2.2 Peptide Synthesis

2.2.1 Instrumentation

All peptides studied in Part II of this dissertation were synthesized on an Applied Biosystems ABI-433A peptide synthesizer. The ABI-433A peptide synthesizer uses a batch mode with vortex mixing, which is more effective compared to the continuous mode.[1] The peptide synthesizer has online conductivity monitoring and feedback control, which extends the length of the deprotection and subsequent coupling time when the

deprotection reaction rate is slow. Specifically, the instrument monitors the conductivity due to the piperidine-carbamate salt produced by the removal of the Fmoc protecting group (see Figure 2.1). Alternatively, the progress of the deprotection reaction can be followed by monitoring the UV absorbance of the released Fmoc group at 301 nm in the form of fulvene-piperidine adduct (see Figure 2.1). In synthesizing the peptides reported here, the instrument was set to monitor conductivity of the piperidine-carbamate salt.

2.2.2 Solid-Phase Peptide Synthesis Overview

Solid-phase peptide synthesis (SPPS) has been the most efficient method for synthesizing peptides since its introduction in 1963 by Bruce Merrifield.[2] In SPPS, the growing peptide chain is covalently bound to an insoluble support, whereas liquid-phase reagents and by-products of synthesis are flushed away. The peptide remains covalently attached to the bead until cleaved during the cleavage step, as will be discussed latter.

Fmoc (9-Fluorenylmethoxycarbonyl) and t-Boc (tert-butoxycarbonyl) are the two major forms of SPPS of peptides. T-Boc amino acid derivatives had been used dominantly for the SPPS[3-6] until Fmoc chemistry was introduced to overcome problems with t-Boc chemistry. One problem of t-Boc chemistry is that repetitive TFA treatment to remove t-Boc from a growing peptide chain might catalyze side reactions and cleave the peptide chain prematurely. Another problem is that the use of hydrofluoric acid to remove side-chain protecting groups and the peptide from the resin at the end of the synthesis can be dangerous. In Fmoc synthesis, the growing peptide is subjected to mild base treatment using piperidine to remove the Fmoc group, and TFA is required only for the final deprotection and cleavage from the resin. The base-labile Fmoc group is used to
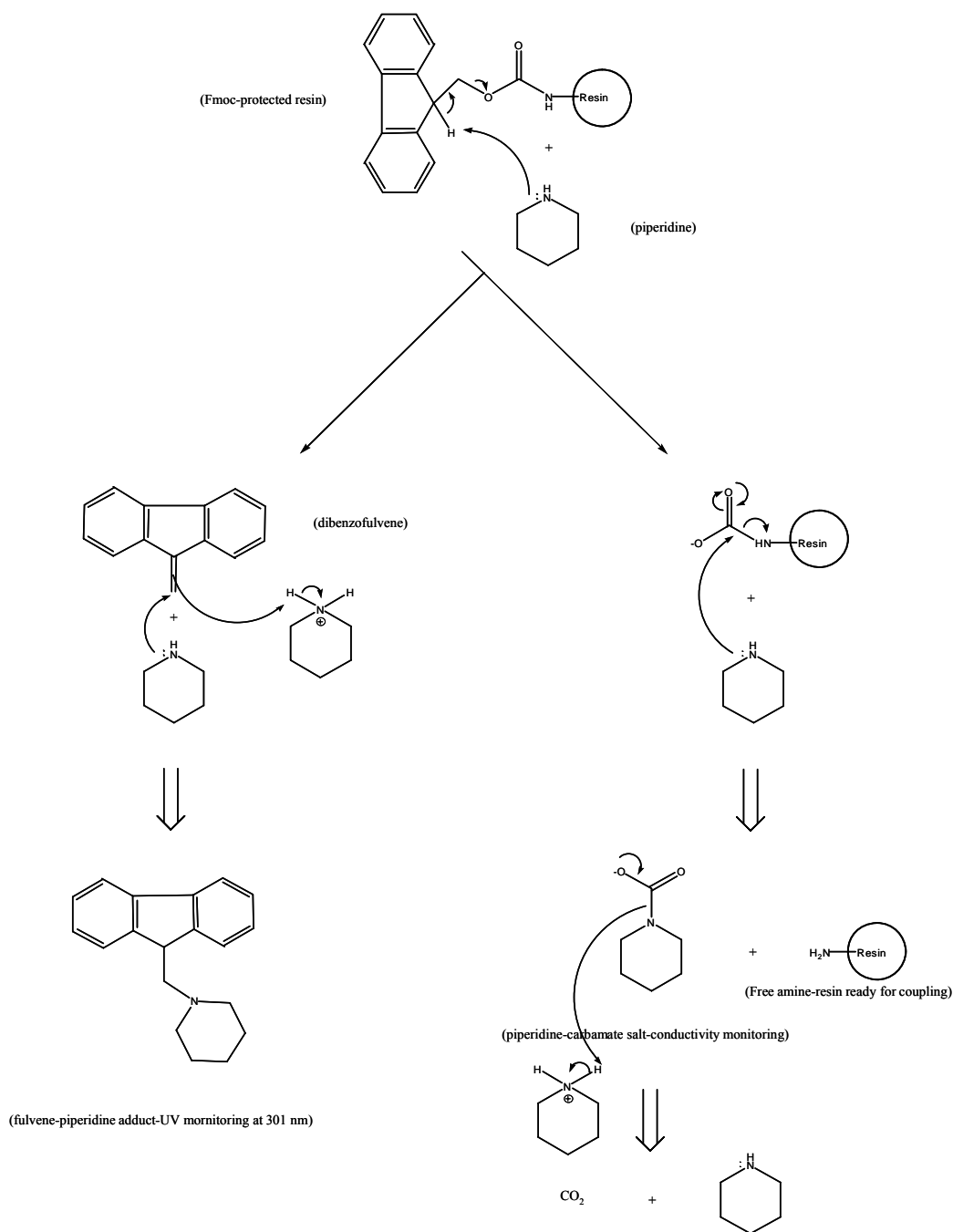
Figure 2.1. Deprotection of the Fmoc protecting group on resin support. The removal of the Fmoc group from the amino acid residue after it has coupled to the resin support and the final deprotection after the last cycle as shown in Scheme 2.1 were carried out in the same way. The instrument was set to monitor conductivity of the piperidine-carbamate salt.

protect the α-amino groups of resin and amino acid residues. Comparison experiments between the Fmoc and t-Boc approaches indicate that Fmoc chemistry is more reliable and tends to give the desired peptides in better purities.[7]

In SPPS, the reactive side-chain groups of many amino acids need to be protected during peptide synthesis to avoid unwanted side reactions. For example, protection of the thiol group of cysteine is imperative to avoid uncontrolled formation of disulphide bridges. The carboxyl groups in the side chains of aspartic and glutamic acids, as another example, must be protected in order to achieve unambiguous activation. To avoid formation of branched peptides resulting from coupling of the ε-amino group of the lysine side-chain to the activated amino acid, for example, the ε-amino group, is protected. The choice of side-chain protecting groups depends on the type of functional groups on the amino acid side chains. For instance, the thiol group of cysteine was protected using triphenylmethyl (Trt) protecting group (Figure 2.2.A); the side-chain carboxyl groups of aspartic and glutamic acids were protected with the tert-butyl (tBu) protecting group (Figure 2.2.B); and the side chain amino group of lysine was protected with t-butoxycarbonyl (t-Boc) (Figure 2.2.C) in the synthesis of peptides studied in Chapter 3-4. The side-chain protecting groups remain intact until cleaved as will be discussed latter in the peptide cleavage section.

2.2.3 Fmoc Solid-Phase Peptide Synthesis

Fmoc chemistry was utilized to synthesize peptides for cis/trans isomerization studies reported in this dissertation. The step-by-step formation of a peptide in SPPS using Fmoc methodology is shown in Scheme 2.1. First, the Fmoc protecting group on

(A)

Fmoc-cysteine with Trt side-chain protection

(B)

Fmoc-aspartic acid with t-butylester protection

(C)

Fmoc-lysine with t-Boc protection
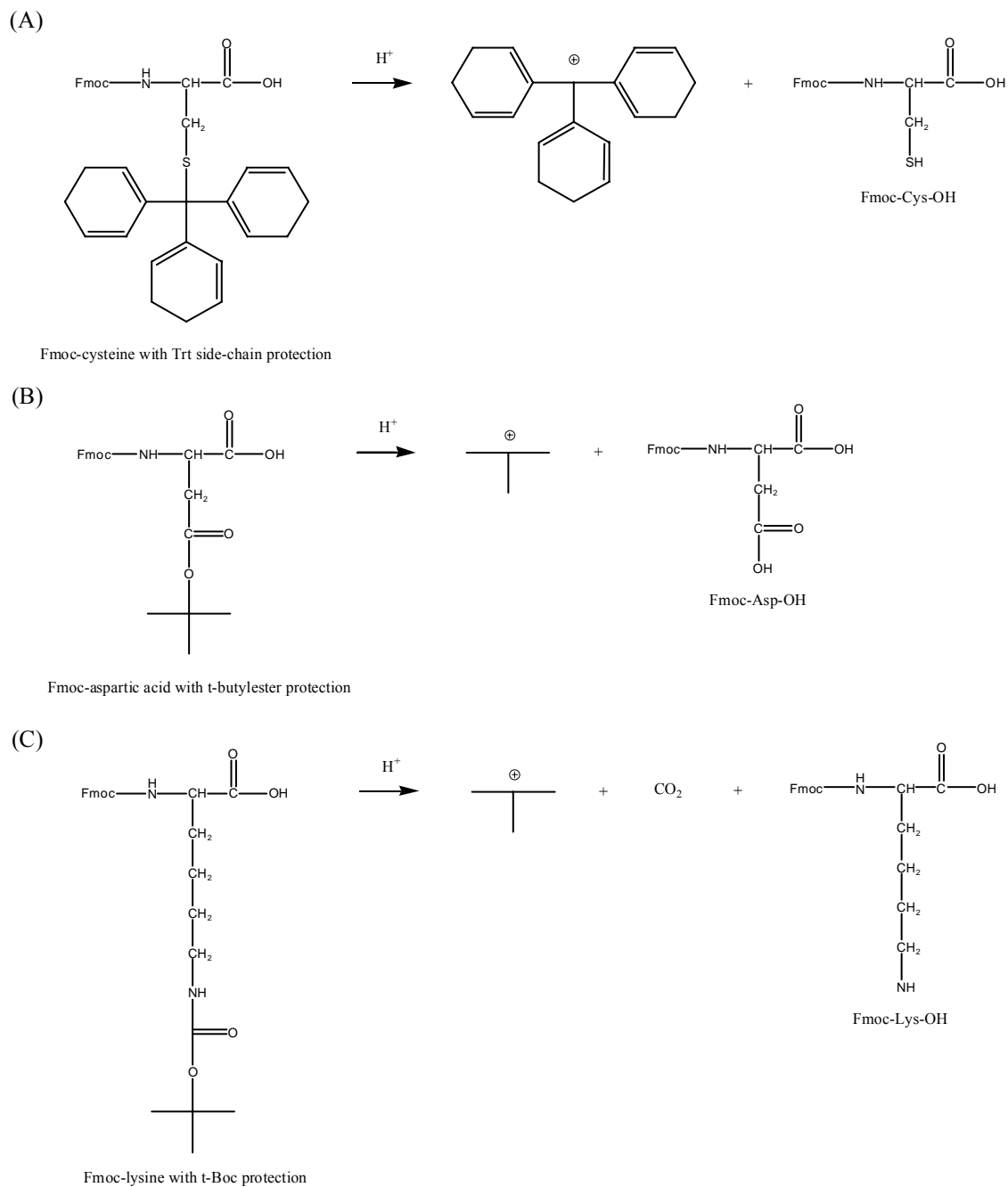
Figure 2.2. Side-chain protected Fmoc-amino acids. The Trt group is cleaved, yielding a tertiary carbocation. TFA cleavage of the t-Bu and t-Boc groups both yield a t-Butyl cation.
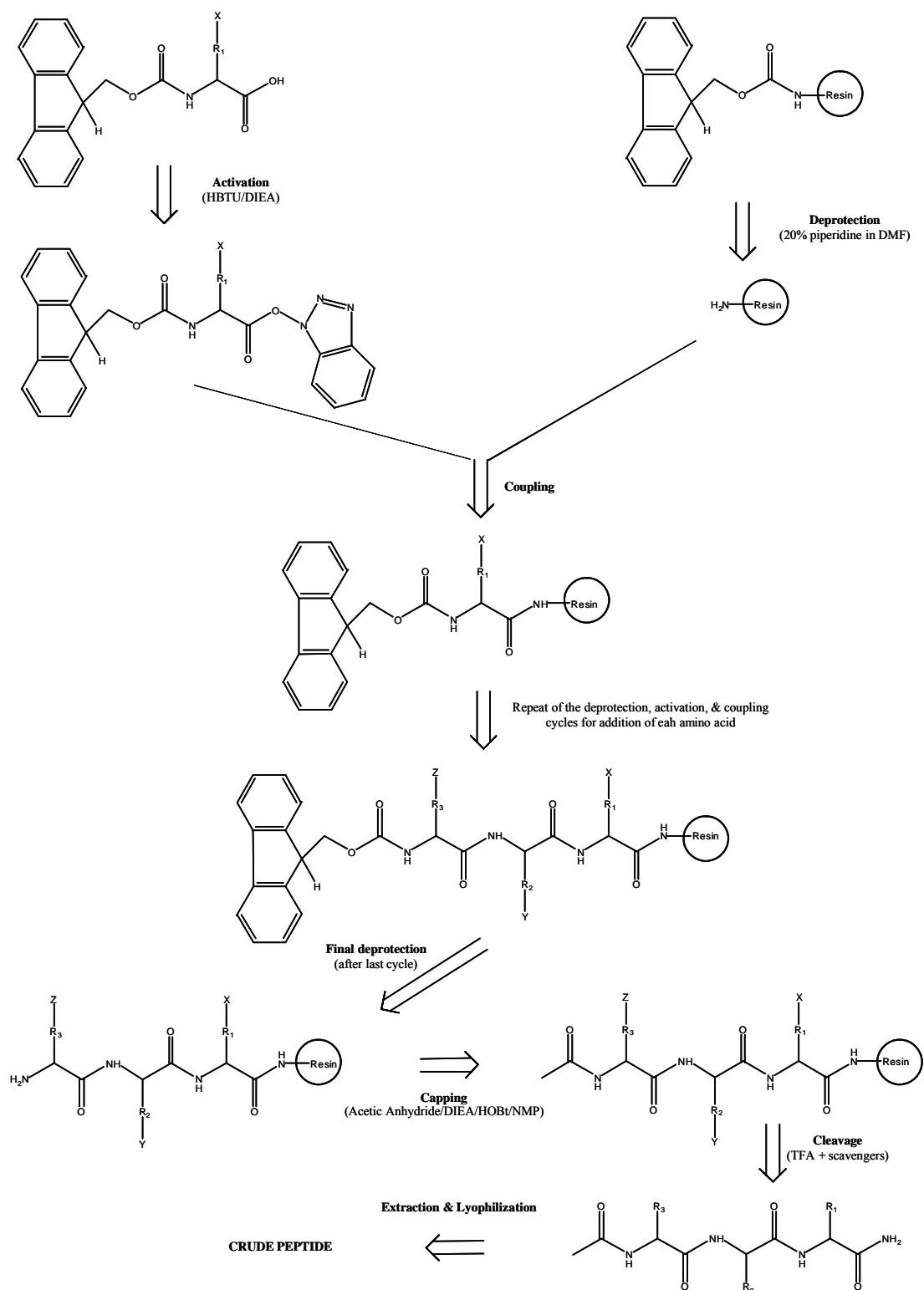
Scheme 2.1. The reaction scheme in solid phase peptide synthesis. X, Y and Z represent side chain protecting groups of amino acid residues.

the resin is removed with 20% PIP/DMF to provide a free N-terminal amino group to couple with an incoming amino acid (AA) (Figure 2.1). Prior to coupling to the free amino group of the resin, the carboxylic acid group of each incoming AA residue was activated with HBTU/DIEA to convert it into a reactive acylating reagent, thus enhancing the electrophilicity of the carboxylate carbon, which then makes it susceptible to nucleophilic attack by the α-amino terminus of the resin via a nucleophilic acyl substitution reaction. It should be noted that a 5-fold excess of each amino acid residue was used in order to obtain an efficient yield. To avoid formation of deletion sequence peptides, the capping step was done following each coupling step to capture any unreacted α-amino group of the growing peptide chain in order to prevent it from coupling to the next added AA. Acetic anhydride was used as the capping reagent. The deprotection, activation and coupling cycles were repeated until the desired peptide sequence was obtained. After the last AA residue was coupled, a final Fmoc deprotection was performed followed by acetylation of the N-terminus of the synthesized peptide.

2.3 Cleavage and Deprotection of Synthesized Peptides

After the desired peptide was made, the support-bound peptide was removed from the synthesizer and was washed with methanol to remove the DMF. The removal of DMF is necessary because the presence of DMF will reduce the TFA concentration in the cleavage cocktail, resulting in a less efficient cleavage reaction and low yields. To remove the amino acid side chain protecting groups and at the same time, to separate the peptide from the resin support in order to obtain a peptide amide, the support-bound peptide was treated with a cleavage cocktail composed of 88% TFA, 4.2% H_2O, 5.8%

phenol, and 2% triisopropylsilane (TIPS) by volume.[8, 9] This cleavage cocktail was used in the cleavage and deprotection of all the peptides synthesized in Part II of this dissertation. Scavengers (H_2O, phenol, & TIPS) were used to capture any carbocation (i.e. t-Boc & t-Bu carbocations which may have formed under acidic conditions during TFA cleavage and deprotection) to prevent them from alkylating reactive side-chain groups.

Each 0.1 gram of resin-bound peptide was allowed to react with 3 mL of the cocktail for about 4 hours. The concentration of TFA, types of scavengers and reaction time were mainly dictated by the amino acid composition of the peptide and the type of support. At the end of the cleavage time, the filtrate was collected under the vacuum through a porous glass filter with medium porosity. To ensure the complete removal of the peptide from the support, an additional 1-2 mL of TFA was used to rinse the resin. Next, methyl t-butyl ether with a volume of about 10 times the volume of the filtrate was added to the separation funnel containing the filtrate to extract scavenged side chain protecting groups and unreacted scavengers (i.e. phenol & TIPS) from the cleavage cocktail as well as to precipitate the peptide out of the cleavage mixture. The precipitated peptide was transferred to a 50 mL plastic tube and was centrifuged. The ether solution on top was combined with the solution remaining inside the separation funnel. The combined solution was extracted 3 times with 10 mL of H_2O each time and the aqueous layer at the bottom containing the peptide was combined with the crude peptide.

2.4 Lyophilization

Solvents used to cleave peptides after synthesis including TFA, MTBE, and

methanol are volatile, which depresses the freezing point of water causing it to melt. Thus, they were blown off first with nitrogen gas before the crude peptide solution was frozen with dry ice and then lyophilized. Most synthesized peptides were in a white powder after lyophilization.

2.5 Reduction of Disulfide Bonds

The peptides all contain two cysteine residues. The crude peptide obtained from SPPS is generally partially oxidized to the disulfide form due to exposure to air. To convert the crude peptide all to the reduce dithiol form, the disulfide bonds were reduced by addition of an excess amount ($\sim$ 10-fold) of dithiolthreitol (DTT), a chemical reducing agent, to the crude peptide solution followed by pH adjustment to $\sim$ 7.5. The crude peptide-DTT solution was allowed to react for $\sim$ 1 hour to reduce the disulfide bond by thiol/disulfide exchange. It should be noted that the pH of the peptide solution should not exceed 8.0, otherwise polymerization may take place.[10] After reacting for $\sim$ 1 hour, the pH was adjusted to $\sim$ 3.0 followed by immediate reverse-phase HPLC purification to prevent peptides from being air-oxidized again.

2.6 Oxidation of Cysteine-Containing Peptides

All cyclic disulfide-bridged peptides studied in this dissertation were prepared by oxidation of the crude peptides obtained from SPPS with trans-$[Pt(en)_2Cl_2]^{2+}$, where en = ethylenediamine (Figure 2.3). The oxidizing agent was discovered in our lab by Dr. Tiesheng Shi.[10] Trans-$[Pt(en)_2Cl_2]^{2+}$ forms intramolecular disulfide bonds rapidly and quantitatively with high selectivity.

5-10 mM crude reduced peptide solution was prepared in 50 mM phosphate
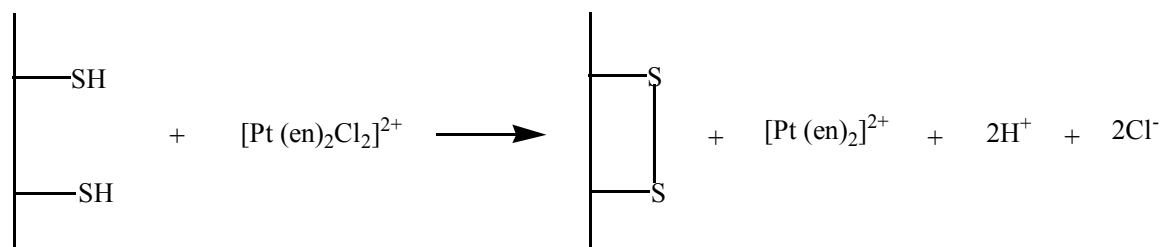
Figure 2.3. Oxidation of dithiol peptides by trans-$[Pt(en)_2Cl_2]^{2+}$, where en =

ethylenediamine, to form an intramolecular disulfide bond in peptides. [Ref. 10].

buffer, pH ~ 4. A 2-4 fold excess of $[Pt(en)_2Cl_2]^{2+}$ powder was then added to the peptide

solution, and the solution pH was adjusted to ~ 3. The peptide solution was allowed to

react for ~ 1 hour, after which formation of disulfide bond was confirmed by MALDI-

TOF mass spectrometry. The crude cyclic disulfide peptide was then purified by

reversed-phase HPLC. $[Pt(en)_2Cl_2]^{2+}$ and its reduction product $[Pt(en)_2]^{2+}$ are inert and

nontoxic and are readily separated from the peptide.

2.7 Peptide Purification by Reversed-Phase HPLC

The crude peptides were purified on a Varian HPLC using a Vydac C_{18} semi-prep

reversed phase column (10 x 250 mm). Elution from the column was monitored at a

wavelength where the amide bond absorbs (215 nm). Peptides were eluted from the

column with a gradient of mobile phases A and B. Mobile phase A was 0.1% TFA in

H_2O (pH 2.11), and mobile phase B was 0.1% TFA in acetonitrile. Mobile phase A was

filtered via a 0.45 μm nylon membrane. For the separations of all the synthesized

peptides, optimum retention time and resolution were achieved with the use of a linear

gradient of 2-30% mobile phase B in 30 minutes.

It should be noted that 0.1% TFA (pK_A ~ 0.30) was added to mobile phases to

improve peak resolution as well as to prevent peak tailing. Using TFA as an ion pairing

reagent is common practice in reversed-phase separation of peptides and proteins in order

to overcome peak broadening and tailing, which presumably result from mixed-mode

interactions of peptide molecules having a variety of polar, ionic and hydrophobic sites

with hydrophobic groups (C_{18} groups) and residual hydroxyl groups on the silica bonded

stationary phase.[11] TFA is believed to exert its effects by pairing with the positively

charged and polar groups on peptides and proteins to mask these sites from interacting

with polar silanol (SiOH, $pK_A \sim 3.5$) groups on the stationary phase. Similarly, TFA may

mask unbonded polar regions of the adsorbent and thus prevents silanol groups from

interacting with peptide molecules.

2.8 MALDI-TOF Mass Spectrometry

Identities of crude peptides after cleavage and pure peptides isolated by reversed-

phase HPLC were confirmed on an Applied Biosystems, Voyager-DE STR

Biospectrometry Workstation with a MALDI (Matrix Assisted Laser Desorption /

Ionization), an ionization source, and a TOF (time of flight) mass analyzer. The mass

spectrometer is equipped with a 337 nm nitrogen laser and a reflectron. An accelerating

voltage of 20 kV and a 100 ns extraction delay were used. The laser intensity was set

between 2000 and 2400 (arbitrary scale).

α–cyano-4-hydroxycinnamic acid (CHCA) was used as the matrix for MALDI

ionization. An excess amount of CHCA was added to 50 μL of 0.1% TFA in 50:50 (v/v)

acetonitrile/methanol solution to prepare a saturated matrix solution. 1 μL of peptide

solution was mixed with 9 μL of CHCA saturated solution. Then 1 μL of the mixture

solution was spotted on a 100-well Applied Biosystems MALDI plate and air dried.

The matrix is excited by a high intensity laser pulse of short duration and the

energy absorbed by the matrix in turn causes the analyte to desorb and ionize. Generated

ions enter a vacuum where they are accelerated toward the detector under a strong

electric field. The flight time taken for particular ions to reach the detector is measured by

an analyzer. The flight time of an ion is related to its mass-to-charge ratio (m/z). Thus,

mass spectra can be generated from simple time measurements. A delay extraction of 100 ns was used to compensate for the initial velocity variation of ions of the same m/z so that they can arrive simultaneously at the detector.

2.9 ^{1}H NMR Experiments

2.9.1 Sample Preparation

5-10 mM pure peptide (either the acyclic dithiol or cyclic disulfide form purified by reversed-phase HPLC) solution in 90% H_2O / 10% D_2O at pH ~ 3.0 with a sample volume of 320 μL was prepared for the NMR study of cis/trans isomerization. For the reduced dithiol peptide, a 3-fold excess of deuterated DTT was added to the peptide solution to ensure the peptide wasn't air-oxidized. 0.1M HCl and 0.1 M NaOH were used to adjust the pH of dithiol peptide solutions to ~ 7.5. The peptide solution was allowed to react with DTT for about 1 hour and the pH was then adjusted to ~ 3.0. The peptide solution was filtered through a 0.45 μm MicroSpin filter to remove particulates before it was transferred to the Shigemi NMR tube. The sample solution was degassed with N_2 for ½ hour. NMR experiments on the reduced peptide were conducted immediately after the sample was degassed to avoid partial oxidation by air.

It should be noted that solutions of some of the dithiol peptides were prepared by adding an excess amount of deuterated DTT to the solution used for NMR experiments on the oxidized peptide after it was transferred from the NMR tube to a 1 mL Eppendorf vial. Preparing a reduced peptide NMR sample in this way was a lot quicker as compared to HPLC purification followed by lyophilization to obtain a sample of the pure reduced peptide. Success in converting the oxidized peptide to the reduced form was confirmed

by MALDI-TOF MS.

2.9.2 One-Dimensional NMR Experiments

1-D ^{1}H NMR spectra of peptide samples were measured using the presat pulse

sequence and parameters described in Chapter 2 of Part I of this dissertation.

2.9.3 The TOtal Correlation SpectroscopY (TOCSY) Experiments

In part II of this thesis, the TOCSY experiment was used to assign ^{1}H NMR

spectra of the peptides. Subspectra were obtained for the amino acids in the peptide. The

TOCSY experiment allows one to correlate all the protons within each amino acid

residue in a peptide based on scalar (through-bond) ^{1}H-^{1}H spin-spin coupling. Figure

2.4.A shows the connections between protons within each amino acid as a result of

magnetization transfer. It should be noted that the protons of each amino acid form an

isolated spin system as there is no magnetization being transferred across the carbonyl

group in the TOCSY experiment.

By taking a trace through the cross peak at the amide resonance, a 1-D

subspectrum corresponding to a specific amino acid residue of a peptide sequence can be

obtained. For example, a trace through the resonance of an amide proton, gives the

subspectrum shown in Figure 2.4.C, which serves to identify the amino acid giving this

subspectrum to be an alanine residue by comparing the chemical shift of each resonance

with reference values.

2.9.4 The Rotating Frame Overhauser Effect SpectroscopY (ROESY) Experiments

The ROESY experiment was used to establish the sequence of amino acid

residues in peptides based on dipolar (through-space) connectivities. The sequential

(A)

(B)   F1 (ppm)   (C)

F2 (ppm)
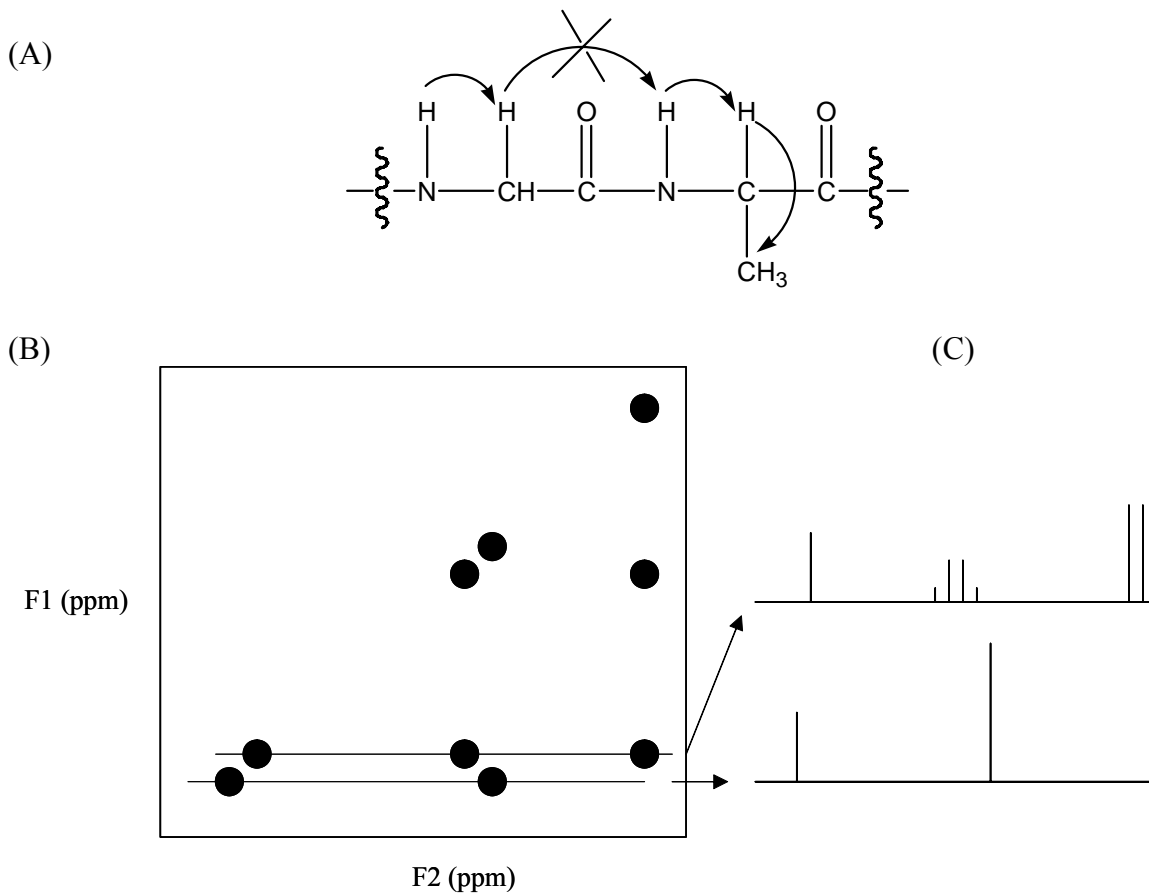
Figure 2.4. (A) Diagram of a dipeptide sequence, illustrating the through-bond

magnetization transfer within the isolated spin system of each amino acid residue in the

TOCSY experiment. The arrows demonstrate the relay of magnetization. No

magnetization transfer occurs across the carbonyl group of the peptide bond in the

TOCSY experiment, as indicated by the cross sign. (B) The hypothetical TOCSY

spectrum of the dipeptide shown in (A). (C) 1-D subspectra obtained by taking traces at

the chemical shifts of the amide resonances, which serve as fingerprint to determine the

identities of the amino acids.

assignment of resonances to amino acid residues is based on sequential cross peaks N_iH-$C_{\alpha i}H$ and $C_{\alpha i}H$- $N_{i+1}H$ as illustrated in Figure 2.5. The pulse sequence and parameters used in the ROESY experiment are presented in Chapter 2 of Part I.

2.9.5 Inversion-Magnetization Transfer Experiments

The inversion-magnetization technique was used to obtain rate constants for cis→trans isomerization.[12-14] Since the rate of interchange between the cis and trans isomers by rotation around the amide bond is slow on the NMR chemical shift time scale, both isomers can be observed. However, exchange can be observed on the magnetization transfer time scale. The basic requirement is that the spin-lattice relaxation time (T_1) of a specific proton of the cis and trans isomer be ≥ the half life of the cis and trans isomers. In the inversion-magnetization transfer experiment, the magnetization giving one of the resonances in a pair of cis/trans exchanging resonances is inverted, and transfer of the inverted magnetization to the other resonance is monitored as a function of time. To achieve the maximum net effect of transfer of inversion on resonance intensity, the more intense trans resonance was selectively inverted and the intensity of the cis resonance was measured as a function of a variable mixing delay. The inversion transfer pulse sequence is 90^o_x-τ-90^o_x-t-$90^o_{\pm x,\pm y}$ -acquisition where τ is a fixed delay time which equals $1/(2|v_t$-$v_c|)$; v_t-v_c is the separation of the resonances for the trans and cis isomers in Hz in the 1-D ^1H NMR spectrum, and t is a variable mixing delay during which magnetization transfer takes place by interchange between the cis and trans isomers. A 1-D ^1H NMR spectrum was first acquired, and then the transmitter was placed on the more intense trans resonance. A well-resolved pair of cis/trans resonances is needed for the inversion-

(A)

$C_{\alpha i}H$-$N_{i+1}H$ $C_{\alpha i+1}H$-$N_{i+2}H$ $C_{\alpha i+2}H$-$N_{i+3}H$

N_iH-$C_{\alpha i}H$ $N_{i+1}H$-$C_{\alpha i+1}H$ $N_{i+2}H$-$C_{\alpha i+2}H$ $N_{i+3}H$-$C_{\alpha i+3}H$

(B)

$C_{\alpha i+1}H$

$C_{\alpha i+2}H$

$C\alpha H$

$C_{\alpha i+3}H$

$C_{\alpha i}H$

$N_{i+3}H$ $N_{i+2}H$ $N_{i+1}H$ N_iH

NH
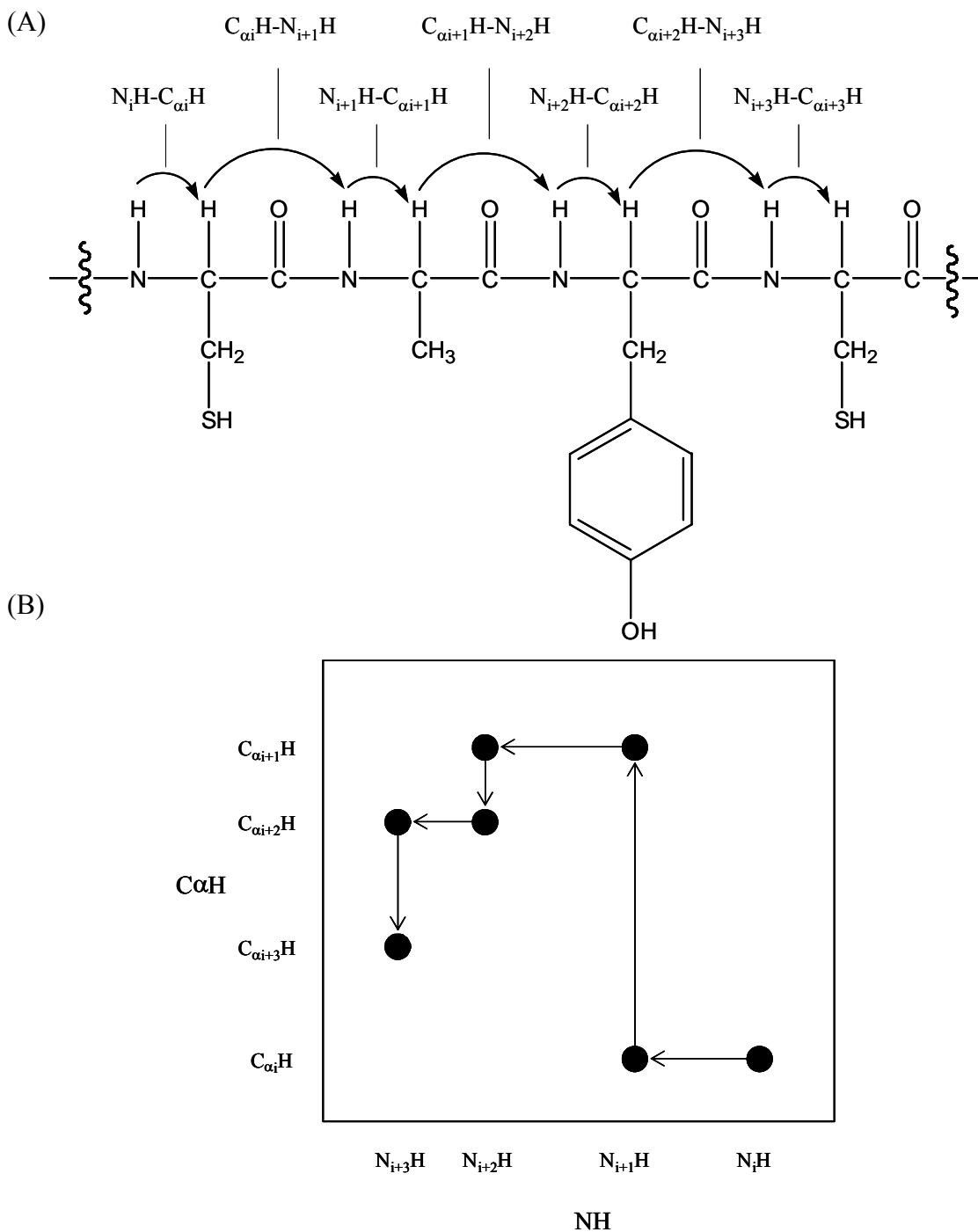
Figure 2.5. (A) Diagram of a typical tetrapeptide sequence, showing the through-space magnetization transfer in the ROESY experiment. The arrows demonstrate the magnetization transfer by through-space dipolar coupling. (B) A schematic diagram of the 2-D ROESY spectrum of the peptide sequence shown in (A). The arrows show how the peptide sequence is assigned.

magnetization transfer experiment.

Figure 2.6 shows a vector diagram to illustrate the behavior of the magnetization for the trans and cis isomers during the magnetization transfer experiment. The first 90°_{x} pulse is applied to place magnetization of both the trans (A) and the cis (B) isomers onto the +y axis. During the fixed delay time τ following the first 90°_{x} pulse, the trans resonance does not precess in the rotating frame since the transmitter is set on the trans resonance. The magnetization of the cis isomer; however, has precessed 180° to the –y axis at the end of the delay period τ. A second 90°_{x} pulse is applied which tips the magnetization B for the cis resonance to be aligned along the +z axis, and the trans magnetization A to be aligned along the –z axis. At this point, the trans resonance has been selectively inverted. During the variable mixing delay t, magnetization transfer takes place between A and B by chemical exchange. As a result of magnetization transfer, the trans resonance begins to return to its equilibrium intensity, via transfer of positive magnetization from the cis resonance and also spin-lattice T_1 relaxation, while the cis resonance first decreases because of chemical exchange and then recovers to its equilibrium intensity by T_1 relaxation as the mixing time is increased. Following the mixing delay, a 90° read pulse places the magnetization vectors A and B into the transverse plane and the free induction decay is acquired. To illustrate, a typical inversion-magnetization transfer data set is shown in Figure 2.7.

The mixing delay was arrayed with values ranging from 0.0001 second to at least 5 times the longest T_1 of the cis/trans pair of resonances that was used. For each t value, 64-256 transients were collected; in the case of secondary amide peptide bonds, 1024
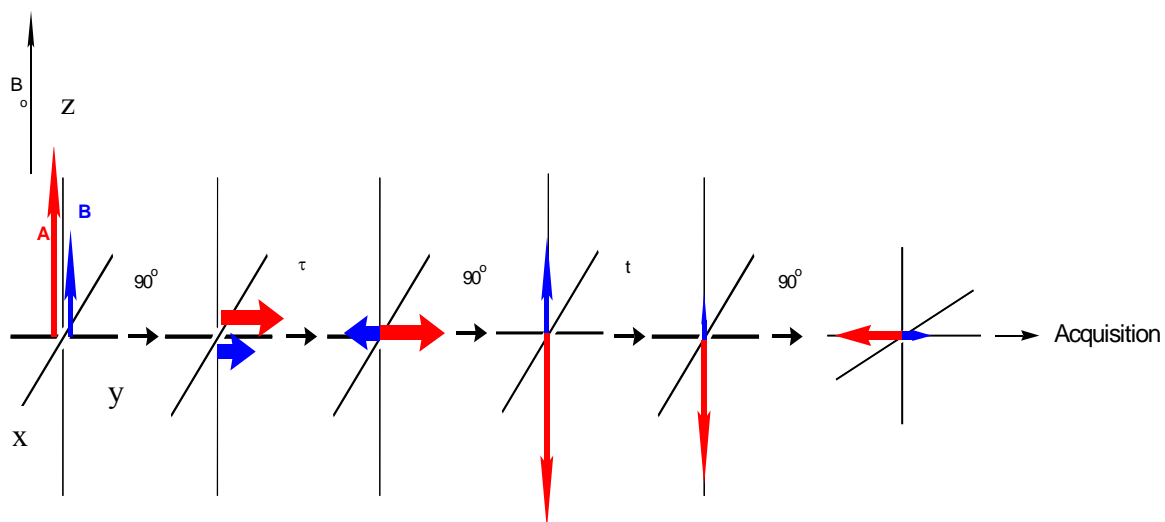
Figure 2.6. Vector diagram showing the magnetization for the trans and cis isomers during the inversion-magnetization transfer experiment for studying the kinetics of cis/trans isomerization of secondary amide bonds in peptides and tertiary amide bonds in peptide/peptoid hybrids. A represents the trans isomer and B represents the cis form.

transients were collected due to low abundance of the cis isomer.

2.9.6 Inversion-Magnetization Transfer Data Analysis

Due to the slow rotation around the peptide bond, two sets of resonances in the ^{1}H

NMR spectrum are expected to be seen: one from the cis isomer and the other from the

trans isomer. Equilibrium constants for cis/trans isomerization (K_{eq}=[trans]/[cis]=k_{ct}/k_{tc},

where k_{ct} is the rate constant for cis→trans exchange and k_{tc} is the rate constant for

trans→cis exchange) were determined from the integrated intensities of the same

cis/trans pair of resonances used in the inversion-magnetization transfer experiments. The

resonance intensities were obtained from standard 1-D ^{1}H NMR spectra.

Rate constants for cis→trans interconversion, k_{ct}, were derived from the

inversion-magnetization transfer data by use of the inversion-magnetization transfer

method described in reference 15. Concisely, the calculation of k_{ct} involves a nonlinear

least-squares fit of the inversion-magnetization transfer data to an equation (see

Appendix 1) that expresses the resonance intensity as a function of mixing time in terms

of known and adjustable parameters, including k_{ct}.

For some peptides reported in this thesis, the rate constants k_{ct} at 25 ^{o}C, were

obtained directly from inversion-magnetization transfer data measured at 25 ^{o}C since

cis/trans isomerization was sufficiently fast. However, in most cases, temperatures higher

than 25°C were needed to bring the rates of cis/trans isomerization onto the

magnetization-transfer time scale. To obtain values for k_{ct} at 25 ^{o}C, rate constants were

measured over a range of elevated temperatures. By plotting ln(k_{ct}/T) vs 1/T, activation

parameters $\Delta H_{ct}^{\neq}$ and $\Delta S_{ct}^{\neq}$ were obtained from the Eyring equation:

$$\ln\frac{k_{ct}}{T} = (-\frac{\Delta H_{ct}^{\ddagger}}{R})\frac{1}{T} + \frac{\Delta S_{ct}^{\ddagger}}{R} + \ln\frac{k_B}{h}$$

where K_B is the Boltzmann constant (1.381×10^{-23} J/K), h is Planck's constant (6.626×10^{-34} J.S), and R is the gas constant (8.315 J.K^{-1}.mol^{-1}). The values for activation parameters derived from the slope and intercept of the Eyring plot were then used to calculate the rate constant k_{ct} at 25 ^{o}C. The rate constant for trans→cis isomerization, k_{tc}, was then obtained from K_{eq} and k_{ct} ($k_{tc}=k_{ct}/K_{eq}$). The values for $\Delta G_{ct}^{\neq}$ at 25 ^{o}C were calculated from the values for $\Delta H_{ct}^{\neq}$ and $\Delta S_{ct}^{\neq}$ ($\Delta G_{ct}^{\neq} = \Delta H_{ct}^{\neq} - T\Delta S_{ct}^{\neq}$).

To illustrate, Figure 2.7 shows the intensities of the resonances for the acetyl methyl protons of the cis and trans isomers of the dithiol form of Ac-Cys-Sar-(His)$_2$-(Ala)$_3$-Cys-NH$_2$ as a function of the length of the mixing time, obtained from the inversion-magnetization experiment measured at 50 ^{o}C. Figure 2.8 shows the integrated intensity of the resonance for the acetyl methyl protons of the cis isomer of the dithiol form of Ac-Cys-Sar-(His)$_2$-(Ala)$_3$-Cys-NH$_2$ as a function of the mixing time at 50 ^{o}C. The smooth curve through the points is the theoretical curve obtained from the nonlinear least squares fit of the data to the equation in Appendix 1.

cis

trans

10^{-4} Mixing Time (sec)   20
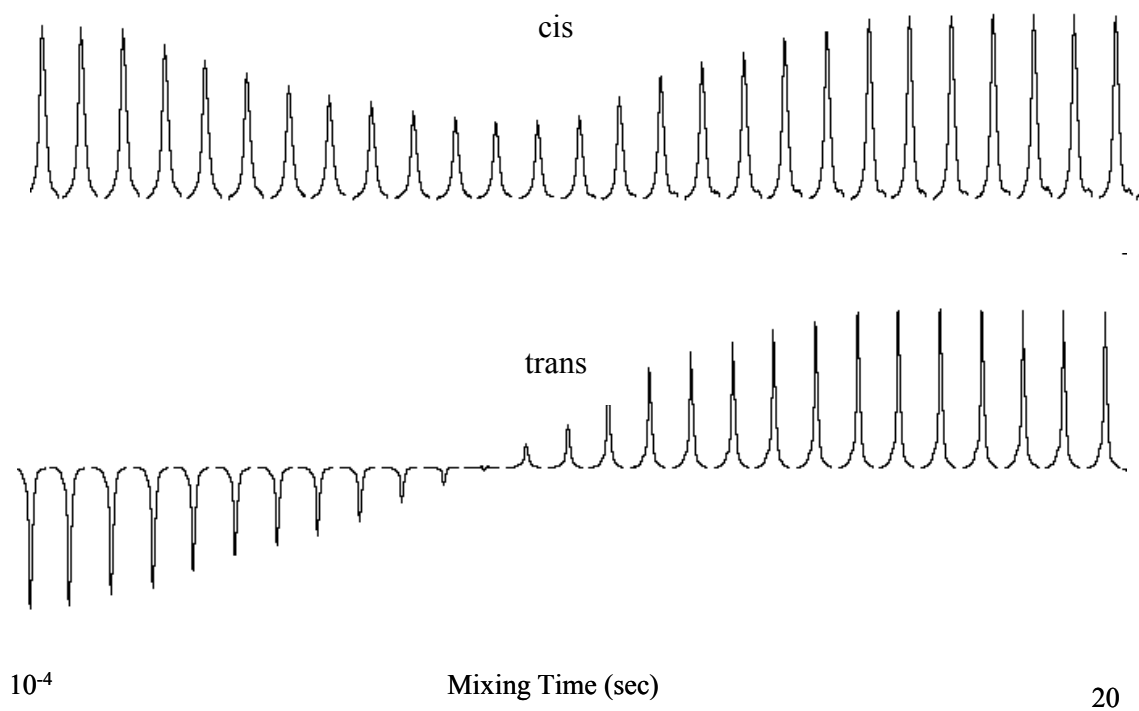
Figure 2.7. Intensities of the resonances for the acetyl methyl protons of the cis and trans isomers of the dithiol form of Ac-Cys-Sar-(His)$_2$-(Ala)$_3$-Cys-NH$_2$ as a function of the length of the mixing time, obtained from the inversion-magnetization experiment. The data are for 6 mM dithiol Ac-Cys-Sar-(His)$_2$-(Ala)$_3$-Cys-NH$_2$ in 90% H$_2$O / 10% D$_2$O at pH 2.91 and 50 °C.
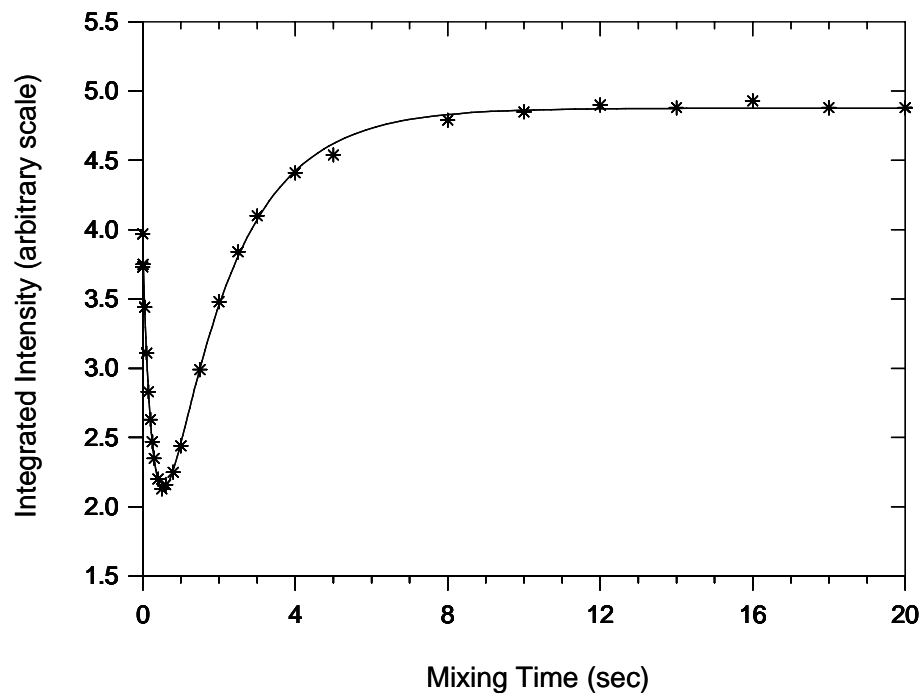
Figure 2.8. Integrated intensities of the resonance for the acetyl methyl protons of the cis isomer of the dithiol form of Ac-Cys-Sar-(His)$_2$-(Ala)$_3$-Cys-NH$_2$ as a function of the mixing time. The data are for 6 mM dithiol Ac-Cys-Sar-(His)$_2$-(Ala)$_3$-Cys-NH$_2$ in 90% H$_2$O / 10% D$_2$O at pH 2.91 and 50 ^{o}C. The smooth curve through the points is the theoretical curve calculated using the parameters obtained by nonlinear least-squares analysis of the inversion-magnetization transfer data. $k_{ct} = 0.153 \pm 0.005$ s^{-1} and $k_{tc} = 0.041 \pm 0.001$ s^{-1}.

References

1. Applied Biosystem Inc., Foster City, CA, *Introduction to Cleavage Techniques*, **1990**.

2. Merrifield, R. B. *J. of Am. Chem. Soc*. **1963**, *85*, 2149-2153.

3. Atherton, E.; Sheppard, R. C. *Solid Phase Peptide Synthesis: A Practical Approach*. IRL Press: Oxford, **1989**.

4. Fields, G. *Methods in Enzymology: Solid Phase Peptide Synthesis*, Academic Press, New York, **1997**.

5. Pennington, M. W.; Dunn, B. M. *Peptide Synthesis Protocols*. Humana Press, Totowa, NJ, **1994**, 35.

6. Jones, J. *The Chemical Synthesis of Peptides*. Clarendon Press, Oxford, **1994**, 52-100.

7. Fields, G. B. *Int. J. Peptide Protein Res.* **1990**, *35*, 161.

8. King, D. S.; Fields, C. G.; Fields, G. B. *J. of Peptide Protein Res*. **1990**, *115*, 1497-1498.

9. Pearson, D. A.; Blanchette, M.; Baker, M. L.; Guindon, C. A. *Tetrahedron Lett*., **1989**, *30*, 2739-2742.

10. Shi, T.; Rabenstein, D. L. *J. Am. Chem. Soc*. **2000**, *122*, 6809-6815.

11. Nawrocki, J. *J. of Chromatography A*, **1997**, *779*, 29-71.

12. Larive, C. K.; Guerra, L.; Rabenstein, D. L. *J. Am. Chem. Soc*. **1992**, *114*, 7331-7337.

13. Larive, C. K.; Rabenstein, D. L. *J. Am. Chem. Soc*. **1993**, *115*, 2833-2836.

14. Rabenstein, D. L.; Shi, T.; Spain, S. *J. Am. Chem. Soc*. **2000**, *122*, 2401-2402.

15. Mariappan, S. V. S.; Rabenstein, D. L. *J. Magn. Reson*. **1992**, *100*, 183-188.

Chapter 3

Cis/Trans Isomerization Kinetics and Equilibria of the Peptidyl-Sarcosyl Amide Bond in Peptide/Peptoid Hybrids

3.1 Introduction

Interest in peptoids as potential pharmaceuticals has focused primarily on di- and tri-peptoid ligands.[1, 2] In this work, we are studying peptide/peptoid hybrids in which one amino acid of the peptide sequence is a peptoid monomer (N-methyl glycine; sarcosine, Sar) to better understand the conformational properties of peptide/peptoid hybrids in solution, in particular the kinetics and equilibria of cis/trans isomerization by rotation around cysteine-sarcosine amide bonds. One feature of peptide/peptoid hybrids is that both the cis and trans conformation across the Cys-Sar peptide bonds are populated. However, it is unlikely that all configurational isomers of peptide/peptoid hybrids are biologically active (i.e. that they all induce a biological action) due to the high specificity of ligand-receptor binding. Therefore, the distribution and kinetics of interchange among configurational isomers of peptide/peptoid hybrids are of interest.

Many peptide hormones (e.g. oxytocine & vasopressin) and peptide toxins (e.g. ShK toxin & Charybdotoxin) contain one or more intramolecular disulfide bonds, which are critical for biological activity. Conformational constraints imposed on the peptide backbone by the intramolecular disulfide bond result in an increase in bioactivity and selectivity as well as improved bioavailability.[3] Cyclic disulfide peptides are less prone to enzymatic degradation.[4] Disulfide-bridged peptides are used as scaffolds to optimize potency and selectivity of drug candidates in the development of new drug leads.[4,5] Thus,

to mimic properties of bioactive cyclic disulfide peptides, peptide/peptoid hybrids studied in this dissertation were designed to contain one intramolecular disulfide bond.

This chapter reports the kinetics, thermodynamics and equilibria of cis/trans isomerization across the Cys-Sar amide bonds in a series of peptide/peptoid hybrids (Table 3.1) of the sequence Ac-Cys-Sar-His-Xaa-Ala-Ala-Ala-Cys-NH$_2$, where Xaa is His, Gly, Lys, Phe, Asp and Glu, to determine the effect of amino acid sequence on the kinetics and equilibria of cis/trans isomerization. The peptide/peptoid hybrids were studied in both their reduced linear dithiol and oxidized cyclic disulfide forms. To illustrate the cis/trans isomerization, the cis and trans conformational isomers across the Cys-Sar peptide bond of the disulfide form of Ac-Cys-Sar-His-Xaa-Ala-Ala-Ala-Cys-NH$_2$ are shown in Figure 3.1.

The kinetics, thermodynamic and equilibria of cis/trans isomerization of the Cys-Sar peptide bonds in a related series of peptide/peptoid hybrids (Table 3.2) of the sequence Ac-Cys-Sar-(Ala)$_x$-His-(Ala)$_y$-Cys-NH$_2$, x = 0-4 and y = 4-0, are also reported in this chapter. These peptide/peptoid hybrids were studied to explore the effect of the position of the histidine residue on the populations of the cis and trans isomers and the rates of cis/trans isomerization. These hybrids were also studied in both their linear dithiol and cyclic disulfide forms.

The kinetics, thermodynamic and equilibria of cis/trans isomerization across the Xaa-Sar peptide bonds in a third series of peptide/peptoid hybrids (Table 3.3) in which the Sar residue is moved along the peptide sequence Ac-Cys-Sar-His-(Ala)$_3$-Cys-NH$_2$, Ac-Cys-His-Sar-(Ala)$_3$-Cys-NH$_2$, etc., are also presented in this chapter. The goal is to

291

Peptide/Peptoid hybrids	Amino acid sequence	Resonances used in inversion-magnetization transfer experiment
1a	Ac-C-Sar-H-H-(A)$_3$-C-NH$_2$	acetyl-CH$_3$
1b	Ac-C-Sar-H-H-(A)$_3$-C-NH$_2$	Sar CH$_3$
2a	Ac-C-Sar-H-G-(A)$_3$-C-NH$_2$	acetyl-CH$_3$
2b	Ac-C-Sar-H-G-(A)$_3$-C-NH$_2$	acetyl-CH$_3$
3a	Ac-C-Sar-H-K-(A)$_3$-C-NH$_2$	acetyl-CH$_3$
3b	Ac-C-Sar-H-K-(A)$_3$-C-NH$_2$	Sar CH$_3$
4a	Ac-C-Sar-H-F-(A)$_3$-C-NH$_2$	acetyl-CH$_3$
4b	Ac-C-Sar-H-F-(A)$_3$-C-NH$_2$	acetyl-CH$_3$
5a	Ac-C-Sar-H-D-(A)$_3$-C-NH$_2$	acetyl-CH$_3$
5b	Ac-C-Sar-H-D-(A)$_3$-C-NH$_2$	acetyl-CH$_3$
6a	Ac-C-Sar-H-E-(A)$_3$-C-NH$_2$	acetyl-CH$_3$
6b	Ac-C-Sar-H-E-(A)$_3$-C-NH$_2$	acetyl-CH$_3$

Table 3.1. Sarcosine-containing peptide/peptoid hybrids of the sequence Ac-Cys-Sar-His-Xaa-Ala-Ala-Ala-Cys-NH$_2$, where Xaa is His, Gly, Lys, Phe, Asp, and Glu. Also shown in the Table are the resonances used in inversion-magnetization transfer experiments.
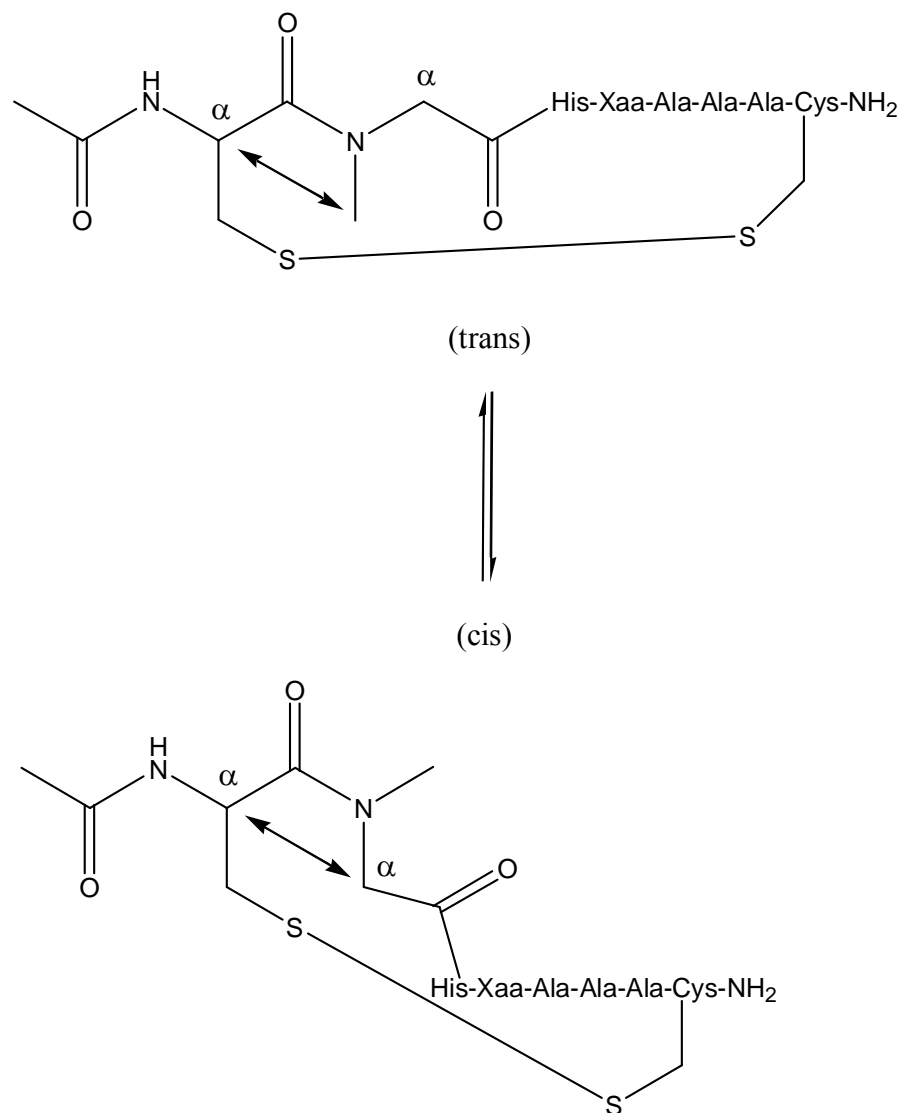
Figure 3.1. The cis and trans isomers for the disulfide form of Ac-Cys-Sar-His-Xaa-(Ala)$_3$-Cys-NH$_2$, where Xaa represents His, Gly, Lys, Phe, Asp or Glu. The cis/trans conformation refers to the cis or trans position of the α-carbon of Cys^1 and the α-carbon of Sar^2 across the C(O)-N amide bond as shown. The arrows indicate the dipolar ROESY cross peaks (Cys^1 C$_\alpha$H-Sar^2 CH$_3$ and Cys^1 C$_\alpha$H-Sar^2 C$_\alpha$H) used to assign the cis and trans isomers across the Cys-Sar peptide bond.

Peptide/Peptoid hybrids	Amino acid sequence	Resonances used in inversion-magnetization transfer experiment
7a	Ac-C-Sar-H-(A)$_4$-C-NH$_2$	acetyl-CH$_3$
7b	Ac-C̲-Sar-H-(A)$_4$-C̲-NH$_2$	acetyl-CH$_3$
8a	Ac-C-Sar-A-H-(A)$_3$-C-NH$_2$	acetyl-CH$_3$
8b	Ac-C̲-Sar-A-H-(A)$_3$-C̲-NH$_2$	Sar CH$_3$
9a	Ac-C-Sar-(A)$_2$-H-(A)$_2$-C-NH$_2$	acetyl-CH$_3$
9b	Ac-C̲-Sar-(A)$_2$-H-(A)$_2$-C̲-NH$_2$	acetyl-CH$_3$
10a	Ac-C-Sar-(A)$_3$-H-A-C-NH$_2$	acetyl-CH$_3$
10b	Ac-C̲-Sar-(A)$_3$-H-A-C̲-NH$_2$	Sar CH$_3$
11a	Ac-C-Sar-(A)$_4$-H-C-NH$_2$	acetyl-CH$_3$
11b	Ac-C̲-Sar-(A)$_4$-H-C̲-NH$_2$	Sar CH$_3$

Table 3.2. Sarcosine-containing peptide/peptoid hybrids of the sequence Ac-Cys-Sar-(Ala)$_x$-His-(Ala)$_y$-Cys-NH$_2$, x = 0-4 and y = 4-0. Also shown in the Table are the resonances used in inversion-magnetization transfer experiments.

Peptide/Peptoid hybrids	Amino acid sequence	Resonances used in inversion-magnetization transfer experiment
12a	Ac-C-Sar-H-(A)$_3$-C-NH$_2$	acetyl-CH$_3$
12b	Ac-C-Sar-H-(A)$_3$-C-NH$_2$	acetyl-CH$_3$
13a	Ac-C-H-Sar-(A)$_3$-C-NH$_2$	Sar CH$_3$
13b	Ac-C-H-Sar-(A)$_3$-C-NH$_2$	Sar CH$_3$
14a	Ac-C-H-A-Sar-(A)$_2$-C-NH$_2$	Sar CH$_3$
14b	Ac-C-H-A-Sar-(A)$_2$-C-NH$_2$	Sar CH$_3$
15a	Ac-C-H-(A)$_2$-Sar-A-C-NH$_2$	Sar CH$_3$
15b	Ac-C-H-(A)$_2$-Sar-A-C-NH$_2$	Sar CH$_3$
16a	Ac-C-H-(A)$_3$-Sar-C-NH$_2$	Sar CH$_3$
16b	Ac-C-H-(A)$_3$-Sar-C-NH$_2$	Sar CH$_3$

Table 3.3. Sarcosine-containing peptide/peptoid hybrids in which the Sar residue is moved along the peptide sequence Ac-Cys-Sar-His-(Ala)$_3$-Cys-NH$_2$, Ac-Cys-His-Sar-(Ala)$_3$-Cys-NH$_2$, etc. Also shown in the Table are the resonances used in inversion-magnetization transfer experiments.

determine the effect of the amino acid preceding the Sar residue on the kinetics and equilibria of cis/trans isomerization. These hybrids were also studied in both their dithiol and disulfide forms.

3.2 Results

3.2.1 Assignment of Resonances of the Cis and Trans Isomers of Sarcosine-Containing Peptide/Peptoid Hybrids

Because interconversion between cis and trans isomers by rotation around the Xaa-Sar peptide bond is slow on the NMR time scale, resonances for both isomers were observed for all peptide/peptoid hybrids reported in this chapter. To illustrate, the 1-D ^{1}H NMR spectrum of the disulfide form of Ac-Cys-Sar-(His)$_2$-(Ala)$_3$-Cys-NH$_2$ in 90% H$_2$O/10% D$_2$O at pH 2.99 and 25 ^{o}C, and an expansion of the amide NH region of the 1-D spectrum, are shown in Figure 3.2. The spectrum was measured by the standard single pulse sequence with suppression of the water resonance by presaturation. The spectrum consists of two sets of resonances, one slightly more intense than the other, as illustrated by the resonances for the amide NH protons. To illustrate the resonance assignment procedure, the assignment of the two sets of resonances for the disulfide form of Ac-Cys-Sar-(His)$_2$-(Ala)$_3$-Cys-NH$_2$ will be presented in detail. The assignment procedure involved first identification of the amino acid residues giving the NH resonances, then determination of the conformation across the Cys-Sar peptide bond, and finally assignment of the resonances to specific residues in the hybrid sequence.

To identify the amino acid residues giving the NH resonances, a 2-D TOCSY experiment was performed. A full 2-D TOCSY spectrum of the disulfide form of Ac-
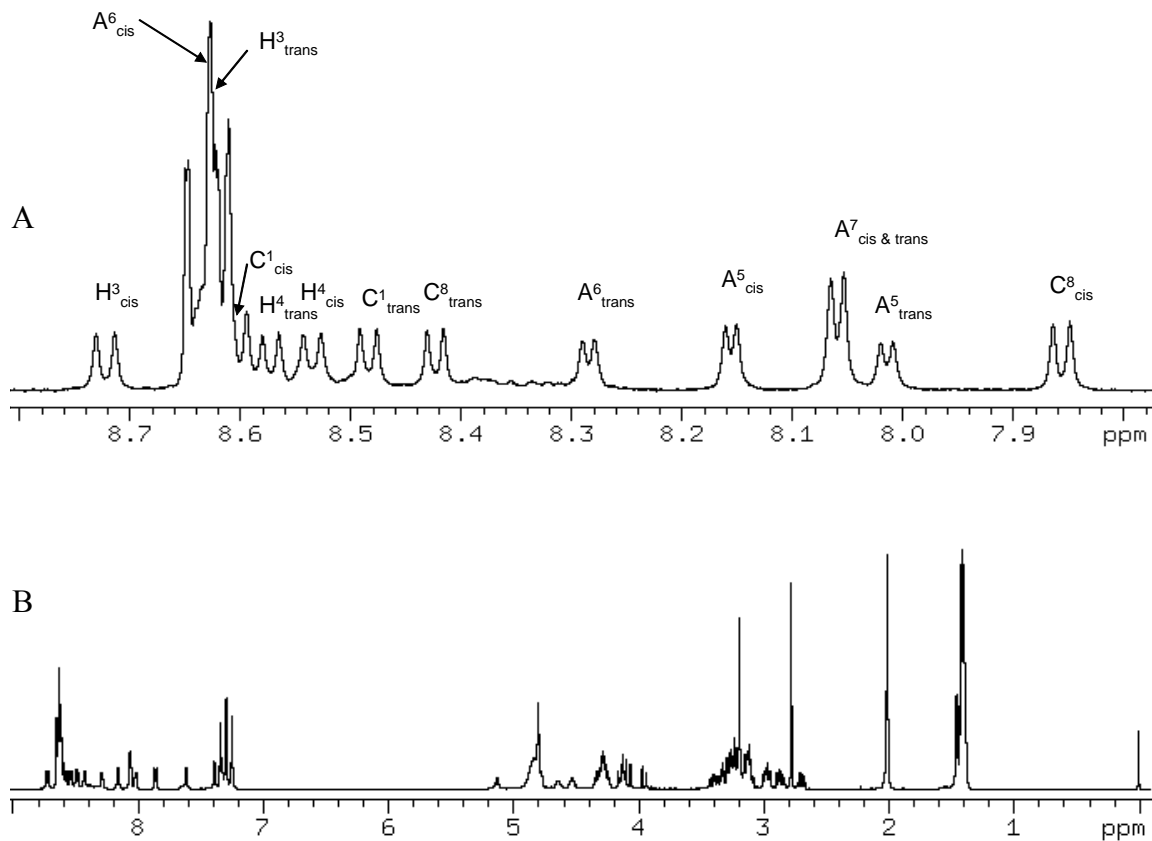
Figure 3.2. (A) The amide NH region of the 500 MHz ^{1}H NMR spectrum of a 5.8 mM solution of the disulfide form of Ac-Cys-Sar-(His)$_2$-(Ala)$_3$-Cys-NH$_2$ in 90% H$_2$O/10% D$_2$O at pH 2.99 and 25 ^{o}C. The spectrum was measured with the single pulse method, with suppression of the H$_2$O resonance by presaturation. The amide NH resonances are assigned to specific residues and by the conformation of the Cys-Sar peptide bond. (B) The full 1-D spectrum.

Cys-Sar-(His)$_2$-(Ala)$_3$-Cys-NH$_2$ in 90% H$_2$O/10% D$_2$O at pH 2.99 and 25 ^{o}C, together

with the corresponding 1-D spectrum, is shown in Figure 3.3. Due to overlap of

resonances in the amide NH region, a BASHD-TOCSY spectrum was measured, with F$_1$-

band selection and F$_1$-homonuclear decoupling of the amide backbone NH region. Figure

3.4 shows the NH (F$_1$)-full (F$_2$) region of the BASHD-TOCSY spectrum of the disulfide

form of Ac-Cys-Sar-(His)$_2$-(Ala)$_3$-Cys-NH$_2$, together with the corresponding region of

the 1-D spectrum plotted across the top. The bottom of Figure 3.4 shows the same NH

(F$_1$)-full (F$_2$) region of the TOCSY spectrum in Figure 3.3 to illustrate the higher

resolution achieved with the BASHD-TOCSY experiment. Plotted in Figure 3.5 are

subspectra obtained by taking traces through the backbone amide NH resonancces in the

BASHD-TOCSY spectrum in Figure 3.4 at the indicated chemical shifts. Each 1-D

subspectrum shown represents a fingerprint of the amino acid residue in the hybrid. By

comparing with literature chemical shift values, identities of all of amino acid residues of

both cis and trans isomers of the disulfide form of Ac-Cys-Sar-(His)$_2$-(Ala)$_3$-Cys-NH$_2$

were determined.

With the identities of the amino acid residues giving the amide NH resonances in

hand, the next step was to identify resonances of the cis and trans configurational

isomers. The trans conformation across the Cys-Sar peptide bond of the disulfide form of

Ac-Cys-Sar-(His)$_2$-(Ala)$_3$-Cys-NH$_2$ was established by the pair of negative (through

space) NOE cross peaks at 3.192 ppm (F$_1$), 5.123 ppm (F$_2$) and 5.123 ppm (F$_1$), 3.192

ppm (F$_2$) between the Cys^1 C$_\alpha$H and Sar^2 CH$_3$ protons in the ROESY spectrum in Figure

3.6. Also plotted in Figure 3.6 is the corresponding region of the 1-D spectrum. NOE
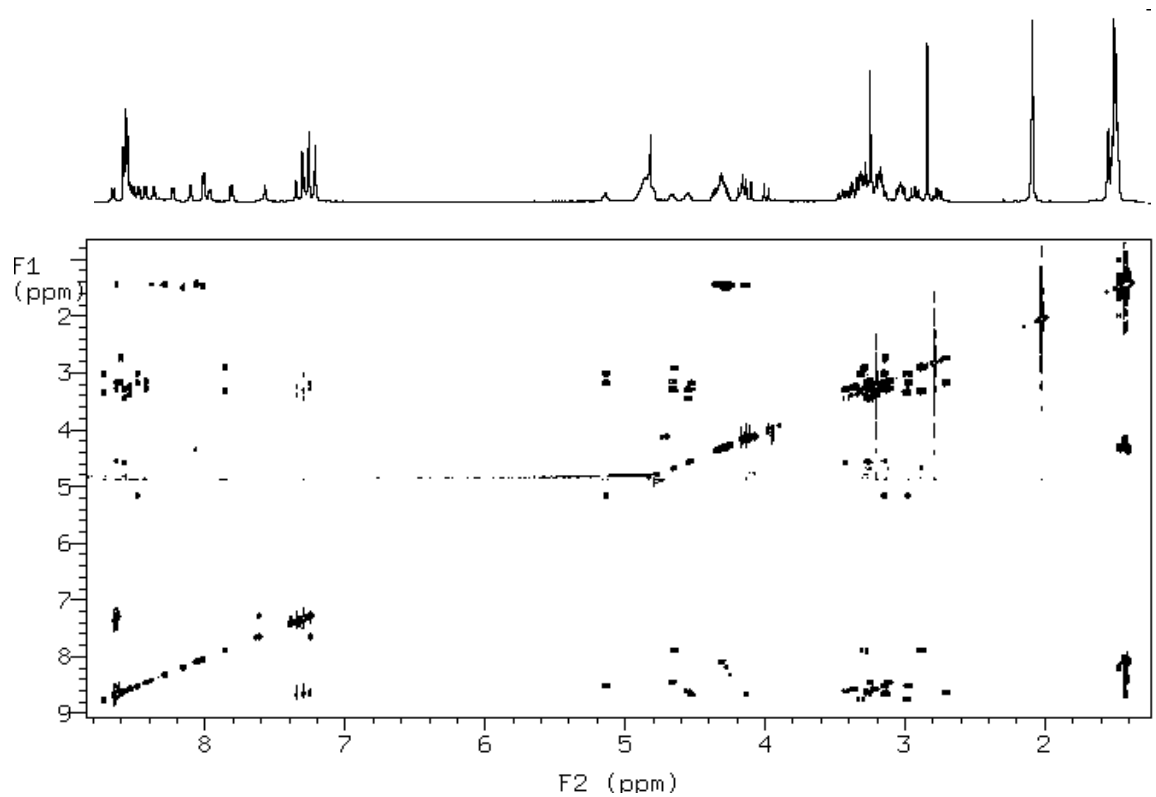
Figure 3.3. The full 2-D TOCSY spectrum of the disulfide form of Ac-Cys-Sar-(His)$_2$-(Ala)$_3$-Cys-NH$_2$ in 90% H$_2$O/10% D$_2$O at pH 2.99 and 25 ^{o}C.
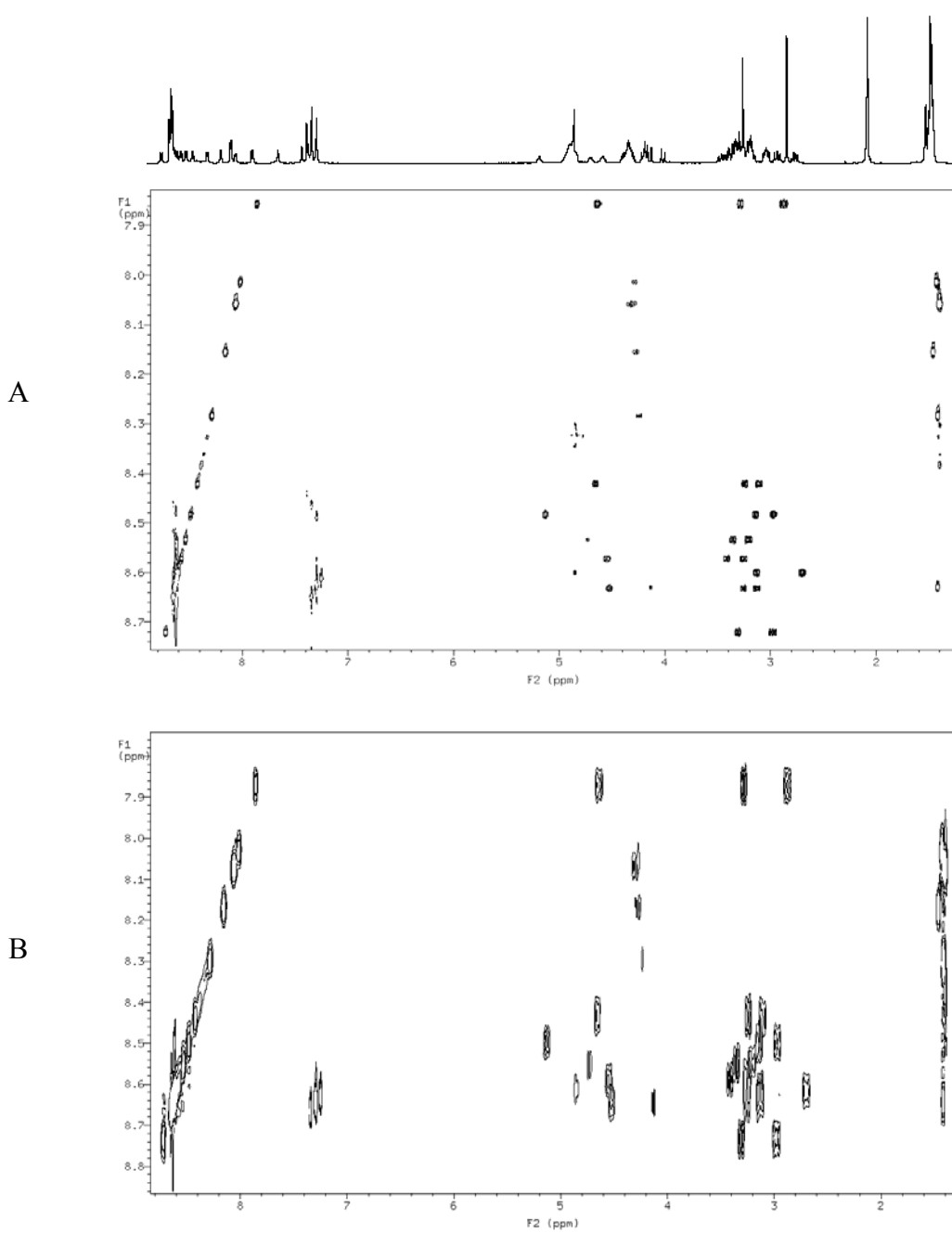
Figure 3.4. The NH (F_1)-full (F_2) region of (A) the BASHD-TOCSY spectrum of the disulfide form of Ac-Cys-Sar-(His)$_2$-(Ala)$_3$-Cys-NH$_2$ in 90% H$_2$O/10% D$_2$O at pH 2.99 and 25 ^{o}C, measured with F_1-band selection and F_1-homonuclear decoupling of the NH region. (B) Portion of the TOCSY spectrum in Figure 3.3 of the same peptide/peptoid hybrid solution.
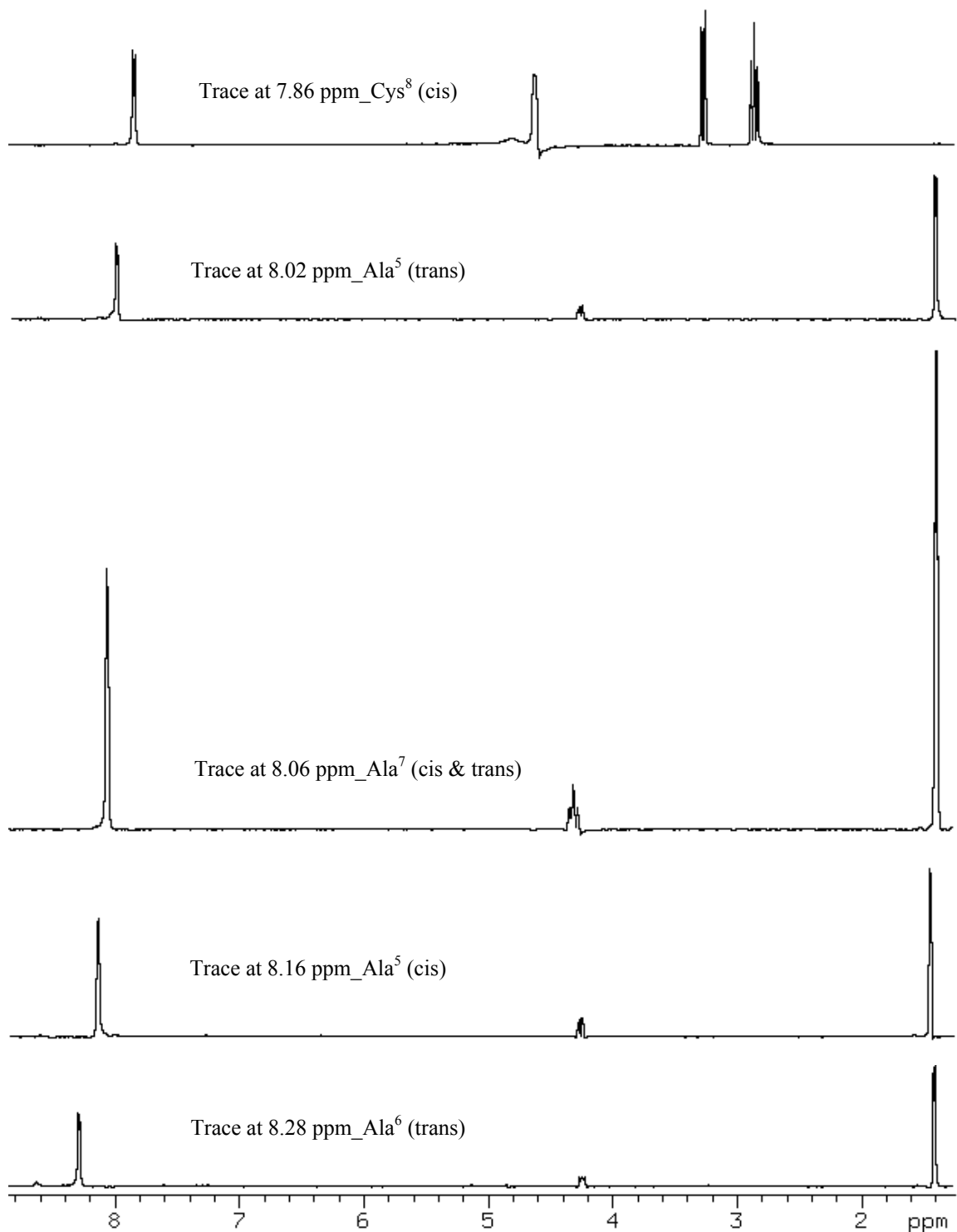
Figure 3.5. Subspectra obtained by taking traces through the backbone amide NH resonancces in the BASHD-TOCSY spectrum shown in Figure 3.4 at the indicated chemical shifts in the F_1 dimension. Traces were plotted using the same scale.

Trace at 8.42 ppm_Cys^8 (trans)

Trace at 8.48 ppm_Cys^1 (trans)

Trace at 8.53 ppm_His^4 (cis)

Trace at 8.57 ppm_His^4 (trans)

Amide NH resonance for Cys^1 (cis) plus the H$_2$ resonance for His^3 (trans)

Trace at 8.60 ppm_Cys^1 (cis)

Amide NH resonances for His^3 (trans) & Ala^6 (cis) plus the H$_2$ resonance for His^3 (cis)

Trace at 8.63 ppm_His^3 (trans) & Ala^6 (cis)

Trace at 8.72 ppm_His^3 (cis)
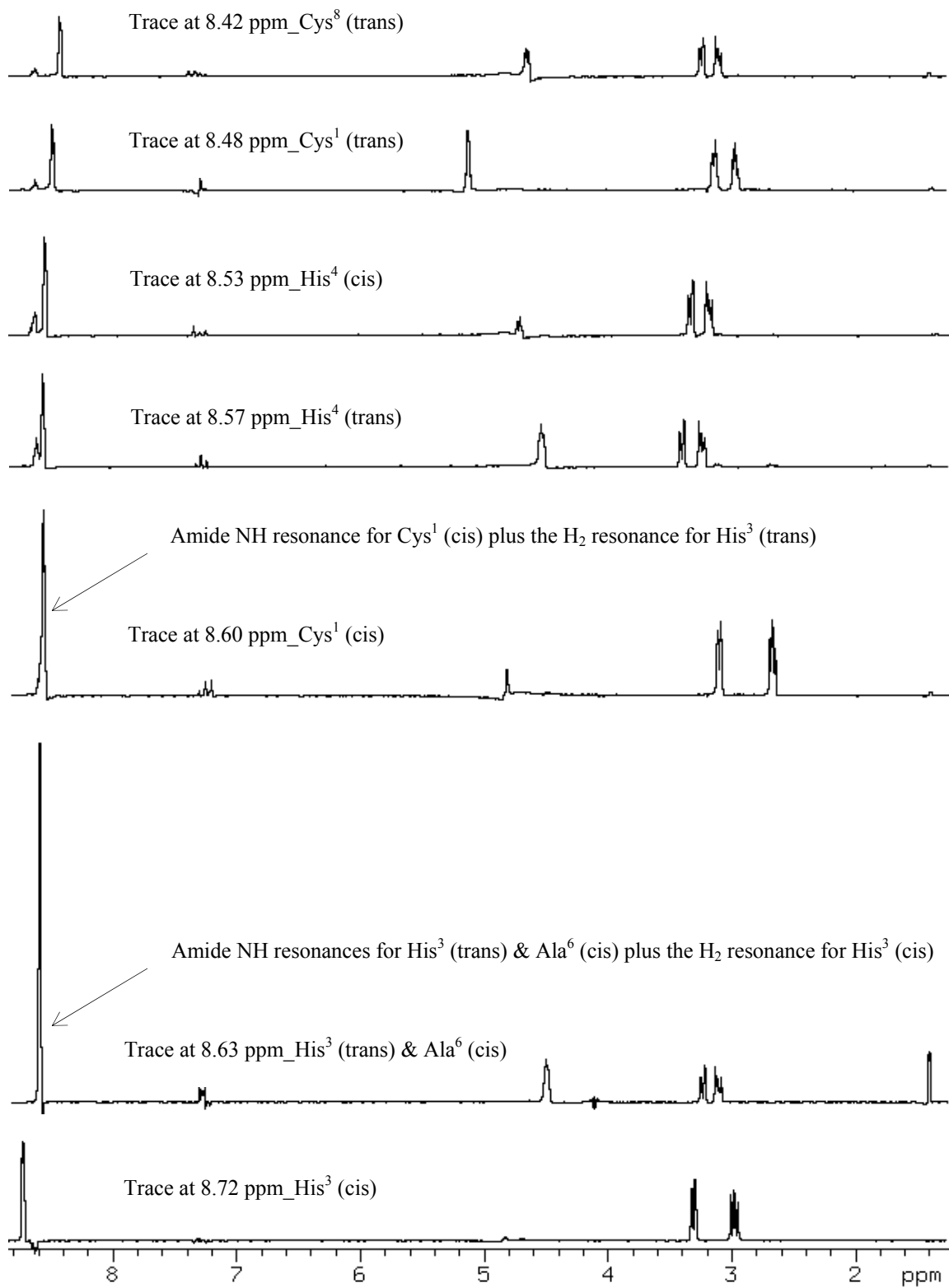
Figure 3.5. (Continued)
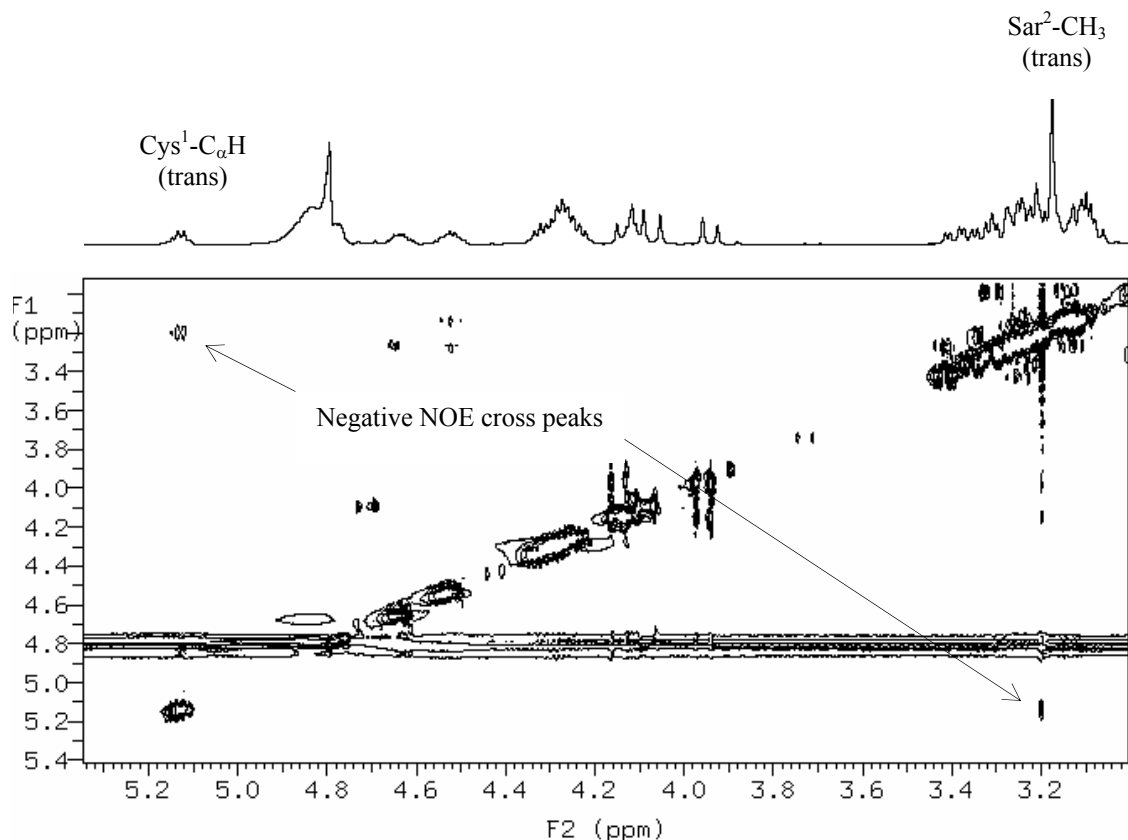
Figure 3.6. A portion of the ROESY spectrum (bottom) of the disulfide form of Ac-Cys-Sar-(His)$_2$-(Ala)$_3$-Cys-NH$_2$ in 90% H$_2$O/10% D$_2$O at pH 2.99 and 25 ^{o}C with the corresponding region of the 1-D spectrum plotted across the top. Negative NOE cross peaks between the Cys[1] C$_\alpha$H resonance at 5.123 ppm and the Sar[2] CH$_3$ resonance at 3.192 ppm establishes that these two resonances are for the configurational isomer having the trans conformation across the Cys[1]-Sar[2] peptide bond.

cross peaks between the Cys^1 C$_\alpha$H and Sar^2 CH$_3$ resonances indicate that the amide NH resonance at 8.480 ppm in Figure 3.2 is for the trans isomer of Cys^1 NH, as evidenced by the TOCSY cross peak between the Cys^1 C$_\alpha$H and Cys^1 NH.

The 1.8-2.2 ppm region of the 1-D spectrum of the disulfide form of Ac-Cys-Sar-(His)$_2$-(Ala)$_3$-Cys-NH$_2$ is shown at the top of Figure 3.7. There are two resonances, a strong resonance at 2.005 ppm and a less intense resonance at 2.011 ppm. The two resonances are for the N-terminal acetyl methyl protons. The less intense acetyl methyl resonance is for the trans isomer, as evidenced by the cross peak for the acetyl CH$_3$-Cys^1 NH NOE connectivity at 8.480 ppm (F$_1$) and 2.011 ppm (F$_2$) shown in the amide NH-acetyl CH$_3$ portion of the 2-D ROESY spectrum plotted at the bottom of Figure 3.7. The resonances at 2.005 ppm and 2.011 ppm are connected by chemical exchange, as evidenced by the magnetization-transfer data obtained at 65 °C in Figure 3.8. Magnetization transfer experiments are discussed in detail in Sections 3.2.3 and 3.2.4. This fact confirms that the more intense acetyl methyl resonance at 2.005 ppm corresponds to the cis isomer. The amide NH resonance at 8.600 ppm in Figure 3.7 therefore corresponds to the cis isomer of Cys^1 NH, as evidenced by the cross peak at 8.600 ppm (F$_1$) and 2.005 ppm (F$_2$).

Positive (exchange) cross peaks between the strong resonance of Sar CH$_3$ at 2.777 ppm and the weaker resonance of Sar CH$_3$ at 3.192 ppm in Figure 3.9 provide further evidence that the cis and trans isomers are in a dynamic equilibrium. The cis conformation across the Cys-Sar peptide bond of the disulfide form of Ac-Cys-Sar-(His)$_2$-(Ala)$_3$-Cys-NH$_2$ theoretically can be established using negative NOE cross peaks
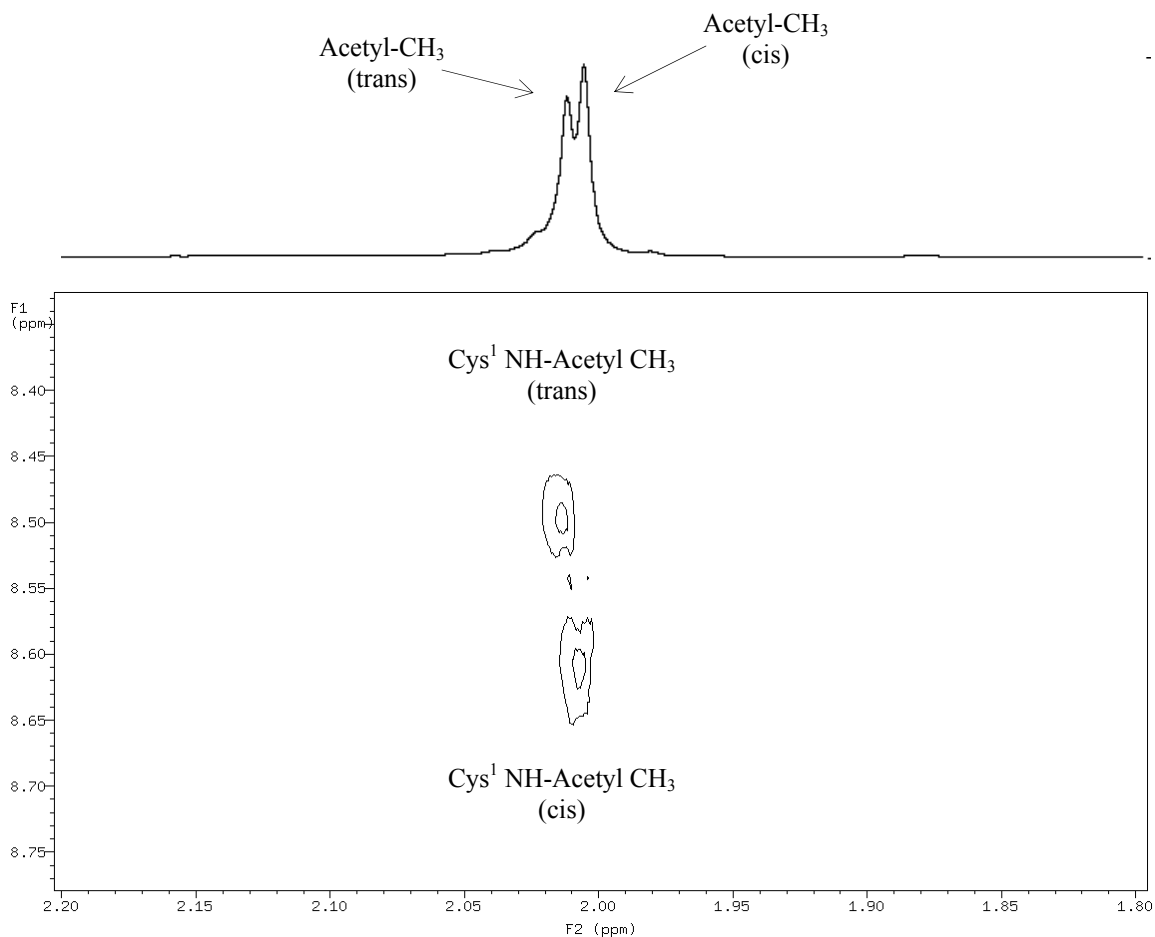
Figure 3.7. The NH-acetyl CH_3 region of the ROESY spectrum of the disulfide form of Ac-Cys-Sar-(His)$_2$-(Ala)$_3$-Cys-NH$_2$ in 90% H_2O/10% D_2O at pH 2.99 and 25 ^{o}C. The acetyl methyl protons region of the 1-D spectrum measured by the single pulse method is plotted across the top. The top negative NOE was observed between the trans resonance for the acetyl methyl protons at 2.011 ppm and the trans resonance for the Cys[1]-NH proton at 8.480 ppm. The bottom negative NOE was between the cis resonance for the acetyl methyl protons at 2.005 ppm and the cis resonance for the Cys[1]-NH proton at 8.600 ppm.

0.0001 0.001 0.01 0.05 0.1 0.15 0.2 0.25 0.3 0.4 0.5 0.6 0.8 1 1.5 2 2.5 3 4 5 8
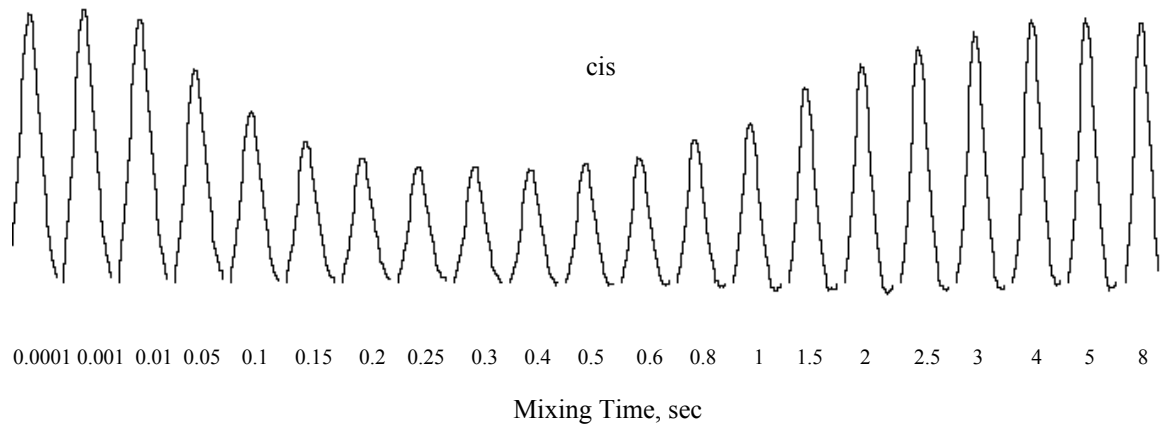
Mixing Time, sec

Figure 3.8. Intensity of the resonance assigned to the acetyl methyl protons of the cis isomer of the disulfide form of Ac-Cys-Sar-(His)$_2$-(Ala)$_3$-Cys-NH$_2$ as a function of the length of the mixing time, obtained from the inversion-magnetization transfer experiment. The data are for 6 mM disulfide Ac-Cys-Sar-(His)$_2$-(Ala)$_3$-Cys-NH$_2$ in 90% H$_2$O/10% D$_2$O at pH 2.99 and 65 $^{\circ}$C.
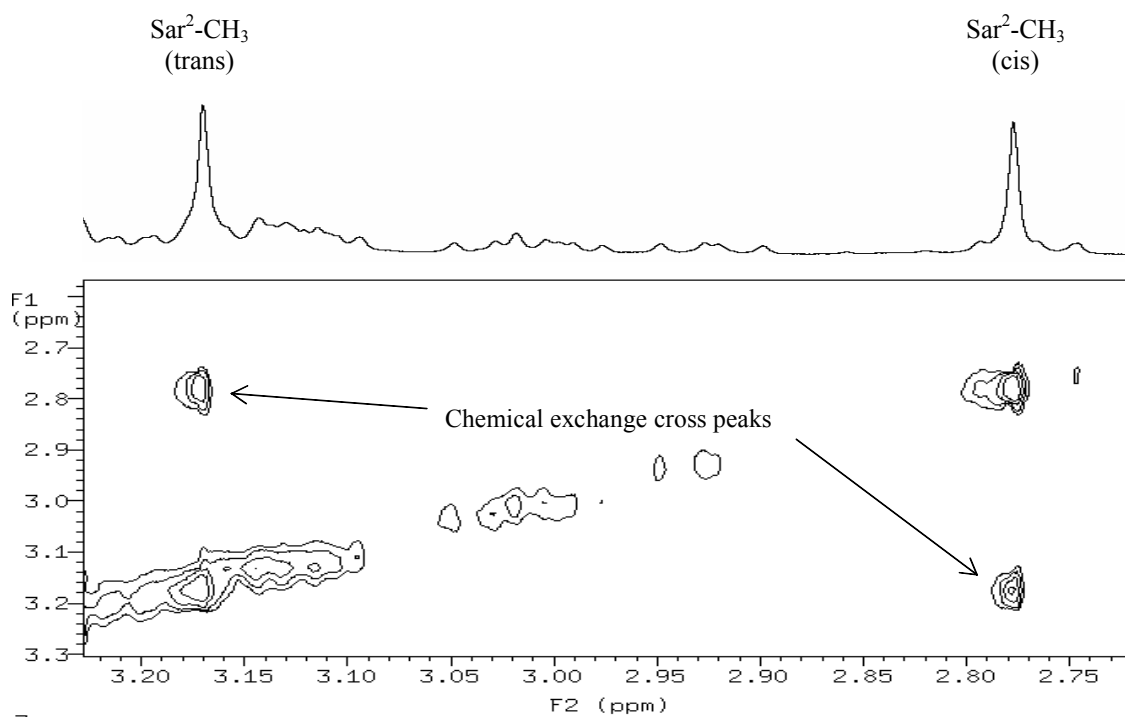
Figure 3.9. A portion of the ROESY spectrum of the disulfide form of Ac-Cys-Sar-$(His)_2$-$(Ala)_3$-Cys-NH_2 in 90% H_2O/10% D_2O at pH 2.99 and 65 ^{o}C. The chemical exchange cross peaks between Sar^2 CH_3 resonances for the cis and trans isomers are labeled with arrows. The cross peaks provide evidence that the cis and trans isomers across the Cys-Sar peptide bond are in a dynamic equilibrium.

between the Cys[1] C$_\alpha$H and Sar[2] C$_\alpha$H resonances (see Figure 3.1). However, for this particular hybrid, the expected NOE between the resonances at 4.850 ppm and 4.080 ppm is not detected because the Cys[1] C$_\alpha$H resonance is close to the water resonance and thus its intensity is suppressed by presaturation.

The completed sequential assignments for the identified amino acids from the TOCSY spectrum for both cis and trans isomers of the disulfide form of Ac-Cys-Sar- (His)$_2$-(Ala)$_3$-Cys-NH$_2$ were achieved using dipolar (negative) cross peaks obtained from both the ROESY and BASHD-ROESY spectra. The spectral resolution in the C$_\alpha$H-NH region of the 2-D ROESY spectrum in Figure 3.10 was increased significantly with the use of the BASHD-ROESY experiment as a result of an increase in the digital resolution in the F$_1$ dimension due to band selection of both the backbone amide NH and C$_\alpha$H regions together with the collapse of multiplets to singlets. Figure 3.11 shows the NH (F$_1$)-C$_\alpha$H (F$_2$) region of the BASHD-ROESY spectrum, measured with F$_1$-band selection and F$_1$-homonuclear decoupling of the NH region. Figure 3.12 shows the C$_\alpha$H (F$_1$)-NH (F$_2$) region of the BASHD-ROESY spectrum, measured with F$_1$-band selection and F$_1$-homonuclear decoupling of the C$_\alpha$H region.

The sequential assignment of resonances for the cis isomer of the disulfide form of Ac-Cys-Sar-(His)$_2$-(Ala)$_3$-Cys-NH$_2$ begins with the acetyl resonance for the cis isomer, which was established by a negative NOE at 8.600 ppm (F$_1$) and 2.005 ppm (F$_2$) in Figure 3.7. The Cys[1]-Sar[2] connectivity was not established because the expected cross peak for the Cys[1] C$_\alpha$H-Sar[2] C$_\alpha$H NOE connectivity at 4.850 ppm (F$_1$) and 4.080 ppm (F$_2$) was not detected, as discussed above. The presence of the cross peak at 4.080 ppm (F$_1$)
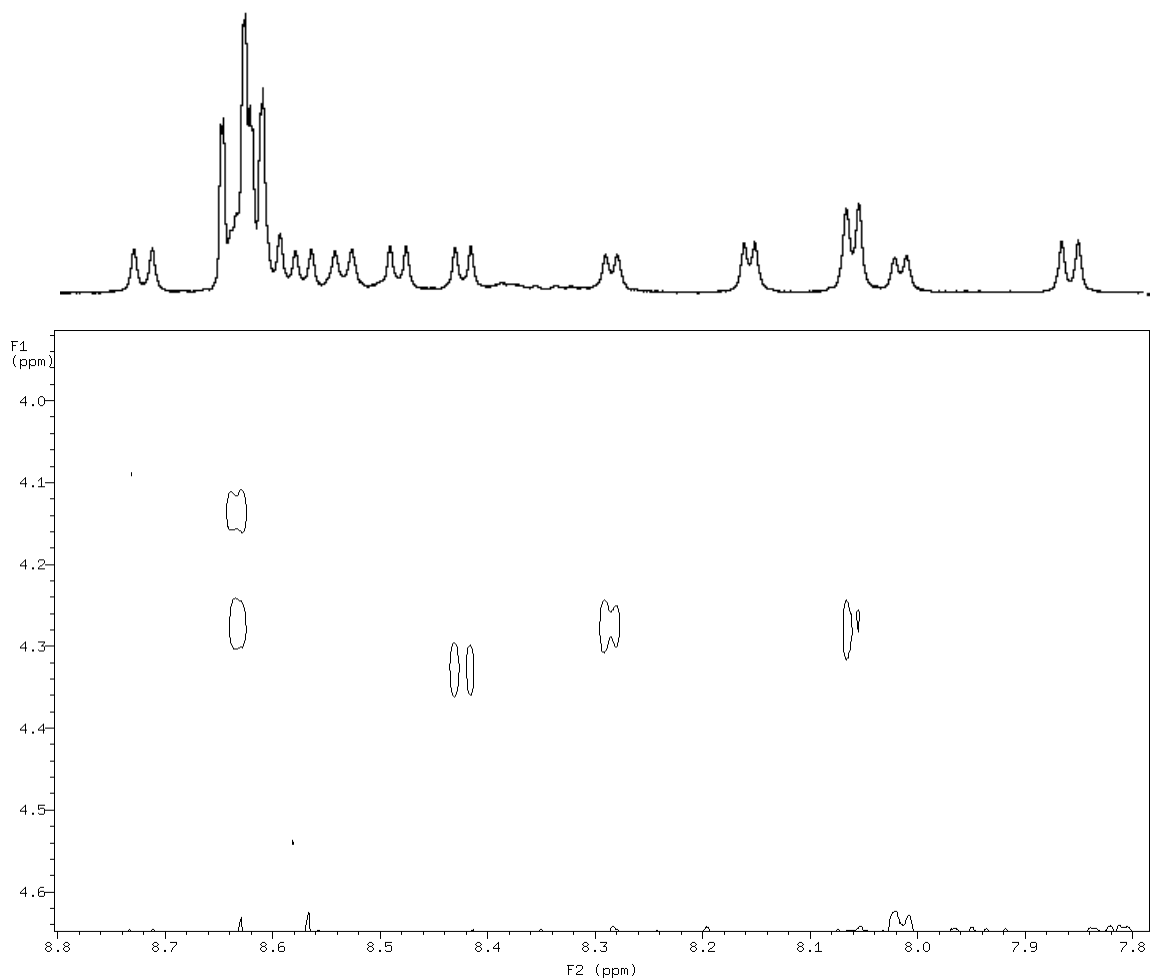
Figure 3.10. The $C_\alpha H$ (F_1)-NH (F_2) region of the ROESY spectrum of the disulfide form of Ac-Cys-Sar-(His)$_2$-(Ala)$_3$-Cys-NH$_2$ in 90% H$_2$O/10% D$_2$O at pH 2.99 and 25 ^{o}C with the corresponding region of the 1-D spectrum plotted across the top.
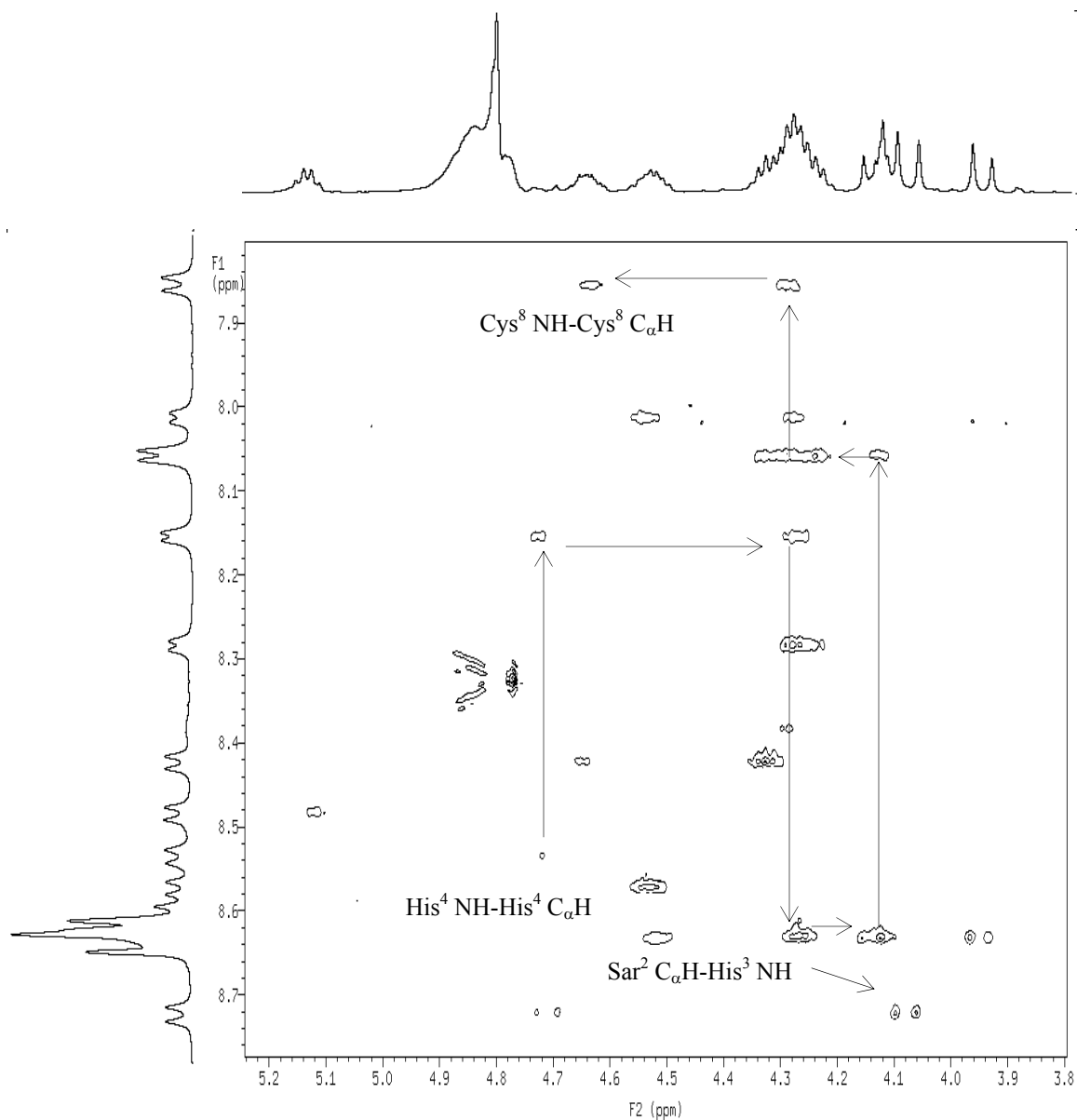
Figure 3.11. The NH (F_1)-C_αH (F_2) region of the BASHD-ROESY spectrum of the disulfide form of Ac-Cys-Sar-(His)$_2$-(Ala)$_3$-Cys-NH$_2$ in 90% H$_2$O/10% D$_2$O at pH 2.99 and 25 ^{o}C, measured with F_1-band selection and F_1-homonuclear decoupling of the NH region, showing the sequential connectivity traced out by the NH- C_αH cross peaks for the cis isomer.
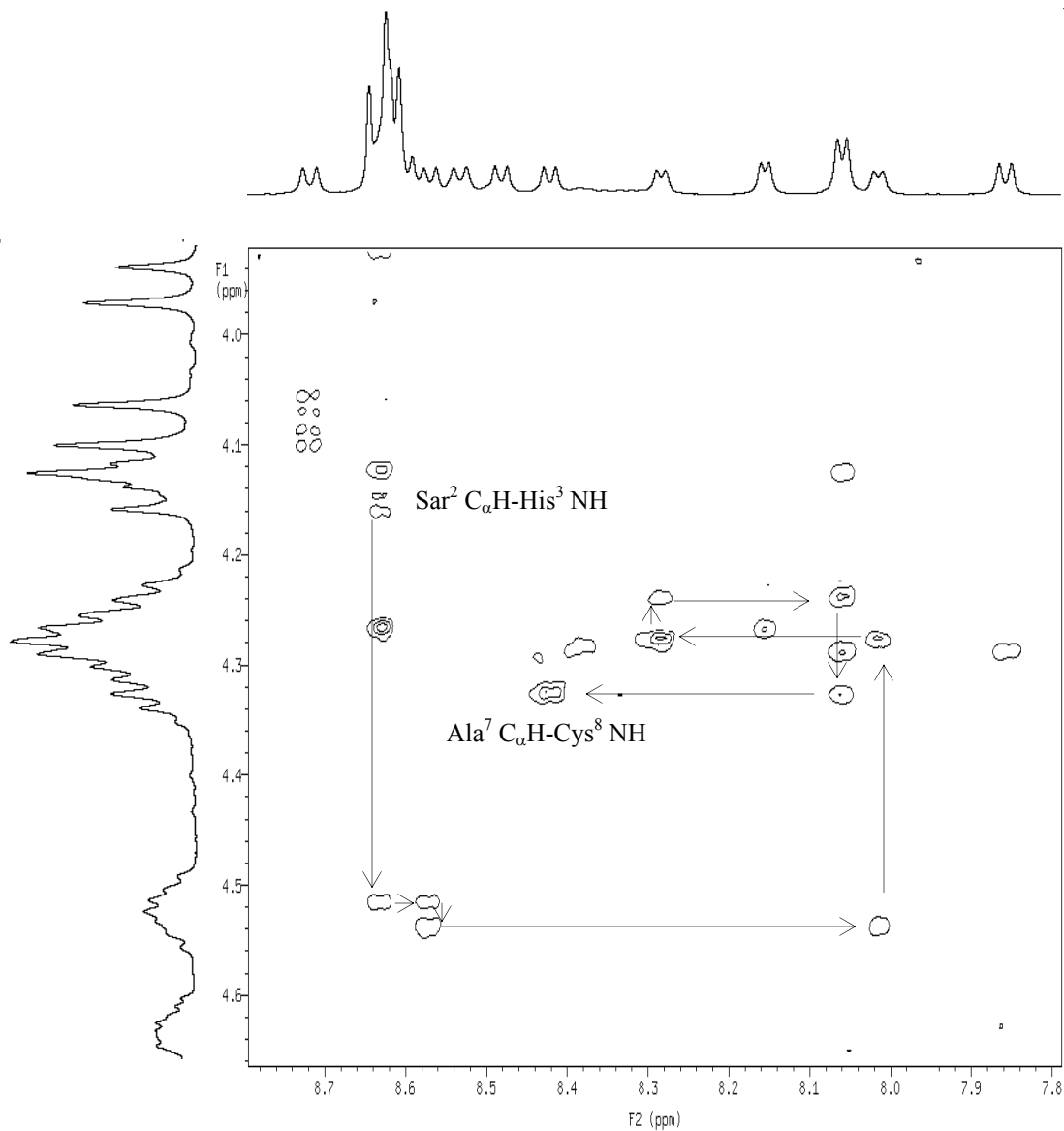
Figure 3.12. The $C_\alpha H$ (F_1)-NH (F_2) region of the BASHD-ROESY spectrum of the disulfide form of Ac-Cys-Sar-(His)$_2$-(Ala)$_3$-Cys-NH$_2$ in 90% H$_2$O/10% D$_2$O at pH 2.99 and 25 $^\circ$C, measured with F_1-band selection and F_1-homonuclear decoupling of the $C_\alpha H$ region, showing the sequential connectivity traced out by the NH- $C_\alpha H$ cross peaks for the trans isomer.

and 8.720 ppm (F_2) for the Sar^2 C$_\alpha$H-His^3 NH NOE connectivity in Figure 3.11 established the Sar^2-His^3 connectivity. The His^3-His^4 connectivity was not established because the intensity of the C$_\alpha$H resonance of His^3 at 4.821 ppm was suppressed by presaturation. The sequential connectivity beginning with His^4 NH-His^4 C$_\alpha$H and ending with Cys^8 NH-Cys^8 C$_\alpha$H can be found in Figure 3.11.

The sequential assignment of resonances for the trans isomer of the disulfide form of Ac-Cys-Sar-(His)$_2$-(Ala)$_3$-Cys-NH$_2$ begins with the acetyl-Cys^1 NH sequential connectivity, which was established by a negative NOE at 8.480 ppm (F_1) and 2.011 ppm (F_2) in Figure 3.7. The Cys^1-Sar^2 connectivity was assigned by the pair of cross peaks at 3.192 ppm (F_1), 5.123 ppm (F_2) and 5.123 ppm (F_1), 3.192 ppm (F_2) between Cys^1 C$_\alpha$H and Sar^2 CH$_3$ in Figure 3.6. The sequential connectivity of Sar^2 to His^3 was established by the cross peaks at 3.951 ppm (F_1), 8.628 ppm (F_2) and 4.141 ppm (F_1), 8.628 ppm (F_2) for the Sar^2 C$_\alpha$H-His^3 NH NOE connectivity in Figure 3.12. It should be noted that there are two protons bonded to the alpha-carbon of sarcosine residue, which are coupled to each other giving rise to the two doublets of an AB pattern. The sequential connectivity beginning with Sar^2 C$_\alpha$H-His^3 NH and ending with Ala^7 C$_\alpha$H-Cys^8 NH is diagramed in Figure 3.12.

Resonances assignments for all protons of the cis and trans isomers of the disulfide form of Ac-Cys-Sar-(His)$_2$-(Ala)$_3$-Cys-NH$_2$ in 90% H$_2$O/10% D$_2$O at pH 2.99 and 25 °C are reported in Table 3.4.

Residue	NH amide	αH	βH	Others
Cys^1(trans)	8.480	5.123	3.134, 2.962	
Sar^2(trans)		4.141, 3.951		N(CH$_3$) 3.192
His^3(trans)	8.628	4.516	3.247, 3.121	H$_2$ 8.610
				H$_4$ 7.243
His^4(trans)	8.571	4.538	3.407, 3.245	H$_2$ 8.619
				H$_4$ 7.293
Ala^5(trans)	8.012	4.277	1.421	
Ala^6(trans)	8.281	4.236	1.407	
Ala^7(trans)	8.055	4.325	1.385	
Cys^8(trans)	8.419	4.645	3.235, 3.100	
Acetyl CH$_3$(trans)				2.011
Amide NH$_2$ (trans)				N(H$_2$) 7.609, 7.322
Cys^1(cis)	8.600	4.850	3.123, 2.691	
Sar^2(cis)		4.080		N(CH$_3$) 2.777
His^3(cis)	8.720	4.821	3.302, 2.972	H$_2$ 8.623
				H$_4$ 7.286
His^4(cis)	8.532	4.723	3.347, 3.200	H$_2$ 8.648
				H$_4$ 7.341
Ala^5(cis)	8.153	4.266	1.452	
Ala^6(cis)	8.626	4.124	1.408	
Ala^7(cis)	8.053	4.287	1.397	
Cys^8(cis)	7.854	4.629	3.277, 2.866	
Acetyl CH$_3$(cis)				2.005
Amide NH$_2$ (cis)				N(H$_2$) 7.385, 7.242

Table 3.4. Assignment of proton resonances for the disulfide form of Ac-Cys-Sar-(His)$_2$-(Ala)$_3$-Cys-NH$_2$ in 90 % H$_2$O/10 % D$_2$O at pH 2.99 and 25 ^{o}C.

3.2.2 Equilibria of Cis/Trans Isomerization of Sarcosine-Containing Peptide/Peptoid Hybrids

In the previous section, evidence was presented demonstrating that sarcosine-containing peptide/peptoid hybrids exist in solution as a mixture of cis and trans isomers across the C-N bond of the Xaa-Sar peptide bond. Equilibrium constants (K_{eq} = [trans]/[cis]) for cis/trans isomerization for all the peptide/peptoid hybrids reported in this chapter were determined and are summarized in Tables 3.5, 3.6 and 3.7. The relative concentration of the cis and trans isomers was determined from the relative integrated intensities of a cis/trans pair of resonances (Tables 3.1, 3.2 and 3.3). The resonance intensities were obtained from the single pulse spectrum. For instance, the populations of the cis and trans isomers of the disulfide form of Ac-Cys-Sar-(His)$_2$-(Ala)$_3$-Cys-NH$_2$ were calculated to be 51.8% and 48.2%, respectively, using these relative populations in the standard 1-D ^{1}H NMR spectrum at 25 °C in Figure 3.2. The equilibrium constant was calculated to be 0.93.

3.2.3 Interconversion of the Cis and Trans Isomers of Sarcosine-Containing Peptide/Peptoid Hybrids by Chemical Exchange

The kinetics of interconversion between the cis and trans isomers by rotation around the Xaa-Sar peptide bond for the three series of peptide/peptoid hybrids were studied using NMR inversion-magnetization transfer experiments. The magnetization transfer data obtained are then used to characterize the dynamics of cis/trans isomerization as will be discussed in the next section.

To determine rate constants for Xaa-Sar cis/trans isomerization by the inversion-

Hybrids	K_{eq}	% cis	k_{ct}, s^{-1}	k_{tc}, s^{-1}	$\Delta H_{ct}^{\ddagger}$ kcal.mol^{-1}	$\Delta S_{ct}^{\ddagger}$ cal.mol^{-1}K^{-1}	$\Delta G_{ct}^{\ddagger}$ kcal.mol^{-1}
1a	3.74±0.04	21.1%	0.153±0.005	0.041±0.001	15.5±0.3	-10.2±0.9	18.5±0.3
1b	0.93±0.01	51.8%	0.041±0.006	0.044±0.001	19.8±0.5	1.4±0.4	19.4±0.5
2a	3.22±0.02	23.7%	0.175±0.008	0.054±0.003	13.5±0.3	-16.7±0.9	18.5±0.3
2b	0.79±0.01	55.9%	0.050±0.003	0.063±0.003	15.1±1.1	-13.5±3.5	19.1±1.1
3a	2.89±0.02	25.7%	0.269±0.014	0.093±0.005	8.2±1.1	-33.6±3.4	18.2±1.1
3b	1.16±0.01	46.2%	0.038±0.003	0.033±0.003	19.5±0.2	0.3±0.5	19.4±0.2
4a	3.57±0.03	21.9%	0.129±0.010	0.061±0.003	12.8±0.5	-18.7±1.4	18.4±0.5
4b	0.53±0.01	65.5%	0.114±0.008	0.217±0.015	10.3±1.1	-26.9±3.4	18.3±1.1
5a	3.39±0.03	22.8%	0.138±0.004	0.041±0.001	15.5±0.1	-10.6±0.1	18.7±0.1
5b	0.34±0.02	74.4%	0.019±0.001	0.055±0.002	17.1±0.9	-7.0±2.6	19.2±0.9
6a	3.35±0.04	23.0%	0.104±0.007	0.031±0.002	17.6±0.2	-3.9±0.6	18.8±0.2
6b	0.45±0.01	69.1%	0.037±0.003	0.082±0.007	15.2±1.3	-12.6±3.8	19.0±1.3

Table 3.5. Equilibrium constants, population of the cis conformation, rate constants, and activation parameters for cis/trans isomerization of the Cys-Sar peptide bond for hybrids in Table 3.2. The rate and equilibrium constants and ΔG are for 25 ^{o}C. Rate constants were obtained by extrapolation to 25 ^{o}C using the activation parameters determined from the rate data measured at higher temperature.

Hybrids	K_{eq}	% cis	k_{ct}, s^{-1}	k_{tc}, s^{-1}	$\Delta H_{ct}^{\ddagger}$ kcal.mol^{-1}	$\Delta S_{ct}^{\ddagger}$ cal.mol^{-1}K^{-1}	$\Delta G_{ct}^{\ddagger}$ kcal.mol^{-1}
7a	3.27±0.03	23.4%	0.150±0.020	0.046±0.006	15.1±0.8	-11.0±2.0	18.0±1.0
7b	0.52±0.01	66.0%	0.047±0.005	0.091±0.010	15.2±0.6	-12.0±2.0	18.8±1.0
8a	2.70±0.02	27.0%	0.160±0.009	0.059±0.003	13.8±0.3	-15.8±0.8	18.5±0.3
8b	1.21±0.01	45.2%	0.054±0.002	0.045±0.002	18.3±0.7	-3.0±2.3	19.2±0.7
9a	2.76±0.03	26.6%	0.134±0.008	0.049±0.003	14.6±0.7	-13.5±2.1	18.6±0.7
9b	1.56±0.01	39.0%	0.061±0.003	0.039±0.002	18.2±0.2	-3.1±0.6	19.1±0.2
10a	2.82±0.02	26.2%	0.192±0.010	0.068±0.004	11.5±3.0	-23.4±9.4	18.5±3.0
10b	1.47±0.01	40.5%	0.108±0.004	0.073±0.003	14.8±0.3	-13.4±0.8	18.8±0.3
11a	2.91±0.03	25.6%	0.147±0.009	0.051±0.003	13.7±0.1	-16.5±0.4	18.6±0.1
11b	1.56±0.01	39.1%	0.103±0.003	0.066±0.002	15.7±0.8	-10.5±2.3	18.8±0.8

Table 3.6. Equilibrium constants, population of the cis conformation, rate constants, and activation parameters for cis/trans isomerization of the Cys-Sar peptide bond for hybrids in Table 3.3. The rate and equilibrium constants and ΔG are for 25 ^{o}C. Rate constants were obtained by extrapolation to 25 ^{o}C using the activation parameters determined from the rate data measured at higher temperature.

Hybrids	K_{eq}	% cis	k_{ct}, s^{-1}	k_{tc}, s^{-1}	$\Delta H_{ct}^{\neq}$ kcal.mol^{-1}	$\Delta S_{ct}^{\neq}$ cal.mol^{-1}K^{-1}	$\Delta G_{ct}^{\neq}$ kcal.mol^{-1}
12a	3.20±0.02	23.8%	0.180±0.020	0.056±0.006	11.1±0.9	-25.0±3.0	18.6±1.0
12b	0.15±0.02	86.8%	0.004±0.001	0.025±0.004	22.6±0.6	10.0±2.0	19.6±0.8
13a	2.66±0.04	27.3%	0.081±0.003	0.030±0.001	16.1±0.3	-9.7±1.0	19.0±0.3
13b	1.21±0.05	45.2%	0.013±0.001	0.011±0.001	22.1±0.7	6.7±2.0	20.1±0.7
14a	2.39±0.04	29.5%	0.159±0.013	0.067±0.006	11.9±1.0	-22.4±3.1	18.6±1.0
14b	0.75±0.03	57.3%	0.031±0.002	0.041±0.003	19.0±0.8	-1.7±2.4	19.5±0.8
15a	2.44±0.03	29.1%	0.109±0.002	0.045±0.001	16.8±0.2	-6.7±0.7	18.8±0.2
15b	2.32±0.02	30.1%	0.137±0.004	0.059±0.002	16.6±0.1	-6.9±0.3	18.7±0.1
16a	3.17±0.05	24.0%	0.084±0.002	0.026±0.001	19.0±0.4	0.4±1.4	18.9±0.4
16b	6.63±0.08	13.1%	0.237±0.007	0.036±0.001	18.1±0.7	-0.6±2.2	18.3±0.7

Table 3.7. Equilibrium constants, population of the cis conformation, rate constants, and activation parameters for cis/trans isomerization across the Cys-Sar peptide bond for hybrids in Table 3.4. The rate and equilibrium constants, and ΔG are for 25 °C. Rate constants were obtained by extrapolation to 25 °C using the activation parameters determined from the rate data measured at higher temperature.

magnetization transfer method, a pair of well-resolved resonances for the cis and trans isomers is required. In the inversion-magnetization transfer experiment, the more intense resonance of the pair, which often is the trans isomer resonance, is selectively inverted, and the transfer of inversion to the less intense cis resonance is monitored. An example of spectra obtained with the inversion-magnetization transfer experiment for determination of cis/trans isomerization rate constants for the disulfide form of Ac-Cys-Sar-(His)$_2$-(Ala)$_3$-Cys-NH$_2$ in 90% H$_2$O/10% D$_2$O at pH 2.91 and 65 $^{\circ}$C are shown in Figure 3.13. The resonance for the sarcosine methyl protons of the trans isomer was inverted and the transfer of inversion to the resonance for the cis isomer was monitored as a function of the delay time in the pulse sequence, during which exchange between the cis and trans isomers takes place. It also should be noted that the dependence of the intensities of the cis and trans resonances on mixing time in Figure 3.13 provides the most conclusive evidence for the presence of cis and trans isomers with respect to the Xaa-Sar peptide bond.

It is interesting to note that exchange cross peaks that reflect cis/trans isomerization of the Cys-Sar amide bond are also observed for the Cys[1], Ala[5], Ala[6], and Cys[8] amide protons as well as for the amide NH$_2$ protons (see Figures 3.14 and 3.15). Resonances in Figures 3.14 and 3.15 are assigned to specific residues by following resonances assigned at 25 $^{\circ}$C as temperature is increased from 25 $^{\circ}$C to 65 $^{\circ}$C (Figures 3.16 and 3.17). It should be noted that resonances for the backbone amide NH and C-terminal NH$_2$ protons of the cis and trans isomers of the disulfide form of Ac-Cys-Sar-(His)$_2$-(Ala)$_3$-Cys-NH$_2$ in Figure 3.16 and 3.17 shift upfield with increasing temperature.

trans

cis

0.001 0.010 0.050 0.100 0.150 0.200 0.250 0.300 0.400 0.500 0.600 0.800 1.000 1.500 2.000 2.500 3.000 4.000 5.000 8.000
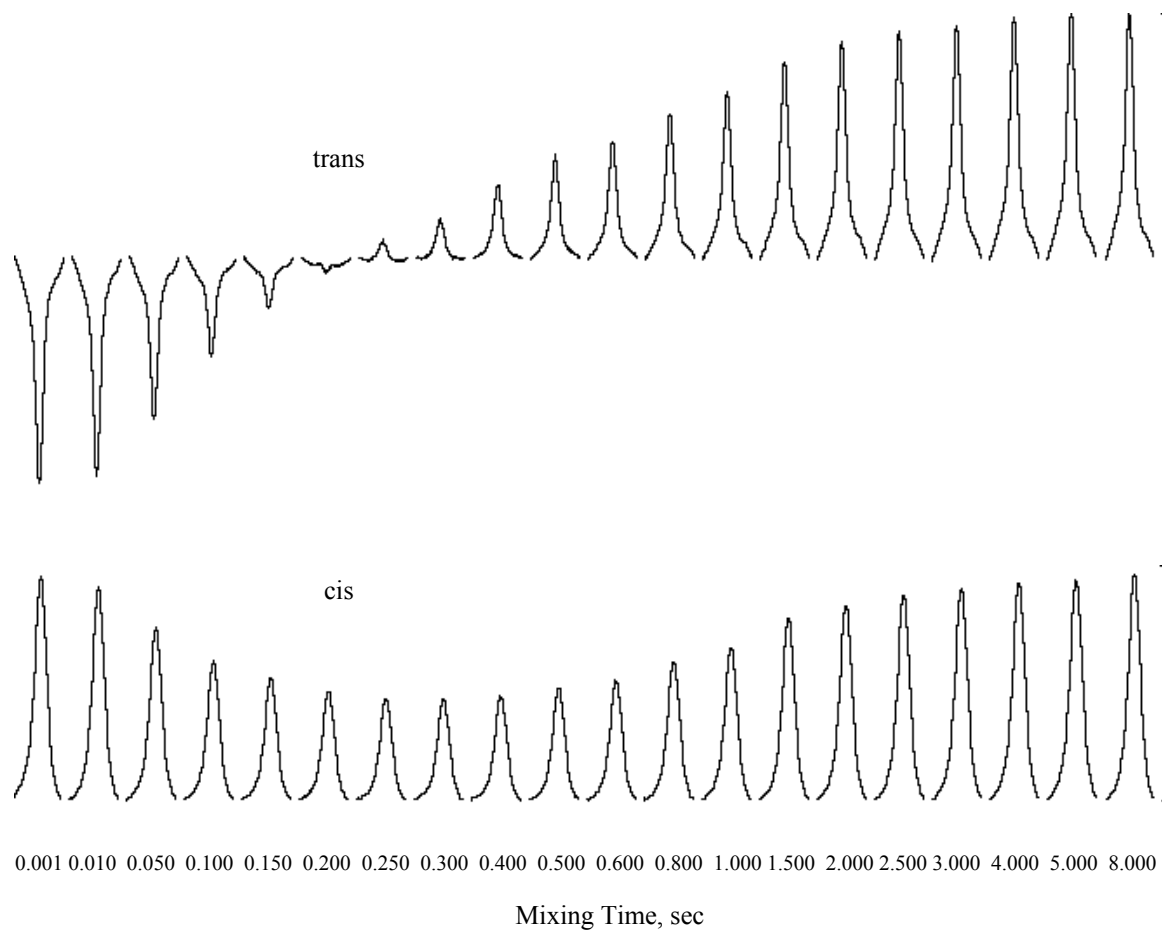
Mixing Time, sec

Figure 3.13. Intensities of the resonances for the sarcosine methyl protons of the cis and trans isomers of the disulfide form of Ac-Cys-Sar-$(His)_2$-$(Ala)_3$-Cys-NH_2 as a function of the length of the mixing time in the inversion-magnetization transfer experiment. The data are for 6 mM cyclic Ac-Cys-Sar-$(His)_2$-$(Ala)_3$-Cys-NH_2 in 90% H_2O/10% D_2O at pH 2.99 and 65 ^{o}C.
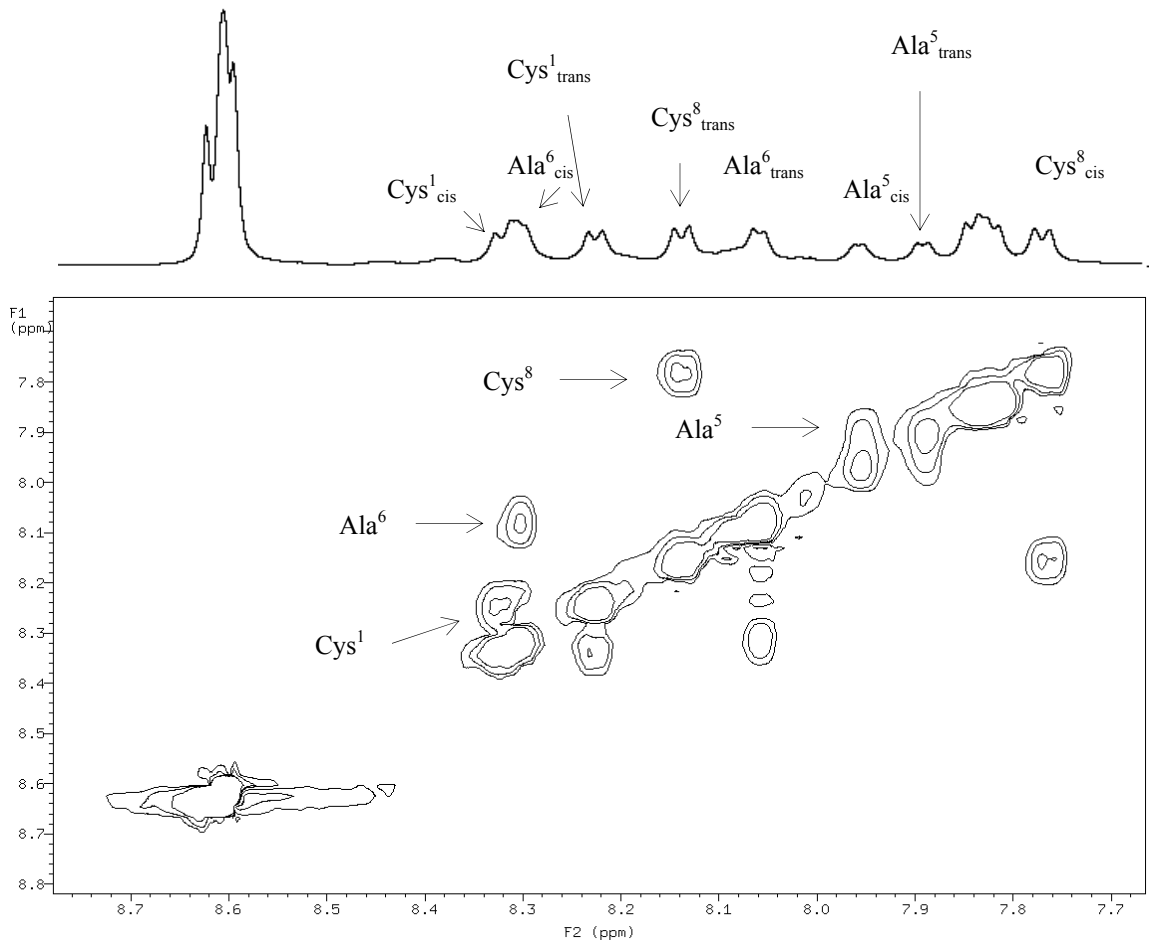
Figure 3.14. The amide NH proton region of the ROESY spectrum of Ac-Cys-Sar-(His)$_2$-(Ala)$_3$-Cys-NH$_2$ in 90% H$_2$O/10% D$_2$O at pH 2.99 and 65 °C. Only positive contours are plotted. The amide protons giving rise to the positive (exchange) cross peaks are identified. The corresponding region of the 1-D spectrum, measured by the single pulse method, is plotted across the top.
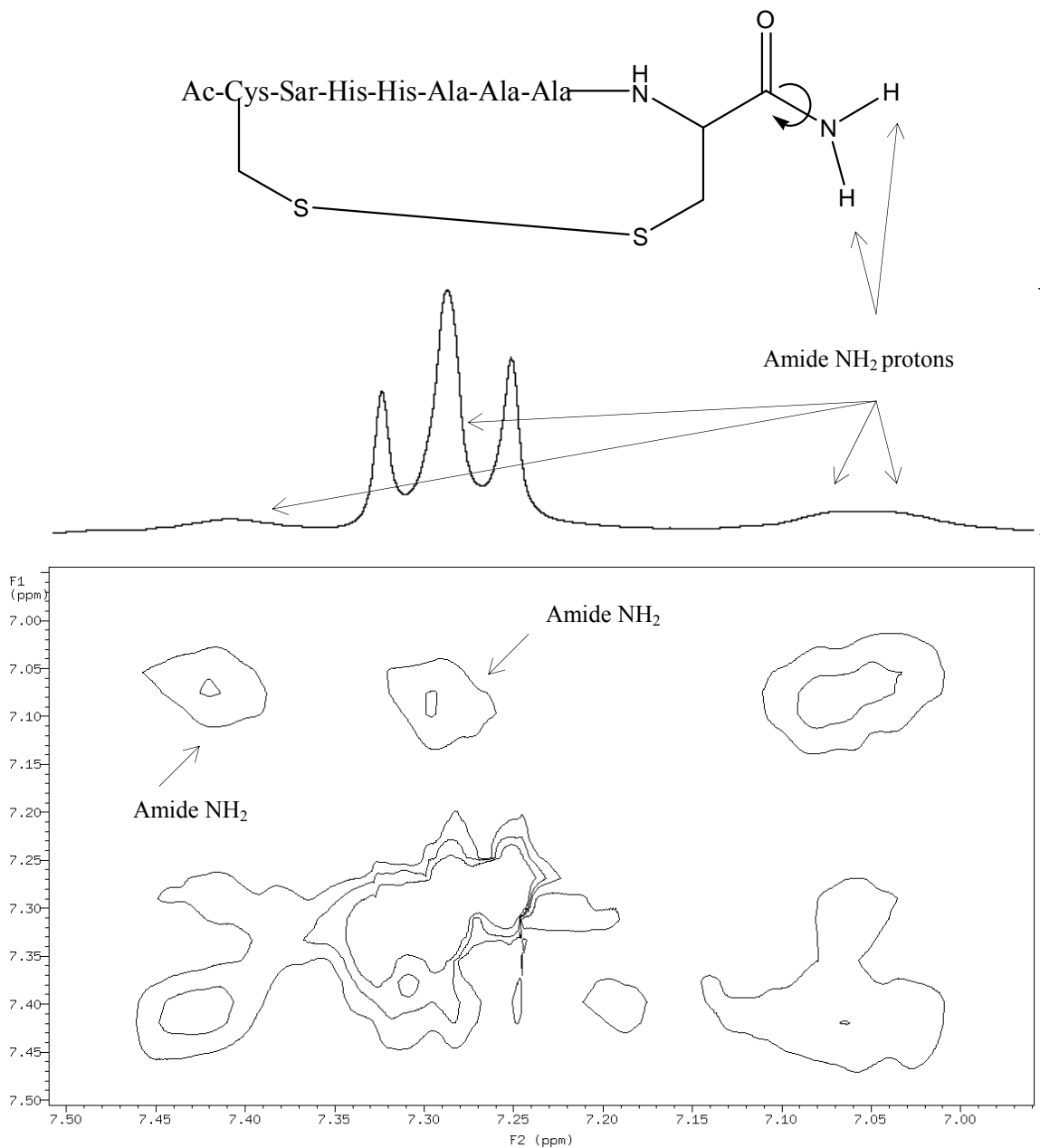
Figure 3.15. The aromatic region of the ROESY spectrum of Ac-Cys-Sar-(His)$_2$-(Ala)$_3$-Cys-NH$_2$ in 90% H$_2$O/10% D$_2$O at pH 2.99 and 65 °C. Only positive contours are plotted. The amide NH$_2$ protons at the carboxy terminus giving rise to the positive (exchange) cross peaks are identified. The corresponding region of the 1-D spectrum, measured by the single pulse method, is plotted across the top.
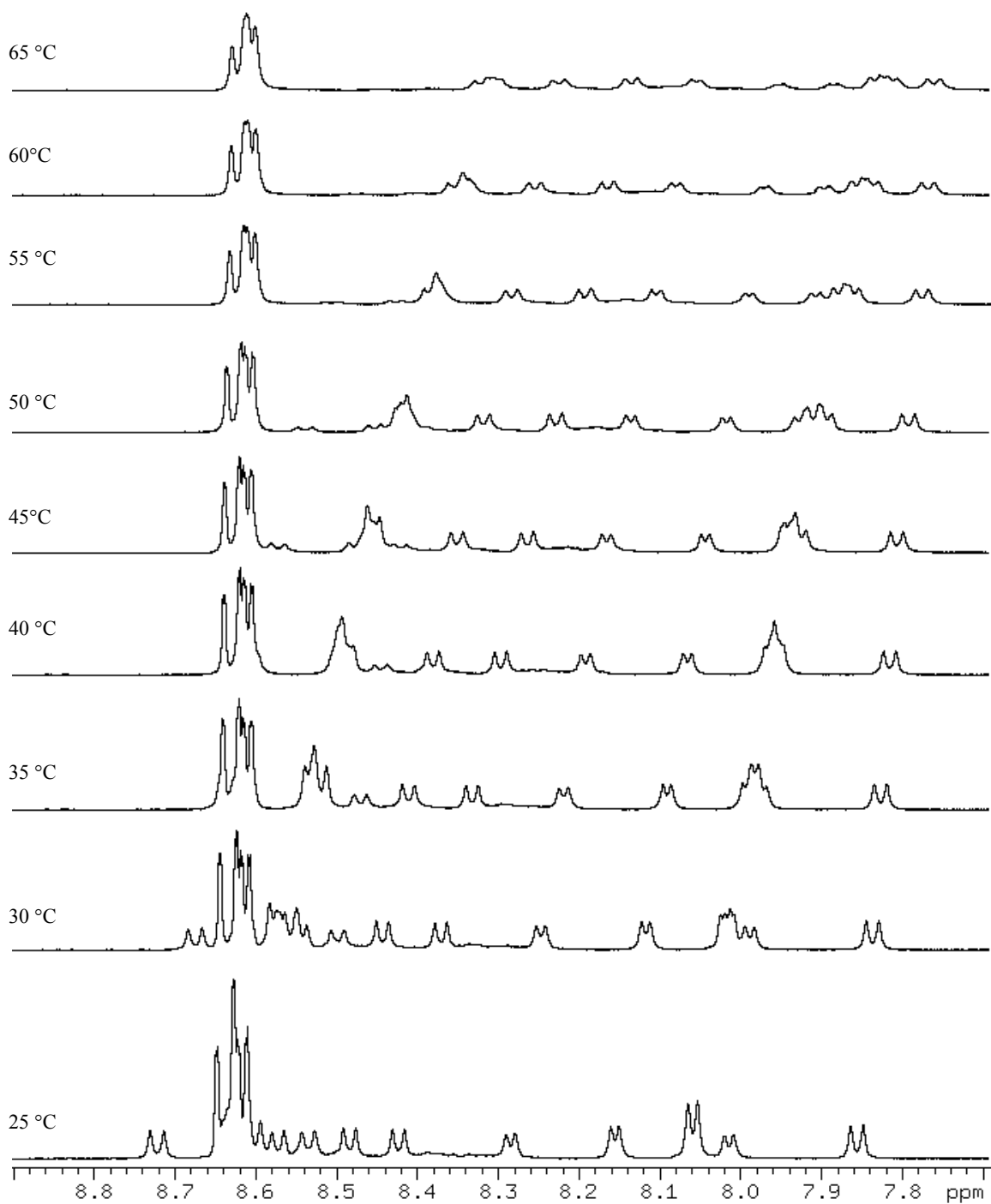
Figure 3.16. 1-D ^{1}H NMR spectra of the disulfide form of Ac-Cys-Sar-(His)$_2$-(Ala)$_3$-Cys-NH$_2$ in 90% H$_2$O/10% D$_2$O at pH 2.99, showing temperature dependence of the amide NH protons. Spectra were plotted using the same scale.
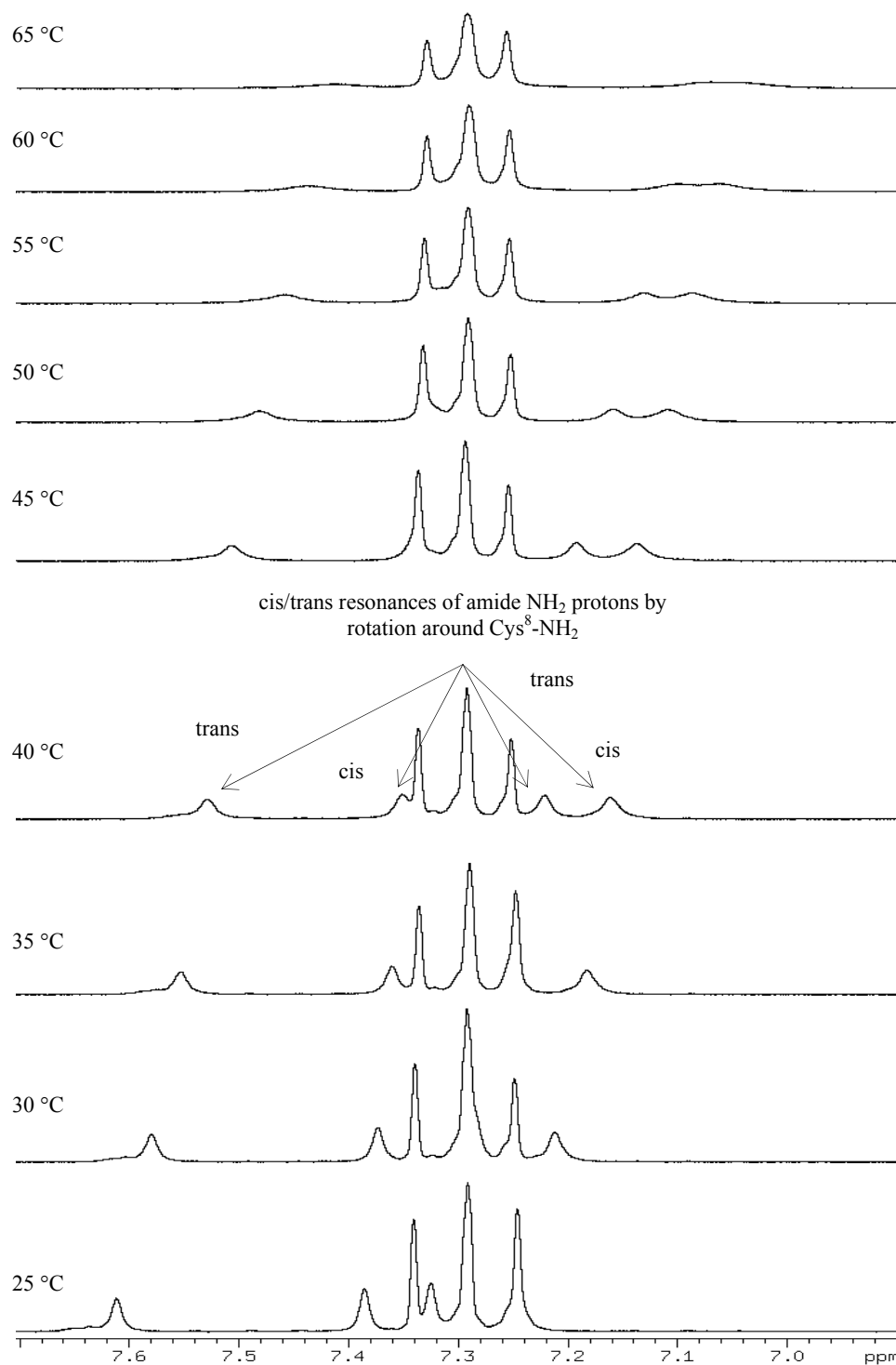
Figure 3.17. 1-D ^{1}H NMR spectra of the disulfide form of Ac-Cys-Sar-(His)$_2$-(Ala)$_3$-Cys-NH$_2$ in 90% H$_2$O/10% D$_2$O at pH 2.99, showing temperature dependence of the amide NH$_2$ protons. Spectra were plotted using the same scale.

The temperature dependence of the chemical shifts of amide protons was first reported in 1969 by Ohnishi and Urry.[6] The observed upfield shift of the amide protons as the temperature is increased is thought to be a result of more and more hydrogen bonds (N-H…O) being broken as the temperature is increased.[7]

The cis/trans pairs of resonances used to characterize the cis/trans isomerization of all peptide/peptoid hybrids reported here are listed in Tables 3.1, 3.2, and 3.3.

3.2.4 Kinetics of Cis/Trans Isomerization of Sarcosine-Containing Peptide/Peptoid Hybrids by Chemical Exchange

To determine the rate constant for cis→trans isomerization (k_{ct}) for sarcosine-containing peptide/peptoid hybrids, the dependence of the intensity of the cis isomer resonance on mixing time was fit using the nonlinear least squares analysis method described in reference 8. To illustrate, the nonlinear least squares fit of the inversion-magnetization transfer data plotted in Figure 3.13 is presented in Figure 3.18. The smooth curve through the points is the theoretical curve obtained by nonlinear least-squares analysis of the data. To bring the rates of cis/trans isomerization of the disulfide form of Ac-Cys-Sar-(His)$_2$-(Ala)$_3$-Cys-NH$_2$ onto the magnetization-transfer time scale, the k_{ct} rate constants were measured at 50, 55, 60, and 65 °C. The k_{ct} value for the disulfide form of Ac-Cys-Sar-(His)$_2$-(Ala)$_3$-Cys-NH$_2$ at 25 °C reported in Table 3.5 was calculated using the activation parameters obtained from the values of k_{ct} at the higher temperatures. The trans→cis isomerization rate constant (k_{tc}) at 25 °C, was calculated from K_{eq} and k_{ct} (k_{tc} = k_{ct}/K_{eq}).

The rate constants for the interconversion of the cis isomer to the trans isomer and
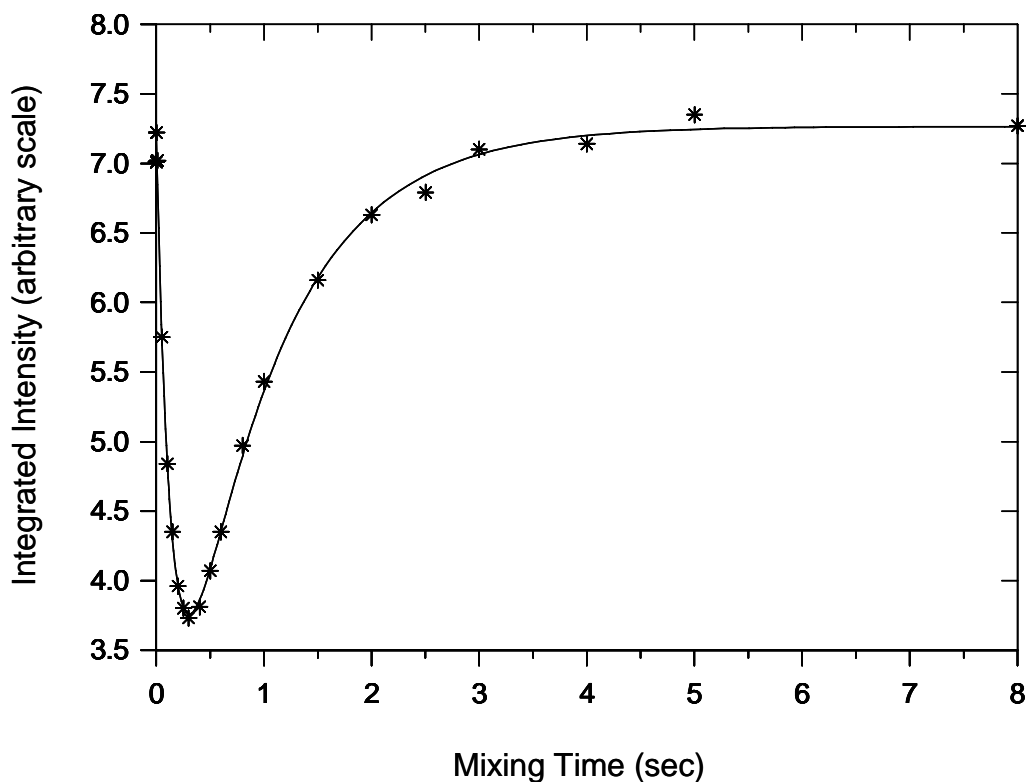
Figure 3.18. Integrated intensities of the resonance for the sarcosine methyl protons of the cis isomer of the disulfide form of Ac-Cys-Sar-(His)$_2$-(Ala)$_3$-Cys-NH$_2$ as a function of the mixing time t in the inversion-magnetization transfer pulse sequence. The inversion-magnetization transfer data are for 6 mM disulfide Ac-Cys-Sar-(His)$_2$-(Ala)$_3$-Cys-NH$_2$ in 90% H$_2$O/10% D$_2$O at pH 2.99 and 65 °C. The smooth curve through the points is the theoretical curve obtained by nonlinear least-squares analysis of the data.

vice versa at 25 °C for all peptide/peptoid hybrids studied are summarized in Tables 3.5, 3.6 and 3.7. It should be noted that rate constants at 25 °C were obtained indirectly since their rates at 25 °C are slow relative to the magnetization-transfer time scale.

3.2.5 Thermodynamics of Cis/Trans Isomerization of Sarcosine-Containing Peptide/Peptoid Hybrids

Activation parameters $\Delta H_{ct}^{\neq}$ and $\Delta S_{ct}^{\neq}$ were obtained from the Eyring plot of $\ln(k_{ct}/T)$ vs $1/T$ as discussed in Chapter 2. The Gibbs free energy at 25 °C, $\Delta G_{ct}^{\neq}$, is calculated from $\Delta H_{ct}^{\neq}$ and $\Delta S_{ct}^{\neq}$ ($\Delta G_{ct}^{\neq} = \Delta H_{ct}^{\neq} - T\Delta S_{ct}^{\neq}$).

The activation parameters for interconversion of the cis isomer to the trans isomer for all peptide/peptoid hybrids studied are presented in Tables 3.5, 3.6 and 3.7.

3.3 Discussion

The equilibrium constants in Tables 3.5, 3.6, and 3.7 indicate that the cis and trans conformations across the Xaa-Sar peptide bonds for the peptide/peptoid hybrids in Tables 3.1, 3.2 and 3.3 are both highly populated in both the cyclic disulfide and acyclic dithiol forms. The cis population of acyclic hybrids 1a-16a ranges from 21.1% to 29.5%, whereas the cis population of cyclic hybrids 1b-16b ranges from 30.1% to 86.8%, with the only exception being hybrid 16b with a cis population of 13.1%. The results indicate that formation of the intramolecular disulfide bond favors the cis conformation, presumably due to the existence of secondary structure in solution for the cyclic hybrids as a result of constraints imposed by the disulfide bond on the conformation of the peptide backbone.

The results in Table 3.5 indicate that amino acid sequence has a significant effect

on the population of the cis conformation across the Cys-Sar peptide bond in the cyclic disulfide peptide/peptoid hybrids of the sequence Ac-Cys-Sar-His-Xaa-Ala-Ala-Ala-Cys-NH$_2$. The cis population for hybrids 1b-6b ranges from 46.2% to 74.4%. The highest cis population of 74.4% was found for 5b when Xaa in the amino acid sequence is aspartic acid. The result suggests that the protonated carboxylate group on aspartic acid side chain (pK$_a$ = 3.86) is probably involved in hydrogen bonding (C=O…H) with the peptide backbone carbonyl oxygen within the disulfide-bridged ring due to being constrained by the disulfide bond. The population of the cis isomers of the linear dithiol hybrids 1a-6a, on the other hand, is very much independent of the amino acid sequence (21.1% - 25.7%).

The results in Table 3.5 also indicate that the formation of the disulfide bond slows down the rate of cis→trans interconversion (k$_{ct}$) for hybrids 1b-6b. The rate constant k$_{ct}$ is smaller by 73% for 1b, 71% for 2b, 86% for 3b, 12% for 4b, 86% for 5b, and 64% for 6b. Among the rates k$_{ct}$ for cyclic hybrids, the rate k$_{ct}$ of 4b is the fastest one. Additionally, the rate constant of trans→cis interconversion (k$_{tc}$) of 4b is 3.6-fold larger than that of 4a. The results suggest that the presence of phenylalanine in the hybrid sequence together with the formation of the disulfide bond somehow lowers the relative energy of the transition state and hence resulting in an increase in the rates of both k$_{ct}$ and k$_{tc}$.

Additionally, analysis of the rate constants k$_{ct}$ and k$_{tc}$ for cyclic hybrids 1b-6b in Table 3.5 reveals that the presence of the stericly hindered aromatic side chain group of phenylalanine in hybrid 4b makes the rate of interchange (k$_{ct}$ and k$_{tc}$) between cis and

trans isomers of 4b ~ 3 to 7-fold faster than other cyclic hybrids. Generally, for cyclic disulfide hybrids 1b-6b, rate constant for cis→trans is decreased much more than rate constant for trans→cis. That is, there is a relative increase in the kinetic stability of the cis conformation in the disulfide form. In contrast, for acyclic dithiol hybrids 1a-6a, rate constant for cis→trans is increased much more than rate constant for trans→cis. That is, there is a relative increase in the kinetic stability of the trans conformation in the dithiol form. Additional analysis of the rate constants k_{ct} and k_{tc} for acyclic hybrids 1a-6a in Table 3.5 reveals that the presence of the ammonium group of the lysine side chain in hybrid 3a accelerates the rate of interchange k_{ct} and k_{tc} of 3a by ~ 3-fold faster than other acyclic hybrids.

The results in Table 3.6 show that for the related series of peptide/peptoid hybrids of the sequence Ac-Cys-Sar-$(Ala)_x$-His-$(Ala)_y$-Cys-NH$_2$, x = 0-4 and y = 4-0, the cis population of the cyclic disulfide hybrids drops from 66% for 7b to 39.1% for 11b when the histidyl residue moves away from sarcosine toward Cys^8. This signifies a great influence of positively charged amino acids located in sequence segments adjacent to sarcosine on the cis population. Unlike a big variation in the percent cis for hybrids 7b-11b, the variation in the cis population for the reduced linear dithiol hybrids 7a-11a is smaller, ranging from 23.4% to 27.0%. The larger cis population for cyclic hybrids 7b-11b suggests that the steric constraints imposed by the formation of the disulfide bond facilitate formation of secondary structure, which in turn favors the cis conformation.

Analysis of the rates k_{ct} for hybrids 7b-11b in Table 3.6 indicates that the rate k_{ct} for 7b-9b is 56%, 50%, and 44% slower than that of 10b, respectively. The results

indicate that the presence of the stericly hindered imidazolium side chain group of the histidyl residue following sarcosine in the sequence of 7b decreases the rate k_{ct} across the Cys-Sar amide bond to the greatest extent. Similarly, the rate k_{ct} of 11b is 5% slower than that of 10b because of steric repulsion between the imidazolium side chain of the histidyl residue and the side chain of Cys^8. In short, for hybrids 10b and 11b, where the histidyl residue is several residues away from Sar, the rate constant k_{ct} for the Cys-Sar peptide bond increases by ~ 2-fold.

Analysis of the rates for hybrids 7b, 10b and 11b shows that the rate constant k_{tc} is larger by factors of 2.0 for 7b, 1.1 for 10b, and 1.3 for 11b, while rate constant k_{ct} is smaller by 69% for 7b, 44% for 10b and 30% for 11b. The results indicate that rate enhancements for the Cys-Sar peptide bond are different from rate enhancements for the Cys-Pro peptide bond in cyclic disulfide peptides 1b-3b, 5b and 6b in reference 9 (see Table 3.8) in which the rates k_{ct} and k_{tc} are both enhanced. Analysis of the rates for acyclic hybrids 7a-11a in Table 3.6 indicates that the rates k_{ct} and k_{tc} of 10a are faster than those of hybrids 7a-9a and 11a by a factor of ~ 1.3, presumably as a result of the minimum steric repulsion in 10a upon having the histidyl residue located at the right place in its sequence. The rates obtained indicate that the position of the histidyl residue in the amino acid sequence affects the rates of cis/trans isomerization for both acyclic and cyclic hybrids.

In general, for cyclic disulfide hybrids 7b-11b, rate constants for cis→trans isomeriztion are increased much more than rate constants for trans→cis isomerization, with the only exception being 7b. That is, there is a relative increase in the kinetic

Peptides	Amino acid sequence	K_{eq}	k_{ct}, s^{-1}	k_{tc}, s^{-1}
1b	Ac-Cys-Pro-Phe-Cys-NH$_2$	9.8±0.2	0.43±0.03	0.044±0.004
2b	Ac-Thr-Cys-Pro-Phe-Cys-Arg-NH$_2$	17.7±0.3	0.48±0.07	0.027±0.01
3b	Ac-Cys-Pro-His-Cys-NH$_2$	6.5±0.3	0.46±0.03	0.071±0.006
5b	Ac-Cys-Pro-Gly-Cys-NH$_2$	50±5	0.34±0.03	0.007±0.001
6b	Ac-Cys-Pro-Leu-Cys-NH$_2$	11.0±0.1	0.26±0.03	0.024±0.003
8a	Ac-Cys-Gly-Pro-Cys-NH$_2$	7.4±0.2	0.061±0.006	0.008±0.001

Table 3.8. Equilibrium constants and rate constants for cis/trans isomerization of the Xaa-Pro peptide bond. The equilibrium and rate constants are for 25 ^{o}C. [Ref. 9].

stability of the trans conformation in the dithiol form.. Similarly, for acyclic dithiol hybrids 7a-11a, rate constants for cis→trans isomerization are increased much more than rate constants for trans→cis isomerization. That is, there is a relative increase in the kinetic stability of the trans conformation in the dithiol form.

The results in Table 3.7 show that for the series of peptide/peptoid hybrids in Table 3.4, the position of sarcosine in the cyclic disulfide ring greatly influences the population of the cis and trans isomers. In fact, the movement of the Sar residue causes the cis population of disulfide-bridged hybrids 12b-16b to vary in the range 13.1% - 86.8%. The population of the cis isomer for linear hybrids 12a-16a varies between 23.8% and 29.5%. A small abnormal cis population of 13.1% for hybrids 16b indicates a tremendous decrease in the kinetic stability of the cis isomer.

The results in Table 3.7 for hybrids 15 and 16 clearly indicate that, even though the peptide backbone is constrained by the disulfide bond, the rate of cis/trans isomerization of the Ala-Sar peptide bond is significantly faster for the cyclic disulfide hybrids 15b and 16b as compared to that of acyclic dithiol hybrids 15a and 16a. Rate constant k_{ct} is larger by factors of 1.3 for 15b and 2.8 for 16b, while rate constant k_{tc} is larger by factors of 1.3 for 15b and 1.4 for 16b. Compared to rate constants for cis/trans isomerization of the Gly-Pro peptide bond for the acyclic dithiol peptide 8a in reference 8, rate constant k_{ct} of 16a (0.084 s^{-1}), for example, is larger than that of 8a (0.061 s^{-1}) by a factor of 1.4, while rate constant k_{tc} of 16a (0.026 s^{-1}) is larger than that of 8a (0.008 s^{-1}) by a factor of 3.2. The faster rates for cis/trans isomerization of the Ala-Sar peptide bond for hybrids 15a and 16a relative to that of peptide 8a in reference 9 (see Table 3.8) are

reasonable since rotation around the Ala-Sar amide bond is less sterically hindered than rotation around the Gly-Pro peptide bond where nitrogen is part of the five-member ring of the proline. In other words, rates of cis/trans isomerization of the Ala-Sar peptide bond of the acyclic dithiol hybrids 15a and 16a are normal, while those of the cyclic disulfide hybrids 15b and 16b are unexpectedly fast.

Acceleration of cis→trans isomerization (k_{ct}) the rates k_{ct} and k_{tc} for hybrids 15b and 16b could be due to conformational constraints imposed on the peptide backbone by the intramolecular disulfide bond that position the lone pair of electrons on the nitrogen of sarcosine close to the amide NH proton of either Ala^3 or Ala^5 so that hydrogen bonding can take place. A hydrogen bond might form in the transition state where the sarcosine nitrogen is sp^3 hybridized. Formation of an intramolecular hydrogen bond would lower the rotational energy barrier, which in turn would enhance the rates for cis/trans isomerization of the Ala-Sar peptide bond for hybrids 15b and 16b. It is interesting to note that k_{ct} for hybrid 16b is ~ 59-fold, 18-fold, 8-fold and 2-fold larger than those of hybrids 12b, 13b, 14b and 15b, respectively. The rate constants k_{ct} and k_{tc} for cyclic hybrids 12b-14b in Table 3.7 are significantly smaller than those for acyclic hybrids 12a-14a.

Generally, for cyclic disulfide hybrids 15b and 16b, the rate constant for cis→trans isomerization is increased much more than rate constant for trans→cis. That is, there is a relative increase in the kinetic stability of the trans conformation in the disulfide form. The opposite is true for hybrids 12b and 14b. For dithiol hybrids 12a-16a, rate constant for cis→trans is increased much more than rate constant for trans→cis. That is,

there is a relative increase in the kinetic stability of the trans conformation in the dithiol form.

3.4 Summary

Evidence was presented that peptide/peptoid hybrids exist in solution as a mixture of cis and trans isomers with respect to the peptidyl-sarcosyl peptide bond. The rates of cis/trans isomerization of the peptidyl-sarcosyl peptide bond in cyclic disulfide-bridged hybrids 4b, 6b, 7b, 15b, and 16b in Tables 3.1, 3.2, and 3.3 are significantly faster than the dithiol hybrids 4a, 6a, 7a, 15a, and 16a even though the peptide backbone being constrained by the disulfide bond. The enhanced rates of cis/trans isomerization presumably result from formation of an intramolecular hydrogen bond that stabilizes the sarcosine nitrogen in the transition state or it could simply be due to ring strain. The results in Table 3.5 clearly show that the type of amino acid (Xaa) in the peptide sequence significantly affects both the cis population and rates of cis/trans isomerization of the Cys-Sar peptide bond of the disulfide form of Ac-Cys-Sar-His-Xaa-Ala-Ala-Ala-Cys-NH_2 peptide/peptoid hybrids. The results in Table 3.6 indicate the great influence of the position of positively charged amino acids (i.e. histidine) in the sequence on the cis population as well as on the rates k_{ct} and k_{tc} for cyclic disulfide hybrids of the sequence Ac-Cys-Sar-(Ala)$_x$-His-(Ala)$_y$-Cys-NH_2, x = 0-4 and y = 4-0. The results in Table 3.7 show that the position of sarcosine in the amino acid sequence tremendously affects the rate of interchange between the cis and trans isomers by rotation around the sarcosyl peptide bonds as well as the cis population for cyclic hybrids in Table 3.3.

3.5 References

1. Gibbons, J. A.; Hancock, A. A. ; Vitt, C. R. ; Knepper, S. ; Buckner, S. A.; Brune, M. E.; Milicic, I.; Kerwin, J. F., Jr.; Richter, L. S.; Taylor, E. W.; Spear, K. L.; Zuckermann, R. N.; Spellmeyer, D. C.; Braeckman, R. A.; Moos, W. H. *J. Pharmacol. Exp. Ther*. **1996**, *277*, 885-899.

2. Zuckermann, R. N.; Martin, E. J.; Spellmeyer, D. C.; Stauber, G. B.; Shoemaker, K. R.; Kerr, J. M.; Figliozzi, G. M.; Goff, D. A.; Siani, M. A.; Simon, R. J.; Banville, S. C.; Brown, E. G.; Wang, L.; Richter, L. S.; Moos, W. H. *J. Med Chem.* **1999**, *7*, 1781-1785.

3. Li, P.; Roller, P. P.; Xu, J. *Curr. Org. Chem*. **2002**, *6*, 411-440.

4. Cochran, A. G.; Tong, R. T.; Starovasnik, M. A.; Park, E. J.; McDowell, R. S.; Theaker, J. E.; Skelton, N. J. *J. Am. Chem. Soc*. **2001**, *123*, 625-632.

5. Russel, S. J.; Blandl, T.; Skelton, N. J. ; Cochran, A. G. *J. Am. Chem. Soc*. **2003**, *125*, 388-395.

6. Ohnishi, M; Urry, D. W. *Biochem. Biophys. Res. Commun*. **1969**, *36*, 194-202.

7. Cordier, F.; Grzesiek, S. *J. Mol. Biol*. **2002**, *715*, 739-752.

8. Maripaan, S. V. S.; Rabenstein, D. L. *J. Mag. Reson*. **1992**.

9. Shi, T.; Spain, S. M.; Rabenstein, D. L. *J. Am. Chem. Soc*. **2004**, *126*, 790-796.

Chapter 4

Cis/Trans Isomerization Kinetics and Equilibria of Secondary Amide Bonds in Proline-Free Peptides

4.1 Introduction

Secondary amide peptide bond isomerization plays a critical role for differentiating between biological active and inactive protein states.[1-3] The average percent cis of secondary amide peptide bonds was found to be 0.03% in 399 protein structures.[4] However, the overall cis content from a large number of normal peptide bonds in the protein is big enough to significantly slow down the folding process. For example, proline-free tendamistat variant, a small protein of 74 amino acids, was found to have a cis content of 5.0% in the unfolded state.[5] Thus, studies of cis/trans isomerization by rotation around the secondary and tertiary amide peptide bond in peptides and proteins are of interest to many researchers. Results from cis/trans isomerization studies provide information about the kinetics and thermodynamics that dictate the formation of folding intermediates, which in turn helps researchers to understand the chemical interactions that make protein folding possible as well as to understand more about how proteins are folded within the cell so that misfolding of proteins resulting in Alzheimer's and Parkinson's diseases, for example, can be prevented.

Aromatic side chains of tyrosine and phenylalanine in the Tyr-Pro-Phe moiety were found to cause an upfield shift for resonances of the $C_\alpha H$, $C_\beta H$, $C_\gamma H$, and $C_\delta H$ protons of proline from 0.17 ppm to 1.51 ppm due to an increase in shielding from the ring current effect.[6] In the case where only a single aromatic amino acid residue followed proline, only the $C_\gamma H$ proton of proline is shifted upfield.[6] More recently, the resonance

for the $C_\beta H$ protons of alanine preceding or following Tyr or Phe in tyrosine- and phenylalanine-containing peptides was found to shift upfield, making it possible to quantify cis/trans isomerization of secondary amide peptide bonds by NMR line shape analysis and inversion-magnetization transfer experiments.[7, 8]

The proper refolding of denatured disulfide-containing proteins, especially for proteins having two disulfide bonds and more (e.g. insulin and tendamistat), depends on correct formation of the disulfide bonds as they are in the native state. Thioredoxin (TRX), a powerful disulfide oxido-reductase, an enzyme that catalyzes the transfer of electrons from one molecule to another, can carry out a wide spectrum of redox reactions in the cell, including disulfide bond formation (oxidation) and breakage (reduction), and shuffling (isomerization) of disulfide bonds in proteins with incorrect disulfide bonds via a dithiol-disulfide exchange mechanism.[9, 10] Members of the TRX family have at least one domain containing the redox-active motif Cys-Xaa-Xaa-Cys, where Xaa represents two other amino acids.[10, 11] During the redox process, the cysteine residues of the motif can act as electron acceptors in their disulfide form or electron donors in their dithiol form. During the exchange of electrons with disulfide-containing proteins the Cys-Xaa-Xaa-Cys catalytic motif switches reversibly between the two redox states. The redox equilibrium reaction can be represented as:

Cys-Xaa-Xaa-Cys + Protein (S-S) $\rightleftharpoons$ Cys-Xaa-Xaa-Cys + Protein (-SH -SH)

For example, oxido-reductase ERp57, a member of thioredoxin, involved in the formation and breaking of disulfide bonds in assembling proteins within the endoplasmic reticulum, contains the redox-active motif Cys-Gly-His-Cys.[12] Mutation of either

cysteine residue at the two ends of the motif abolished reductase activity of ERp57, whereas substitution of the two central Xaa residues partially retained its redox potential and enzyme activity.

In this work, the kinetics, thermodynamics and equilibria of cis/trans isomerization across Xaa-Xaa secondary amide peptide bonds in a series of model peptides for oxido-reductase enzymes with the Cys-Xaa-Xaa-Cys active site motif were studied, where Xaa is Ala, Tyr and Phe (Table 4.1). It should be noted that peptides 1-4 in Table 4.1 contain the histidyl residue to improve peptide solubility, and that the amino terminus of the peptides is acetylated, giving the final sequence of Ac-Cys-Xaa-Xaa-Cys-His-NH$_2$. The effects of the type and position of the central Xaa residues on the kinetics and equilibria of cis/trans isomerization will be presented in this chapter. The peptides 1-4 were studied in both their reduced linear dithiol and oxidized cyclic disulfide forms. To illustrate the cis/trans isomerization, the cis and trans conformational isomers across the Tyr-Ala peptide bond of the disulfide form of Ac-Cys-Tyr-Ala-Cys-His-NH$_2$ are shown in Figure 4.1.

4.2 Results

4.2.1 Assignment of Resonances of the Trans Isomer of Proline-Free Peptides

Because interconversion between cis and trans isomers by rotation around Xaa-Xaa secondary amide peptide bond is slow on the NMR time scale, resonances for both isomers were observed for all peptides reported in this chapter. To illustrate, the CH$_3$-alanine region of the 1-D ^{1}H NMR spectrum of the disulfide form of Ac-Cys-Tyr-Ala-Cys-His-NH$_2$ in 90% H$_2$O/10% D$_2$O at pH 2.991 and 25 ^{o}C is shown in Figure 4.2. Also

Peptides	Amino acid sequence	Resonances used in inversion-magnetization transfer experiment
1a	Ac-C-A-Y-C-H-NH$_2$	Ala CH$_3$
1b	Ac-C-A-Y-C-H-NH$_2$	Ala CH$_3$
2a	Ac-C-Y-A-C-H-NH$_2$	Ala CH$_3$
2b	Ac-C-Y-A-C-H-NH$_2$	Ala CH$_3$
3a	Ac-C-A-F-C-H-NH$_2$	Ala CH$_3$
3b	Ac-C-A-F-C-H-NH$_2$	Ala CH$_3$
4a	Ac-C-F-A-C-H-NH$_2$	Ala CH$_3$
4b	Ac-C-F-A-C-H-NH$_2$	Ala CH$_3$

Table 4.1. Peptides synthesized and studied in this research. Also shown in the Table are the resonances used in inversion-magnetization transfer experiments.
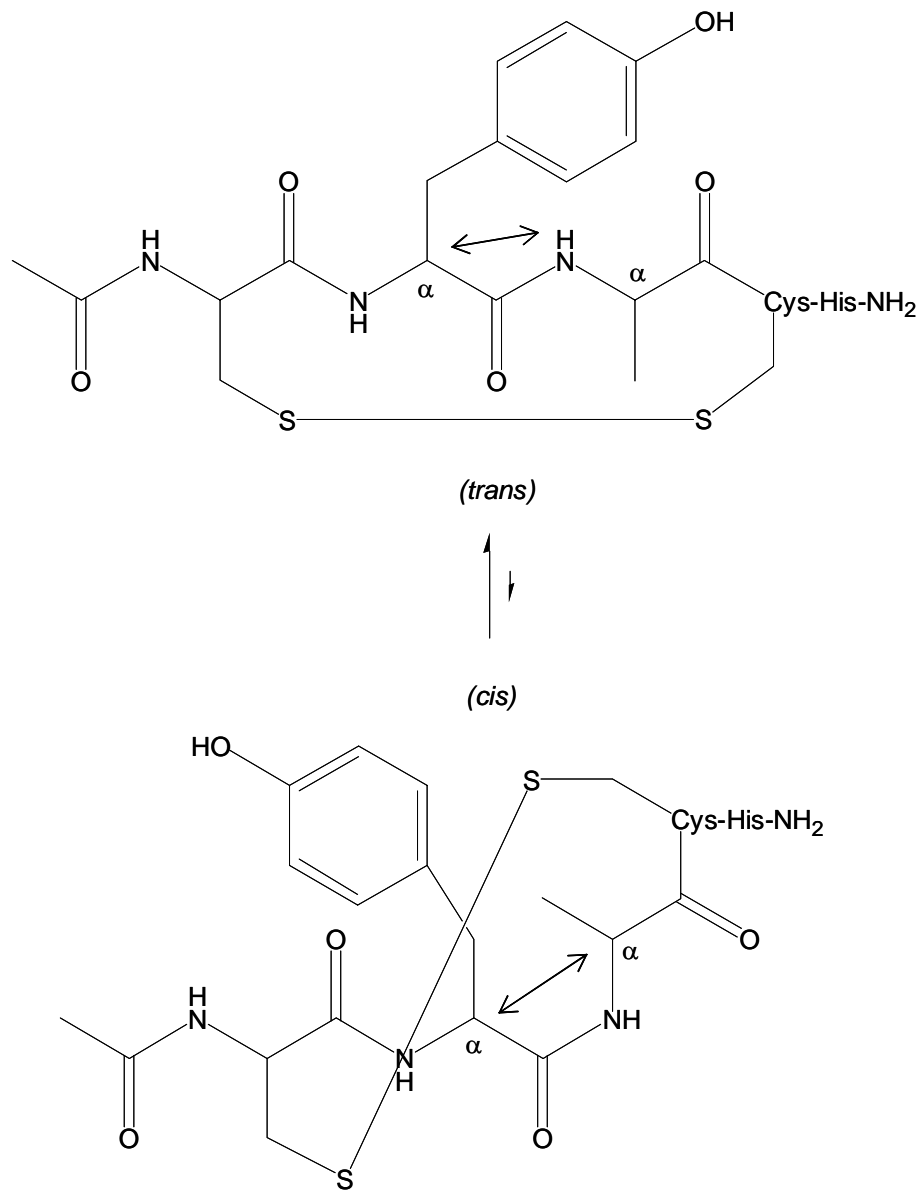
Figure 4.1. The cis and trans isomers for the disulfide form of Ac-Cys-Tyr-Ala-Cys-His-NH$_2$. The cis/trans conformation refers to the cis or trans position of the α-carbon of Tyr^2 and the α-carbon of Ala^3 across the C(O)-N amide bond as shown. The arrows indicate the dipolar ROESY cross peaks (Tyr^2 C$_\alpha$H-Ala^3 NH and Tyr^2 C$_\alpha$H-Ala^3 C$_\alpha$H) used to assign the cis and trans isomers across the Tyr-Ala peptide bond.
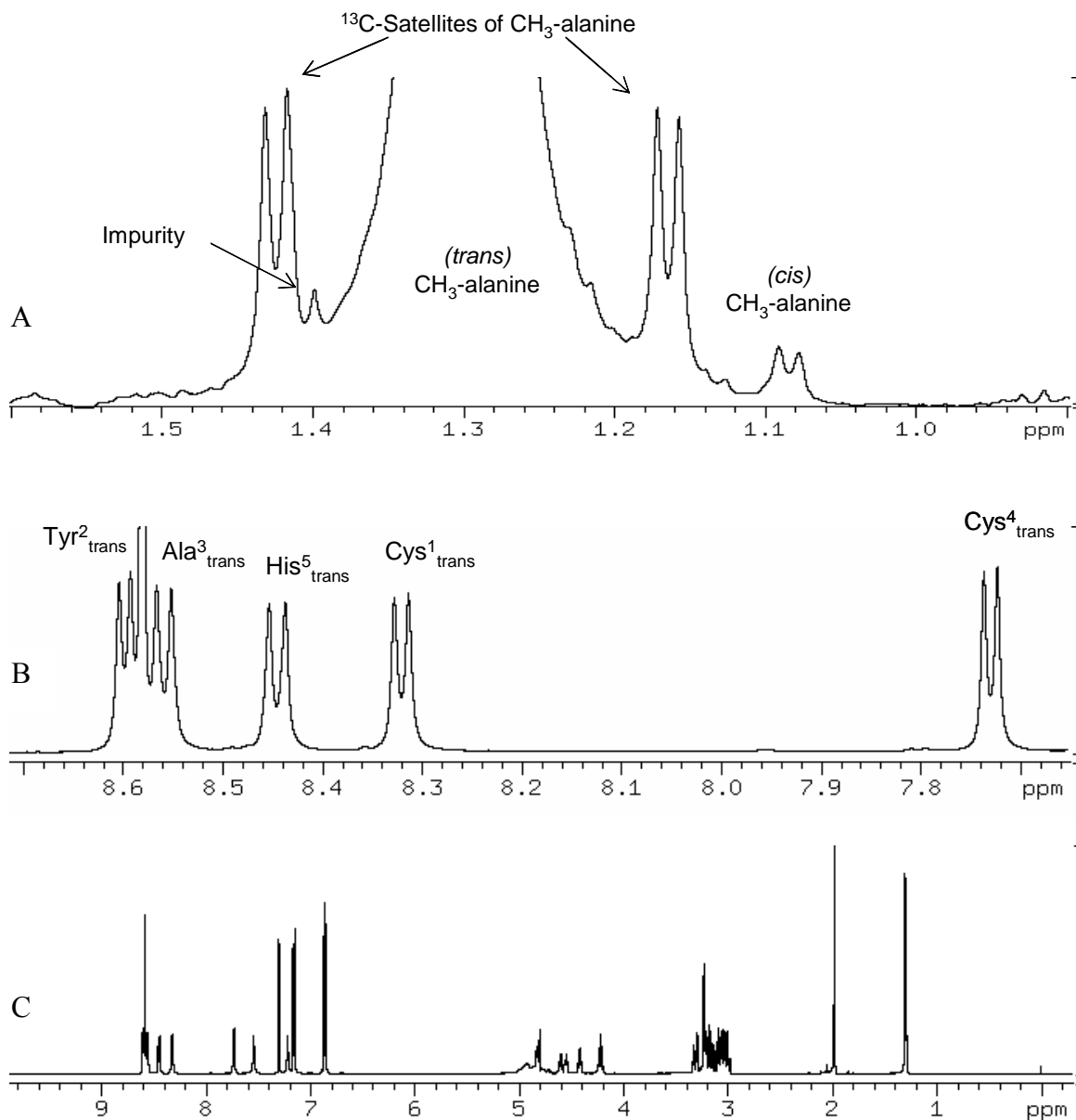
Figure 4.2. (A) The CH_3-alanine region; (B) The amide NH region; (C) The full 1-D ^1H NMR spectrum of a 22 mM solution of the disulfide form of Ac-Cys-Tyr-Ala-Cys-His-NH_2 in 90% H_2O/10% D_2O at pH 2.91 and 25 ^oC. The spectrum was measured with the single pulse method, with suppression of the H_2O resonance by presaturation. The trans signal of the alanine methyl protons was cut off to show the existence of the cis signal. The amide NH resonances are assigned to specific residues and by the conformation of the Tyr-Ala peptide bond.

plotted in Figure 4.2 are an expansion of the amide NH region and a full 1-D spectrum. The spectrum was measured by the standard single pulse sequence with suppression of the water resonance by presaturation. The spectrum consists of two sets of resonances, one greatly more intense than the other, as illustrated by the cis and trans resonances for alanine CH_3 protons in Figure 4.2. To illustrate the resonance assignment procedure, the assignment of the more intense set of resonances for the disulfide form of Ac-Cys-Tyr-Ala-Cys-His-NH$_2$ will be presented in detail. The assignment of the other set of resonances is impossible because of its extremely low percent cis of 0.07%. The assignment procedure for the more intense set of resonances involved first identification of the amino acid residues giving the NH resonances, then determination of the conformation across the Tyr-Ala peptide bond, and finally assignment of the resonances to specific residues in the peptide sequence.

To identify the amino acid residues giving the NH resonances, a 2-D BASHD-TOCSY experiment was measured with F_1-band selection and F_1-homonuclear decoupling of the amide backbone NH region because of overlap of resonances in the amide NH region. Figure 4.3 shows the NH (F_1)-full (F_2) region of the BASHD-TOCSY spectrum of the disulfide form of Ac-Cys-Tyr-Ala-Cys-His-NH$_2$, together with the corresponding region of the 1-D spectrum plotted across the top. Plotted in Figure 4.4 are subspectra obtained by taking traces through the backbone amide NH resonancces in the BASHD-TOCSY spectrum in Figure 4.3 at the indicated chemical shifts. Each 1-D subspectrum shown represents a fingerprint of the amino acid residue in the peptide. By comparing with literature chemical shift values, identities of all of the amino acid
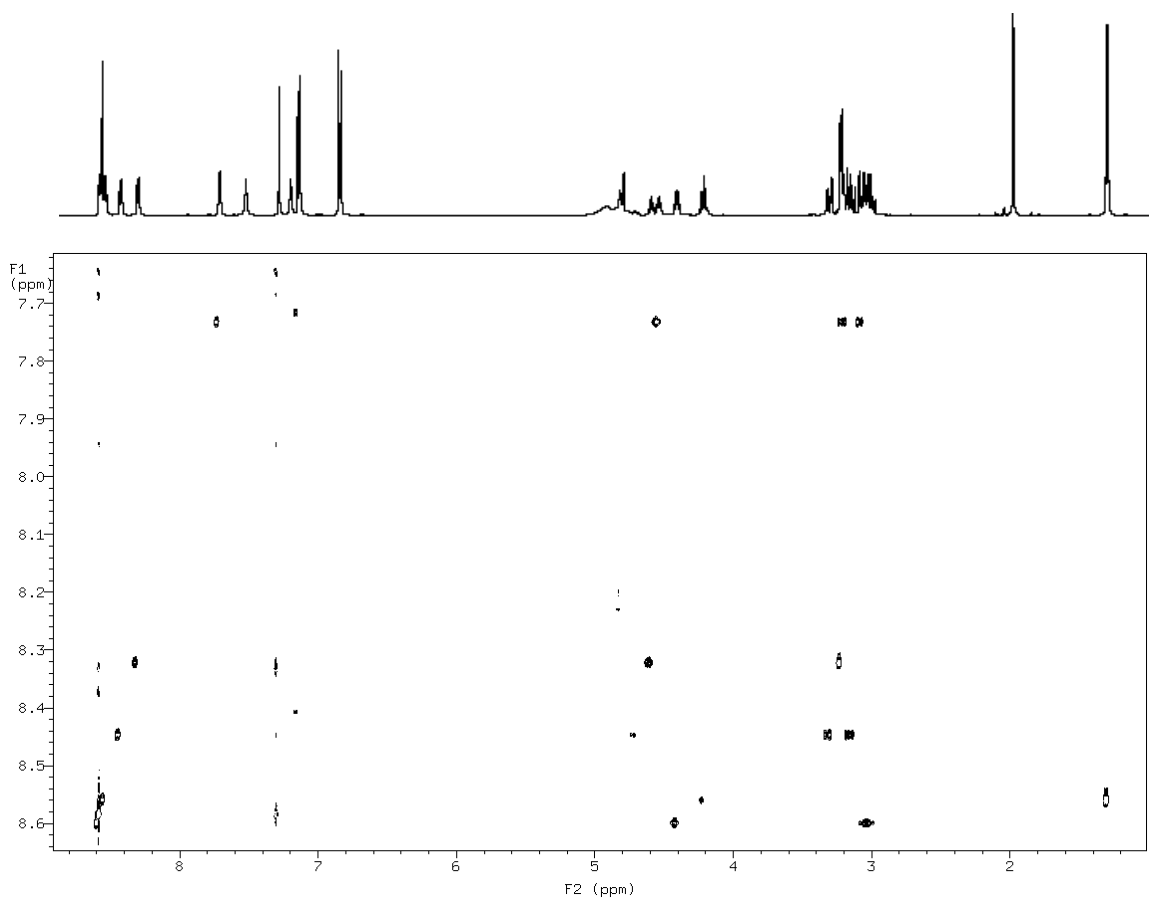
Figure 4.3. The NH (F$_1$)-full (F$_2$) region of the BASHD-TOCSY spectrum of the disulfide form of Ac-Cys-Tyr-Ala-Cys-His-NH$_2$ in 90% H$_2$O/10% D$_2$O at pH 2.91 and 25$^{\text{o}}$C, measured with F$_1$-band selection and F$_1$-homonuclear decoupling of the NH region.

Trace at 7.73 ppm_Cys[4] (trans)

Trace at 8.32 ppm_Cys[1] (trans)

Trace at 8.45 ppm_His[5] (trans)

Trace at 8.56 ppm_Ala[3] (trans)

Trace at 8.60 ppm_Tyr[2] (trans)
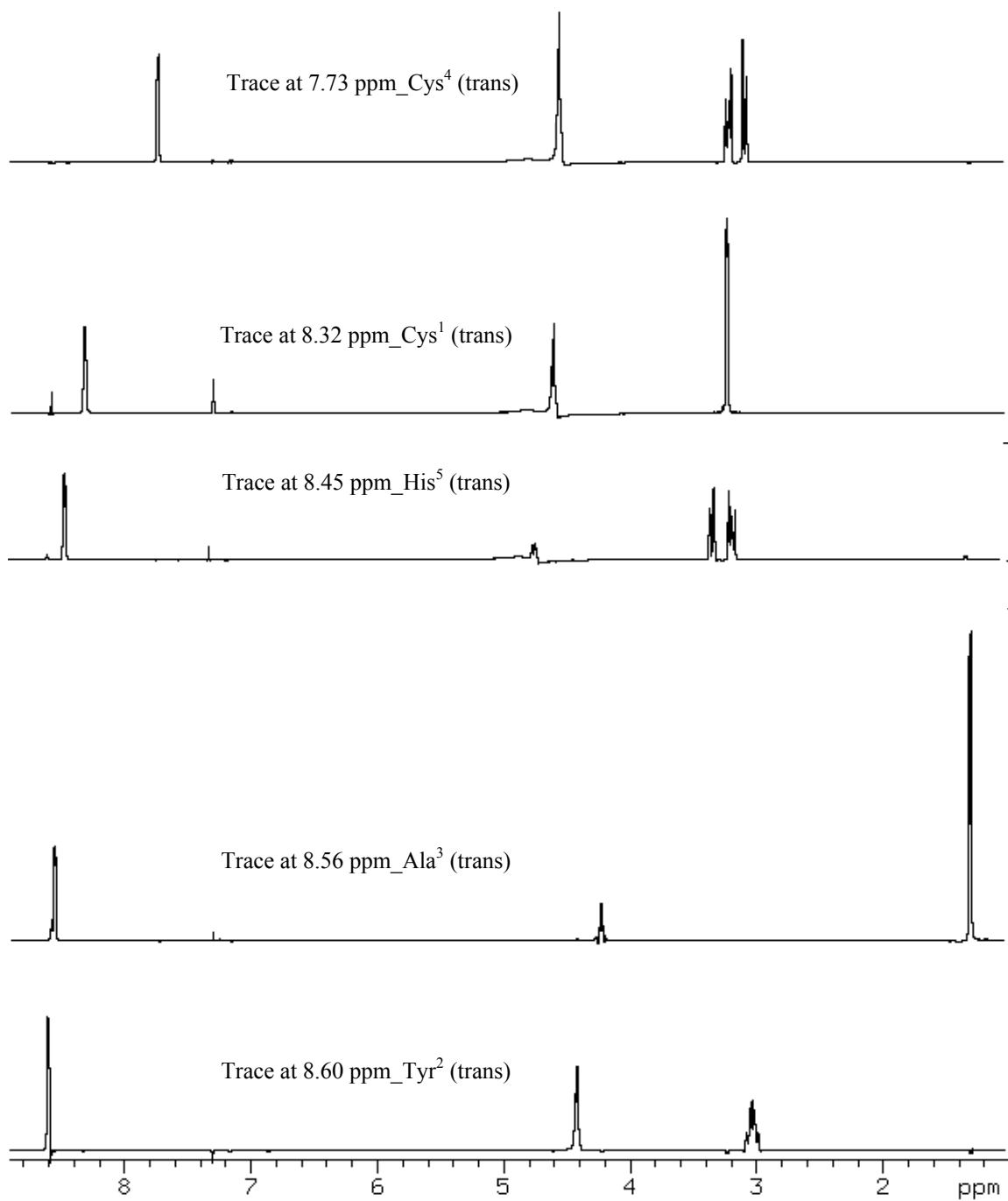
Figure 4.4. Subspectra obtained by taking traces through the backbone amide NH resonancces in the BASHD-TOCSY spectrum shown in Figure 4.3 at the indicated chemical shifts in the F_1 dimension. Traces were plotted using the same scale.

residues of the trans isomer of the disulfide form of Ac-Cys-Tyr-Ala-Cys-His-NH$_2$ were determined.

The cis/trans isomerization across the Tyr-Ala peptide bond and the completed sequential assignments for the identified amino acids from the BASHD-TOCSY spectrum for the trans isomer of the disulfide form of Ac-Cys-Tyr-Ala-Cys-His-NH$_2$ were established using dipolar (negative) cross peaks obtained from both the ROESY and BASHD-ROESY spectra. A full 2-D ROESY spectrum of the disulfide form of Ac-Cys-Tyr-Ala-Cys-His-NH$_2$ in 90% H$_2$O/10% D$_2$O at pH 2.91 and 25 $^{\circ}$C is shown in Figure 4.5. The bottom of Figure 4.5 shows the NH (F$_1$)-C$_\alpha$H (F$_2$) region of the upper full ROESY spectrum. The cross peak in the rectangle in Figure 4.5 is composed of two cross peaks (see Figure 4.6) because the chemical shift difference between amide protons of the trans isomers of Tyr (8.598 ppm) and Ala (8.559 ppm) is small (~2 Hz). Figure 4.6 shows the NH (F$_1$)-C$_\alpha$H (F$_2$) region of the BASHD-ROESY spectrum, measured with F$_1$-band selection and F$_1$-homonuclear decoupling of the NH region.

With the identities of the amino acid residues giving the amide NH resonances and the ROESY and BASHD-ROESY spectra in hand, the next step was to verify that there are two sets of resonances for isomers of the same peptide in dynamic equilibrium. The trans conformation across the Tyr-Ala peptide bond of the disulfide form of Ac-Cys-Tyr-Ala-Cys-His-NH$_2$ was established by the negative (through space) NOE cross peak at 8.550 ppm (F$_1$) and 4.417 ppm (F$_2$) between the Tyr C$_\alpha$H and Ala NH protons in the BASHD-ROESY spectrum in Figure 4.6. The cis conformation across the Tyr-Ala peptide bond of the disulfide form of Ac-Cys-Tyr-Ala-Cys-His-NH$_2$ was established by
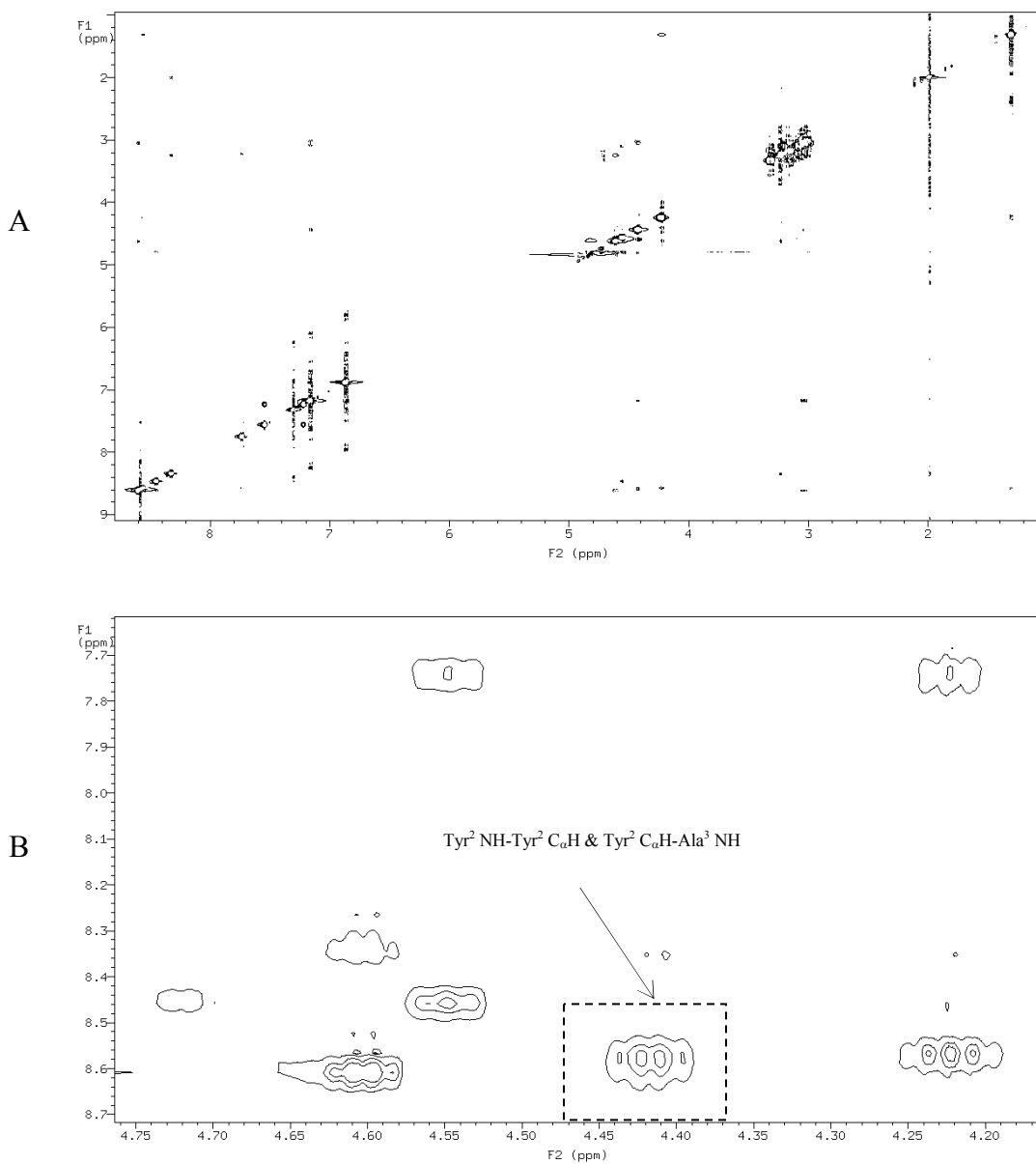
Figure 4.5. (A) The full ROESY spectrum of the disulfide form of Ac-Cys-Tyr-Ala-Cys-His-NH$_2$ in 90% H$_2$O/10% D$_2$O at pH 2.91 and 25 ^{o}C. (B) The NH (F$_1$)-C$_\alpha$H (F$_2$) region of (A). The cross peak in the rectangle is composed of two cross peaks Tyr^2 NH-Tyr^2 C$_\alpha$H and Tyr^2 C$_\alpha$H-Ala^3 NH (see Figure 4.6).
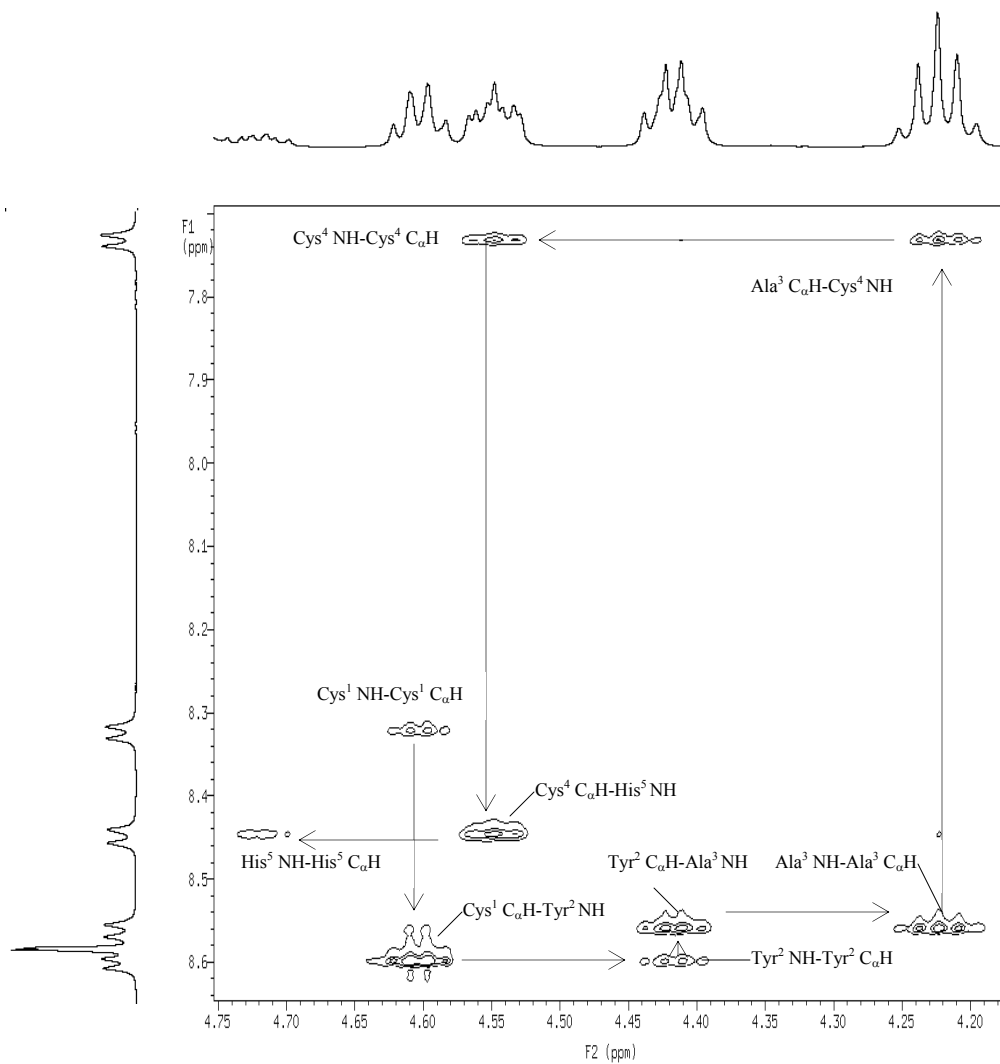
Figure 4.6. The NH (F_1)-C_αH (F_2) region of the BASHD-ROESY spectrum of the
disulfide form of Ac-Cys-Tyr-Ala-Cys-His-NH$_2$ in 90% H$_2$O/10% D$_2$O at pH 2.91 and
25 °C, measured with F_1-band selection and F_1-homonuclear decoupling of the NH
region, showing the sequential connectivity traced out by the NH-C_αH cross peaks for the
trans isomer.
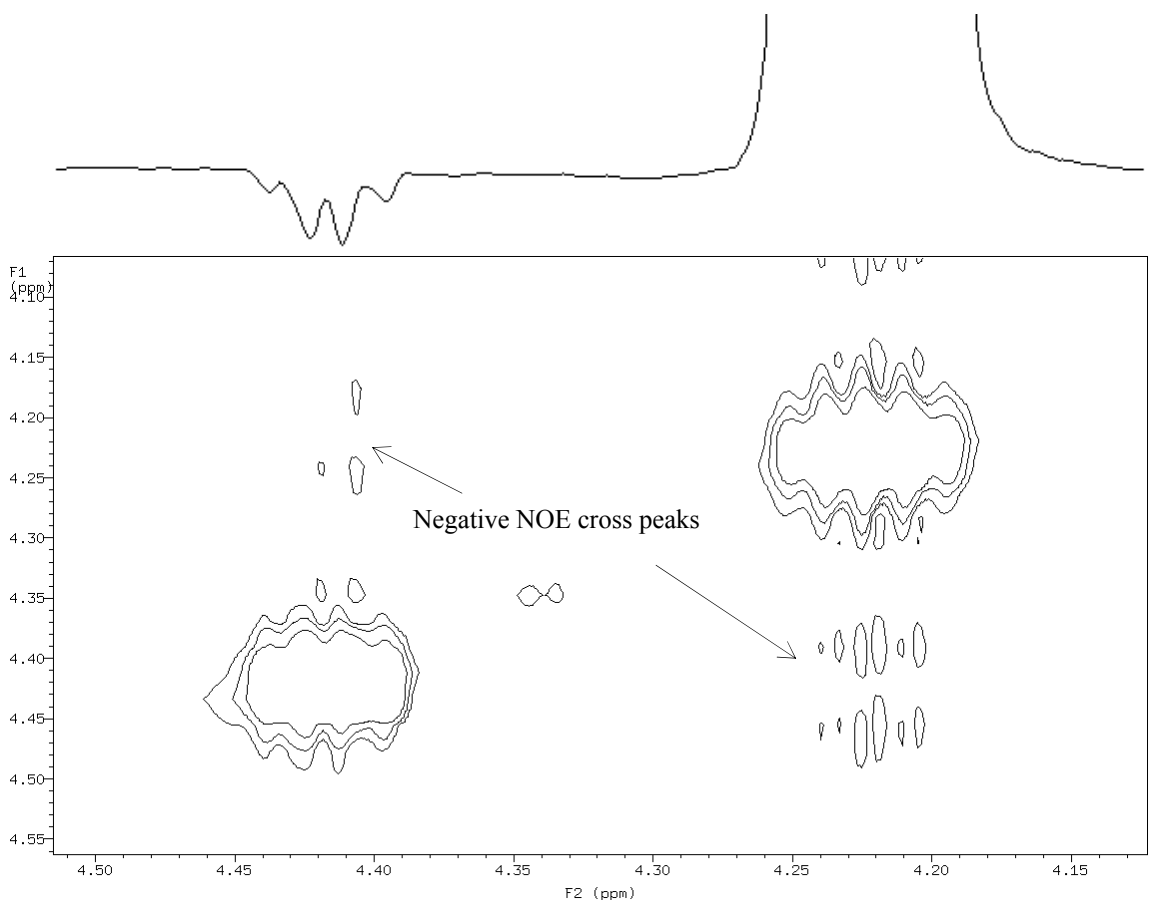
Figure 4.7. The $C_\alpha H$ (F_1)-$C_\alpha H$ (F_2) region of the ROESY spectrum of the disulfide form of Ac-Cys-Tyr-Ala-Cys-His-NH$_2$ in 90% H$_2$O/10% D$_2$O at pH 2.91 and 25 $^\circ$C with the subspectrum plotted across the top obtained by taking trace at 4.222 ppm in the F_1 dimension. The pair of negative NOE cross peaks at 4.222 ppm (F_1), 4.417 ppm (F_2) and 4.417 ppm (F_1), 4.222 ppm (F_2) between the Tyr^2 $C_\alpha H$ and Ala^3 $C_\alpha H$ protons establish that these two resonances are for the configurational isomer having the cis conformation across the Tyr-Ala peptide bond.

the pair of negative NOE cross peaks at 4.222 ppm (F_1), 4.417 ppm (F_2) and 4.417 ppm (F_1), 4.222 ppm (F_2) between the Tyr $C_\alpha H$ and Ala $C_\alpha H$ protons from the $C_\alpha H$ (F_1)-$C_\alpha H$ (F_2) region of the ROESY spectrum in Figure 4.7. The results in Figure 4.9 from the inversion-magnetization transfer experiment in Section 4.2.3 for the disulfide form of Ac-Cys-Tyr-Ala-Cys-His-NH$_2$ provides further evidence that the peptide is in dynamic equilibrium between cis and trans conformations. It is obvious that all amide NH resonances in the amide region in Figure 4.2 are for the trans conformer since the trans conformation across secondary amide peptide bond is much more abundant than the cis conformation due to steric strains between the two C_α atoms of adjacent amino acid residues (see Figure 4.1). Additionally, cyclic disulfide-bridged peptide Ac-Cys-Tyr-Ala-Cys-His-NH$_2$ most likely favors formation of the trans conformation as result of ring constraint imposed on the peptide backbone by the disulfide bond.

The sequential assignment of resonances for the trans isomer of the disulfide form of Ac-Cys-Tyr-Ala-Cys-His-NH$_2$ begins with the acetyl resonance for the trans isomer, which was established by a negative NOE at 1.978 ppm (F_1) and 8.321 ppm (F_2) from the acetyl CH$_3$ (F_1)-NH (F_2) region of the ROESY spectrum in Figure 4.8. The Cys^1-Tyr^2 connectivity was established by the Cys^1 $C_\alpha H$-Tyr^2 NH NOE connectivity at 8.598 ppm (F_1) and 4.603 ppm (F_2) in Figure 4.6. The presence of the cross peak at 8.559 ppm (F_1) and 4.417 ppm (F_2) for the Tyr^2 $C_\alpha H$-Ala^3 NH NOE connectivity in Figure 4.6 established the Tyr^2-Ala^3 connectivity. The completed sequential connectivity is diagramed in Figure 4.6.

Resonances assignments for all protons of the trans isomer of the disulfide form
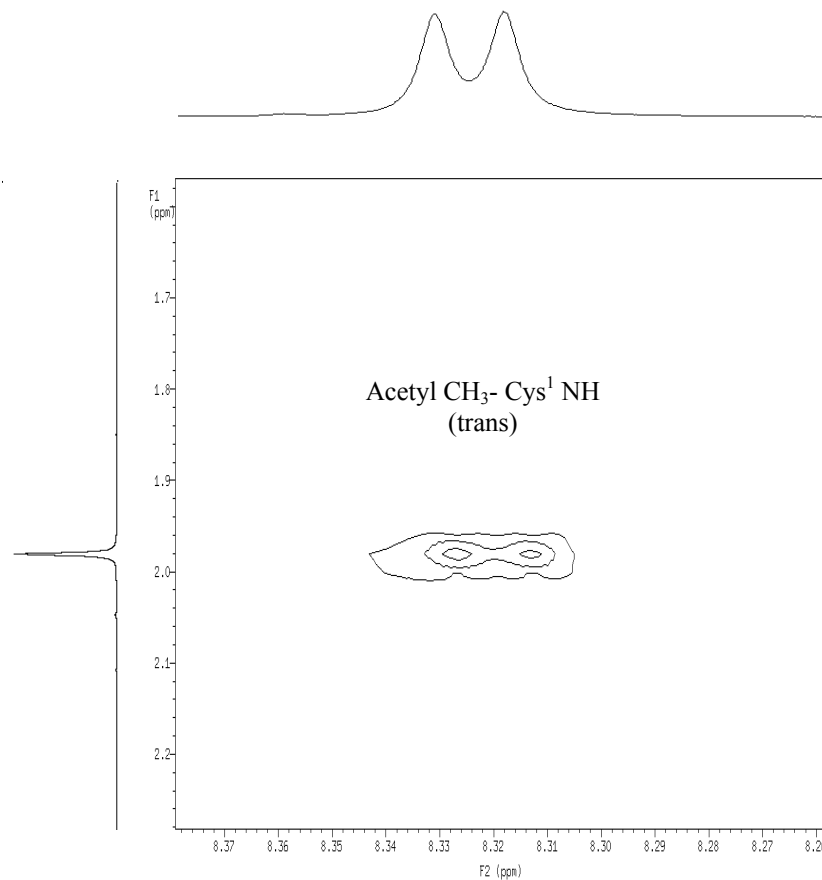
Figure 4.8. The acetyl CH_3 (F_1)-NH (F_2) region of the ROESY spectrum of the disulfide form of Ac-Cys-Tyr-Ala-Cys-His-NH_2 the in 90% H_2O/10% D_2O at pH 2.91 and 25 ^{o}C. The negative NOE observed between the resonance for the acetyl methyl protons at 1.978 ppm and the resonance for the Cys[1]NH proton at 8.321 ppm establishes the N-terminal acetyl-Cys[1] connectivity for the trans isomer across the Tyr-Ala peptide bond.

of Ac-Cys-Tyr-Ala-Cys-His-NH$_2$ in 90% H$_2$O/10% D$_2$O at pH 2.91 and 25 °C are

reported in Table 4.2.

4.2.2 Equilibria of Cis/Trans Isomerization of Proline-Free Peptides

In the previous section, evidence was presented demonstrating that peptides exist

in solution as a mixture of cis and trans isomers across the C-N bond of Xaa-Xaa

secondary amide peptide bond. Equilibrium constants (K_{eq} = [trans]/[cis]) for cis/trans

isomerization for all the peptides reported in this chapter were determined and are

summarized in Table 4.3. The relative concentration of the cis and trans isomers was

determined from the indirect relative mass of a cis/trans pair of resonances. Specifically,

the ^{13}C satellite peak of the trans alanine CH$_3$ signal and the cis alanine CH$_3$ peak were

plotted using the same scale and were weighed. Knowing that the intensity of the two ^{13}C

satellite signals equals 1.1% of the intensity of the trans alanine CH$_3$ signal, the mass of

the trans alanine CH$_3$ peak was then obtained from the mass of the ^{13}C satellite peak. For

instance, the populations of the cis and trans isomers of the disulfide form of Ac-Cys-

Tyr-Ala-Cys-His-NH$_2$ were calculated to be 0.07% and 99.93%, respectively, using the

relative populations in the standard 1-D ^{1}H NMR spectrum at 25 °C in Figure 4.2. The

equilibrium constant was calculated to be 1369.

4.2.3 Interconversion of the Cis and Trans Isomers of Proline-Free Peptides by Chemical Exchange

The kinetics of interconversion between the cis and trans isomers by rotation

around Xaa-Xaa peptide bond for peptides 1-4 in Table 4.1 were studied using NMR

inversion-magnetization transfer experiments. The magnetization transfer data obtained

Residue	NH amide	αH	βH	δH	ϵH	Others
Cys^1(trans)	8.321	4.603	3.227			
Tyr^2(trans)	8.598	4.417	3.001, 3.057	7.155	6.858	
Ala^3(trans)	8.559	4.222	1.296			
Cys^4(trans)	7.730	4.547	3.078, 3.206			
His^5(trans)	8.445	4.721	3.153, 3.311			H$_2$ 8.580
						H$_4$ 7.298
Acetyl CH$_3$(trans)						1.978
Amide NH$_2$(trans)						N(H$_2$) 7.214, 7.539

Table 4.2. Assignment of proton resonances for the disulfide form of Ac-Cys-Tyr-Ala-Cys-His-NH$_2$ in 90 % H$_2$O/10 % D$_2$O at pH 2.91 and 25 $^{\circ}$C.

Peptides	K_{eq}	% cis	k_{ct}, s^{-1}	k_{tc} x 10^{-3} s^{-1}	$\Delta H_{ct}^{\ddagger}$ kcal.mol^{-1}	$\Delta S_{ct}^{\ddagger}$ cal.mol^{-1}K^{-1}	$\Delta G_{ct}^{\ddagger}$ kcal.mol^{-1}
1a	1586±111	0.06%	1.953±0.089	1.2±0.1	n.d.	n.d.	n.d.
1b	1123±105	0.09%	0.601±0.031	0.5±0.1	22.1±0.7	14.5±2.2	17.8±0.7
2a	1298±90	0.08%	1.400±0.049	1.1±0.1	n.d.	n.d.	n.d.
2b	1369±92	0.07%	1.254±0.082	0.9±0.1	n.d.	n.d.	n.d.
3a	1148±103	0.09%	0.863±0.060	0.7±0.1	n.d.	n.d.	n.d.
3b	1019±101	1.00%	0.367±0.054	0.4±0.1	24.1±1.1	20.3±3.6	18.1±1.1
4a	1470±96	0.07%	1.235±0.079	0.8±0.1	n.d.	n.d.	n.d.
4b	942±89	0.11%	1.066±0.131	1.1±0.2	25.4±0.3	26.8±0.9	17.4±0.3

n.d., not determined because rate constant was obtained at a single temperature, 25 °C.

Table 4.3. Equilibrium constants, population of the cis conformation, rate constants, and activation parameters for cis/trans isomerization of the secondary amide peptide bonds for peptides in Table 4.1. The rate and equilibrium constants, and ΔG are for 25 °C. Some rate constants were obtained by extrapolation to 25 °C using the activation parameters determined from the rate data measured at higher temperature. Other rate constants were determined directly.

are then used to characterize the dynamics of cis/trans isomerization as will be discussed in the next section.

To determine rate constants for Xaa-Xaa cis/trans isomerization by the inversion-magnetization transfer method, a pair of well-resolved resonances for the cis and trans isomers is required. In the inversion-magnetization transfer experiment, the more intense resonance of the pair, which is always the trans isomer resonance for peptides 1-4, is selectively inverted, and the transfer of inversion to the less intense cis resonance is monitored. An example of spectra obtained with the magnetization transfer experiment for determination of cis/trans isomerization rate constants for the disulfide form of Ac-Cys-Tyr-Ala-Cys-His-NH$_2$ in 90% H$_2$O/10% D$_2$O at pH 2.91 and 30 $^{\circ}$C are shown in Figure 4.9. The resonance for the alanine methyl protons of the trans isomer was inverted and the transfer of inversion to the resonance for the corresponding cis isomer was monitored as a function of the delay time in the pulse sequence, during which exchange between the cis and trans isomers takes place. It also should be noted that the dependence of the intensities of the cis and trans resonances on mixing time in Figure 4.9 provides the most conclusive evidence for the presence of cis and trans isomers with respect to the Tyr-Ala peptide bond.

The cis/trans pairs of resonances used to characterize the cis/trans isomerization of all peptides reported here are listed in Table 4.1.

4.2.4 Kinetics of Cis/Trans Isomerization of Proline-Free Peptides by Chemical Exchange

To determine the rate constant for cis→trans isomerization (k$_{ct}$) for peptides in

trans

cis

0.0001   0.0100   0.1000   0.2500   0.4000   0.6000   0.8000   1.0000   1.5000   2.0000   3.0000   4.0000   5.0000   6.0000
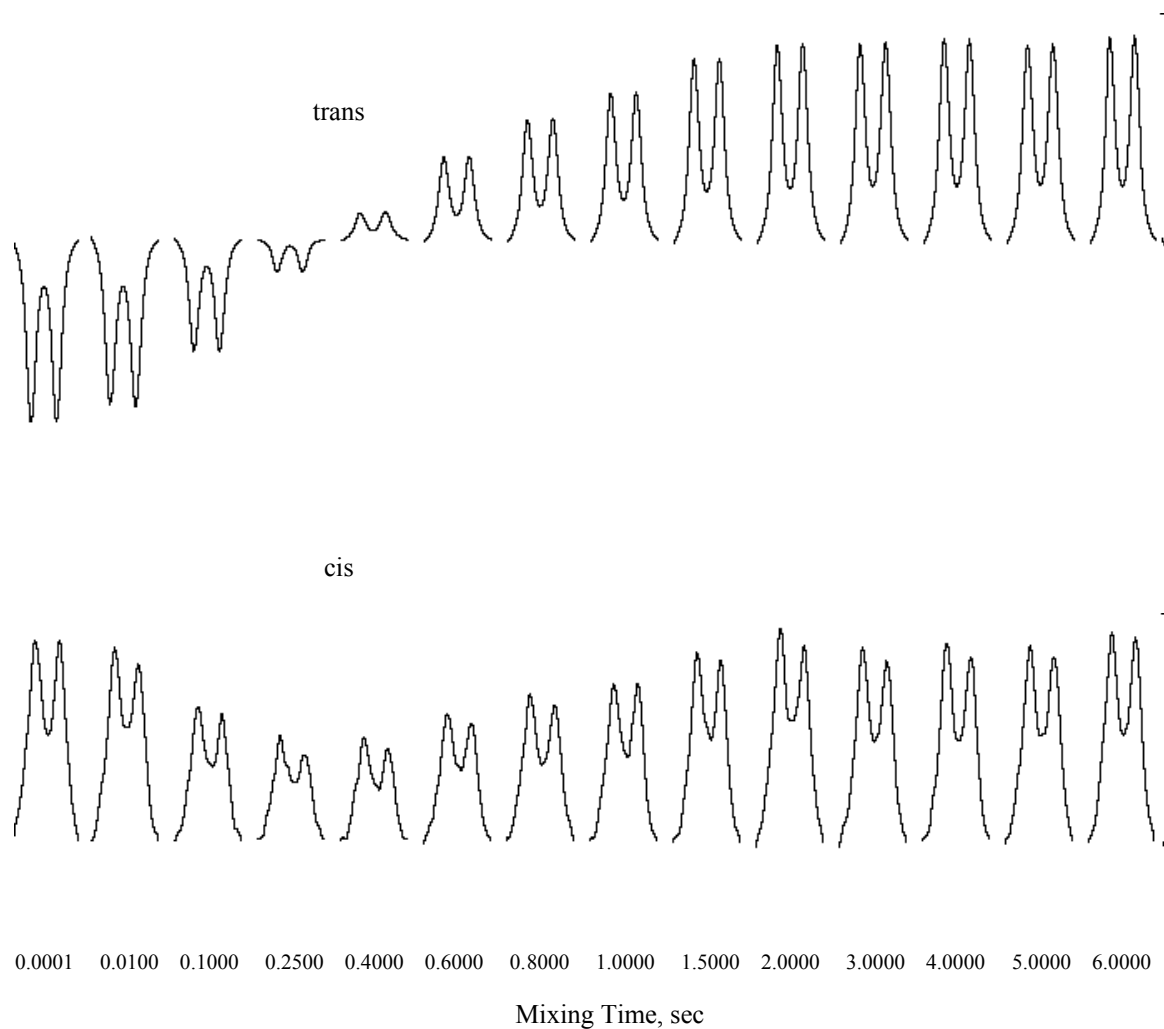
Mixing Time, sec

Figure 4.9. Intensities of the resonances for the alanine methyl protons of the cis and trans isomers of the disulfide form of Ac-Cys-Tyr-Ala-Cys-His-NH$_2$ as a function of the length of the mixing time in the inversion-magnetization transfer experiment. The data are for 22 mM disulfide Ac-Cys-Tyr-Ala-Cys-His-NH$_2$ in 90% H$_2$O/10% D$_2$O at pH 2.91 and 30 ^{o}C. The trans and cis resonances are plotted on different scales.

Table 4.1, the dependence of the intensity of the cis isomer resonance on mixing time was fit using the nonlinear least squares analysis method described in reference 13. To illustrate, the nonlinear least squares fit of the inversion- magnetization transfer data plotted in Figure 4.9 is presented in Figure 4.10. The smooth curve through the points is the theoretical curve obtained by nonlinear least-squares analysis of the data. The k_{ct} rate constant for the disulfide form of Ac-Cys-Tyr-Ala-Cys-His-NH$_2$ was measured directly at 25 °C. The trans→cis isomerization rate constant (k_{tc}) at 25 °C, was then calculated from K_{eq} and k_{ct} ($k_{tc} = k_{ct}/K_{eq}$).

The rate constants for interconversion of the cis isomer to the trans isomer and vice versa at 25 °C for all peptides studied are summarized in Table 4.3. It should be noted that rate constants at 25 °C for peptides 1b, 3b and 4b were obtained indirectly since their rates at 25 °C are slow relative to the magnetization-transfer time scale. To bring their rates of cis/trans isomerization onto the magnetization-transfer time scale, experiments were performed at higher temperatures. Rate constants were measured over a range of elevated temperatures. The k_{ct} values for peptides 1b, 3b and 4b at 25 °C were then calculated using the activation parameters obtained from the k_{ct} values at higher temperatures.

4.2.5 Thermodynamics of Cis/Trans Isomerization of Proline-Free Peptides

Activation parameters $\Delta H_{ct}^{\neq}$ and $\Delta S_{ct}^{\neq}$ were obtained from the Eyring plot of $\ln(k_{ct}/T)$ vs $1/T$ as discussed in Chapter 2. The Gibbs free energy at 25 °C, $\Delta G_{ct}^{\neq}$, is calculated from $\Delta H_{ct}^{\neq}$ and $\Delta S_{ct}^{\neq}$ ($\Delta G_{ct}^{\neq} = \Delta H_{ct}^{\neq} - T\Delta S_{ct}^{\neq}$).

The activation parameters for interconversion of the cis isomer to the trans isomer
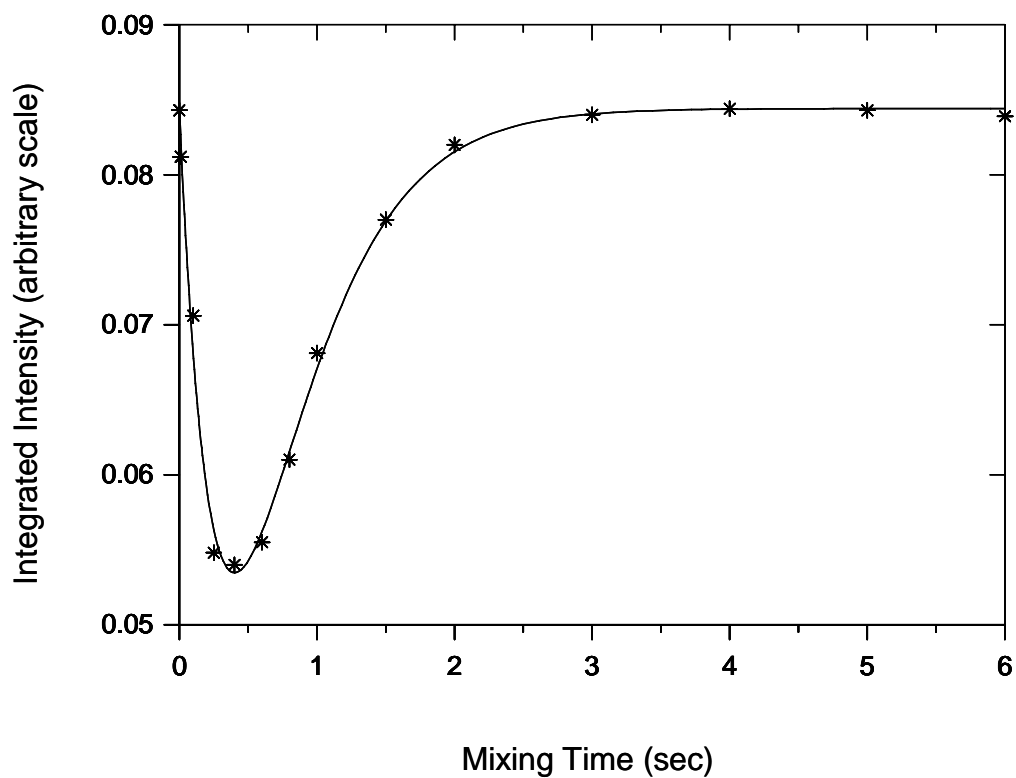
Figure 4.10. Integrated intensities of the resonance for the alanine methyl protons of the cis isomer of the disulfide form of Ac-Cys-Tyr-Ala-Cys-His-NH$_2$ as a function of the mixing time t in the inversion-magnetization transfer pulse sequence. The inversion-magnetization transfer data are for 22 mM disulfide Ac-Cys-Tyr-Ala-Cys-His-NH$_2$ in 90% H$_2$O/10% D$_2$O at pH 2.91 and 25 $^{\circ}$C. The smooth curve through the points is the theoretical curve obtained by nonlinear least-squares analysis of the data.

for all peptides studied are presented in Table 4.3.

4.3 Discussion

The results in Table 4.3 indicate that the population of cis isomers is about the same for both the linear dithiol and cyclic disulfide forms for all the peptides 1-4. Analysis of the rate constants for all the dithiol and disulfide peptides in Table 4.3 shows that the rate constant for trans→cis interconversion is decreased much more than the rate constant for cis→trans interconversion. That is, there is a relative increase in the kinetic stability of the trans conformation in both the dithiol and disulfide forms. Formation of the disulfide bond slows down the rate of cis→trans interconversion (k_{ct}) for peptides 1b-4b, as expected, due to steric constraints and reduced flexibility of the peptide backbones within the disulfide-bridged rings. The rate constant k_{ct} is smaller by 69% for 1b, 10% for 2b, 57% for 3b, and 14% for 4b.

Analysis of the rate constants k_{ct} and k_{tc} for disulfide peptides 1b and 2b in Table 4.3 shows that the rate k_{ct} for 2b is 2.1-fold faster than that of 1b, while the rate k_{tc} for 2b is 1.8-fold faster than that of 1b. Similarly analysis of the rate constants k_{ct} and k_{tc} for disulfide peptides 3b and 4b in Table 4.3 shows that the rate k_{ct} for 4b is 2.9-fold faster than that of 3b, while the rate k_{tc} for 4b is 2.8-fold faster than that of 3b. The analyzed results here show that the rates k_{ct} and k_{tc} are both enhanced for peptides 2b and 4b where alanine is adjacent to Cys[4], suggesting the effect of the amino acid sequence on rate constant for disulfide peptides 1b-4b.

The rate constant k_{ct} and the population of cis conformers for peptides 1a and 2a were compared with the rate constants k_{ct} for proline-free tendamistat[5], RNase T_1

variant[14] and oligopeptides containing tyrosine[7] (Table 4.4). The k_{ct} values for peptides 1a and 2a obtained here is consistent with the rate values of other oligopeptides and proteins. However, the cis content of 1a and 2a is smaller compared to others.

4.4 Summary

The results of quantitative kinetic and thermodynamic studies of secondary amide peptide bond isomerization for a series of model peptides for oxido-reductase enzymes of the Cys-Xaa-Xaa-Cys motif as well as the corresponding cyclic disulfide-bridged peptides reported here may contribute to a better understanding of cis/trans isomerization of secondary amide peptide bond, which in turn may serve as a probe to better understanding the refolding of unfolded proline-free proteins.

	This work		Tendamistat[1]	RNase T$_1$ Variant[2]	Peptides[3]			
	AcCAYCHNH$_2$	AcCYACHNH$_2$			AAYA		AAYAA	
					Ala-Tyr	Tyr-Ala	Ala-Tyr	Tyr-Ala
Relevant bond	Ala-Tyr	Tyr-Ala	n.d.	Tyr-Ala	Ala-Tyr	Tyr-Ala	Ala-Tyr	Tyr-Ala
Percent cis	0.06	0.08	5.0	0.17	0.16	0.19	0.14	0.11
K$_{cis \rightarrow trans}$ (s^{-1})	2.0 ± 0.1	1.4 ± 0.1	2.5 ± 0.2	1.4	1.6	0.5	2.4	1.8

Table 4.4. Comparison of kinetic parameters for secondary amide peptide bond cis/trans isomerization. Rate constants were all determined at 25 °C. (1) Ref. 5; (2) Ref. 14; (3) Ref. 7; n.d., not determined.

4.5 References

1. Heroux, A.; White, E. L.; Ross, L. J.; Davis, R. L.; Borhani, D. W. *Biochemistry* **1999**, *38*, 14495-14506.

2. Stoddard, B. L.; Pietrokovski, S. *Nat. Struct. Biol*. **1998**, *5*, 3-5.

3. Poland, B. W.; Xu, M. Q. ; Quiocho, F. A. *J. Biol. Chem*. **2000**, *275*, 16408-16413.

4. Hobohm, U. ; Sander, C. *Protein Sci*. **1994**, *3*, 522-524.

5. Pappenberger, Gunter; Aygun, H.; Engels, J. W.; Reimer, U.; Fischer, G.; Kiefhaber, T. *Nature Struct. Biol*. **2001**, *8*, 452-458.

6. Yao, J.; Feher, V. A.; Espejo, B. F.; Reymond, M. T.; Wright, P. E.; Dyson, H. J. *J. Mol. Biol*. **1994**, *243*, 736-753.

7. Scherer, G.; Kramer, M. L.; Schutkowski, M.; Reimer, U.; Fischer, G. *J. Am. Chem. Soc.* **1998**, *120*, 5568-5574.

8. Mayr, L. M.; Willbold, D.; Rosch, P.; Schmid, F. X. *J. Mol. Biol*. **1994**, *240*, 288-293.

9. Koivunen, P. ; Helaakoski, T. ; Annunen, P. ; Veijola, J.; Raisanen, S. ; Pihlajaniemi, T. ; Kivirikko, K. I. *Biochem. J.* **1996**, *316*, 599-605.

10. Ferrari, D. M.; Soling, H. D. *Biochem. J.* **1999**, *339*, 1-10.

11. Chivers, P. T.; Laboissiere, M. C. A. ; Raines, R. T. *The EMBO J.* **1996**, *15*, 2659-2667.

12. Beynon-Jones, S. M. ; Antoniou, A. N. ; Powis, S. J. *FEBS Letters* **2006**, *580*, 1897-1902.

13. Maripaan, S. V. S.; Rabenstein, D. L. *J. Mag. Reson*. **1992**.

14. Mayr, L. M.; Willbold, D.; Rosch, P.; Schmid, F. X. *J. Mol. Biol*. **1994**, *240*, 288-293.

Rate constants were obtained for cis→trans interconversion by fitting the
resonance intensity versus mixing time data to an equation, which accounts for transfer of
magnetization by chemical exchange and T1 relaxation.

A nonlinear least square fit was performed on the observed signal by using the
Scientist Program. The model used is presented below, where I0B is the initial intensity
of the cis resonance, IEB is its equilibrium intensity, KEQ is the equilibrium constant for
the cis→trans process, which is equals to [trans]/[cis], K1 is rate constant for the
cis→trans isomerization reaction, and T1A and T1B are the spin-lattice relaxation time
for the trans and cis isomers, respectively.

```
//MicroMath Scientist Cis/Trans Isomerization Model
IndVars: T
DepVars: IAT
Params: K1, I0A, T1A, T1B, IEA

I0B=-2
IEB=2

KEQ=1
A=K1+K1/KEQ+1/T1A+1/T1B
B=(K1/KEQ)/T1A+K1/T1B+1/(T1A*T1B)
C=K1/KEQ*(I0A+I0B)+IEA/T1A+I0A/T1B
D=K1/KEQ*(IEA/T1A+IEB/T1B)+IEA/(T1A*T1B)
L1=-(-A+SQRT(A*A-4*B))/2
L2=-(-A-SQRT(A*A-4*B))/2
PH1=(L1*L1-L1*(C/I0A)+(D/I0A))/(L1*(L2-L1))
PH2=(L2*L2-L2*(C/I0A)+(D/I0A))/(L2*(L1-L2))
IAT=I0A*(IEA/I0A-PH1*EXP((-L1)*T)-PH2*EXP((-L2)*T))

***
```